



Jerome J. Connor · Susan Faraji

Fundamentals of Structural Engineering

 Springer

Fundamentals of Structural Engineering

Jerome J. Connor • Susan Faraji

Fundamentals of Structural Engineering



Jerome J. Connor
Department of Civil
& Environmental Engineering
Massachusetts Institute of Technology
Cambridge, MA, USA

Susan Faraji
Department of Civil
& Environmental Engineering
University of Massachusetts-Lowell
Lowell, MA, USA

ISBN 978-1-4614-3261-6

ISBN 978-1-4614-3262-3 (eBook)

DOI 10.1007/978-1-4614-3262-3

Springer New York Heidelberg Dordrecht London

Library of Congress Control Number: 2012940713

© Springer Science+Business Media, LLC 2013

This work is subject to copyright. All rights are reserved by the Publisher, whether the whole or part of the material is concerned, specifically the rights of translation, reprinting, reuse of illustrations, recitation, broadcasting, reproduction on microfilms or in any other physical way, and transmission or information storage and retrieval, electronic adaptation, computer software, or by similar or dissimilar methodology now known or hereafter developed. Exempted from this legal reservation are brief excerpts in connection with reviews or scholarly analysis or material supplied specifically for the purpose of being entered and executed on a computer system, for exclusive use by the purchaser of the work. Duplication of this publication or parts thereof is permitted only under the provisions of the Copyright Law of the Publisher's location, in its current version, and permission for use must always be obtained from Springer. Permissions for use may be obtained through RightsLink at the Copyright Clearance Center. Violations are liable to prosecution under the respective Copyright Law.

The use of general descriptive names, registered names, trademarks, service marks, etc. in this publication does not imply, even in the absence of a specific statement, that such names are exempt from the relevant protective laws and regulations and therefore free for general use.

While the advice and information in this book are believed to be true and accurate at the date of publication, neither the authors nor the editors nor the publisher can accept any legal responsibility for any errors or omissions that may be made. The publisher makes no warranty, express or implied, with respect to the material contained herein.

Printed on acid-free paper

Springer is part of Springer Science+Business Media (www.springer.com)

Preface

Audience

The intended audience of this book is that of students majoring in civil engineering or architecture who have been exposed to the basic concepts of engineering mechanics and mechanics of materials. The book is sufficiently comprehensive to be used for both elementary and higher level undergraduate structures subjects. In addition, it can serve students as a valuable resource as they study for the engineering certification examination and as a reference later in their careers. Practicing professionals will also find the book useful for self-study, for review for the professional registration examination, and as a reference book.

Motivation

The availability of inexpensive digital computers and user-friendly structural engineering software has revolutionized the practice of structural engineering. Engineers now routinely employ computer-based procedures throughout the various phases of the analysis and design detailing processes. As a result, with these tools engineers can now deal with more complex structures than in the past. Given that these tools are now essential in engineering practice, the critical question facing faculty involved in the teaching of structural engineering is “How the traditional teaching paradigm should be modified for the computer age?” We believe that more exposure to computer-based analysis is needed at an early stage in the course development. However, since the phrase “garbage in garbage out” is especially relevant for computer-based analysis, we also believe that the student needs to develop, through formal training in analysis methodology, the ability to estimate qualitatively the behavior of a structure subjected to a given loading and to confirm qualitative estimates with some simple manual computations.

Based on a review of the current structural engineering academic literature, it appears that the current set of undergraduate textbooks are focused mainly on either (i) teaching manual analysis methods and applying them to simple idealized structures or (ii) reformulating structural analysis methods in terms of matrix notation. The first approach is based on the premise that intuition about structural behavior is developed as one works through the manual computations, which, at times, may seem exhaustive. The second approach provides the basis for developing and understanding computer software codes but does not contribute toward developing intuition about structural behavior.

Clearly there is a need for a text that provides a balanced treatment of both classical and modern computer-based analysis methods in a seamless way and also stresses the development of an intuitive understanding of structural behavior. Engineers reason about behavior using simple models and intuition that they have acquired through problem-solving experience. The approach adopted in this text is to develop this type of intuition through computer simulation which allows one to rapidly explore how the structure responds to changes in geometry and physical parameters. We believe this approach better prepares the reader for the practice of structural engineering.

Objectives

Structural engineers have two major responsibilities during the design process. First, they must synthesize the structural system, i.e., select the geometry and the type of structural members that make up the structure. Second, they must size the members such that the structure can comfortably support the design loading. Creating a structural concept requires a deep knowledge of structural behavior. Sizing the members requires information about the internal forces resulting from the loading. These data are acquired through intelligent application of analysis methods, mainly computer-based methods. With these responsibilities in mind, we have selected the following objectives for this book:

- *Develop the reader's ability to analyze structures using manual computational procedures.*
- *Educate the reader about structural behavior.* We believe that a strong analytical background based on classical analysis methodology combined with computer simulation facilitates the development of an understanding of structural behavior.
- *Provide the reader with an in-depth exposure to computer-based analysis methods.* Show how computer-based methods can be used to determine, with minimal effort, how structures respond to loads and also how to establish the extreme values of design variables required for design detailing.
- *Develop the reader's ability to validate computer-based predictions of structural response.*

-
- *Provide the reader with idealization strategies for reducing complex structures to simple structural models.*
 - *Develop an appreciation for and an awareness of the limitations of using simple structural models to predict structural behavior through examples which illustrate behavioral trends as structures become more complex.*
-

Organization

We have organized this text into three parts. Parts I and II are intended to provide the student with the necessary computational tools and also to develop an understanding of structural behavior by covering analysis methodologies, ranging from traditional classical methods through computer-based methods, for skeletal type structures, i.e., structures composed of one-dimensional slender members. Part I deals with statically determinate structures; statically indeterminate structures are covered in Part II. Certain classical methods which we consider redundant have been omitted. Some approximate methods which are useful for estimating the response using hand computations have been included. Part III is devoted to structural engineering issues for a range of structures frequently encountered in practice. Emphasis is placed on structural idealization; how one identifies critical loading patterns; and how one generates the extreme values of design variables corresponding to a combination of gravity, live, wind, earthquake loading, and support settlement using computer software systems.

A Web site containing computer analysis files for certain examples and homework problems is provided. This information can be accessed at <http://extras.springer.com>

Brief descriptions of the subject content for each part are presented below.

Part I discusses statically determinate structures. We start with an introduction to structural engineering. Statically determinate structures are introduced next. The treatment is limited to linear elastic behavior and static loading. Separate chapters are devoted to different skeletal structural types such as trusses, beams, frames, cables, curved members, footings, and retaining walls. Each chapter is self-contained in that all the related analysis issues for the particular structural type are discussed and illustrated. For example, the chapter on beams deals with constructing shear and moment diagrams, methods for computing the deflection due to bending, influence lines, force envelopes, and symmetry properties. We find it convenient from a pedagogical perspective to concentrate the related material in one location. It is also convenient for the reader since now there is a single source point for knowledge about each structural type rather than having the knowledge distributed throughout the text. We start with trusses since they involve the least amount of theory. The material on frames is based on beam theory so it is logical to present it directly after beam theory. Cables and curved members are special structural types that generally receive a lower priority, due to time constraints, when selecting a syllabus for an introductory course.

We have included these topics here, as well as a treatment of footings and retaining walls, because they are statically determinate structures. We revisit these structures later in Part III.

Part II presents methods for analyzing statically indeterminate structures and applies these methods to a broad range of structural types. Two classical analysis methods are described, namely the force (also referred to as the flexibility) method and the displacement (or stiffness) method are presented. We also present some approximate analysis methods that are based on various types of force and stiffness assumptions. These methods are useful for estimating the structural response due to lateral loads using simple hand computations. Lastly, we reformulate the traditional displacement method as a finite element method using matrix notation. The finite element formulation (FEM) is the basis of most existing structural analysis software packages. Our objectives here are twofold: First, we want to enable the reader to be able to use FEM methods in an *intelligent way*, and second, we want the reader to develop an understanding of structural behavior by applying analysis methods to a broad range of determinate and indeterminate skeletal structures. *We believe that using computer analysis software as a simulation tool to explore structural behavior is a very effective way of building up a knowledge base of behavioral modes, especially for the types of structures commonly employed in practice.*

Part III discusses typical structural engineering problems. Our objective here is to expose the reader to a select set of activities that are now routinely carried out by structural engineers using structural engineering software. These activities are related to the approach followed to establish the “values” for the design variables. Defining these values is the key step in the engineering design process; once they are known, one can proceed to the design detailing phase. Specific chapters deal with horizontal structures such as multi-span girder, arch, and cable-stayed bridge systems; modeling of three-dimensional vertical structures subjected to lateral loading; and vertical structures such as low and high rise buildings subjected to gravity loading. The topics cover constructing idealized structural models; establishing the critical design loading patterns for a combination of gravity and live loading; using analysis software to compute the corresponding design values for the idealized structures; defining the lateral loading due to wind and earthquake excitation for buildings; and estimating the three-dimensional response of low rise buildings subjected to seismic and wind loadings.

The Web site provides input files for examples and selected homework problems. Computer solutions are generated for certain example problems contained in the text using Mathcad [29], Matlab [30], and GTSTRUDL® [31]. The corresponding input files for these problems are available on extras.springer.com. In addition, a number of homework problems requiring computer solutions are included in the various chapters. Providing this information avoids the need for the student to be trained on the software.

Course Suggestions

The following suggestions apply for students majoring in either civil engineering or architecture. Depending on the time available, we suggest organizing the material into either a two-semester or a three-semester sequence of subjects.

Our recommendations for the three-semester sequence are as follows:

Structures I

The goal of this subject is to provide the skills for the analysis of statically determinate trusses, beams, frames, and cables, and to introduce some computer-based analysis methods.

Chapters 1, 2, part of 3, part of 4, and the first part of 5

Structures II

The objectives of this subject are to present both classical and computer-based analysis methods for statically indeterminate structures such as multi-span beams, gable frames, arches, and cable-stayed structures subjected to various loadings. The emphasis is on using analysis methods to develop an understanding of the behavior of structures.

Chapters 9, 10, 11, 12, 6, and the last part of 5

Structures III

This subject is intended to serve as an introduction to the practice of structural engineering. The material is presented as case studies for the two most common types of structures, bridges, and buildings. Issues such as geometrical configurations, idealized structural models, types and distribution of loadings, determination of the values of the design variables such as the peak moment in a beam, and force envelopes are discussed. Both the superstructure and the substructure components are considered. Extensive use of computer software is made throughout the subject. Recitation classes dealing with the design detailing of steel and concrete elements can be taught in parallel with the lectures.

Chapters 13, 14, 15, 7, and 8

The makeup of the two-semester sequence depends on how much background in mechanics and elementary structures the typical student has and the goal of the undergraduate program. One possibility is to teach Structures I and II described above. Another possible option is to combine Structures I and II into a single subject offering together with Structures III. A suggested combined subject is listed below.

Structures (Combined I + II)

Chapters 3, 4 (partial), 9 (partial), 10, 11, and 12

Features of the Text

Organization by Structural Type

The chapters are organized such that an individual chapter contains all the information pertaining to a particular structural type. We believe this organization facilitates access to information. Since the basic principles are generic, it also reinforces these principles throughout the development of successive chapters.

Classical Analysis Methods

In-depth coverage of classical analysis methods with numerous examples helps students learn fundamental concepts and develop a “feel” and context for structural behavior.

Analysis by Hand Computation

The book helps teach students to do simple hand computing, so that as they move into doing more complex computational analysis, they can quickly check that their computer-generated results make sense.

Gradual Introduction of Computer Analysis

The text provides students with a gradual transition from classical methods to computational methods, with examples and homework problems designed to bring students along by incorporating computational methods when most appropriate.

Finite Element Methods

In-depth coverage of finite element methods for skeletal structures. Input files are available for all relevant example problems and homework exercises, so that students can more easily use the software.

Detailed Sample Problems

Sample problems in each chapter illustrate detailed solutions to structural analysis problems, including some problems illustrating computer analysis. Most of the sample problems are based on real scenarios that students will encounter in professional practice.

Units

Both SI and customary US units are used in the examples and homework problems.

Homework Problems That Build Students' Skills

An extensive set of homework problems for each chapter provides students with more exposure to the concepts and skills developed in the chapters. The difficulty level is varied so that students can build confidence by starting with simple problems, and advancing toward more complex problems.

Comprehensive Breadth and Depth, Practical Topics

The comprehensive breadth and depth of this text means it may be used for two or more courses, so it is useful to students for their courses and as a professional reference. Special topics such as the simplifications associated with symmetry and anti-symmetry, arch type structures, and cable-stayed structures are topics that a practicing structural engineer needs to be familiar with.

Acknowledgements

We would like to thank our spouses Barbara Connor and Richard Hennessey for their patience and moral support over the seemingly endless time required to complete this text. We are most appreciative. We would also like to thank our colleagues and students who provided us with many valuable suggestions concerning the content and organization of the text. We are especially indebted to Dr. Moneer Tewfik and Dr. Carlos Brebbia for their constructive criticisms and enthusiastic support as the text was evolving into its final form.

Contents

| | | |
|---------------|-----------------------------------------------------------|----------|
| Part I | Statically Determinate Structures | 1 |
| 1 | Introduction to Structural Engineering | 3 |
| 1.1 | Types of Structures and Structural Components | 4 |
| 1.1.1 | Structural Components | 4 |
| 1.1.2 | Types of Structures | 4 |
| 1.2 | Critical Concerns of Structural Engineering | 7 |
| 1.2.1 | Reactions | 10 |
| 1.2.2 | Initial Stability | 10 |
| 1.2.3 | Loss of Stability Due to Material Failure | 12 |
| 1.2.4 | Buckling Failure Mode | 13 |
| 1.2.5 | Priorities for Stability | 14 |
| 1.3 | Types of Loads | 14 |
| 1.3.1 | Source of Loads | 15 |
| 1.3.2 | Properties of Loadings | 17 |
| 1.3.3 | Gravity Live Loads | 19 |
| 1.3.4 | Wind Loading | 20 |
| 1.3.5 | Snow Loading | 26 |
| 1.3.6 | Earthquake Loading | 28 |
| 1.4 | Structural Design Philosophy | 30 |
| 1.5 | Basic Analytical Tools of Structural Analysis | 31 |
| 1.5.1 | Concept of Equilibrium-Concurrent Force System | 32 |
| 1.5.2 | Concept of Equilibrium: Non-concurrent Force System | 33 |
| 1.5.3 | Idealized Structure: Free Body Diagrams | 35 |
| 1.5.4 | Internal Forces | 35 |
| 1.5.5 | Deformations and Displacements | 38 |
| 1.5.6 | Structural Behavior; Structural Analysis | 39 |
| 1.5.7 | The Importance of Displacements | 45 |
| 1.6 | Summary | 47 |
| 1.6.1 | Objectives of the Chapter | 47 |
| 1.6.2 | Key Issues and Concepts Introduced | 47 |

| | | |
|----------|-----------------------------------------------------------------------------------|-----|
| 2 | Statically Determinate Truss Structures | 51 |
| 2.1 | Introduction: Types of Truss Structures | 51 |
| 2.1.1 | Structural Idealization | 54 |
| 2.1.2 | Historical Background | 54 |
| 2.2 | Analysis of Planar Trusses | 61 |
| 2.2.1 | Equilibrium Considerations | 61 |
| 2.2.2 | Statically Determinate Planar Trusses | 62 |
| 2.2.3 | Stability Criterion | 63 |
| 2.2.4 | Method of Joints: Planar Trusses | 67 |
| 2.2.5 | Method of Sections | 83 |
| 2.2.6 | Complex Trusses | 94 |
| 2.3 | Computation of Deflections | 100 |
| 2.3.1 | Introduction | 100 |
| 2.3.2 | Force–Deformation Relationship | 100 |
| 2.3.3 | Deformation–Displacement Relations | 102 |
| 2.3.4 | Method of Virtual Forces | 105 |
| 2.4 | Influence Lines | 117 |
| 2.5 | Analysis of Three-Dimensional Trusses | 132 |
| 2.5.1 | Introduction | 132 |
| 2.5.2 | Restraining Rigid Body Motion | 133 |
| 2.5.3 | Static Determinacy | 137 |
| 2.5.4 | Method of Joints for 3-D Trusses | 139 |
| 2.6 | Matrix Formulation: Equilibrium Analysis of Statically Determinate 3-D Trusses | 150 |
| 2.6.1 | Notation | 150 |
| 2.6.2 | Member–Node Incidence | 152 |
| 2.6.3 | Force Equilibrium Equations | 152 |
| 2.6.4 | Stability | 154 |
| 2.6.5 | Matrix Formulation: Computation of Displacements | 154 |
| 2.7 | Summary | 161 |
| 2.7.1 | Objectives of the Chapter | 161 |
| 2.7.2 | Key Facts and Concepts | 161 |
| 2.8 | Problems | 162 |
| 3 | Statically Determinate Beams | 185 |
| 3.1 | Definition of a Prismatic Beam | 185 |
| 3.2 | Stability and Determinacy of Beams: Planar Bending | 188 |
| 3.2.1 | Fixed Support: Planar Loading | 190 |
| 3.2.2 | Hinged Support: Planar Loading | 190 |
| 3.2.3 | Roller Support: Planar Loading | 191 |
| 3.2.4 | 3-D Fixed Support | 192 |
| 3.2.5 | 3-D Hinged Support | 192 |
| 3.2.6 | 3-D Roller Support: Z Direction | 192 |
| 3.2.7 | Static Determinacy: Planar Beam Systems | 193 |
| 3.2.8 | Unstable Support Arrangements | 193 |

| | | |
|----------|-------------------------------------------------------------------------------|------------|
| 3.2.9 | Beam with Multiple Supports | 193 |
| 3.2.10 | Beam with a Moment Release | 194 |
| 3.3 | Reactions: Planar Loading | 196 |
| 3.4 | Internal Forces: Planar Loading | 204 |
| 3.5 | Differential Equations of Equilibrium: Planar Loading | 213 |
| 3.6 | Displacement and Deformation of Slender Beams: Planar Loading | 235 |
| 3.6.1 | Moment: Curvature Relationship | 237 |
| 3.6.2 | Qualitative Reasoning about Deflected Shapes | 238 |
| 3.6.3 | Moment Area Theorems | 243 |
| 3.6.4 | Computing Displacements with the Conjugate Beam Method | 254 |
| 3.6.5 | Computing Displacements with the Method of Virtual Forces | 259 |
| 3.6.6 | Computing Displacements for Non-prismatic Members | 270 |
| 3.7 | Deformation–Displacement Relations for Deep Beams: Planar Loading | 274 |
| 3.8 | Torsion of Prismatic Members | 277 |
| 3.9 | Symmetry and Anti-symmetry | 280 |
| 3.9.1 | Symmetry and Anti-symmetry: Shear and Moment Diagrams | 280 |
| 3.9.2 | Symmetry and Anti-Symmetry: Deflected Shapes | 283 |
| 3.10 | Influence Lines and Force Envelopes for Statically Determinate Beams | 287 |
| 3.10.1 | The Engineering Process | 287 |
| 3.10.2 | Influence Lines | 290 |
| 3.10.3 | Force Envelopes | 316 |
| 3.11 | Summary | 329 |
| 3.11.1 | Objectives of the Chapter | 329 |
| 3.11.2 | Key Facts and Concepts | 329 |
| 3.12 | Problems | 330 |
| 4 | Statically Determinate Plane Frames | 355 |
| 4.1 | Definition of Plane Frames | 355 |
| 4.2 | Statical Determinacy: Planar Loading | 357 |
| 4.3 | Analysis of Statically Determinate Frames | 360 |
| 4.3.1 | Behavior of Portal Frames: Analytical Solution | 373 |
| 4.4 | Pitched Roof Frames | 378 |
| 4.4.1 | Member Loads | 378 |
| 4.4.2 | Analytical Solutions for Pitched Roof Frames | 381 |
| 4.5 | A-Frames | 396 |

| | | |
|----------|----------------------------------------------------------------------|------------|
| 4.6 | Deflection of Frames Using the Principle of Virtual Forces | 399 |
| 4.7 | Deflection Profiles: Plane Frame Structures | 412 |
| 4.8 | Computer-Based Analysis: Plane Frames | 415 |
| 4.9 | Plane Frames: Out of Plane Loading | 415 |
| 4.10 | Summary | 419 |
| 4.10.1 | Objectives | 419 |
| 4.10.2 | Key Concepts | 420 |
| 4.11 | Problems | 420 |
| 5 | Cable Structures | 443 |
| 5.1 | Introduction | 443 |
| 5.2 | Cables Subjected to Concentrated Loads | 445 |
| 5.2.1 | Horizontal Cables | 445 |
| 5.2.2 | Inclined Cables | 453 |
| 5.3 | Cables Subjected to Distributed Loading | 458 |
| 5.3.1 | Horizontal Cable: Uniform Loading per Horizontal Projection | 458 |
| 5.3.2 | Inclined Cables | 460 |
| 5.4 | Advanced Topics | 464 |
| 5.4.1 | Arc Length | 464 |
| 5.4.2 | Equivalent Axial Stiffness | 468 |
| 5.4.3 | Equivalent Axial Stiffness for an Inclined Cable | 471 |
| 5.4.4 | Cable Shape Under Self Weight: Catenary | 474 |
| 5.5 | Summary | 478 |
| 5.5.1 | Objectives | 478 |
| 5.5.2 | Key Concepts | 478 |
| 5.6 | Problems | 479 |
| 6 | Statically Determinate Curved Members | 489 |
| 6.1 | A Brief History of Arch-Type Structures | 489 |
| 6.2 | Modeling of Arch Structures | 494 |
| 6.3 | Internal Forces in Curved Members | 498 |
| 6.4 | Parabolic Geometry | 503 |
| 6.5 | Method of Virtual Forces for Curved Members | 510 |
| 6.5.1 | Non-shallow Slender Curved Members | 511 |
| 6.5.2 | Shallow Slender Curved Members | 511 |
| 6.5.3 | Circular Curved Member | 515 |
| 6.6 | Analysis of Three-Hinged Arches | 518 |
| 6.7 | Summary | 533 |
| 6.7.1 | Objectives | 533 |
| 6.7.2 | Key Factors and Concepts | 534 |
| 6.8 | Problems | 534 |

| | |
|-------------------------------------------------------------------------------------------------|-----|
| 7 Shallow Foundations | 545 |
| 7.1 Introduction | 545 |
| 7.1.1 Types of Foundations | 545 |
| 7.1.2 Types of Shallow Foundations | 546 |
| 7.1.3 Soil Pressure Distribution | 547 |
| 7.2 An Analytical Method for Evaluating the Soil Pressure Distribution under a Footing | 550 |
| 7.3 Dimensioning a Single Rectangular Footing | 554 |
| 7.4 Dimensioning Combined Footings | 565 |
| 7.5 Dimensioning Strap Footings | 575 |
| 7.6 Summary | 587 |
| 7.6.1 Objectives of the Chapter | 587 |
| 7.7 Problems | 587 |
| 8 Vertical Retaining Wall Structures | 599 |
| 8.1 Introduction | 599 |
| 8.1.1 Types of Retaining Walls | 599 |
| 8.1.2 Gravity Walls | 600 |
| 8.1.3 Cantilever Walls | 601 |
| 8.2 Force Due to the Backfill Material | 601 |
| 8.2.1 Different Types of Materials | 601 |
| 8.2.2 Rankine Theory: Active Soil Pressure | 604 |
| 8.3 Stability Analysis of Retaining Walls | 605 |
| 8.4 Pressure Distribution Under the Wall Footing | 611 |
| 8.5 Critical Sections for Design of Cantilever Walls | 623 |
| 8.6 Summary | 627 |
| 8.6.1 Objectives of the Chapter | 627 |
| 8.6.2 Key Concepts and Facts | 627 |
| 8.7 Problems | 628 |
| Part II Statically Indeterminate Structures | 633 |
| 9 The Force Method | 635 |
| 9.1 Introduction | 635 |
| 9.2 Maxwell's Law of Reciprocal Displacements | 644 |
| 9.3 Application of the Force Method to Beam-Type Structures | 647 |
| 9.3.1 Beam with Yielding Supports | 654 |
| 9.3.2 Fixed-Ended Beams | 668 |
| 9.3.3 Analytical Solutions for Multi-span Beams | 673 |
| 9.4 Application to Arch-Type Structures | 683 |
| 9.5 Application to Frame-Type Structures | 693 |
| 9.5.1 General Approach | 694 |
| 9.5.2 Portal Frames | 695 |
| 9.5.3 Pitched Roof Frames | 707 |

| | | |
|-----------|---------------------------------------------------------------------------------------------------|------------|
| 9.6 | Indeterminate Trusses | 712 |
| 9.7 | Summary | 719 |
| 9.7.1 | Objectives | 719 |
| 9.7.2 | Key Factors and Concepts | 720 |
| 9.8 | Problems | 720 |
| 10 | The Displacement Method | 737 |
| 10.1 | Introduction | 737 |
| 10.2 | Displacement Method Applied to a Plane Truss | 739 |
| 10.3 | Member Equations for Frame-Type Structures | 742 |
| 10.4 | The Displacement Method Applied to Beam Structures | 747 |
| 10.4.1 | Two Span Beams | 747 |
| 10.5 | The Displacement Method Applied to Rigid Frames | 775 |
| 10.5.1 | Portal Frames: Symmetrical Loading | 779 |
| 10.5.2 | Portal Frames Anti-symmetrical Loading | 781 |
| 10.6 | The Moment Distribution Solution Procedure for Multi-span Beams | 788 |
| 10.6.1 | Introduction | 788 |
| 10.6.2 | Incorporation of Moment Releases at Supports | 793 |
| 10.6.3 | Moment Distribution for Multiple Free Nodes | 795 |
| 10.7 | Moment Distribution: Frame Structures | 800 |
| 10.7.1 | Frames: No Sideway | 800 |
| 10.7.2 | Frames with Sideway | 809 |
| 10.8 | Plane Frames: Out of Plane Loading | 821 |
| 10.8.1 | Slope-Deflection Equations: Out of Plane Loading | 821 |
| 10.9 | Summary | 826 |
| 10.9.1 | Objectives | 826 |
| 10.9.2 | Key Factors and Concepts | 826 |
| 10.10 | Problems | 827 |
| 11 | Approximate Methods for Estimating Forces in Statically Indeterminate Structures | 843 |
| 11.1 | Introduction | 843 |
| 11.2 | Multi-span Beams: Gravity Loading | 844 |
| 11.2.1 | Basic Data-Moment Diagrams | 844 |
| 11.2.2 | Quantitative Reasoning Based on Relative Stiffness | 845 |
| 11.3 | Multistory Rigid Frames: Gravity Loading | 847 |
| 11.4 | Multistory Rigid Frames: Lateral Loading | 849 |
| 11.4.1 | Portal Method | 850 |
| 11.4.2 | Shear Stiffness Method: Low-Rise Rigid Frames | 857 |
| 11.4.3 | Low-Rise Rigid Frames with Bracing | 863 |

| | | |
|----------------------------------------------------------|---------------------------------------------------------------------------------|------------|
| 11.5 | High-Rise Rigid Frames: The Cantilever Method | 870 |
| 11.6 | Summary | 876 |
| 11.6.1 | Objectives of the Chapter | 876 |
| 11.6.2 | Key Concepts | 876 |
| 11.7 | Problems | 876 |
| 12 | Finite Element Displacement Method for Framed Structures | 885 |
| 12.1 | Introduction | 885 |
| 12.2 | Key Steps of the Finite Element Displacement Method for Member Systems | 886 |
| 12.3 | Matrix Formulation of the Member Equations: Planar Behavior | 887 |
| 12.4 | Local and Global Reference Frames | 890 |
| 12.5 | Nodal Force Equilibrium Equations | 893 |
| 12.6 | Introduction of Nodal Supports | 900 |
| 12.6.1 | Systematic Approach | 901 |
| 12.7 | Specialized Formulation for Beam and Truss Structures | 916 |
| 12.7.1 | The Steps Involved for Plane Truss Structures | 917 |
| 12.7.2 | The Steps Involved for Beam Structures with Transverse Loading | 923 |
| 12.8 | Three-Dimensional Formulation | 935 |
| 12.9 | Summary | 938 |
| 12.9.1 | Objectives | 938 |
| 12.10 | Problems | 939 |
| Part III Practice of Structural Engineering | | 953 |
| 13 | Multi-span Horizontal Structures | 955 |
| 13.1 | The Engineering Process for Girders | 955 |
| 13.2 | Influence Lines for Indeterminate Beams Using Müller-Breslau Principle | 957 |
| 13.3 | Engineering Issues for Multi-span Girder Bridges | 962 |
| 13.3.1 | Geometric Configurations | 962 |
| 13.3.2 | Choice of Span Lengths | 965 |
| 13.3.3 | Live Loads for Multi-span Highway Bridge Girders: Moment Envelopes | 968 |
| 13.3.4 | Loading Due to Support Settlements | 972 |
| 13.4 | Case Studies | 976 |
| 13.4.1 | Case Study I: A Three-Span Continuous Girder Bridge | 976 |
| 13.4.2 | Case Study II: Two-Hinged Parabolic Arch Response: Truck Loading | 982 |

| | | |
|-----------|---------------------------------------------------------------------------------------------|-------------|
| 13.4.3 | Case Study III: Three-Span Parabolic Arch Response: Truck Loading | 985 |
| 13.4.4 | Case Study IV: Cable-Stayed Bridge | 986 |
| 13.5 | Summary | 992 |
| 13.5.1 | Objectives | 992 |
| 13.5.2 | Key Facts and Concepts | 992 |
| 13.6 | Problems | 992 |
| 14 | Lateral Load Issues for Buildings | 999 |
| 14.1 | Types of Multistory Building Systems | 999 |
| 14.2 | Treatment of Lateral Loading | 1001 |
| 14.2.1 | Wind Loading | 1002 |
| 14.2.2 | Earthquake Loading | 1003 |
| 14.3 | Building Response Under Lateral Loads | 1011 |
| 14.3.1 | Center of Twist: One Story Frame | 1012 |
| 14.3.2 | Center of Mass: One Story Frame | 1026 |
| 14.3.3 | One Story Frame: General Response | 1029 |
| 14.3.4 | Multistory Response | 1032 |
| 14.3.5 | Matrix Formulation: Shear Beam Model | 1035 |
| 14.4 | Response of Symmetrical Buildings | 1039 |
| 14.5 | Summary | 1056 |
| 14.5.1 | Objectives | 1056 |
| 14.5.2 | Key Facts and Concepts | 1057 |
| 14.6 | Problems | 1057 |
| 15 | Vertical Loads on Multistory Buildings | 1069 |
| 15.1 | Loads on Frames | 1069 |
| 15.2 | Treatment of Gravity Floor Loads | 1071 |
| 15.3 | Live Load Patterns for Frame Structures | 1074 |
| 15.4 | A Case Study: Four-Story Building | 1087 |
| 15.4.1 | Building Details and Objectives | 1087 |
| 15.5 | Analysis Procedures for Bracing Scheme | 1089 |
| 15.5.1 | Case (1) Frames Are Braced in Both N–S and E–W Directions: Building Details | 1089 |
| 15.5.2 | Case (1) Beam Properties in the N–S and E–W Directions | 1091 |
| 15.5.3 | Case (1) Bracing Systems | 1093 |
| 15.5.4 | Case (1) Interior Columns | 1097 |
| 15.5.5 | Summary for Case (1) | 1098 |
| 15.5.6 | Case (2) Frames Are Rigid in the N–S Direction but Remain Braced in the E–W Direction | 1098 |
| 15.5.7 | Strategy for N–S Beams and Columns | 1098 |
| 15.5.8 | Live Load Patterns | 1102 |

| | | |
|-------------------|----------------------------|------|
| 15.5.9 | Moment Diagrams | 1102 |
| 15.5.10 | Design Values | 1107 |
| 15.5.11 | Summary for Case (2) | 1112 |
| 15.6 | Summary | 1112 |
| 15.6.1 | Objectives | 1112 |
| 15.6.2 | Key Concepts | 1112 |
| 15.7 | Problems | 1113 |
| References | | 1121 |
| Index | | 1123 |

Photo Credits

Chapter 1

Fig. 1.1c Offshore Platform, Brazil. This image was produced by Agência Brasil, a public Brazilian news agency and published under a Creative Commons Attribution License. It was accessed in February 2012 from [http://en.wikipedia.org/wiki/File:Oil_platform_P-51_\(Brazil\).jpg](http://en.wikipedia.org/wiki/File:Oil_platform_P-51_(Brazil).jpg)

Fig. 1.1a Skyscraper under construction in Kutuzovsky Prospekt, Moscow, Russia. This image, created by Denghu, is licensed under a Creative Commons Attribution 3.0 Unported License. The image was accessed in April 2012 from http://commons.wikimedia.org/wiki/File:Skyscraper_Kutuzovsky_Prospekt_Moscow.jpg

Fig. 1.8 Millau Viaduct, Author: Delphine DE ANDRIA Date: 18.11.2007, from FreeMages. Accessed May 2012 from <http://www.freemages.co.uk/browse/photo-916-millau-viaduct.html>. This work is licensed under a Creative Commons Attribution 3.0 Unported License.

Chapter 2

Fig. 2.13 Three-dimensional truss of roof system. This image of the lead shot tower in Melbourne, Australia, created by freeaussiestock.com, is licensed under a Creative Commons Attribution 3.0 Unported License. The image was accessed in February 2012 from http://freeaussiestock.com/free/Victoria/Melbourne/slides/shot_tower.htm

Chapter 5

Fig. 5.1 Clifton Suspension bridge, England. Picture taken by Adrian Pingstone in October 2003 and placed in the public domain. Accessed in February 2012 from <http://commons.wikimedia.org/wiki/File:Clifton.bridge.arp.750pix.jpg>

Fig. 5.5 Munich Olympic stadium, view from Olympic Tower. Picture taken by Arad Mojtabaei in July 2008 and placed in the public domain. Accessed in May 2012 from http://commons.wikimedia.org/wiki/File:Olympiastadion_Muenchen.jpg

Fig. 5.21 Millau Viaduct, Author: Delphine DE ANDRIA, Date: 18.11.2007, from FreeMages. Accessed in May 2012 from <http://www.freemages.co.uk/browse/photo-916-millau-viaduct.html>. This work is licensed under a Creative Commons Attribution 3.0 Unported License.

Chapter 6

Fig. 6.5 Alcantara Toledo Bridge, Puente de Alcántara, Toledo, Spain. This image was originally posted to Flickr on December 19, 2006 and published under a Creative Commons Attribution License. It was accessed in February 2012 from http://commons.wikimedia.org/wiki/File:Puente_Alcantara_toledo.jpg

Fig. 6.7 Eads Bridge, USA. This image was originally posted to Flickr by Kopper at <http://flickr.com/photos/94086509@N00/2745897992>. It was reviewed on January 18, 2011 (2011-01-18) by the FlickreviewR robot and confirmed to be licensed under the terms of the cc-by-2.0 (Creative Commons Attribution 2.0). It was accessed in February 2012 from http://commons.wikimedia.org/wiki/File:Eads_Bridge-1.jpg

Fig. 6.8 Salginatobel Bridge, Switzerland. Bild (Figure) 1.4-45 Ansicht der Salginatobelbrücke. P. 81 in Mehlhorn, G. et al. "Brückenbau auf dem Weg vom Altertum zum modernen Brückenbau," in Handbuch Brücken. Gerhard Mehlhorn (Ed). Berlin, Heidelberg. Springer-Verlag (2010)

Fig. 6.9a New Gorge Arch, West Virginia. This image was originally posted to Flickr by nukeit1 at <http://flickr.com/photos/88893304@N00/244750516>. It was reviewed on November 14, 2007 (2007-11-14) by the FlickreviewR robot and confirmed to be licensed under the terms of the cc-by-2.0 (Creative Commons Attribution 2.0). It was accessed in February 2012 from http://commons.wikimedia.org/wiki/File>New_River_Gorge_Bridge_West_Virginia_244750516.jpg

Chapter 8

Fig. 8.4 Gravity retaining wall. Courtesy of HNTB Corporation, 31 St. James Avenue, Suite 300 Boston, MA 02116, USA

Chapter 13

Fig. 13.1a Multi-span curved steel box girder bridge. Courtesy of HNTB Corporation, 31 St. James Avenue, Suite 300, Boston, MA 02116, USA

Fig. 13.1c The John James Audubon Bridge crossing the Mississippi River. This image is credited to the Louisiana TIMED Managers and was accessed in April 2012 from http://commons.wikimedia.org/wiki/File:Audubon_Bridge2.jpg

Fig. 13.34 Typical cable-stayed scheme. This work has been released into the public domain by its author, Kelly C. Cook. This applies worldwide. The image was accessed in February 2012 from http://commons.wikimedia.org/wiki/File:Sunshine_Skyway_from_Tampa_Bay.jpeg

Problem 13.9 Puente del Alamillo in Seville, Spain. This work has been released into the public domain by its author, Consorcio Turismo Sevilla. This applies worldwide. The image was accessed in March 2012 from http://en.wikipedia.org/wiki/File:Puente_del_Alamillo.jpg

Part I

Statically Determinate Structures

A structure is an assemblage of components which are connected in such a way that the structure can withstand the action of loads that are applied to it. These loads may be due to gravity, wind, ground shaking, impact, temperature, or other environmental sources. Structures are everywhere in the built environment. Buildings, bridges, tunnels, storage tanks, and transmission lines are examples of a “structure.” Structural engineering is the discipline which is concerned with identifying the loads that a structure may experience over its expected life, determining a suitable arrangement of structural members, selecting the material and dimensions of the members, defining the assembly process, and lastly monitoring the structure as it is being assembled and possibly also over its life.

In Part I, we first present an overview of structural engineering so that the reader can develop an appreciation for the broad range of tasks that structural engineers carry out and the challenges that they face in creating structures which perform satisfactorily under the loadings that they are subjected to. We then discuss a particular sub-group of structures called statically determinate structures. This sub-group is relatively easy to deal with analytically since only equilibrium concepts are involved. Also, most structures belong to this category. Trusses, beams, frames, cables, curved members, shallow foundations, and vertical retaining walls are described in separate chapters. The last two topics are not normally covered in elementary texts but we have included them here for completeness.

In general, all structures can be classified as either statically determinate or statically indeterminate. Part II describes techniques for dealing with statically indeterminate structures.

Part III describes how the methodologies presented in Parts I and II are applied to “engineer” various types of bridges and buildings. This section is intended to identify the key issues involved in structural engineering practice.

Overview

A structure is an assemblage of components which are connected in such a way that the structure can withstand the action of loads that are applied to it. These loads may be due to gravity, wind, ground shaking, impact, temperature, or other environmental sources. Examples of structures employed in civil infrastructure are buildings, bridges, dams, tunnels, storage tanks, and transmission line towers. Non-civil applications include aerospace structures such as airplane fuselages, missiles; naval structures such as ships, offshore platforms; and automotive structures such as cars and trucks. Structural engineering is the discipline which is concerned with identifying the loads that a structure may experience over its expected life, determining a suitable arrangement of structural members, selecting the material and dimensions of the members, defining the assembly process, and lastly monitoring the structure as it is being assembled and possibly also over its life.

In this chapter, we describe first the various types of structures. Each structure is categorized according to its particular function and the configuration of its components. We then discuss the critical issues that a structural Engineer needs to address when designing or assessing the adequacy of a structure. The most important issue is preventing failure, especially a sudden catastrophic failure. We describe various modes of failures: initial instability, material failure, and buckling of individual structural components. In order to carry out a structural design, one needs to specify the loading which is also a critical concern. Fortunately, the technical literature contains considerable information about loadings. We present here an overview of the nature of the different loads and establish their relative importance for the most common civil structures. Conventional structural design philosophy and the different approaches for implementing this design strategy are described next. Lastly we briefly discuss some basic analytical methods of structural engineering and describe how they are applied to analyze structures.

1.1 Types of Structures and Structural Components

Structures are everywhere in the built environment. Buildings, bridges, tunnels, storage tanks, and transmission lines are examples of a “structure.” Structures differ in their *makeup* (i.e., the type and configuration of the components), and also in their *function*. Our approach to describing a structure is based on identifying a set of attributes which relate to these properties.

1.1.1 Structural Components

The components are the basic building blocks of a structure. We refer to them as structural elements. Elements are classified into two categories according to their geometry [1]:

1. *Line Elements*—The geometry is essentially one-dimensional, i.e., one dimension is large with respect to the other two dimensions. Examples are cables, beams, columns, and arches. Another term for a line element is member.
2. *Surface Elements*—One dimension is small in comparison to the other two dimensions. The elements are plate-like. Examples are flat plates, curved plates, and shells such as spherical, cylindrical, and hyperbolic paraboloids.

1.1.2 Types of Structures

A structure is classified according to its function and the type of elements used to make up the structure. Typical structures and their corresponding functions are listed in Table 1.1 and illustrated in Fig. 1.1.

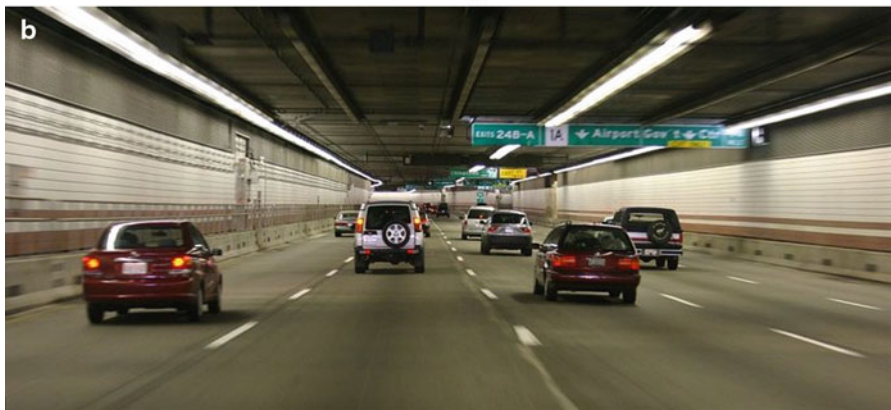
A classification according to makeup is listed in Table 1.2 and illustrated in Fig. 1.2.

Table 1.1 Structures classified by function

| Structural type | Function |
|-----------------|------------------------------------------------------------------------------------------------|
| Building | Provide shelter above ground |
| Bridge | Provide means of traversing above ground over a site |
| Tunnel | Provide means of traversing underground through a site |
| Tower | Support transmission lines and broadcasting devices |
| Retaining walls | Retain earth or other material |
| Containments | Provide means of storage of materials, also enclose dangerous devices such as nuclear reactors |
| Platforms | Provide a platform for storage of materials and machinery either onshore or offshore |



Building



Tunnel

Fig. 1.1 Examples of typical structures classified by function



Offshore platforms



Bridge

Fig. 1.1 (continued)

1.2 Critical Concerns of Structural Engineering

Of primary concern to a Structural engineer is ensuring that the structure *will not collapse* when subjected to its design loading. This requires firstly that the engineer properly identify the extreme loading that the structure may experience over

Table 1.2 Structures classified by makeup

| Structural type | Composition |
|-----------------|-------------------------------------------------------------------------------------------------------------------------------------------------------------------------------------------------------------------------------------------------------------------|
| Frame | <ul style="list-style-type: none"> Composed of members rigidly or semi-rigidly connected in rectangular or triangular patterns May be contained in a single plane (plane frame, plane grid), or in a 3D configuration (space frame) |
| Truss | <ul style="list-style-type: none"> A type of framed structure where the members are Connected together at their ends with frictionless pins (plane or space truss) |
| Girder/Beam | <ul style="list-style-type: none"> Composed of straight members connected sequentially (end to end) An additional descriptor related to the type of member cross section is used Examples are plate girders, box girders, and tub girders |
| Arch | Curved beams (usually in one plane) |
| Cable | <ul style="list-style-type: none"> Composed of cables and possibly other types of elements such as girders Examples are cable-stayed bridges and tensioned grids |
| Shell | <ul style="list-style-type: none"> Composed of surface elements and possibly also line elements such as beams The elements may be flat (plate structures) or curved (spherical or cylindrical roof structures) |



Fig. 1.2 Examples of typical structures classified by makeup

Frame



Bridge girder



Space truss



Shell

Fig. 1.2 (continued)



Arch bridge



Cable-girder system (suspension bridge)

Fig. 1.2 (continued)

its design life and secondly, ensure that the forces generated internally within the structure due to external loading combined *satisfy the conditions for force equilibrium*. In general, a structure will deform, i.e., change its shape, when loaded. It may also move as a rigid body if not properly restrained. Certain structures such as airplanes and automobiles are designed to move. However, civil structures are generally limited to small motion due to deformation, and *rigid* body motion is prohibited. Identifying the design loads is discussed later in this chapter. We focus here on the force equilibrium requirement for civil structures.

1.2.1 Reactions

Civil structures are connected to the ground at certain points called supports. When the external loading is applied to the structure, the supports develop forces which oppose the tendency of the structure to move. These forces are called reactions [2]. The nature and number of reactions depends on the type of support. Figure 1.3 shows the most common types of idealized structural supports for any planar structure. A roller support allows motion in the longitudinal direction but not in the transverse direction. A hinge prevents motion in both the longitudinal and transverse directions but allows rotation about the pin connection. Lastly, the clamped (fixed) support restrains rotation as well as translation with 2 reaction forces and one moment. Three-dimensional supports are similar in nature. There is an increase from 2 to 3 and from 3 to 6 in the number of reactions for the 3D hinge and a clamped supports.

1.2.2 Initial Stability

If either the number or nature of the reactions is insufficient to satisfy the equilibrium conditions, the structure is said to be initially unstable. Figure 1.4a illustrates this case. The structure consists of a triangular arrangement of members that are pinned at their ends. This combination of members forms a rigid body. However, the arrangement is supported on two roller supports, which offer no resistance to horizontal motion, and consequently the structure is initially unstable. This situation can be corrected by changing one of the roller supports to a hinge support, as shown in Fig. 1.4b. In general, a rigid body is initially stable when translational and rotational motions are prevented in three mutually orthogonal directions.

Even when the structure is adequately supported, it still may be initially unstable if the members are not properly connected together to provide sufficient internal forces to resist the applied external forces. Consider the four member pin-connected planar structure shown in Fig. 1.5a. The horizontal force, P , cannot be transmitted

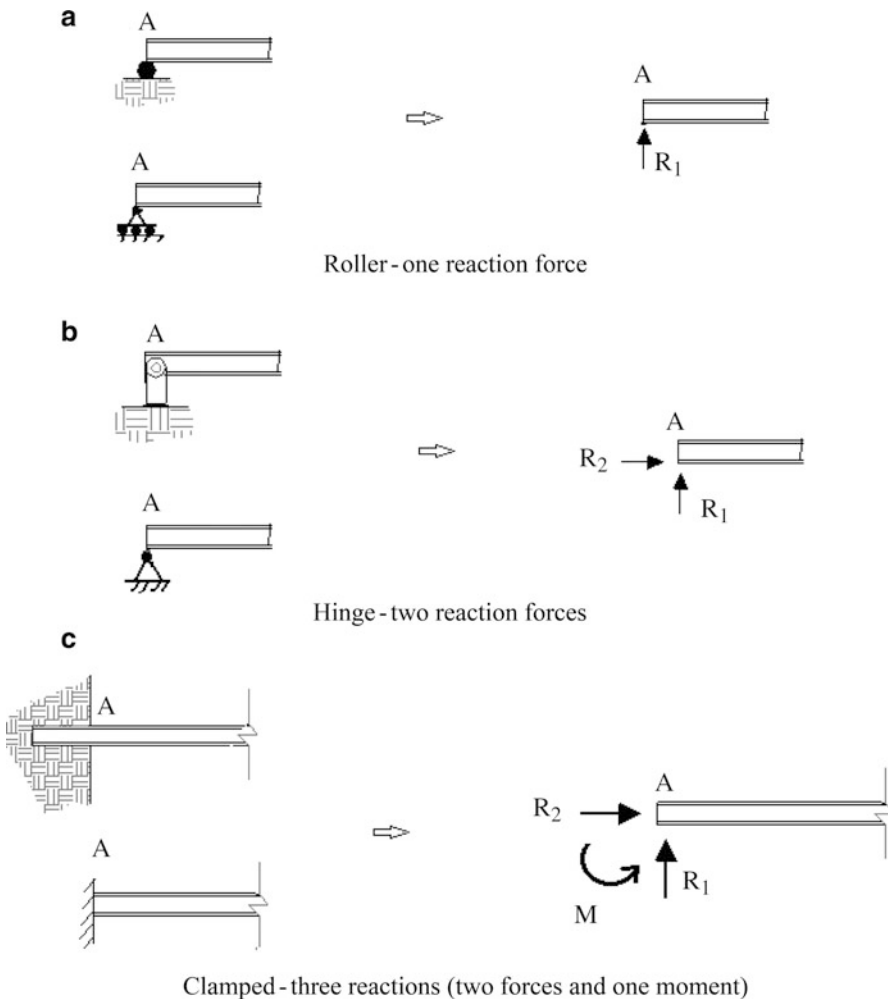


Fig. 1.3 Typical supports for planar structures

to the support since the force in member 1-2 is vertical and therefore cannot have a horizontal component. Adding a diagonal member, either 1-3 or 2-4, would make the structure stable.

In summary, initial instability can occur either due to a *lack of appropriate supports* or to an *inadequate arrangement of members*. The test for initial instability is whether there are sufficient reactions and internal member forces to equilibrate the applied external loads. Assuming the structure is initially stable, there still may be a problem if certain structural components fail under the action of the extreme loading and cause the structure to *lose* its ability to carry load. In what follows, we discuss various failure scenarios for structures which are loaded.

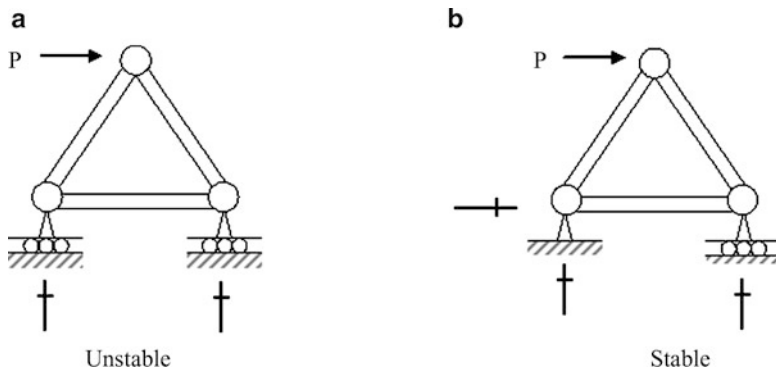


Fig. 1.4 Examples of unstable and stable support conditions—planar structure

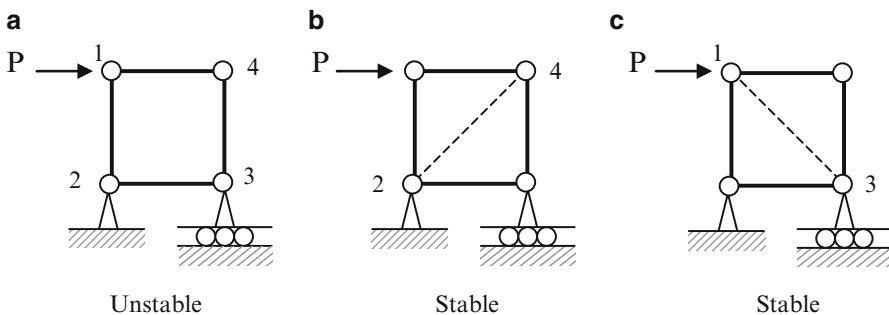


Fig. 1.5 Stabilizing an initially unstable planar structure

1.2.3 Loss of Stability Due to Material Failure

In the first scenario, the level of stress in a component reaches the ultimate stress for the material, causing a material failure, which, in turn, triggers a failure of the component. This type of failure depends on the stress-strain relationship for the material. Figure 1.6 illustrates the tensile stress-extensional strain response of tension specimens fabricated from two different types of materials [3, 4]. The behavior of the first material is essentially linear up to a peak stress, σ_f , at which point the material fractures and loses its ability to carry any load. This behavior is referred to as *brittle behavior* and obviously is not desirable from a structural behavior perspective.

The second response is completely different. The initial behavior is linear up to a certain stress value defined as the yield stress, σ_y . For further straining, the stress remains essentially constant. Eventually, the material stiffens and ultimately fails at a level of strain which is considerably greater than the yield strain, ϵ_y . This behavior is typical for *ductile* materials such as the steels used in civil structures. In practice, the maximum allowable strain is limited to a multiple of the yield strain. This factor

is called the ductility ratio (μ) and is on the order of 5. Ductile behavior is obviously more desirable since a member fabricated out of a ductile material does not lose its load capacity when yielding occurs. However, it cannot carry additional loading after yielding since the resistance remains constant.

From a design perspective, the Structural Engineer must *avoid* brittle behavior since it can result in *sudden* catastrophic failure. Ductile behavior and the associated inelastic deformation are acceptable provided that the ductility demand is within the design limit. Limit state design is a paradigm for dimensioning structural components that assumes the component is at its limit deformation state and calculates the force capacity based on the yield stress [24].

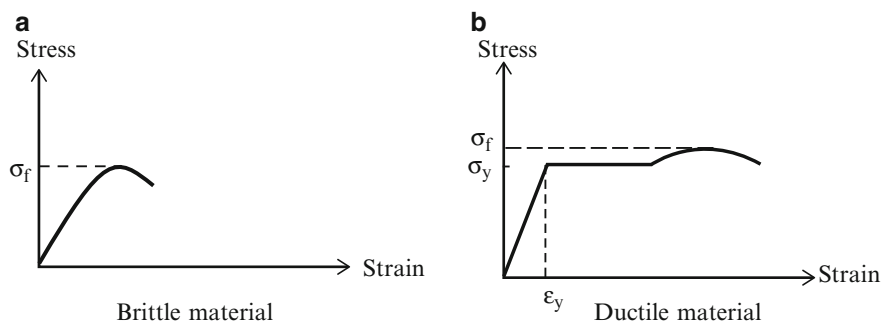


Fig. 1.6 Stress–strain behavior of brittle and ductile materials

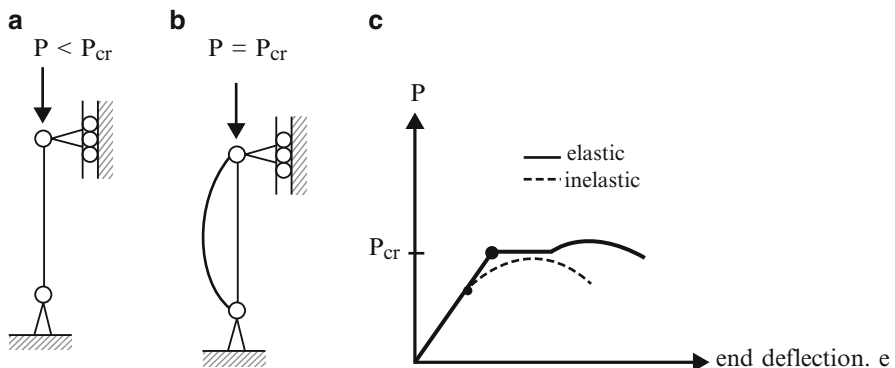


Fig. 1.7 Behavior of a flexible member

1.2.4 Buckling Failure Mode

Another possible failure scenario for a structural component is buckling. Buckling is a phenomenon associated with long slender members subjected to compressive loading [3, 4]. We illustrate this behavior using the member shown in Fig. 1.7a.

As the axial loading is increased, the member remains straight until a critical load value is reached. At this point, the member adopts a deflected configuration (Fig. 1.7b) with the load remaining constant. The member force remains essentially constant as the end deflection, e , is increased (Fig. 1.9c). This load deflection behavior is similar to inelastic action in the sense that the member experiences a large deflection with essentially no increase in load. For flexible members, the critical load for buckling (P_{cr}) is generally less than the axial compressive strength based on yielding, *therefore buckling usually controls the design.*

1.2.5 Priorities for Stability

Finally, summarizing and prioritizing the different concerns discussed in the previous sections, the highest priority is ensuring the structure is initially stable. If not stable, the structure will fail under an infinitesimal load. The second priority is avoiding buckling of the members. Buckling can result in large deformation and significant loss in load capacity for a member, which could cause the structure to lose its ability to support the applied loading. The third priority is limiting inelastic deformation of members under the extreme design loading. Although there is no loss in load capacity, the member cannot provide any additional load capacity, and therefore the deformation will increase significantly when the external loading is increased. We discuss this topic further in Sect. 1.4 where we present design philosophies.

1.3 Types of Loads

As described above, structures must be proportioned so that they will not fail or deform excessively under the loads they may be subjected to over their expected life. Therefore, it is critical that the nature and magnitude of the loads they may experience be accurately defined. Usually there are a number of different loads, and the question as to which loads may occur simultaneously needs to be addressed when specifying the design loading. In general, the structural engineer works with codes, which specify design loadings for various types of structures. General building codes such as the “International Building Code” [12] specify the requirements of governmental agencies for minimum design loads for structures and minimum standards for construction. Professional technical societies such as the American Society of Civil Engineers (ASCE) [8], the American Concrete Institute (ACI) [11], the American Institute of Steel construction (AISC) [9], and the British Standards Institute (BSI) [22] publish detailed technical standards that are also used to establish design loads and structural performance requirements. In what follows, we present an overview of the nature of the different loads and provide a sense of their relative importance for the most common civil structures.

1.3.1 Source of Loads

Loads are caused by various actions: the interaction of the structure with the natural environment; carrying out the function they are expected to perform; construction of the structure; and terrorist activities.

1.3.1.1 Interaction with the Environment

Interaction with the natural environment generates the following types of loads:

- Gravity—gravitational force associated with mass
- Snow—gravity type loading
- Wind—steady flow, gusts
- Earthquake—ground shaking resulting from a seismic event
- Water—scour, hydrostatic pressure, wave impact
- Ice—scour, impact
- Earth pressure—soil-structure interaction for foundations and underground structures
- Thermal—seasonal temperature variations

The relative importance of these sources depends on the nature of the structure and the geographical location of the site. For example, building design is generally governed by gravity, snow, wind, and possibly earthquake loads. Low-rise buildings in arctic regions tend to be governed by snow loading. Underground basement structures and tunnels are designed for earth pressure, hydrostatic pressure, and possibly earthquake loads. Gravity is the dominant source of load for bridge structures. Wave and ice action control the design of offshore platforms in coastal arctic waters such as the coasts of Alaska and Newfoundland. Structures located in California need to be designed for high seismic load. Structures located in Florida need to be designed for high wind load due to hurricanes. Thermal loads occur when structural elements are exposed to temperature change and are not allowed to expand or contract.

1.3.1.2 Function

Function-related loads are structure specific. For bridges, vehicular traffic consisting of cars, trucks, and trains generates gravity-type load, in addition to the self-weight load. Office buildings are intended to provide shelter for people and office equipment. A uniformly distributed gravity floor load is specified according to the nature of the occupancy of the building. Legal offices and libraries tend to have a larger design floor loading since they normally have more storage files than a normal office. Containment structures usually store materials such as liquids and granular solids. The associated loading is a distributed internal pressure which may vary over the height of the structure.

1.3.1.3 Construction

Construction loading depends on the process followed to assemble the structure. Detailed force analyses at various stages of the construction are required for complex structures such as segmented long-span bridges for which the erection



Fig. 1.8 Millau viaduct

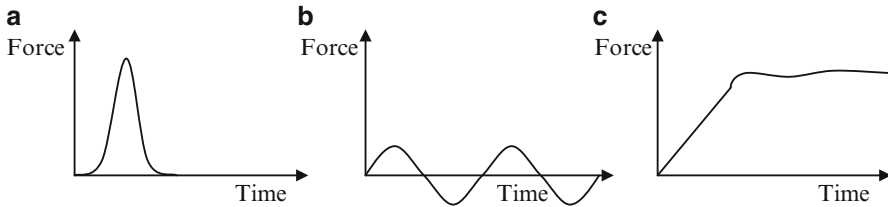
loading dominates the design. The structural engineer is responsible for approving the construction loads when separate firms carry out engineering and construction. A present trend is for a single organization to carry out both the engineering design and construction (the design-build paradigm where engineering companies and construction companies form a joint venture for the specific project). In this case, a team consisting of structural engineers and construction engineers jointly carries out the design. An example of this type of partnering is the construction of the Millau Viaduct in southwestern France, shown in Fig. 1.8. The spans were constructed by cantilevering segments out from existing piers, a technically challenging operation that required constant monitoring. The bridge piers are the highest in the world: the central pier is 280 m high.

1.3.1.4 Terrorist Loads

Terrorist loads are a new problem for structural engineers, driven primarily by the need to protect essential facilities from terrorist groups. Design criteria are continuously evolving, and tend to be directed more at providing multilevel defense barriers to prevent incidents, rather than to design for a specific incident. Clearly, there are certain incidents that a structure cannot be designed to safely handle, such as the plane impacts that destroyed the World Trade Center Towers. Examining progressive collapse mechanisms is now required for significant buildings, and is the responsibility of the structural engineer.

Table 1.3 Loading attributes

| Attribute | Value |
|-----------------------|------------------------------------------|
| Duration | Temporary or permanent |
| Spatial distribution | Concentrated or distributed |
| Temporal distribution | Impulsive; cyclic; quasi-static |
| Degree of certainty | Return period; probability of occurrence |

**Fig. 1.9** Temporal variation of loading. (a) Impulsive. (b) Cyclic. (c) Quasi-static

1.3.2 Properties of Loadings

The previous discussion was focused on the source of loadings, i.e., environmental, functional, construction, and terrorist activity. Loadings are also characterized by attributes, which relate to properties of the loads. Table 1.3 lists the most relevant attributes and their possible values.

Duration relates to the time period over which the loading is applied. Long-term loads, such as self weight are referred to as dead loads. Loads whose magnitude or location changes are called temporary loads. Examples of temporary loads are the weight of vehicles crossing a bridge, stored items in buildings, wind and seismic loads, and construction loads.

Most loads are represented as being applied over a finite area. For example, a line of trucks is represented with an equivalent uniformly distributed load. However, there are cases where the loaded area is small, and it is more convenient to treat the load as being concentrated at a particular point. A member partially supported by cables such as a cable-stayed girder is an example of concentrated loading.

Temporal distribution refers to the rate of change of the magnitude of the temporary loading with time. An impulsive load is characterized by a rapid increase over a very short duration and then a drop off. Figure 1.9 illustrates this case. Examples are forces due to collisions, dropped masses, brittle fracture material failures, and slamming action due to waves breaking on a structure. Cyclic loading alternates in direction (+ and -) and the period may change for successive cycles. The limiting case of cyclic loading is harmonic excitation where the amplitude and period are constant. Seismic excitation is cyclic. Rotating machinery such as printing presses, electric generators, and turbines produce harmonic excitation on their supports when they are not properly balanced. Quasi-static loading is characterized by a relatively slow build

Table 1.4 Occupancy categories

| Category | Description |
|----------|--------------------------------------------------------------------------------------|
| I | Structures that represent a low hazard to human life in the event of a failure |
| II | All structures outside of Categories I, III, and IV |
| III | Structures that represent a substantial hazard to human life in the event of failure |
| IV | Essential structures. Failure not allowed |

up of magnitude, reaching essentially a steady state. Because they are applied slowly, there is no appreciable dynamic amplification and the structure responds as if the load was a *static* load. Steady winds are treated as quasi-static; wind gusts are impulsive. Wind may also produce a periodic loading resulting from vortex shedding. We discuss this phenomenon later in this section.

The design life of a structure is that time period over which the structure is expected to function without any loss in operational capacity. Civil structures have long design lives vs. other structures such as motorcars, airplanes, and computers. A typical building structure can last several centuries. Bridges are exposed to more severe environmental actions, and tend to last a shorter period, say 50–75 years. The current design philosophy is to extend the useful life of bridges to at least 100 years. The Millau viaduct shown in Fig. 1.8 is intended to function at its full design capacity for at least 125 years.

Given that the natural environment varies continuously, the structural engineer is faced with a difficult problem: the most critical natural event, such as a windstorm or an earthquake that is likely to occur during the design life of the structure located at a particular site needs to be identified. To handle this problem, natural events are modeled as stochastic processes. The data for a particular event, say wind velocity at location x , is arranged according to return period which can be interpreted as the average time interval between occurrences of the event. One speaks of the 10-year wind, the 50-year wind, the 100-year wind, etc. Government agencies have compiled this data, which is incorporated in design codes. Given the design life and the value of return period chosen for the structure, the probability of the structure experiencing the chosen event is estimated as the ratio of the design life to the return period. For example, a building with a 50-year design life has a 50 % chance of experiencing the 100-year event during its lifetime. Typical design return periods are ≈ 50 years for wind loads and between 500 and 2,500 years for severe seismic loads.

Specifying a loading having a higher return period reduces the probability of occurrence of that load intensity over the design life. Another strategy for establishing design loads associated with uncertain natural events is to increase the load magnitude according to the importance of the structure. Importance is related to the nature of occupancy of the structure. In ASCE Standards 7-05 [8], four occupancy categories are defined using the *potential hazard to human life in the event of a failure* as a basis. They are listed in Table 1.4 for reference.

The factor used to increase the loading is called the importance factor, and denoted by I . Table 1.5 lists the values of I recommended by ASCE 7-05 [8] for each category and type of loading.

Table 1.5 Values of I

| Category | Wind | | | |
|----------|----------------|------------|------|------------|
| | Non-horizontal | Horizontal | Snow | Earthquake |
| I | 0.87 | 0.77 | 0.80 | 1.00 |
| II | 1.00 | 1.00 | 1.00 | 1.00 |
| III | 1.15 | 1.15 | 1.10 | 1.25 |
| IV | 1.15 | 1.15 | 1.20 | 1.50 |

Table 1.6 Uniformly distributed live loads (ASCE 7-05)

| Occupancy | Magnitude lbs/ft ² (kN/m ²) |
|-------------------------|----------------------------------------------------|
| Computer equipment | 150 (7.18) |
| Dormitories | 80 (3.83) |
| File room | 125 (6.00) |
| Court rooms | 50–100 (2.4–4.79) |
| Scientific laboratories | 100 (4.79) |
| Public rooms | 100 (4.79) |
| Rest rooms | 60 (2.87) |
| Laundries | 150 (7.18) |
| Foundries | 600 (28.73) |
| Ice manufacturing | 300 (14.36) |
| Transformer rooms | 200 (9.58) |
| Storage, hay or grain | 300 (14.36) |

For example, one increases the earthquake loading by 50 % for an essential structure (category 4).

1.3.3 Gravity Live Loads

Gravitational loads are the dominant loads for bridges and low-rise buildings located in areas where the seismic activity is moderate. They act in the downward vertical direction and are generally a combination of fixed (dead) and temporary (live) loads. The dead load is due to the weight of the construction materials and permanently fixed equipment incorporated into the structure. As mentioned earlier, temporary live loads depend on the function of the structure. Typical values of live loads for buildings are listed in Table 1.6. A reasonable estimate of live load for office/residential facilities is $\approx 100 \text{ lbs/ft}^2$ (4.8 kN/m^2). Industrial facilities have higher live loadings, ranging up to 600 lbs/ft^2 for foundries.

Live loading for bridges is specified in terms of standard truck loads. In the USA, bridge loads are defined by the American Association of State Highway and Transportation Officials (AASHTO) [10]. They consist of a combination of the Design truck or tandem, and Design lane load.

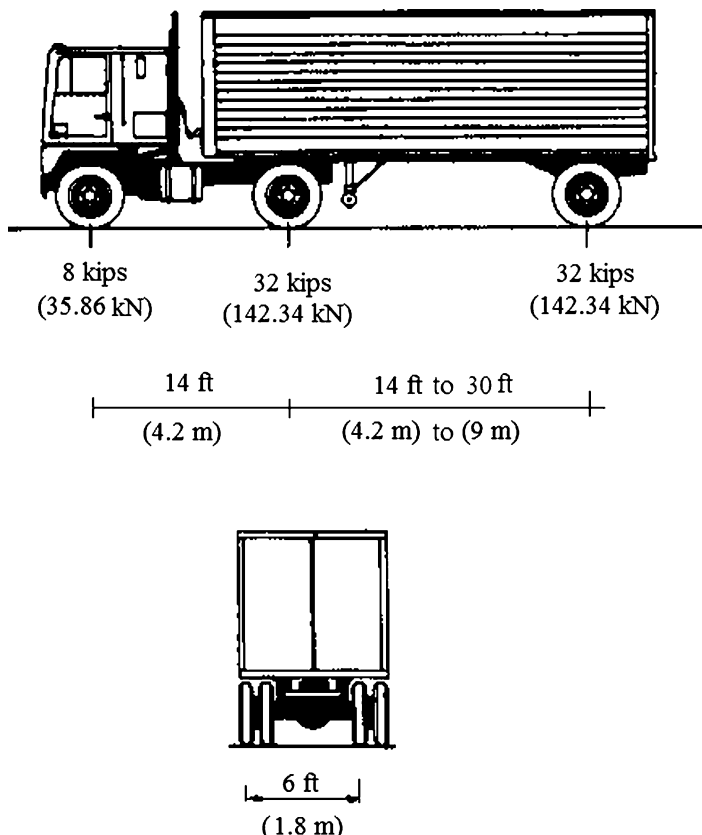


Fig. 1.10 Characteristics of the AASHTO Design Truck

The design truck loading has a total weight of 72 kip (323 kN), with a variable axle spacing is shown in Fig. 1.10.

The design tandem shall consist of a pair of 25 kip (112 kN) axles spaced 4 ft (1.2 m) apart. The transverse spacing of wheels shall be taken as 6 ft (1.83 m).

The design lane load shall consist of a load of 0.64 kip/ft² (30.64 kN/m²) uniformly distributed in the longitudinal direction and uniformly distributed over a 10 ft (3 m) width in the transverse direction.

1.3.4 Wind Loading

1.3.4.1 Wind Pressure Distribution

The effect of wind acting on a building is represented by a pressure loading distributed over the exterior surface. This pressure loading depends on the geometry of the structure and the geographic location of the site. Figure 1.11 illustrates the

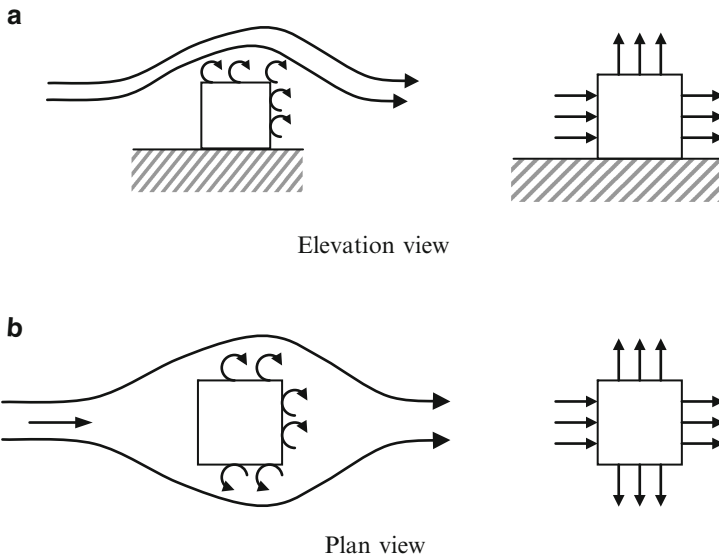


Fig. 1.11 Flow lines and pressure distributions due to wind

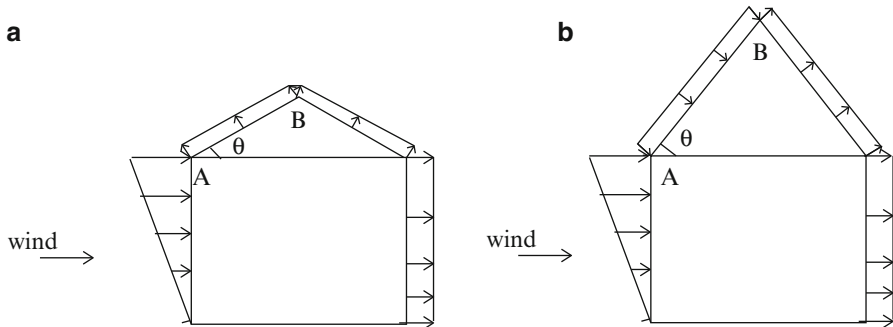


Fig. 1.12 Wind pressure profiles for a gable roof. (a) $\theta < 45^\circ$. (b) $\theta > 45^\circ$

flow past a low-rise, single story, flat roof structure. The sharp corners such as at point A causes flow separation, resulting in eddies forming and turbulence zones on the flat roof, side faces, and leeward face. The sense of the pressure is positive (inward) on the incident face and negative (outward) in the turbulence zones.

In general, the magnitude of the pressure varies over the faces, and depends on both the shape of the structure and the design wind velocity at the site. The influence of shape is illustrated by Fig. 1.12, which shows the effect of roof angle on the pressure distribution. When $\theta > 45^\circ$, there is a transition from negative to positive pressure on face AB of the inclined roof. This shift is due to the flow separation point moving from A to B for steeply inclined roofs.

1.3.4.2 Wind Velocity

The effect of the site is characterized firstly by the topography at the site, and secondly by the regional wind environment. Exposure categories are defined to describe the local topography and to establish the level of exposure to wind. ASCE 7-05 adopts the following definitions of exposure categories.

Category B: Site located within an urban or suburban area having numerous closely spaced obstructions similar in size to a single family dwelling, and extending at least 2,600 ft from the site.

Category D: Site located in a flat unobstructed area or on a water surface outside hurricane prone regions, and extending at least 5,000 ft from the site.

Category C: All cases where exposure categories B and D do not apply.

Regional wind environments are represented by maps containing wind speed data for a specified return period and exposure category. Figure 1.13 shows US data for the 50-year wind speed observed at 10 m elevation corresponding to Exposure C. The higher wind speeds along the East and Gulf Coasts reflects the occurrence of hurricanes in these regions. Typical 50-year wind speeds are on the order of 100 miles per hour (45 m/s).

Given a site, one can establish the 50-year wind speed at 10 m elevation using Fig. 1.13. In general, the wind velocity increases with distance from the ground. A typical approximation is a power law:

$$V(z) = \bar{V} \left(\frac{z}{\bar{z}} \right)^{1/\alpha} \quad (1.1)$$

where z is the elevation above the ground, \bar{V} is the velocity measured at elevation \bar{z} , and $\alpha \approx 7$. For US data, one takes $\bar{z}=10$ m and \bar{V} given by Fig. 1.13.

1.3.4.3 Pressure Profiles

The next step is to establish the vertical pressure distribution associated with this velocity distribution, and then modify it to account for the shape of the building. Pressure and velocity are related by Bernoulli's Equation, which is a statement of conservation of energy. Specialized for steady irrotational inviscid flow of a weightless fluid, the Law states that [13]

$$E = \text{Energy per unit volume} = p + \frac{1}{2} \rho V^2 \quad (1.2)$$

is constant along a streamline. Here, p is the pressure energy, ρ is the mass density, and $1/2\rho V^2$ is the kinetic energy per unit volume. Assuming the pressure is zero in the free stream flow regime away from the structure, and taking point (1) in the free stream and point (2) at the structure, one obtains

$$p_2 = \frac{1}{2} \rho (V_1^2 - V_2^2) \quad (1.3)$$

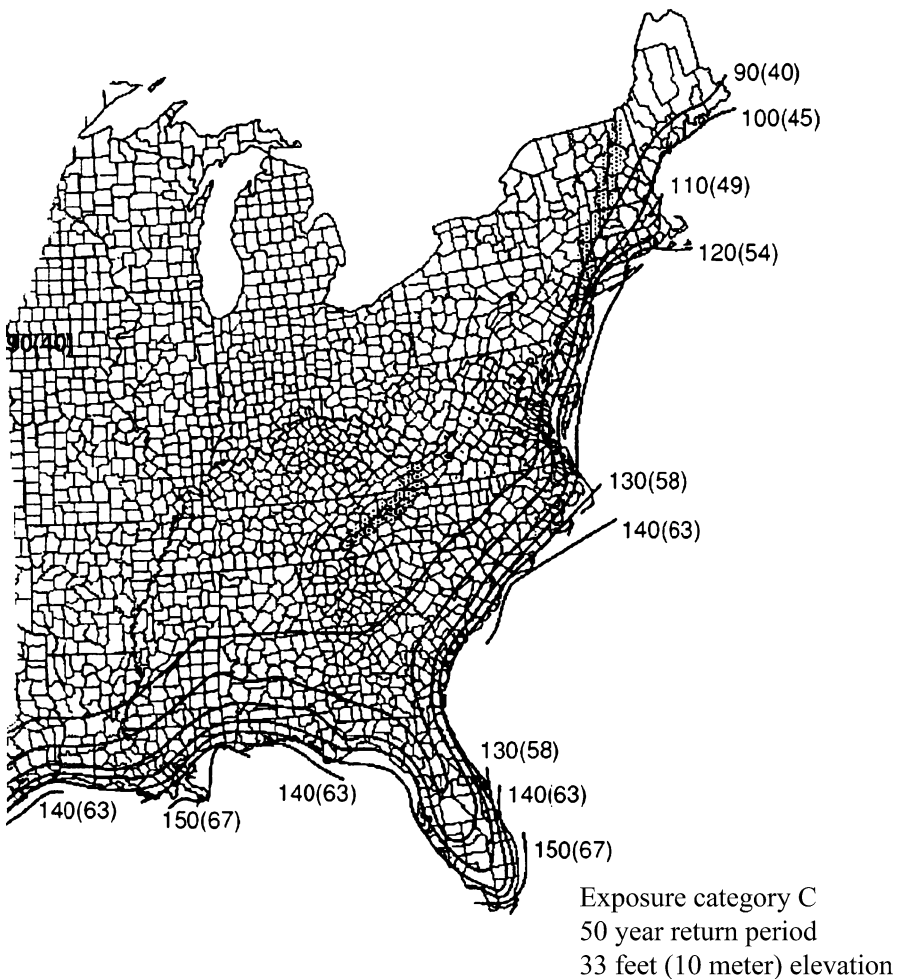


Fig. 1.13 Basic Wind Speed miles per hour (meter per second) for the East coast of USA

The free stream velocity, V_1 , is defined by (1.1). Considering the flow to be stopped by the structure, ($V_2 \approx 0$), it follows that the maximum pressure energy associated with the free stream velocity is estimated as

$$(p_2)_{\max} = \frac{1}{2} \rho V_1^2 = p_{\text{stag}} \quad (1.4)$$

This pressure is called the stagnation pressure and is generally expressed in terms of the reference velocity, \bar{V} , at $z = 10$ m and a function $k(z)$ which defines the vertical distribution.

$$p_{\text{stag}} = \frac{1}{2} \rho \bar{V}^2 k(z) \quad (1.5)$$

ASCE 7-05 tabulates values of $k(z)$ vs. z .

The actual pressure distribution is influenced by the geometric shape which tends to change both the magnitude and sense of the pressure. Figures 1.11 and 1.12 illustrate this effect for flat and gable roof structures. Design codes handle this aspect by introducing “shape” factors for different regions of the structural surface. They also include a gust factor for “dynamic” loading, and an importance factor for the structure. The final expression for the design pressure has the following general form:

$$P_{\text{design}} = I G C_p(z) p_{\text{stag}} \quad (1.6)$$

where $C_p(z)$ is the pressure coefficient that accounts for the shape, G is the gust factor, and I is the importance factor corresponding to the occupancy category. Values for these parameters are code dependent. The determination of the design pressure can be labor intensive if one wants to account fully for the spatial distribution of design pressure. A reasonable estimate can be obtained using the simplified procedure illustrated in the following example which is appropriate for low-rise buildings.

Example 1.1 Wind pressure distribution on a low-rise gable roof structure

Given: The structure shown in Fig. E1.1a. There are four surface areas included in the sketch. Zone (1) is the windward face, zone (2) is the leeward face, and zones (3) and (4) are on the gable roof.

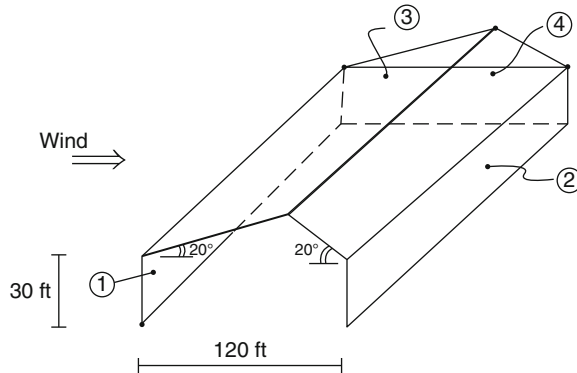


Fig. E1.1a

Determine: The wind pressure distribution on the interior zone away from the ends. Assume

$$\bar{V} = 100 \text{ mph} \text{ and exposure } C$$

Solution: Applying (1.5) leads to

$$p_{\text{stag}} = (0.00256)(10^4)k(z) = 25.6k(z)(\text{lb}/\text{ft}^2)$$

Values of $k(z)$ and the corresponding p_{stag} are listed below

| z (ft) | $k(z)$ | p_{stag} (lb/ft^2) |
|----------|--------|-----------------------------------------------|
| 15 | 0.85 | 21.8 |
| 20 | 0.90 | 23.0 |
| 25 | 0.94 | 24.1 |
| 30 | 0.98 | 25.1 |

We assume the structure is Category III and use $I = 1.15$. For low-rise buildings with $h < 60$ ft, the factors G and C_p are combined and specified as constant for each zone. Using data from ASCE 7-05, the values are

| Zone | GC_p | IGC_p |
|------|--------|---------|
| 1 | 0.53 | 0.609 |
| 2 | -0.43 | -0.495 |
| 3 | -0.69 | -0.794 |
| 4 | -0.48 | -0.552 |

Lastly, we compute the design pressure using (1.6). The ASCE 7-05 code assumes that p_{design} varies on the windward force (zone 1), but specifies constant distributions for the other zones. The details are listed below.

| | |
|--------|----------------------------------------------------------------|
| Zone 1 | $p_{\text{design}} = 0.609 (25.6) k(z) = 15.59 k(z)$ |
| Zone 2 | $p_{\text{design}} = -0.495 (25.6) k(30) = -12.42 \text{ psf}$ |
| Zone 3 | $p_{\text{design}} = -0.791 (25.6) k(30) = -19.92 \text{ psf}$ |
| Zone 4 | $p_{\text{design}} = -0.552 (25.6) k(30) = -13.85 \text{ psf}$ |

Pressure distributions generated with (1.6) define the quasi-static wind load, which acts predominately in the horizontal (lateral) direction. For low-rise buildings, gravity loads are the dominant loads and generally control the structural dimensioning process for vertical members. Since the wind loads are horizontal, whereas the gravity loads are vertical, lateral structural bracing systems such as shown in Fig. 1.14 need to be incorporated in certain types of structures such as a braced frames. This topic is addressed further in Chaps. 11, 14, and 15.

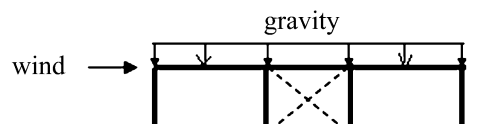
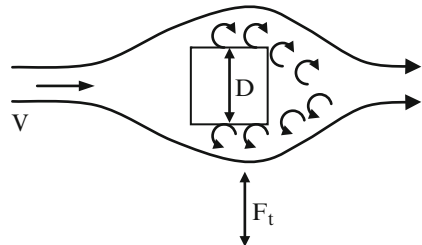


Fig. 1.14 Lateral bracing system

Fig. 1.15 Vortex shedding patterns—plan view



1.3.4.4 Vortex Shedding Pressure

The action of a steady wind on a structure is represented by quasi-static forces. However, a steady wind also creates periodic forces due to the shedding of vortices from the turbulence zones at the leeward face [13]. Consider the rectangular cross section plan view shown in Fig. 1.15. As the incident flow velocity increases, eddies are created at the upper and lower surfaces and exit downstream. This shedding pattern develops a cyclic mode, shedding alternately between the upper and lower surfaces, which result in an antisymmetric pressure distribution. The net effect is a periodic force, F_t , acting in the transverse direction with frequency, f_s . An estimate for the shedding frequency is

$$f_s(\text{cycles per second}) \approx \frac{0.2V}{D} \quad (1.7)$$

where D is a representative dimension in the transverse direction and V is the free stream velocity. Vortex shedding is a major concern for tall buildings and slender long-span horizontal structures since these structures are flexible and consequently more susceptible to transverse periodic excitation with a frequency close to f_s . Low-rise buildings are stiffer and relatively insensitive to vortex shedding-induced transverse motion.

1.3.5 Snow Loading

Design snow loads for a structure are based on ground snow load data for the region where the structure is located. Snow loads act on the roof zones of structures. For a flat roof, defined as a roof with a slope angle less than 5° , the snow load is represented as a uniform downward pressure, p_f . The magnitude of p_f depends on the exposure category and regional environment at the site, as well as the importance of the structure. We express p_f as

$$p_f = Cp_g \quad (1.8)$$

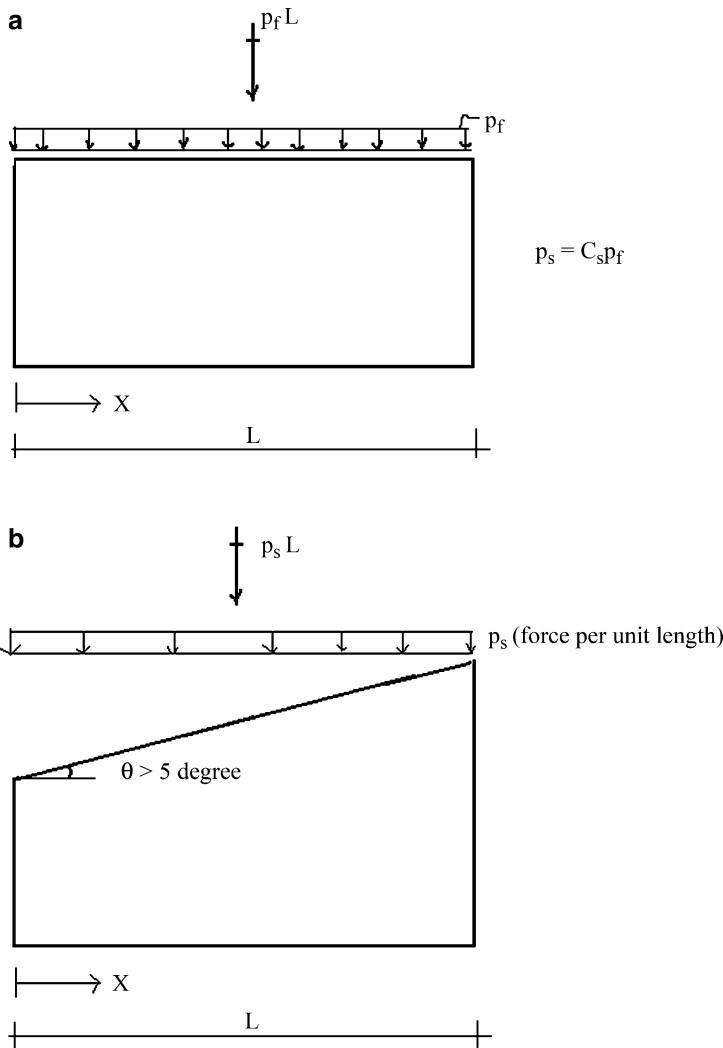


Fig. 1.16 Snow loadings on sloped and flat roofs. (a) Flat roof. (b) Sloped roof

where p_g is the ground snow pressure given by Fig. 1.16a and C is a factor that incorporates the exposure and importance parameters. A typical value of C is ≈ 1 . The ground snow pressure varies from 0 in the southeastern zone of the USA up to ≈ 100 psf in northern New England.

A sloped roof is defined as a roof with a slope angle greater than 5° . The snow load on a sloped roof is expressed in terms of the *horizontal projected area* rather than the actual surface area. Figure 1.16b illustrates this definition.

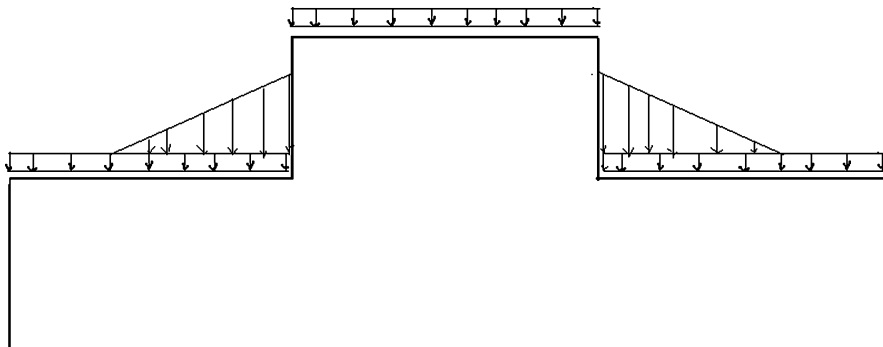


Fig. 1.17 Snow drift profiles

The sloped roof pressure depends on the slope angle as well as the other parameters mentioned earlier.

$$p_s = C_s p_f \quad (1.9)$$

where C_s is a slope coefficient. In general, $C_s \leq 1$. For $\theta < \approx 30^\circ$, one usually assumes $C_s \approx 1$ and takes $p_s \approx p_f$.

When the roof has projections as illustrated in Fig. 1.17, a nonuniform snow loading can result due to the drifting on both the windward and leeward faces produced by wind. Drifts are modeled as triangular surcharge loadings. The details are code dependent.

1.3.6 Earthquake Loading

The structural engineer's task is to design structures such that they can resist earthquake the ground shaking associated with an earthquake without collapsing. Since an earthquake may occur anytime during the design life, the first task is to identify the magnitude of peak ground acceleration (ρ_{ga}) that has a specified probability of occurrence during the design life. A common value is 2 % probability of occurrence in 50 years, which corresponds to a return period of 2,500 years. Earthquake ground motion is site specific in that it depends on the location and soil conditions for the site. Sites near known faults and sites on soft soils such as soft clay experience more intense ground motion. Factors such as the importance of the building, the geographic location of the site, and the type of soil must be taken into account when specifying the design magnitude for ρ_{ga} .

In order to understand how buildings respond to ground motion, one needs to examine the dynamic response. Consider the three-story frame shown in Fig. 1.18a. We approximate it with the simple beam/mass system defined in Fig. 1.18b. This approximation, known as a single degree-of-freedom model, provides useful information concerning the influence of certain structural properties on the response.

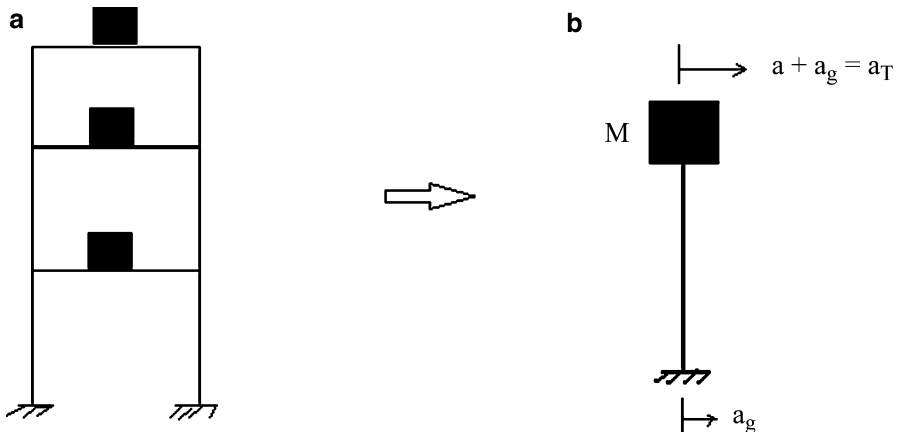


Fig. 1.18 A typical three-story frame and the corresponding one degree-of-freedom model.

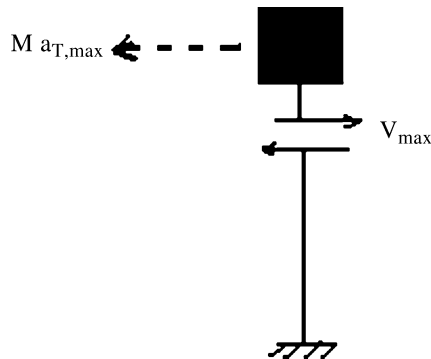
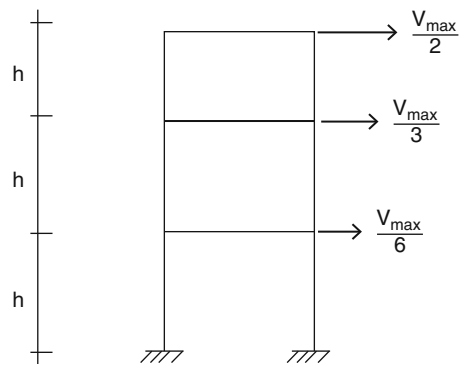


Fig. 1.19 Peak lateral inertia force

The ground acceleration is defined as a_g . This motion causes the mass to vibrate. We define $a_{T,\max}$ as the peak total acceleration of the mass (Fig. 1.19). If the frame is very stiff, $a_{T,\max}$ is essentially equal to $a_{g,\max}$, the peak ground acceleration. When the frame is very flexible, $a_{T,\max}$ is small in comparison to $a_{g,\max}$. It follows that the stiffness of the structure has a significant influence on the peak total acceleration response. The peak acceleration also depends on the geographic location and the soil conditions at the site. Data concerning earthquake accelerations is published by the US Geological Survey on their Web site [17]. This site contains an extensive set of earthquake ground motion records for the USA and other major seismically active regions throughout the world.

Fig. 1.20 Seismic lateral load profile



The motion of the mass generates an inertia force which is resisted by the lateral shear force in the system. The maximum value of the lateral shear force is denoted as V_{\max} .

$$V_{\max} = Ma_{T,\max} = W \left(\frac{a_{T,\max}}{g} \right) \quad (1.10)$$

Given the structural weight, W , and the peak total acceleration, one can estimate the peak total lateral load that the structure will experience due to seismic excitation. This load is assumed to be distributed linearly throughout the height of the structure, as indicated in Fig. 1.20, and used to generate an initial structural design. The final design is checked with more refined dynamic analysis. Seismic Design is an advanced topic within the field of Structural Engineering. We will discuss this topic in more detail in Chap. 14.

1.4 Structural Design Philosophy

Conventional structural design philosophy is based on satisfying two requirements, namely safety and serviceability [8]. Safety relates to extreme loadings, which have a very low probability of occurrence, on the order of 2 %, during a structure's life, and is concerned with the collapse of the structure, major damage to the structure and its contents, and loss of life. The most important priority is ensuring sufficient structural integrity so that sudden collapse is avoided. Serviceability pertains to medium to large loadings, which may occur during the structure's lifetime. For service loadings, the structure should remain operational. It should suffer minimal damage, and furthermore, the motion experienced by the structure should not exceed specified comfort levels for humans and motion-sensitive equipment mounted on the structure. Typical occurrence probabilities for service loads range from 10 to 50 %.

Safety concerns are satisfied by requiring the resistance, i.e., the strength of the individual structural elements to be greater than the demand associated with the extreme loading. Once the structure is dimensioned, the stiffness properties are derived and used to check the various serviceability constraints such as elastic behavior. Iteration is usually necessary for convergence to an acceptable structural design. This approach is referred to as strength-based design since the elements are dimensioned initially according to strength requirements.

Applying a strength-based approach for preliminary design is appropriate when strength is the dominant design requirement. In the past, most structural design problems have fallen in this category. However, the following developments have occurred recently that limit the effectiveness of the strength-based approach. Firstly, the trend toward more flexible structures such as tall buildings and long-span horizontal structures has resulted in more structural motion under service loading, thus shifting the emphasis toward serviceability. Secondly, some new types of facilities such as micro device manufacturing centers and hospital operating centers have more severe design constraints on motion than the typical civil structure. For example, the environment for micro device manufacturing must be essentially motion free. Thirdly, recent advances in material science and engineering have resulted in significant increases in the strength of traditional civil engineering materials. However, the material stiffness has not increased at the same rate. The lag in material stiffness vs. material strength has led to a problem with satisfying the requirements on the various motion parameters. Indeed, for very high strength materials, the motion requirements control the design. Fourthly, experience with recent earthquakes has shown that the cost of repairing structural damage due to inelastic deformation was considerably greater than anticipated. This finding has resulted in a trend toward decreasing the reliance on inelastic deformation to dissipate energy and shifting to other type of energy dissipating and energy absorption mechanisms.

Performance-based design [14] is an alternate design paradigm that addresses these issues. The approach takes as its primary objective the satisfaction of motion-related design requirements such as restrictions on displacement and acceleration and seeks the optimal deployment of material stiffness and motion control devices to achieve these design targets as well as satisfy the constraints on strength and elastic behavior. Limit state design can be interpreted as a form of performance-based design where the structure is allowed to experience a specific amount of inelastic deformation under the extreme loading.

1.5 Basic Analytical Tools of Structural Analysis

Engineering a structure involves not only dimensioning the structure but also evaluating whether the structure's response under the construction and design loadings satisfy the specified design criteria. Response evaluation is commonly referred to as structural analysis and is carried out with certain analytical methods developed in the field of Engineering Mechanics and adopted for structural systems. In this section, we review these methods and illustrate their application to some simple structures.

Most of this material is covered in textbooks dealing with Statics and Mechanics of Materials [2–4] and Structural Analysis [5–7]. Heyman's text [15] contains an excellent description of the “underlying science of Structural Engineering.”

1.5.1 Concept of Equilibrium-Concurrent Force System

We begin with a discussion of equilibrium conditions for solid bodies. This topic is relevant to structural engineering since structures are solid bodies subjected to loads, and we need to ensure that a structure remain at rest, i.e., that it is in a state of equilibrium.

The simplest case is a body subjected to a set of concurrent forces. By definition, the lines of action of the forces comprising a concurrent force system intersect at a common point. Figure 1.21 illustrates this case. For static equilibrium, the resultant of the force system must be a null vector.

$$\vec{R} = \vec{F}_1 + \vec{F}_2 + \vec{F}_3 = \vec{0} \quad (1.11)$$

We convert the vector equilibrium over to a set of algebraic equations by resolving the force vectors into their components with respect to an arbitrary set of orthogonal directions (X, Y, Z). This operation leads to

$$\begin{aligned} \sum_{i=1}^3 F_{i,x} &= F_{1,x} + F_{2,x} + F_{3,x} = 0 \\ \sum_{i=1}^3 F_{i,Y} &= F_{1,Y} + F_{2,Y} + F_{3,Y} = 0 \\ \sum_{i=1}^3 F_{i,z} &= F_{1,z} + F_{2,z} + F_{3,z} = 0 \end{aligned} \quad (1.12)$$

We find it more convenient to work with (1.12) rather than (1.11).

When all the force vectors are in one plane, say the $X-Y$ plane, the force system is called a planar force system and (1.12) reduces to 2 equations. Most of the force systems that we deal with will be planar systems.

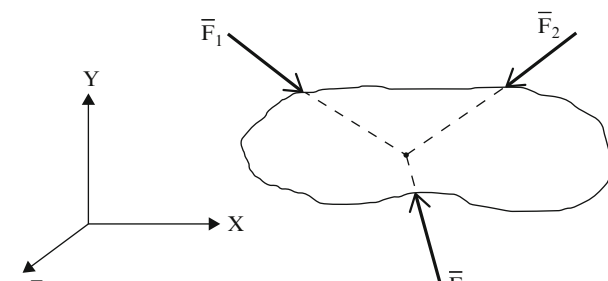


Fig. 1.21 Concurrent force system

1.5.2 Concept of Equilibrium: Non-concurrent Force System

The next level of complexity is a body subjected to a non-concurrent planar force system. Referring to Fig. 1.22, the forces tend to rotate the body as well as translate it. Static equilibrium requires the resultant force vector to vanish and, in addition, the resultant moment vector about an arbitrary point to vanish.

$$\begin{aligned}\vec{R} &= \vec{F_1} + \vec{F_2} + \vec{F_3} = \vec{0} \\ \vec{M}_0 &= \vec{0}\end{aligned}\quad (1.13)$$

Resolving the force and moment vectors into their X , Y , Z components leads to six scalar equations, three for force and three for moment.

When the force system is planar, say in the X - Y plane, the equations (1.13) reduce to three scalar equations

$$\begin{aligned}\sum_{i=1}^3 F_{i,x} &= 0 \\ \sum_{i=1}^3 F_{i,y} &= 0 \\ \sum M_O &= 0\end{aligned}\quad (1.14)$$

where O is an arbitrary point in the x - y plane. Note that now for a planar system there are three equilibrium conditions vs. two for a concurrent system. Note also that since there are three equilibrium equations, one needs to apply three restraints to prevent planar rigid body motion.

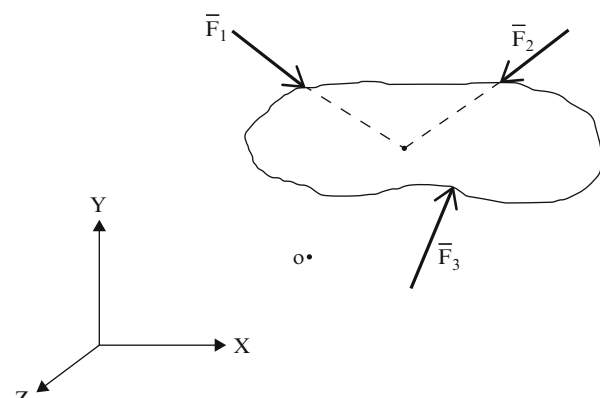
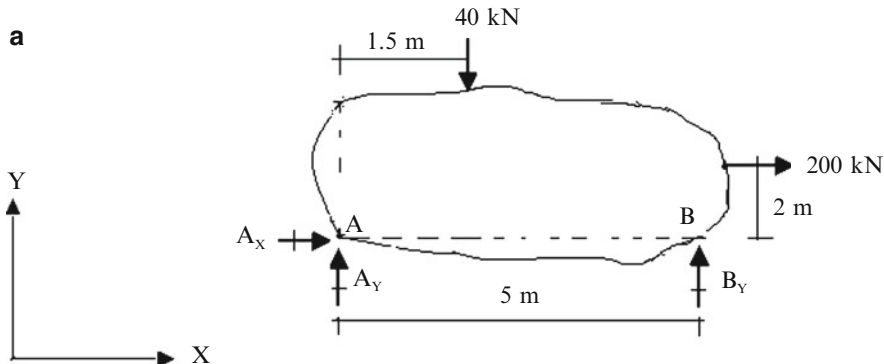


Fig. 1.22 Non-concurrent force system

Example 1.2 Equilibrium equations

Given: The rigid body and force system shown in Fig. E1.2a. Forces A_x , A_Y , and B_Y are unknown.

**Fig. E1.2a**

Determine: The forces A_x , A_Y , and B_Y

Solution: We sum moments about A, and solve for B_Y

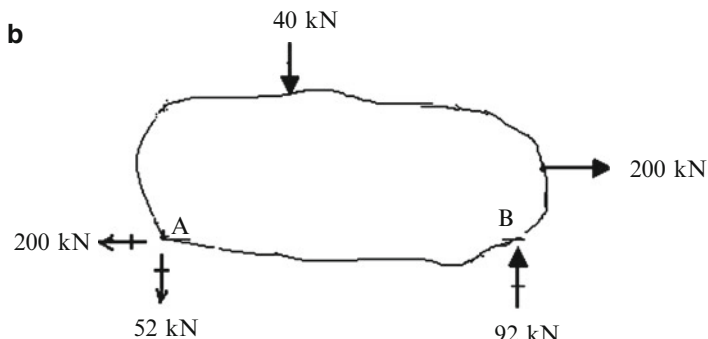
$$\sum M_A = -40(1.5) - 200(2) + B_Y(5) = 0$$

$$B_Y = +92 \Rightarrow B_Y = 92 \text{ kN} \uparrow$$

Next, summing forces in the X and Y directions leads to (Fig. E1.2b)

$$\sum F_x \rightarrow^+ = A_x + 200 = 0 \Rightarrow A_x = -200 \Rightarrow A_x = 200 \text{ kN} \leftarrow$$

$$\sum F_y \uparrow^+ = A_Y + 92 - 40 = 0 \Rightarrow A_Y = -52 \Rightarrow A_Y = 52 \text{ kN} \downarrow$$

**Fig. E1.2b**

1.5.3 Idealized Structure: Free Body Diagrams

Generating an idealization of an actual structure is the key step in applying the equilibrium equations. Given a structure acted upon by external loads and constrained against motion by supports, one idealizes the structure by identifying the external loads and supports, and replacing the supports with their corresponding unknown reaction forces. This process is called constructing the free body diagram (FBD). Figures 1.23a, b illustrate the details involved.

One applies the equilibrium equations to the FBD. Note that this diagram has 4 unknown reaction forces. Since there are only three equilibrium equations, one cannot determine all the reaction forces using only the equilibrium conditions. In this case, we say that the structure is *statically indeterminate*.

Constructing a FBD is *an essential step* in applying the equilibrium equations. The process is particularly useful when the structure is actually a collection of interconnected structural components such as a framed structure. One first generates a FBD for the entire structure and then works with separate FBD's for the individual members. We illustrate this approach throughout the text.

1.5.4 Internal Forces

Consider the body shown in Fig. 1.24a. Suppose we pass a cutting plane as indicated and separate the two segments. We represent the action of body “n” on

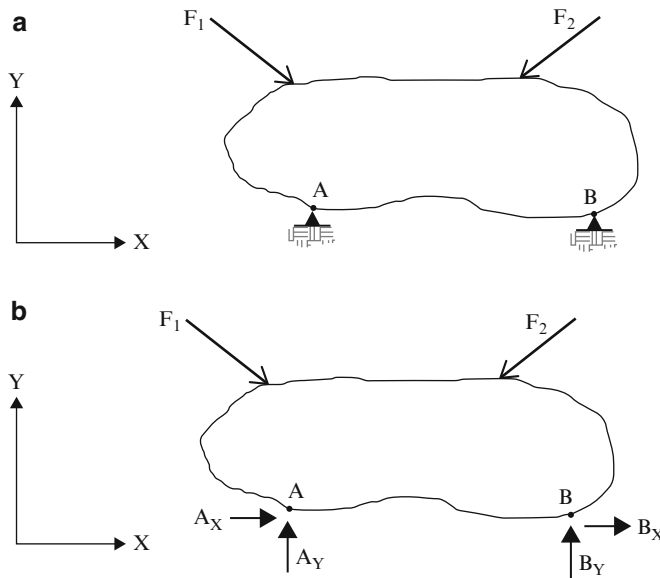


Fig. 1.23 Constructing the Free Body Diagram (FBD)

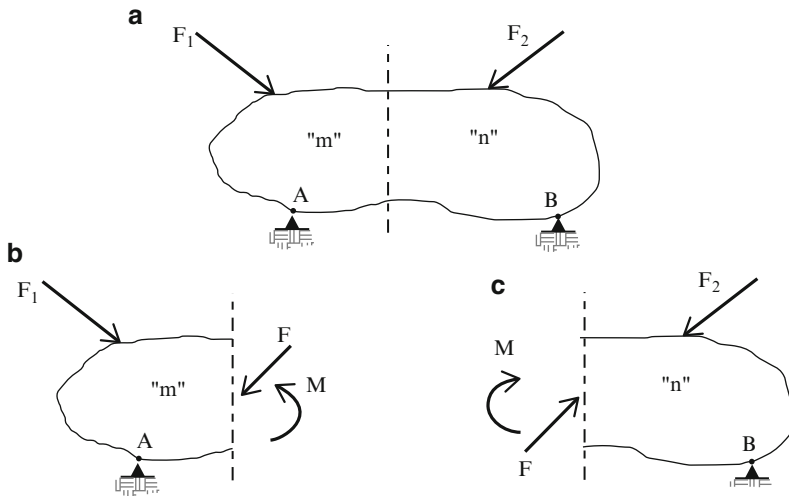


Fig. 1.24 Definition of internal forces

body "m" by a force \vec{F} and moment \vec{M} . From Newton's third law, the action of body m on body n is opposite in sense.

Once the reaction forces are known, we can determine \vec{F} and \vec{M} by applying the equilibrium conditions to either segment. These force quantities are called "internal forces" in contrast to the reactions which are "external forces." Note that the magnitude of the internal forces varies with the location of the cutting plane. The following example illustrates the process of computing internal forces.

Example 1.3

Given: The body and loading shown in Fig. E1.3a.

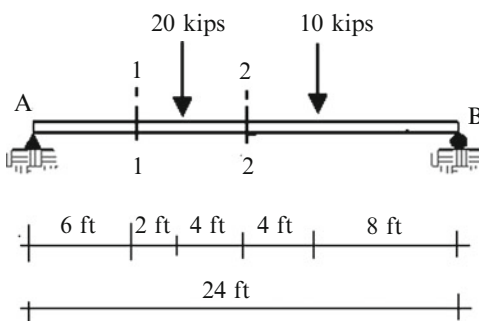
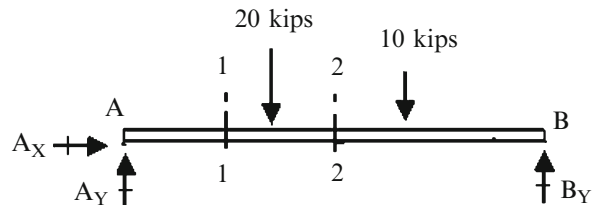


Fig. E1.3a

Determine: The internal forces at Sects. 1.1 and 2.2

Solution: First we determine the reactions at A and B by applying the equilibrium conditions to entire body AB (Fig. E1.3b).

Fig. E1.3b

The static equilibrium equations are

$$\sum F_x = 0 \quad A_x = 0$$

$$\sum F_y = 0 \quad A_y + B_y = 30$$

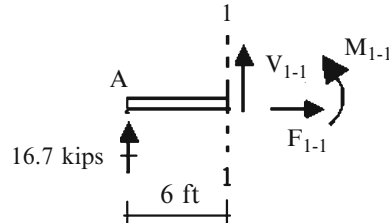
$$\sum M_{\text{about } A} = 0 \quad 8(20) + 16(10) - 24B_y = 0$$

We solve for B_y , $B_y = \frac{20}{3} + \frac{2}{3}(10) = 13.3 \text{ kip } \uparrow$

and then $A_y \quad A_y = 16.7 \text{ kip } \uparrow$

Next, we work with the free body diagrams shown below. We replace the internal \vec{F} with its normal and tangential components, F and V (Figs. E1.3c, d).

Fig. E1.3c Left segment-cutting plane 1-1



Applying the equilibrium conditions to the above segment leads to

$$\sum F_x \rightarrow^+ F_{1-1} = 0$$

$$\sum F_y \uparrow^+ = 0 \quad V_{1-1} + 16.7 = 0 \Rightarrow V_{1-1} = 16.7 \text{ kip } \downarrow$$

$$\sum M_{\text{about } 1-1} = 0 \quad M_{1-1} - 16.7(6) = 0 \Rightarrow M_{1-1} = 100.2 \text{ kip ft counterclockwise}$$

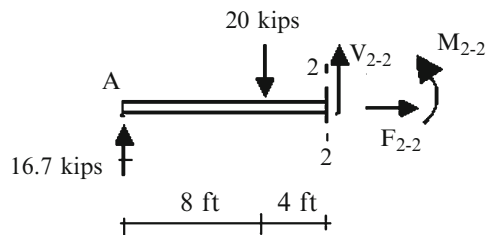
Applying the equilibrium conditions to the segment shown below leads to

$$\sum F_x \rightarrow^+ F_{2-2} = 0$$

$$\sum F_y \uparrow^+ = 0 \quad V_{2-2} - 20 + 16.7 = 0 \Rightarrow V_{2-2} = 3.3 \text{ kip } \uparrow$$

$$\sum M_{\text{about } 2-2} = 0 \quad M_{2-2} - 12(16.7) + 4(20) = 0 \Rightarrow M_{2-2} = 120.4 \text{ kip ft counterclockwise}$$

Fig. E1.3d Left segment-cutting plane 2-2



Note that the sense of V_{1-1} and V_{2-2} are opposite.

1.5.5 Deformations and Displacements

When a body is subjected to external loads, internal forces are developed in order to maintain equilibrium between the internal segments. These forces produce stresses which in turn produce strains that cause the body to change its shape and displace from its unloaded position.

Consider the member shown in Fig. 1.25. We apply an axial force which generates the axial stress, σ , equal to

$$\sigma = \frac{F}{A} \quad (1.15)$$

where A is the cross-sectional area. The resulting strain depends on E , the modulus of elasticity for the material [3] and [4].

$$\varepsilon = \frac{\sigma}{E} \quad (1.16)$$

Extensional strain is defined as the change in length.

$$\varepsilon = \frac{\Delta L}{L} \quad (1.17)$$

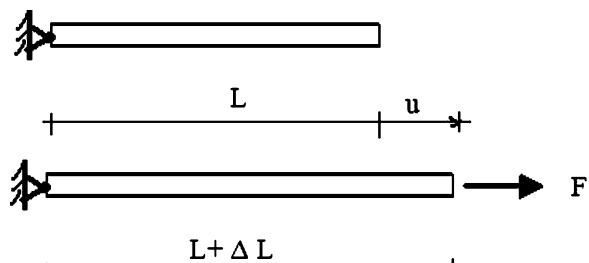


Fig. 1.25 Unreformed and deformed states

Then,

$$\Delta L = L\varepsilon = \left(\frac{L}{AE} \right) F \quad (1.18)$$

We refer to the movement due to strain as the displacement and denote it by u . It follows that $\Delta L \equiv u$. Finally, we write (1.18) as

$$u = \left(\frac{L}{AE} \right) F \quad (1.19)$$

Strains are generally referred to as deformations since they relate to a change in shape. This example illustrates that displacements are a consequence of deformations which are due to forces. Note that deformations are dimensionless quantities whereas displacements have geometric units such as either length (translation) or angle (rotation). The coefficient of F in (1.19) has units of displacement/force. We interpret this coefficient as a measure of the flexibility of the member. Here we are defining flexibility as displacement/unit force. The inverse of flexibility is called stiffness. Stiffness relates the force required to introduce a unit displacement. Inverting (1.19) leads to

$$F = \left(\frac{AE}{L} \right) u \quad (1.20)$$

It follows that the stiffness of an axial loaded member is equal to $\frac{AE}{L}$.

Stiffness and flexibility are important concept in Structural Engineering. We use them to reason qualitatively about the change in behavior of a structure when we introduce modifications to the geometry and structural members. Obviously, to reduce displacements, one makes the structure stiffer. How this is achieved is one of the themes of this text.

1.5.6 Structural Behavior; Structural Analysis

When a structure is subjected to an external loading, it responds by developing internal forces which lead to internal stresses. The stresses generate strains, resulting in displacements from the initial unloaded position. Figure 1.26 illustrates the displacement process for a beam type member subjected to a transverse loading. This process is continued until the internal stresses reach a level at which the external loading is equilibrated by the internal forces. The final displacement profile corresponds to this equilibrium state.

Structural analysis is concerned with quantifying the response of structures subjected to external loading. The scope includes determining the magnitude of

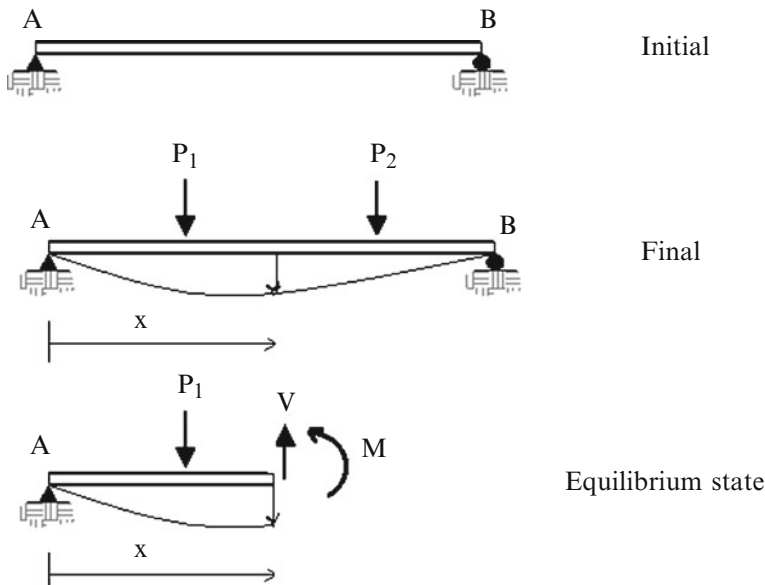


Fig. 1.26 Simple beam response

the reactions, internal forces, and displacements. The analysis is generally carried out in the following order.

1.5.6.1 Study Forces

In the study of forces, we apply the equilibrium equations to various Free Body Diagrams. We work initially with the FBD for the structure treated as a single body, and determine the reactions. Once the reactions are known, we select various cutting planes and determine the corresponding internal forces. This phase involves some heuristic knowledge as to “the best” choice of cutting planes.

1.5.6.2 Study Displacements

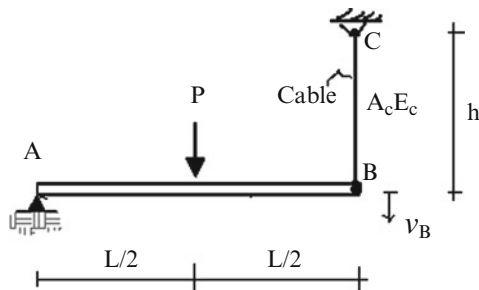
Displacements are the geometric measures that define the position of the structure under the applied external loading. Displacements are a consequence of internal stresses and are usually expressed in terms of the internal forces. The form of the “Force-displacement” relations depends on the type of structural member, e.g., a truss member, a beam, etc. We discuss this topic in more detail in Chaps. 2 and 3. In what follows, we illustrate these computations for some fairly simple structures.

Example 1.4

Given: The structure defined in Fig. E1.4a. Member AB is a beam type member. It is connected to a hinge support at A, and supported at B by a cable, BC.

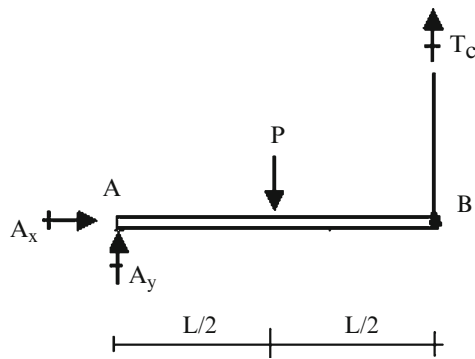
Determine: The reactions, cable tension, and vertical displacement at B . Assume $E_c = 200 \text{ GPa}$, $A_c = 600 \text{ mm}^2$, $h = 4 \text{ m}$, $L = 10 \text{ m}$, and $P = 80 \text{ kN}$

Fig. E1.4a



Solution: We start with the free body diagram of the entire structure shown in Fig. E1.4b. We note that the cable force is tension. Requiring the sum of the moments of the forces with respect to point A to vanish leads to the T_c

Fig. E1.4b



$$\sum M_{\text{about } A} = \frac{L}{2}P - LT_c = 0$$

↓

$$T_c = \frac{P}{2}$$

Next, we determine the reactions at A using force summations.

$$\begin{aligned}\sum F_y &= 0 \quad A_y + T_c - P = 0 \Rightarrow A_y = \frac{P}{2} \\ \sum F_x &= 0 \quad A_x = 0\end{aligned}$$

The vertical displacement of B is equal to the extension of the cable. Noting (1.19), the expression for v_B is

$$v_B = \left(\frac{h}{A_c E_c} \right) T_c = \frac{h}{A_c E_c} \left(\frac{P}{2} \right) = \frac{4,000}{(600)(200)} \left(\frac{80}{2} \right) = 1.33 \text{ mm } \downarrow$$

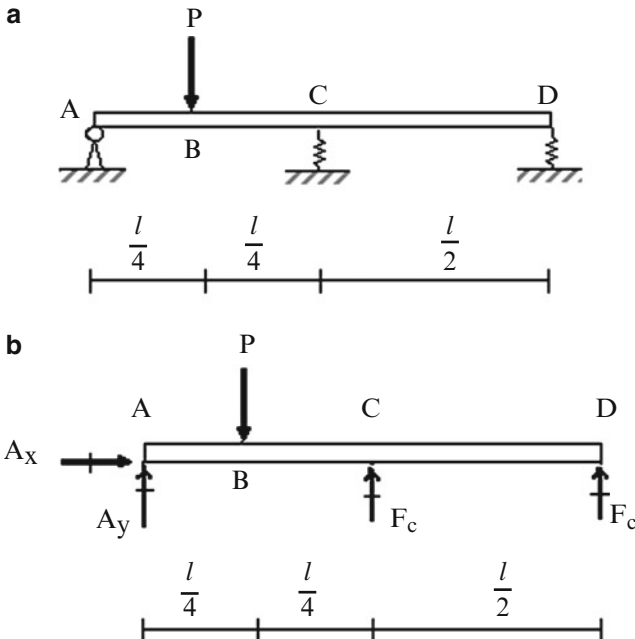


Fig. 1.27 Rigid member on springs

In what follows, we illustrate the application of the general analysis procedure to the idealized structure defined in Fig. 1.27. Member ABCD is considered to be rigid. It is supported by a hinge at A and springs at C and D. The force, P , is constant. Replacing the hinge support and springs with their corresponding forces results in the free body diagram shown in Fig. 1.27b. There are four unknown forces; A_x , A_y , F_c , and F_d . Setting the resultant force equal to zero leads to

$$\begin{aligned} A_x &= 0 \\ A_y + F_c + F_d &= P \end{aligned} \tag{1.21}$$

Next, we require that the moment vanish at A.

$$\frac{l}{4}P = \frac{l}{2}F_c + lF_d \tag{1.22}$$

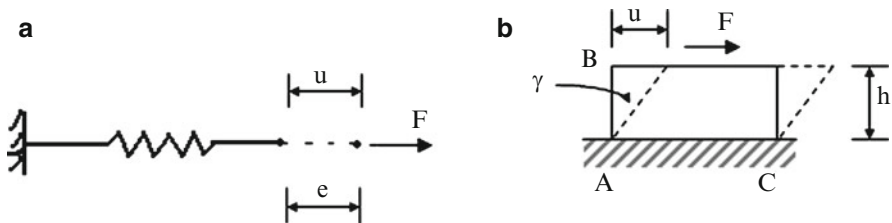


Fig. 1.28 Deformation modes. (a) Extension. (b) Shear

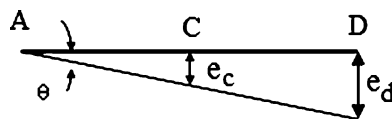


Fig. 1.29 Deformation-displacement relations

Since there are more force unknowns than force equilibrium equations, the structure is statically indeterminate.

We generate additional equations by examining how the structure deforms. Deformation is a consequence of applying a force to a material. Deformation is associated with a change in shape. Figure 1.28 illustrates various deformation modes: the first is extension of a spring; the second is shear. A rigid body is an idealized case: the deformations are considered to be negligible.

An important phase in the analysis of a deformable body is the study of deformations. One first identifies the displacement variables that define the “deformed” position and then, using geometric analysis, establishes the expressions relating the deformations of the deformable structural elements with the displacements. We illustrate this process for the structure defined in Fig. 1.29.

Member ABCD is assumed to be rigid and therefore remains straight when the load is applied. Deformation occurs in the springs at C and D, causing ABCD to rotate about the hinge at A. There is only one independent displacement variable. We take it to be the rotation angle θ shown in Fig. 1.29. With this choice of sense, the springs compress. When θ is small, the spring deformations can be approximated as linear functions of θ . This approximation is valid for most cases.

$$\begin{aligned} e_c &= \left(\frac{l}{2}\right)\theta \\ e_d &= l\theta \end{aligned} \tag{1.23}$$

The last step in the analysis involves relating the deformations and the corresponding internal forces. For this example structure, the internal forces are the spring forces, F_c and F_d . In general, the relationship between the force and deformation of a component is a function of the makeup of the component (i.e., the

material used and the geometry of the component). Here, we assume the behavior is linear and write

$$\begin{aligned} F_c &= k_c e_c \\ F_d &= k_d e_d \end{aligned} \quad (1.24)$$

where k_c , and k_d are the spring stiffness factors. Note that the units of k are force/length since e has units of length.

At this point, we have completed the formulation phase. There are seven equations, (1.21)–(1.23), relating the seven variables consisting of the four forces, one displacement, and two deformations. Therefore, the problem is solvable. How one proceeds through the solution phase depends on what variables one want to determine first.

Starting with (1.23), we observe that the reaction A_v can be determined once the spring forces are known. Therefore, we hold this equation in reserve, and focus on the remaining equations. We can combine (1.23) and (1.24) by substituting for the deformations. The resulting equations together with (1.24) are

$$F_c = \left(k_c \frac{l}{2} \right) \theta, \quad F_d = (k_d l) \theta \quad (1.25a)$$

$$\frac{l}{4} P = \frac{l}{2} F_c + l F_d \quad (1.25b)$$

The most convenient strategy is to substitute for F_c, F_d in the second equation. Then,

$$\frac{l}{4} P = l \left(\frac{1}{4} k_c + k_d \right) l \theta$$

and

$$\theta = \frac{P}{(4k_d + k_c)l} \quad (1.26)$$

Finally, the spring forces corresponding to this value of θ are

$$\begin{aligned} F_c &= \frac{k_c}{2(4k_d + k_c)} P \\ F_d &= \frac{k_d}{(4k_d + k_c)} P \end{aligned} \quad (1.27)$$

An alternate strategy is to solve first for one of the spring forces. Suppose we take F_c as the primary force variable. Using (1.25b), we solve for F_c .

$$F_c = \frac{1}{2} P - 2F_d \quad (1.28)$$

Another equation relating F_c and F_d is obtained by eliminating θ in (2.23a). The steps are

$$\theta = \frac{1}{k_c(l/2)} F_c \quad (1.29)$$

and

$$F_d = \frac{2k_d}{k_c} F_c \quad (1.30)$$

Equation (1.30) represents a constraint on the spring forces. The deformations of the springs are not arbitrary; they must satisfy (1.23), which can be written as:

$$e_d = 2e_c \quad (1.31)$$

Finally, substituting for F_d in (1.28) and solving for F_c leads to

$$F_c = \left(\frac{1/2}{1 + 4k_d/k_c} \right) P \quad (1.32)$$

The rotation angle is determined with (1.29) and F_c with (1.30).

We refer to the first solution procedure as the *displacement or stiffness method*. It is relatively simple to execute since it involves only substitution. Most of the structural analysis computer programs are based on this method. The second procedure is called the *force or flexibility method*. Some manipulation of the equations is required when the structure is statically indeterminate and consequently the method is somewhat more difficult to apply in this case. However, the Force Method is more convenient to apply than the displacement method when the structure is statically determinate, since the forces can be determined using only the equilibrium equations. The approach we present in part I of the text is based on the Force Method. Later in part II, we present the Force and Displacement methods in more detail in Chaps. 9 and 10.

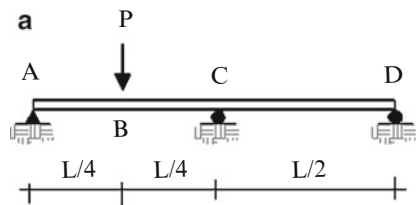
1.5.7 The Importance of Displacements

Displacements are important for two reasons. Firstly, the serviceability requirement for structures is usually specified as a limit on the magnitude of certain displacements. Secondly, for indeterminate structures, one cannot determine the internal forces using only the equations of static equilibrium. One needs to consider the displacements and internal forces simultaneously. This topic is addressed in part II of the text. The following example illustrates one of the strategies employed for a statically indeterminate beam.

Example 1.5 A statically indeterminate beam

Given: The beam shown in Fig. E1.5a.

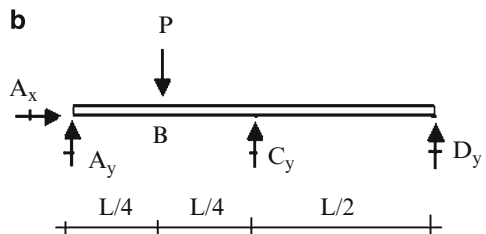
Fig. E1.5a



Determine: The reactions.

Solution: First, we construct the free body diagram for the beam (Figs. E1.5b, c).

Fig. E1.5b



Considering summation of forces in the X and Y directions and summation of moments about A , we obtain the following three equations.

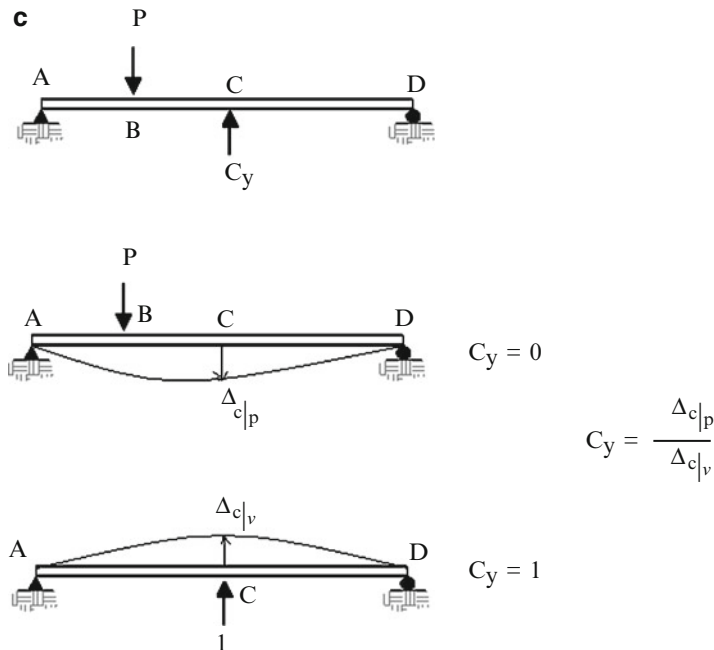
$$\sum F_x \rightarrow^+ \Rightarrow A_x = 0$$

$$\sum F_y \uparrow^+ = 0 \Rightarrow A_y + C_y + D_y = P$$

$$\sum M_{\text{about } A} = 0 \Rightarrow \frac{L}{4}P = \frac{L}{2}C_y + LD_y$$

We have only two equations for the three vertical reactions, A_y , C_y , and D_y . Therefore, we *cannot* determine their magnitude using only the force equilibrium equations.

The Force (or Flexibility) method for this problem is based on releasing one of the roller supports, say support C, replacing it with an unknown force, C_y , and allowing point C to move vertically under the action of the applied loads. First, we take $C_y = 0$ and apply P . Point C moves an amount $\Delta_{c|p}$ shown in the Figure below. Then, we take $P = 0$, $C_y = 1$, and determine $\Delta_{c|v}$ the corresponding movement at C due to a unit upward force at C. Assuming the support at C is unyielding, the net movement must be zero. Therefore, we increase the force C_y until this condition is satisfied. Once C_y is known, we can find the remaining forces using the equations of static equilibrium. In order to carry out this solution procedure, one needs to have a method for computing displacements of beams. These methods are described in Chap. 3.

**Fig. E1.5c**

1.6 Summary

1.6.1 Objectives of the Chapter

- Provide an overview of the set of issues that a structural engineer needs to address as a practicing professional engineer.
- Introduce the basic analytical methods of structural analysis and describe how they are applied to determine the response of a structure.

1.6.2 Key Issues and Concepts Introduced

- A structure is an assemblage of structural components which are arranged in such a way that the structure can withstand the action of the loads that are applied to it. Structures are classified according to their makeup such as trusses, frames and their function such as bridges, office buildings.
- The primary concern of a structural engineer is to ensure that the structure *will not collapse* during its expected lifetime. This requires firstly that the engineer properly identify the extreme loading that the structure is likely to experience over its design life, and secondly, that the structure is dimensioned so that it has adequate capacity to resist the extreme loading.

- Structures are restrained against rigid body motion by supports. When the structure is loaded, reaction forces are developed by the supports. A minimum of three non-concurrent reaction forces are necessary to prevent rigid body motion for a planar structure.
- Initial instability occurs when the reactions are insufficient or the members are not properly arranged to resist applied external forces. In this case, the structure will fail under an infinitesimal load. This condition can be corrected by modifying the supports or including additional members.
- Loss of stability under loading can occur when a primary structural member loses its capacity to carry load due to either elastic buckling or failure of the material. There are two modes of material failure: “brittle” and “ductile.” Brittle failure occurs suddenly with a complete loss in load capacity. One should avoid this mechanism. Ductile failure is evidenced by substantial inelastic deformation and loss in stiffness. The limit state design procedure allows for a limited amount of inelastic deformation.
- Loads applied to civil structures are categorized according to direction. Vertical loads are due to gravitational forces and are defined in terms of the weight of objects. Lateral loads are produced by natural events such as wind and earthquake. The relative importance of these loads depends on the nature of the structure and the geographical location of the site.
- Loads are also generated during the construction of the structure. The design loading for certain types of structures such as segmented concrete girders is controlled by the construction process. Most structural failures occur during the construction process.
- Loads are also classified according to the time period over which the loads are applied. Long-term loads, such as self weight, are called “dead” loads. Loads whose magnitude or location changes are called “live” loads. Typical live loads are produced by vehicles crossing bridges, and people occupying buildings.
- Extreme loads such as wind and earthquakes are defined in terms of their return period, which is interpreted as the average time interval between occurrences of the event. One speaks of the 50 year wind, the 50 year earthquake, etc. The magnitude of the load increases with increasing return period.
- The design life of a structure is the time period over which the structure is expected to function without any loss in functionality. Bridges are designed to last at least 100 years. Industrial buildings are expected to have design lives usually greater than 100 years. The probability that a structure will experience an extreme event over its design life is approximately equal to the ratio of the design life to the return period.
- The effect of wind acting on a building is represented by a pressure loading distributed over the external surfaces. The magnitude and spatial variation of the pressure depends on the shape of the building and the local wind environment. Positive pressure is generated on windward vertical faces and steeply inclined roofs. Turbulence zones occur on flat roof and leeward faces, and result in negative pressure.

- Design codes specify procedures for computing the spatial distribution of wind pressure given the expected extreme wind velocity at the geographic location. The wind velocity tends to be larger in coastal regions. A typical wind velocity for coastal regions of the USA is 100 miles per hour. The corresponding wind pressure is approximately 20 psf.
- Snow loading is represented as a uniform download pressure acting on the roof zones of a structure. Design snow pressure is based on ground snow data for the region where the structure is located. Snow is an important loading for the northern part of the USA, Canada, and Eastern Europe.
- Earthquakes produce sudden intense short-term ground motion which causes structures to vibrate. The lateral floor loading is due to the inertia forces associated with the acceleration generated by the ground shaking and is generally expressed as $(W_f/g)a_{\max}$ where W_f is the floor weight and a_{\max} is the peak value of floor acceleration. Seismic engineering is specialized technical area which is beyond the scope of this textbook. However, the reader should be knowledgeable of the general seismic design strategy.
- Conventional structural design philosophy is based on satisfying two requirements: safety and serviceability. Safety relates to extreme loading, and is concerned with preventing collapse and loss of life. Safety is achieved by providing more resistance than is required for the extreme loading. Serviceability relates to loading which occur during the structure's lifetime. One needs to ensure that the structure remains operational and has no damage.
- Motion-Based Design, also called performance-based design, is an alternate design methodology that takes as its primary objective the satisfaction of motion-related design requirements such as displacement and acceleration. The goal here is to provide sufficient stiffness and energy dissipation mechanisms to limit the motion under extreme loading.
- Structural analysis is concerned with quantifying the response of a structure subjected to external loading. This effort involves determining the reactions, internal forces, and displacement profiles. One generally carries out the analysis in two steps: study of forces and study of displacements. In the study of forces, one applies the force equilibrium equations to isolate segments of the structure called Free Body Diagrams. Selecting appropriate Free Body Diagrams is a skill acquired through practice. In the study of displacements, one first uses a geometric-based approach to express the deformation measures in terms of displacement measures. The displacement measures are then related to the internal forces by introducing certain material properties such as the elastic modulus. These relations allow one to determine the displacements, given the internal forces. We apply this approach throughout part II of the text. It provides the basis for the analysis of statically indeterminate structures.

Overview

We begin this chapter by reviewing the historical development of truss structures. Trusses have played a key role in the expansion of the highway and railroad systems during the past two centuries. From a mechanics perspective, they are ideal structures for introducing the concepts of equilibrium and displacement. We deal first with the issues of stability and static determinacy, and then move on to describe manual and computer-based techniques for determining the internal forces generated by external loads. A computational scheme for determining the displacements of truss structures is presented next. Given a structure, one needs information concerning how the internal forces vary as the external live load is repositioned on the structure for the design phase. This type of information is provided by an influence line. We introduce influence lines in the last section of this chapter and illustrate how they are constructed for typical trusses. This book focuses on linear elastic structural analysis. Although nonlinear structural analysis is playing an increasingly more important role in structural design, we believe an understanding of linear analysis is essential before discussing the topic of nonlinear analysis.

2.1 Introduction: Types of Truss Structures

Simple two-dimensional (2-D) truss structures are formed by combining one-dimensional linear members to create a triangular pattern. One starts with a triangular unit, and then adds a pair of members to form an additional triangular unit. This process is repeated until the complete structure is assembled. Figure 2.1 illustrates this process for the case where all the members are contained in a single plane. Such structures are called *plane* trusses; the nodes are also called “*Joints*.”

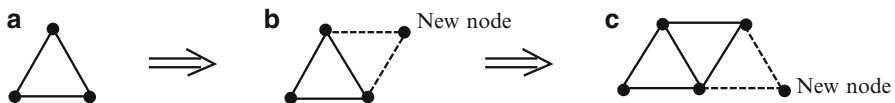


Fig. 2.1 Simple planar truss construction

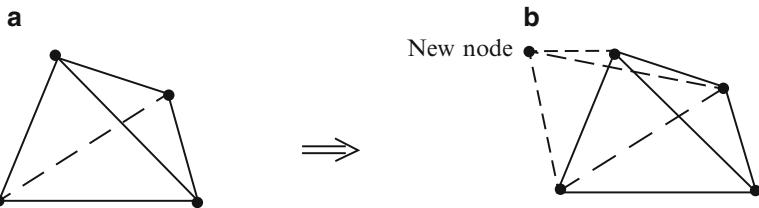


Fig. 2.2 Simple space truss construction

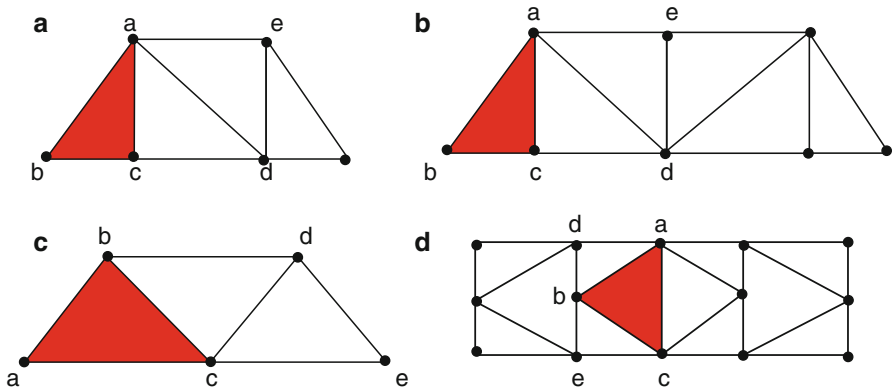


Fig. 2.3 Simple planar trusses

Three members connected at their ends form a rigid structure in the sense that, when loaded, the change in shape of the structure is due only to the deformation of the members. It follows that a structure constructed in the manner described above is also rigid provided that the structure is suitably supported.

Simple three-dimensional (3-D) space trusses are composed of tetrahedral units. Starting with a tetrahedral unit, one forms an additional tetrahedral unit by adding three linear elements, as illustrated in Fig. 2.2. When the structure is suitably supported to prevent rigid body motion, the assemblage is rigid. The question of suitable supports is addressed later in the chapter.

Examples of simple planar trusses are shown in Fig. 2.3. Starting with the initial triangle abc, one adds the nodes d, e, etc.

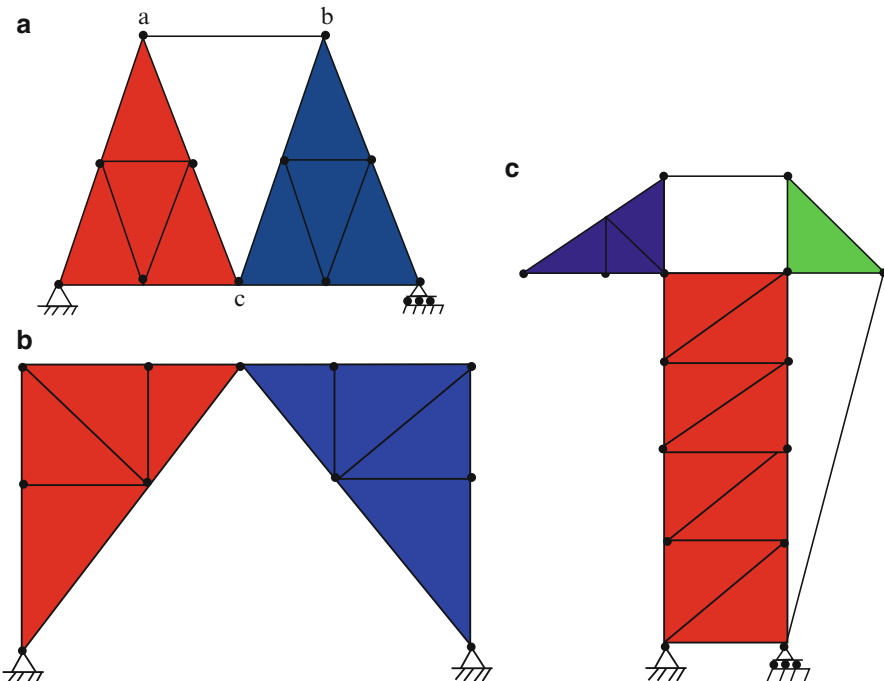


Fig. 2.4 Compound planar trusses

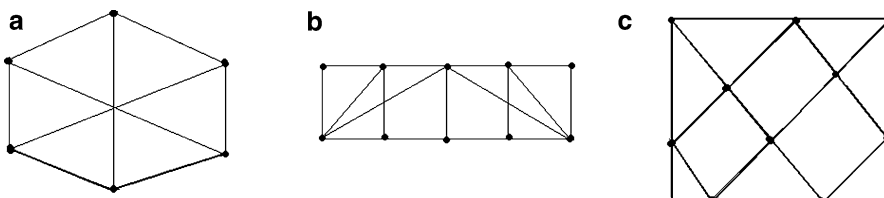


Fig. 2.5 Complex planar trusses

Trusses may also be constructed by using simple trusses as the “members,” connected together by additional bars or joints. These structures are called *compound trusses*. Figure 2.4 shows several examples of compound trusses, where the simple trusses are shown as shaded areas.

A truss geometry that does not fall in either the simple or compound category is called a complex truss [23]. Examples are shown in Fig. 2.5. This type of truss is not used as frequently as either simple or compound trusses.

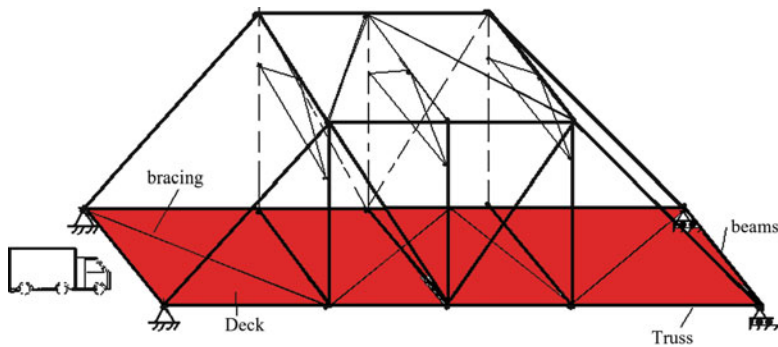


Fig. 2.6 Single span truss bridge system

2.1.1 Structural Idealization

Trusses are components of larger structural systems, such as buildings, bridges, and towers. In order to evaluate the behavior under loading, one needs to identify the main structural components of the system and determine how the external load is transmitted from one component to another. This process is called “structural idealization,” it is a key step in the analysis process. In what follows, we illustrate idealization strategies for typical bridges and roof systems.

Figure 2.6 shows a typical single span truss bridge system. The key components are the two simple planar trusses, the lateral bracing systems at the top, sides, and bottom levels and the flooring system consisting of floor stringers/beams and deck slab. Loading applied to the deck slab is transmitted through the stringer/beam system to the bottom nodes of the two planar trusses. The major percentage of the analysis effort is concerned with analyzing a simple truss for dead weight, wind, and traffic loading.

Roofing system for buildings such as warehouses, shopping centers, and sports facilities employ trusses to support the roof envelope. Figure 2.7 illustrates a scheme for a typical roofing system for a single-story industrial building. The roof system consists of steel decking attached to purlins which, in turn, are supported at the top nodes of the planar trusses. Loading applied to the roof area in a bay is transmitted through the purlins to the trusses adjacent to the bay, and eventually to the supports. Bracing is incorporated to carry the lateral loading which may act either in the longitudinal or transverse direction. The primary effort for this structural system is concerned with analyzing a single planar roof truss for the tributary area loading applied at the top chord nodes.

2.1.2 Historical Background

The first application of truss type structures is believed to be in Egyptian boats built between 3,100 and 2,700 BC. Egyptian boat builders used trusses constructed by

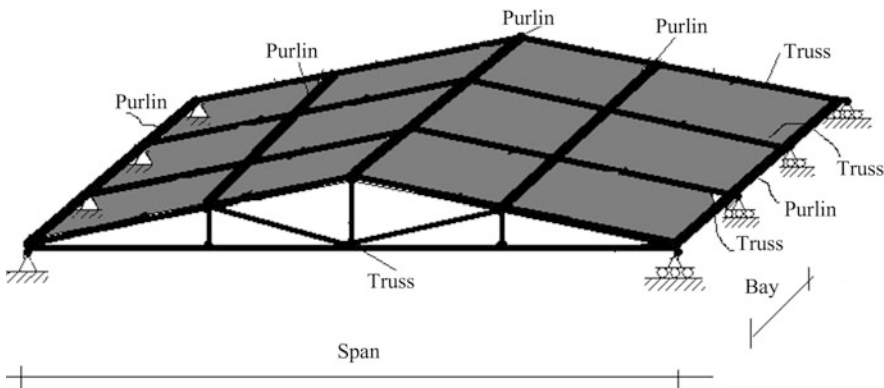


Fig. 2.7 Typical industrial building roofing system

tying the members together with vines to form the sides and attached the outer hull to these structures (Garrison, 1991). The Romans used wood trusses for bridges and roofs. Examples are a bridge over the Danube (circa 106 AD) and the entrance to the Pantheon (circa 120 AD). The next time frame is that of the Middle Ages. Examples of trusses are found in English cathedrals (Salisbury Cathedral, circa 1258 AD) and great halls (Westminster Palace, circa 1400). Deployment of wooden trusses continued through the Gothic and Renaissance periods, mainly to support roofs. The Engineers of these time periods intuitively understood the rigidity provided by the triangular form, but lacked a theory that they could apply to evaluate the response for a given load.

A major contribution to the theory is the work of Leonardo daVinci (1452–1519), who formulated the concepts of force and moment as vectors and showed that forces can be combined using a graphical construction that is now called the force parallelogram. From the early 1600s to the mid-1800s, many advances in the development of a scientific basis for a theory of structures were made. Key contributors were Newton (1642–1729), Hooke (1635–1703), Galileo Galilei (first useable formula for strength of a cantilever beam-1638), Euler (theory of buckling of columns-1757), Bernoulli (bending deformation of a beam-1741), Navier (produced an integrated theory of Structural Mechanics—1826), and Möbius (published the *Textbook of Statics*—1837).

Wooden bridge truss structures were popular in the early 1800s, especially in the USA. There are many examples of covered wooden bridges in Vermont and New Hampshire. Figure 2.8 illustrates some typical structural schemes.

There was a flourishing industry in New England producing wooden bridge trusses, many of which were exported to Europe. As with many emerging technologies, competition from other emerging technologies occurred and eventually took over the market for the product. The first impetus for change was the Industrial Revolution which occurred in the early 1800s. The concept of the railroad

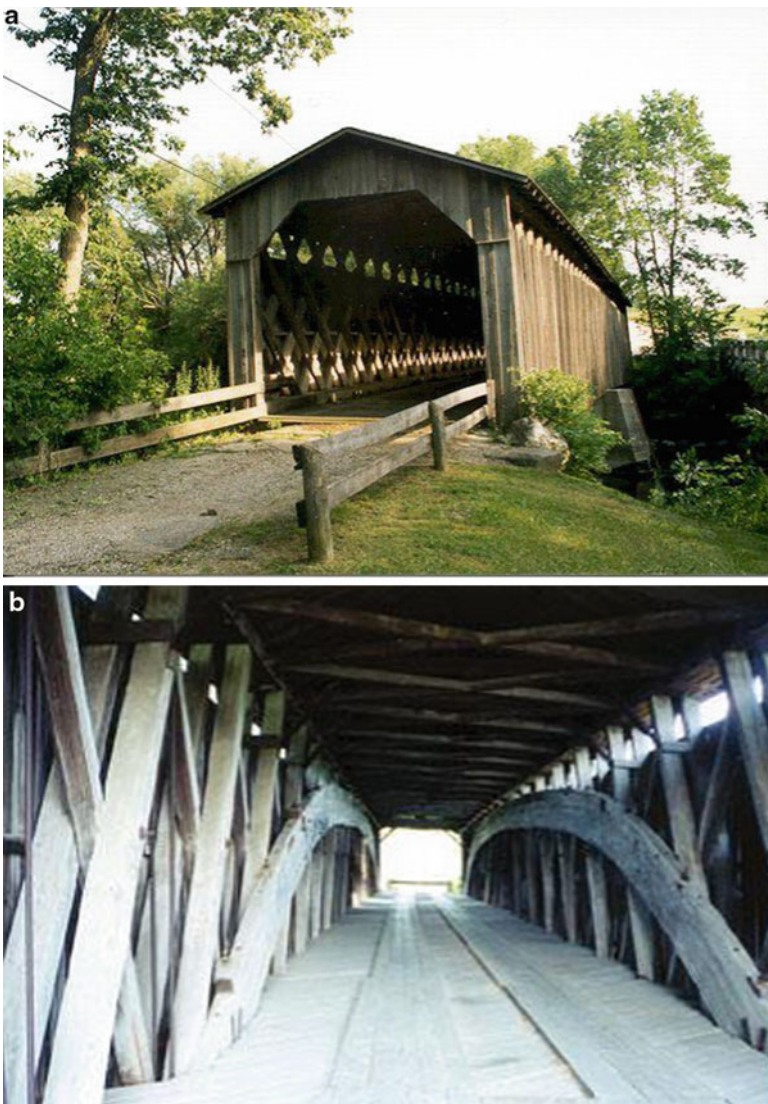


Fig. 2.8 Covered wood bridges

was invented during this period. This invention created a demand for more robust and more durable bridges to carry the heavier moving loads over longer spans. Cost also became an issue. Up to this time, wooden bridges were designed to carry light pedestrian and horse and carriage traffic over relatively short spans. Their expected life was short, but since they used local materials and local labor, they were not expensive and durability was not an issue. However, they were not adequate for the railroad traffic and other solutions were needed.

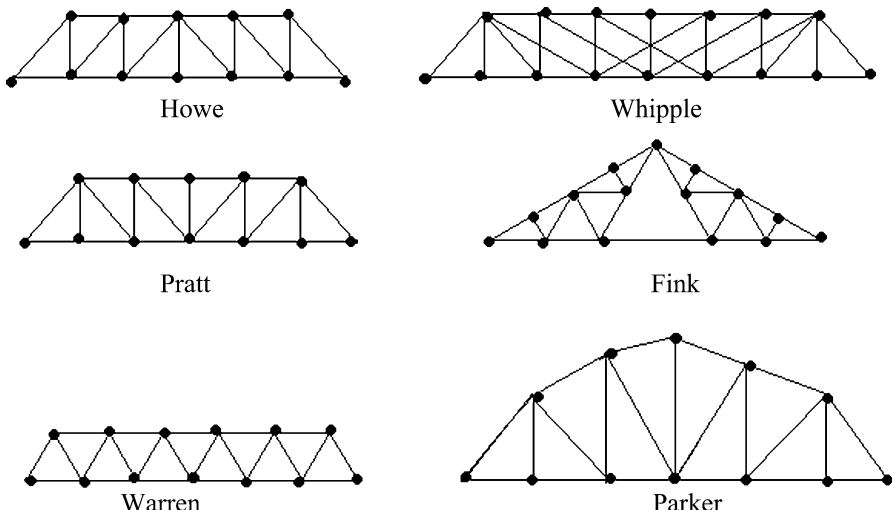


Fig. 2.9 Examples of named trusses

Another technology that was evolving in the late 1700s was iron making. Processes for making cast and wrought iron cheaper than existing methods were developed in the 1780s. Methods for shaping wrought iron into shapes that could be used as truss members were also invented simultaneously. These inventions set the stage for the use of iron members in trusses during the early 1800s. Initially, wrought iron was used for tension elements and wood for compression elements. Gradually, cast iron replaced wood for compression elements. The first all iron truss bridge in the USA was built in 1840 by Squire Whipple, a leading bridge designer in the USA at that time. He is also known for his book *Essay on Bridge Building*, published in 1847, the first publication on Structural Theory by an US author. Some other designers active in the 1840s were W. Howe, T. Pratt, A. Fink in North America and J. Warren in the UK. Trusses of this era were given the name of the individual who designed or constructed them. Examples are shown in Fig. 2.9.

Starting around 1850, iron trusses were used not only for bridges but also for other long-span structures such as market halls, exhibition buildings, and railway stations. Notable examples are the Crystal Palace, the Eiffel tower and the Saint Pancras station (Fig. 2.10).

During the period from 1850 to 1870, an improved version of iron called steel was invented. This material was much stronger than cast iron; more ductile than wrought iron, and quickly displaced iron as the material of choice. The first all steel truss bridge in the USA was built for the Chicago and Alton Railroad in 1879. The structure consisted of a series of Whipple trusses with a total length of 1,500 ft spanning over the Mississippi River at Glasgow, Missouri. The first major long-span steel bridge was the Firth of Forth Bridge built in Scotland in 1890. Another similar cantilever style truss bridge was built over the St Lawrence River in Quebec,

Canada in 1919. The initial steel structures used eyebars and pins. Rivets replaced pins as connectors in the late 1800s.

High-strength bolts and welding are now used to connect the structural members in today's modern steel constructions. Figure 2.11 illustrates typical bolted and welded connections. Connection details are usually designed by the steel fabricator and checked by the structural engineer. The goal in connection design is to minimize steel erection time (Fig. 2.12).

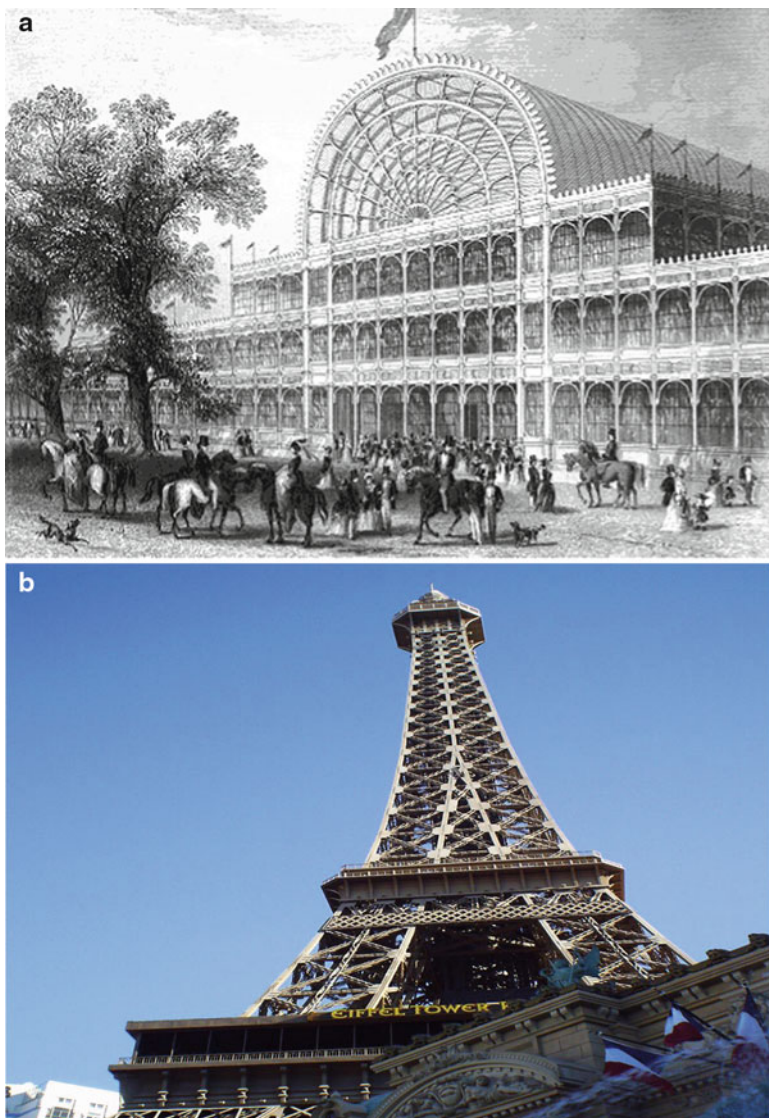


Fig. 2.10 Examples of structures made of iron trusses. (a) Crystal Palace. (b) Eiffel Tower. (c) Saint Pancras station

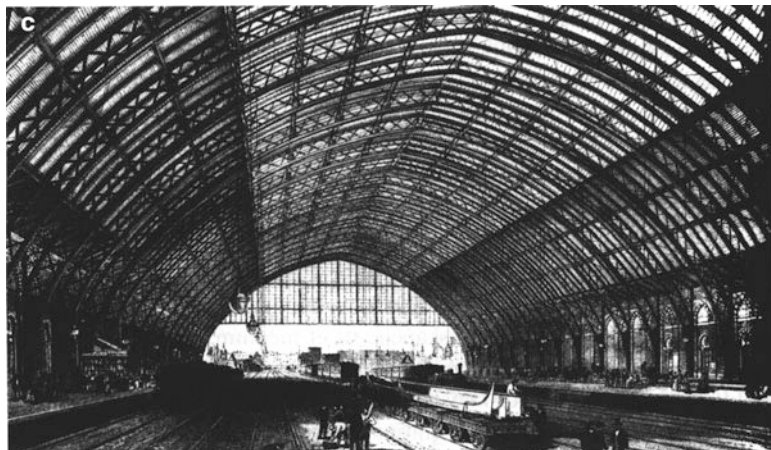


Fig. 2.10 (continued)

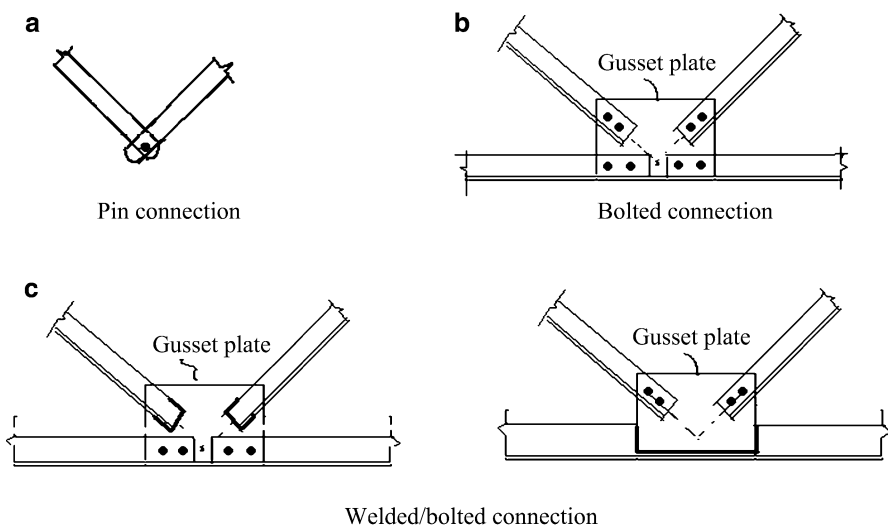


Fig. 2.11 Typical pin joint connections

Steel truss bridges were the dominant choice for long-span crossings until the mid-1900s when another structural form, the cable-stayed bridge, emerged as a competitor. Cable-stayed bridges have essentially captured the market for spans up to about 900 m. Segmented concrete girder construction has also emerged as a major competitor for somewhat shorter spans. Plane trusses now are used mainly for prefabricated joists, for gable roof systems, and for spanning long interior



Fig. 2.12 Example of early steel bridges—Firth of Forth Bridge, Scotland



Fig. 2.13 Three-dimensional truss roof system

distances in buildings and sporting facilities such as convention halls and stadiums. Three-dimensional space trusses are used in dome type structures such as shown in Fig. 2.13, and also for towers. One of the most notable examples of the space truss concept is the Eiffel tower in Paris, France.

2.2 Analysis of Planar Trusses

In this section, we focus on introducing analysis and behavior issues for planar trusses. The discussion is extended in the next section to deal with three-dimensional space structures.

The analysis of trusses is based on the following idealizations that ensure that the forces in the members are purely axial:

1. The loads and displacement restraints are applied only at the nodes.
2. The members are connected with frictionless pins so that the members can rotate freely and no moment exists at the ends.
3. The stress due to the weight of the members is small in comparison to the stress due to the applied loads.
4. Each member is straight and is arranged such that its centroidal axis coincides with the line connecting the nodal points.

With these restrictions, it follows that a member is subjected only to an axial force at each end. These forces are equal in magnitude and their line of action coincides with the centroidal axis of the member. There is only one unknown per member, the magnitude of the force. The resulting state is uniform axial stress throughout the member. Depending on the loading, the member force may be either tension or compression. Figure 2.14 illustrates free body diagrams for a truss member and its associated nodes.

2.2.1 Equilibrium Considerations

Each node of a plane truss is acted upon by a set of coplanar concurrent forces. There are no moments since the pins are frictionless and the lines of action of the forces intersect at the node. For equilibrium of a node, the resultant force vector must vanish. In Squire Whipple's time (1840s), equilibrium was enforced using Leonardo da Vinci's graphical method based on the force polygon. Now, one applies an analytical approach based on resolving the force vectors into

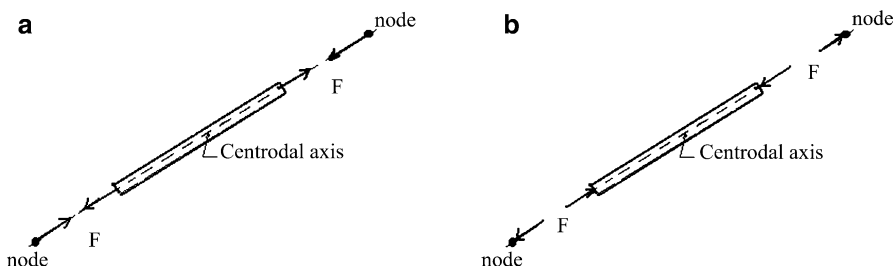
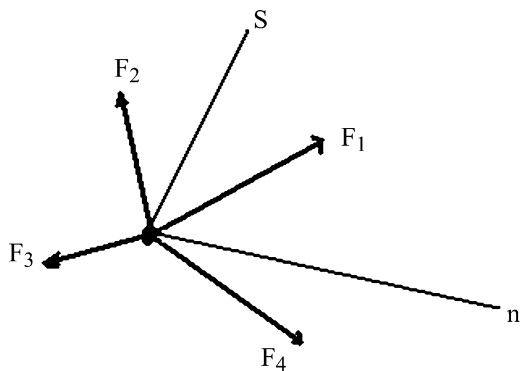


Fig. 2.14 Free body diagram of a truss member and its associated nodes. (a) Tension. (b) Compression

Fig. 2.15 Concurrent force system at a node



components and summing the components. The corresponding scalar equilibrium equations are

$$\sum F_n = 0 \quad \sum F_s = 0 \quad (2.1)$$

where n and s are two arbitrary nonparallel directions in the plane. Figure 2.15 illustrates this notation.

2.2.2 Statically Determinate Planar Trusses

In general, three motion restraints are required to prevent rigid body motion of a planar truss. Two of these restraints may be parallel. However the third restraint cannot be parallel to the other two restraints since, in this case, the truss could translate in the direction normal to the parallel restraint direction. Each restraint generates an unknown force, called a reaction. Therefore, the minimum number of reactions is 3.

Examples of typical support motion restraints and the corresponding reactions are shown in Fig. 2.16.

There are two scalar equilibrium equations per node for a plane truss. Assuming that there are j nodes, it follows that there are a total of $2j$ equilibrium equations available to determine the force unknowns. We suppose there are m members and r reactions. Then, since each member and each reaction involves only one unknown force magnitude, the total number of force unknowns is equal to $m + r$.

When the number of force unknowns is equal to the number of equilibrium equations, the structure is said to be *statically determinate*. If $m + r < 2j$, the truss is unstable since there are an insufficient number of either member forces or reactions or possibly both to equilibrate the applied loads. A word of caution: a statically determinate truss may also be unstable if the reactions are not properly aligned so as to prevent rigid body motion of the truss. We discuss this point in

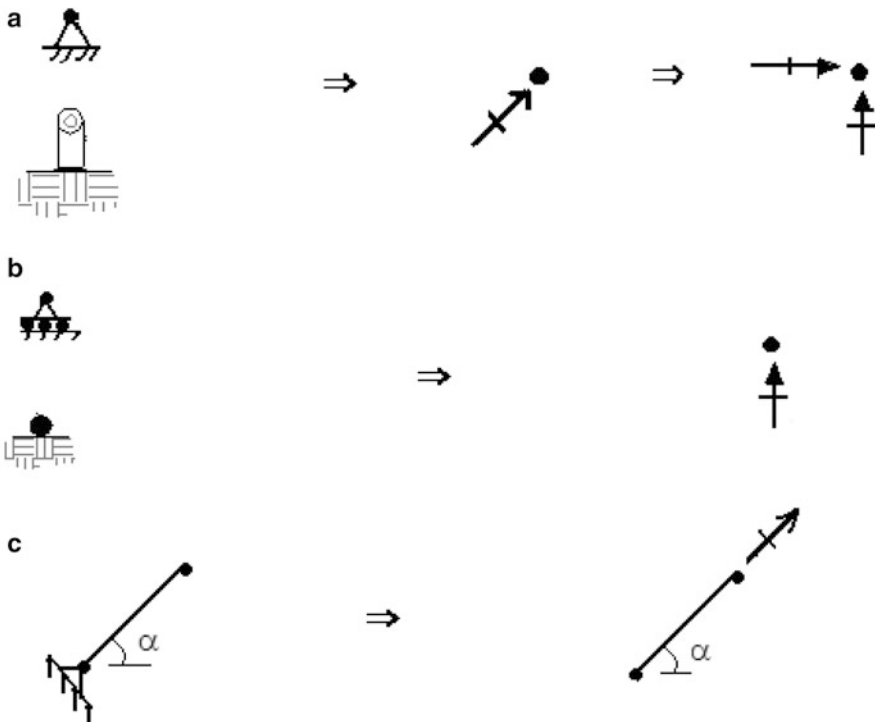


Fig. 2.16 Types of supports for planar trusses. (a) Hinge Support (two restraints \Rightarrow 2 reactions). (b) Roller Support (1 restraint \Rightarrow 1 reaction). (c) Rigid link

more detail in the following section. It follows that a plane truss is statically determinate, unstable, or indeterminate when

$$\begin{aligned} m + r = 2j & \text{ Statically determinate} \\ m + r < 2j & \text{ Unstable} \\ m + r > 2j & \text{ Statically indeterminate} \end{aligned} \quad (2.2)$$

2.2.3 Stability Criterion

In this section, we examine in more detail the question of whether a planar truss structure is initially stable. Assuming a plane truss has m members, r reactions, and j joints, there are $2j$ force equilibrium equations that relate the known (given) joint loads and the $(m + r)$ unknown forces. If $m + r < 2j$, the number of force unknowns is less than the number of equilibrium equations that the forces must satisfy. Mathematically, the problem is said to be under determined or inconsistent.

One cannot find the exact solution for an arbitrary loading, except in the trivial case where the magnitude of all the loads is zero, and consequently the forces are zero. Once a nontrivial load is applied, the structure cannot resist it, and motion ensues. The descriptor “initial instability” is used to denote this condition.

Even when $m + r = 2j$, a truss may still be unstable if the motion restraints are not properly arranged to prevent rigid body motion of the structure. There may be an insufficient number of restraints or the restraints may be aligned in such a way that rotation of a segment is possible. The stability of a complex truss depends on the geometrical arrangements of the members. Even though the truss satisfies the condition, $m + r = 2j$, and has sufficient restraints, it still may be unstable. The instability condition becomes evident when one attempts to determine the member forces using the $2j$ force equilibrium equations. The solution is not unique when the structure is unstable.

When $m + r > 2j$ and the structure is suitably restrained against rigid body motion, the structure is said to be statically indeterminate. This terminology follows from the fact that now there are more force unknowns than equilibrium equations, and not all the forces can be determined with only equilibrium considerations. One needs some additional equations. We address this type of problem in Part II.

In what follows, we illustrate the initial stability criteria with typical examples. Stability can be defined in a more rigorous way using certain concepts of linear algebra, a branch of mathematics that deals with linear algebraic equations. This approach is discussed in Sect. 2.4

Example 2.1 Simple trusses

Given: The structures shown in Fig. E2.1a–d

Determine: Whether the structures are initially stable, determinate or indeterminate.

Solutions:

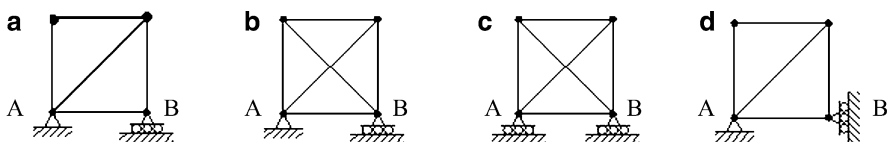


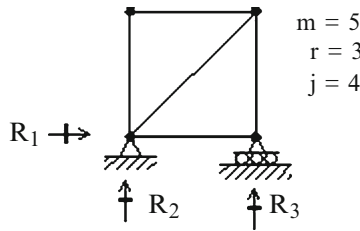
Fig. E2.1

Case (a): There are five members, three reactions, and four nodes. Then applying (2.2)

$$m + r = 8$$

$$2j = 8$$

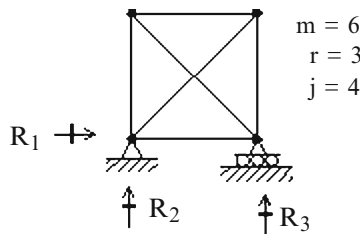
The structure is determinate and initially stable.



Case (b):

$$m + r = 9$$

$$2j = 8$$

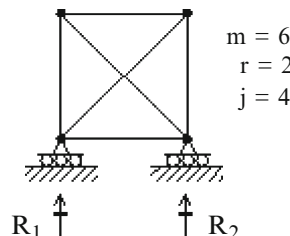


There is one extra force and therefore the structure is initially stable and indeterminate to the first degree.

Case(c): The stability criterion appears to be satisfied.

$$m + r = 8$$

$$2j = 8$$

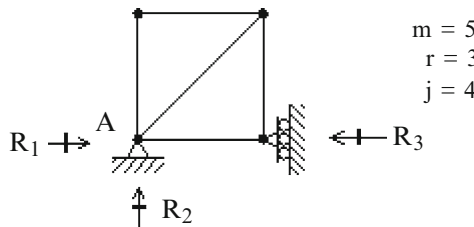


However, the number of supports is insufficient to prevent rigid body motion in the horizontal direction. Therefore the structure is initially unstable.

Case (d): The stability criterion appears to be satisfied.

$$m + r = 8$$

$$2j = 8$$



However, the three displacement restraints are concurrent (point A) and therefore the structure can rotate at point A. It follows that the structure is initially unstable.

Example 2.2 A compound truss

Given: The structure shown in Fig. E2.2a. This compound truss is actually a combination of two simple trusses.

Determine: Is the structure statically determinate?

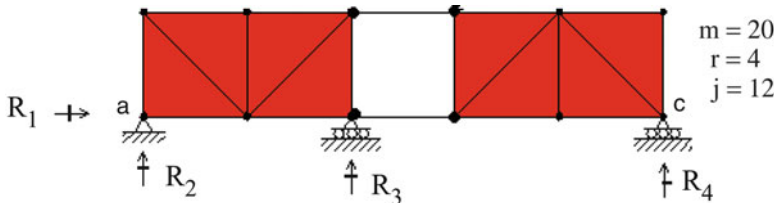


Fig. E2.2a

Solution: The structure is statically determinate and stable.

$$m + r = 24$$

$$2j = 24$$

Example 2.3 A complex truss

Given: The complex truss defined in Fig. E2.3a.

Determine: Is the truss statically determinate?

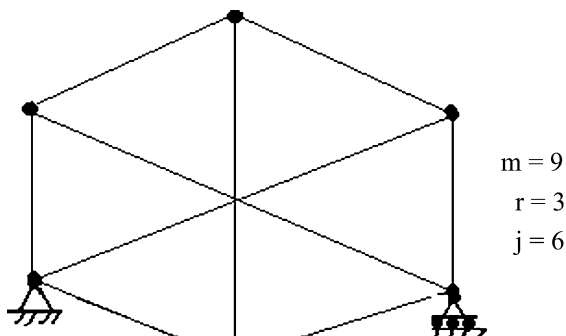


Fig. E2.3a

Solution: There are three restraints, six joints, and nine members.

$$m + r = 12$$

$$2j = 12$$

The truss appears to be stable. Note that the condition, $m + r = 2j$ is *necessary* but not *sufficient* to ensure stability of this truss. Sufficient conditions are discussed further in Sect. 2.4.

In what follows, we describe two classical hand computation-based procedures for finding the member forces in *simple* and *compound* trusses due to an applied loading. These approaches are useful for gaining insight as to how loads are carried by structures. That is the most important aspect of structural engineering that one needs to master in order to be a successful practitioner. Also, although most current structural analysis is computer based, one still needs to be able to assess the computer-generated results with a simple independent hand computation.

2.2.4 Method of Joints: Planar Trusses

Each joint of a plane truss is subjected to a concurrent force system. Since there are two equilibrium equations for a 2-D concurrent force system, one can solve for at most two force unknowns at a particular joint. The strategy for the method of joints is to proceed from joint to joint, starting with the free body diagram of a joint that has only two unknowns, solving for these unknowns, and then using this newly acquired force information to identify another eligible joint. One continues until equilibrium has been enforced at all the joints. When all the joints are in equilibrium, the total structure will be in equilibrium. This analysis procedure was first described in Squire Whipple's 1840 Essay on Bridge Building.

Enforcing the equilibrium conditions is simplified if one works with the force components referred to a common reference frame. Once one component is known, it is a simple step to determine the magnitude of the other component and the force. As an illustration, we consider the member shown in Fig. 2.17. The ratio of force components is equal to the ratio of the projected lengths. This equality follows from the fact that the direction of the force is the same as the direction of the line. Here, we are taking the horizontal and vertical directions as the common reference frame.

$$\frac{F_y}{F_x} = \frac{L_y}{L_x} = \tan \theta$$

Similarly, the force is determined using

$$F = \frac{F_x}{\cos \theta} = \frac{F_y}{\sin \theta}$$

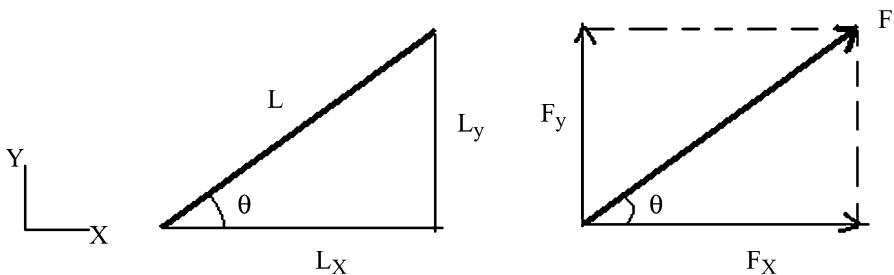


Fig. 2.17 Force components

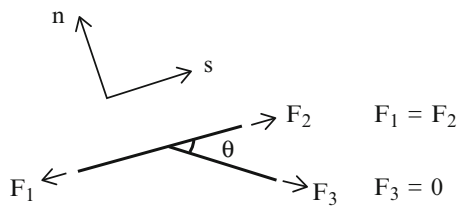


Fig. 2.18 Zero force member

Another simplification is possible when the joint has only three members, two of which are colinear, and there is *no* applied load at the joint. Figure 2.18 illustrates this case. There is only one force acting at an angle to the direction of the two common members, and equilibrium in the normal direction (n) requires the magnitude of this force to be zero. The other two forces must have the same magnitude.

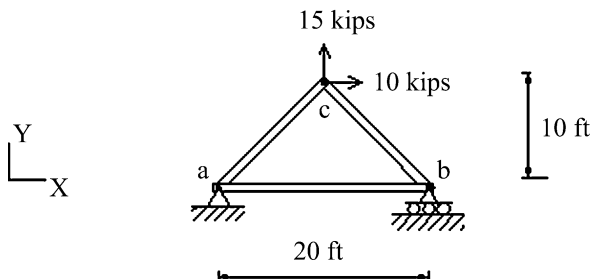
When applying the method of joints, it is convenient to first determine the reactions by enforcing global equilibrium on the total structure. With the reactions known, it may be easier to locate a joint having only two unknown member forces.

In what follows, we present a set of examples that illustrate how the method of joints is efficiently applied.

Example 2.4 Three member truss analyzed by the methods of joints

Given: The truss and loading defined by Fig. E2.4a.

Determine: The reactions and member forces.

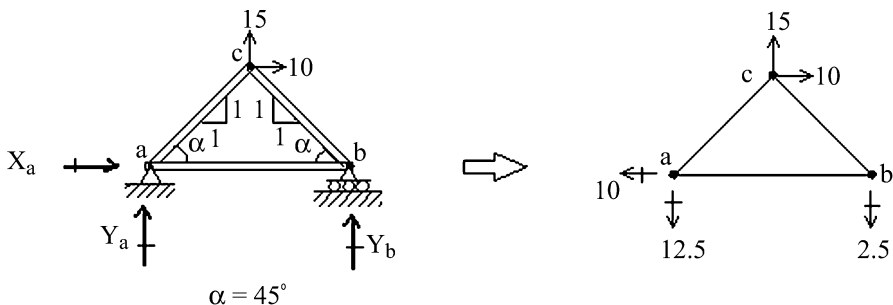
**Fig. E2.4a**

Solution: We first find the reactions at joints a and b. Moment summation about joint a leads to the y reaction at b. Force summations provide the remaining two reaction forces. The results are shown below (Fig. E2.4b).

$$\sum M_a = 0 \quad \Rightarrow \quad 10(10) - 15(10) - Y_b(20) = 0 \quad \Rightarrow \quad Y_b = -2.5 \quad \therefore Y_b = 2.5 \text{ kip} \downarrow$$

$$\sum F_x = 0 \rightarrow + \quad X_a + 10 = 0 \quad \Rightarrow \quad X_a = -10 \quad \therefore X_a = 10 \text{ kip} \leftarrow$$

$$\sum F_y = 0 \uparrow + \quad Y_a + 15 - 2.5 = 0 \quad \Rightarrow \quad Y_a = -12.5 \quad \therefore Y_a = 12.5 \text{ kip} \downarrow$$

**Fig. E2.4b** Reactions

One can start at any joint since they all have just two unknown member forces. We pick joint b (Fig. E2.4c). Summation of forces in the y direction gives $F_{bc,y} = 2.5 \text{ kip}$. Then summing forces in the x direction requires F_{ba} being compressive and equal to 2.5 kip. We indicate a tensile member force with an arrow pointing away from the joint. The opposite sense is used for compression. One converts the force components to the force magnitude using the Pythagorean Theorem, $F = \sqrt{F_x^2 + F_y^2}$.

$$\sum F_y = 0 \quad F_{bc,y} = 2.5 \uparrow \text{ Then } F_{bc,x} = 2.5 \leftarrow \therefore F_{bc} = 2.5\sqrt{2} \text{ kip (Tension)}$$

$$\sum F_x = 0 \quad F_{ba} = 2.5 \text{ kip (Compression)}$$

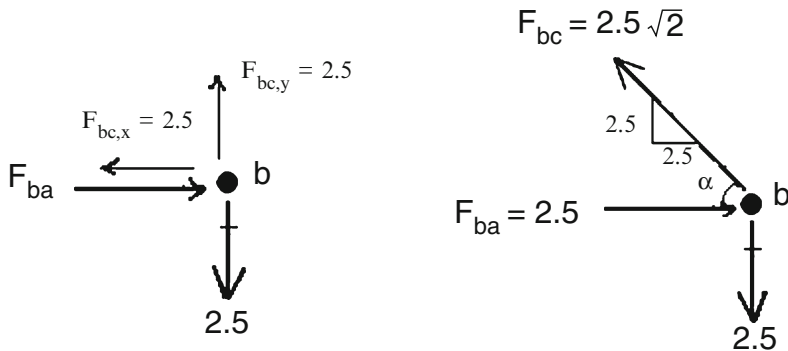


Fig. E2.4c Joint b

There is only one unknown member force left, F_{ca} . One can work with either joint a or joint c. We pick joint c. The free body diagram for joint c is shown in Fig. E2.4d. Equilibrium in the x direction requires $F_{ca,x} = 12.5$ kip.

$$\sum F_x = 0 \quad F_{ca,x} = 12.5 \leftarrow \therefore F_{ca} = 12.5\sqrt{2} \text{ kip (Tension)}$$

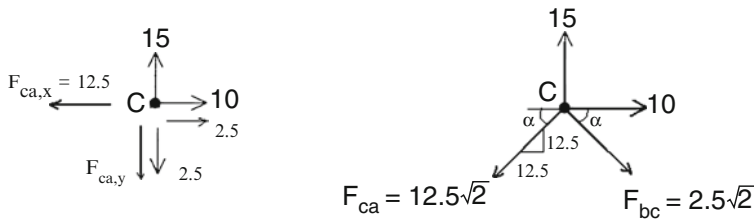
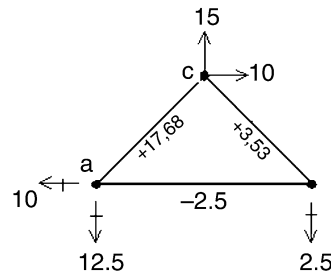


Fig. E2.4d Joint C

Note that in this example we do not need to use the remaining equilibrium equations (one for joint c and two for joint a) since we used instead three global

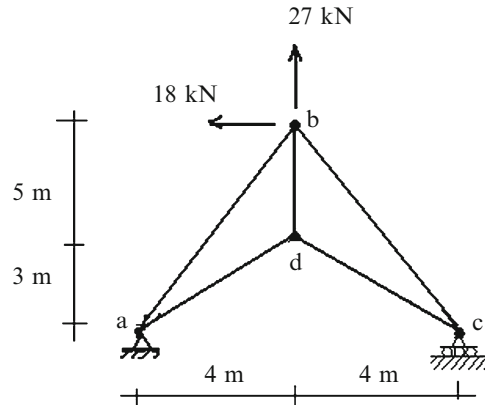
equilibrium equations to calculate the reactions. The total number of joint equilibrium equations is equal to six (two per joint \times three joints). If we use three equations for global equilibrium, there are only three independent equations left to apply to the joints. The final results are shown on the sketch below. Tensile forces are denoted with a + sign, and compressive forces with a - sign.

Fig. E2.4e

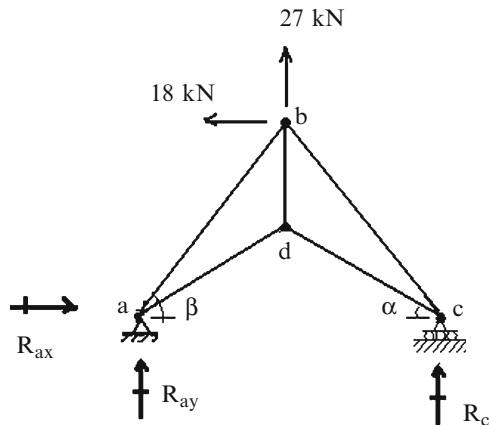
Example 2.5 Five member truss analyzed by the methods of joints

Given: The truss defined in Fig. E2.5a.

Determine: The reactions and member forces for the loading shown.

Fig. E2.5a

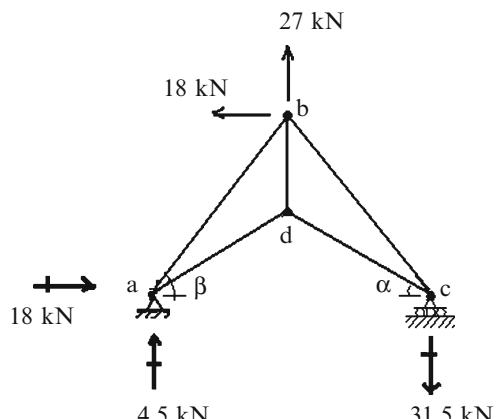
Solution: We first find the reactions and then proceed starting with joint a, and then moving to joints c and d.

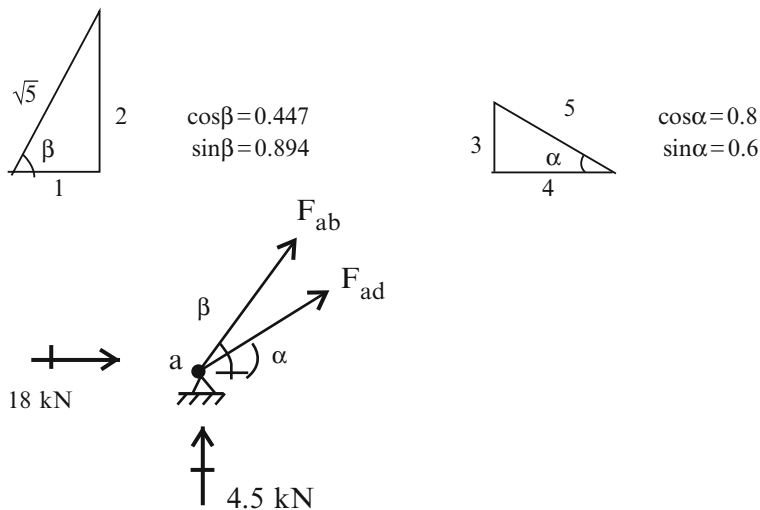
Fig. E2.5b

$$\sum M_a = 0 \xrightarrow{+} -10(10) - 18(8) + R_c(8) = 0 \Rightarrow R_c = -31.5 \quad \therefore R_c = 31.5 \text{ kip} \downarrow$$

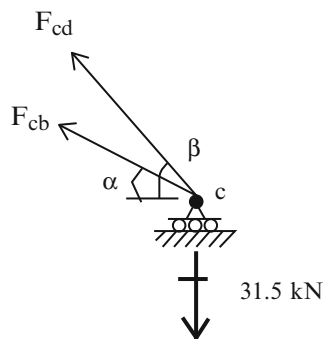
$$\sum F_x = 0 \rightarrow + R_{ax} - 18 = 0 \Rightarrow R_{ax} = 18 \quad \therefore R_{ax} = 18 \text{ kip} \rightarrow$$

$$\sum F_y = 0 \uparrow + R_{ay} + 27 - 31.5 = 0 \Rightarrow R_{ay} = 4.5 \quad \therefore R_{ay} = 4.5 \text{ kip} \uparrow$$

**Fig. E2.5c**

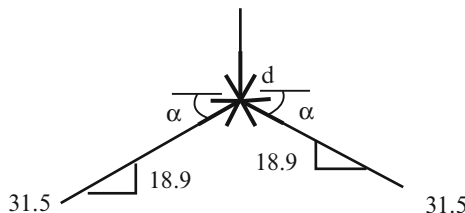


$$\begin{cases} \sum F_x = 0 & F_{ad} \cos \alpha + F_{ab} \cos \beta + 18 = 0 \\ \sum F_y = 0 & F_{ad} \sin \alpha + F_{ab} \sin \beta + 4.5 = 0 \end{cases} \Rightarrow \begin{cases} F_{ad} = -31.5 \text{ kN} \\ F_{ab} = 16.1 \text{ kN} \end{cases}$$



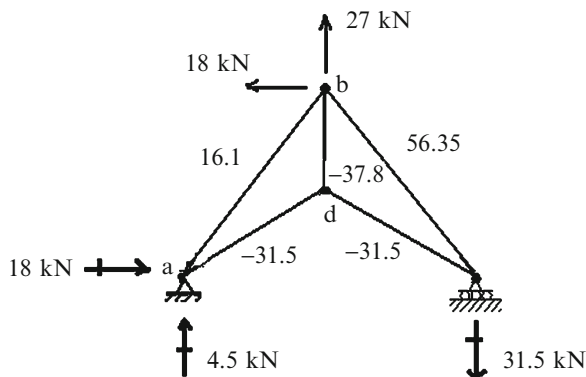
$$\begin{cases} \sum F_x = 0 & F_{cd} \cos \alpha + F_{cb} \cos \beta = 0 \\ \sum F_y = 0 & F_{cd} \sin \alpha + F_{cb} \sin \beta - 31.5 = 0 \end{cases} \Rightarrow \begin{cases} F_{cd} = -31.5 \text{ kN} \\ F_{cb} = 56.35 \text{ kN} \end{cases}$$

$$F_{bd} = 37.8$$



$$\sum F_y = 0 \quad F_{bd} = 37.8 \text{ kN} \text{ (Compression)}$$

The final forces are listed below.



Example 2.6 Five member truss analyzed by the methods of joints

Given: The truss defined in Fig. E2.6a.

Determine: The reactions and member forces for the loading shown.

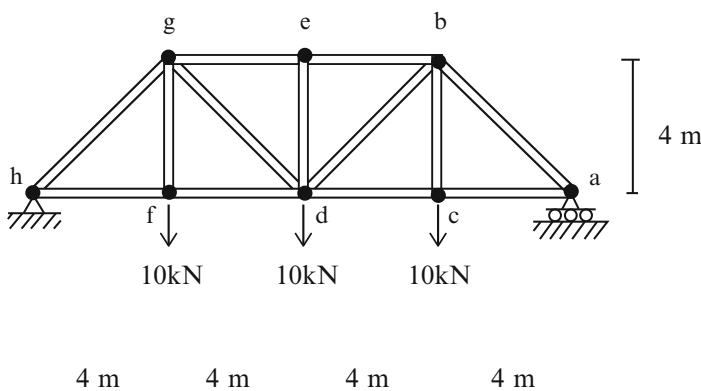


Fig. E2.6a Bridge truss

Solution: We note that the structure and loading are symmetrical with respect to a vertical axis through points e and d. It follows that the forces in symmetrically located members are equal and therefore we need to find the forces in only $\frac{1}{2}$ of the structure. Joints c, e, and f are special in the sense that two incident members are co-linear. Then, noting Fig. 2.18,

$$F_{cb} = 10 \text{ kN (Tension)} \quad F_{ed} = 0 \quad F_{fg} = 10 \text{ kN (Tension)}$$

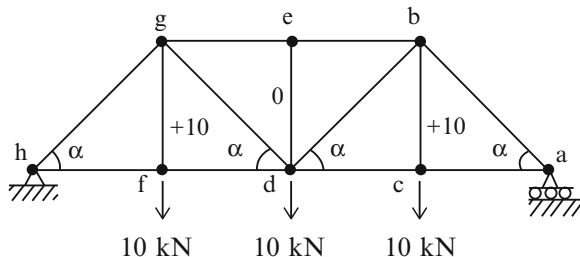


Fig. E2.6b

There are multiple options. We can first find the reactions and then proceed inward, starting with joint a, and then moving to joints c and b. An alternate approach would be to start at joint d, find the y component of F_{bd} , and then move to joint b.

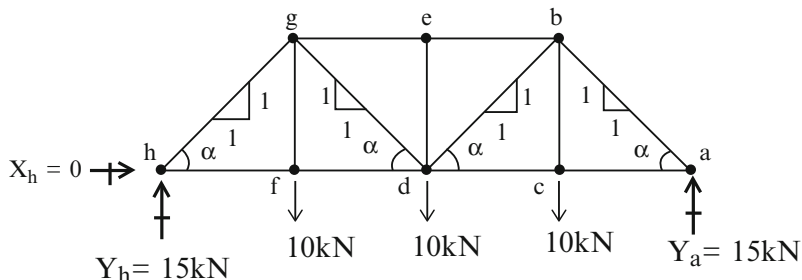


Fig. E2.6c Reactions

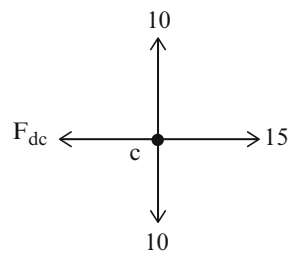
We list the results for the first approach below. We first find $F_{ba,y}$ with the vertical equilibrium condition at joint a. Then we find F_{ac} from the horizontal component of F_{ba} .

$$\begin{aligned} \sum F_y &= 0 \quad F_{ba,y} = 15 \text{ kN} \downarrow \text{Then } F_{ba,x} = 15 \text{ kN} \rightarrow \\ &\therefore F_{ba} = 15\sqrt{2} \text{ kN (Compression)} \end{aligned}$$

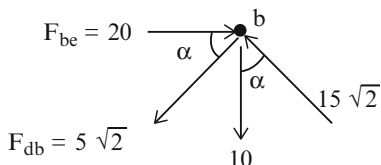
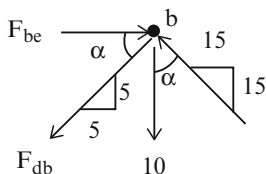
$$\sum F_x = 0 \quad F_{ac} = 15 \text{ kN (Tension)}$$

**Fig. E2.6d** Joint a

At joint c, we note from the sketch that $F_{dc} = 15 \text{ kN}$ (Tension).

Fig. E2.6e Joint c

At joint b, we note from the sketch that F_{db} must be in tension and F_{be} must be in compression.

**Fig. E2.6f** Joint b

We first find $F_{db,y}$ with the vertical equilibrium condition at joint b.

$$\sum F_y = 0 \quad F_{db,y} = 5 \downarrow$$

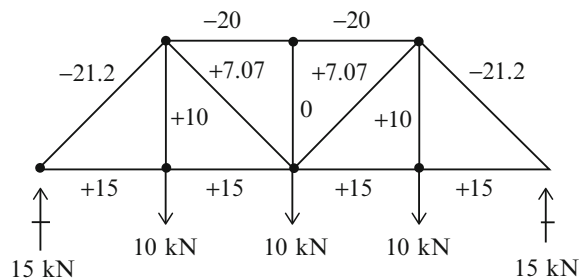
Then $F_{db,x} = 5 \leftarrow \therefore F_{db} = 5\sqrt{2} \text{ kN}$ (Tension)

Then we apply the horizontal equilibrium equation at joint b.

$$\sum F_x = 0 \quad F_{be} = 20 \text{ kN (Compression)}$$

The resultant member forces are shown below. Note that, for this loading, the members in the top zone (the top chord) are in compression and the bottom chord members are in tension. The interior vertical and diagonal members are in tension. When iron was used as a structural material, cast iron, which is relatively weak in tension, was employed for the top chord members and wrought iron, which is relatively strong in tension, for the verticals, diagonals, and bottom chord members.

Fig. E2.6g



If the truss structure is inverted as shown below, the sense of the member forces is also reversed. This geometric arrangement is preferred for bridge crossings when the clearance below the structure is not a problem.

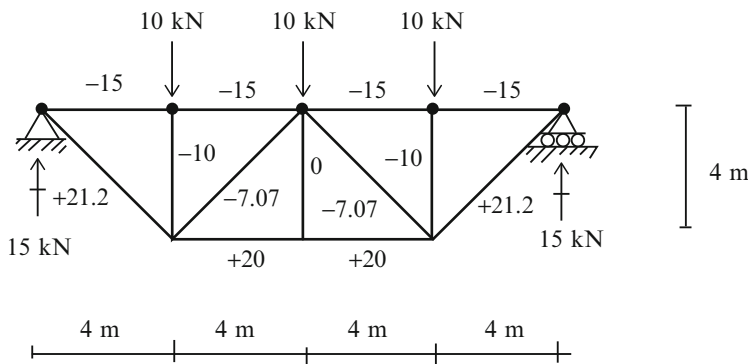


Fig. E2.6h

Example 2.7 A cantilever truss analyzed by methods of joints

Given: The truss and loading defined by Fig. E2.7a.

Determine: The member forces for the loading shown.

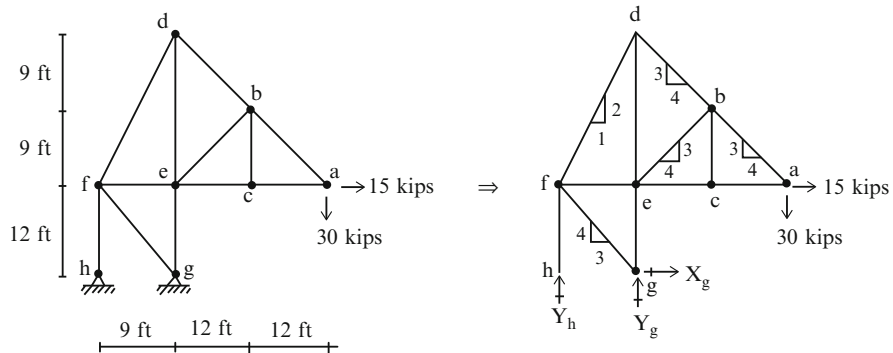


Fig. E2.7a

Solution: First we determine the zero force members. Starting at joint c, we observe that $F_{cb} = 0$. Then moving to joint b, it follows that $F_{be} = 0$.

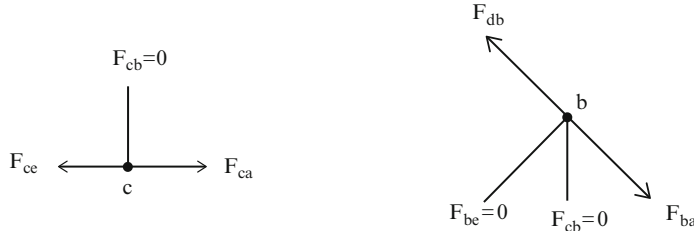


Fig. E2.7b Zero force members

In this case, we do not need to first find the reactions. We can start at joint a.

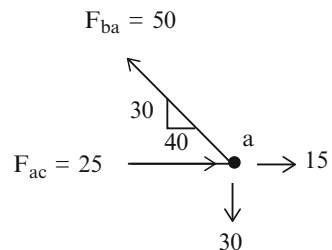


Fig. E2.7c Joint a

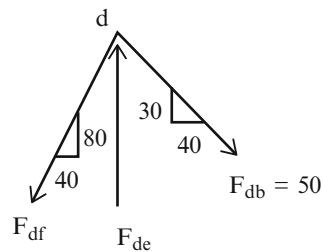
$$\sum F_y = 0 \quad F_{ba,y} = 30 \rightarrow F_{ba,x} = 40 \quad \therefore F_{ba} = 50 \text{ kip (Tension)}$$

Given F_{ba} , we determine F_{ac}

$$\sum F_x = 0 \quad F_{ac} = 25 \text{ kip (Compression)}$$

Next, we move to joint d and determine F_{df}

Fig. E2.7d Joint d



$$\sum F_x = 0 \quad F_{df,x} = 40 \quad \therefore F_{df,y} = 80 \quad F_{df} = 40\sqrt{5} \text{ kip (Tension)}$$

With F_{df} known, we can determine F_{de}

$$\sum F_y = 0 \quad F_{de} = 110 \text{ kip (Compression)}$$

At joint e, we determine F_{ef} and F_{eg} .

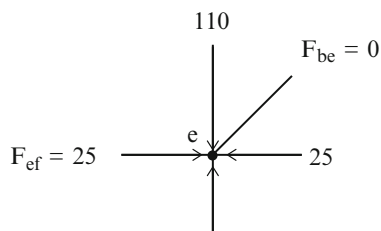


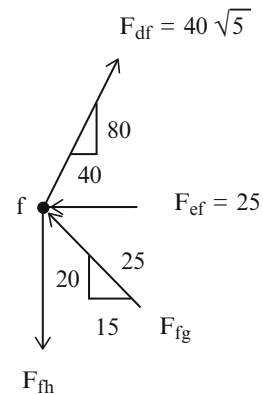
Fig. E2.7e Joint e

The last joint is joint f. We first determine $F_{fg,x}$

$$\sum F_x = 0 \quad F_{fg,x} = 15 \quad \therefore F_{fg,y} = 20 \quad F_{fg} = 25 \text{ kip (Compression)}$$

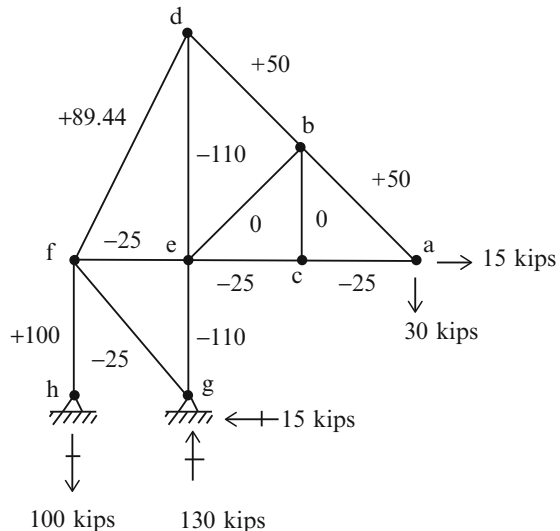
Then $\sum F_y = 0$ $F_{fh} = 100 \text{ kip}$ (Tension)

Fig. E2.7f Joint f



The final forces are listed below.

Fig. E2.7g

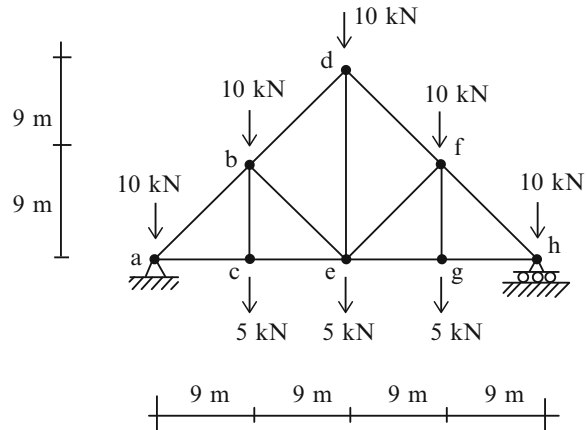


Example 2.8 Gable roof truss analyzed by the method of joints

Given: The truss and loading defined by Fig. E2.8a.

Determine: The member forces.

Fig. E2.8a



Solution: Fig. E2.8a shows a typical truss structure for supporting roof (top joints) and ceiling (bottom joints) loads. Members cb and gf function to transfer loads to the top joints (b and f). Their force magnitudes are

$$F_{bc} = 5 \text{ kN (Tension)} \quad F_{gf} = 5 \text{ kN (Tension)}$$

All the remaining joints have at least three unknown member forces and reactions. Therefore, we start the analysis by first finding the reactions.

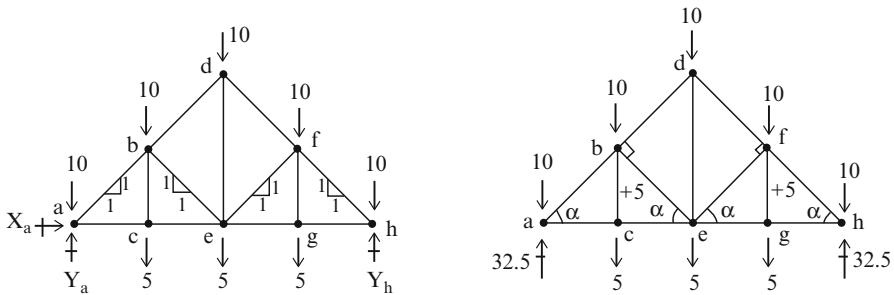
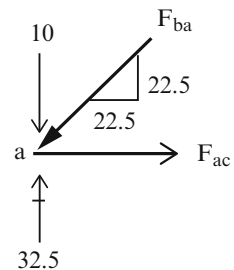


Fig. E2.8b Reactions

Given the reactions, we start at joint a. Force F_{ba} must be compression and $F_{ba,y} = 22.5 \downarrow$. Then, $F_{ba,x} = 22.5 \leftarrow$ and $F_{ba} = 22.5\sqrt{2}$ kN (Compression). It follows that, F_{ac} is in tension and equal to 22.5 kN.

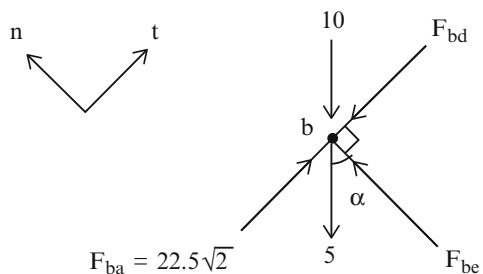
Fig. E2.8c Joint a

We then move on to joint b. Members ab and bd are co-linear, and member be is normal to this common direction. Summing forces in the normal direction results in

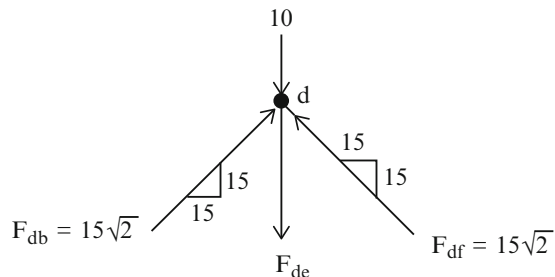
$$\sum F_n = 0 \quad F_{be} = (10 + 5) \cos \alpha = 15 \frac{\sqrt{2}}{2} \text{ kN (Compression)}$$

Next, summing forces in the tangential direction leads to F_{bd} .

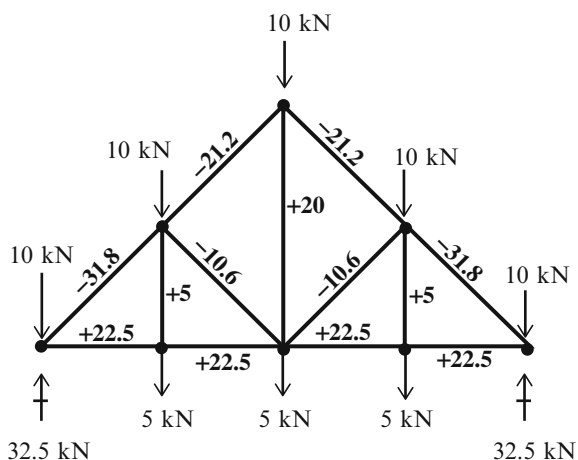
$$\sum F_t = 0 \quad F_{bd} = 22.5\sqrt{2} - (10 + 5) \cos \alpha = 15\sqrt{2} \text{ kN (Compression)}$$

Fig. E2.8d Joint b

The last force is F_{de} . We use joint d shown in Fig. E2.8e. Summing forces in the y direction leads to $F_{de} = 20 \text{ kN (tension)}$

Fig. E2.8e Joint d

The final forces are listed below.

Fig. E2.8f

2.2.5 Method of Sections

If one wants to determine only the force in a particular member, applying the method of joints might not be convenient since in general it involves first finding the force in other members. For example, consider the truss shown in Fig. 2.19a. Suppose the force in member ef is desired. One possible strategy is to first determine the reactions at joint a, then proceed to joints b, c, d, and lastly e where the Y component of F_{ef} can be determined once F_{ed} is known. Another possible strategy is to start at joint j, and then proceed to joints i, h, g, and f. Either approach requires some preliminary computation that provides information on forces that may or may not be of interest.

The method of sections is an analysis procedure that avoids this preliminary computation. One passes a cutting plane through the truss, isolates either the left or

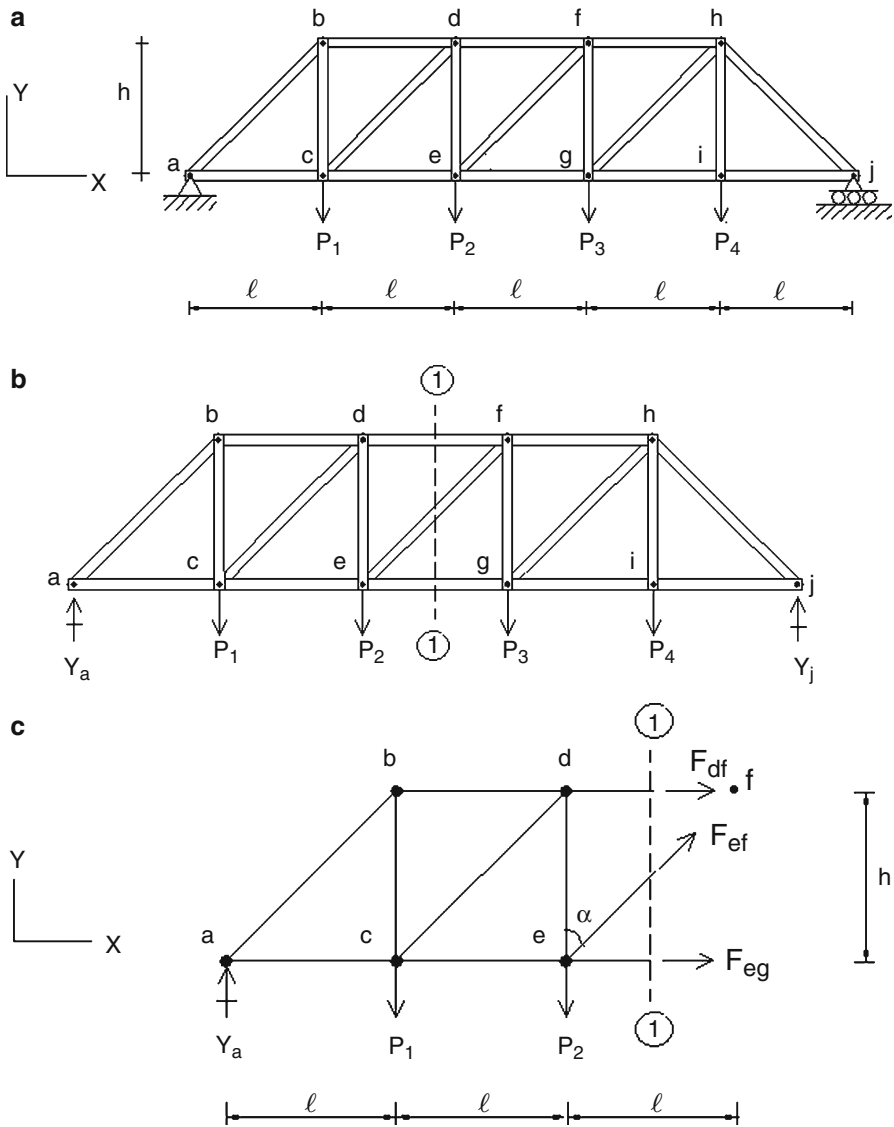


Fig. 2.19 (a) An example of a truss. (b) Cutting vertical plane. (c) Truss segment for method of sections

right segment, and applies the equilibrium equations for a rigid body to the segment. The choice of cutting plane is critical. It must cut the particular member whose force is desired, and other members that are concurrent. This restriction is necessary since there are only three equilibrium equations for planar loading, and therefore, one can only determine three unknowns.

We illustrate this method for the truss defined in Fig. 2.19a. We start by determining the reaction at a. To determine F_{ef} we use the vertical cutting plane 1-1 and consider the left segment shown in Fig. 2.19c. Summing forces in the Y direction leads to:

$$\sum F_y = 0 \quad \uparrow^+ \quad F_{ef} \cos \alpha x = P_1 + P_2 - Y_a \quad (2.3)$$

We point out here that the function of the diagonal members is to equilibrate the unbalanced vertical forces at the sections along the longitudinal axis. These forces are called “shear” forces.

If the force in member df is desired, one can use the moment equilibrium condition with respect to joint e which is the point of concurrency for members ef and eg.

$$\sum M_{\text{about } e} = 0 \quad hF_{df} = \ell P_1 - 2\ell Y_a \quad (2.4)$$

Similarly, for member eg, we use moment equilibrium about joint f:

$$\sum M_{\text{about } f} = 0 \quad hF_{eg} = 3\ell Y_a - 2\ell P_1 - \ell P_2 \quad (2.5)$$

For parallel chord trusses (top and bottom chords are parallel), the function of the chords is to equilibrate the unbalanced moments at the various sections. One chord force is compressive, the other force is tensile. For downward vertical loading, the top chord is generally in compression, and the bottom is in tension. The method of section is convenient in the sense that it allows one to easily identify the sense of a particular member force.

Example 2.9 Application of the method of sections to a parallel chord truss

Given: The structure and loading shown in Fig. E2.9a

Determine: The force in members F_{gd} , F_{gf} , and F_{dc} . Use the method of sections.

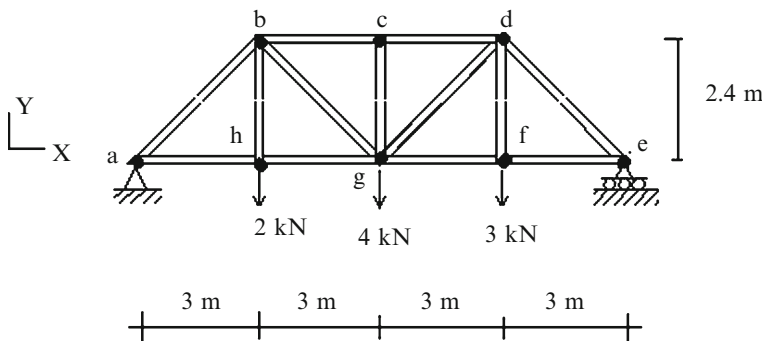


Fig. E2.9a

Solution: We start by determining the reactions.

$$\sum M_a = 0 \quad \text{→} \quad 2(3) + 4(6) + 3(9) - Y_e (12) = 0 \quad \Rightarrow \quad Y_e = 4.75 \text{ kN} \uparrow$$

$$\sum F_x = 0 \rightarrow + \quad X_a = 0$$

$$\sum F_y = 0 \uparrow + \quad Y_a + 4.75 - 2 - 4 - 3 = 0 \quad \Rightarrow \quad Y_a = 4.25 \text{ kN} \uparrow$$

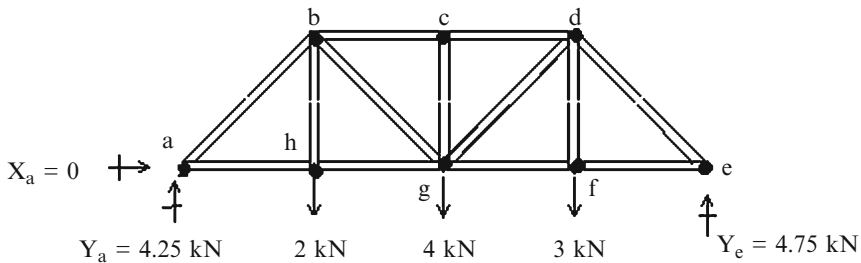


Fig. E2.9b

Then, we pass a vertical cutting plane through the panel between joints d and c and consider the left segment. Enforcing equilibrium leads to:

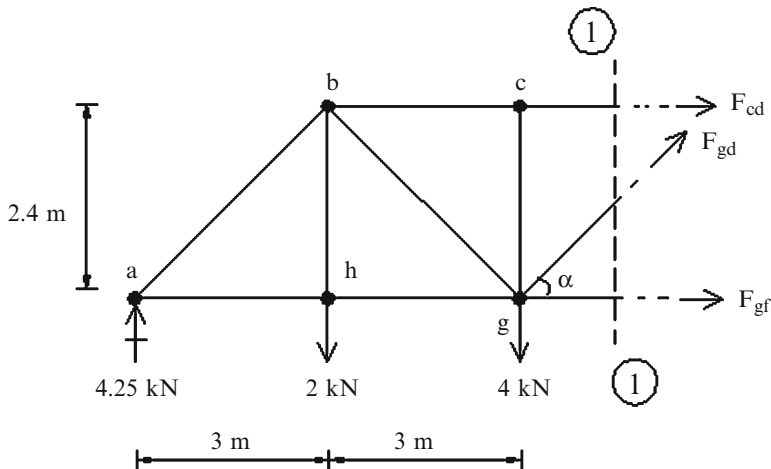


Fig. E2.9c

$$\sum F_y = 0 \quad F_{gd,y} = 1.75 \uparrow$$

Therefore $F_{gd,x} = 2.1875$ Therefore $F_{gd} = 2.8 \text{ kN}$ (Tension)

$$\sum M_{atg} = 0 \quad F_{cd}(2.4) - 2(3) + 4.25(6) = 0 \quad F_{cd} = -8.125$$

Therefore $F_{cd} = 8.125 \text{ kN}$ (Compression)

$$\sum F_x = 0 \quad F_{gf} - 8.125 + 2.1875 = 0 \quad F_{gf} = +5.9375$$

Therefore $F_{gf} = 5.9375 \text{ kN}$ (Tension).

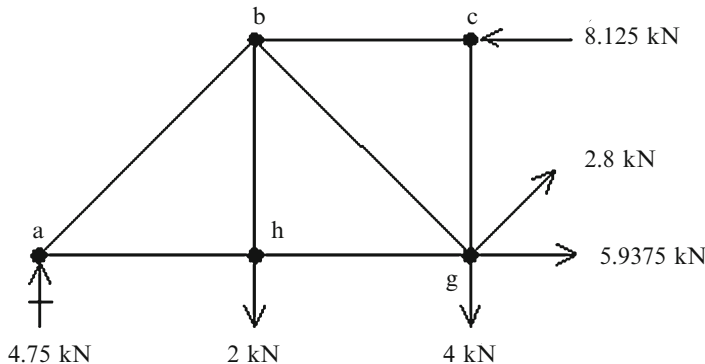


Fig. E2.9d

Example 2.10 The method of sections applied to a roof truss

Given: The structure shown in Fig. E2.10a.

Determine: The member forces F_{db} , F_{be} , and F_{ce} .

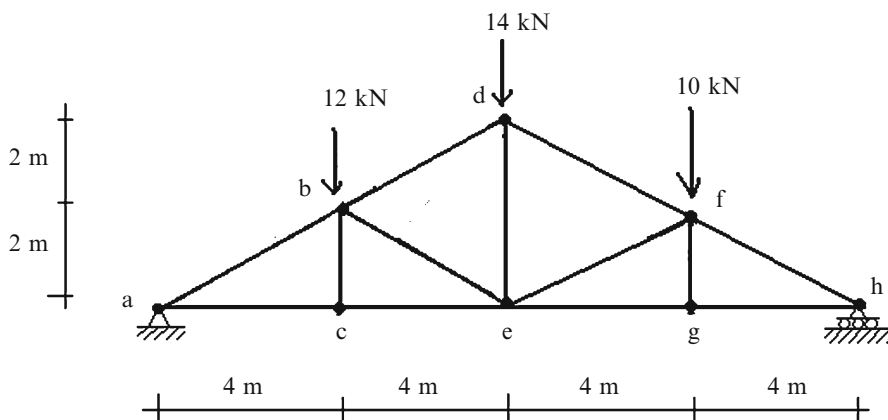


Fig. E2.10a

Solution: We determine the reactions first.

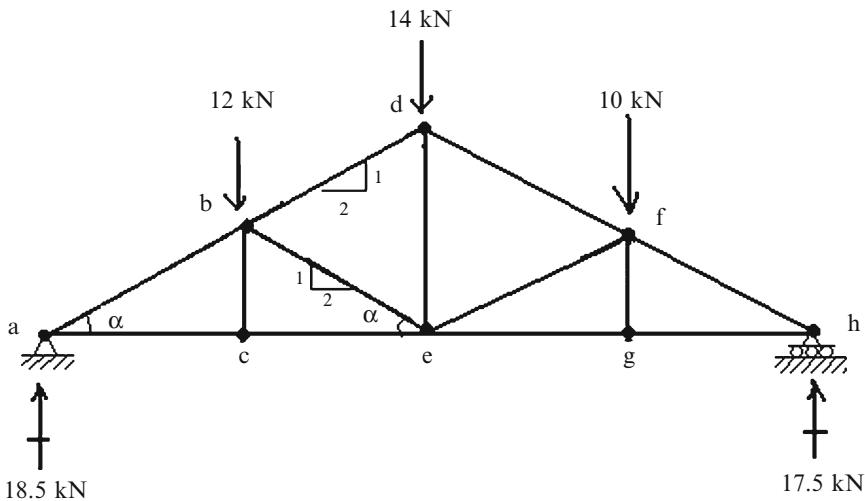


Fig. E2.10b

To determine the member forces F_{db} , F_{be} , and F_{ce} , we use a vertical cutting plane. The appropriate segment is shown below. Various options are possible. We choose first to determine F_{db} by summing moments about e. Then summing moments about b leads to F_{ce} . Lastly we can find F_{be} by summing either X or Y forces.

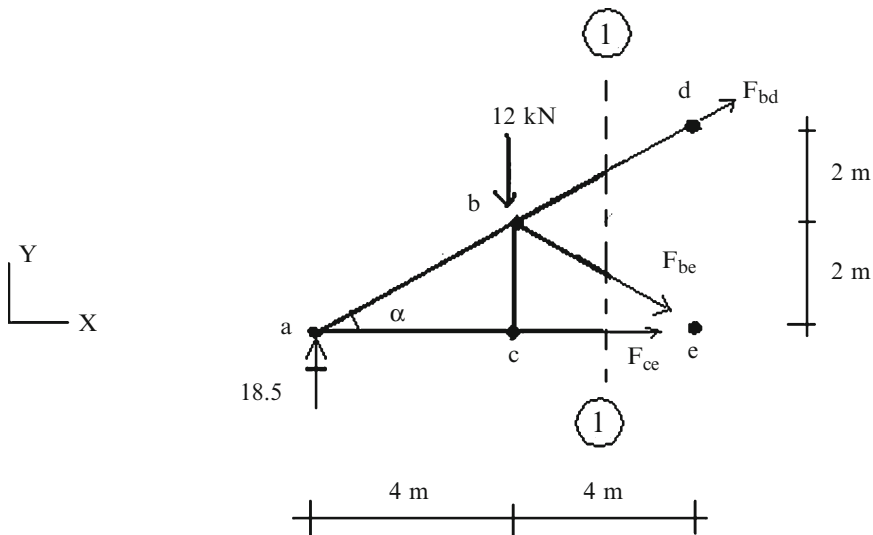


Fig. E2.10c

The calculations for this analysis procedure are listed below:

$$1. \sum M_e = 0 \quad \text{at } e \quad 4 F_{bd,x} + (18.5) 8 - (12) 4 = 0$$

$$F_{bd,x} = -25 \quad F_{bd} = \frac{F_{bd,x}}{\cos \alpha} = 27.95 \text{ kN (Compression)}$$

$$2. \sum M_b = 0 \quad \text{at } b \quad -2 F_{ce} + (18.5) 4 = 0$$

$$F_{ce} = 37 \text{ kN (Tension)}$$

$$3. \sum F_Y = 0 \uparrow + \quad -F_{be,y} - 12 - 12.5 + 18.5 = 0$$

$$F_{be,y} = -6 \quad \Rightarrow \quad F_{be} = \frac{F_{be,y}}{\sin \alpha} = 13.41 \text{ kN (Compression)}$$

Example 2.11 Analysis of K-type trusses with the method of sections

Given: The truss defined in Fig. E2.11a.

Determine: The member forces F_{ab} , F_{be} , F_{ed} , and F_{cd} .

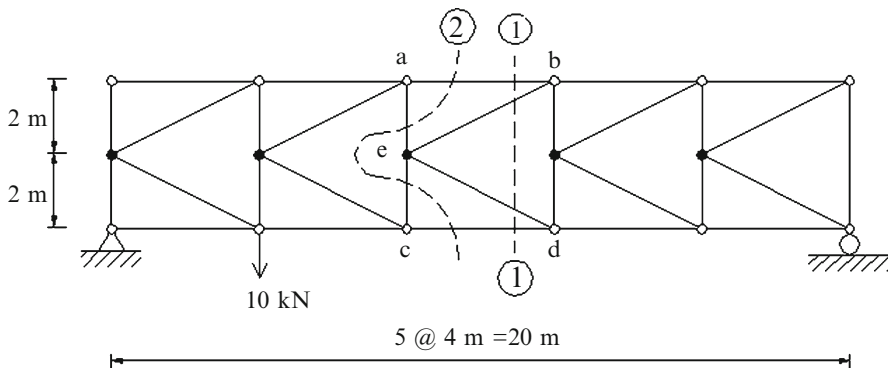
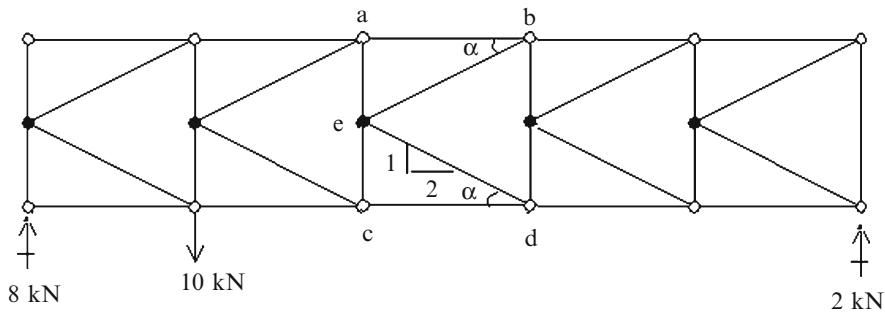
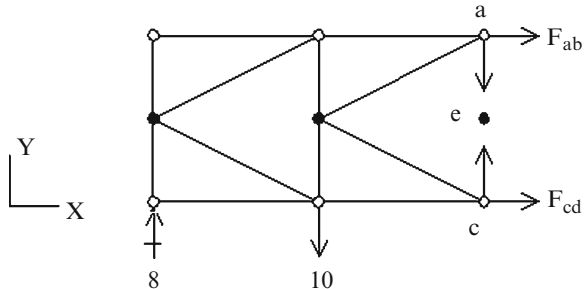


Fig. E2.11a

Solution: We determine reactions first.

A vertical section such as ①—① cuts four unknown forces and does not lead to a solution. There are no vertical cutting planes that involve only three unknown forces. Therefore, one has to be more creative with the choice of planes. For this type of truss, plane ②—② is the appropriate choice. Isolating the left segment and summing moments about joint c results in F_{ab} :

$$\sum M_c = 0 \quad \text{at } c \quad 4 F_{ab} - 10(4) + 8(8) = 0 \rightarrow F_{ab} = -6 \quad \therefore F_{ab} = 6 \text{ kN (Compression)}$$

**Fig. E2.11b****Fig. E2.11c**

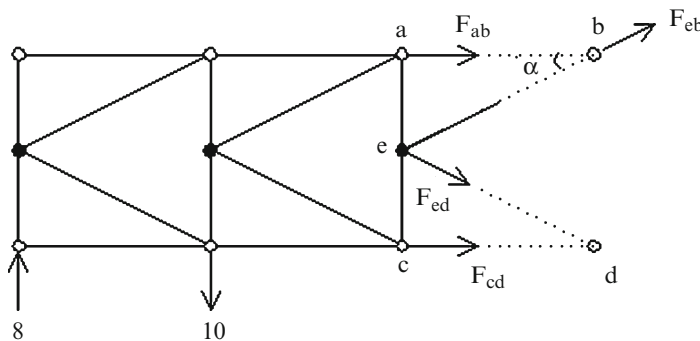
Then summing *X* forces,

$$\sum F_x = 0 \quad F_{cd} = -F_{ab} = +6 \quad \therefore F_{cd} = 6 \text{ kN (Tension)}$$

The diagonal forces F_{eb} and F_{ed} are found using section ①—①. Summing moments about joint d leads to F_{eb} :

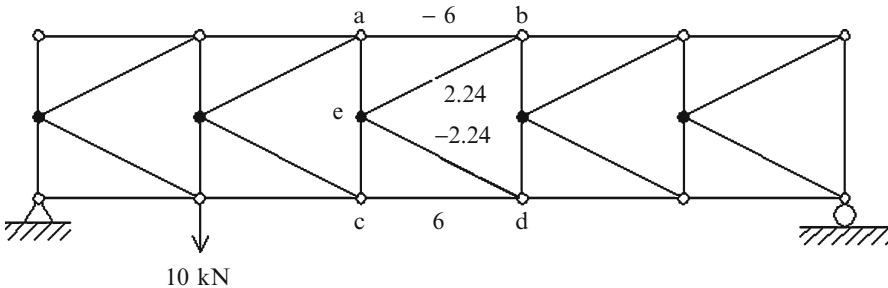
$$\sum M_d = 0 \quad \Rightarrow \quad 4(F_{ab} + F_{eb,x}) - 10(8) + 8(12) = 0 \quad 4(-6 + F_{eb,x}) + 16 = 0$$

$$F_{eb,x} = +2 \quad \therefore F_{eb} = \frac{F_{ed,x}}{\cos \alpha} = 2.24 \text{ kN (Tension)}$$

**Fig. E2.11d**

We find F_{ed} by summing x forces, and noting that the horizontal components of the chord forces must cancel.

$$\sum F_x = 0 \quad F_{ed,x} = -F_{ed,x} \quad \therefore F_{ed} = 2.24 \text{ kN (Compression)}$$

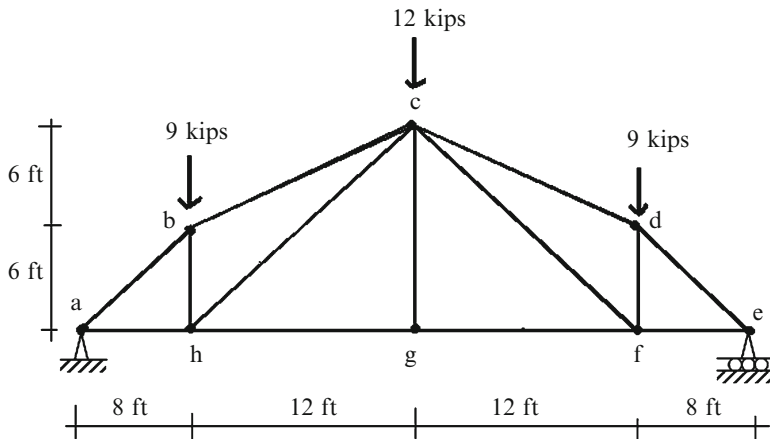
**Fig. E2.11e**

If one wants all the member forces, one can apply multiple cutting planes or combinations of the method of joints and method of sections. How one proceeds is a matter of personal preference.

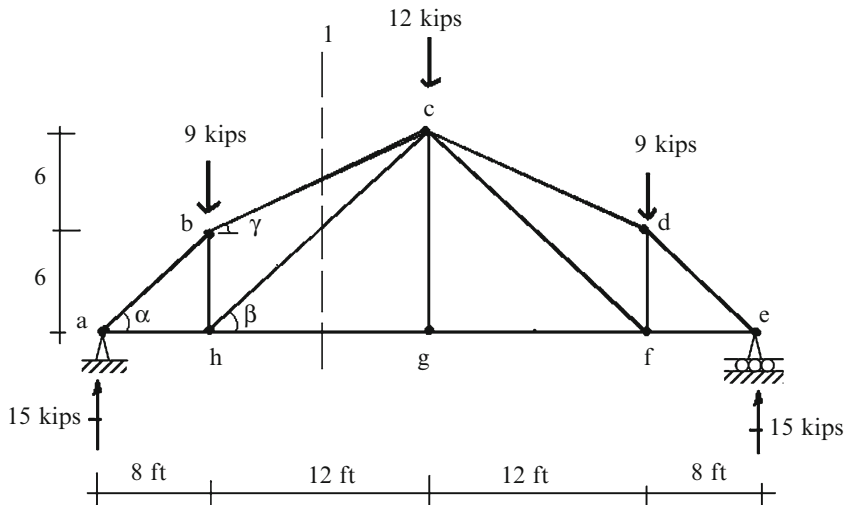
Example 2.12 A hybrid analysis strategy

Given: The truss defined in Fig. E2.12a

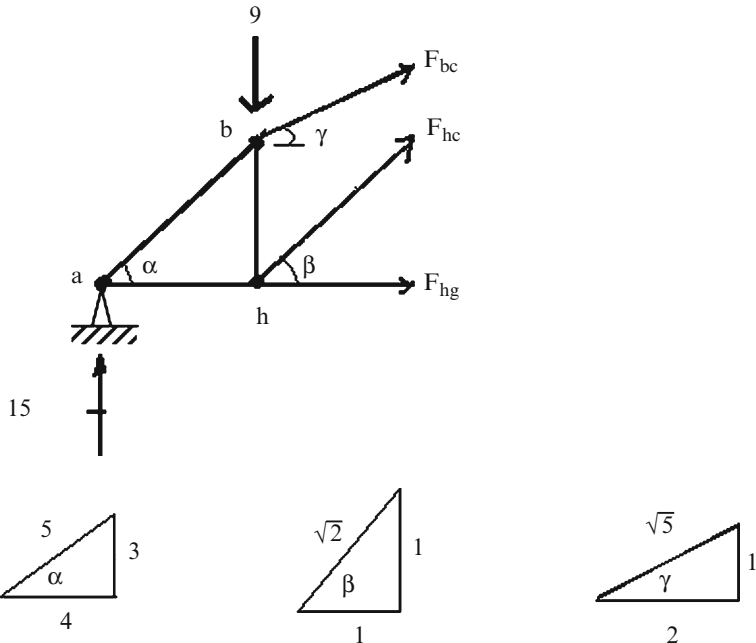
Determine: All the member forces using a combination of the method of joints and the method of sections.

**Fig. E2.12a**

Solution: We note that the structure and loading are symmetrical with respect to a vertical axis through points c and g. It follows that the forces in symmetrically located members are equal and therefore we need to find the forces in only $\frac{1}{2}$ of the structure. We start by determining the reactions. The member forces F_{bc} , F_{hc} , and F_{hg} can be determined by passing vertical cutting plane 1-1 and enforcing the equilibrium equations.

**Fig. E2.12b**

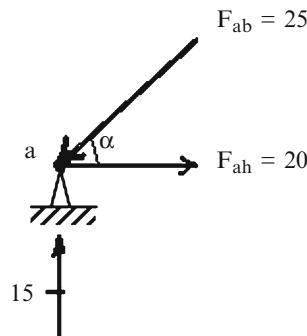
Considering the left segment and enforcing equilibrium leads to:
Section 1-1:



$$\begin{aligned}\sum M_{at\ h} &= 0 \quad (F_{bc} \cos \gamma)(6) + 15(8) = 0 \quad F_{bc} = 10\sqrt{5} \text{ kip (Compresion)} \\ \sum F_y &= 0 \quad F_{hc} = 4\sqrt{2} \text{ kip (Tension)} \\ \sum F_x &= 0 \quad F_{hg} = 16 \text{ kip (Tension)}\end{aligned}$$

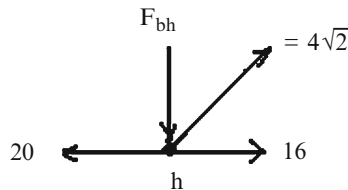
We then enforce equilibrium at joints a and h.

Equilibrium at joint a:



$$\sum F_y = 0 \quad F_{ab,y} = 15 \downarrow \quad \therefore F_{ab} = 25 \text{ kip (Compression)}$$

Equilibrium at joint h:



$$\sum F_y = 0 \quad F_{bh} = -F_{ch,y} = 4 \text{ kip (Compression)}$$

The final member forces are listed below.

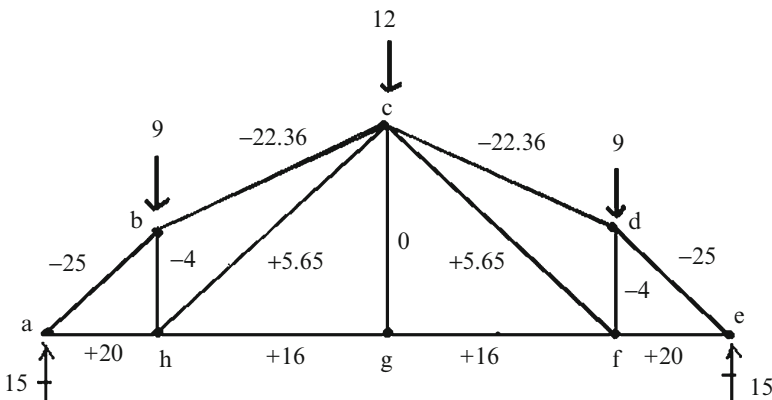


Fig. E2.12c

2.2.6 Complex Trusses

Complex trusses are defined as truss structures that cannot be classified as either simple or compound trusses. In order to determine the member forces, one has to establish the complete set of nodal force equilibrium equations expressed in terms of the member forces. If the truss is statically determinate, the number of equations will be equal to the number of force unknowns, and theoretically one can solve these equations for the force unknowns. However, if one cannot determine the member forces, the truss is said to be geometrically unstable. Static determinacy is a necessary but not sufficient condition for stability. In what follows, we expand on this point.

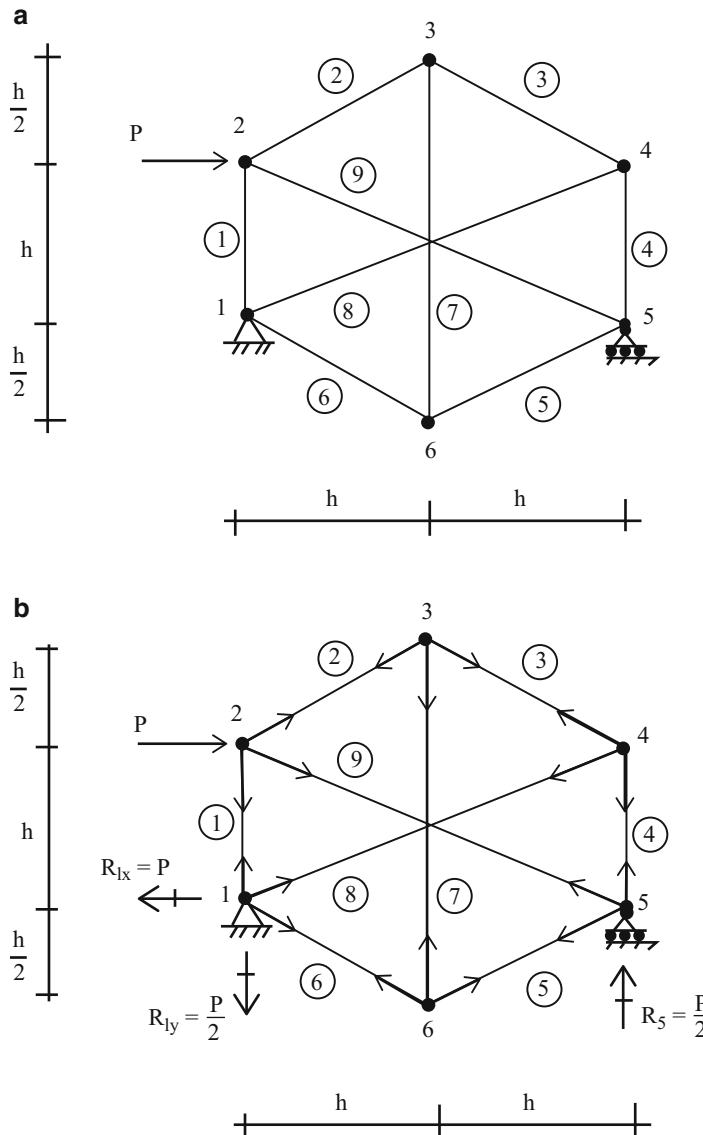


Fig. 2.20 (a). (b) Reactions. (c). (d). (e). (f) member forces

Consider the planar truss shown in Fig. 2.20a. There are nine members, three reactions, and six nodes. Then,

$$2j = 12$$

$$m + r = 9 + 3 = 12$$

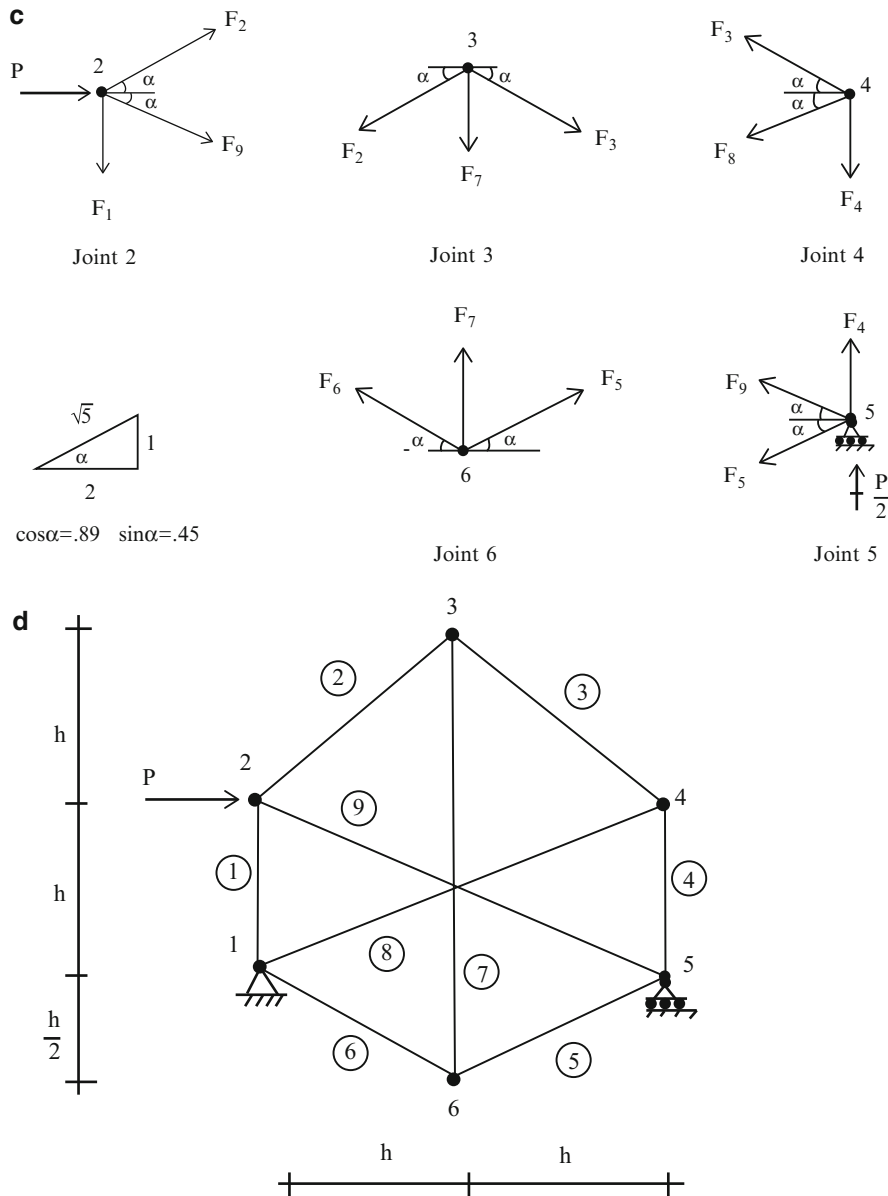
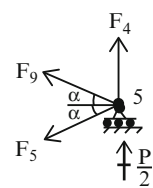
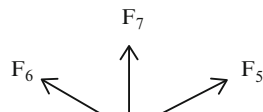
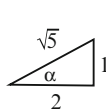
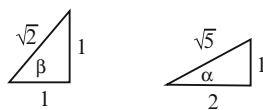
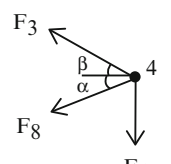
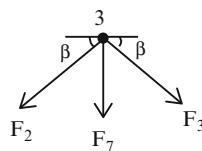
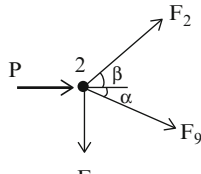


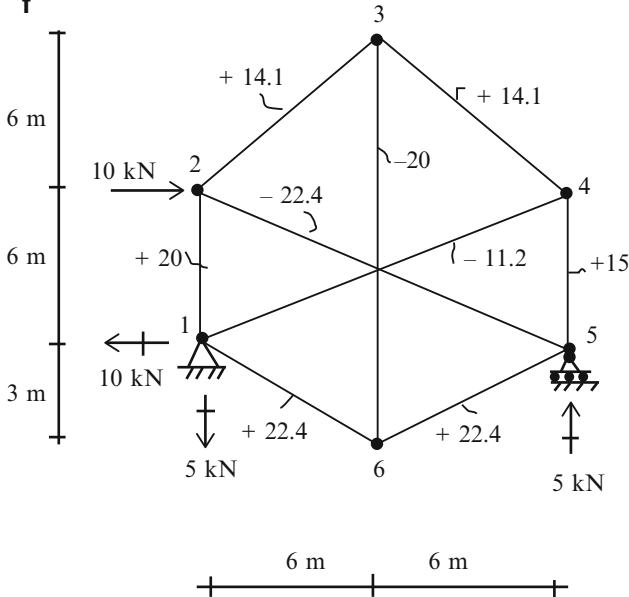
Fig. 2.20 (continued)

and the truss is statically determinate. It also has a sufficient number of reactions to prevent rigid body motions.

We use 3 of the 12 equilibrium equations to determine the reactions, leaving 9 equations available to solve for the 9 member forces.

e

$$\cos\beta = \sin\beta = .71 \quad \cos\alpha = .89 \quad \sin\alpha = .45$$

f

$$\begin{aligned}
 F_1 &= 20 \text{ kN} \\
 F_2 &= 14.1 \text{ kN} \\
 F_3 &= 14.1 \text{ kN} \\
 F_4 &= 15 \text{ kN} \\
 F_5 &= 22.4 \text{ kN} \\
 F_6 &= 22.4 \text{ kN} \\
 F_7 &= -20 \text{ kN} \\
 F_8 &= -11.2 \text{ kN} \\
 F_9 &= -22.4 \text{ kN}
 \end{aligned}$$

Fig. 2.20 (continued)

$$\begin{aligned}
 \sum F_x &= 0 & R_{1x} &= P \leftarrow \\
 \sum M_{at1} &= 0 & R_5 &= \frac{P}{2} \uparrow \\
 \sum F_y &= 0 & R_{1y} &= \frac{P}{2} \downarrow
 \end{aligned}$$

Enforcing equilibrium at joints 2–6 results in the following nine equations:

$$\begin{aligned}
 \text{Joint 2} & \left\{ \begin{array}{l} \sum F_x = 0 \\ \sum F_y = 0 \end{array} \right. \quad \begin{array}{l} 0.89F_2 + 0.894F_9 = -P \\ -F_1 + 0.45F_2 - 0.45F_9 = 0 \end{array} \\
 \text{Joint 3} & \left\{ \begin{array}{l} \sum F_x = 0 \\ \sum F_y = 0 \end{array} \right. \quad \begin{array}{l} 0.89F_2 - 0.89F_3 = 0 \\ 0.45F_2 + 0.45F_3 + F_7 = 0 \end{array} \\
 \text{Joint 4} & \left\{ \begin{array}{l} \sum F_x = 0 \\ \sum F_y = 0 \end{array} \right. \quad \begin{array}{l} 0.89F_3 + 0.89F_8 = 0 \\ 0.45F_3 - F_4 - 0.45F_8 = 0 \end{array} \\
 \text{Joint 5} & \left\{ \begin{array}{l} \sum F_x = 0 \\ \sum F_y = 0 \end{array} \right. \quad \begin{array}{l} 0.89F_5 + 0.89F_9 = 0 \\ F_4 - 0.45F_5 + 0.45F_9 = -\frac{P}{2} \end{array} \\
 \text{Joint 6} & \left\{ \sum F_x = 0.89F_5 - 0.89F_6 = 0 \right\}
 \end{aligned} \tag{2.6}$$

We express (2.6) in matrix form

$$\mathbf{BF} = \mathbf{P} \tag{2.7}$$

where

$$\mathbf{F} = \begin{Bmatrix} F_1 \\ F_2 \\ F_3 \\ F_4 \\ F_5 \\ F_6 \\ F_7 \\ F_8 \\ F_9 \end{Bmatrix} \quad \mathbf{P} = \begin{Bmatrix} -P_1 \\ 0 \\ 0 \\ 0 \\ 0 \\ 0 \\ 0 \\ -\frac{P}{2} \\ 0 \end{Bmatrix}$$

$$\mathbf{B} = \begin{bmatrix} 0 & 0.89 & 0 & 0 & 0 & 0 & 0 & 0 & 0.89 \\ -1 & 0.45 & 0 & 0 & 0 & 0 & 0 & 0 & -0.45 \\ 0 & 0.89 & -0.89 & 0 & 0 & 0 & 0 & 0 & 0 \\ 0 & 0.45 & 0.45 & 0 & 0 & 0 & 1 & 0 & 0 \\ 0 & 0 & 0.89 & 0 & 0 & 0 & 0 & 0.89 & 0 \\ 0 & 0 & 0.45 & -1 & 0 & 0 & 0 & -0.45 & 0 \\ 0 & 0 & 0 & 0 & 0.89 & 0 & 0 & 0 & 0.89 \\ 0 & 0 & 0 & 1 & -0.45 & 0 & 0 & 0 & 0.45 \\ 0 & 0 & 0 & 0 & 0.89 & -0.89 & 0 & 0 & 0 \end{bmatrix}$$

The coefficient matrix, \mathbf{B} is singular (the determinate of \mathbf{B} equals 0). Therefore, a unique solution for the unknown forces does not exist for an arbitrary nodal load. The truss is said to be geometrically unstable since the elements of \mathbf{B} depend only on the geometric pattern.

In order to eliminate the instability, one needs to change the geometry. We modify the truss by changing the vertical position of node 3 as shown in Fig. 2.20d. The individual nodal force systems are defined in Fig. 2.20e and the corresponding nodal force equilibrium equations are listed in (2.8).

$$\begin{aligned} \text{Joint 2} & \left\{ \begin{array}{l} \sum F_x = 0 \quad 0.71F_2 + 0.89F_9 = -P \\ \sum F_y = 0 \quad -F_1 + 0.71F_2 - 0.45F_9 = 0 \end{array} \right. \\ \text{Joint 3} & \left\{ \begin{array}{l} \sum F_x = 0 \quad 0.71F_2 - 0.71F_3 = 0 \\ \sum F_y = 0 \quad 0.71F_2 + 0.71F_3 + F_7 = 0 \end{array} \right. \\ \text{Joint 4} & \left\{ \begin{array}{l} \sum F_x = 0 \quad 0.71F_3 + 0.89F_8 = 0 \\ \sum F_y = 0 \quad 0.71F_3 - F_4 - 0.45F_8 = 0 \end{array} \right. \\ \text{Joint 5} & \left\{ \begin{array}{l} \sum F_x = 0 \quad 0.89F_5 + 0.89F_9 = 0 \\ \sum F_y = 0 \quad F_4 - 0.45F_5 + 0.45F_9 = -\frac{P}{2} \end{array} \right. \\ \text{Joint 6} & \left\{ \sum F_x = 0 \quad 0.89F_5 - 0.89F_6 = 0 \right. \end{aligned} \tag{2.8}$$

In this case, the coefficient matrix \mathbf{B} is nonsingular ($\det \mathbf{B} \neq 0$), and it follows that the structure is geometrically stable:

$$\mathbf{B} = \begin{bmatrix} 0 & 0.71 & 0 & 0 & 0 & 0 & 0 & 0 & 0.89 \\ -1 & 0.71 & 0 & 0 & 0 & 0 & 0 & 0 & -0.45 \\ 0 & 0.71 & -0.71 & 0 & 0 & 0 & 0 & 0 & 0 \\ 0 & 0.71 & 0.71 & 0 & 0 & 0 & 1 & 0 & 0 \\ 0 & 0 & 0.71 & 0 & 0 & 0 & 0 & 0.89 & 0 \\ 0 & 0 & 0.71 & -1 & 0 & 0 & 0 & -0.45 & 0 \\ 0 & 0 & 0 & 0 & 0.89 & 0 & 0 & 0 & 0.89 \\ 0 & 0 & 0 & 1 & -0.45 & 0 & 0 & 0 & 0.45 \\ 0 & 0 & 0 & 0 & 0.89 & -0.89 & 0 & 0 & 0 \end{bmatrix}$$

Solving (2.8) using a computer software system leads to member forces listed below.

$$\mathbf{F} = \mathbf{B}^{-1} \mathbf{P} = \left\{ \begin{array}{l} 2P \\ 1.41P \\ 1.41P \\ 1.5P \\ 2.24P \\ 2.24P \\ -2P \\ -1.12P \\ -2.24P \end{array} \right\} \Rightarrow \left\{ \begin{array}{l} F_1 = 2P \\ F_2 = 1.41P \\ F_3 = 1.41P \\ F_4 = 1.5P \\ F_5 = 2.24P \\ F_6 = 2.24P \\ F_7 = -2P \\ F_8 = -1.12P \\ F_9 = -2.24P \end{array} \right.$$

For $P = 10$ kN and $h = 6$ m, the member forces are listed in Fig. 2.20f.

Assembling the nodal force equilibrium equations usually is a tedious operation, especially for three-dimensional space structures. The process can be automated by using matrix operations. We will describe one approach later in Sect. 2.6.

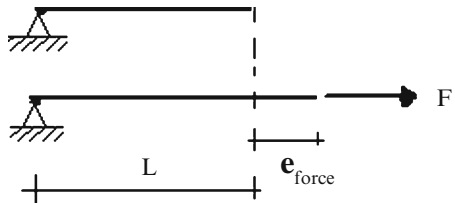
2.3 Computation of Deflections

2.3.1 Introduction

The deflections of the joints are due to the change in length of the members that make up the truss. Each member is subjected to an axial force which produces, depending on the sense, either an extension or a contraction along the member. We call these movements “axial deformation.” The study of deflection involves two steps. Firstly, we determine the axial deformation due to the applied loading. This step involves introducing the material properties for the members. Secondly, we need to relate the deflections to the axial deformations. This step is purely geometric. In what follows, we develop procedures for determining the axial deformation due to an axial force, and the deflections resulting from a set of axial deformations. The latter procedure is carried out here using a manual computation scheme. A computer-based scheme is described in the next section.

2.3.2 Force–Deformation Relationship

Consider the axially loaded member shown in Fig. 2.21. We suppose an axial force, F , is applied, and the member extends an amount e . Assuming the material is linear elastic, e is a linear function of F . We estimate the proportionality factor by first determining the stress, then the strain, and lastly the extension. We discussed this approach in Chap. 1. The steps are briefly reviewed here.

Fig. 2.21

1. Stress

$$\sigma = \frac{F}{A}$$

where A is the cross-sectional area

2. Strain

$$\varepsilon = \frac{\sigma}{E} = \frac{F}{AE}$$

where E is young's modulus

3. Extension

$$e_{\text{force}} = L\varepsilon = \frac{FL}{AE}$$

where L is the member length

The member may also experience an extension due to a temperature change or a fabrication error. Introducing these additional terms, the total extension is expressed as

$$e = e_{\text{force}} + e_{\text{temperature}} + e_{\text{fabrication error}} \quad (2.9)$$

where

$$e_{\text{force}} = \frac{FL}{AE}$$

$$e_{\text{temperature}} = \alpha \Delta T L$$

$$e_{\text{fabrication error}} = e_0$$

α is the coefficient of thermal expansion, ΔT is the temperature change, and e_0 represents the fabrication error. The *total extension*, e , is the quantity that produces the displacement of the node.

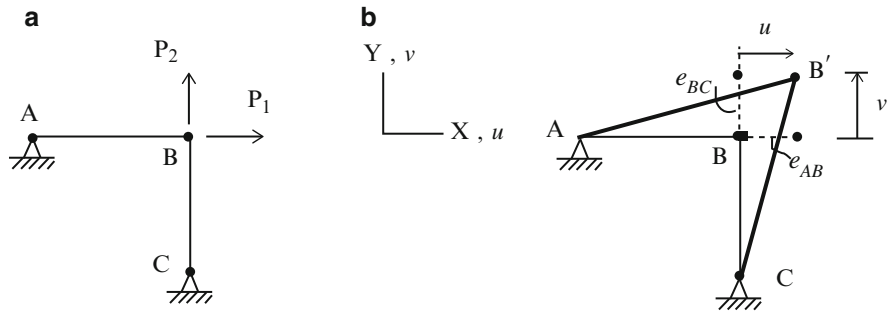


Fig. 2.22 Initial and deformed geometries. (a) Initial geometry. (b) Deformed configuration

2.3.3 Deformation–Displacement Relations

Consider the planar truss structure shown in Fig. 2.22. Suppose the members experience deformation and one wants to determine the final position of node B. Our approach is based on first temporarily disconnecting the members at B, allowing the member deformations to occur, and then rotating the members such that they are reconnected. The movements of the nodes from the original configuration to the new configuration are defined as the displacements. These quantities are usually referred to a global reference frame having axes X and Y and corresponding displacement components u and v .

For structural materials such as steel, the extensions are small in comparison to the original length. Then, the member rotations will also be small. Noting Fig. 2.22b, and the above assumptions, it follows that the displacements are related to the deformations by

$$\begin{aligned} u &\approx e_{AB} \\ v &\approx e_{BC} \end{aligned} \quad (2.10)$$

The simplicity of this results is due to the fact that the structure's geometry is simple (the members are orthogonal to the coordinate axes).

We consider the single member AB defined in Fig. 2.23. Our strategy is to track the motion of the end B as it experiences an extension, e . The final length is $(L + e)$ where e is the extension. We assume $\Delta\theta$ is small and project the final length onto the original direction. This step provides a first order estimate for the extension in terms of the nodal displacements.

$$e \approx u \cos\theta + v \sin\theta \quad (2.11)$$

We consider next a two member planar truss shown in Fig. 2.24. Since the member orientations are arbitrary, the deformation–displacement relations will involve all the displacement components.

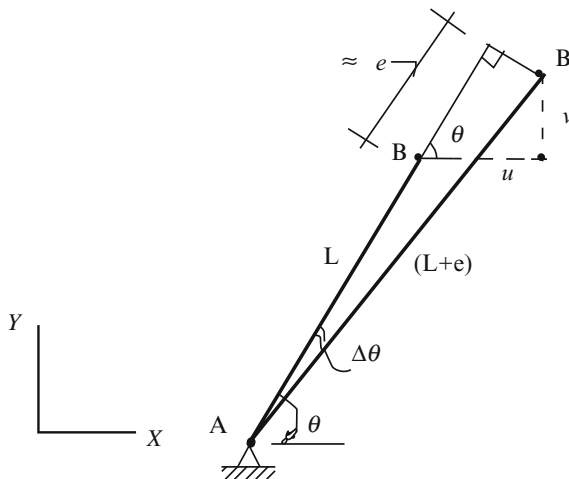


Fig. 2.23 Extension displacement relationships

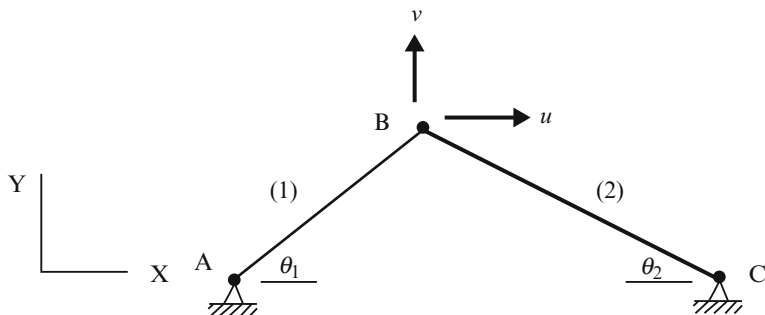


Fig. 2.24 Geometry—two member truss

Applying (2.11) to the above structure leads to

$$\begin{aligned} e_1 &= u \cos\theta_1 + v \sin\theta_1 \\ e_2 &= -u \cos\theta_2 + v \sin\theta_2 \end{aligned} \quad (2.12)$$

Given the member forces, one computes the extensions e_1 and e_2 and finally determines the displacements by solving (2.12).

$$\begin{aligned} u &= e_1 \frac{\sin\theta_2}{\sin\theta_1 \cos\theta_2 + \cos\theta_1 \sin\theta_2} - e_2 \frac{\sin\theta_1}{\sin\theta_1 \cos\theta_2 + \cos\theta_1 \sin\theta_2} \\ v &= e_1 \frac{\cos\theta_2}{\sin\theta_1 \cos\theta_2 + \cos\theta_1 \sin\theta_2} + e_2 \frac{\cos\theta_1}{\sin\theta_1 \cos\theta_2 + \cos\theta_1 \sin\theta_2} \end{aligned}$$

Example 2.13 Calculation of displacements

Given: The structure defined in Fig. E2.13a.

Determine: The displacement components u and v at joint 2. $E = 29,000$ ksi, $h = 10$ ft. $A = 2$ in. 2

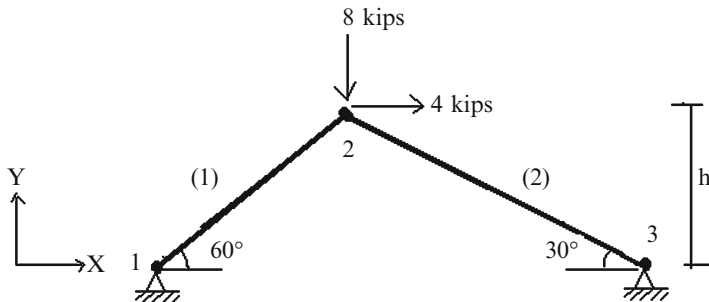


Fig. E2.13a

Solution: We apply the equilibrium equation to joint 2 to determine the member forces.

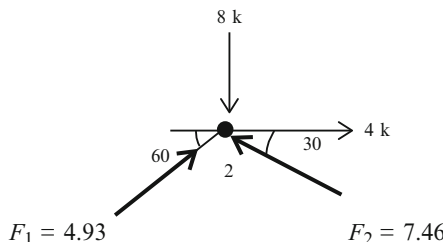


Fig. E2.13b

Then we determine member extensions.

$$e_1 = \frac{F_1 L_1}{A_1 E} = \frac{(-4.93)(11.547 \times 12)}{2(29,000)} = -0.018 \text{ in.}$$

$$e_2 = \frac{F_2 L_2}{A_2 E} = \frac{(-7.46)(20 \times 12)}{2(29,000)} = -0.02 \text{ in.}$$

Evaluating the coefficients in (2.12) for this geometry leads to

$$0.5 u_2 + 0.866 v_2 = -0.018$$

$$-0.866 u_2 + 0.5 v_2 = -0.02$$

Solving for u_2 and v_2 , we obtain

$$\begin{aligned} u_2 &= +0.008 \text{ in. or } u_2 = 0.008 \text{ in.} \rightarrow \\ v_2 &= -0.026 \text{ in. or } v_2 = 0.026 \text{ in.} \downarrow \end{aligned}$$

2.3.4 Method of Virtual Forces

The formulation described in the previous section is not convenient for manual computation, even for fairly simple trusses. However, there is an alternative procedure called the Virtual Force Method, which avoids the need to solve simultaneous equations. Engineers prefer this approach since it is based on executing a set of force equilibrium analyses, a task that they are more familiar with.

The Method of Virtual Forces is a procedure for determining the deflection at a particular point in a structure given that the member forces are known. A general proof of the method can be found in [16]. We apply the method here for truss type structures. Later in the following chapters, we apply the procedure to beam and frame type structures. The method is restricted to static loading and geometrically linear behavior, i.e., where the displacements are small. This is not a serious restriction for civil structures such as building and bridges.

Consider a typical truss shown in Fig. 2.25a. Suppose the deflection, d_A , in a specified direction at point A is desired. One applies a virtual force, δP_A , at A in the specified desired direction and computes the corresponding member forces, δF , and reactions, δR , using only the static equilibrium equations. Usually one takes δP_A to be a unit load. Note that this virtual force system is “specialized” for the particular displacement that one is seeking. The displacement is determined using the following expression:

$$d_A \delta P_A = \sum_{\text{members}} e \delta F - \sum_{\text{reactions}} \bar{d} \delta R \quad (2.13)$$

where e is the total extension defined by (2.9), \bar{d} is the support movement, and δR the corresponding reaction. When the supports are unyielding, $\bar{d} = 0$, and the statement simplifies to

$$d_A \delta P_A = \sum_{\text{members}} e \delta F \quad (2.14)$$

Given the actual forces, one evaluates e with (2.9), then determines the product, $e \delta F$, and lastly sums over the members. Applying (2.13) is equivalent to solving the set of simultaneous equations relating the deformations and the displacements. The following example illustrates this point.

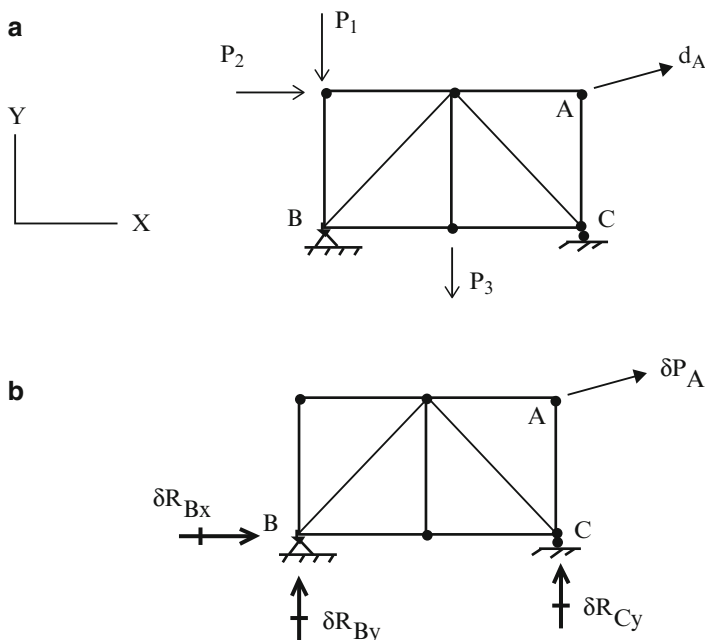


Fig. 2.25 (a) Desired deflection—Actual Force System F. (b) Virtual Force System δF

Example 2.14 Computation of Deflection—Virtual Force Method

Given: The plane truss shown in Fig. E2.14a. Assume $A = 1,300 \text{ mm}^2$ and $E = 200 \text{ GPa}$.

Determine: The horizontal displacement at c (u_c).

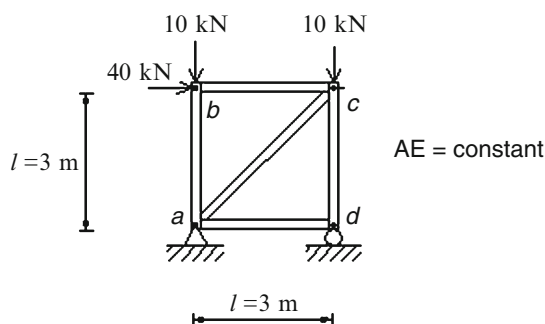


Fig. E2.14a Geometry and loading

Solution: Applying (2.14), the horizontal displacement at node c (u_c) is determined with

$$u_c \delta P = \sum e \delta F = \sum \left(\frac{Fl}{AE} \right) \delta F$$

Fig. E2.14b Actual forces, F

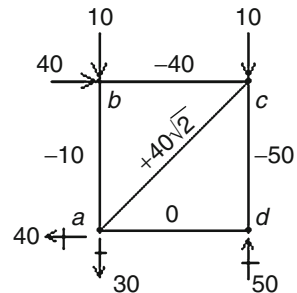
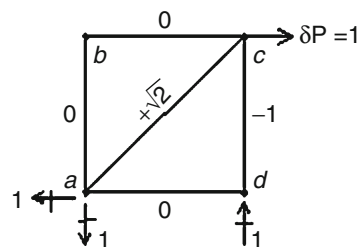


Fig. E2.14c Virtual forces, δF



The actual and virtual forces are listed below.

Using this data, and assuming AE is constant, the computation proceeds as follows:

| Member | L | F | δF | $e = \frac{fl}{AE}$ | $e\delta F$ |
|--------|-------------|--------------|------------|---------------------|---------------------------|
| ab | l | -10 | 0 | $-10 \frac{l}{AE}$ | 0 |
| bc | l | -40 | 0 | $-40 \frac{l}{AE}$ | 0 |
| cd | l | -50 | -1 | $-50 \frac{l}{AE}$ | $50 \frac{l}{AE}$ |
| da | l | 0 | 0 | 0 | 0 |
| ac | $l\sqrt{2}$ | $40\sqrt{2}$ | $\sqrt{2}$ | $80 \frac{l}{AE}$ | $80\sqrt{2} \frac{l}{AE}$ |

$$u_c = \sum e_{\text{force}} \delta F = \frac{l}{AE} (80\sqrt{2} + 50)$$

The plus sign indicates the deflection is in the direction of the unit load. For $A = 1,300 \text{ mm}^2$, $E = 200 \text{ GPa}$, and $l = 3 \text{ m}$, the displacement is

$$u_c = \frac{3(10^3)}{1,300(200)} (80\sqrt{2} + 50) = 1.88 \text{ mm} \rightarrow$$

We point out that the virtual force (δF) results identify which member deformations contribute to the corresponding deflection. In this case, only two member deformations contribute to the horizontal displacement.

Example 2.15 Computation of Deflection—Virtual Force Method

Given: The plane truss shown in Fig. E2.15a. Assume $E = 200 \text{ GPa}$.

Determine: The value of A required to limit the vertical displacement at e (v_e) to be equal to 10 mm.

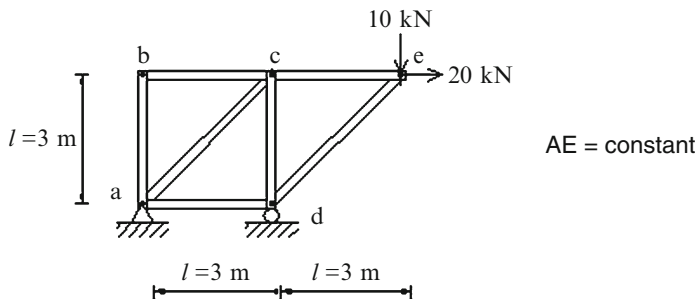


Fig. E2.15a Geometry and loading

Solution: Following (2.14) the horizontal displacement at node c (u_c) is determined with

$$v_e \delta P = \sum e_{\text{force}} \delta F = \sum \left(\frac{Fl}{AE} \right) \delta F$$

The actual and virtual forces are listed below.

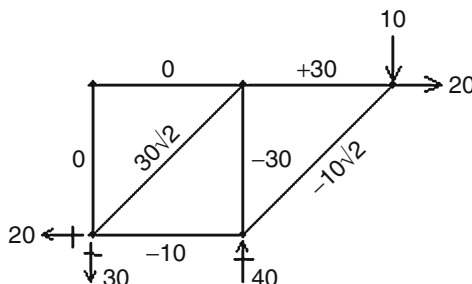
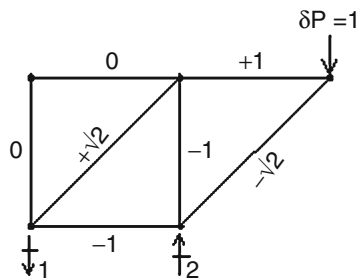


Fig. E2.15b Actual forces, F

**Fig. E2.15c** Virtual forces, δF

Using this data, and assuming AE is constant, the following computations are carried out:

| Member | L | F | δF | $e = \frac{FL}{AE}$ | $e\delta F$ |
|--------|-------------|---------------|-------------|---------------------|----------------------------------------------------|
| ab | l | 0 | 0 | 0 | 0 |
| bc | l | 0 | 0 | 0 | 0 |
| cd | l | -30 | -1 | $-30 \frac{l}{AE}$ | $30 \frac{l}{AE}$ |
| da | l | -10 | -1 | $-10 \frac{l}{AE}$ | $10 \frac{l}{AE}$ |
| ac | $l\sqrt{2}$ | $30\sqrt{2}$ | $\sqrt{2}$ | $60 \frac{l}{AE}$ | $60\sqrt{2} \frac{l}{AE}$ |
| ce | l | 30 | 1 | $30 \frac{l}{AE}$ | $30 \frac{l}{AE}$ |
| ed | $l\sqrt{2}$ | $-10\sqrt{2}$ | $-\sqrt{2}$ | $-20 \frac{l}{AE}$ | $20\sqrt{2} \frac{l}{AE}$ |
| | | | | | $\sum e \delta F = \frac{l}{AE} (80\sqrt{2} + 70)$ |

$$v_e = \sum e_{\text{force}} \delta F = \frac{l}{AE} (80\sqrt{2} + 70)$$

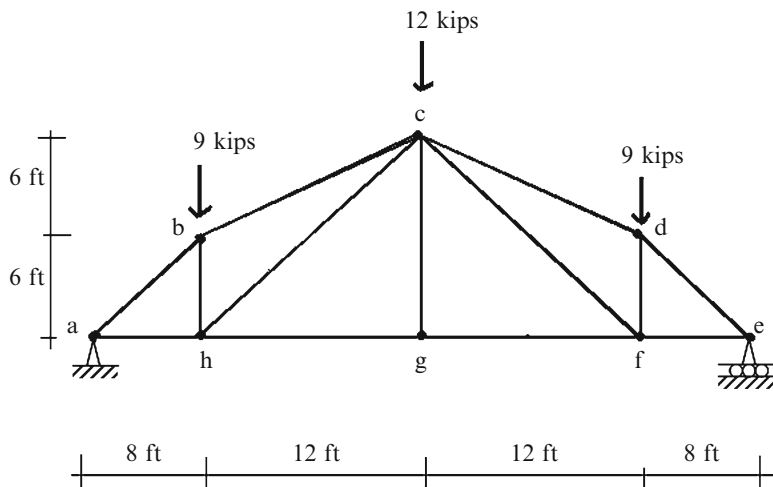
The plus sign indicates the deflection is in the direction of the unit load. For, $E = 200$ GPa, and $l = 3,000$ mm, the required area is

$$A_{\text{required}} = \frac{l}{v_e E} (80\sqrt{2} + 70) = \frac{(3,000)}{10(200)} (80\sqrt{2} + 70) = 275 \text{ mm}^2$$

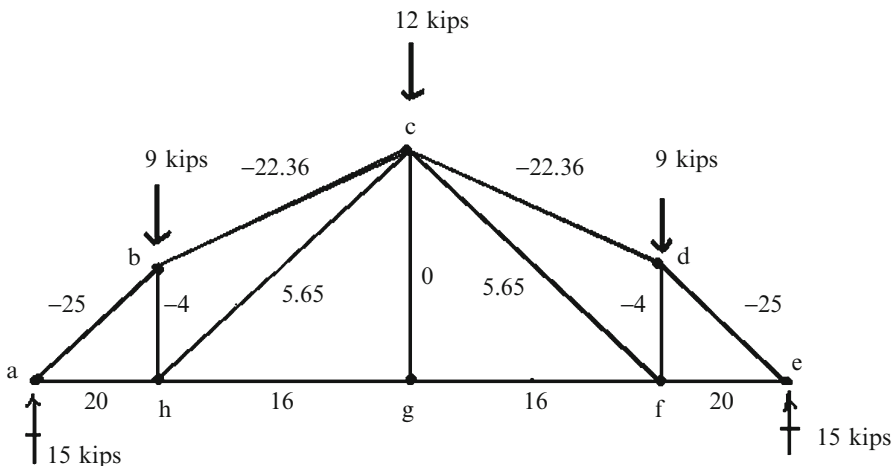
Example 2.16 Computation of Deflection—Virtual Force Method

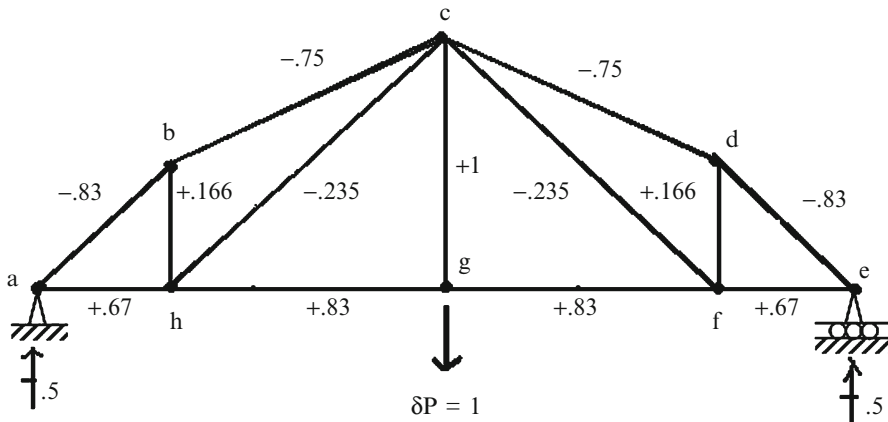
Given: The plane truss shown in Fig. E2.16a. Member bc and cf also have fabrication error of +0.5 in.

Determine: The vertical component of the displacement at joint g (v_g). Take $A = 2 \text{ in.}^2$ and $E = 29,000$ ksi for all the members.

**Fig. E2.16a**

Solution: The actual and virtual forces are listed below.

**Fig. E2.16b** Actual forces, F

**Fig. E2.16c** Virtual forces, δF

| Member | $L_{in.}$ | L/A | F | δF_v | $\frac{L}{A}F$ | δF_v | $e_{0in.}$ | e_0 | δF_v |
|--------------------------------------|-----------|-------|--------|--------------|----------------|--------------|-------------------------------|---------|--------------|
| ab | 120 | 60 | -25 | -0.83 | 1,245 | | 0 | 0 | |
| bc | 161 | 80.5 | -22.36 | -0.75 | 1,350 | | +0.5 | -0.375 | |
| cd | 161 | 80.5 | -22.36 | -0.75 | 1,350 | | 0 | 0 | |
| de | 120 | 60 | -25 | -0.83 | 1,245 | | 0 | 0 | |
| ef | 96 | 48 | 20 | 0.67 | 643 | | 0 | 0 | |
| fg | 144 | 72 | 16 | 0.83 | 960 | | 0 | 0 | |
| gh | 144 | 72 | 16 | 0.83 | 960 | | 0 | 0 | |
| ha | 96 | 48 | 20 | 0.67 | 643 | | 0 | 0 | |
| bh | 72 | 36 | -4 | 0.166 | -24 | | 0 | 0 | |
| cg | 144 | 72 | 0 | 1 | 0 | | 0 | 0 | |
| df | 72 | 36 | -4 | 0.166 | -24 | | 0 | 0 | |
| ch | 203.6 | 101.8 | 5.65 | -0.235 | -135.7 | | 0 | 0 | |
| cf | 203.6 | 101.8 | 5.65 | -0.235 | -135.7 | | +0.5 | -1.1175 | |
| $\sum \frac{L}{A}F \delta F = 8,077$ | | | | | | | $\sum e_0 \delta F_v = -0.49$ | | |

$$v_{g\text{load}} = \sum e_{\text{force}} \delta F = \sum \left(\frac{L}{AE} F \right) \delta F = \frac{8,077}{29,000} = +0.278 \text{ in.} \Rightarrow v_{g\text{load}} 0.28 \text{ in.} \downarrow$$

$$v_g \text{ fabrication error} = \sum e_0 \delta F = -0.49 \text{ in.} \Rightarrow v_g \text{ fabrication error} = 0.49 \text{ in.} \uparrow$$

$$v_{g(\text{load+fabrication})} = +0.278 - 0.49 = -0.21 \text{ in.} \Rightarrow v_{g(\text{load+fabrication})} = 0.21 \text{ in.} \uparrow$$

Example 2.17 Deflection of a gable truss

Given: The plane truss shown in Fig. E2.17a. The truss has variable cross sections, such that $A = 6,500 \text{ mm}^2$ for top chord members, $A = 3,900 \text{ mm}^2$ for bottom chord members, $A = 1,300 \text{ mm}^2$ for diagonal members, and $A = 650 \text{ mm}^2$ for vertical members and $E = 200 \text{ GPa}$.

Determine: The vertical displacement of node j (v_j) and the horizontal displacement of node g (u_g).

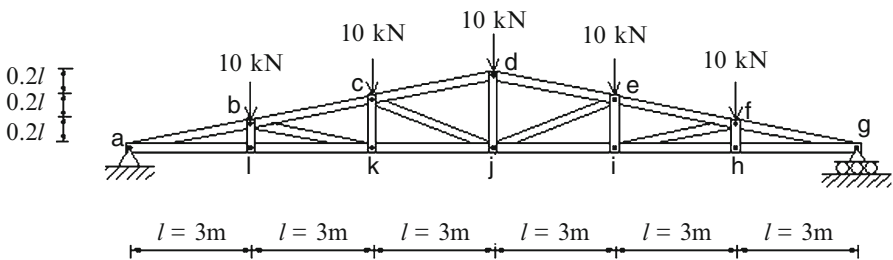


Fig. E2.17a Geometry and loading

Solution: The actual and virtual forces are listed below.

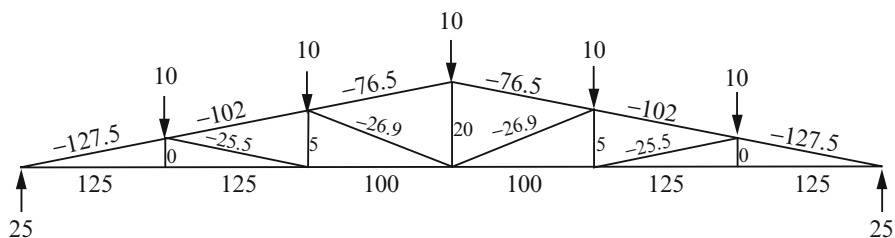


Fig. E2.17b Actual forces F

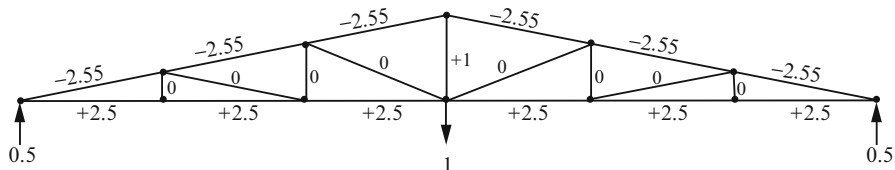


Fig. E2.17c Virtual forces δF_v

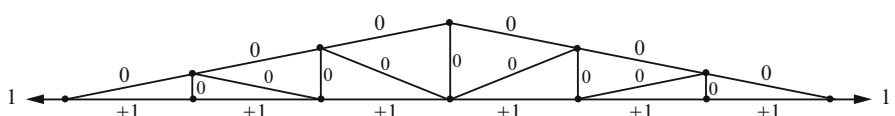


Fig. E2.17d Virtual forces δF_u

The computations are organized using the spread sheet format listed below. Note that the upper and lower chords and only the central member contribute to the central vertical deflection. And only the lower chord contributes to the horizontal support deflection. The plus sign indicates the deflection is in the direction of the unit load.

| Member | L mm | A mm 2 | L/A | F kN | δF_u | δF_v | $(L/A) F \delta F_u$ | $(L/A) F \delta F_v$ |
|--------|--------|-------------|-------|--------|--------------|--------------|----------------------|----------------------|
| ab | 3,059 | 6,500 | 0.47 | -127.5 | 0.0 | -2.55 | 0 | 152.8 |
| bc | 3,059 | 6,500 | 0.47 | -102.0 | 0.0 | -2.55 | 0 | 122.2 |
| cd | 3,059 | 6,500 | 0.47 | -76.5 | 0.0 | -2.55 | 0 | 91.7 |
| de | 3,059 | 6,500 | 0.47 | -76.5 | 0.0 | -2.55 | 0 | 91.7 |
| ef | 3,059 | 6,500 | 0.47 | -102.0 | 0.0 | -2.55 | 0 | 122.2 |
| fg | 3,059 | 6,500 | 0.47 | -127.5 | 0.0 | -2.55 | 0 | 152.8 |
| gh | 3,000 | 3,900 | 0.77 | 125.0 | 1.0 | 2.5 | 96.2 | 240.6 |
| hi | 3,000 | 3,900 | 0.77 | 125.0 | 1.0 | 2.5 | 96.2 | 240.6 |
| ij | 3,000 | 3,900 | 0.77 | 100.0 | 1.0 | 2.5 | 77 | 192.5 |
| jk | 3,000 | 3,900 | 0.77 | 100.0 | 1.0 | 2.5 | 77 | 192.5 |
| kl | 3,000 | 3,900 | 0.77 | 125.0 | 1.0 | 2.5 | 96.2 | 240.6 |
| la | 3,000 | 3,900 | 0.77 | 125.0 | 1.0 | 2.5 | 96.2 | 240.6 |
| bl | 600 | 650 | 0.92 | 0.0 | 0.0 | 0.0 | 0 | 0 |
| ck | 1,200 | 650 | 1.85 | 5.0 | 0.0 | 0.0 | 0 | 0 |
| dj | 1,800 | 650 | 2.77 | 20.0 | 0.0 | 1.0 | 0 | 55.4 |
| ei | 1,200 | 650 | 1.85 | 5.0 | 0.0 | 0.0 | 0 | 0 |
| fh | 600 | 650 | 0.92 | 0.0 | 0.0 | 0.0 | 0 | 0 |
| bk | 3,059 | 1,300 | 2.35 | -25.5 | 0.0 | 0.0 | 0 | 0 |
| cj | 3,231 | 1,300 | 2.48 | -26.9 | 0.0 | 0.0 | 0 | 0 |
| ej | 3,231 | 1,300 | 2.48 | -26.9 | 0.0 | 0.0 | 0 | 0 |
| fi | 3,059 | 650 | 4.71 | -25.5 | 0.0 | 0.0 | 0 | 0 |

The remaining computations involve dividing by E .

$$\sum \left(\left(\frac{L}{A} \right) F \delta F_u \right) = 538.8 \text{ kN/mm}$$

$$\therefore u_g = \sum e_{\text{force}} \delta F = \frac{1}{E} \sum \left(\left(\frac{L}{A} \right) F \delta F_u \right) = 538.8 / 200 = 2.69 \text{ mm} \rightarrow$$

$$\sum \left(\left(\frac{L}{A} \right) F \delta F_v \right) = 2,136.2 \text{ kN/mm}$$

$$\therefore v_j = \sum e_{\text{force}} \delta F = \frac{1}{E} \sum \left(\left(\frac{L}{A} \right) F \delta F_v \right) = 2,136.2 / 200 = 10.7 \text{ mm} \downarrow$$

We pointed out earlier that the distribution of member forces depends on the orientation of the diagonal members. We illustrate this behavior by reversing the diagonal pattern for the truss defined in Fig. E2.17a. The member forces corresponding to the same loading are listed in Fig. E2.17e. Suppose the vertical deflection at mid-span is desired. The corresponding virtual force system is shown in Fig. E2.17f.

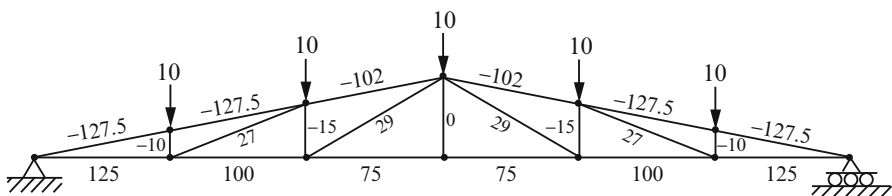


Fig. E2.17e Diagonal pattern reversed—Actual forces F

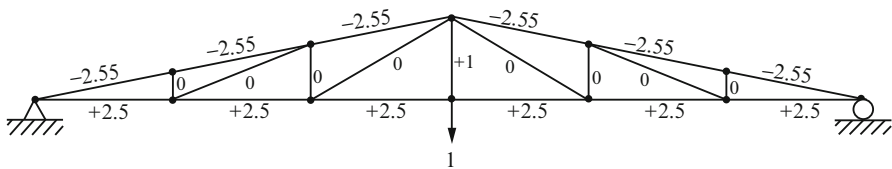


Fig. E2.17f Diagonal pattern reversed—Virtual forces δF

| Member | L mm | A mm 2 | L/A | F kN | δF_v | $(L/A)F \delta F_v$ |
|--------|--------|-------------|-------|--------|--------------|---------------------|
| ab | 3,059 | 6,500 | 0.47 | -127.5 | -2.55 | 153 |
| bc | 3,059 | 6,500 | 0.47 | -127.5 | -2.55 | 153 |
| cd | 3,059 | 6,500 | 0.47 | -102 | -2.55 | 122.2 |
| de | 3,059 | 6,500 | 0.47 | -102 | -2.55 | 122.2 |
| ef | 3,059 | 6,500 | 0.47 | -127.5 | -2.55 | 153 |
| fg | 3,059 | 6,500 | 0.47 | -127.5 | -2.55 | 153 |
| gh | 3,000 | 3,900 | 0.77 | 125.0 | 2.5 | 240.6 |
| hi | 3,000 | 3,900 | 0.77 | 100 | 2.5 | 192.5 |
| ij | 3,000 | 3,900 | 0.77 | 75 | 2.5 | 144.4 |
| jk | 3,000 | 3,900 | 0.77 | 75 | 2.5 | 144.4 |
| kl | 3,000 | 3,900 | 0.77 | 100 | 2.5 | 192.5 |
| la | 3,000 | 3,900 | 0.77 | 125. | 2.5 | 240.6 |
| bl | 600 | 650 | 0.92 | -10 | 0.0 | 0 |
| ck | 1,200 | 650 | 1.85 | -15 | 0.0 | 0 |
| dj | 1,800 | 650 | 2.77 | 0 | 1.0 | 0 |
| ei | 1,200 | 650 | 1.85 | -15 | 0.0 | 0 |
| fh | 600 | 650 | 0.92 | -10 | 0.0 | 0 |
| bk | 3,059 | 1,300 | 2.35 | 27 | 0.0 | 0 |
| dk | 3,498 | 1,300 | 2.69 | 29 | 0.0 | 0 |
| di | 3,498 | 1,300 | 2.69 | 29 | 0.0 | 0 |
| fi | 3,059 | 1,300 | 2.35 | 27 | 0.0 | 0 |

Using the data listed above, the mid-span deflection calculations are

$$\sum \left(\left(\frac{L}{A} \right) F \delta F_v \right) = 2,011 \text{ kN/mm}$$

$$\therefore v_j = \sum e_{\text{force}} \delta F = \frac{1}{E} \sum \left(\left(\frac{L}{A} \right) F \delta F_v \right) = 2,011 / 200 = 10 \text{ mm} \downarrow$$

The examples presented to this point have been concerned with loads. Structures are also subjected to seasonal (and daily) temperature changes and it is of interest to determine the corresponding nodal displacements. A unique feature of statically determinate structures is their ability to accommodate temperature changes without experiencing member forces. When subjected to a temperature change, a statically determinate structure adjusts its geometry in such a way that there are *no forces introduced in the members*. From a design perspective, this behavior is very desirable since member forces, i.e. stresses, are due only to the loads. However, one may need to compute the deflected shape due to temperature change from some initial state. The effect of temperature change is to produce an additional extension in a truss member given by:

$$e_{\text{temperature}} = \alpha \Delta T \ell$$

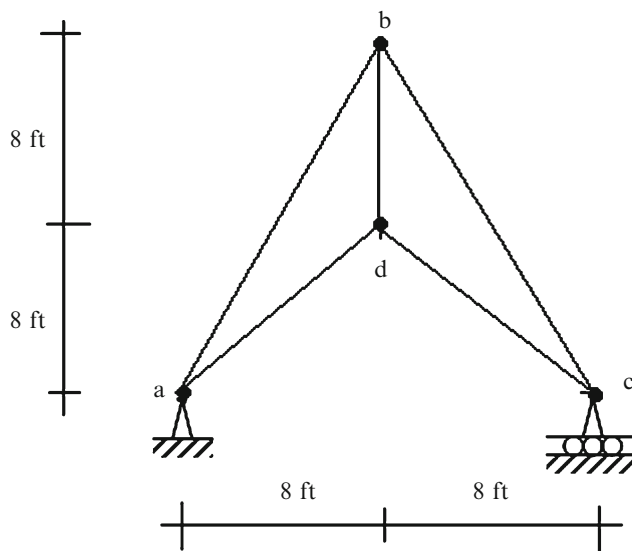
where α is a material property, defined as the coefficient of thermal expansion, and ΔT is the temperature change from the initial state. Then, the form of the Principle of Virtual force specialized for only temperature and unyielding supports reduces to

$$d \delta P = \sum (e_{\text{temperature}})(\delta F) \quad (2.15)$$

The computational procedure is similar to the approach discussed earlier. We evaluate $(\alpha \Delta T) \ell$ for the members. Then, given a desired deflection, we apply the appropriate virtual loading and compute δF for the members. Lastly we evaluate the summation. The following example illustrates the details. This discussion applies only for statically determinate trusses. A temperature change introduces internal forces in statically indeterminate trusses. Analysis procedures for this case are discussed in Chaps. 9 and 10.

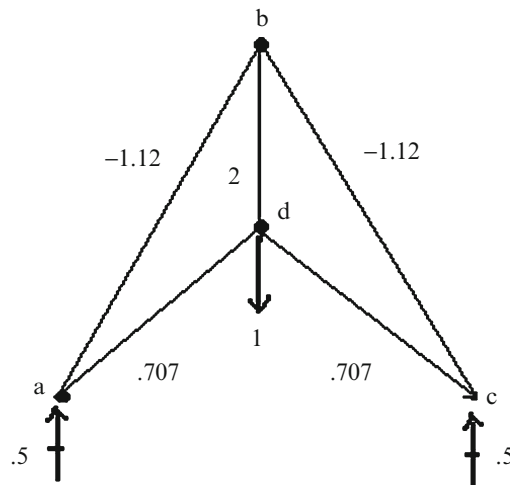
Example 2.18 Computation of deflection due to temperature

Given: The plane truss shown in Fig. E2.18a.

**Fig. E2.18a**

Determine: The vertical displacement at joint d due to temperature increase of $\Delta T = 65 \text{ }^{\circ}\text{F}$ for all members. $A = 2 \text{ in.}^2$, $E = 29,000 \text{ ksi}$ and $\alpha = 6.5(10^{-6})/\text{ }^{\circ}\text{F}$

Solution: The corresponding virtual force system is listed below.

**Fig. E2.18b** Virtual forces δF

| Member | $L_{in.}$ | $e = \alpha \Delta TL$ | δF | $e \delta F$ |
|--------|-----------|------------------------|------------|----------------------------|
| ab | 214.7 | 0.091 | -1.12 | -0.102 |
| bc | 214.7 | 0.091 | -1.12 | -0.102 |
| cd | 135.7 | 0.057 | 0.707 | 0.04 |
| da | 135.7 | 0.057 | 0.707 | 0.04 |
| bd | 96 | 0.041 | 2 | 0.082 |
| | | | | $\sum e \delta F = -0.042$ |

$$v_d = \sum e_{\text{temperature}} \delta F = (\alpha \Delta TL) \delta F = -0.042 \Rightarrow v_d = 0.042 \text{ in. } \uparrow$$

2.4 Influence Lines

Consider the plane bridge truss shown in Fig. 2.26a. To design a particular member, one needs to know the maximum force in the member due to the design loading. The dead loading generally acts over the entire structure, i.e., on all the nodes. For this loading component, one places all the dead load on the structure and carries out a single analysis for the member forces. The live loading, by definition, can act anywhere on the structure and therefore one needs to determine the location of the live loading that produces the maximum force in the member that is being designed. A systematic approach to locating the critical position of the live loading is based on first constructing an influence line for the member force. This construction involves a series of analyses, one for each possible location of live loading. The live load is usually taken as a single force, of unit magnitude, which is moved from node to node across the structure. The resulting influence line is a plot of the member force as a function of the location of the applied load. Figure 2.26b illustrates the possible nodal positions of a vertical load applying to the bottom chord, and the corresponding member forces. Given this data, one can construct an influence line for any of the member forces.

The process described above assumes the loading is a concentrated load applied at the nodes. For bridge structures, the live loading is actually applied to the deck which transmits the load to the transverse beams, and finally to the nodes. The deck is usually simply supported on the transverse beams, so the complete deck-beam system is statically determinate and one can determine the reactions at the nodes using only the equations of statics. We illustrate this computation using the structure shown in Fig. 2.27a. We suppose a truck loading is passing over the span.

Consider the position shown in Fig. 2.27b. The wheel loads act on the deck segments gf and fe. The live load vehicle analysis reduces to just applying loads to the nodes adjacent to the vehicle since the deck segments (gf and fe) are simply supported. Noting Fig. 2.27c the equivalent nodal loads are

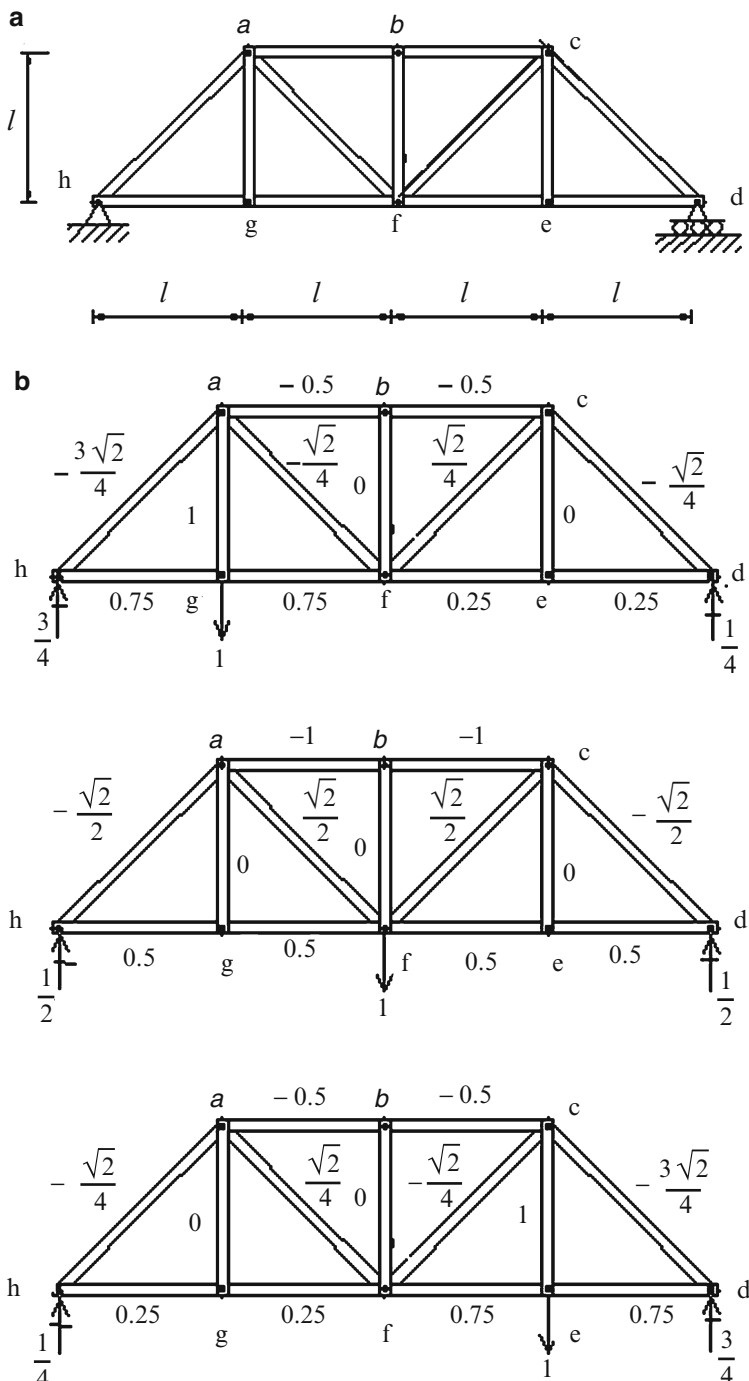


Fig. 2.26 (a) Truss geometry. (b) Load positions and corresponding member forces

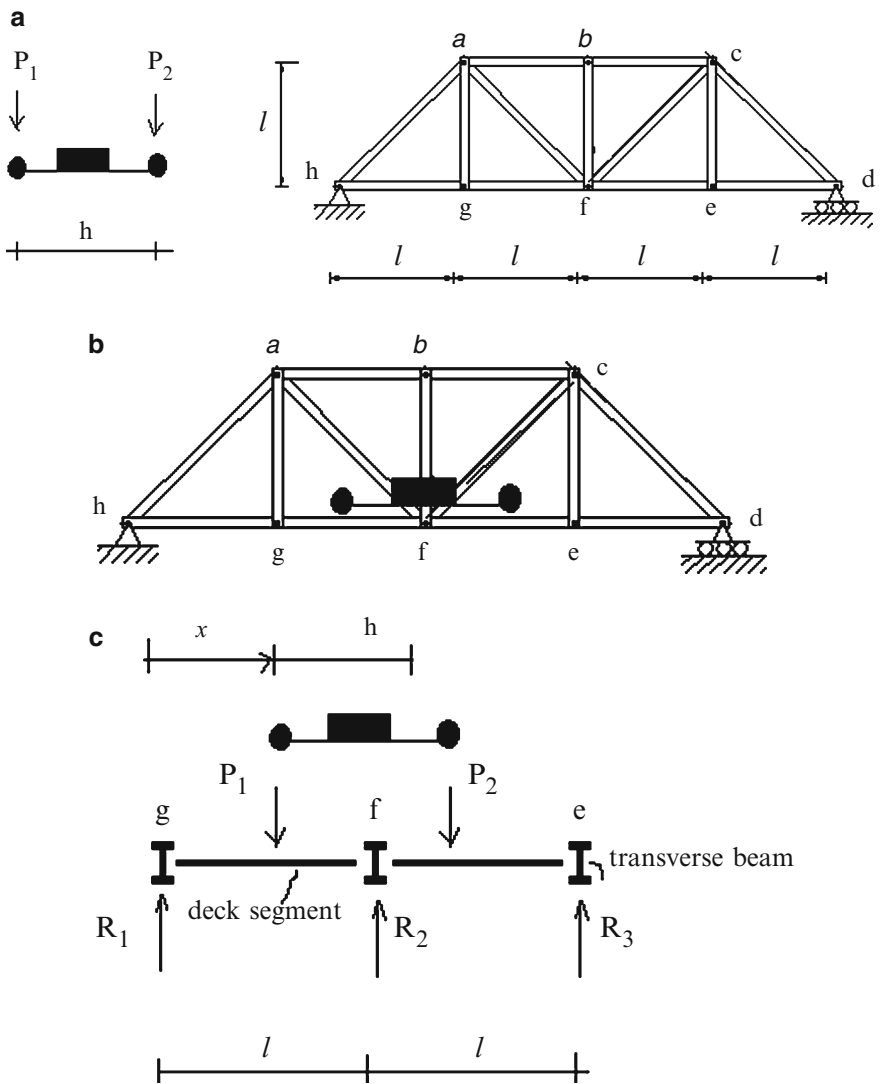


Fig. 2.27 (a) Truss geometry. (b). (c)

$$\begin{aligned}
 R_1 &= \left(1 - \frac{x}{l}\right)P_1 \\
 R_2 &= \left(\frac{x}{l}\right)P_1 + \left(2 - \frac{x}{l} - \frac{h}{l}\right)P_2 \\
 R_3 &= \left(\frac{x}{l} + \frac{h}{l} - 1\right)P_1
 \end{aligned}$$

Note that the reactions are linear functions of x , the position coordinate for the truck.

We define F_j as the force in member j . Applying separate unit loads at nodes g and f leads to $F_j|_g$ and $F_j|_f$. Then, according to the equations listed above, the force due to a unit load at x is

$$F_j|_x = \left(1 - \frac{x}{l}\right)F_j|_g + \left(\frac{x}{l}\right)F_j|_f$$

The most convenient way to present these results is to construct a plot of F_j vs. x where F_j is the force in member j due to a unit load at x , and x is taken to range over the nodes on the bottom chord. We need to apply these loads *only at the nodes* since the plot is *linear* between adjacent nodes. Plots of this type are called influence lines. Figure 2.28a shows the influence line for chord member ab . This visual representation is convenient since one can immediately identify the critical location of the load. For the chord member, ab , the maximum magnitude occurs when the load is applied at mid-span. Also, we note that the force is compression for all locations.

Given an actual loading distribution, one evaluates the contribution of each load, and then sums the contributions. If the actual live load consisted of a uniform loading, then it follows that one would load the entire span. The maximum force due to the truck loading is determined by positioning the truck loads as indicated in Fig. 2.28b. In general, one positions the vehicle such that the maximum vehicle load acts on node f .

The influence line for member fg is plotted in Fig. 2.28c. In this case, the member force is always tension.

The function of the diagonal members is to transmit the vertical forces from node to node along the span. This action is called “shear.” The influence line for a diagonal is different than the influence lines for upper and lower chord members, in that it has both positive and negative values. Figure 2.28d shows the result for diagonal af . A load applied at node g generates compression, whereas loads at nodes f and e produce tension. Lastly, a symmetrically located diagonal with opposite orientation, such as cf vs. af has an influence line that is a rotated version of its corresponding member (see Fig. 2.28d vs. Fig. 2.28e).

Because the influence lines for diagonals have both positive and negative values, one needs to consider two patterns of live load in order to establish the peak value of the member force.

For member af , the extreme values are

Load at node f $F = \sqrt{2}/2$

Load at node g $F = -\sqrt{2}/4$

For member cf , the extreme values are

Loads at node e $F = -\sqrt{2}/4$

Loads at node f $F = \sqrt{2}/2$

If a uniform load is applied, the peak force values for both members will be:

$$F_{\max} = +\sqrt{2}/2$$

As mentioned earlier, diagonal members function to transmit vertical loads to the end supports. We showed above that the sense of the diagonal force depends on the orientation of the member. The sense of the diagonal force is important since slender members behave differently under compression vs. tension. A slender member subjected to compressive load will fail by buckling rather than by yielding since the buckling load is considerably less than the yield force. Therefore, from a design perspective one should avoid using slender compression members. For truss type structures, this problem can be avoided by selecting an appropriate diagonal orientation pattern.

As an example, consider the two diagonal patterns shown in Fig. 2.29a, b. The sense of the member forces due to a uniform live load is indicated by C (compression) and T (tension).

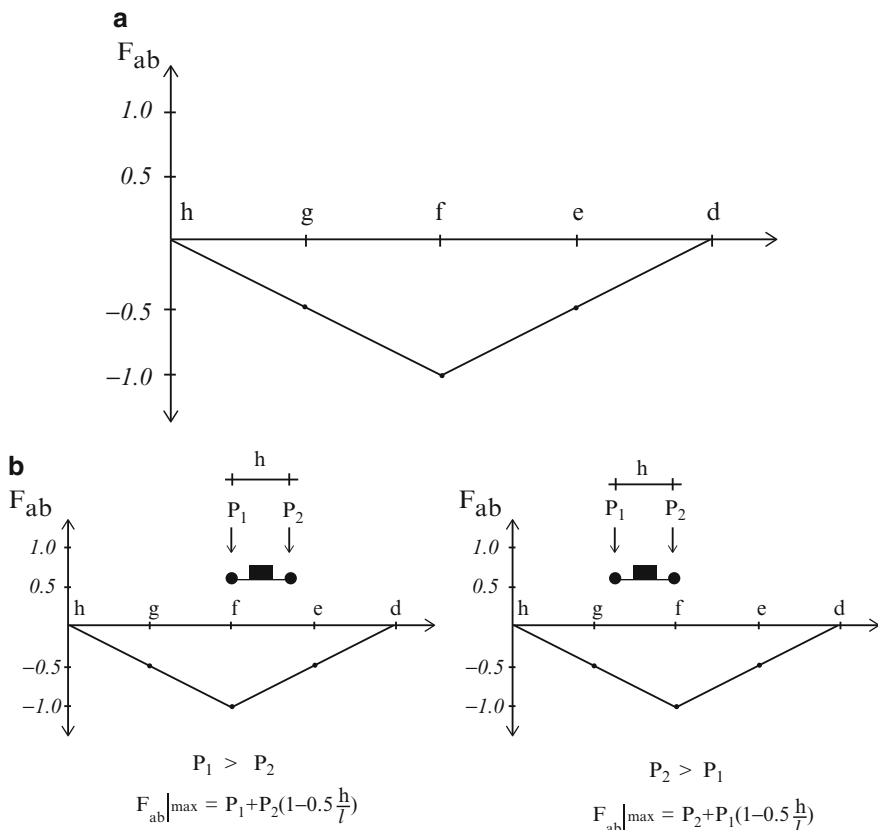
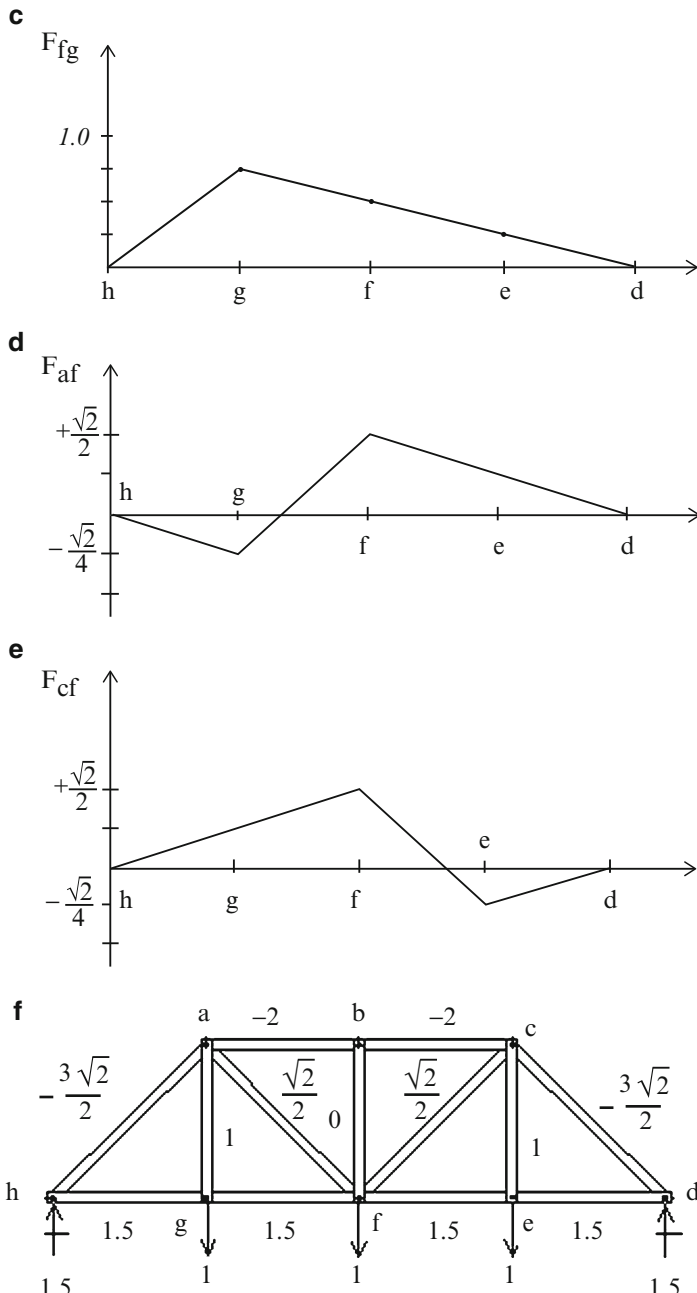


Fig. 2.28 (a) Influence line for cord member ab. (b) Vehicle positioning for $F_{ab}|_{\max}$. (c) Influence line for chord member fg. (d) Influence line for diagonal member af. (e) Influence line for diagonal member cf. (f) Uniform unit load

**Fig. 2.28** (continued)

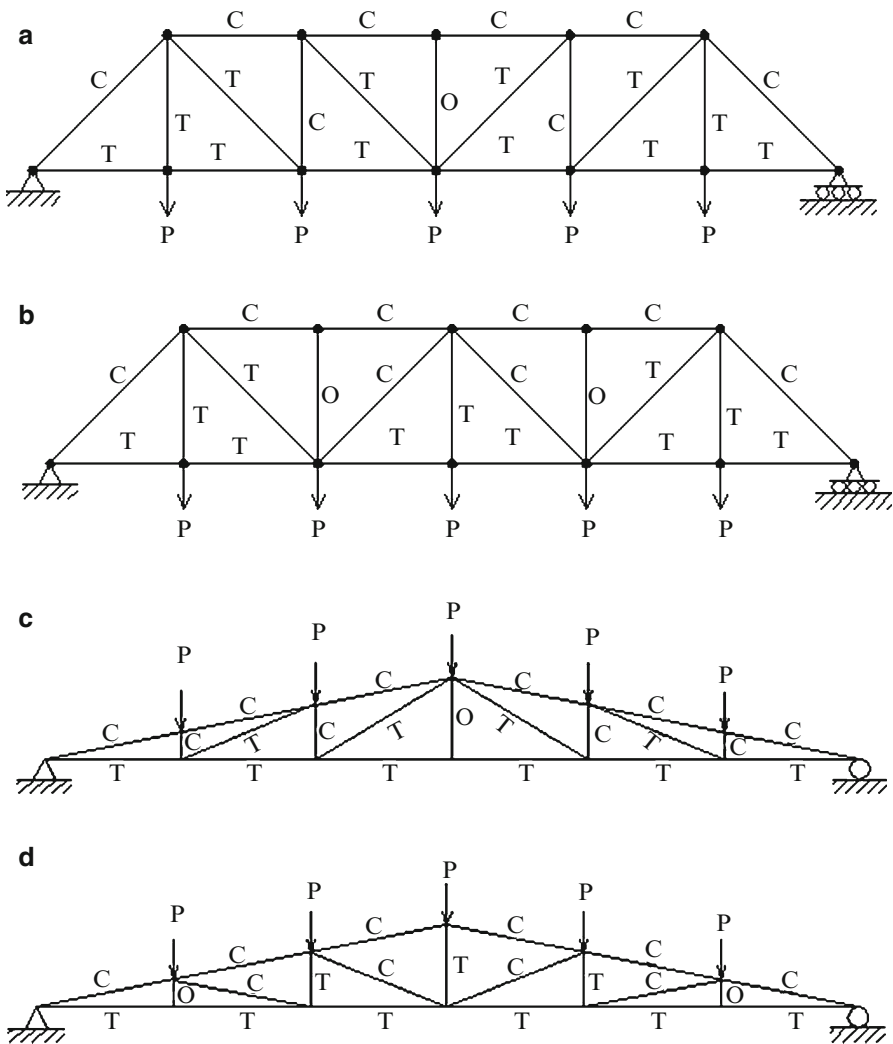


Fig. 2.29 Force pattern for various truss geometries. (a) Pratt Truss. (b) Warren truss. (c) Pratt Truss. (d) Howe Truss

Pattern (a) is more desirable since all the interior diagonals are in tension. However, some of the vertical members are in compression. Pattern (b) has alternating sense for the diagonals; the vertical hangers are all in tension. In general, for both truss types the top chord forces are compression and the bottom chord forces are tension. Figure 2.29c, d show similar results for inclined chord trusses. The designators “Pratt,” “Warren” and “Howe” refer to the individuals who invented these geometrical forms.

Example 2.19

Given: The structure and truck loading shown in Fig. E2.19a.

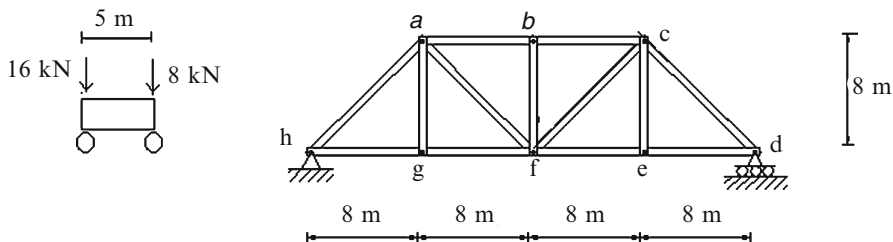


Fig. E2.19a

Determine: The maximum force in members ab and fg due to the truck loading.

Solution: We first determine the influence lines for a unit vertical force applied along the bottom nodes.

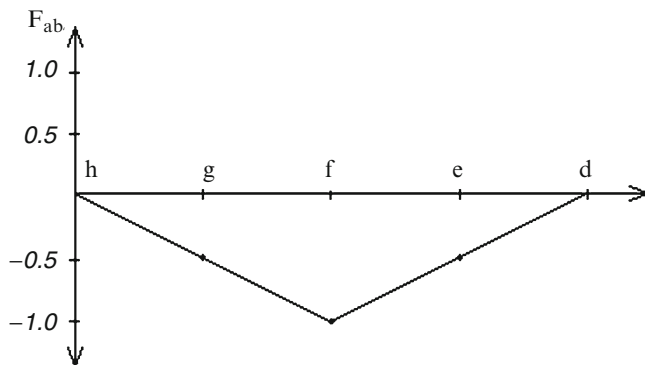


Fig. E2.19b Influence line for member ab

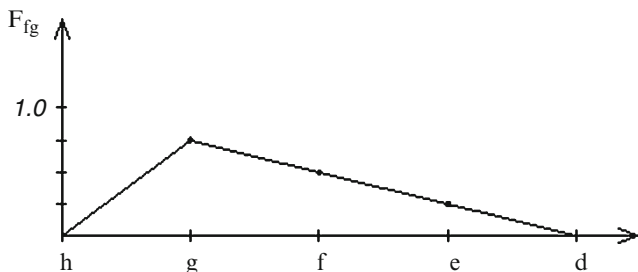
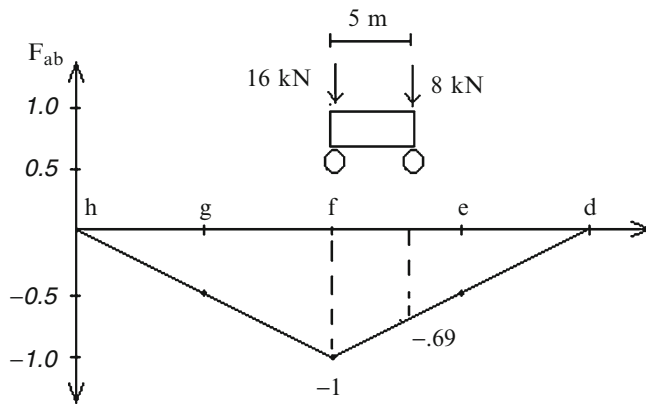
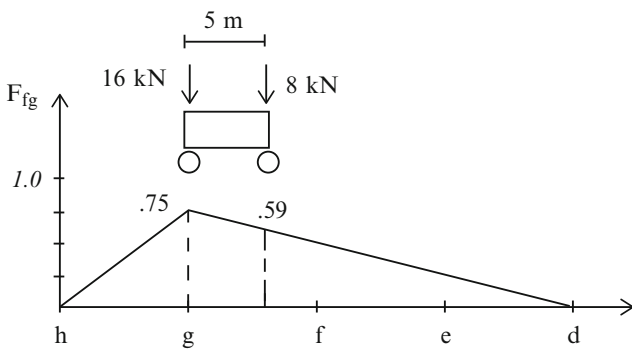


Fig. E2.19c Influence line for member fg

**Fig. E2.19d****Fig. E2.19e**

Then, we position the truck loading as indicated below

$$F_{ab_{\max}} = 16(-1) + 8(-0.69) = -21.52 \quad \therefore F_{ab_{\max}} = 21.52 \text{ kN Compression}$$

$$F_{fg_{\max}} = 16(0.75) + 8(0.59) = +16.72 \quad \therefore F_{fg_{\max}} = 16.72 \text{ kN Tension}$$

Example 2.20 Live load analysis for a gable roof structure

Given: The gable roof structure shown in Fig. E2.20a.

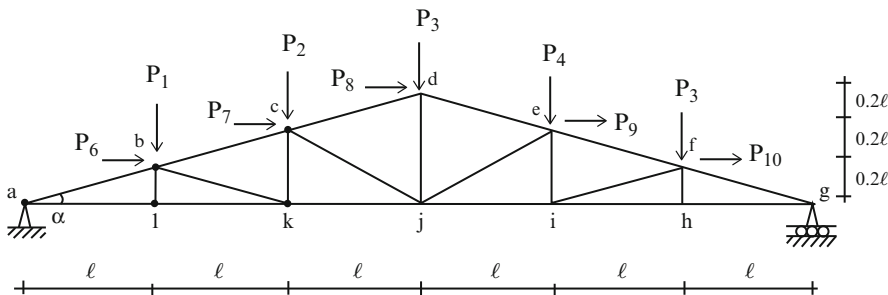


Fig. E2.20a Structural geometry and nodal loads

Determine:

1. Tabulate all the member forces due to the individual unit nodal forces applied to the top chord. We refer to this type of table as a force influence table.
2. Use the force influence table to draw the influence line for member cd.
3. The force in member cd due to the wind load shown in Fig. E2.20b.

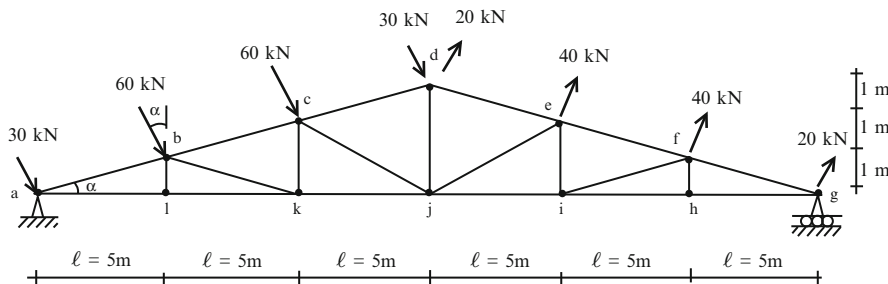


Fig. E2.20b Wind

Solution:

Part (i) The member forces due to the ten individual unit nodal loads are listed in Fig. E2.20c. Computer-based analysis software is usually used for this computation.

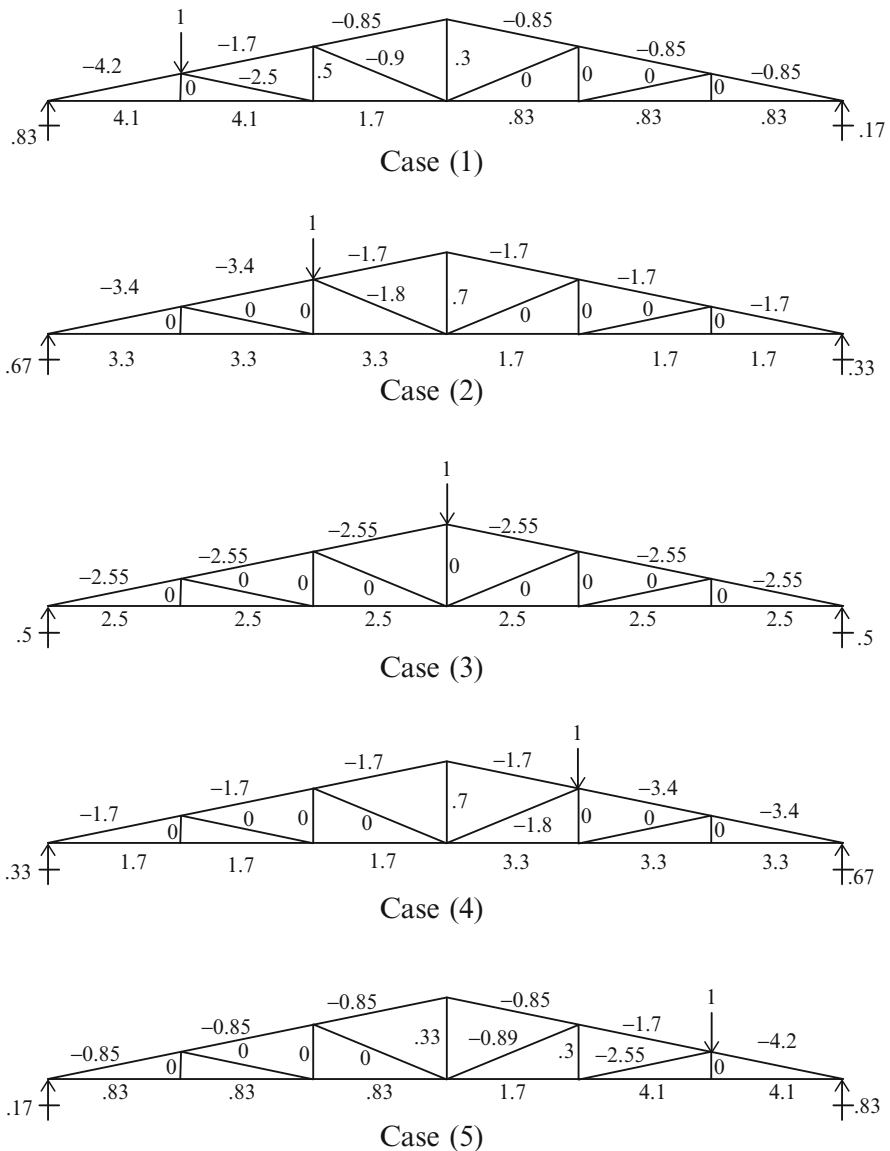
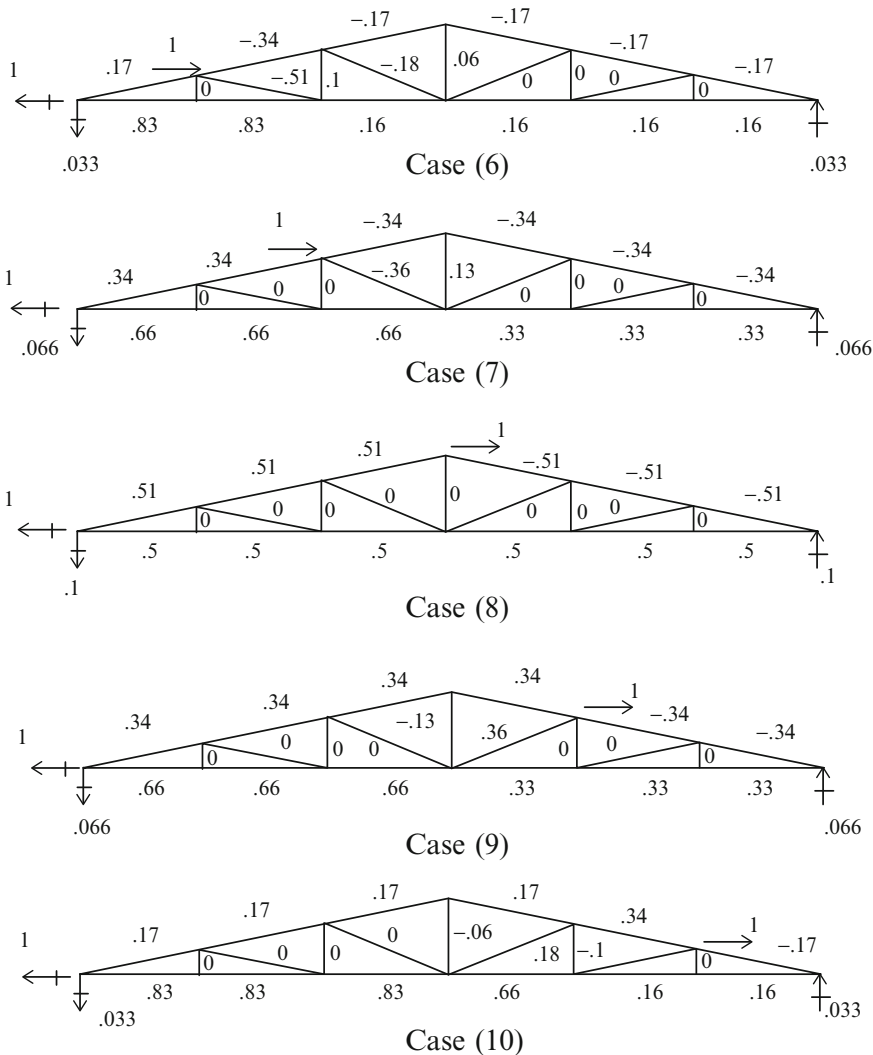


Fig. E2.20c Force results for different load positions

**Fig. E2.20c** (continued)

The complete set of member force results are listed in the following Table. One uses this table in two ways. Firstly, scanning down a column shows the member which is most highly stressed by the loading acting at the position corresponding to the column. Scanning across a row identifies the loading which has the maximum contribution to the member force.

Force Influence Table

| Member | $P_1 = 1$ | $P_2 = 1$ | $P_3 = 1$ | $P_4 = 1$ | $P_5 = 1$ | $P_6 = 1$ | $P_7 = 1$ | $P_8 = 1$ | $P_9 = 1$ | $P_{10} = 1$ |
|--------|-----------|-----------|-----------|-----------|-----------|-----------|-----------|-----------|-----------|--------------|
| ab | -4.2 | -3.4 | -2.55 | -1.7 | -0.85 | 0.17 | 0.34 | 0.51 | 0.34 | 0.17 |
| bc | -1.7 | -3.4 | -2.55 | -1.7 | -0.85 | -0.34 | 0.34 | 0.51 | 0.34 | 0.17 |
| cd | -0.85 | -1.7 | -2.55 | -1.7 | -0.85 | -1.7 | 0.34 | 0.51 | 0.34 | 0.17 |
| de | -0.85 | -1.7 | -2.55 | -1.7 | -0.85 | -1.7 | -0.34 | -0.51 | 0.34 | 0.17 |
| ef | -0.85 | -1.7 | -2.55 | -3.4 | -1.7 | -1.7 | -0.34 | -0.51 | -0.34 | 0.34 |
| fg | -0.85 | -1.7 | -2.55 | -3.4 | -4.2 | -1.7 | -0.34 | -0.51 | -0.34 | -1.7 |
| gh | 0.83 | 0.17 | 2.5 | 3.3 | 4.1 | 0.16 | 0.33 | 0.5 | 0.33 | 0.16 |
| hi | 0.83 | 0.17 | 2.5 | 3.3 | 4.1 | 0.16 | 0.33 | 0.5 | 0.33 | 0.16 |
| ij | 0.83 | 0.17 | 2.5 | 3.3 | 1.7 | 0.16 | 0.33 | 0.5 | 0.33 | 0.66 |
| jk | 1.7 | 3.3 | 2.5 | 1.7 | 0.83 | 0.33 | 0.66 | 0.5 | 0.66 | 0.83 |
| kl | 4.1 | 3.3 | 2.5 | 1.7 | 0.83 | 0.83 | 0.66 | 0.5 | 0.66 | 0.83 |
| la | 4.1 | 3.3 | 2.5 | 1.7 | 0.83 | 0.83 | 0.66 | 0.5 | 0.66 | 0.83 |
| bl | 0 | 0 | 0 | 0 | 0 | 0 | 0 | 0 | 0 | 0 |
| ck | 0.5 | 0 | 0 | 0 | 0.0 | 0.1 | 0 | 0 | 0 | 0 |
| dj | 0.3 | 0.7 | 0 | 0.7 | 0.3 | 0.06 | 0.13 | 0 | -0.13 | -0.06 |
| ei | 0 | 0 | 0 | 0 | 0.5 | 0 | 0 | 0 | 0 | -0.1 |
| fh | 0 | 0 | 0 | 0 | 0 | 0 | 0 | 0 | 0 | 0 |
| bk | -2.5 | 0 | 0 | 0 | 0 | -0.51 | 0 | 0 | 0 | 0 |
| cj | -0.9 | -1.8 | 0 | 0 | 0 | -0.18 | -0.36 | 0 | 0 | 0 |
| je | 0 | 0 | 0 | -0.18 | 0 | 0 | 0 | 0 | 0.36 | 0.18 |
| if | 0 | 0 | 0 | 0 | -0.9 | 0 | 0 | 0 | 0 | 0.51 |

Part (ii) One can interpret the force influence table as representing the complete set of influence lines for the individual members. We use this data it to draw influence line for member cd.

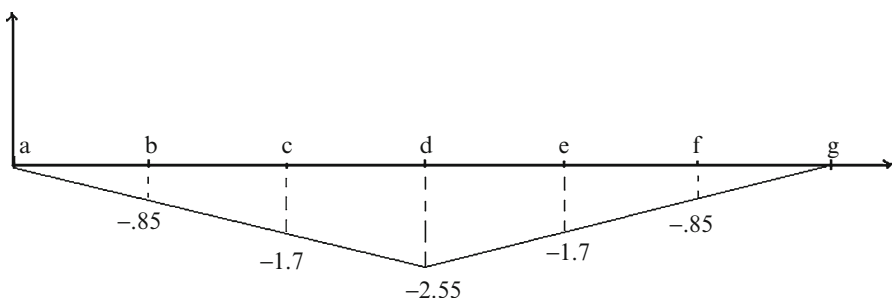


Fig. E2.20d Influence line for member cd—vertical load

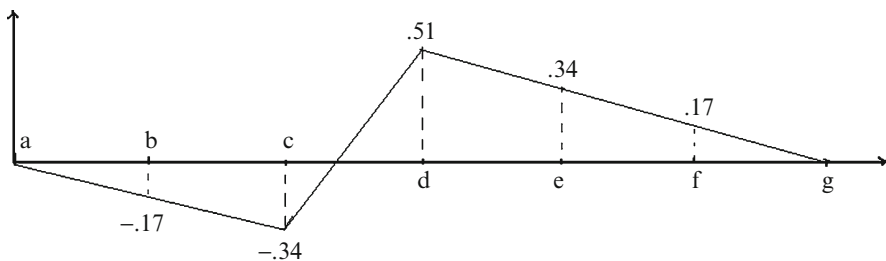


Fig. E2.20e Influence line for member cd—horizontal load

Part (iii) Given an actual wind loading for the upper chord, one scales these force results according to the loading and then combines the scaled results to obtain the member force.

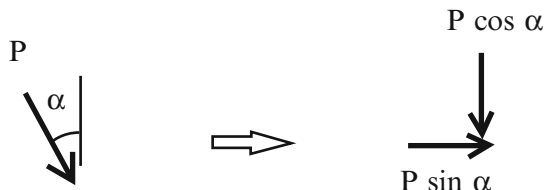


Fig. E2.20f

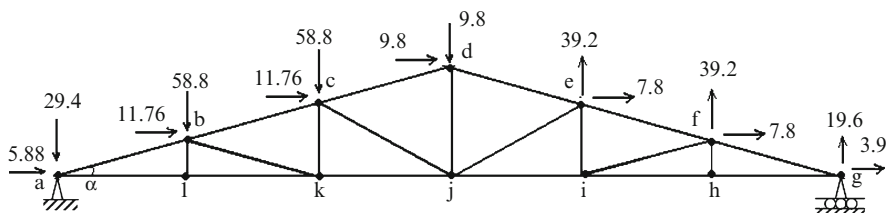
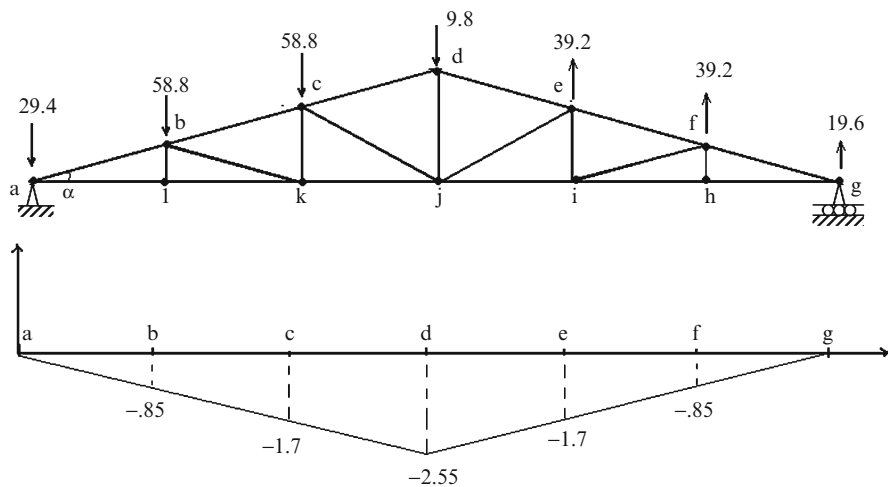
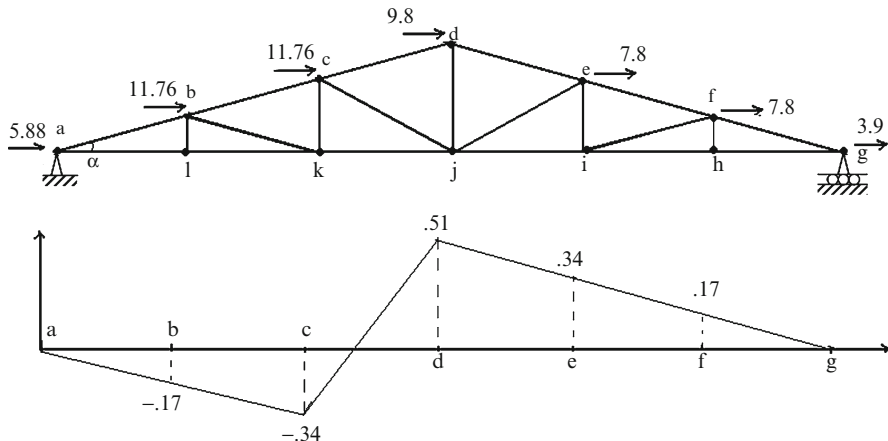


Fig. E2.20g Wind loading

**Fig. E2.20h****Fig. E2.20i**

The corresponding force in member cd is determined as follows:

$$\begin{aligned}
 F_{cd} &= 58.8(-0.85) + 58.8(-1.7) + 9.8(-2.55) - 39.2(-1.7) - 39.2(-0.85) \\
 &\quad + 11.76(-0.17) + 11.76(-0.34) + 9.8(0.51) + 7.8(0.34) + 7.8(0.17) = -72 \\
 \therefore F_{cd} &= 72 \text{ kN Compression}
 \end{aligned}$$

2.5 Analysis of Three-Dimensional Trusses

2.5.1 Introduction

Most structural systems such as highway bridges and roof systems can be considered to be composed of a set of planar trusses. However, there are exceptions, such as towers and domed structures, which cannot be decomposed into planar components and consequently one needs to deal with three-dimensional combinations of members. These structural types are called space structures.

The basic unit for a 3-D space truss is the tetrahedron, a geometrical object composed of 6 members that form 4 triangular faces. Figure 2.30 illustrates this object. We form a 3-D structure by attaching members to existing nodes. Each new node requires 3 members. Provided that the structure is suitably supported with respect to rigid body motion, the displacements that the structure experiences when loaded are due only to deformation of the members.

Space truss structures are used for vertical structures such as towers, and long-span horizontal structures covering areas such as exhibition halls and covered stadiums. They usually are much more complex than simple plane trusses, and therefore more difficult to analyze.

The equilibrium analysis for three-dimensional trusses is similar to that for planar structures except that now there are three force equilibrium equations per node instead of two equations. One can apply either the method of joint or the method of sections. Manual analysis techniques are difficult to apply for large-scale space structures, and one usually resorts to computer-based analysis procedures. Our immediate objectives in this section are to discuss how a space structure needs

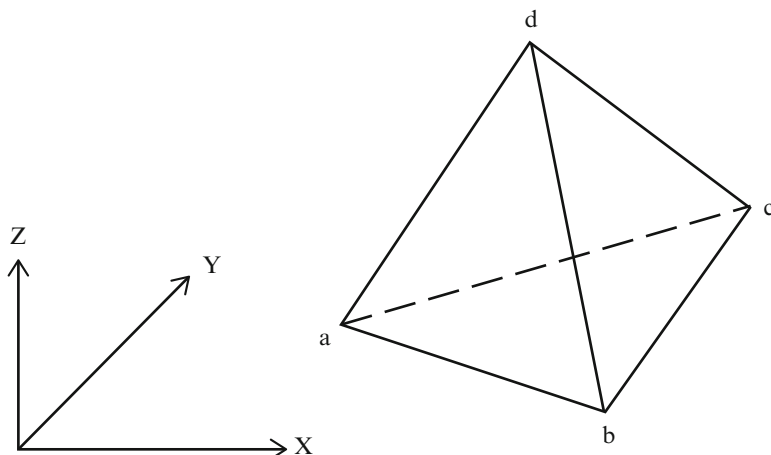


Fig. 2.30 Tetrahedron units for 3-D trusses

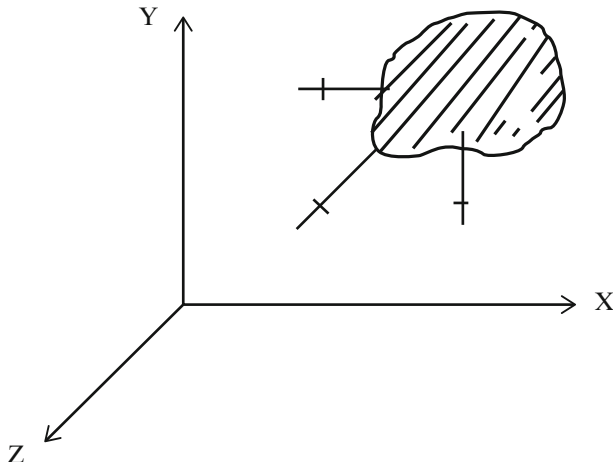


Fig. 2.31 Restraints for a 3-D rigid object

to be restrained in order to prevent rigid body motion, and to illustrate some manual calculations using the methods of joints. We present a computer-based method in the next section.

2.5.2 Restraining Rigid Body Motion

A rigid three-dimensional body requires six motion constraints to be fully constrained; three with respect to translation, and three with respect to rotation. We select an orthogonal reference frame having directions X , Y , and Z . Preventing translation is achieved by constraining motion in the X , Y , and Z directions as illustrated in Fig. 2.31. Even when suitably restrained against translation, the body can rotate and we need to provide additional constraints which eliminate rotation about the X , Y , and Z axes. To prevent rotation about an axis, say the X axis, one applies a translational constraint in a direction which does not pass through X . This rule is used to select three additional constraint directions, making a total of six restraints. If one introduces more than six restraints, the structure is said to be statically indeterminate with respect to the reactions. Various examples illustrating the selection of restraints are listed below (Fig. 2.32).

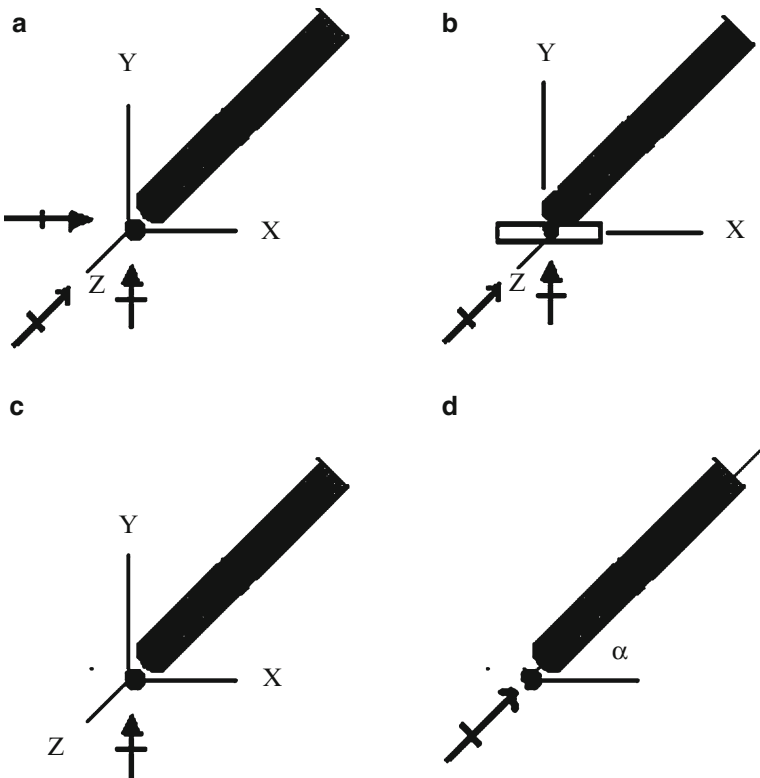


Fig. 2.32 Types of supports for space trusses. (a) Hinge joint. (b) Slotted roller. (c) Roller. (d) Rigid link

Example 2.21 Various restraint schemes

Given: The 3-D truss shown in Fig. E2.21a.

Determine: Possible restraint schemes.

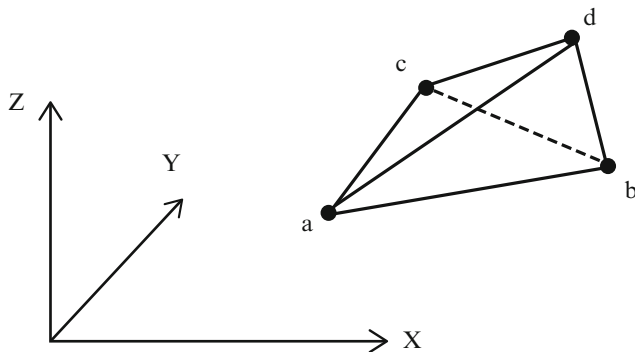


Fig. E2.21a 3-D truss

Solution: The preferred way of displaying 3-D objects is to work with projections on the $X-Y$ and $X-Z$ planes, referred to as the “plan” and “elevation” views. The projections corresponding to the object defined in Fig. E2.21a are shown in Fig. E2.21b.

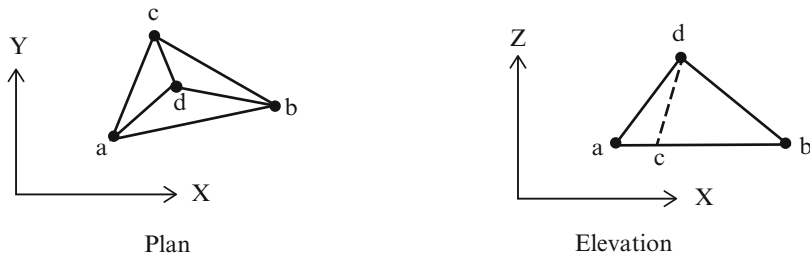


Fig. E2.21b Plan and elevation views

The choice of restraints is not unique. One can employ a 3-D hinge which provides full restraint against translation, or roller type supports which provide restraint against motion in a particular direction. Suppose we place a 3-D hinge at joint a. Then a is “fixed” with respect to translation in the X , Y , and Z directions.

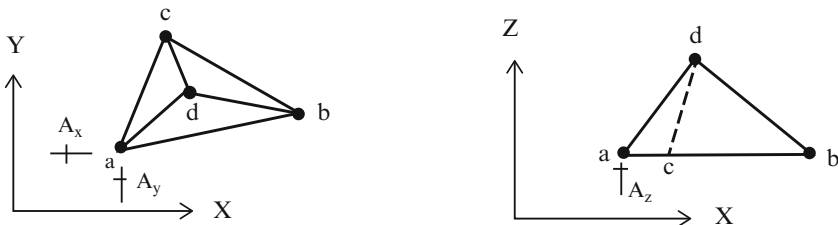


Fig. E2.21c 3-D hinge at a

With these restraints, the body can still rotate about either line a-b or line a-c, or a line parallel to the Z axis through a. The first two modes are controlled with Z restraints applied at b and c. The third node is controlled with either an X or Y restraint applied at either b or c. Figure E2.21d shows the complete set of displacement restraints chosen.

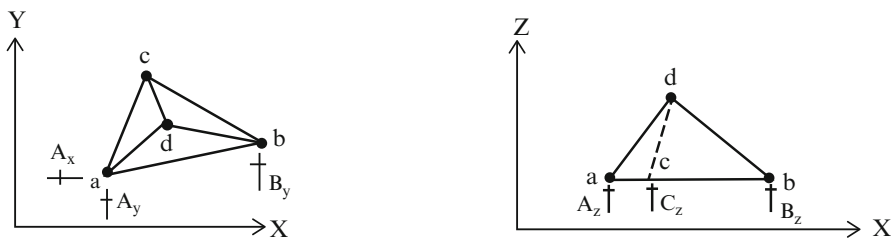


Fig. E2.21d Complete set of restraints

Other possible restraint schemes are shown in Fig. E2.21e–g. Our strategy is to first restrain translation and then deal with the rotation modes.

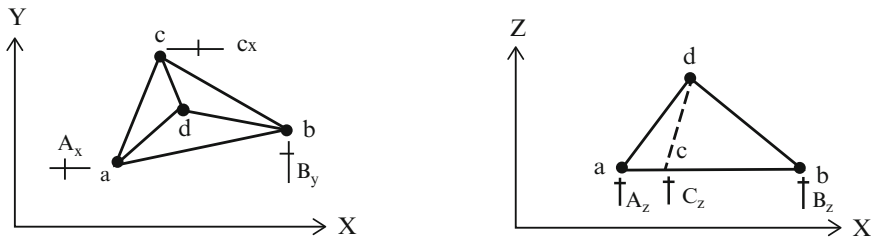


Fig. E2.21e Alternative restraint scheme #1

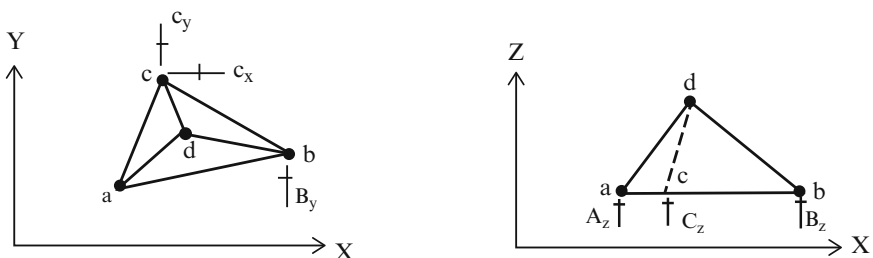


Fig. E2.21f Alternative restraint scheme #2

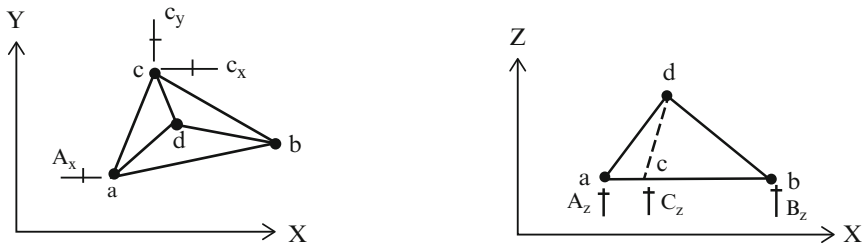


Fig. E2.21g Alternative restraint scheme #3

2.5.3 Static Determinacy

The approach we followed in Sect. 2.2.1 for 2-D Plane trusses is also applicable for 3-D trusses. One just has to include the additional variables associated with shifting from two to three dimensions. Each member of a truss structure has a single force measure, the magnitude of the axial force. However, for 3-D trusses, there are three equilibrium equations per node instead of two for a plane truss. Defining m as the number of members, r as the number of reactions, and j as the number of nodes, it follows that the number of force unknowns and the number of force equilibrium equations available are

$$\begin{aligned} \text{Force Unknowns} &= m + r \\ \text{Force Equilibrium Equations} &= 3j \end{aligned}$$

The structure is statically determinate when $m + r = 3j$. If $m + r > 3j$, there are more force unknowns than available equilibrium equations and the structure is designated as statically indeterminate. Lastly, if $m + r < 3j$, there are less force unknowns than required to withstand an arbitrary nodal loading, and the structure is unstable, i.e., it is incapable of supporting an arbitrarily small loading.

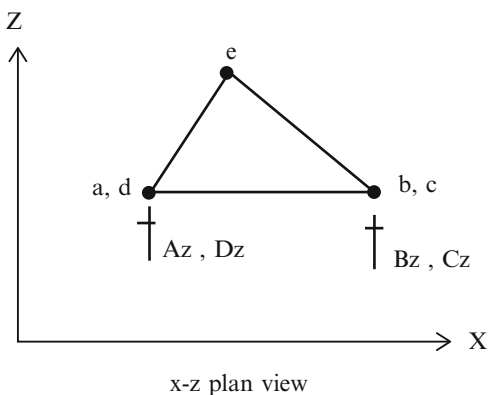
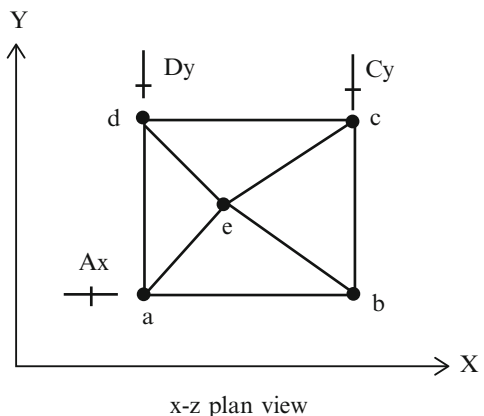
$$m + r = \begin{cases} < 3J & \text{unstable} \\ = 3J & \text{determinate} \\ > 3J & \text{indeterminate} \end{cases}$$

In addition to these criteria, the structure must be suitably restrained against rigid body motion.

Example 2.22 A stable determinate structure

Given: The structure defined in Fig. E2.22a, b.

Fig. E2.22 Plan and elevation views



Determine: The stability

Solution: For the structure shown above, there are eight members, seven reactions, and five joints.

Then

$$m = 8 \quad r = 7 \quad j = 5$$

$m + r \equiv 3j$ and the structure is initially stable.

Example 2.23 An unstable structure

Given: The truss defined in Fig. E2.23a

Determine: The stability

Solution: The number of force unknowns is equal to the number of available force equilibrium equations but the structure has a fundamental flaw. The translation restraints in the X-Y plane are concurrent, i.e., they intersect at a common point, d' , shown in Fig. E2.23b. As a result, the structure cannot resist rotation about a Z axis through d' .

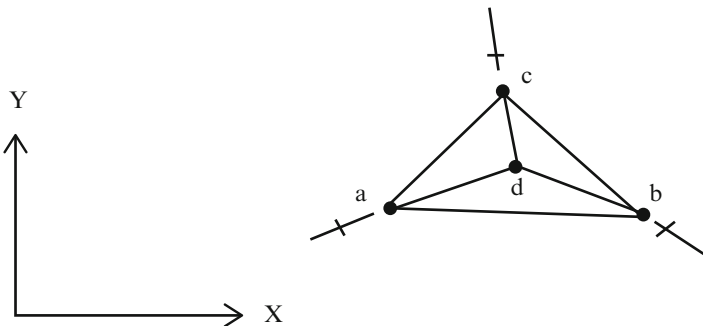


Fig. E2.23a $x-y$ plan view

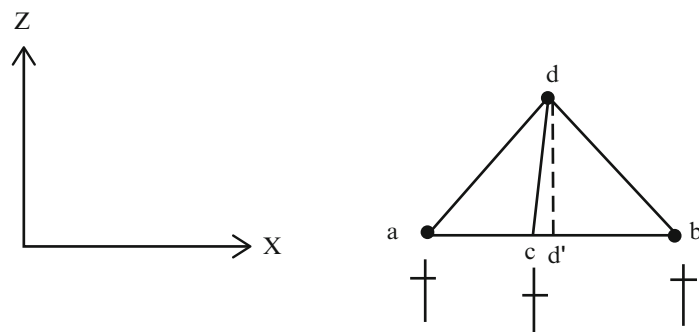


Fig. E2.23b $x-z$ plan view

2.5.4 Method of Joints for 3-D Trusses

Each member of a space truss is assumed to be pinned at its ends to nodes in such a way that there is no bending in the member, only an axial force whose direction coincides with the centroidal axis. The direction of the force is determined by the geometry of the member, so one needs only to determine the magnitude. We find these quantities using force equilibrium equations. Our overall strategy is to first determine the reactions with the global equilibrium conditions. Once the reactions are known, we range over the nodes and establish the nodal force equilibrium equations for each node. This process is similar to the method of joints for Planar Trusses except that now there are three equilibrium equations per node. The member forces are computed by solving the set of nodal force equilibrium equations.

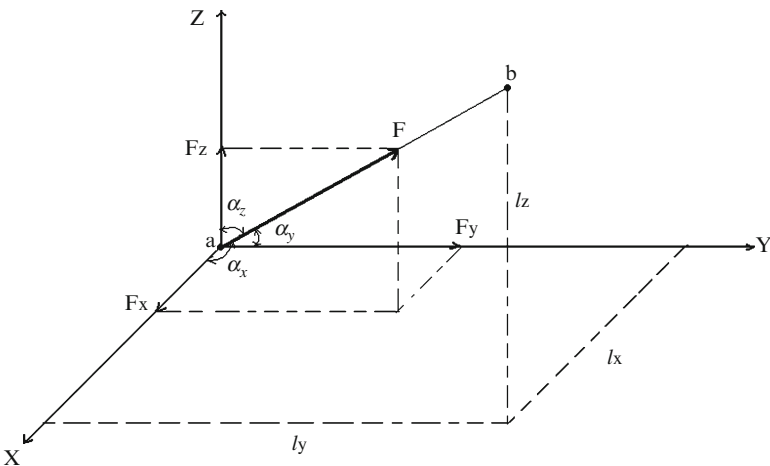


Fig. 2.33 Resolution of a force into its components

Consider the force vector shown in Fig. 2.33. Since the force vector orientation coincides with the direction of the centroidal axis for member ab, the force components are related to the geometric projections of the member length. We resolve the force vector into X , Y , and Z components, and label the components as F_x , F_y , and F_z . Noting the commonality of directions, the force components are related to the force magnitude and geometric projections by

$$\begin{aligned} \frac{F_x}{F} &= \frac{\ell_x}{\ell_{ab}} = \cos \alpha_x = \beta_x \\ \frac{F_y}{F} &= \frac{\ell_y}{\ell_{ab}} = \cos \alpha_y = \beta_y \\ \frac{F_z}{F} &= \frac{\ell_z}{\ell_{ab}} = \cos \alpha_z = \beta_z \end{aligned} \quad (2.16)$$

The coefficients, β_x , β_y , and β_z , are called direction cosines. Given the coordinates of the nodes at each end (a, b), one determines the projection and length using

$$\begin{aligned} l_x &= x_b - x_a \\ l_y &= y_b - y_a \\ l_z &= z_b - z_a \\ l &= \sqrt{l_x^2 + l_y^2 + l_z^2} \end{aligned} \quad (2.17)$$

We are assuming the positive sense of the member is from node a toward node b. These relationships allow one to carry out the equilibrium analysis working initially with the components and then evaluate the force magnitude.

$$F = \sqrt{F_x^2 + F_y^2 + F_z^2} \quad (2.18)$$

We illustrate the analysis process with the following examples. There are many ways to carry out the analysis. Our approach here is based primarily on trying to avoid solving sets of simultaneous equations relating the force magnitudes. However, there are cases where this strategy is not possible.

Example 2.24 Analysis of a tripod structure

Given: The tripod structure shown in Fig. E2.24a, b. The supports at a, b, and c are fully restrained against translation with 3-D hinges.

Determine: The force in each member.

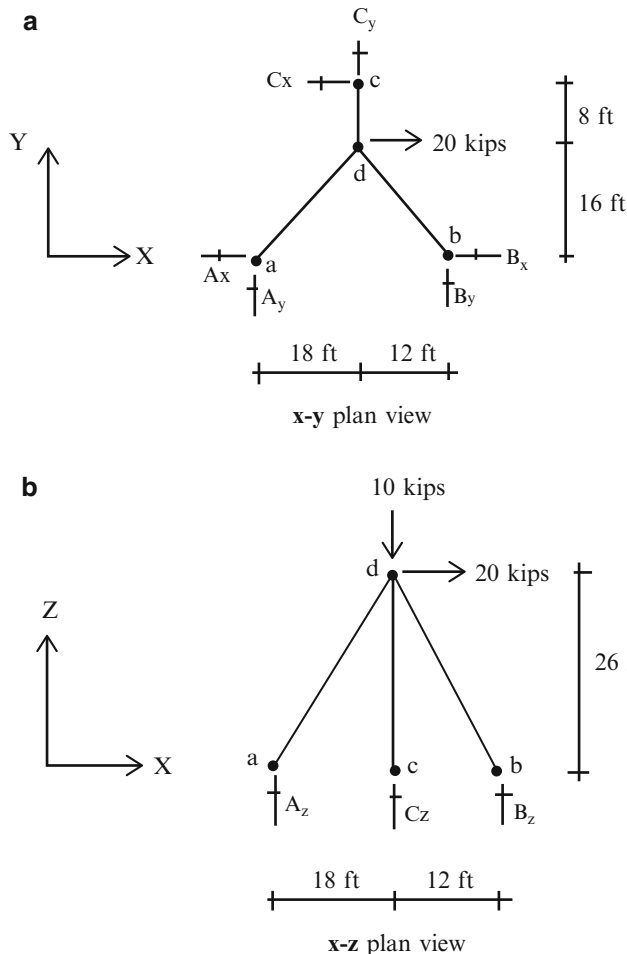


Fig. E2.24 Tripod geometry and supports

Solution: There are three reactions per support, making a total of nine reaction unknowns. Adding the three unknown member forces, raises the total number of force unknowns to 12. Each joint has three force equilibrium equations and there are four joints, so the structure is statically determinate.

The first step is to determine the direction cosines for the members. This data is listed in Table E2.1 below.

We first determine the Z reaction at c by enforcing moment equilibrium about an

Table E2.1

| Member | l_x | l_y | l_z | l | β_x | β_y | β_z |
|--------|-------|-------|-------|------|-----------|-----------|-----------|
| ad | 18 | 16 | 26 | 35.4 | 0.508 | 0.452 | 0.734 |
| bd | -12 | 16 | 26 | 32.8 | -0.366 | 0.488 | 0.793 |
| cd | 0 | -8 | 26 | 27.2 | 0.000 | -0.294 | 0.956 |

X axis through a-b.

$$10(16) - C_z(24) = 0$$

$$C_z = 6.67 \text{ kip } \uparrow$$

The reaction force at c is equal to the z component of the force in member cd. Therefore,

$$F_{cd,z} = -C_z = -6.67$$

$$F_{cd,x} = C_x = 0$$

and

$$C_y = F_{cd,y} = 2.052 \text{ kip } \uparrow$$

$$F_{cd} = -6.98$$

We determine the Y reaction at b by summing moments about the Z axis through a.

$$20(16) + 2.052(18) = 30B_y$$

$$B_y = 11.90 \text{ kip } \uparrow$$

Then,

$$F_{bd,y} = -B_y = -11.90$$

$$F_{bd,x} = \frac{-12}{16}(-11.90) = 8.92 = B_x \leftarrow$$

$$F_{bd,z} = \frac{26}{16}(-11.90) = -19.33$$

$$F_{bd} = -24.39 \text{ (Compression)}$$

Lastly, we sum forces in the Z direction and determine the reaction at A.

$$B_z + C_z + A_z = 10$$

$$A_z = 10 - 26 = -16$$

$$A_z = 16 \text{ kip } \downarrow$$

Then

$$F_{ad,z} = +16 \text{ (Tension)}$$

and

$$F_{ad} = \frac{35.4}{26}(16) = 21.77 \text{ (Tension)}$$

$$A_x = 11.07 \text{ kip } \leftarrow$$

$$A_x = 11.07 \text{ kip } \leftarrow$$

$$A_y = 9.85 \text{ kip } \downarrow$$

We were able to find the member forces working at any time with no more than a single unknown. A more direct but also more computationally intensive approach would be to work with joint d and generate the three force equilibrium equations expressed in terms of the magnitudes of the three member forces. In this approach, we use the direction cosine information listed in Table E2.1 and assume all the member forces are tension. The corresponding force equilibrium equations are

$$\sum F_x = 0 \quad 20 + 0.366F_{bd} - 0.508F_{ad} = 0$$

$$\sum F_y = 0 \quad 0.294F_{cd} - 0.452F_{ad} - 0.488F_{bd} = 0$$

$$\sum F_z = 0 \quad 10 + 0.734F_{ad} + 0.798F_{bd} + 0.956F_{cd} = 0$$

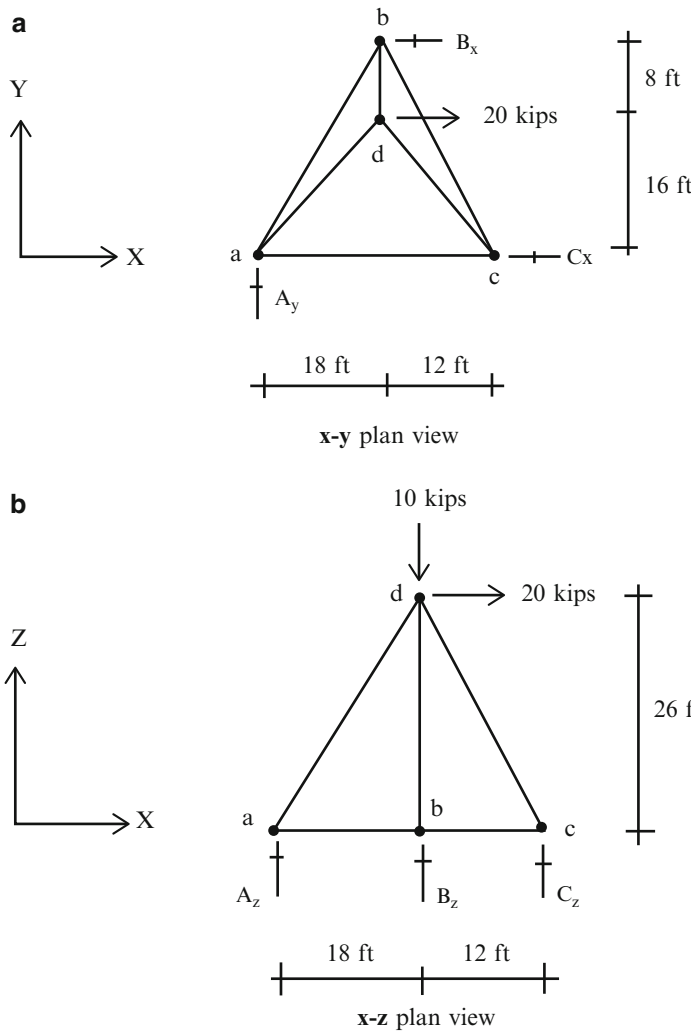
Example 2.25 Analysis of a tetrahedron**Given:** The tetrahedron structure defined in Fig. E2.25a, b.**Determine:** The member forces.**Solution:** There are six reactions (three Z forces, two X forces, and one Y force), six members, and four joints. The determinacy criteria,**Fig. E2.25** Tetrahedron geometry and support

Table E2.2

| Member | l_x | l_y | l_z | l | β_x | β_y | β_z |
|--------|-------|-------|-------|------|-----------|-----------|-----------|
| ab | 18 | 24 | 0 | 30.0 | 0.600 | 0.800 | 0.000 |
| ac | 30 | 0 | 0 | 30.0 | 1.000 | 0.000 | 0.000 |
| bc | 12 | 24 | 0 | 26.8 | 0.447 | 0.895 | 0.000 |
| ad | 18 | 16 | 26 | 25.4 | 0.508 | 0.452 | 0.734 |
| bd | 0 | 8 | 26 | 27.2 | 0.000 | 0.290 | 0.960 |
| cd | 12 | 16 | 26 | 32.8 | 0.366 | 0.488 | 0.793 |

$$3j = m + r \rightarrow 3(4) = 6 + 6$$

is satisfied, so the structure is statically determinate.

We first determine the direction cosines for the members listed in Table E2.2.
Next, we determine the Z reactions at a, b, and c.

$$\sum M_x \text{ at } a=0$$

$$10(16) = 24B_z$$

$$B_z = 6.67 \uparrow$$

$$\sum M_y \text{ at } a=0$$

$$20(26) + 10(18) = 6.67(18) + 30C_z$$

$$C_z = 19.33 \uparrow$$

$$\sum F_z = 0$$

$$19.33 + 6.67 + A_z = 10$$

$$A_z = -16 = 16 \downarrow$$

The Y component at a is determined with: $\Sigma F_y = 0 \therefore A_y = 0$

Then, we enforce $\Sigma M_z = 0$ with respect to a Z axis through a.

$$24B_x = 20(16)$$

$$B_x = 13.34 \leftarrow$$

Lastly, we evaluate C_x

$$\sum F_x = 0 \quad C_x + B_x = 20$$

$$C_x = 6.66 \leftarrow$$

With the reactions known, each of the joints involves only three unknowns, and we can start with any joint. It is most convenient to start with joint c and enforce Z equilibrium.

$$\sum F_z = 0 \quad F_{cd,z} = C_z = 19.33$$

Then

$$F_{cd} = -24.4 \text{ (Compression)}$$

We find F_{cb} by summing Y forces at C .

$$\sum F_y = 0 \quad +F_{cb,y} + F_{cd,y} = 0$$

$$F_{cb,y} = 11.91$$

$$F_{cb} = +13.3 \text{ (Tension)}$$

Then, we find F_{ac} by summing X forces at C .

$$F_{ac} + F_{cb,x} + C_x - F_{cd,x} = 0$$

$$F_{ac} = -3.69 \text{ (Compression)}$$

We move on to joint b. Summing Z forces yields F_{bd}

$$\sum F_z = 0 \quad B_z + F_{bd,z} = 0$$

$$F_{bd,z} = -6.67$$

$$F_{bd} = -6.95 \text{ (Compression)}$$

Summing X (or Y) forces leads to F_{ab}

$$\sum F_x = 0 \quad B_x + F_{ab,x} - F_{cb,x} = 0$$

$$F_{ab,x} = -13.34 + 5.94 = -7.40$$

$$F_{ab} = -12.33 \text{ (Compression)}$$

The last step is to determine F_{ad} by enforcing Z force equilibrium at a.

$$\sum F_z = 0 \quad F_{ad,z} + A_z = 0$$

$$F_{ad,z} = 16$$

$$F_{ad} = +21.8 \text{ (Tension)}$$

We could have solved this problem by establishing the three force equilibrium equations for joint d, and finding F_{ad} , F_{cd} , F_{bd} . Once the reactions are known, we could set up the equations for joints c and b, and solve for the member forces F_{ac} , F_{cb} , and F_{ab} . We follow a different approach to illustrate how one applies the method of joints is a selective manner to a 3-D space truss.

Example 2.26 Displacement computation—3-D truss

Given: The tripod structure defined in Fig. E2.26a, b.

Determine: The displacements at joint d due to loading shown and temperature increase of $\Delta T = 55^{\circ}\text{F}$ for all the members.

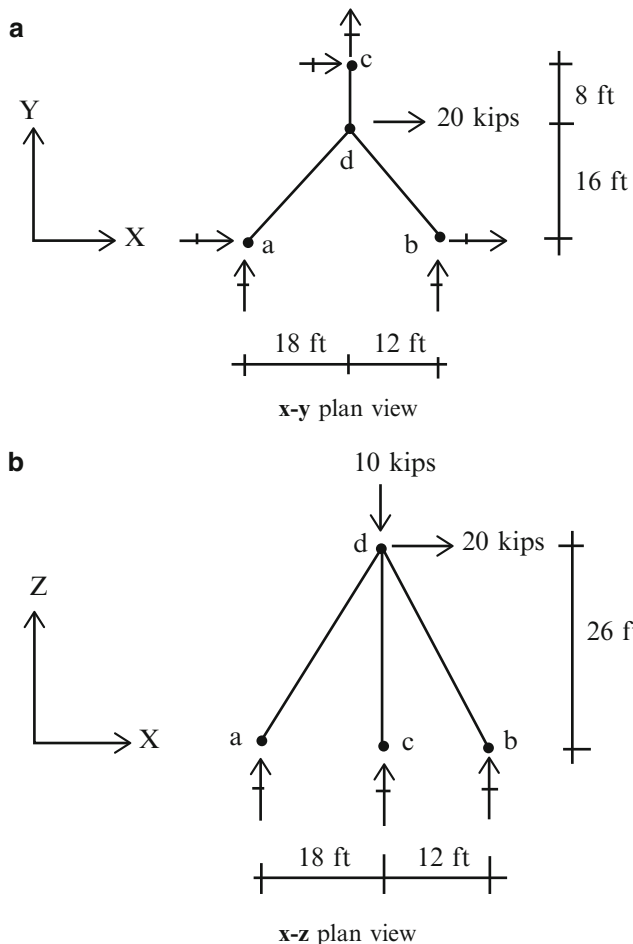


Fig. E2.26 Tripod geometry and supports

Solution: We apply the virtual loads δP_x , δP_y , and δP_z , (see Fig. E2.26c, d) at joint d and determine the corresponding virtual member forces, δF_u , δF_v , and δF_w . The individual displacement components due to loading are determined with:

$$u \ \delta P_x = \sum \frac{Fl}{AE} \ \delta F_u$$

$$v \ \delta P_y = \sum \frac{F\ell}{AE} \ \delta F_v$$

$$w \ \delta P_z = \sum \frac{F\ell}{AE} \ \delta F_w$$

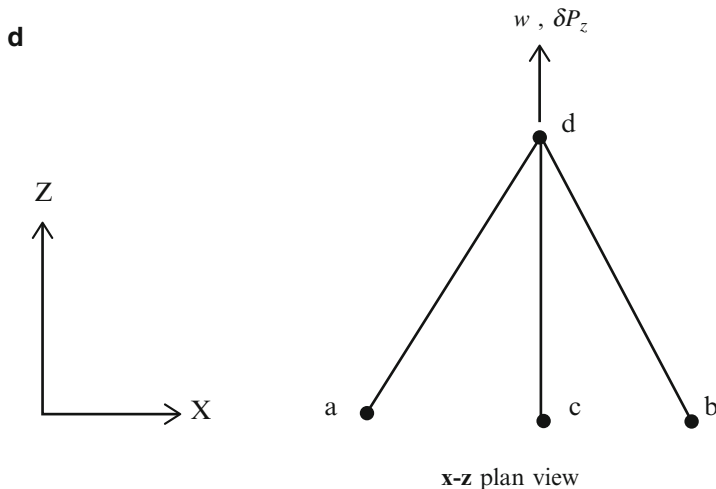
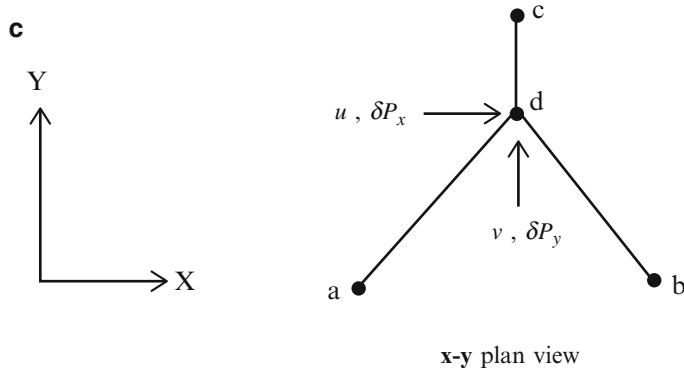


Fig. E2.26 (continued)

For temperature change, we use

$$u \quad \delta P_x = \sum (\alpha \Delta T l) \delta F_u$$

$$v \quad \delta P_y = \sum (\alpha \Delta T l) \delta F_v$$

$$w \quad \delta P_z = \sum (\alpha \Delta T l) \delta F_w$$

The relevant data needed to evaluate these equations is listed below. We use the member forces determined in Example 2.24 and consider a temperature increase of 55 °F. The material properties are $A = 2\text{in}^2 E = 29 \times 10^3 \text{ ksi}$ and $\alpha = 6.6 \times 10^{-6}/\text{°F}$. Note that we need to shift length units over to inches when computing $F\ell/AE$.

| Member | l (ft) | A (in^2) | F | For $\delta P = 1.0$ | | | $\frac{F\ell}{AE}$ (in) | $\alpha l \Delta T$ (in) |
|--------|----------|-----------------------|--------|----------------------|--------------|--------------|-------------------------|--------------------------|
| | | | | δF_u | δF_v | δF_w | | |
| ad | 35.4 | 2.0 | 21.77 | 1.18 | 0.59 | 0.18 | 0.160 | 0.154 |
| bd | 32.8 | 2.0 | -24.39 | -1.09 | 0.82 | 0.25 | -0.165 | 0.143 |
| cd | 27.2 | 2.0 | -6.98 | 0.00 | -1.13 | 0.69 | -0.039 | 0.118 |

The displacements due to loads are

$$u = \sum \frac{Fl}{AE} \delta F_u = (0.160)(1.18) + (-0.165)(-1.09) = 0.37 \text{ in.}$$

$$\begin{aligned} v &= \sum \frac{Fl}{AE} \delta F_v = (0.160)(0.59) + (-0.165)(0.82) + (-0.039)(-1.13) \\ &= 0.0032 \text{ in.} \end{aligned}$$

$$\begin{aligned} w &= \sum \frac{Fl}{AE} \delta F_w = (0.160)(0.18) + (-0.165)(0.25) + (-0.039)(0.69) \\ &= -0.0394 \text{ in.} \end{aligned}$$

A 55 °F temperature increase produces the following displacements:

$$u = \sum (\alpha \Delta T l) \delta F_u = (0.154)(1.18) + (0.143)(-1.09) = 0.026 \text{ in.}$$

$$v = \sum (\alpha \Delta T l) \delta F_v = (0.154)(0.59) + (0.143)(0.82) + (0.118)(-1.13) = 0.075 \text{ in.}$$

$$w = \sum (\alpha \Delta T l) \delta F_w = (0.154)(0.18) + (0.143)(0.25) + (0.118)(0.69) = 0.145 \text{ in.}$$

2.6 Matrix Formulation: Equilibrium Analysis of Statically Determinate 3-D Trusses

Manual techniques are easy to apply for simple geometries, but become more difficult with increasing geometric complexity. The equilibrium analysis approaches described in the previous sections can be formulated as a sequence of matrix operations which can be readily automated for computer-based analysis. In what follows, we describe one approach for the equilibrium analysis of statically determinate 3-D trusses. We present a more general matrix formulation later in Chap. 12.

2.6.1 Notation

A truss is an assembly of nodes that are interconnected with members. It is convenient to define the geometry with respect to a global Cartesian coordinate system, X Y Z , and number the nodes and members sequentially. Figure 2.34 illustrates this scheme. The structure has four nodes and six members.

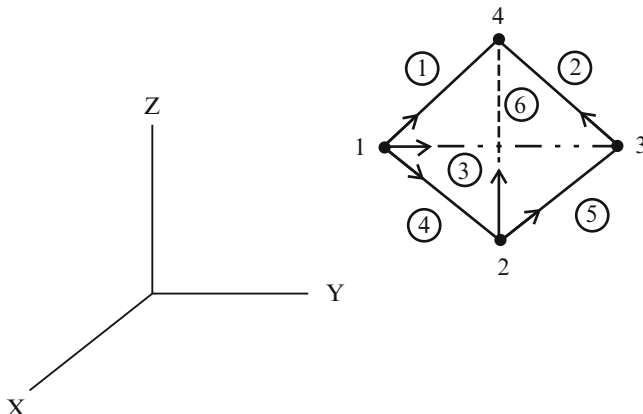
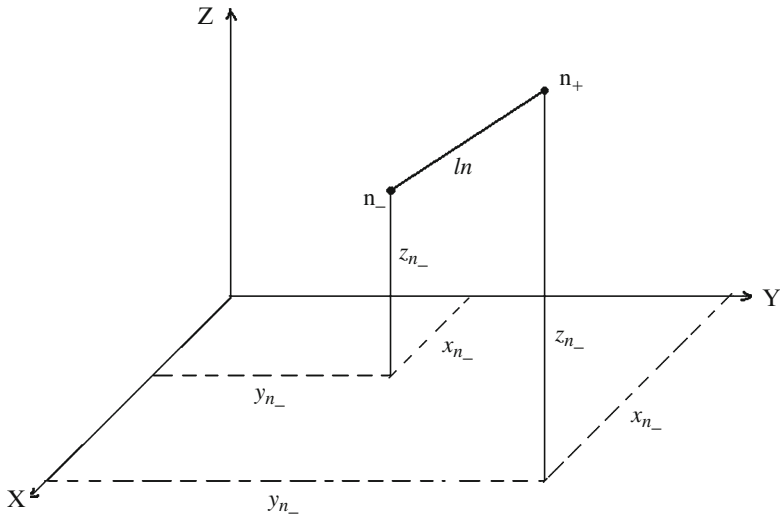


Fig. 2.34

We assume a positive sense for each member and define the direction cosines consistent with the assumed sense. The positive and negative nodes for member n are denoted as n_+ and n_- . Noting (2.16) and (2.17), the direction cosines for member n are determined using

$$\begin{aligned}\frac{x_{n_+} - x_{n_-}}{l_n} &= \beta_{n_x} \\ \frac{y_{n_+} - y_{n_-}}{l_n} &= \beta_{n_y} \\ \frac{z_{n_+} - z_{n_-}}{l_n} &= \beta_{n_z}\end{aligned}\quad (2.19)$$

**Fig. 2.35**

It is convenient to introduce matrix notation at this point (Fig. 2.35). We define the nodal coordinate matrix for node j as

$$\mathbf{x}_j = \begin{Bmatrix} x_j \\ y_j \\ z_j \end{Bmatrix} \quad (2.20)$$

and the direction cosine matrix for member n as β_n .

$$\beta_n = \begin{Bmatrix} \beta_{nx} \\ \beta_{ny} \\ \beta_{nz} \end{Bmatrix} \quad (2.21)$$

With this notation, the matrix form of (2.19) is

$$\beta_n = \frac{1}{l_n} (\mathbf{x}_{n+} - \mathbf{x}_{n-}) \quad (2.22)$$

where

$$l_n^2 = (\mathbf{x}_{n+} - \mathbf{x}_{n-})^T (\mathbf{x}_{n+} - \mathbf{x}_{n-})$$

2.6.2 Member–Node Incidence

The computation of the direction cosines can be automated using the topological data for the members and nodes. This data is represented in tabular form. One lists, for each member, the node numbers for the positive and negative ends of the member. It is commonly referred to as the member–node incidence table. The table corresponding to the structure defined in Fig. 2.34 is listed below. One loops over the members, extracts the nodal coordinates from the global coordinate vector, executes the operation defined by (2.22), and obtains the member direction cosine matrix, β .

| Member | Negative mode | Positive mode1 |
|--------|---------------|----------------|
| 1 | 1 | 4 |
| 2 | 3 | 4 |
| 3 | 1 | 3 |
| 4 | 1 | 2 |
| 5 | 2 | 3 |
| 6 | 2 | 4 |

2.6.3 Force Equilibrium Equations

The force vector for a member points in the positive direction of the member, i.e., from the negative end toward the positive end. Noting (2.16), the set of Cartesian components for member n are listed in the matrix, \mathbf{P}_n , which is related to β_n by

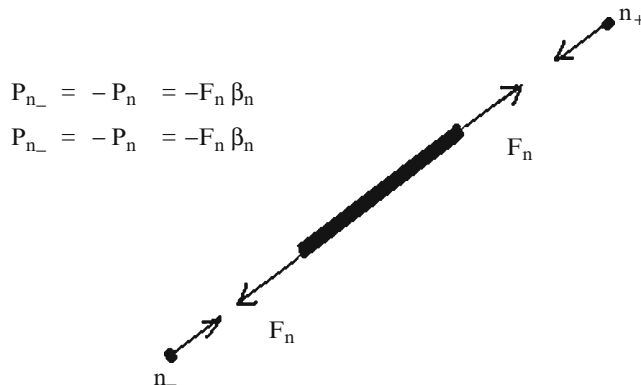
$$\mathbf{P}_n = \begin{Bmatrix} F_x \\ F_y \\ F_z \end{Bmatrix} = F_n \beta_n \quad (2.23)$$

The force components acting on the nodes at the ends of the member are equal to $\pm \mathbf{P}_n$. Figure 2.36 illustrates this distribution.

We generate the set of force equilibrium equations for a node by summing the force matrices acting on the node. Consider node l . Let \mathbf{P}_l be the external force matrix for node l . The matrix equation for node l involves the member force matrices for those members which are positive incident and negative incident on node l .

$$\mathbf{P}_l = \sum_{n_+=l} F_n \beta_n + \sum_{n_-=l} -F_n \beta_n \quad (2.24)$$

This step is carried out for each node. Equation (2.24) requires i scalar equations where $i = 2$ for a plane truss and $i = 3$ for a space truss. We assemble the complete

**Fig. 2.36**

set of equations in partitioned form, taking blocks of i rows. Assuming j nodes and m members, the equations are written as.

$$\mathbf{P}' = \mathbf{B}'\mathbf{F} \quad (2.25)$$

where the dimensions of the global matrices are

$$\mathbf{B}' = (i \text{ times } j) \times m, \quad \mathbf{F} = m \times 1, \quad \mathbf{P}' = (i \text{ times } j) \times 1$$

The algorithms for generating \mathbf{P}' and \mathbf{B}' are

$$\begin{aligned} & \text{For member } n \ (n = 1, 2, \dots, m) \\ & + \beta_n \text{ in partitioned row } n_+, \text{ column } n \\ & - \beta_n \text{ in partitioned row } n_-, \text{ column } n \end{aligned} \left. \right\} \text{of } \mathbf{B}' \quad (2.26)$$

For node l ($l = 1, 2, \dots, j$)
External load P_l in partitioned row l of \mathbf{P}'

These operations can be easily implemented using spread sheet software. The required size of the spread sheet is i times j rows and $m + 1$ columns, (m columns for the member forces and one column for the external nodal loads). Applying (2.26) to the structure shown in Fig. 2.34 and noting the incidence table leads to the following form of \mathbf{B}' .

| | F_1 | F_2 | F_3 | F_4 | F_5 | F_6 | |
|--------|------------|------------|------------|------------|------------|------------|---------|
| Node 1 | $-\beta_1$ | | $-\beta_3$ | $-\beta_4$ | | | + i row |
| Node 2 | | | | $+\beta_4$ | $-\beta_5$ | $-\beta_6$ | |
| Node 3 | | $-\beta_2$ | $+\beta_3$ | | $+\beta_5$ | | |
| Node 4 | $+\beta_1$ | $+\beta_2$ | | | | $+\beta_6$ | |

Certain joint loads correspond to the r reactions which are not initially known. We separate out the rows in \mathbf{B}' and \mathbf{P}' corresponding to the r reactions, resulting in (i times $(j-r)$) rows relating the m force unknowns. The reduced set of equations is expressed as (we drop the prime superscript on β and P to simplify the equation)

$$\mathbf{P} = \mathbf{B} \mathbf{F} \quad (2.27)$$

When the structure is statically determinate, $m = i$ times $(j - r)$, and since the coefficient matrix \mathbf{B} is now square, one can solve for \mathbf{F} . We used a similar approach when discussing complex planar trusses in Sect. 2.2.

2.6.4 Stability

A structure is said to be stable when a unique solution for the member forces exist for a given set of external loads. The relationship between the loading and the resulting member forces is defined by the linear matrix equation, (2.27). Noting Cramer's rule [26], the stability requirement can be expressed as

$$\text{determinant}(\mathbf{B}) \neq 0 \quad (2.28)$$

which is equivalent to requiring \mathbf{B} to be nonsingular. Singularity can be due to an insufficient number or improper orientation of the restraints. It may also arise due to the geometrical pattern of the members. Complex trusses, such as the example discussed in Sect. 2.2, may exhibit this deficiency even though they appear to be stable.

2.6.5 Matrix Formulation: Computation of Displacements

The manual process described in the previous section for computing displacements is not suited for large-scale structures. We faced a similar problem with the analysis of space trusses, and in that case, we resorted to a computer-based scheme.

We follow a similar strategy here. We utilize the matrix notation introduced earlier, and just have to define some additional terms related to deformation and nodal displacement.

Noting (2.11), we see that e involves the direction cosines for the member, and the nodal displacements. Using the notation for the direction cosine matrix defined by (2.15) and also defining \mathbf{u} as the nodal displacement matrix,

$$\begin{aligned}\beta &= \{\beta_x, \beta_y, \beta_z\} \\ \mathbf{u} &= \{u, v, w\}\end{aligned}\quad (2.29)$$

we express the extension e as a matrix product.

$$e = \beta^T \mathbf{u} \quad (2.30)$$

We generalize (2.30) for member n connected to nodes n_+ and n_-

$$e_n = \beta_n^T (\mathbf{u}_{n+} - \mathbf{u}_{n-}) \quad (2.31)$$

Note that this matrix expression applies to both 2-D and 3-D structures.

Following the strategy used to assemble the matrix force equilibrium equations, we assemble the complete set of deformation–displacement relations for the structure. They have the following form

$$\mathbf{e} = (\mathbf{B}')^T \mathbf{U}' \quad (2.32)$$

where

$$\mathbf{U}' = \{u_1, u_2, \dots, u_j\}, \mathbf{e} = \{e_1, e_2, \dots, e_m\}$$

and \mathbf{B}' is defined by (2.20). Note that \mathbf{B}' is the matrix associated with the matrix force equilibrium equations (2.19). Some of the nodal displacements correspond to locations where constraints are applied and their magnitudes are known. When the structure is statically determinate, support movement introduces no deformation, and we can delete these terms from \mathbf{U}' . We also delete the corresponding rows of \mathbf{B}' . These operations lead to the modified equation

$$\mathbf{e} = \mathbf{B}^T \mathbf{U} \quad (2.33)$$

Note that the corresponding modified equilibrium equations have the form $\mathbf{P} = \mathbf{B} \mathbf{F}$.

The duality between these equations is called the “Static-Geometric” analogy. Once \mathbf{F} is known, one determines the extension of a member using

$$e = \left(\frac{L}{AE} \right) F + e_I$$

where \mathbf{e}_I contains terms due to temperature and fabrication error. We express the set of deformations in matrix form

$$\mathbf{e} = \mathbf{f} \mathbf{F} + \mathbf{e}_I \quad (2.34)$$

where \mathbf{f} is a diagonal matrix containing the flexibility coefficients for the members,

$$\mathbf{f} = \begin{bmatrix} \left(\frac{L}{AE}\right)_1 & & \\ & \left(\frac{L}{AE}\right)_2 & \\ & & \left(\frac{L}{AE}\right)_m \end{bmatrix} \quad (2.35)$$

Given \mathbf{P} , one generates \mathbf{B} and, solves for \mathbf{F} ,

$$\mathbf{F} = \mathbf{B}^{-1} \mathbf{P} \quad (2.36)$$

Then we compute \mathbf{e} with (2.34) and lastly solve for \mathbf{U} using,

$$\mathbf{U} = (\mathbf{B}^{-1})^T \mathbf{e} \quad (2.37)$$

This approach can be represented as a series of computer operations. The major computational effort is in assembling and inverting \mathbf{B} . The deflection computation requires minimal additional effort since one needs to compute \mathbf{B}^{-1} in order to determine the member forces.

Using matrix notation, it is relatively straight forward to prove the validity of the Method of Virtual Forces. We apply a virtual force $\delta\mathbf{P}'$ and find the corresponding virtual forces using the matrix equilibrium equations.

$$\delta\mathbf{P}' = \mathbf{B}' \delta\mathbf{F} \quad (2.38)$$

Member forces which satisfy the force equilibrium equations are said to be statically permissible. Note that $\delta\mathbf{P}'$ includes both the external nodal loads and the reactions. The extensions are related to the nodal displacements by (2.32)

$$\mathbf{e} = (\mathbf{B}')^T \mathbf{U}' \quad (2.38a)$$

where \mathbf{U}' contains both the nodal displacements and support movements. We multiply (2.38a) by $\delta\mathbf{F}^T$,

$$\delta\mathbf{F}^T \mathbf{e} = \delta\mathbf{F}^T [(\mathbf{B}')^T \mathbf{U}'] \quad (2.38b)$$

and note the identity,

$$\delta\mathbf{F}^T (\mathbf{B}')^T \equiv [\mathbf{B}' \delta\mathbf{F}]^T \equiv (\delta\mathbf{P}')^T \quad (2.39)$$

Then, (2.38b) takes the form

$$\delta \mathbf{F}^T \mathbf{e} = (\delta \mathbf{P}')^T \mathbf{U}' \quad (2.40)$$

Separating out the prescribed support displacements and reactions, and expanding the matrix products leads to the scalar equation

$$\sum \delta F \cdot e = \sum \delta P \cdot u + \sum \delta R \cdot \bar{u} \quad (2.41)$$

The final form follows when δP is specialized as a single force.

Example 2.27 Planar complex truss

Given: The planar structure shown in Fig. E2.27. Assume equal cross-sectional areas.

Determine:

- (a) The displacements at the nodes. Take $A = 10 \text{ in.}^2$ and $E = 29,000 \text{ ksi}$.
- (b) The value of A required to limit the horizontal displacement to 1.5 in.

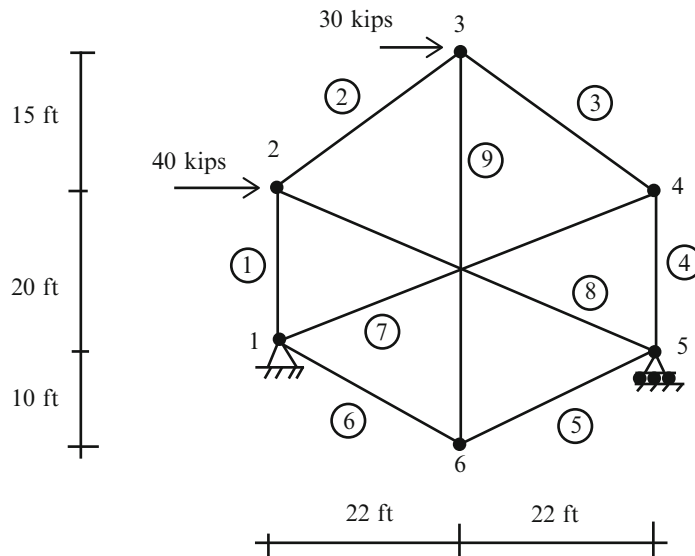


Fig. E2.27

Solution: This truss is a complex truss similar to example discussed in Sect. 2.2.5. One needs to solve the complete set of force equilibrium equations to find the member forces. Therefore, applying the Method of Virtual Forces is not computationally advantageous in this case, so we use a computer-based scheme. The computer method presented above is applicable for both planar and 3-D trusses.

We just need to take $i = 2$ for the planar case. The results for the nodal displacements are listed below.

$$\begin{cases} u_1 = 0 \\ v_1 = 0 \\ u_2 = 4.88 \text{ in.} \\ v_2 = 0.13 \text{ in.} \\ u_3 = 2.34 \text{ in.} \\ v_3 = 4.15 \text{ in.} \\ u_4 = -0.27 \text{ in.} \\ v_4 = 0.09 \text{ in.} \\ u_5 = 4.42 \text{ in.} \\ v_5 = 0 \\ u_6 = 2.2 \text{ in.} \\ v_6 = 4.43 \text{ in.} \end{cases}$$

The area required to limit the maximum displacement to 1.5 in. is

$$A_{\text{required}} = (10) \frac{4.88}{1.5} = 32.53 \text{ in.}^2$$

The revised nodal displacements for $A = 32.53 \text{ in.}^2$ will be

$$\begin{cases} u_1 = 0 \\ v_1 = 0 \\ u_2 = 1.5 \text{ in.} \\ v_2 = 0.04 \text{ in.} \\ u_3 = 0.72 \text{ in.} \\ v_3 = 1.27 \text{ in.} \\ u_4 = -0.08 \text{ in.} \\ v_4 = 0.03 \text{ in.} \\ u_5 = 1.36 \text{ in.} \\ v_5 = 0 \\ u_6 = 0.68 \text{ in.} \\ v_6 = 1.36 \text{ in.} \end{cases}$$

Example 2.28 Space truss

Given: The space structure shown in Fig. E2.28. Assume equal cross-sectional areas. Take $A = 1,300 \text{ mm}^2$ and $E = 200 \text{ GPa}$.

Determine: The member forces, the reactions, and the nodal displacements.

Solution: The joint displacements, the member forces, and the reactions are listed below.

Joint displacements:

$$\begin{aligned} \text{Joint 1} & \left\{ \begin{array}{l} u_1 = 0 \\ v_1 = 4.9 \text{ mm} \\ w_1 = 0 \end{array} \right. \\ \text{Joint 2} & \left\{ \begin{array}{l} u_2 = 0 \\ v_2 = 3.5 \text{ mm} \\ w_2 = 0 \end{array} \right. \\ \text{Joint 3} & \left\{ \begin{array}{l} u_3 = -1.3 \text{ mm} \\ v_3 = 0 \\ w_3 = 0 \end{array} \right. \\ \text{Joint 4} & \left\{ \begin{array}{l} u_4 = 4.5 \text{ mm} \\ v_4 = 8.9 \text{ mm} \\ w_4 = -2.2 \text{ mm} \end{array} \right. \end{aligned}$$

Member forces and reactions:

$$\begin{cases} F_{(1)} = -37.47 \text{ kN} \\ F_{(2)} = 76.94 \text{ kN} \\ F_{(3)} = -38.66 \text{ kN} \\ F_{(4)} = 68.26 \text{ kN} \\ F_{(5)} = -128.27 \text{ kN} \\ F_{(6)} = -9.05 \text{ kN} \end{cases} \quad \begin{cases} R_{1x} = 26.67 \text{ kN} \\ R_{1z} = -50.37 \text{ kN} \\ R_{2x} = -66.67 \text{ kN} \\ R_{2z} = 123.33 \text{ kN} \\ R_{3y} = -60.00 \text{ kN} \\ R_{3z} = 7.04 \text{ kN} \end{cases}$$

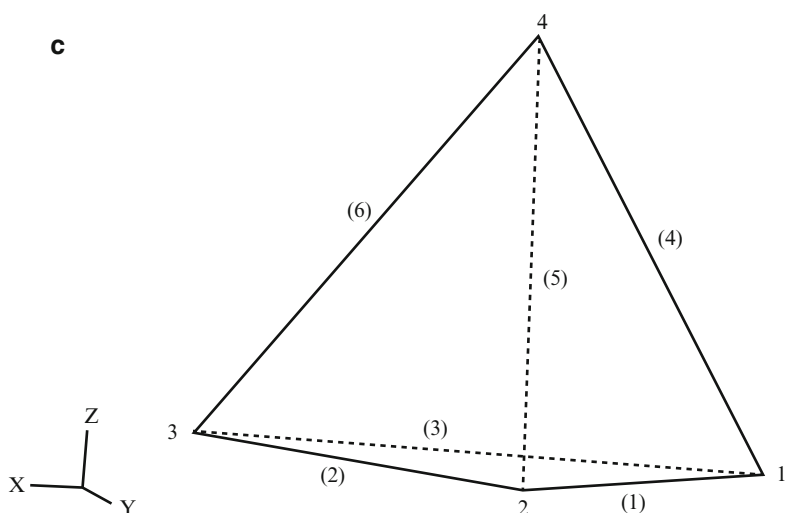
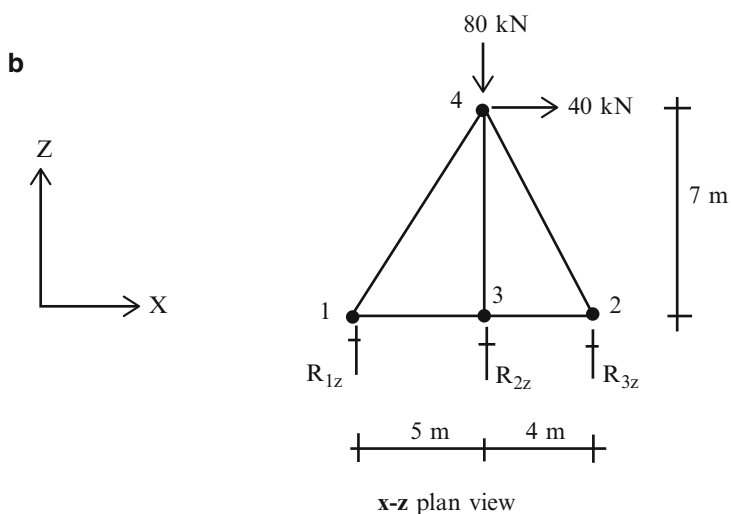
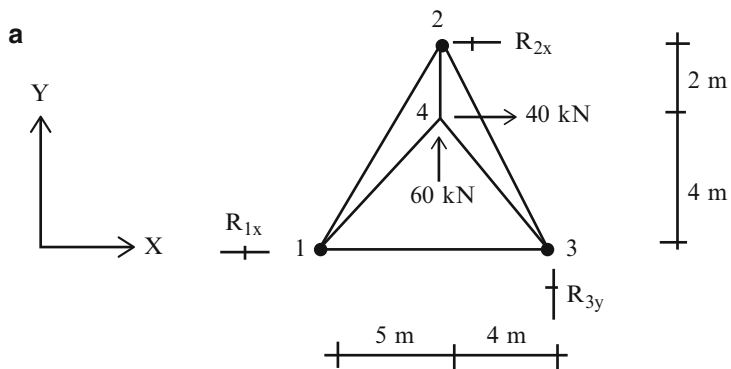


Fig. E2.28

2.7 Summary

2.7.1 Objectives of the Chapter

- To develop a criteria for assessing the initial stability of truss type structures
- To present methods for determining the axial forces in the members of statically determinate trusses
- To present a matrix-based formulation for the analyses of arbitrary statically determinate trusses
- To present methods for computing the displaced configuration of a truss
- To introduce the concept of an influence line and illustrate its application to trusses

2.7.2 Key Facts and Concepts

- The statical determinacy of a plane truss is determined by comparing the number of unknown forces vs. the number of available force equilibrium equations.
- The forces in the members of a statically determinate truss are independent of the member properties such as area and material modulus and support movements.
- The two force analysis procedures are the method of joints and the method of sections. The method of joints strategy proceeds from joint to joint, always working with a joint having a statically determinate force system. This approach generates all the member forces. The method of sections is designed to allow one to determine the force in a particular member. One passes a cutting plane through the structure, selects either segment, and applies the equilibrium conditions. This method requires less computation and generally is easier to apply.
- Given the external loads, one can determine the internal member forces using force equilibrium equations when the truss is statically determinate. The displacements due to the loading can be computed manually using the method of virtual forces. To determine the displacement at a point A in a particular direction, d_a , one applies a virtual force δP_a at point A in the same direction as the desired displacement and computes, using static equilibrium equations, the internal forces δF , and reactions, δR , due to δP_a . The displacement is given by

$$d_a \delta P_a = \sum_{\text{members}} e \delta F - \sum_{\text{reactions}} \bar{d} \delta R$$

where \bar{d} is the prescribed support movement and e is the elongation of the member due to force, temperature change, and initial fabrication error.

$$e = \left(\frac{L}{AE} \right) F + (\alpha \Delta T)L + e_0$$

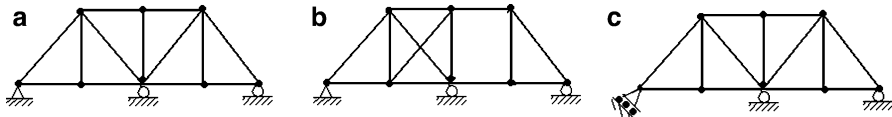
This method is restricted to static loading and small displacements. It is also applicable for statically indeterminate trusses when the member forces are known.

- The concept of influence lines is very useful for dealing with the live loading which can act anywhere on the structure. Given a particular member force and a particular type of live loading, usually a unit vertical loading, the influence line displays graphically the magnitude of the force for various locations of the load. By viewing the plot, one can immediately determine the position of the load that produces the peak magnitude of the member force.

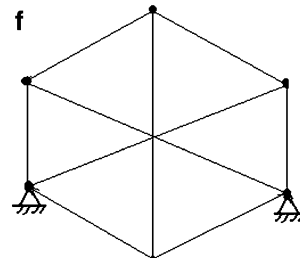
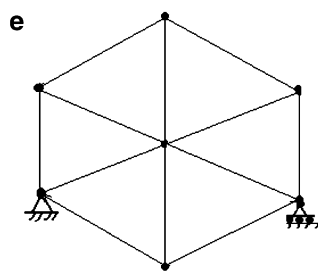
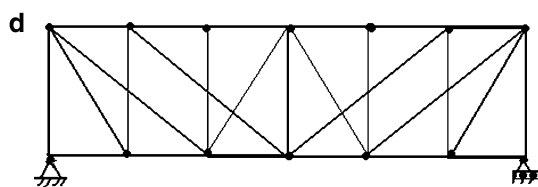
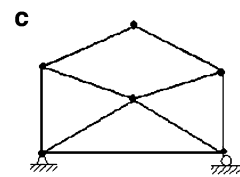
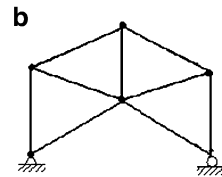
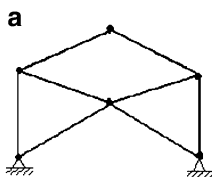
2.8 Problems

Classify each of the following plane trusses defined in Problems 2.1–2.4 as initially stable or unstable. If stable, then classify them as statically determinate or indeterminate. For indeterminate trusses, determine the degree of static indeterminacy.

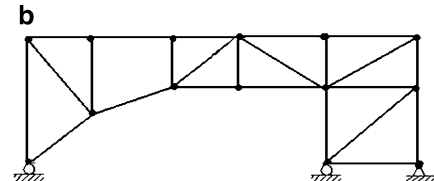
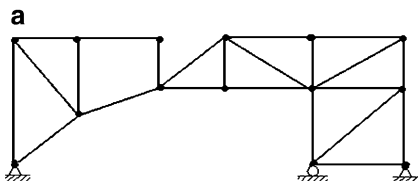
Problem 2.1

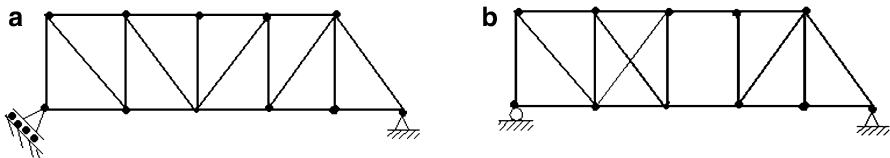


Problem 2.2

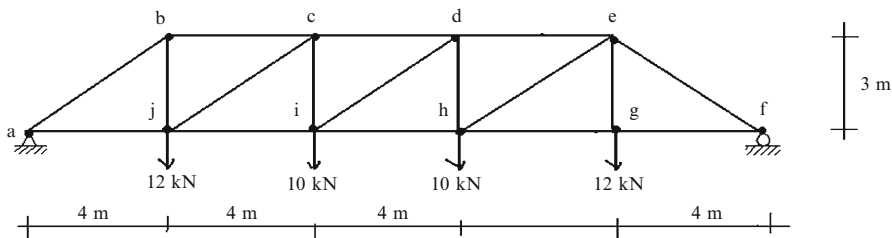
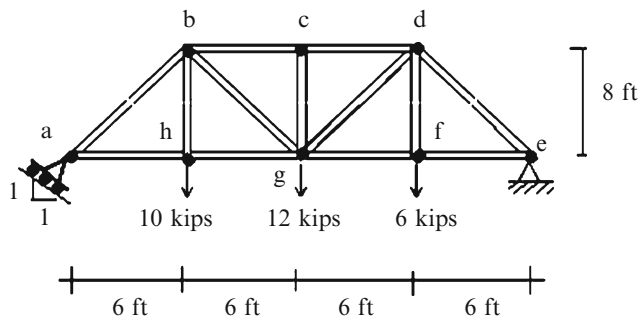


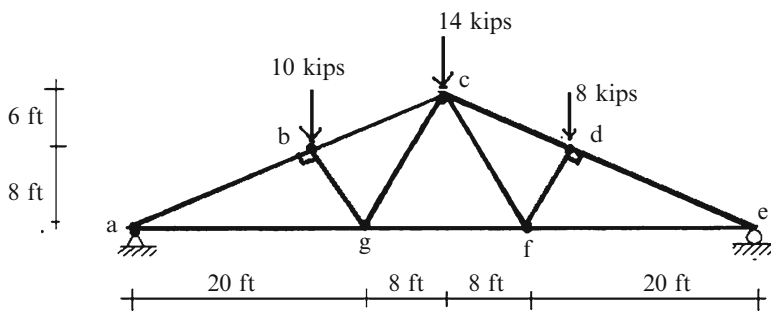
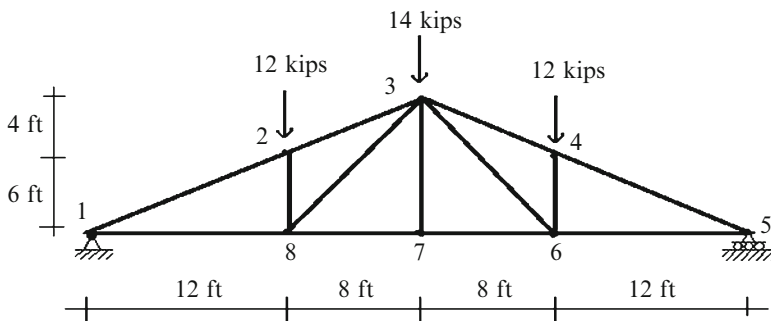
Problem 2.3

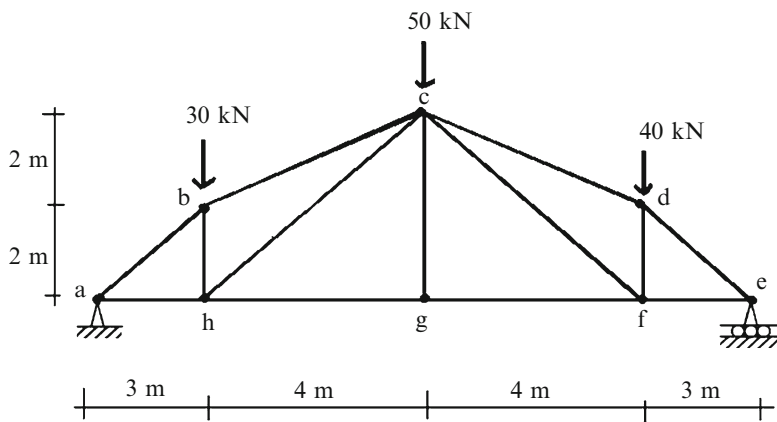
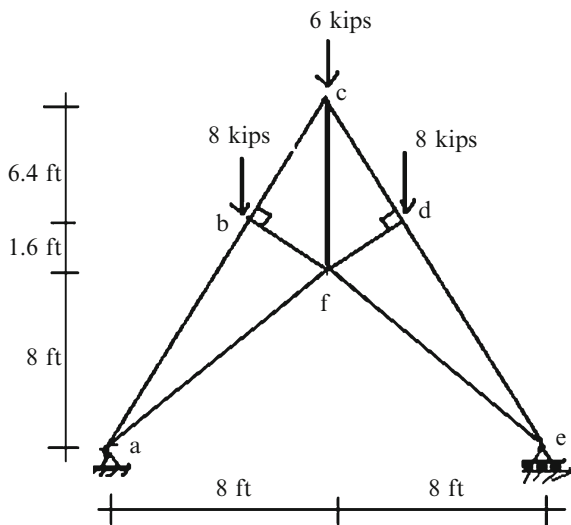


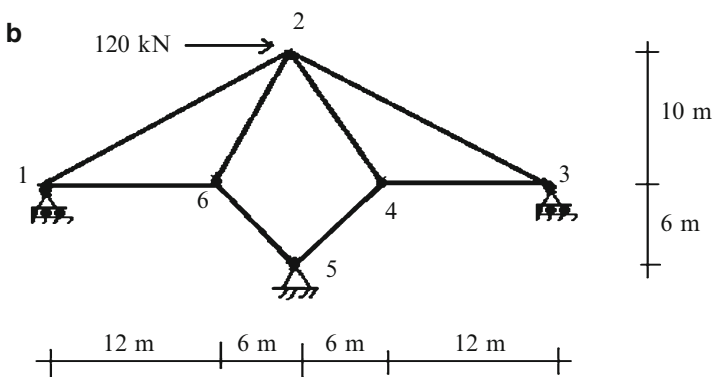
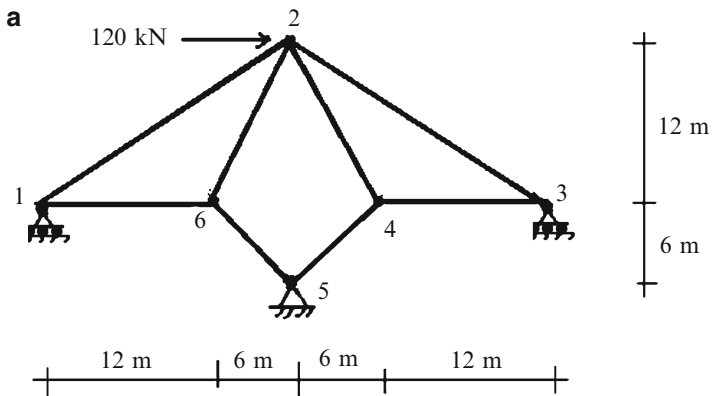
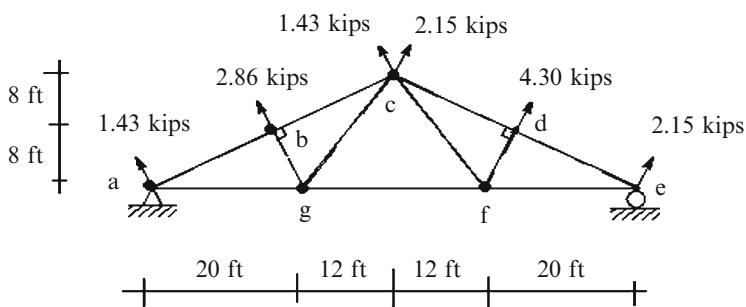
Problem 2.4

Determine all the member forces for the plane trusses defined in Problems 2.5–2.12 using the method of joints.

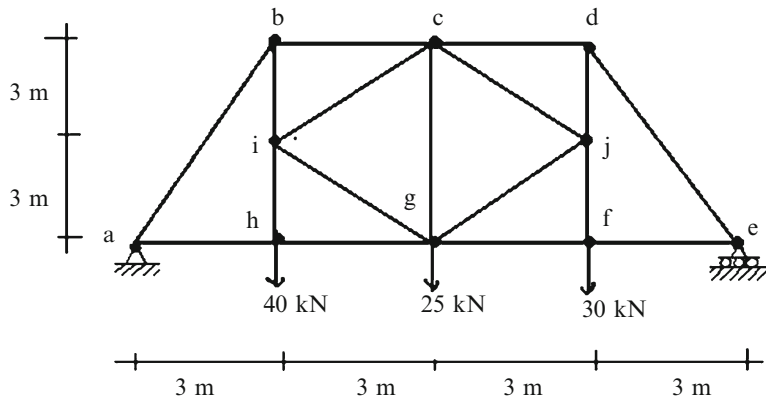
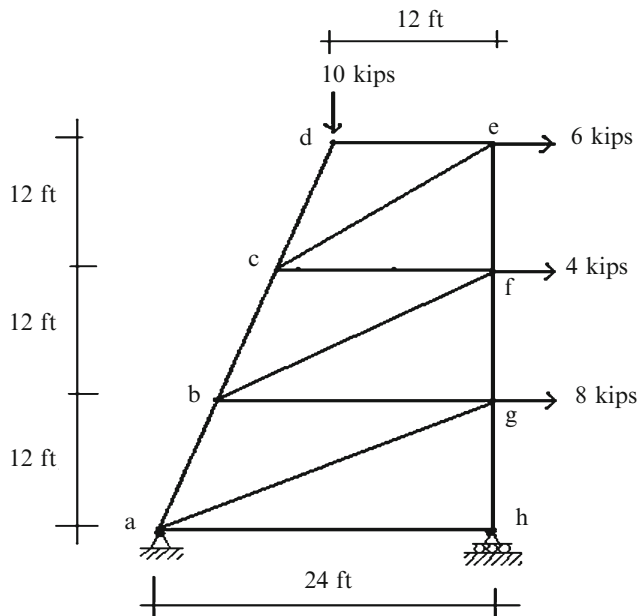
Problem 2.5**Problem 2.6**

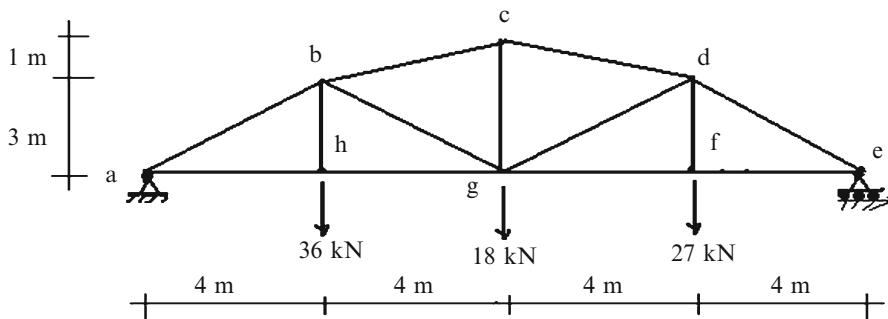
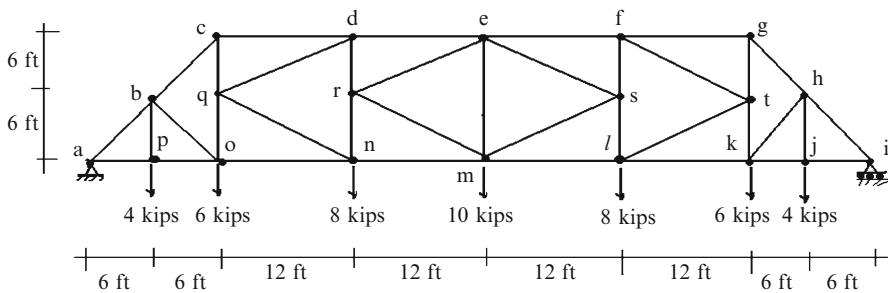
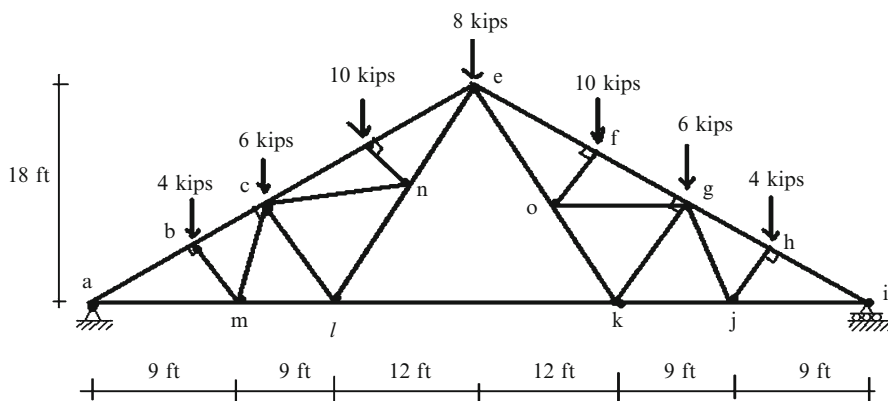
Problem 2.7**Problem 2.8**

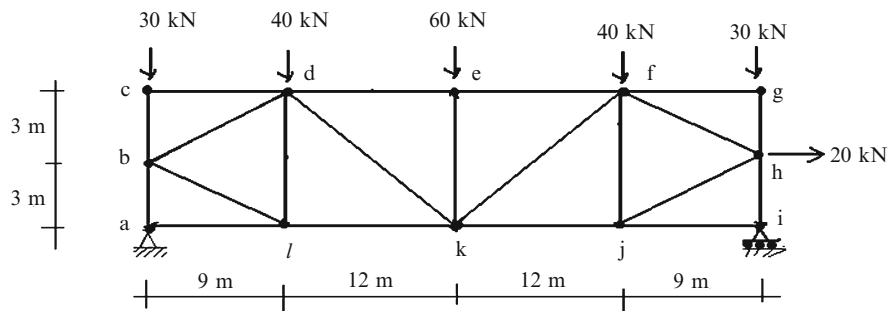
Problem 2.9**Problem 2.10**

Problem 2.11**Problem 2.12**

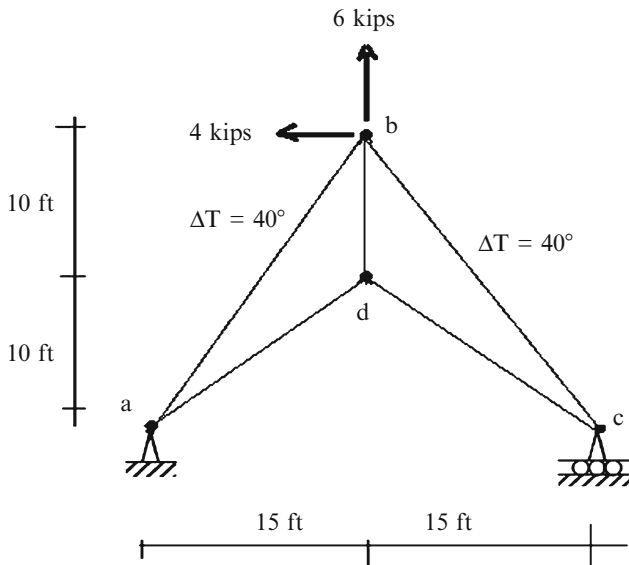
Determine all the member forces for the plane trusses defined in Problems 2.13–2.18 using a combination of the method of joints and the method of sections.

Problem 2.13**Problem 2.14**

Problem 2.15**Problem 2.16****Problem 2.17**

Problem 2.18**Problem 2.19**

Use the principle of virtual forces to determine the horizontal and vertical displacement at joint b due to loading shown and temperature increase of $\Delta T = 40^\circ\text{F}$ for members ab and bc. Assume $A = 1.4 \text{ in.}^2$, $E = 29,000 \text{ ksi}$ and $\alpha = 6.5(10^{-6})/\text{ }^\circ\text{F}$



Problem 2.20

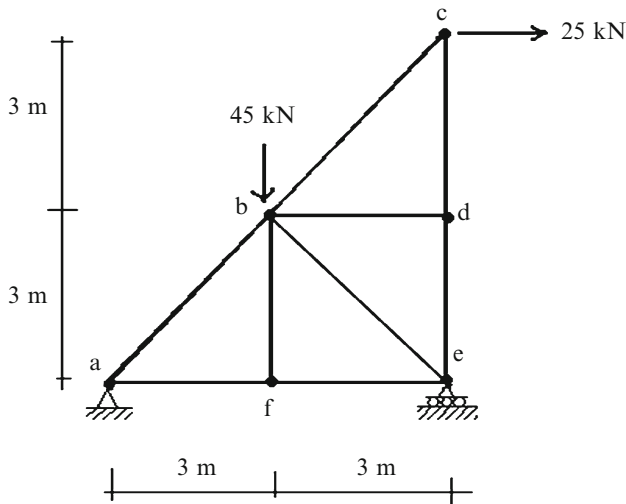
For the plane truss shown, use the principle of virtual forces to determine the vertical displacement at joint b and the horizontal displacement at joint c. $E = 200$ kPa. The areas of the members are as follow:

$$A_{ab} = A_{bc} = A_{be} = 1290 \text{ mm}^2$$

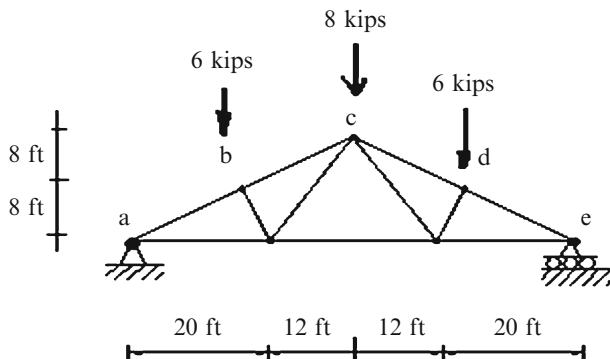
$$A_{bf} = A_{bd} = 645 \text{ mm}^2$$

$$A_{cd} = A_{de} = 1935 \text{ mm}^2$$

$$A_{af} = A_{fe} = 2580 \text{ mm}^2$$

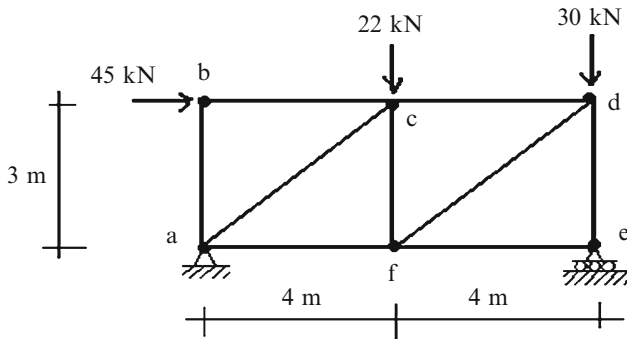
**Problem 2.21**

For the plane truss shown, use the principle of virtual forces to determine the vertical displacement at joint C. Assume $A = 2 \text{ in.}^2$ and $E = 29,000 \text{ ksi}$.



Problem 2.22

For the plane truss shown, use the principle of virtual forces to determine the vertical and horizontal displacement at joint d.



$$A = 1,300 \text{ mm}^2$$

$$E = 200 \text{ GPa}$$

Problem 2.23

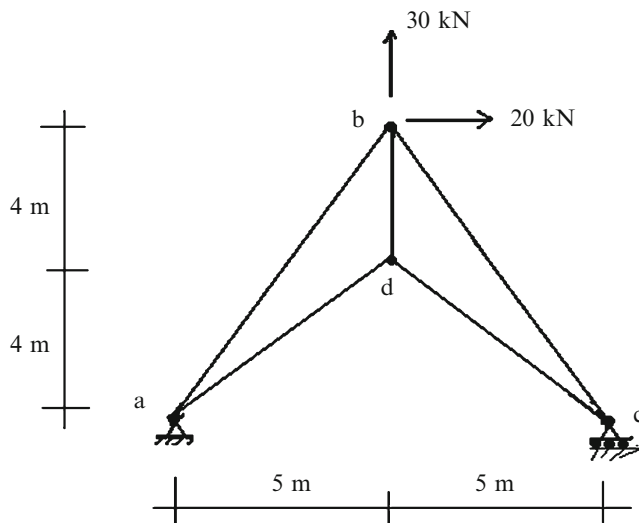
Use the principle of virtual forces to determine the horizontal and vertical displacement at joint b due to:

- (a) Loading shown.
- (b) Temperature increase of $\Delta T = 16^\circ\text{C}$ for members ab and bc.

$$A = 900 \text{ mm}^2$$

$$E = 200 \text{ GPa}$$

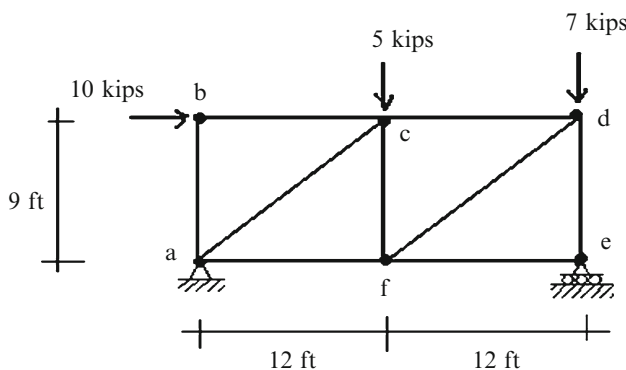
$$\alpha = 12 \times 10^{-6}/^\circ\text{C}$$



Problem 2.24

Use the principal of virtual force method to determine the horizontal component of the displacement at joint d. Assume $A = 0.5 \text{ in.}^2$ and $E = 29,000 \text{ ksi}$.

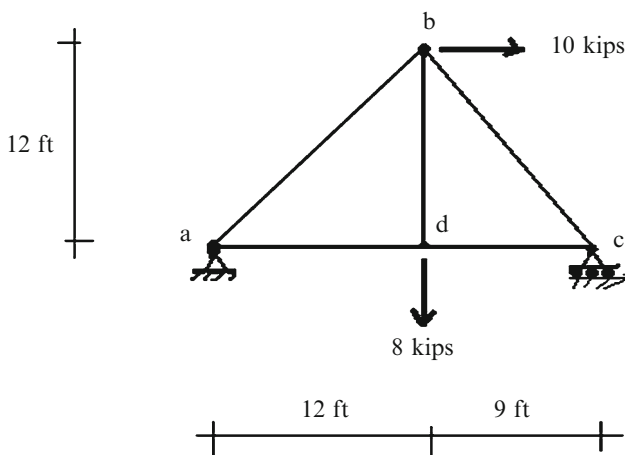
- For the loading shown
- For a fabrication of error of -0.25 in. for members ac and df
- For the summation of loading of Case (i) and Case (ii)



Problem 2.25

Use the principle of virtual forces method to determine the horizontal component of the displacement at joint b. Assume $A = 0.5 \text{ in}^2$, $E = 30,000 \text{ ksi}$, $\alpha = 6.5 \times 10^{-6}/^\circ\text{F}$

- (i) For the loading shown
- (ii) For a temperature increase of $\Delta T = 60^\circ\text{F}$ for all members
- (iii) For the summation of loading of Case (i) and Case (ii)

**Problem 2.26**

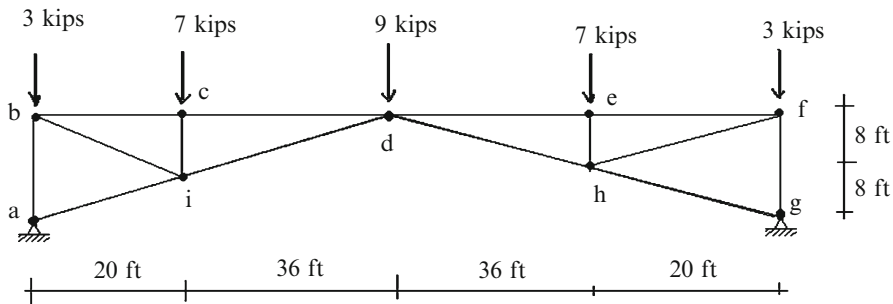
For the plane truss shown in Problem 2.10, use the principle of virtual forces to determine the vertical displacement at joint f.

$$A = 2 \text{ in}^2$$

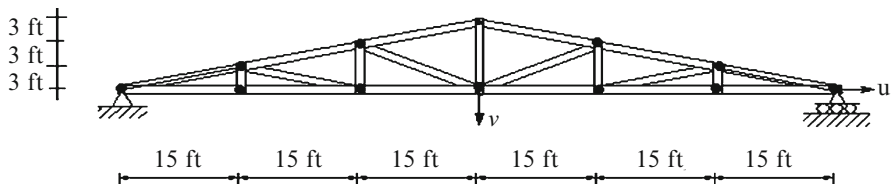
$$E = 29,000 \text{ ksi}$$

Problem 2.27

For the plane truss shown below, determine the required cross-sectional area for the truss members to limit the vertical deflection at d to .56 in. Assume equal cross-sectional areas. $E = 29,000 \text{ ksi}$.

**Problem 2.28**

For the plane truss shown in Problem 2.12, use the principle of virtual forces to determine the vertical displacement at joint g. The areas are 4 in.^2 for top chord members, 3 in.^2 for bottom chord members, and 2 in.^2 for other members. $E = 29,000 \text{ ksi}$.

Problem 2.29

Suppose the top chord members in the truss defined above experience a temperature decrease of 60°F . Determine the resulting displacements, u and v . $A = 2 \text{ in.}^2$, $E = 29,000 \text{ ksi}$ and $\alpha = 6.5 \times 10^{-6}/^\circ\text{F}$.

Problem 2.30

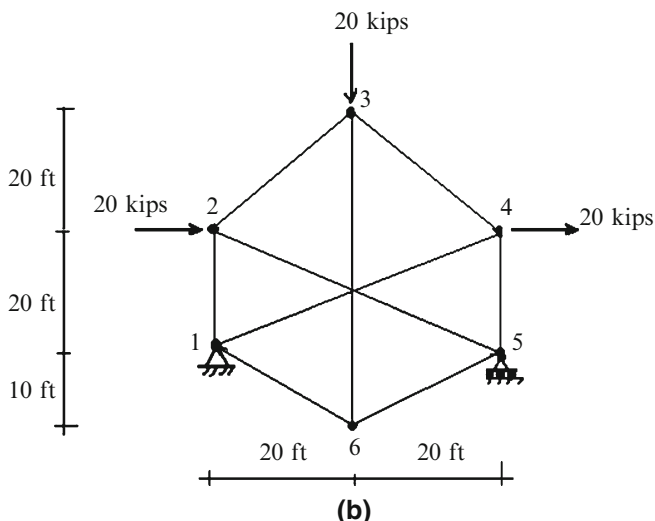
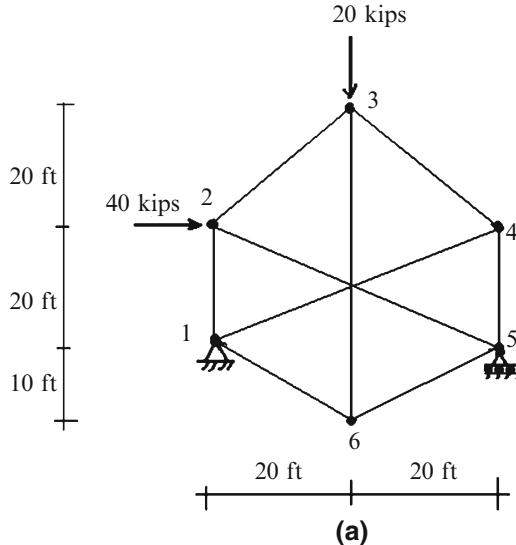
Solve Problem 2.15 using computer software. Assume the cross-sectional areas are equal to A .

- Demonstrate that the member forces are independent of A by generating solutions for different values of A .
- Determine the value of A required to limit the vertical displacement to 50 mm.

Problem 2.31

Consider the complex truss defined below in Figure (a). Use computer software to determine the member forces for the loading shown in Figure (a).

- (a) Assume equal areas
- (b) Take an arbitrary set of areas
- (c) Determine the member forces corresponding to the loading shown in Figure (b). Are the forces similar to the results of part (a). Discuss.

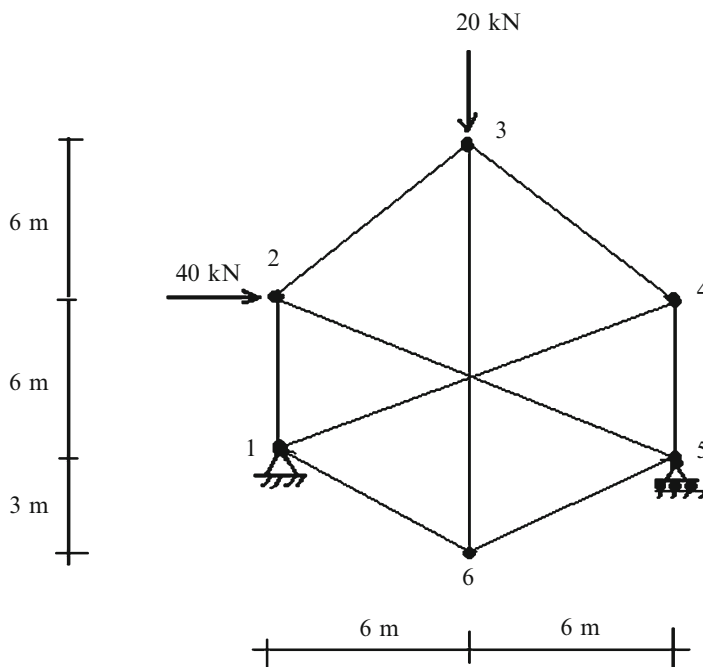


Problem 2.32

Solve Problem 2.11 using computer software. Assuming the cross-sectional areas are equal to A . Demonstrate that the member forces are independent of A by generating solution of different values of A .

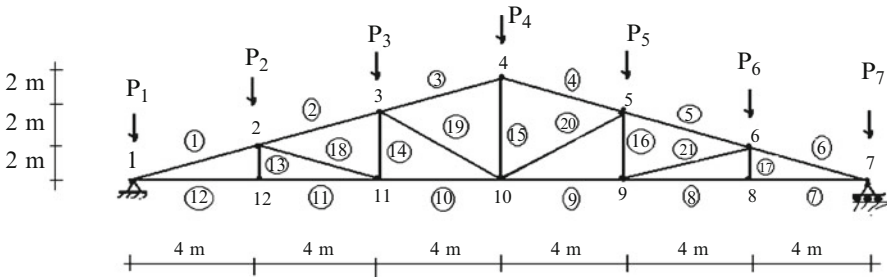
Problem 2.33

Consider the complex truss defined below. Assume equal areas. Use computer software to determine the member forces and joint displacements (limit the maximum joint displacement to 30 mm). $E = 200 \text{ GPa}$.



Problem 2.34

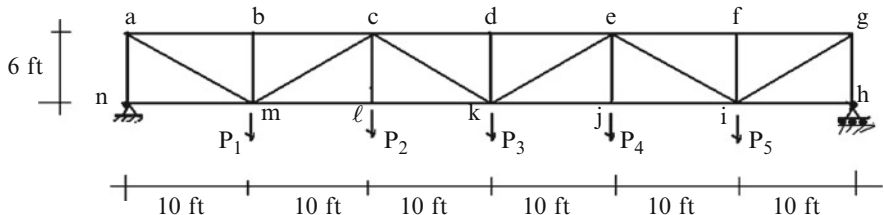
For the truss and the loading shown:



- Tabulate all the member forces due to the individual unit vertical nodal forces applied to the top chord (force influence table). Use computer software.
- Use the force influence table in part (a) to
 - Draw influence lines for members 15, 4, and 20.
 - Calculate the maximum member forces in members 3, 19, 10, and 14 for the following loading: $P_2 = 10 \text{ kN}$, $P_4 = 6 \text{ kN}$, and $P_6 = 8 \text{ kN}$.

Problem 2.35

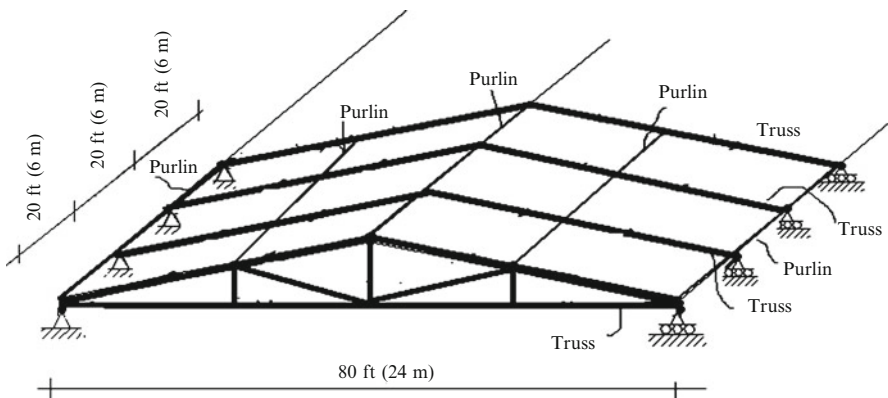
For the truss and the loading shown:



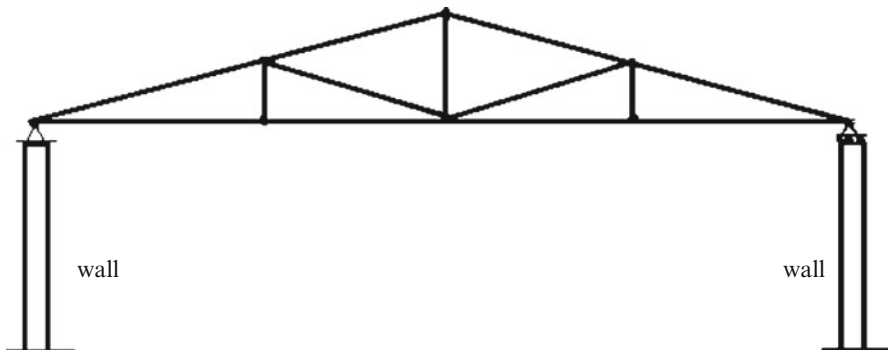
- Tabulate all the member forces due to the individual unit vertical nodal forces applied to the bottom chord (force influence table). Use computer software.
- Use the force influence table in part (a) to
 - Draw influence lines for members bc, cm, and ji.
 - Calculate the maximum member forces in members ke, de, kl, and ei for the loading $P_1 = 8 \text{ kip}$, $P_3 = 10 \text{ kip}$, and $P_4 = 4 \text{ kip}$.

Problem 2.36

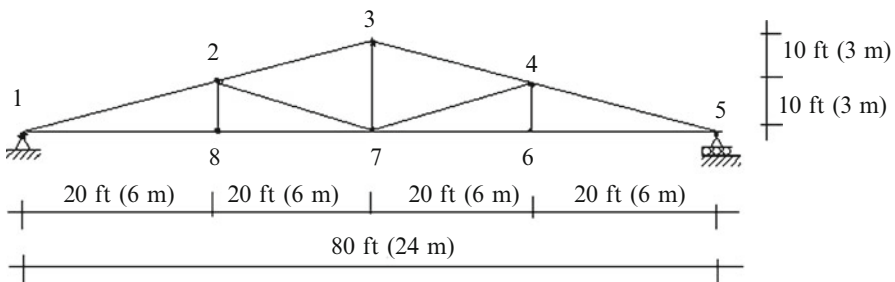
The roof structure shown below consists of trusses spaced uniformly, 20 ft (6 m) on center, along the length of the building and tied together by purlins and x-bracing. The roofing materials are supported by the purlins which span between trusses at the truss joints.



(a) Roof structural make-up



(b) Elevation-typical truss



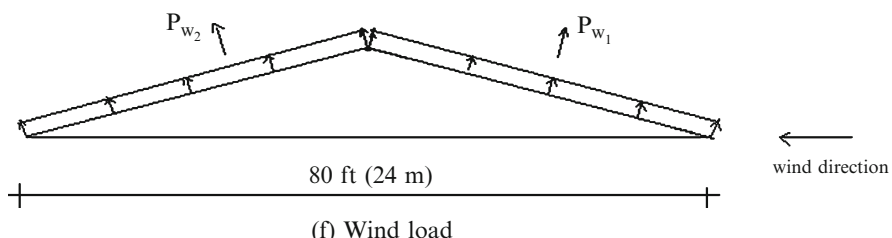
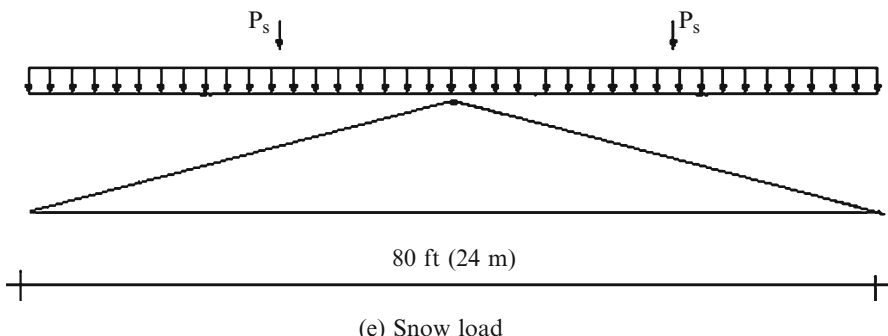
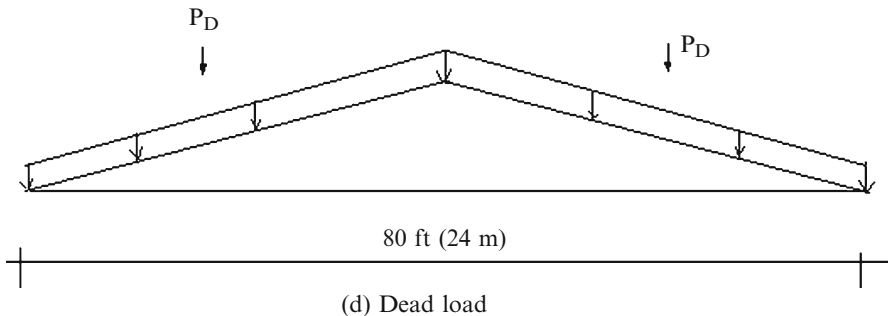
(c) Truss geometry

Consider the following loadings:

Dead load: roof material, purlins, truss members, estimated at 15 psf (720 Pa) of roof surface

Snow load: 20 psf (960 Pa) of horizontal projection of the roof surface

Wind load: windward face 12 psf (575 Pa), leeward face 8 psf (385 Pa) normal to roof surface

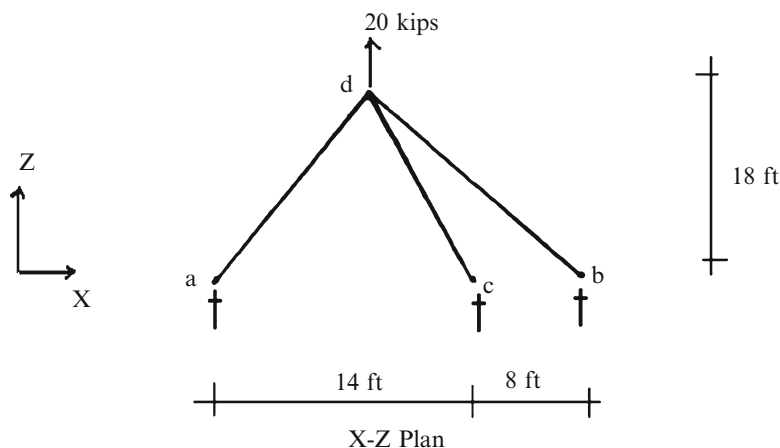
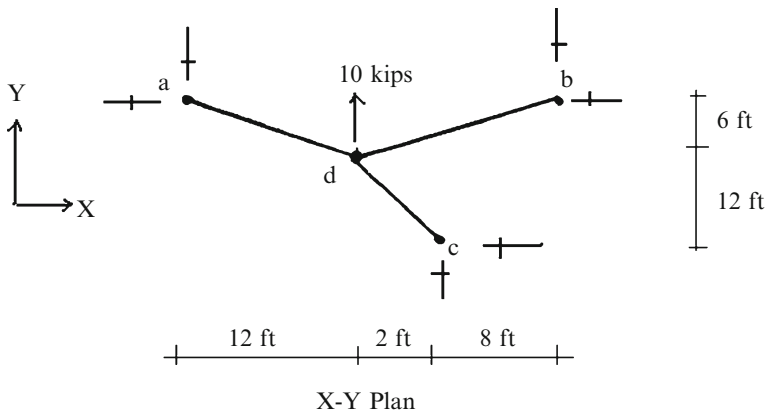


Determine the following quantities for the typical interior truss:

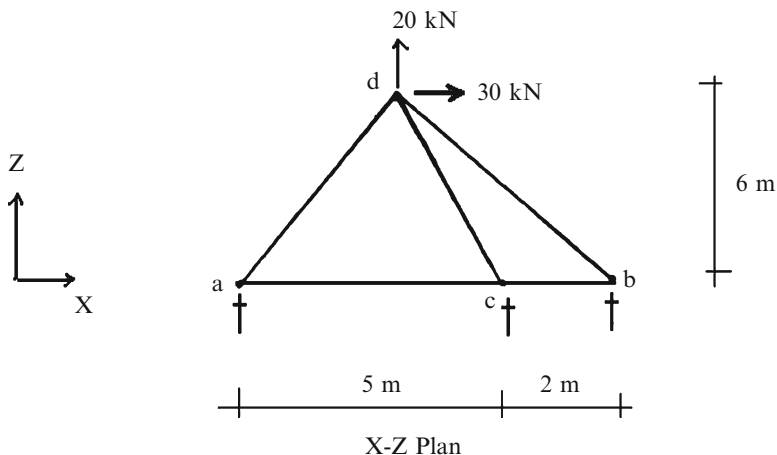
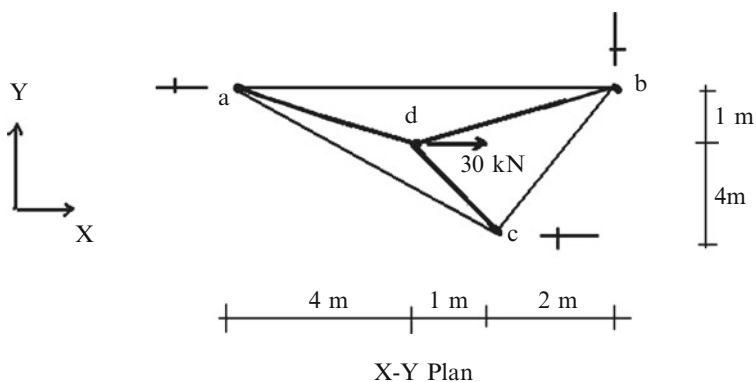
- Compute the truss nodal loads associated with gravity, snow, and wind.
- Use computer software to determine the member forces due to dead load, snow load, and wind. Tabulate the member force results.

Problem 2.37

Determine the member forces for the space truss shown.

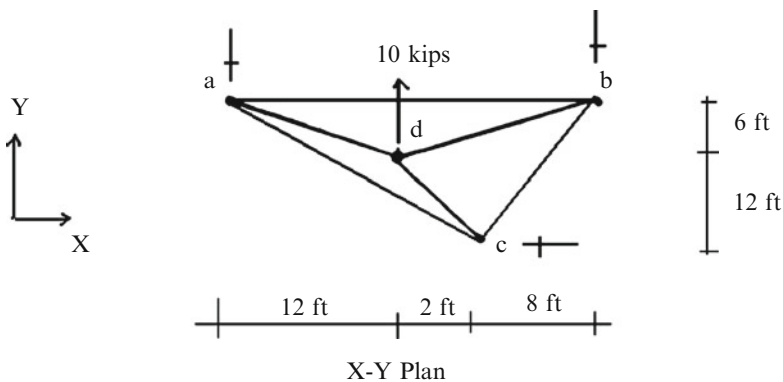
**Problem 2.38**

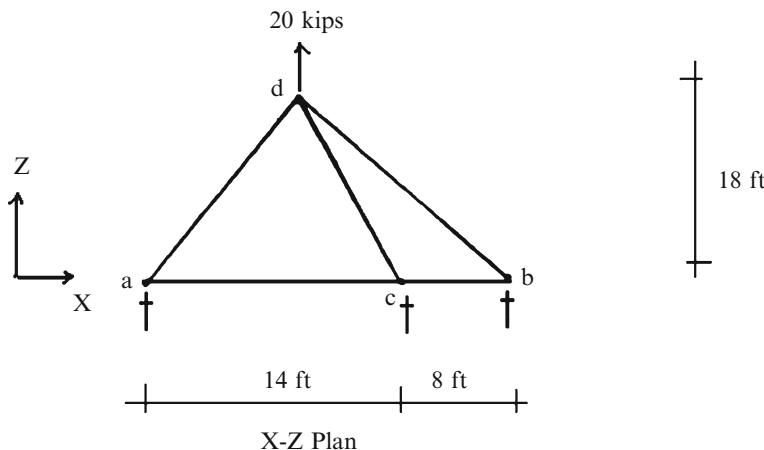
Determine the member forces for the space truss shown.



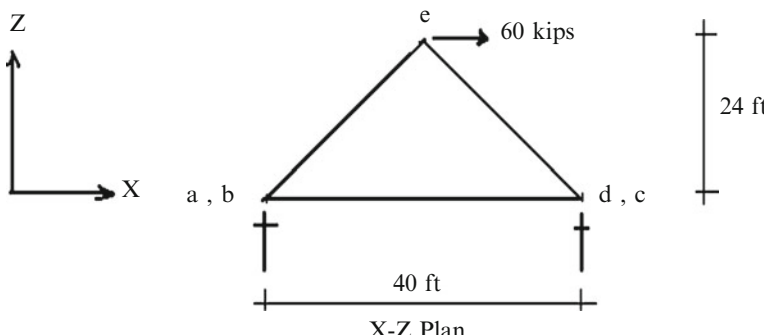
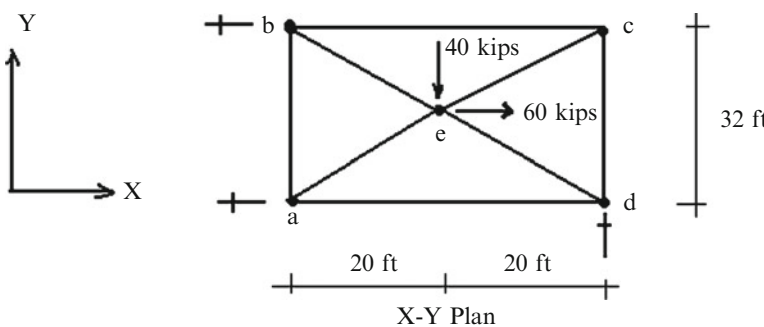
Problem 2.39

Determine the member forces for the space truss shown.



**Problem 2.40**

Determine the member forces for the space truss shown.

**Problem 2.41**

For the space truss shown in Problem 2.37, use the principle of virtual forces to determine the displacements u , v , and w at joint d. $E = 29,000$ ksi and $A = 3.0 \text{ in}^2$

Overview

Our focus in this chapter is on describing how beams behave under transverse loading, i.e., when the loading acts normal to the longitudinal axes. This problem is called the “beam bending” problem. The first step in the analysis of a statically determinate beam is the determination of the reactions. Given the reactions, one can establish the internal forces using equilibrium-based procedures. These forces generate deformations that cause the beam to displace. We discuss in detail the relationship between the internal forces and the corresponding displacements and describe two quantitative analysis procedures for establishing the displacements due to a particular loading. The last section of the chapter presents some basic analysis strategies employed in the design of beams such as influence lines and force envelopes.

3.1 Definition of a Prismatic Beam

Beams are used extensively in structures, primarily in flooring systems for buildings and bridges. They belong to the line element category, i.e. their longitudinal dimension is large in comparison to their cross-sectional dimensions. Whereas truss members are loaded axially, beams are loaded normal to the longitudinal direction, and carry the loading by bending and twisting action. This mode is illustrated in Fig. 3.1. The transverse loading produces transverse deflection, which results in a nonuniform distribution of stress throughout the body.

Most of the applications of beams in building structures involve straight beams with constant cross-section. We refer to this subgroup as prismatic beams. Figure 3.2 defines the geometrical parameters and notation used for prismatic beams. The longitudinal axis passes through the centroid of the cross-section, and the y , z axes are principal inertia directions. The relevant definition equations are

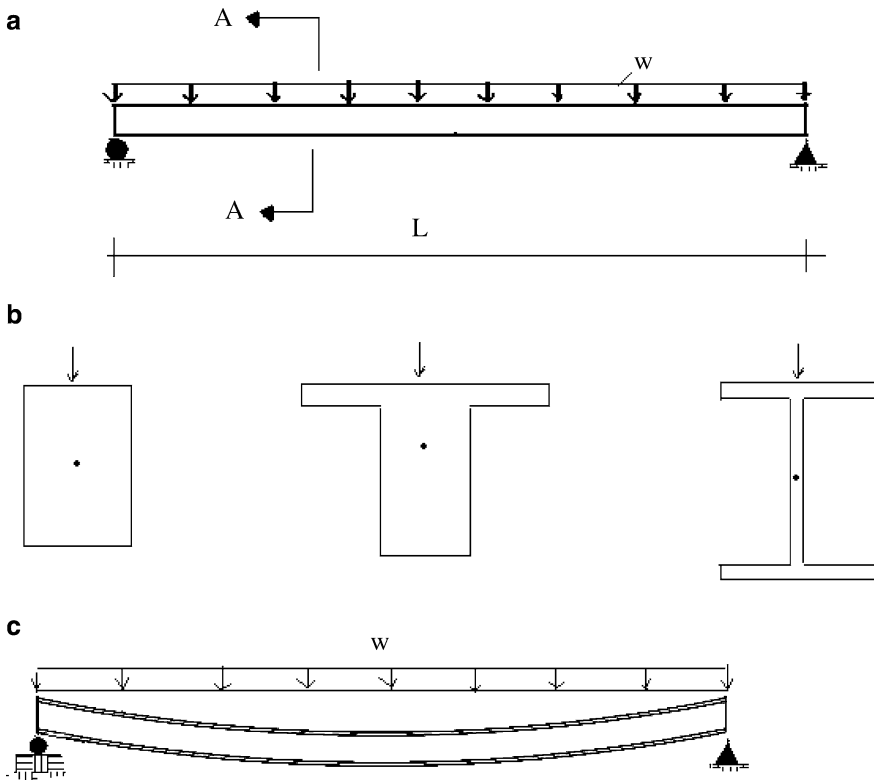


Fig. 3.1 Beam cross-sections and bending mode. (a) Simply supported beam. (b) Section A-A—Cross-section examples. Rectangular, T shape, I shape. (c) Bending mode

$$\int_A ydA = \int_A zdA = \int_A yzdA = 0$$

$$I_z = \int_A y^2 dA \quad (3.1)$$

$$I_y = \int_A z^2 dA$$

These conditions ensure that when the applied loads are in the $x-y$ plane, points on the longitudinal axis will not displace in the z direction. Figure 3.3 illustrates this mode of behavior. For this type of loading, the longitudinal axis becomes a curve $v(x)$ contained in the $x-y$ plane. This type of behavior is called *planar bending*.

There are cases where the line of action of the loading does not pass through the X -axis, such as illustrated in Fig. 3.4. The eccentricity produces a torsional moment about the Z -axis, and the cross-section will rotate as well as deflect. This behavior is called “combined bending and torsion.” A prismatic member acted upon by just a torsional moment will experience only torsional behavior, i.e., the cross-section will just twist.

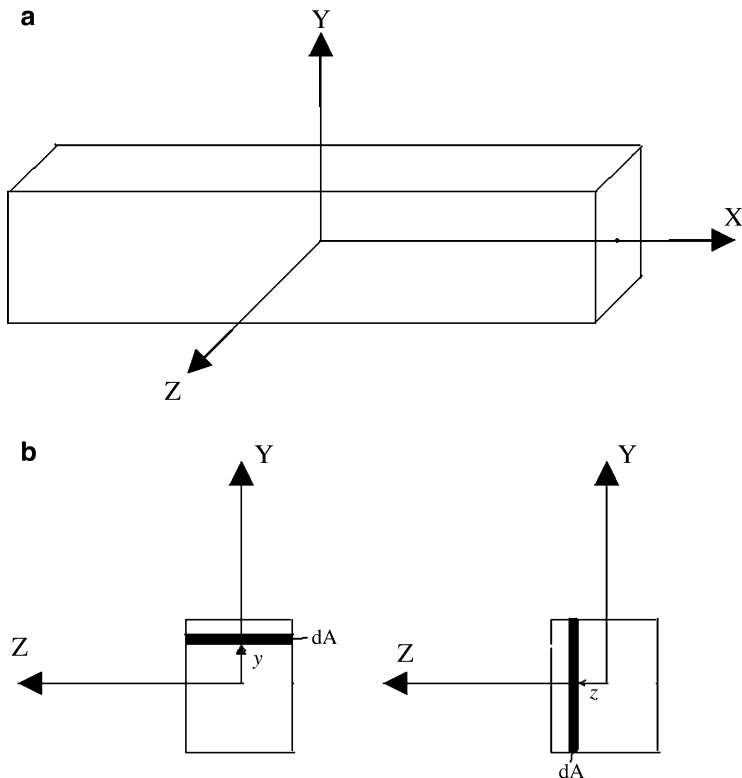


Fig. 3.2 Notations for prismatic beam

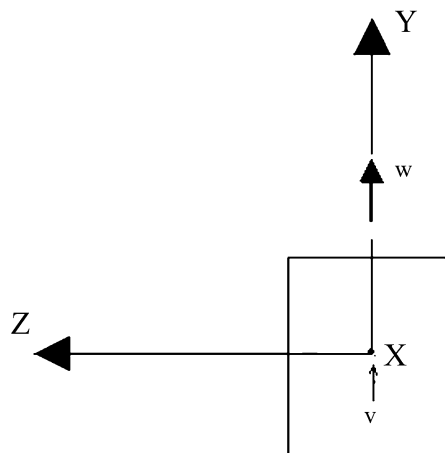


Fig. 3.3 Planar bending mode

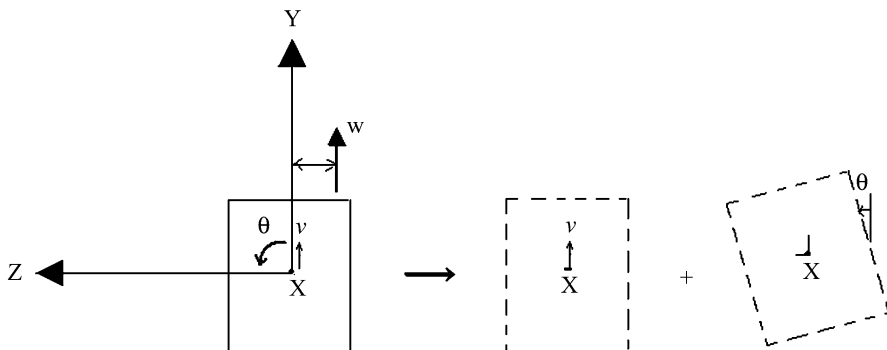


Fig. 3.4 Combined bending and torsion

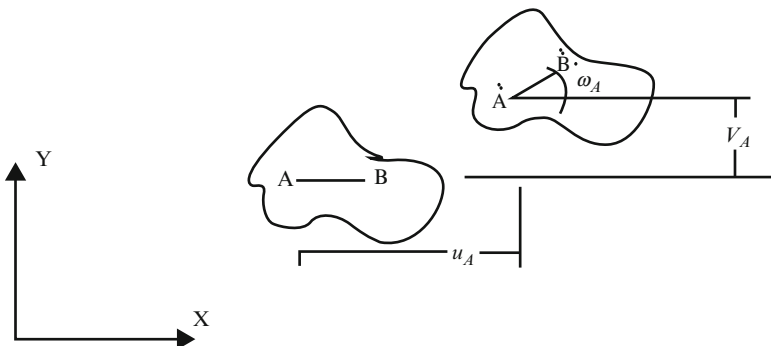
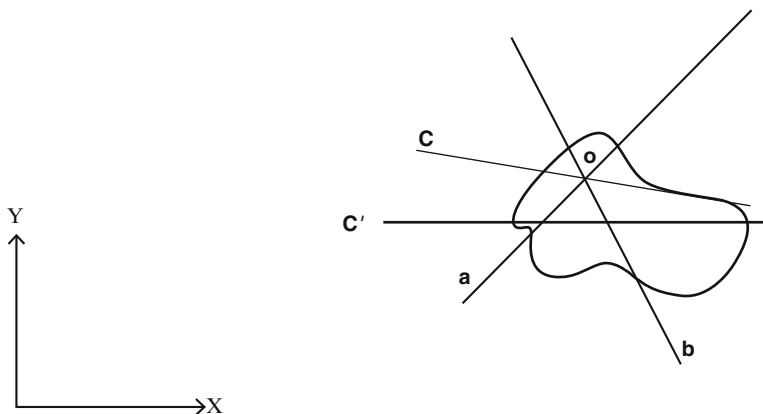
Mechanics of Solids texts deal with stresses and strains in beams. Our objective here is not to redevelop this material but rather to utilize it and formulate a structural theory for beams that will provide the basis for analyzing the behavior of structures composed of beam elements. Since structural theory is founded on Engineering Mechanics Theory, at least one subject dealing with Engineering Mechanics is usually required before studying Structural Theory. We assume that the reader has this level of exposure to Engineering Mechanics.

3.2 Stability and Determinacy of Beams: Planar Bending

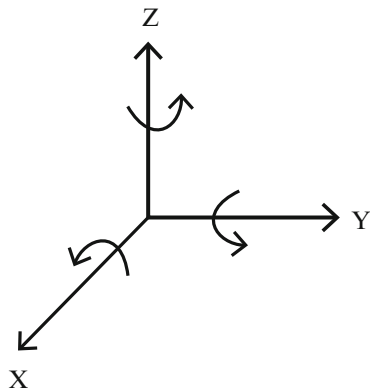
We presented the general concept of stability of a rigid body in Chap. 1 and used the general concept to develop stability criteria for truss-type structures in Chap. 2. In what follows, we examine the stability question for beam-type structures and develop similar criteria. For completeness, we first briefly review the basis for stability discussed in Chap. 1.

Consider the rigid body shown in Fig. 3.5. Assume the body can move only in the x - y plane. There are three types of planar motion for a rigid body: translation in the x direction, u_A , translation in the y direction, v_A , and rotation about an axis normal to the x - y plane, ω_A . A body is said to be stable when rigid body motion is prevented. Therefore, it follows that one must provide three motion constraints to restrain motion in the X - Y plane.

One needs to be careful in selecting the orientation of the three translation constraints. Consider Fig. 3.6, we first choose two directions, “ a ” and “ b ” in the X - Y plane. They intersect at point o . With these two constraints, the only possible rigid body motion is rotation about point o . If we take the third direction as “ c ,” this rotation is not prevented. *Therefore, it follows that the three directions must be nonconcurrent as well as coplanar, i.e., they cannot intersect at a common point.* This implies that they must not be parallel. Any other direction, such as “ c' ” is permissible.

**Fig. 3.5** planar rigid body motions**Fig. 3.6** Concurrent displacement constraints

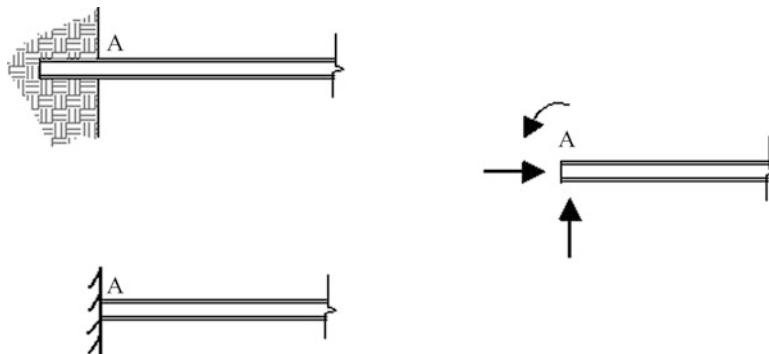
When the loading is arbitrary, the body needs to be constrained against motion in any plane. This requires six constraints, three with respect to translation and three with respect to rotation about the X , Y , and Z direction. The strategy for selecting restraints is similar to the treatment of 3-D truss structures. We point out that for pure rotational loading, only one rotational restraint is required.



Motion constraints produce reaction forces when the body is loaded. The nature of the reaction forces depends on the constraints. Various types of supports for beams subjected to planar bending are illustrated below.

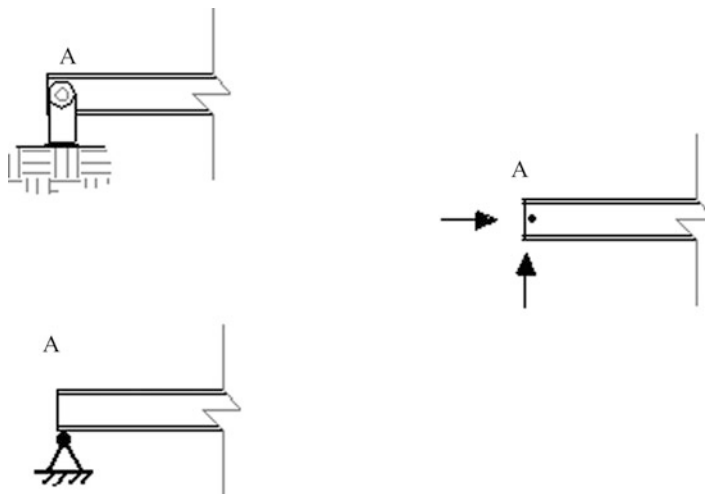
3.2.1 Fixed Support: Planar Loading

The beam is embedded at point A in such a way that the end is prevented from translating or rotating. We say the member is “fixed” at A. The reactions consist of two forces and one moment.



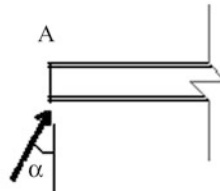
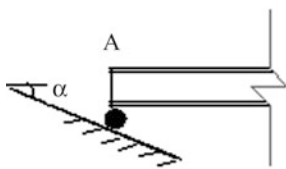
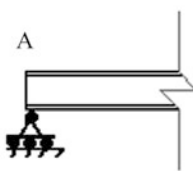
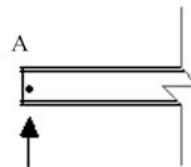
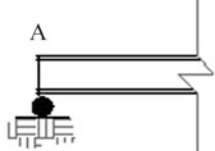
3.2.2 Hinged Support: Planar Loading

Suppose A is to be fully restrained against translation. This can be achieved by pinning the member. Horizontal and vertical reactions are produced.



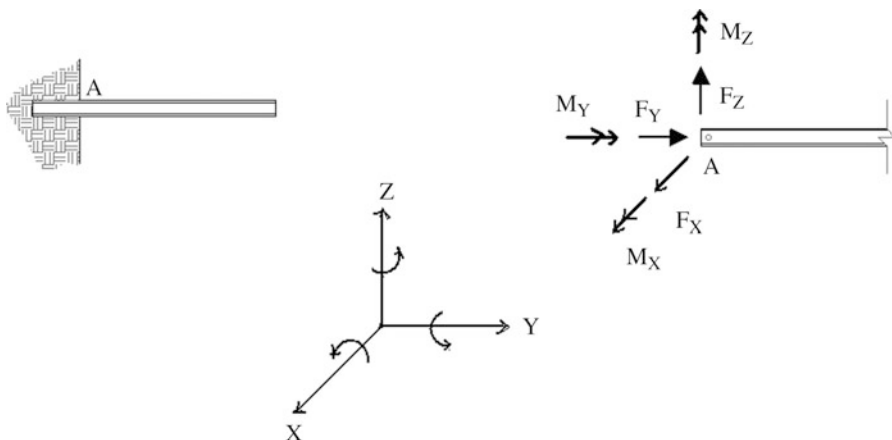
3.2.3 Roller Support: Planar Loading

Suppose A is to be restrained against motion perpendicular to the surface of contact. We add a restraint to A by inserting a device that allows motion parallel to the surface of contact but fully restrains motion in the direction perpendicular to the surface. We refer to this device as a roller. This restraint produces a reaction force perpendicular to the surface of contact.

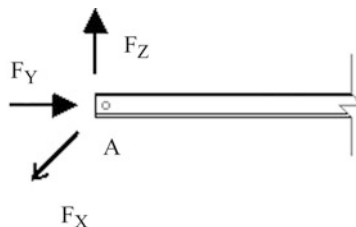


When the loading is three dimensional, additional restraints are required. The supports described above need to be modified to deal with these additional restraints. Typical schemes are shown below.

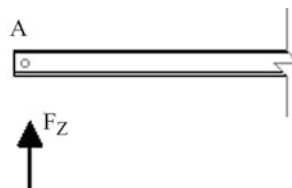
3.2.4 3-D Fixed Support



3.2.5 3-D Hinged Support



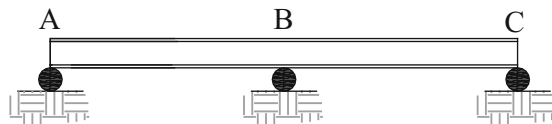
3.2.6 3-D Roller Support: Z Direction



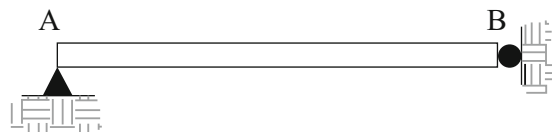
3.2.7 Static Determinacy: Planar Beam Systems

In general, a body restrained with three *nonconcurrent* coplanar displacement constraints is stable for planar loading. When loading is applied, the only motion that occurs is due to deformation of the body resulting from the stresses introduced in the body by the loading. The motion restraints introduce reaction forces. Since there are three equations of force equilibrium for a body, and only three unknown forces, one can determine these force unknowns using only the force equilibrium equations. In this case, we say that the structure is stable and statically determinate. If a body is over restrained, i.e. if there are more than three nonconcurrent displacement restraints, we say that the structure is statically indeterminate. This terminology follows from the fact that now there are more than three force unknowns and consequently one cannot uniquely determine these unknowns with only the three available force equilibrium equations. Statically indeterminate structures require a more rigorous structural theory and therefore we postpone their treatment to part II of the text. In what follows, we present some examples of statically determinate and statically indeterminate planar beams.

3.2.8 Unstable Support Arrangements



The beam shown above has the proper number of constraints, but they are all vertical. There is no constraint against horizontal motion, and therefore the beam is unstable.



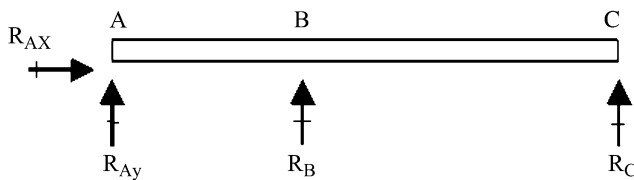
The beam shown above is unstable. The roller support at B constrains motion in the horizontal direction but does not prevent rigid body motion about point A.

3.2.9 Beam with Multiple Supports

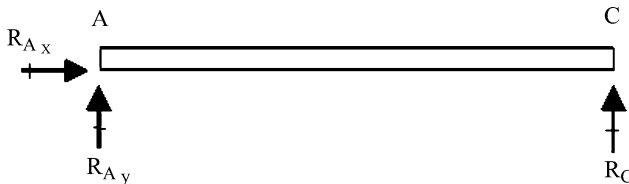
There are three vertical restraints and one horizontal restraint. These restraints produce the four reaction forces shown below.



Fig. 3.7 Two-span beam



One of the vertical restraints is redundant, i.e., is not needed for stability and therefore can be deleted. Deleting the support at B results in the structure shown below.



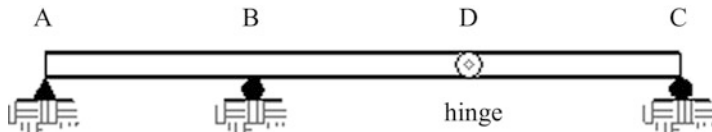
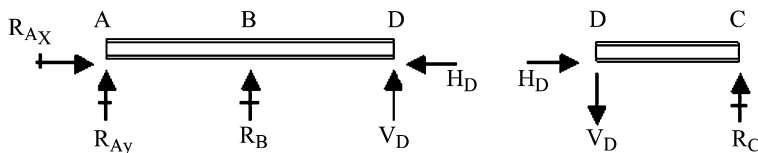
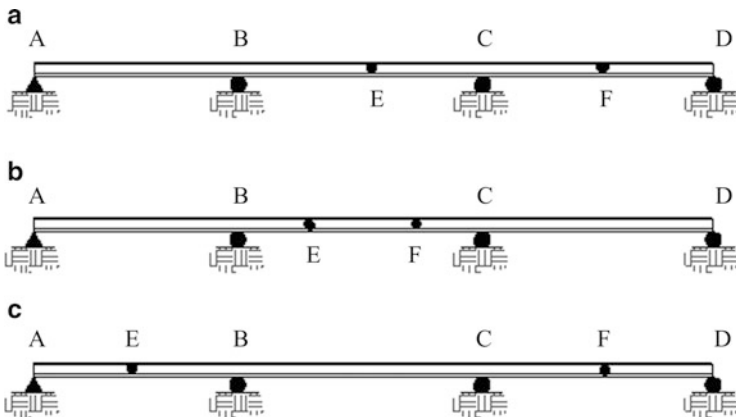
A beam supported only at its ends in a minimal way is referred to as a simple supported beam.



The beam depicted in Fig. 3.7 is called a two-span continuous beam. This beam is statically indeterminate to the first degree. We will show later that multi-span continuous beams are more structurally efficient than simply supported beams in the sense that they deflect less for a given design loading.

3.2.10 Beam with a Moment Release

Suppose we cut the beam shown in Fig. 3.8 at point D and insert a frictionless hinge. We refer to the hinge as a moment release since the moment is zero. The hinge does not restrain rotation at D, and member DC is free to rotate about D. The beam is now statically determinate. The corresponding reaction forces are listed below on the free body diagrams (Fig. 3.9).

**Fig. 3.8** Beam with moment release**Fig. 3.9** Free body diagram for beam with moment release**Fig. 3.10** Three-span beam**Fig. 3.11** Statically determinate versions of three-span beam with moment releases

Member DC is statically determinate since there are only three reaction forces. Once the forces at D are known, the remaining reactions for member ABD can be determined. Therefore, it follows that inserting a hinge at D reduces the static indeterminacy by 1° .

We consider next the three-span continuous beam shown in Fig. 3.10. This structure is indeterminate to the second degree since there are two extra vertical supports. One can reduce the structure to a statically determinate structure by inserting two moment releases. Various possibilities are listed in Fig. 3.11. The optimal location of moment releases is illustrated in Examples 3.29 and 3.30.

3.3 Reactions: Planar Loading

When a structure is subjected to external loads, the displacement restraints develop reaction forces to resist the tendency for motion. If the structure is statically determinate, we can determine these forces using the three global force equilibrium equations for planar loading applied to a body. One selects a set of directions 1-1 and 2-2, where 2-2 is not parallel to 1-1. The steps are

- (i) Summation of forces in direction 1 – 1 = 0
 - (ii) Summation of forces in direction 2 – 2 = 0
where direction 2 – 2 is not parallel to direction 1 – 1
 - (iii) Summation of moments about an arbitrary point, $A = 0$
- (3.2)

One constructs a free body diagram of the structure and applies these equations in such a way as to obtain a set of uncoupled equations, which can be easily solved.

When a statically indeterminate structure has a sufficient number of releases to reduce it to being statically determinate, we proceed in a similar way except that now we need to consider more than one free body. In what follows, we present a series of examples that illustrate the computation of the reactions.

Example 3.1 Beam with two overhangs

Given: The beam shown in Fig. E3.1a.

Determine: The reactions.

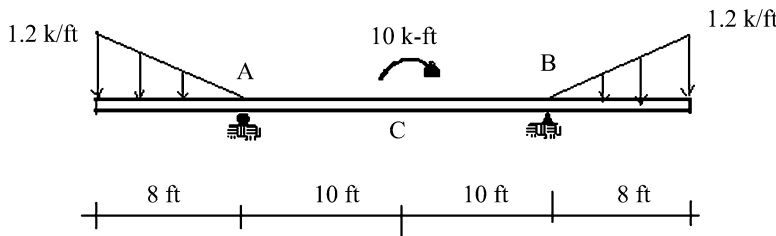


Fig. E3.1a

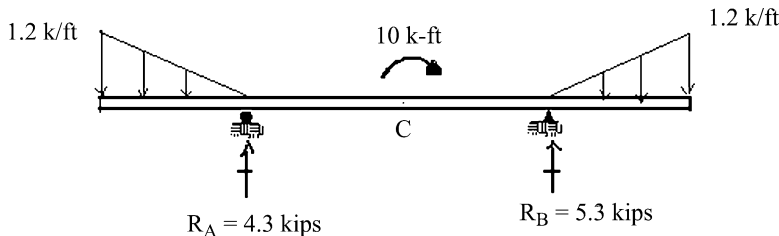
Solution: Summing moments about B leads to the vertical reaction at A.

$$\begin{aligned} \sum M_B &= 0 \\ R_A(20) + 10 + \frac{1}{2}(1.2)(8)\frac{2}{3}(8) - 1.2\left(\frac{8}{2}\right)\left(20 + \frac{2}{3}8\right) &= 0 \\ \therefore R_A &= 4.3 \uparrow \end{aligned}$$

Summing the vertical forces,

$$\sum F_Y = 0 \quad R_B + 4.3 - 1.2\left(\frac{8}{2}\right)(2) = 0 \\ \therefore R_B = 5.3 \uparrow$$

The reactions are listed below.



Example 3.2 Simply supported beam

Given: The beam shown in Fig. E3.2a.

Determine: The reactions.

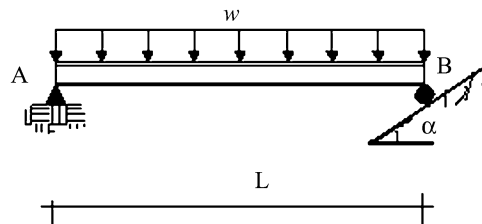


Fig. E3.2a

Solution: As a first step, we construct the free body diagram for the beam. The reaction at B is normal to the inclined surface. We resolve it into horizontal and vertical components using (Fig. E3.2b)

$$R_{By} = R_B \cos \alpha \quad R_{Bx} = R_B \sin \alpha$$

Summing moments about A leads to the vertical reaction at B.

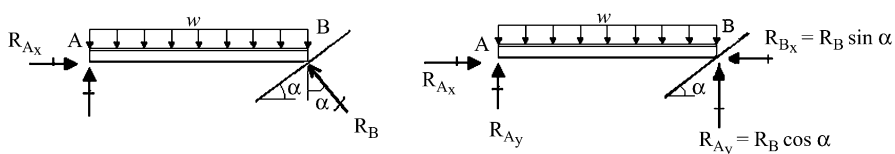


Fig. E3.2b

$$\begin{aligned}\sum M_A &= 0 \\ wL\left(\frac{L}{2}\right) - LR_{By} &= 0 \\ \therefore R_{By} &= \frac{wL}{2} \uparrow\end{aligned}$$

Given R_{By} , we find the reaction R_B

$$R_B = \frac{R_{By}}{\cos \alpha} = \frac{wL}{2 \cos \alpha}$$

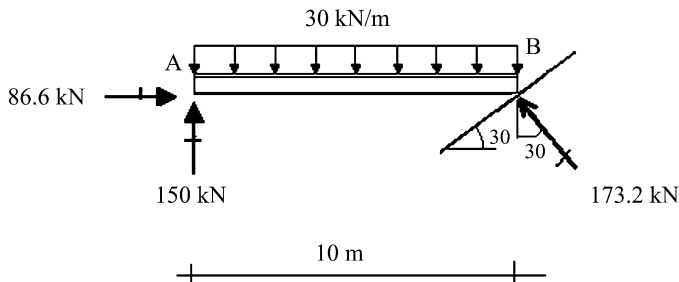
The corresponding horizontal component is

$$R_{Bx} = R_B \sin \alpha = \frac{wL}{2} \tan \alpha \leftarrow$$

We determine the reactions at A using force summations.

$$\begin{aligned}\sum F_x &= 0 \quad R_{Ax} = -R_{Bx} = \frac{wL}{2} \tan \alpha \rightarrow \\ \sum F_y &= 0 \uparrow^+ \quad R_{Ay} + R_{By} - wL = 0 \quad R_{Ay} = \frac{wL}{2} \uparrow\end{aligned}$$

Suppose $w = 30 \text{ kN/m}$, $\alpha = 30^\circ$ and $L = 10 \text{ m}$. The reactions are listed below.



Example 3.3 Two-span beam with a moment release

Given: The beam shown in Fig. E3.3a. There is a moment release at D.

Determine: The reactions.

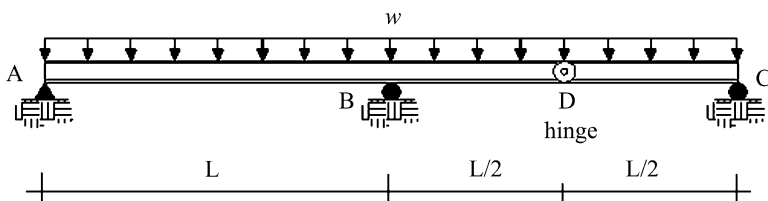
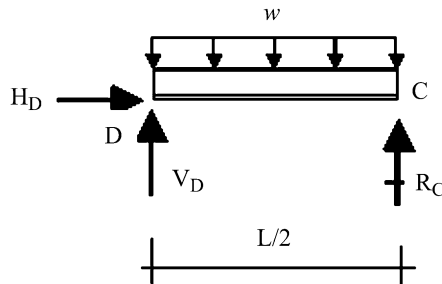


Fig. E3.3a

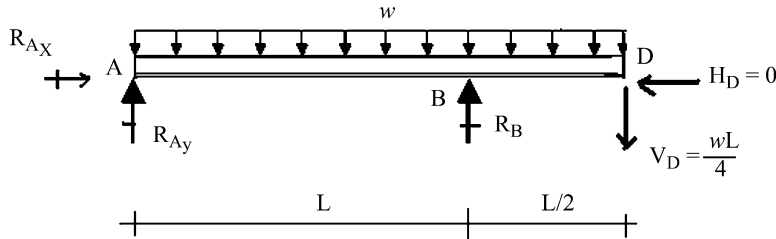
Solution: The most direct way of analyzing this structure is to first work with a free body diagram of beam segment DC.



Applying the equilibrium conditions to this segment results in

$$\begin{aligned}\sum M_D &= 0 \quad R_C = \frac{wL}{4} \uparrow \\ \sum F_Y &= 0 \quad V_D = \frac{wL}{4} \uparrow \\ \sum F_x &= 0 \quad H_D = 0\end{aligned}$$

With the internal forces at D known, we can now proceed with the analysis of segment ABD.



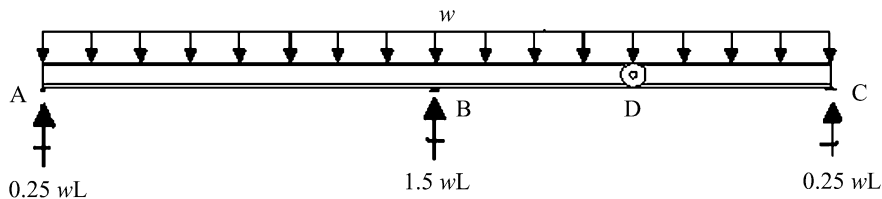
Summing moments about A leads to R_B

$$\begin{aligned}\sum M_A &= 0 \quad (0.75L)(1.5wL) + (1.5L)(0.25wL) - LR_B = 0 \\ R_B &= 1.5wL \uparrow\end{aligned}$$

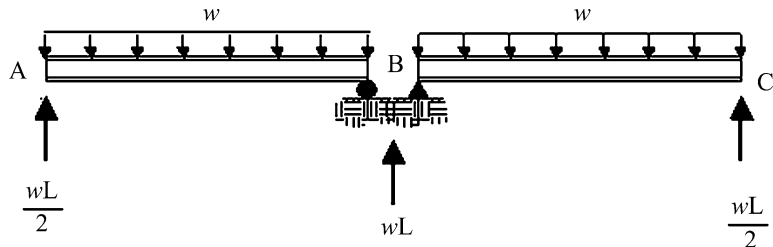
Summing the vertical and horizontal forces,

$$\begin{aligned}\sum F_Y &= 0 \quad R_{Ay} = 1.75wL - R_B = 0.25wL \uparrow \\ \sum F_x &= 0 \quad R_{Ax} = 0\end{aligned}$$

The reactions are listed below.



If the hinge was placed at point B, the structure would act as two simply supported beams, and the reactions would be as shown below.



Example 3.4

Given: The beam shown in Fig. E3.4a.

Determine: The reactions.

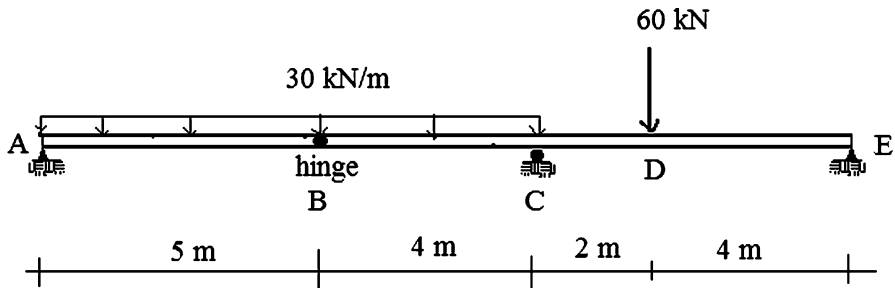
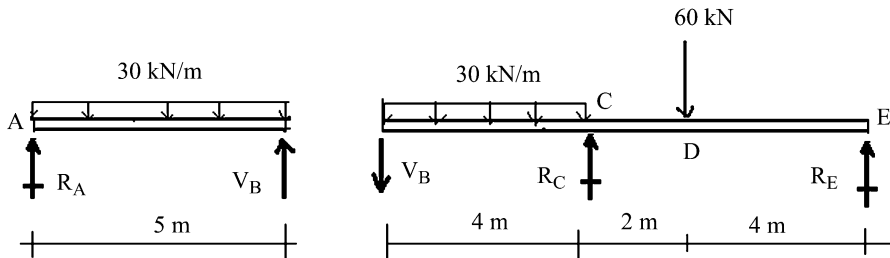
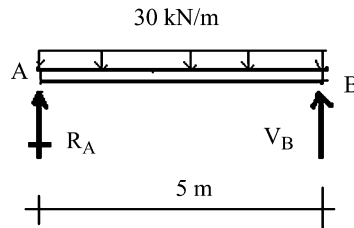


Fig. E3.4a

Solution: we construct the free body diagram for the beam.

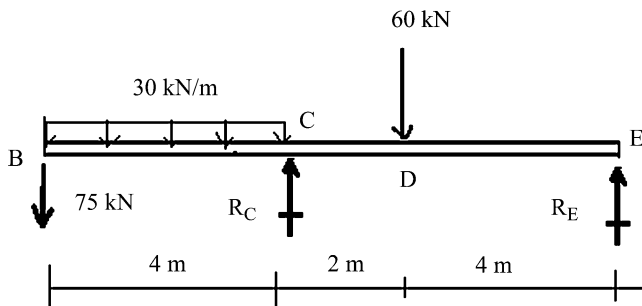


We start with the free body diagram of beam segment AB. Then, with the internal force at B known, we proceed with the analysis of segment BCDE.



$$\begin{aligned}\sum M_B &= 0 \quad R_A = 75 \text{ kN} \uparrow \\ \sum F_Y &= 0 \quad V_B = 75 \text{ kN}\end{aligned}$$

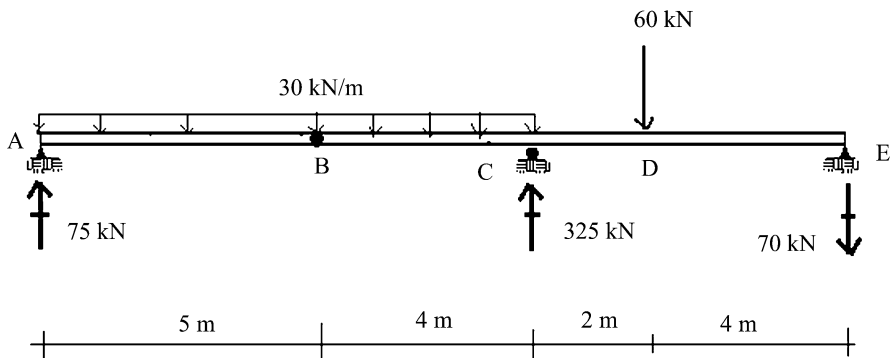
Analysis of segment BCDE:



$$\sum M_C = 0 \quad R_E(6) + 75(4) - 60(2) + \frac{30}{2}(4)^2 = 0 \quad R_E = -70$$

$$\sum F_Y = 0 \uparrow \quad R_C = +325$$

The reactions are listed below.



Example 3.5 Three-span beam with two moment releases

Given: The beam shown in Fig. E3.5a.

Determine: The reactions.

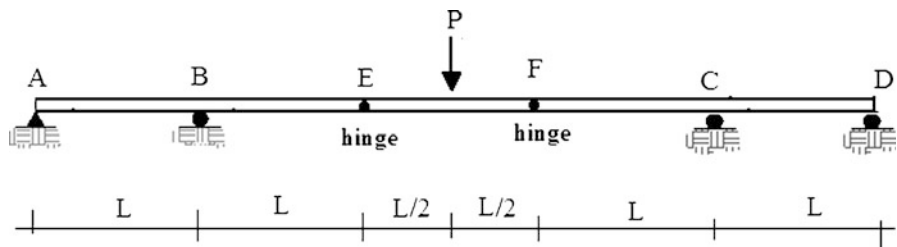
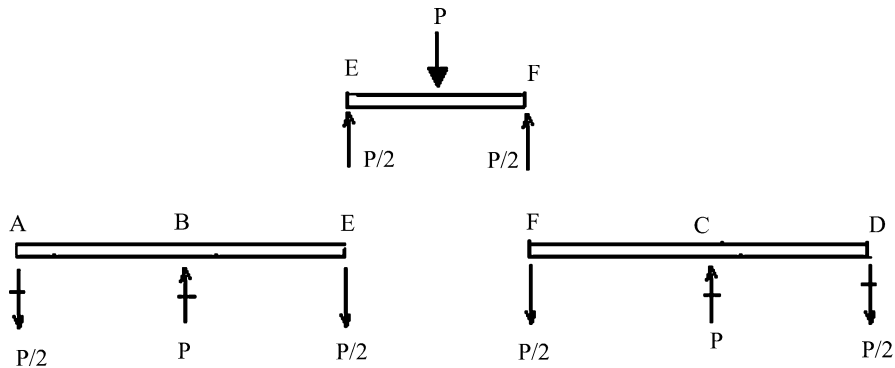
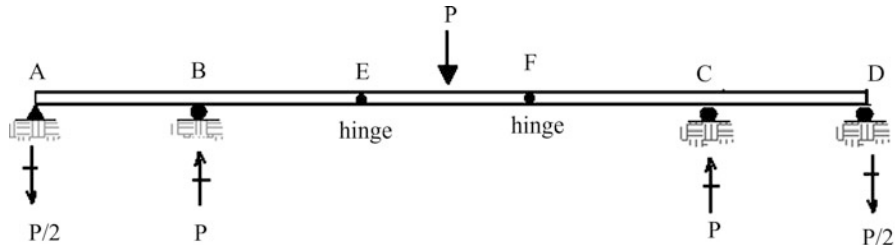


Fig. E3.5a

Solution: We first work with a free body diagram of beam segment EF. Then, with the internal forces at E and F known, we proceed with the analysis of segment ABE and FCD.



The reactions are listed below.



Example 3.6 Horizontal beam supporting a vertical sign

Given: The structure defined in Fig. E3.6a. Member BED is rigidly attached to the beam, ABC. Member FG is simply supported on member BED. Assume member FG has some self-weight, W and is acted upon by a uniform horizontal wind load p . This structure is an idealization of a highway sign supported on a beam.

Determine: The reactions.

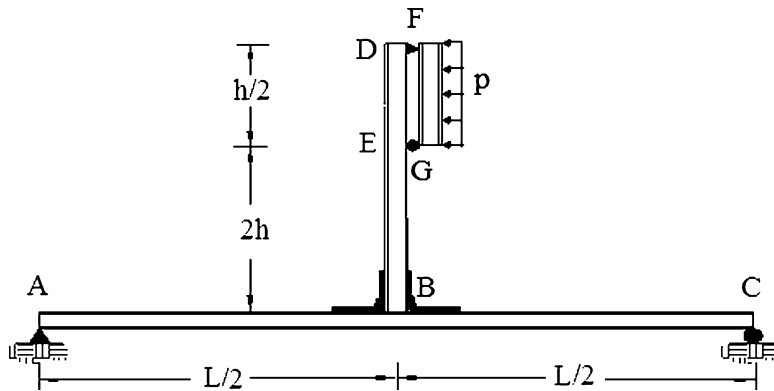
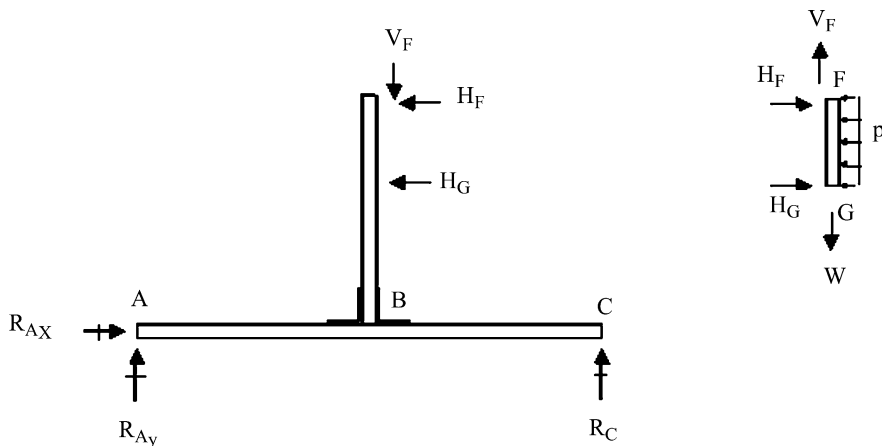


Fig. E3.6a

Solution: We work with two free body diagrams, one for member FG and the other for the remaining part of the structure.

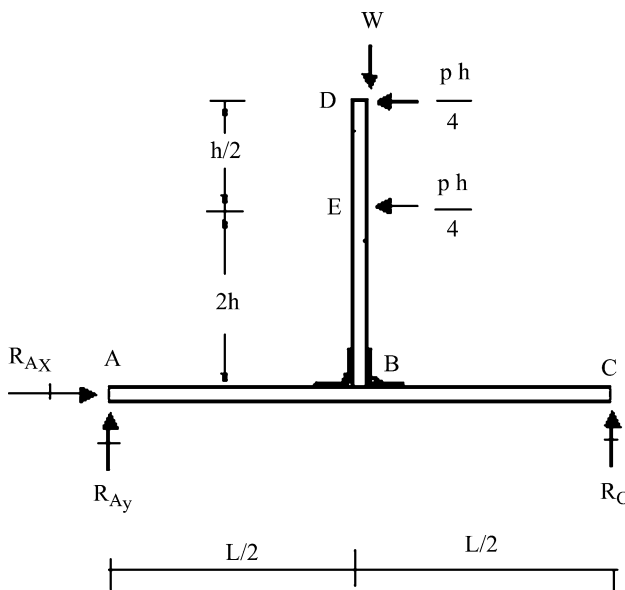


Consider first member FG. Enforcing equilibrium leads to:

$$V_F = W$$

$$H_F = H_G = \frac{ph}{4}$$

Next, we apply these forces to the structure composed of member ABC and member BED. The free body diagram is shown below.



Summing moments about A leads to \$R_C\$

$$\begin{aligned}\sum M_A &= 0 \\ W \frac{L}{2} &= \frac{ph}{4}(2h) + \frac{ph}{4}(2.5h) + R_C L \\ \therefore R_C &= \frac{W}{2} - ph \left(1.125 \frac{h}{L} \right)\end{aligned}$$

The horizontal and vertical reactions at A are

$$\begin{aligned}R_{Ax} &= \frac{ph}{2} \\ R_{Ay} &= \frac{W}{2} + ph \left(1.125 \frac{h}{L} \right)\end{aligned}$$

Note that the vertical reaction at C may become negative if \$ph\$ is large with respect to \$W\$ and \$h\$ is of the order of \$L\$.

3.4 Internal Forces: Planar Loading

We have shown that external loads produce reaction forces. The next question we need to address is: What is the effect of this combination of external loads and reaction forces on the body? We answer this question by examining the equilibrium of an arbitrary segment of the body.

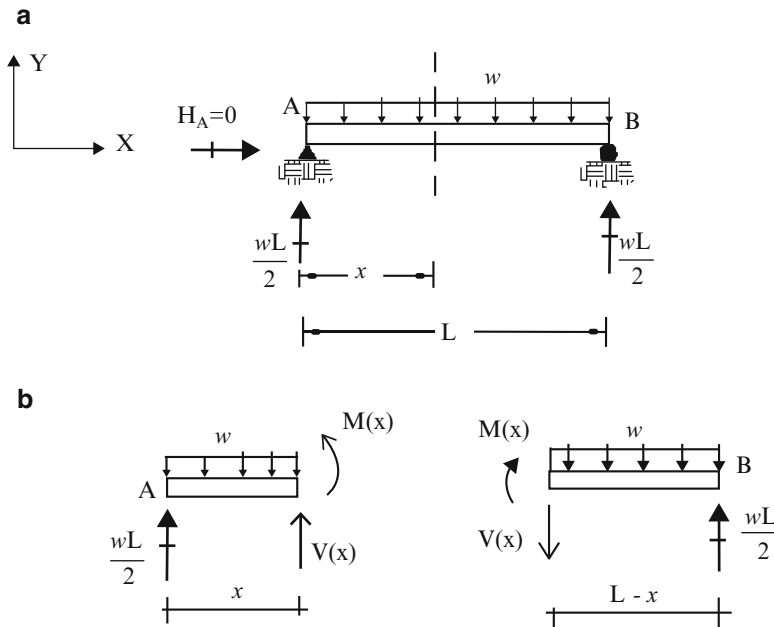


Fig. 3.12 (b) Internal shear and moment

Consider the uniformly loaded, simply supported beam shown in Fig. 3.12a. We pass a cutting plane a distance x from the left end and consider either the left or right segment.

The external loads create a force unbalance. To maintain equilibrium, a vertical force, $V(x)$, and a moment, $M(x)$, are required at the section. We refer to these quantities as the *internal shear force and bending moment*. The magnitudes of $V(x)$ and $M(x)$ for this section are

$$\begin{aligned} V(x) &= -\frac{wL}{2} + wx \\ M(x) &= \frac{wL}{2}x - \frac{wx^2}{2} \end{aligned} \tag{3.3}$$

We need to first define a sign convention for the positive directions of the internal force quantities. This notation is shown in Fig. 3.13 for a positive face, i.e., a face whose outward normal points in the $+X$ direction. The shear force is positive when it points in the $+Y$ direction, and the positive sense for moment is from X to Y . Depending on the external loading, there may also be an axial force. The positive sense for the axial force is taken as the $+X$ direction. These directions are reversed for a negative face.

This sign convention is also used in the matrix formulation of the beam bending problem which is the basis for computer-based analysis software. Historically, some authors use a sign convention for shear which is opposite to this choice. We prefer to employ the above convention since it is consistent with the output of

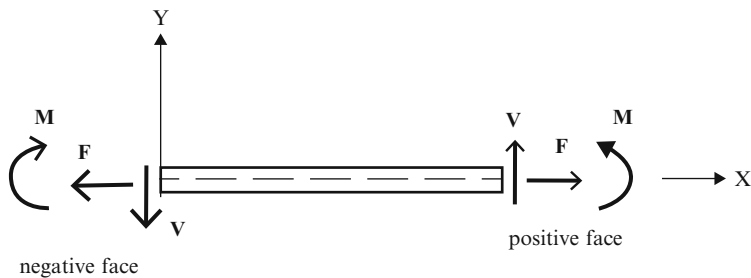


Fig. 3.13 Sign convention for internal forces

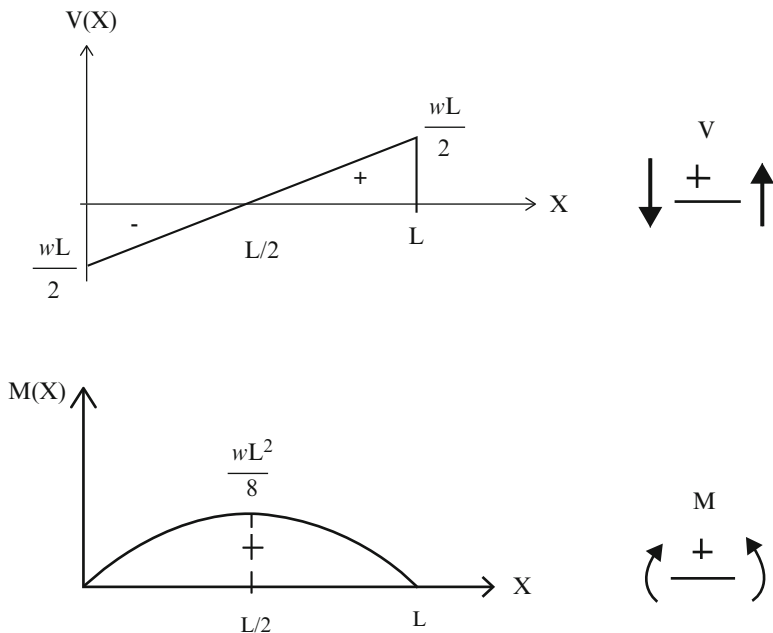


Fig. 3.14 Shear and moment diagrams

structural software systems and therefore allows the reader to transition easily from analytical to digital computation schemes.

Figure 3.14 shows the variation of these quantities over the span. The shear varies linearly with maximum values at the supports. The moment varies parabolically, and the maximum value occurs at mid-span. These plots are called “shear” and “moment” diagrams. Positive moment is plotted on the top face in the USA. In the UK, positive moment is plotted on the bottom face. Again, it is a question of what convention one is most comfortable with.

The maximum bending moment and shear force are used to determine the dimensions of the cross-section. The specific design procedure depends on the material selected, such as wood, steel, or concrete, and the design code adopted.

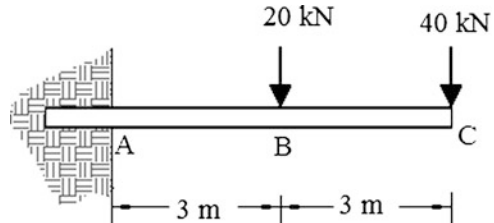
One constructs the internal force distributions by selecting various cutting planes, evaluating the corresponding values, and then extrapolating between the sections. With some experience, one can become very proficient at this operation. We illustrate the process with the following examples.

Example 3.7 Cantilever beam with multiple concentrated loads

Given: The cantilever beam with two concentrated loads shown in Fig. E3.7a.

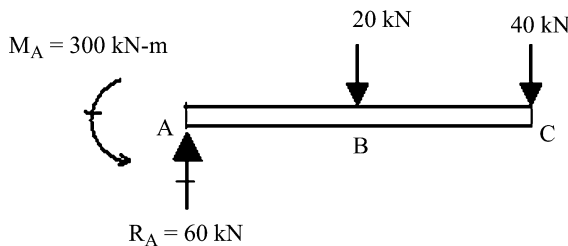
Determine: The shear and moment diagrams.

Fig. E3.7a



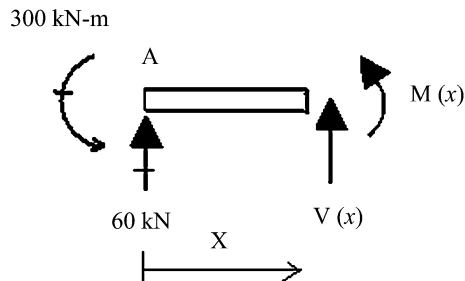
Solution: We first determine the reactions at A by enforcing the equilibrium equations.

$$\begin{aligned}\sum F_y &= 0 \quad R_A - 20 - 40 = 0 \Rightarrow R_A = 60 \text{ kN} \uparrow \\ \sum M_A &= 0 \quad M_A - 20(3) - 40(6) = 0 \Rightarrow M_A = 300 \text{ kN m}\end{aligned}$$



Then we pass a cutting plane between points A and B

$$\begin{aligned}0 \leq x < 3 \quad V(x) &= -60 \\ M(x) &= -300 + 60x\end{aligned}$$

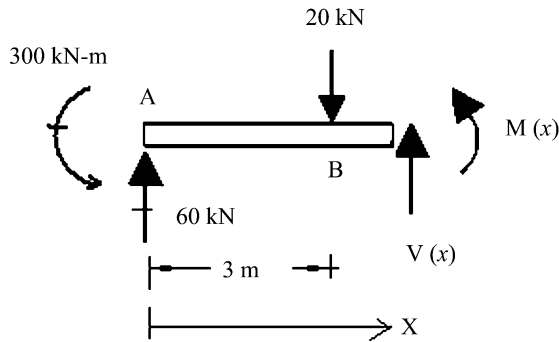


Lastly, we cut between B and C.

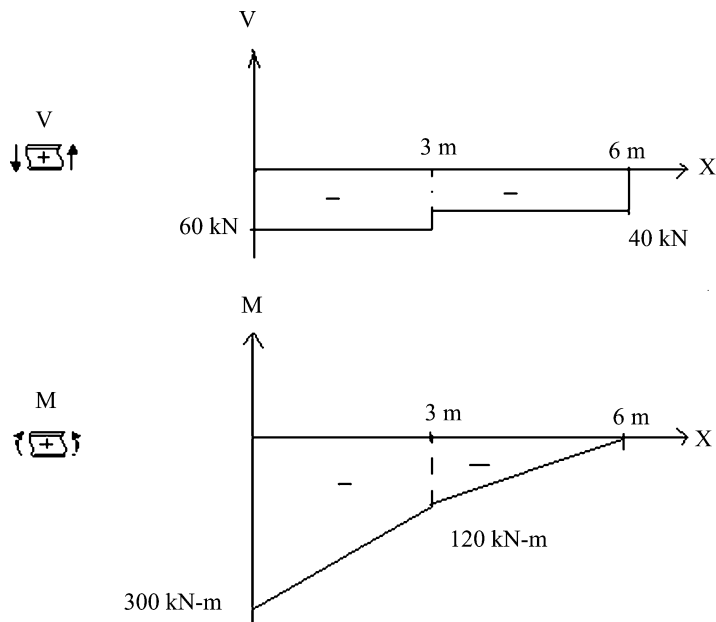
$$3 < x \leq 6$$

$$V(x) = -40$$

$$M(x) = -300 + 60x - 20(x - 3) = 40x - 240$$



The distributions are plotted below.



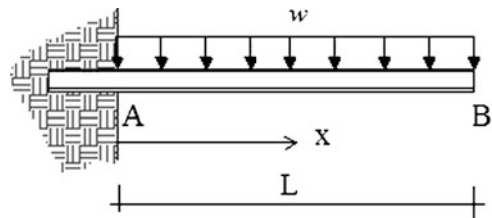
There are some features that we want to point out. Firstly, a concentrated load produces a discontinuity in the form of a “jump” in the shear force, such as at points B and C. Secondly, when the loading consists only of concentrated loads, the shear diagram consists of segments having constant values, and the moment diagram is composed of a set of straight-line segments. We have demonstrated these features here. Later in the next section, we will establish a proof based on equilibrium considerations. A thought question: When would the moment diagram have a jump in the moment value? Hint: Consider Example 3.15.

Example 3.8 Cantilever beam with uniform loading

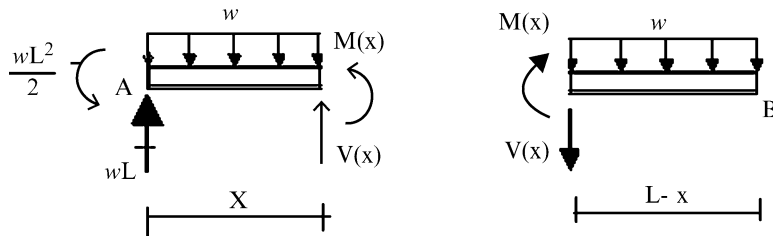
Given: The uniformly loaded cantilever beam shown in Fig. E3.8a.

Determine: The shear and moment distributions.

Fig. E3.8a



Solution: We pass a cutting plane between points A and B. Then we can consider either segment shown below.

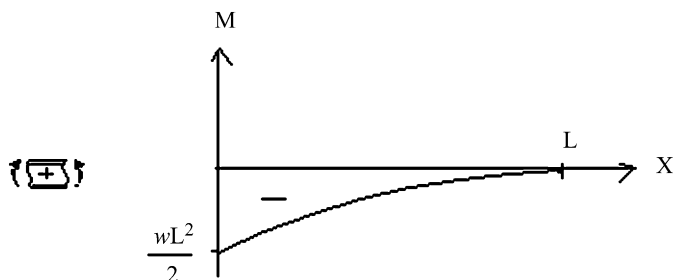
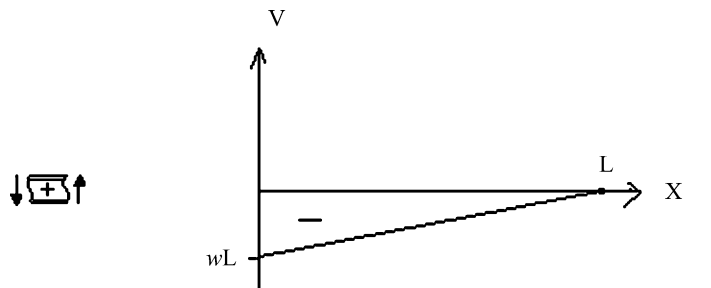


The shear and moment required for equilibrium are

$$0 \leq x \leq L \quad V(x) = -w(L - x)$$

$$M(x) = -\frac{w}{2}(L - x)^2$$

These functions are plotted below. Note that the maximum moment varies as L^2 .

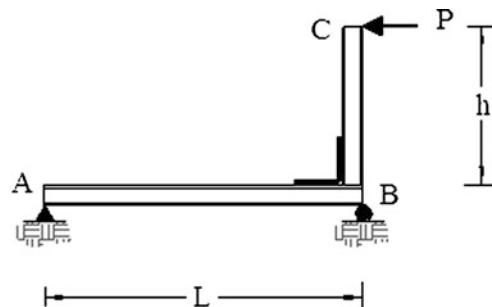


Example 3.9 Beam with an eccentric lateral load

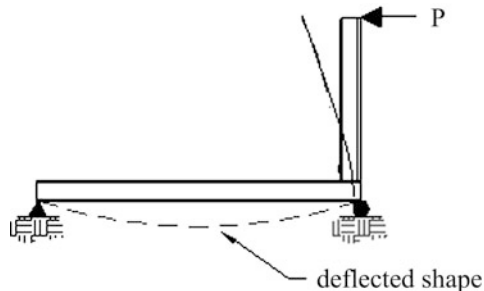
Given: The structure defined in Fig. E3.9a. Member BC is rigidly attached to member AB at B.

Determine: The axial, shear, and moment diagrams.

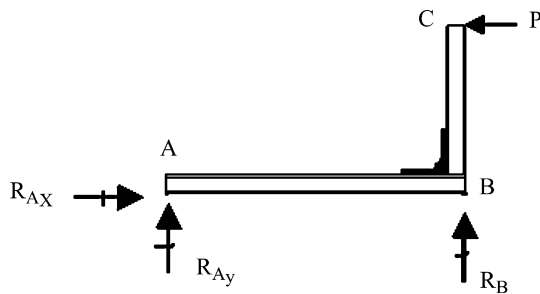
Fig. E3.9a



Solution: Member BC is rigidly attached to the beam, AB, and has a horizontal load applied at its end. The effect of this force is to apply a bending moment at B, which causes beam AB to bend. Figure E3.9b illustrates the deflected shape.

Fig. E3.9b

We determine the reactions first. The free body diagram is shown below.



Moment summation about A leads to

$$\sum M_A = 0$$

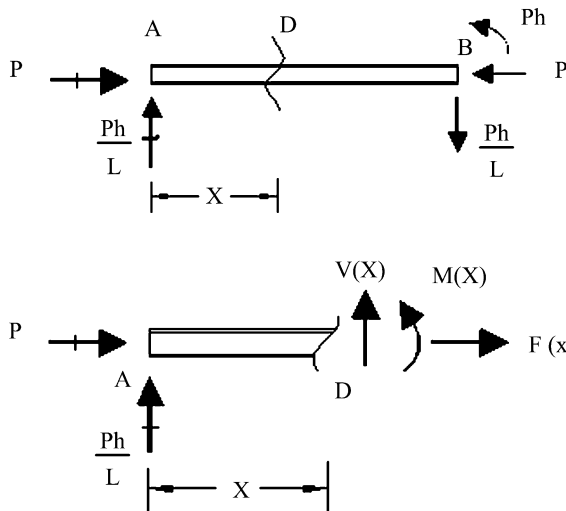
$$R_B L + Ph = 0 \quad \Rightarrow \quad R_B = -\frac{h}{L}P \quad \Rightarrow \quad R_B = \frac{h}{L}P \downarrow$$

The reactions at A required for equilibrium are

$$\sum F_y = 0 \quad R_{Ay} = -V_B = \frac{h}{L}P \quad \Rightarrow \quad R_{Ay} = \frac{h}{L}P \uparrow$$

$$\sum F_x = 0 \quad \Rightarrow \quad R_{Ax} = P \rightarrow$$

Next, we pass a cutting plane at D, isolate the left segment, and enforce equilibrium.



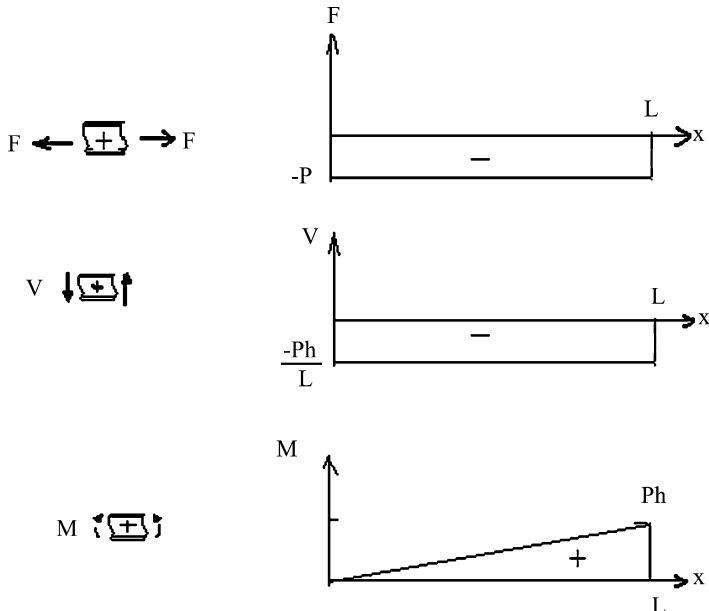
The results are

$$V(x) = -Ph/L$$

$$M(x) = (Ph/L)x$$

$$F(x) = -P$$

The beam is subjected to combined compression and bending: The maximum moment is equal to Ph and occurs at B. This is the critical section for design. Plots of F , V , and M for member AB are shown below.



3.5 Differential Equations of Equilibrium: Planar Loading

The strategy described in the previous section was based on working with a free body diagram of a large segment of the beam and determining the shear and moment by applying the equilibrium equations. We generate the distributions of these quantities by selecting various free body diagrams. This approach is convenient when the loading is fairly simple, i.e., it consists of a combination of concentrated forces and uniformly distributed loadings. For complex distributed loadings expressed as analytic functions, one needs a more systematic approach for enforcing the equilibrium conditions. In what follows, we describe an approach based on applying the equilibrium conditions to a differential element of the beam, resulting in a set of differential equations relating the shear force and moment to the applied distributed loading.

Consider the beam and the differential element shown in Fig. 3.15. We use the same sign convention for V and M as defined in Sect. 3.4. We take the positive sense of the distributed loading to be “downward” since these loadings are generally associated with gravity. Considering V and M to be functions of x , expanding these variables in terms of their differentials, and retaining up to first order terms results in the forces shown in Fig. 3.15b.

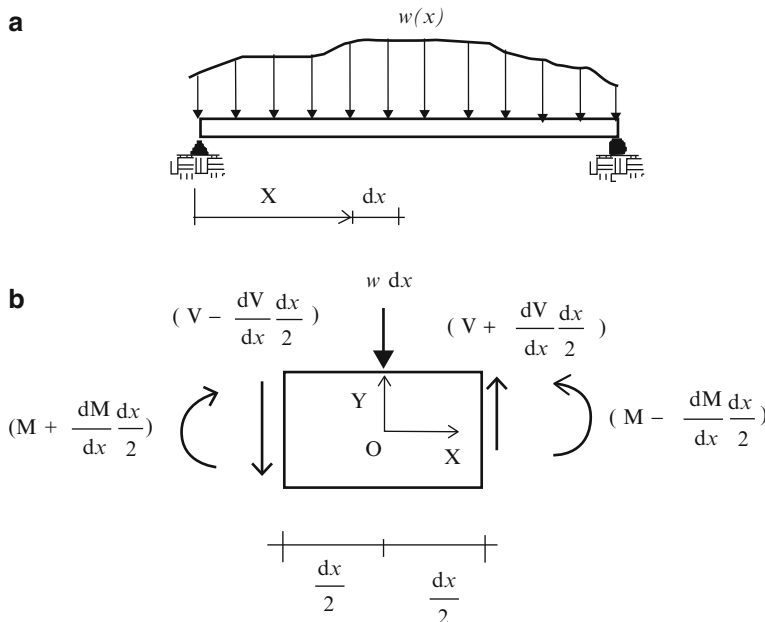


Fig. 3.15 Beam with arbitrary distributed loading. (a) Beam. (b) Differential beam element

Summing forces in the Y direction,

$$V + \frac{dV}{dx} \frac{dx}{2} - \left(V - \frac{dV}{dx} \frac{dx}{2} \right) - w dx = 0$$

and combining terms leads to

$$\left(\frac{dV}{dx} - w \right) dx = 0$$

Lastly, since this equation must be satisfied for arbitrary dx , it follows that

$$\frac{dV}{dx} = w \quad (3.4)$$

In words, “*the rate of change of the shear force is equal to the applied distributed loading.*”

Repeating this analysis for moment summation about point o, the steps are

$$\begin{aligned} M + \frac{dM}{dx} \frac{dx}{2} - \left(M - \frac{dM}{dx} \frac{dx}{2} \right) + \left(V + \frac{dV}{dx} \frac{dx}{2} \right) \frac{dx}{2} + \left(V - \frac{dV}{dx} \frac{dx}{2} \right) \frac{dx}{2} &= 0 \\ \Downarrow \\ \left(\frac{dM}{dx} + V \right) dx &= 0 \\ \Downarrow \\ \frac{dM}{dx} + V &= 0 \\ \Downarrow \\ \frac{dM}{dx} &= -V \end{aligned} \quad (3.5)$$

Equation (3.5) states that “*the rate of change of the bending moment is equal to minus the shear force.*”

These two relations are very useful for checking the consistency of the shear and moment diagrams. One can reason qualitatively about the shape of these diagrams using only information about the loading on a segment of the beam. For example, if $w = 0$, the shear is constant and the moment varies linearly. If $w = \text{constant}$, the shear varies linearly and the moment varies quadratically.

One can establish a set of integral equations by integrating the derivative terms. Consider two points, x_1 and x_2 , on the longitudinal X -axis. Integrating (3.4) and (3.5) between these points leads to

$$V_2 - V_1 = \int_{x_1}^{x_2} w dx \quad (3.6)$$

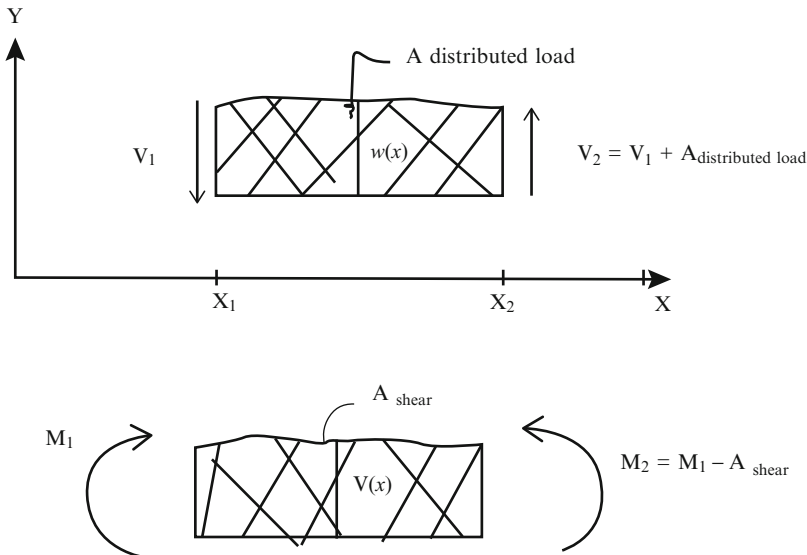


Fig. 3.16 Interpretation of shear and moment in terms of segmental loadings

$$M_2 - M_1 = - \int_{x_1}^{x_2} V \, dx \quad (3.7)$$

The first result can be interpreted as: “*The difference in shear between two points is equal to the area of the distributed loading diagram included between these points.*” The second result relates the *change in moment to the area of the shear diagram*. Figure 3.16 illustrates these interpretations.

The integral forms are useful if one wants to either compute values at discrete points or determine analytical solutions. The differential forms are more convenient for qualitatively reasoning about the shape of the diagrams. We generally use both approaches to construct shear and moment diagrams.

Another useful property that can be established from (3.5) relates to the maximum values of the moment. We know from calculus that extreme values of a continuous function are located at points where the first derivative is zero. Applying this theorem to the moment function, \$M(x)\$, the location \$x^*\$, of an extreme value (either maximum or minimum) of moment is found by solving:

$$\left. \frac{dM}{dx} \right|_{x=x^*} = 0 \quad (3.8)$$

Noting (3.5), it follows that *extreme values of moment occur at points where the shear force is zero*. One first generates the shear diagrams from the applied loading. This process identifies the points of zero shear. If we are interested only in peak values of moment, we can select free body diagrams by passing cutting planes through these locations and apply the equilibrium conditions. This approach is the most direct procedure.

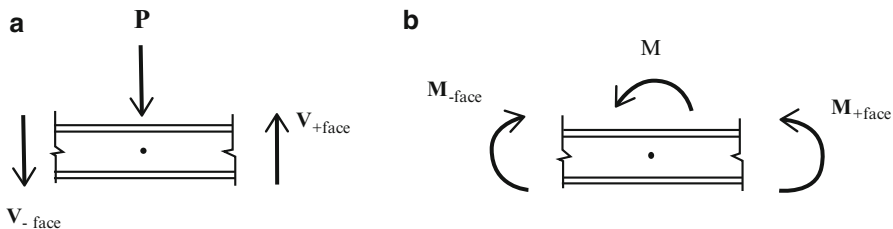


Fig. 3.17 Jump conditions. (a) Shear. (b) Moment

When the loading consists of concentrated forces, the shear diagram has a discontinuity at the point of application of each concentrated force. By considering the equilibrium of a differential element at the point (see Fig. 3.17), one can establish that *the “jump” in shear is equal to the applied load*. Similarly, *the jump in moment is equal to the applied external moment, M* .

$$V_{+face} - V_{-face} = P \quad (3.9)$$

$$M_{+face} - M_{-face} = -M \quad (3.10)$$

One applies (3.6) and (3.7) to generate solutions for the segments adjacent to the discontinuities and uses (3.9) and (3.10) to connect the solutions.

In what follows, we illustrate the application of the differential/integral equation representation to generate shear and moment diagrams. This material overlaps slightly with the material presented in the previous section. Some repetition is useful for reinforcing basic concepts.

Example 3.10 Cantilever beam—triangular loading

Given: A cantilever beam with a triangular distributed loading (Fig. E3.10a).

Determine: $V(x)$ and $M(x)$.

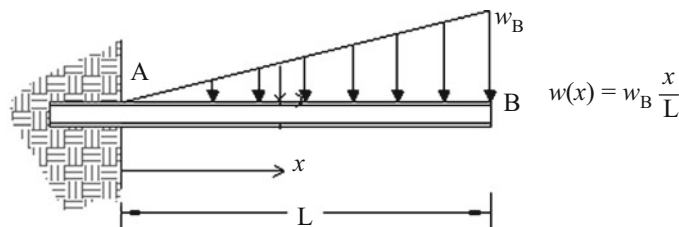


Fig. E3.10a

Solution: First, we determine the reactions at A (Fig. E3.10b)

$$\begin{aligned}\sum F_Y &= 0 \quad V_A = \frac{w_B L}{2} \uparrow \\ \sum M_A &= 0 \quad M_A = \frac{w_B L^2}{3}\end{aligned}$$

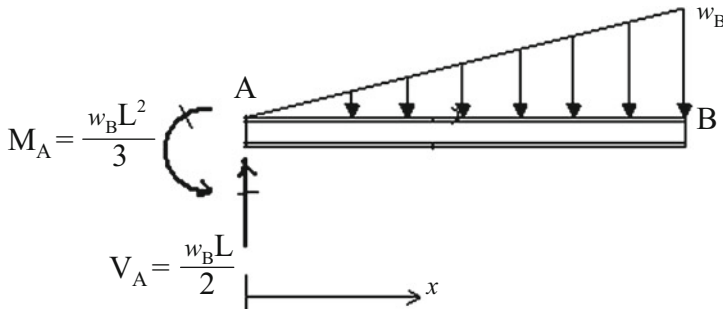


Fig. E3.10b Reactions

Next, we determine the shear, $V(x)$, with (3.5) (Fig. E3.10c). Integrating between points A and x

$$V(x) - V_A = \int_0^x w(x) dx = \int_0^x \frac{w_B x}{L} dx = \frac{w_B x^2}{2L} \Big|_0^x = \frac{w_B x^2}{2L}$$

Noting that $V_A = -\frac{w_B L}{2}$, the solution for $V(x)$ reduces to

$$V(x) = \frac{w_B}{2} \left(-L + \frac{x^2}{L} \right)$$

We determine the moment, $M(x)$, with (3.6)

$$M(x) - M_A = - \int_0^x V(x) dx = \int_0^x \frac{w_B}{2} \left(L - \frac{x^2}{L} \right) dx = \frac{w_B}{2} \left(Lx - \frac{x^3}{3L} \right)$$

Noting that $M_A = -\frac{w_B L^2}{3}$, one obtains

$$M(x) = w_B \left(-\frac{x^3}{6L} + \frac{Lx}{2} - \frac{L^2}{3} \right)$$

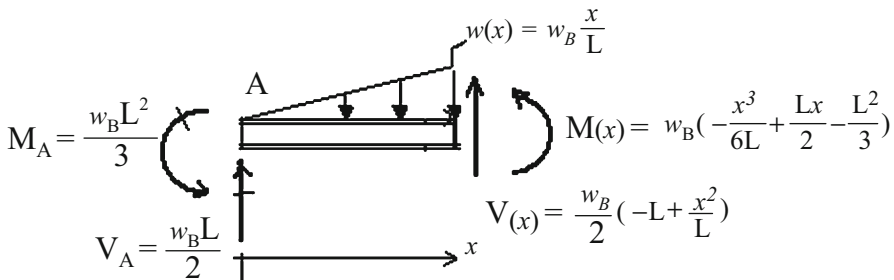
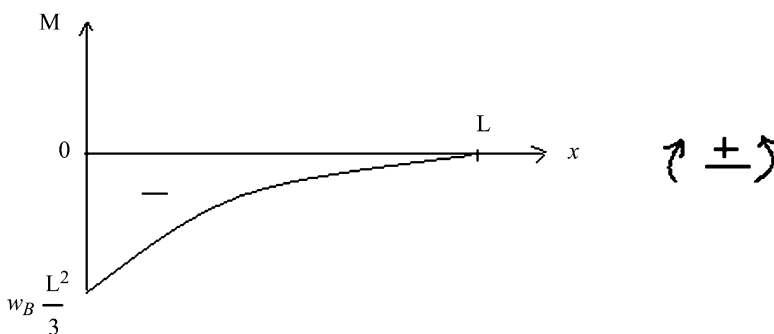
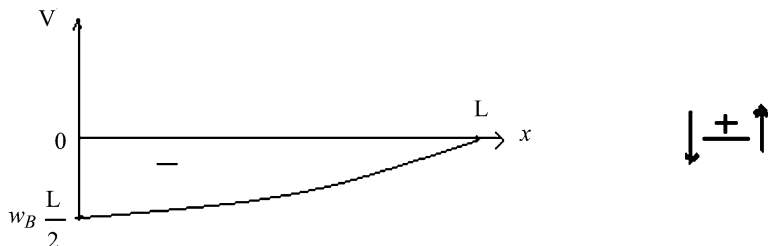


Fig. E3.10c Internal shear and moment

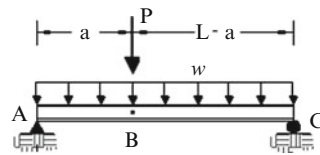
The shear and moment distribution are plotted below. Note that the peak values of shear and moment occur at $x = 0$. Also note that the boundary conditions at B are $V_B = M_B = 0$ since this cross-section is free, i.e., unrestrained and unloaded.



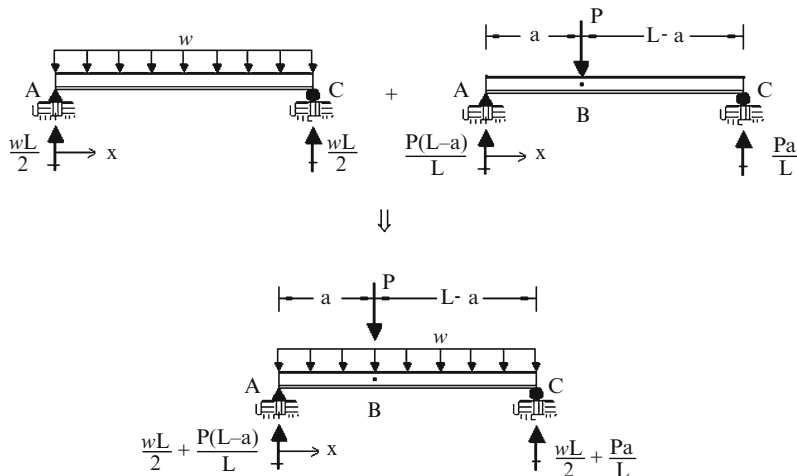
Example 3.11 Distributed and concentrated loads

Given: The beam and loading defined in Fig. E3.11a.

Determine: $V(x)$ and $M(x)$.

**Fig. E3.11a**

Solution: This example illustrates how to deal with a combination of distributed and concentrated loads. We separate the distributed and the concentrated loads and then superimpose the results (Fig. E3.11b).

**Fig. E3.11b** Reactions

We consider first the segment AB. Applying (3.6) and (3.7), and noting the boundary conditions at $x = 0$, the distributions for $0 \leq x < a$ are

$$V(x) = -\frac{wL}{2} - \frac{(L-a)P}{L} + wx$$

$$M(x) = \frac{wL}{2}x + \frac{P(L-a)}{L}x - \frac{1}{2}wx^2$$

The values of V and M just to the left of point B are

$$V_{B-} = -\frac{wL}{2} + wa - \frac{P(L-a)}{L}$$

$$M_{B-} = \frac{wL}{2}a - \frac{1}{2}wa^2 + \frac{P(L-a)}{L}a$$

Applying (3.9) and (3.10) for the jump conditions at B, and noting signs, the quantities just to the right of B are

$$V_{B+} = P + V_{B-} = -\frac{wL}{2} + wa - \frac{Pa}{L}$$

$$M_{B+} = M_{B-} = \frac{wL}{2}a - \frac{1}{2}wa^2 + \frac{P(L-a)}{L}a$$

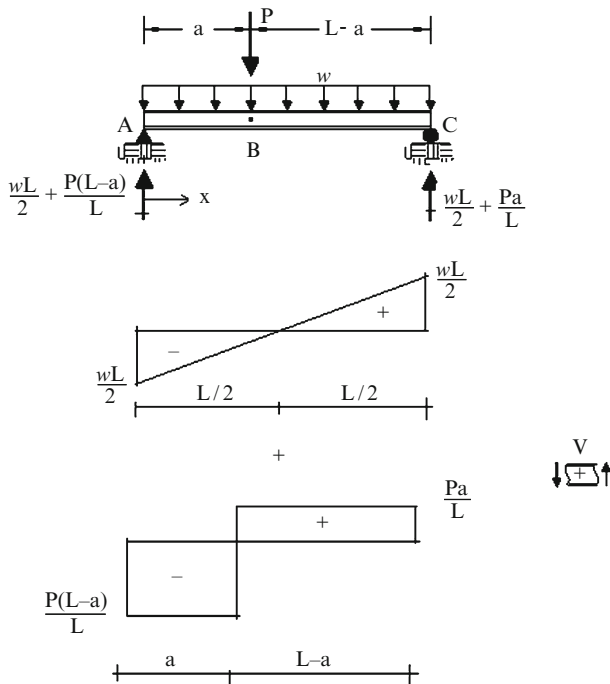
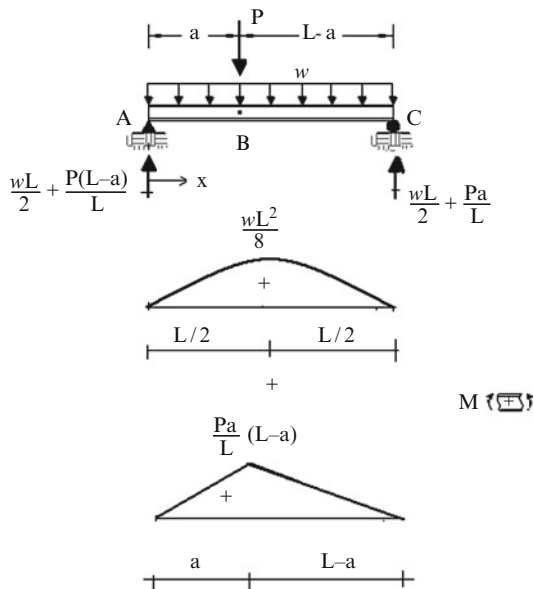
Note that there is no jump in moment for this example.

Applying (3.6) and (3.7), these expressions for $a < x \leq L$ expand to

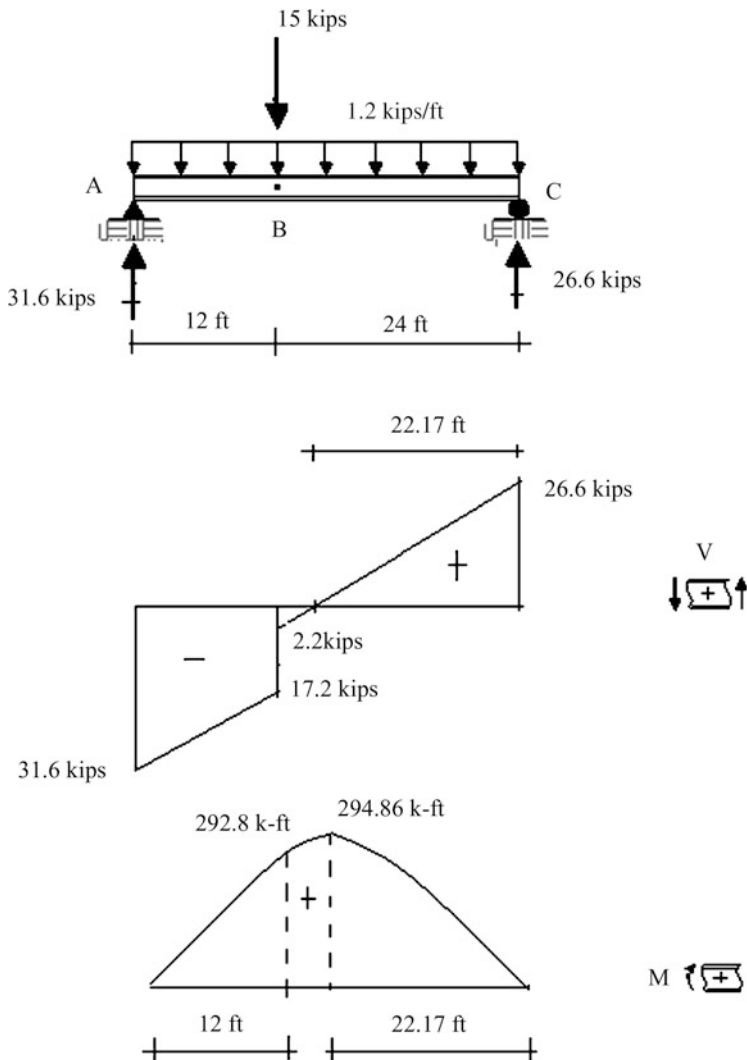
$$V(x) = \frac{Pa}{L} - \frac{wL}{2} + wx$$

$$M(x) = Pa - \frac{Pax}{L} + \frac{wLx}{2} - \frac{wx^2}{2}$$

The approach we followed here is general and applies for all loadings. It is fairly straightforward to establish the expressions for the regions $0 \leq x < a$ and $a < x \leq L$. An easier way to obtain the shear and moment diagrams for this example would be to generate separate diagrams for the two types of loadings and then superimpose the results. The individual shear and moment diagrams are plotted below (Figs. E3.11c, d).

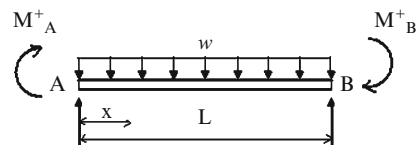
**Fig. E3.11c** Shear diagrams**Fig. E3.11d** Moment diagrams

Suppose $P = 15$ kip, $a = 12$ ft, $L = 36$ ft and $w = 1.2$ kip/ft. The combined shear and moment diagrams are plotted below.



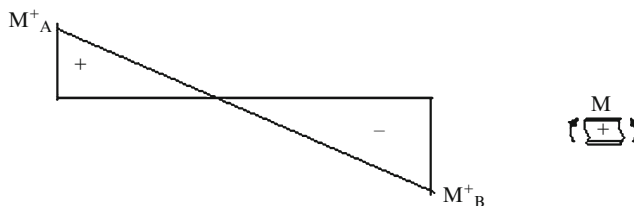
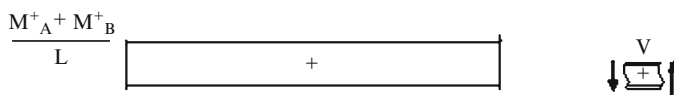
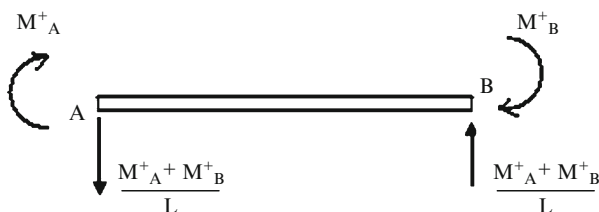
Example 3.12 Uniform loading combined with end moments

Given: A simply supported beam subjected to a uniform loading and bending moments at the ends. This is a typical case for a floor beam in a rigid building frame, i.e., where the beam-column connections apply moment to the ends of the beam (Fig. E3.12a).

Fig. E3.12a

Determine: The location and magnitude of the maximum moment.

Solution: We consider separate loadings and then superimpose the results. The solution due to the end moment is (Fig. E3.12b)

**Fig. E3.12b**

The uniform loading provides the following distribution (Fig. E3.12c):

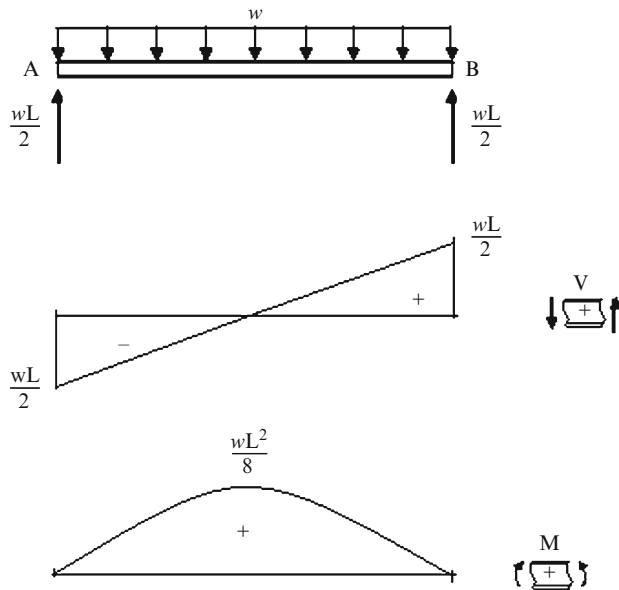


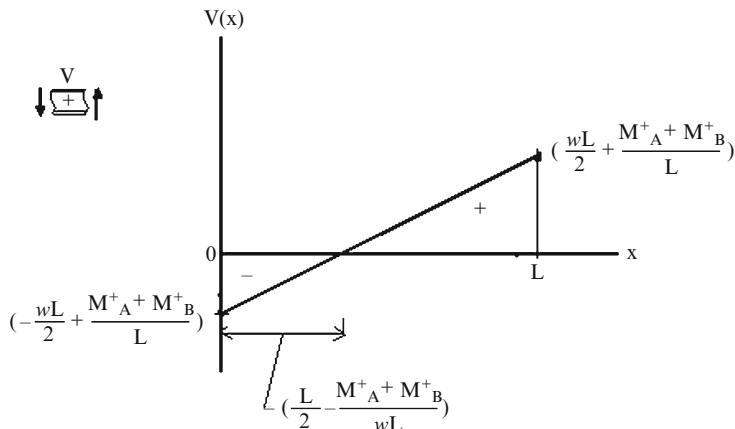
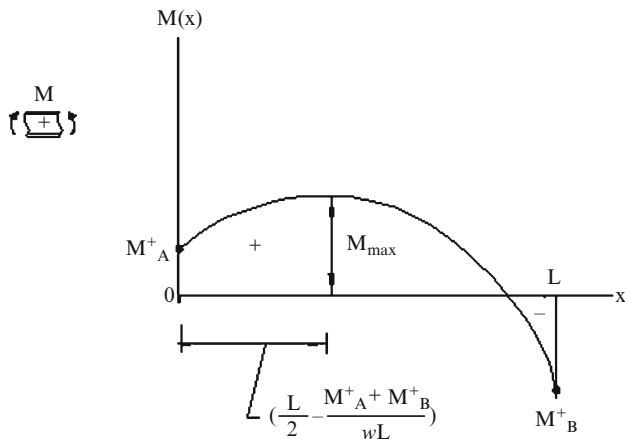
Fig. E3.12c

Combining these solutions leads to the analytical solution

$$V(x) = -\frac{wL}{2} + wx + \frac{M_A^* + M_B^*}{L}$$

$$M(x) = M_A^* - \frac{M_A^* + M_B^*}{L}x + \frac{wL}{2}x - \frac{wx^2}{2}$$

These functions are plotted below (Figs. E3.12d, e).

**Fig. E3.12d****Fig. E3.12e**

The peak moment occurs where the shear is zero. Noting the plot of $V(x)$, the shear is zero at x_{\max} .

$$\begin{aligned} V &= 0 \\ \Downarrow \\ x_{\max} &= \frac{L}{2} - \frac{M_A^* + M_B^*}{wL} \end{aligned}$$

The form of the solution suggests that we express the sum of the end moments as

$$M_A^* + M_B^* = \frac{\alpha}{2} wL^2$$

where α is a dimensionless parameter. Substituting for this term, the equation simplifies to

$$x_{\max} = \frac{L}{2}(1 - \alpha)$$

Lastly, we determine M_{\max} using this value for x .

$$M_{\max} = M_A^* + \frac{wL^2}{8}(1 - \alpha)^2$$

Given w and the end moments, one evaluates α ,

$$\alpha = \frac{\frac{M_A^* + M_B^*}{wL^2}}{2}$$

and then M_{\max} . When $\alpha = \pm 1$, the peak moment occurs at an end point and equals the applied end moment.

The case where the end moments are equal in magnitude but opposite in sense is of considerable interest. One sets $M_A^* = -M_B^* = -M^*$, and it follows that $\alpha = 0$. The moment diagram is symmetrical with respect to the centerline. The peak negative values of moment occur at the end points; the peak positive moment occurs at the center point of the span (Fig. E3.12f).

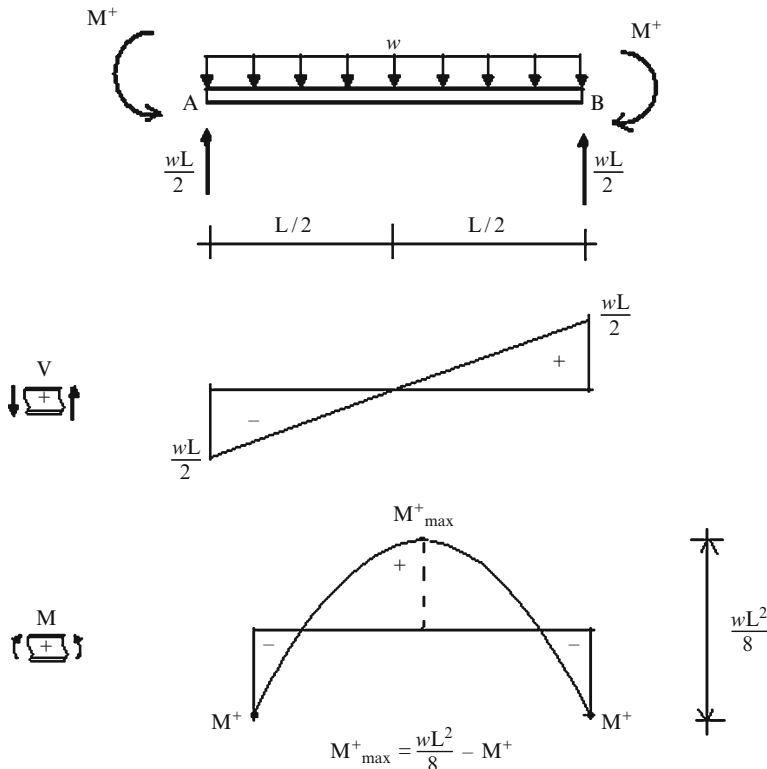


Fig. E3.12f

When there is no end restraint, $M^* = 0$. Then $M_{\max}^+ = wL^2/8$. The effect of end restraint is to *reduce* the positive moment and introduce a negative moment at the ends. This behavior is typical for rigid frames such as building frames subjected to gravity loading. We examine this behavior in more detail in Chap. 15.

Example 3.13

Given: The beam shown in Fig. E3.13a

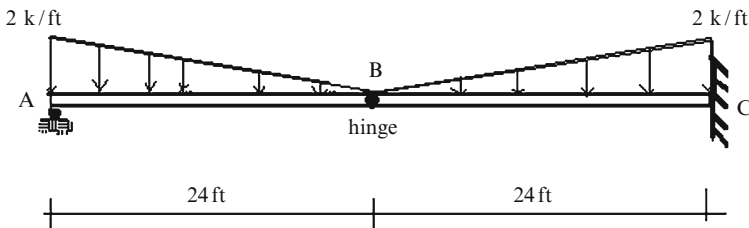


Fig. E3.13a

Determine: The reactions, shear, and bending moment distributions.

Solution: We draw the free body diagram of beam segment AB. Applying the equilibrium conditions to this segment results in (Fig. E3.13b)

$$\begin{aligned}\sum M_A &= 0 \quad V_B(24) - (2)\frac{(24)}{2}\frac{(24)}{3} = 0 \quad V_B = 8 \text{ kip} \\ \sum F_y &= 0 \quad R_A - (2)\frac{(24)}{2} + 8 = 0 \quad R_A = 16 \text{ kip}\end{aligned}$$

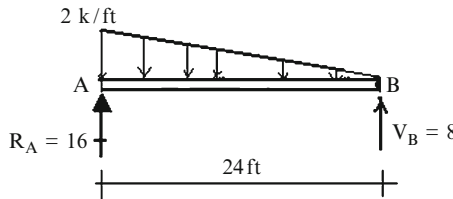
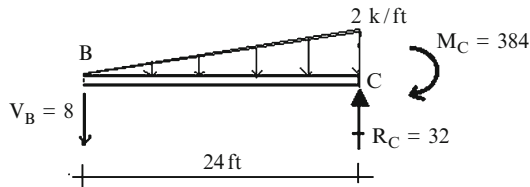


Fig. E3.13b Segment AB

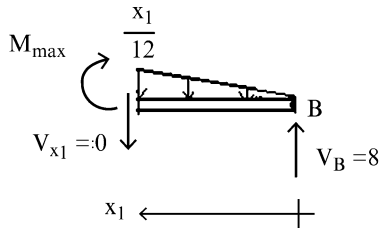
With the internal force at B known, one can now proceed with the analysis of segment BC (Fig. E3.13c).

$$\begin{aligned}\sum F_Y &= 0 \quad -(2)\frac{(24)}{2} - 8 + R_C = 0 \quad \Rightarrow \quad R_C = 32 \text{ kip } \uparrow \\ \sum M_C &= 0 \quad -M_C + 8(24) + (2)\frac{(24)}{2}\frac{(24)}{3} = 0 \quad \Rightarrow \quad M_C = 384 \text{ kip ft clockwise}\end{aligned}$$

**Fig. E3.13c** Segment BC

The peak moment occurs where the shear is zero.

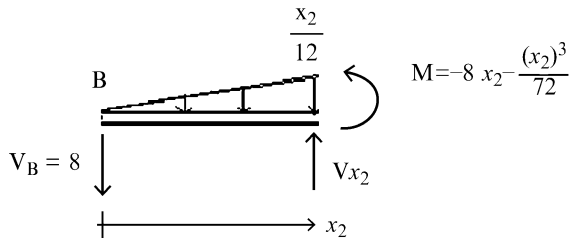
Segment AB:



$$\sum F_y = 0 \quad 8 - \frac{1}{2} \left(\frac{x_1}{12} \right) x_1 = 0 \quad \rightarrow \quad x_1 = 13.85 \text{ ft}$$

$$\therefore M_{\max} = 8(13.85) - (13.85) \left(\frac{13.85}{12} \right) \frac{1}{2} \left(\frac{13.85}{3} \right) = +73.9 \text{ kip ft}$$

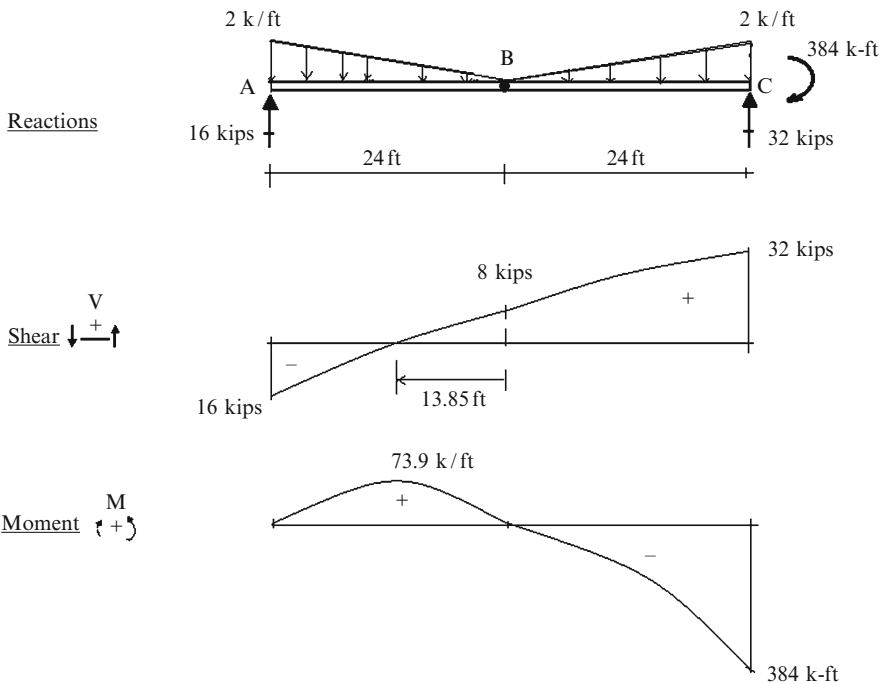
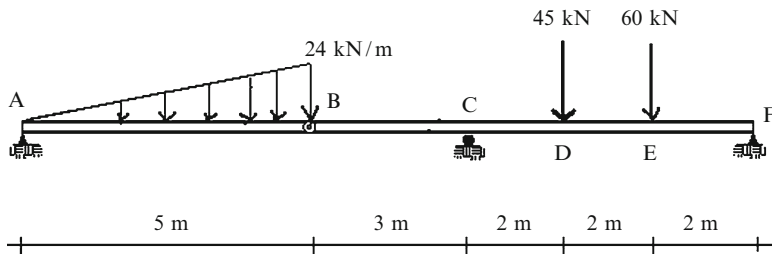
Segment BC:



$$\sum F_y = 0 \quad V_{x2} = 8 + \frac{1}{2} \left(\frac{x_2}{12} \right) x_2 \neq 0$$

\therefore Therefore, there is no peak moment between B and C.

The shear and bending moment diagrams are listed below (Fig. E3.13d).

**Fig. E3.13d****Example 3.14****Given:** The beam shown in Fig. E3.14a**Fig. E3.14a****Determine:** The reactions, and the shear and bending moment distributions.**Solution:** Applying the equilibrium conditions to the free body diagram of beam segment AB results in (Fig. E3.14b)

$$\sum F_x = 0 \quad R_{AX} = 0$$

$$\sum M_A = 0 \quad V_B(5) - (24)\left(\frac{5}{2}\right)\left(\frac{2}{3}\right)(5) = 0 \quad V_B = 40 \uparrow$$

$$\sum F_y = 0 \quad R_{AY} + 40 - (24)\left(\frac{5}{2}\right) = 0 \quad R_{AY} = 20 \uparrow$$

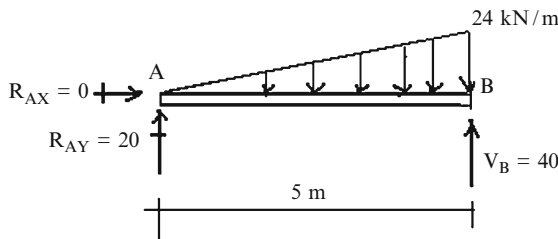


Fig. E3.14b Segment AB

With the internal force at B known, one can now proceed with the analysis of segment BCDEF (Fig. E3.14c).

$$\begin{aligned} \sum M_F &= 0 \quad R_C(6) - 40(9) - 45(4) - 60(2) = 0 \quad R_C = 110 \uparrow \\ \sum F_y &= 0 \quad R_F + 110 - 60 - 45 - 40 = 0 \quad R_F = 35 \uparrow \end{aligned}$$

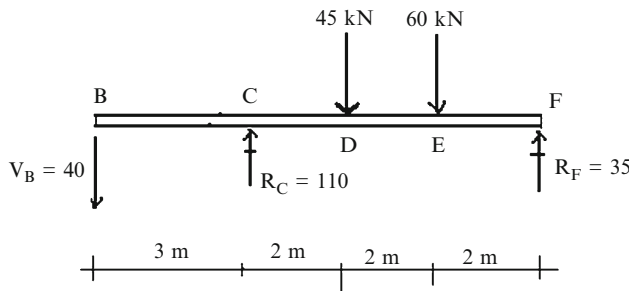
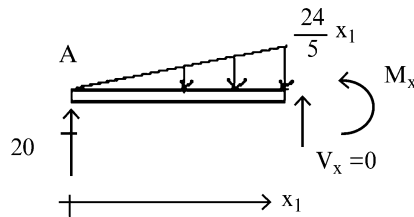


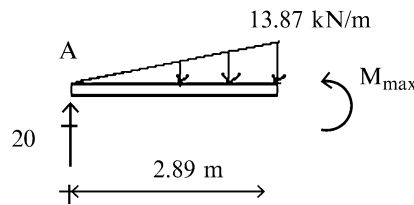
Fig. E3.14c

The last step invokes establishing the expressions for V and M .
The peak moment occurs where the shear is zero.

Segment AB:

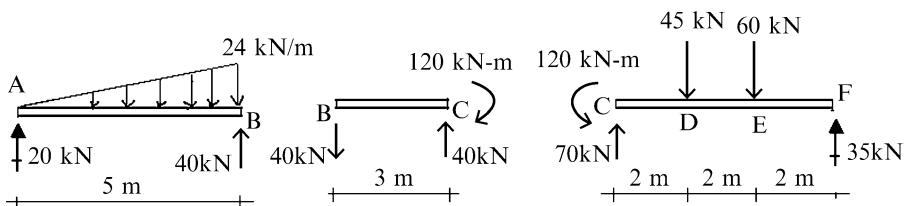


$$\sum F_y = 0 \quad 20 - \frac{1}{2} \left(\frac{24}{5} x_1 \right) x_1 = 0 \quad \rightarrow \quad x_1 = 2.89 \text{ m}$$

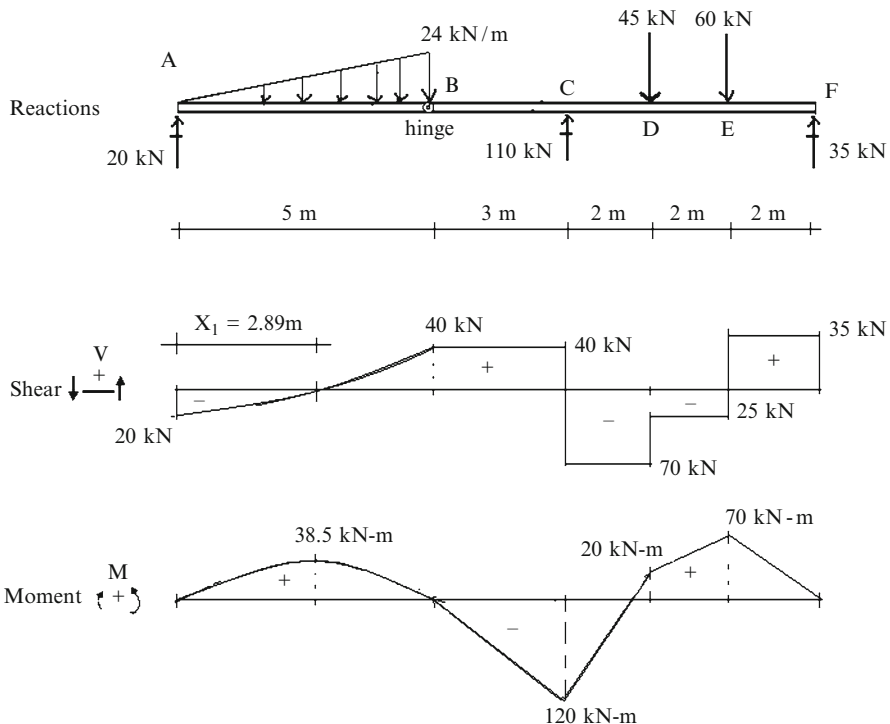
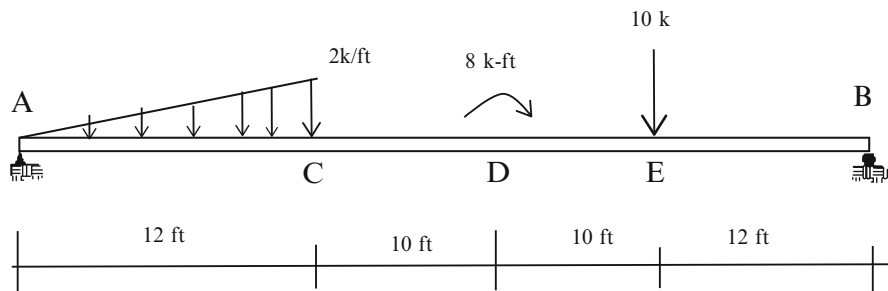


$$\therefore M_{\max} = 20(2.89) - \frac{1}{2}(2.89)(13.87) \frac{1}{3}(2.89) = +38.5 \text{ kNm}$$

Next, we determine the remaining end moments and end shears for segments AB, BC, and CF using the equilibrium equations for the members.



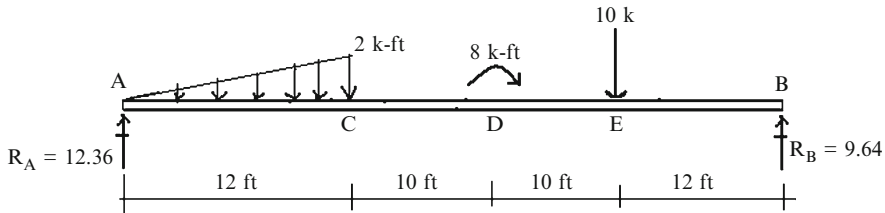
The reactions, shear, and bending moment distributions are listed below. Note that the moment distribution for segment AB is a cubic function (Fig. E3.14d).

**Fig. E3.14d***Example 3.15***Given:** The beam shown in Fig. E3.15a**Determine:** The reactions, and the shear and bending moment distributions.**Fig. E3.15a**

Solution: We first determine the reaction at B using $\sum M_A = 0$. We then compute the reaction at A by summing forces in the Y direction (Fig. E3.15b).

$$\sum M_A = 0 \quad -R_B(44) + (2)\left(\frac{12}{2}\right)\frac{2}{3}(12) + 8 + 10(32) = 0 \quad R_B = 9.64 \uparrow$$

$$\sum F_Y = 0 \quad R_A - 2\left(\frac{12}{2}\right) - 10 + 9.64 = 0 \quad R_A = 12.36 \uparrow$$

**Fig. E3.15b**

Applying (3.7) to the different segments results in:
Segment EB

$$M_B - M_E = - \int_{E \rightarrow B} V dx = -9.64(12) = -115.68$$

$$M_B = 0 \quad \therefore M_E = 115.68 \text{ kip ft}$$

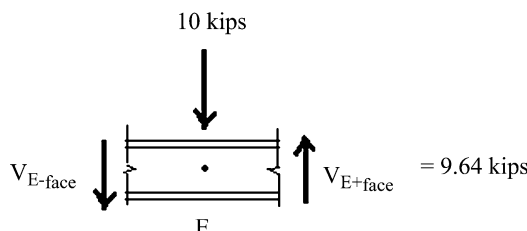
Segment DE

$$M_E - M_D = - \int_{E \rightarrow B} V dx = -(-0.36)(10) = 3.6$$

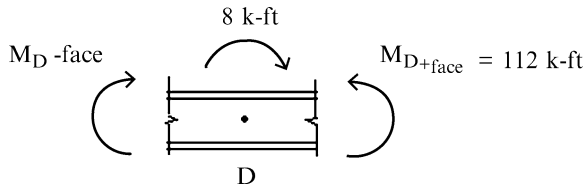
$$M_E = 115.68 \quad \therefore M_D = 112 \text{ kip ft}$$

Note that there is a jump in the shear at E.

$$\sum F_y = 0 \quad V_{E-\text{face}} - 9.64 + 10 = 0 \quad V_{E-\text{face}} = -0.36 \quad V_{E+\text{face}} = 0.36 \uparrow \text{kip}$$



Note that there is a jump in the bending moment at D.



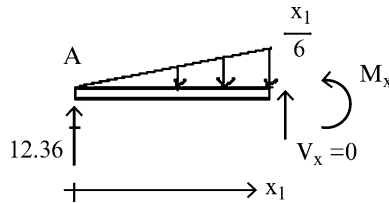
$$\sum M = 0 \quad M_{D\text{-face}} + 8 - 112 = 0 \quad M_{D\text{-face}} = 104 \text{ kip ft}$$

Segment CD

$$M_D - M_C = - \int_{E \rightarrow B} V dx = -(-0.36)(10) = 3.6$$

$$M_D = 104. \quad \therefore M_C = 100.4 \text{ kip ft}$$

Segment AC

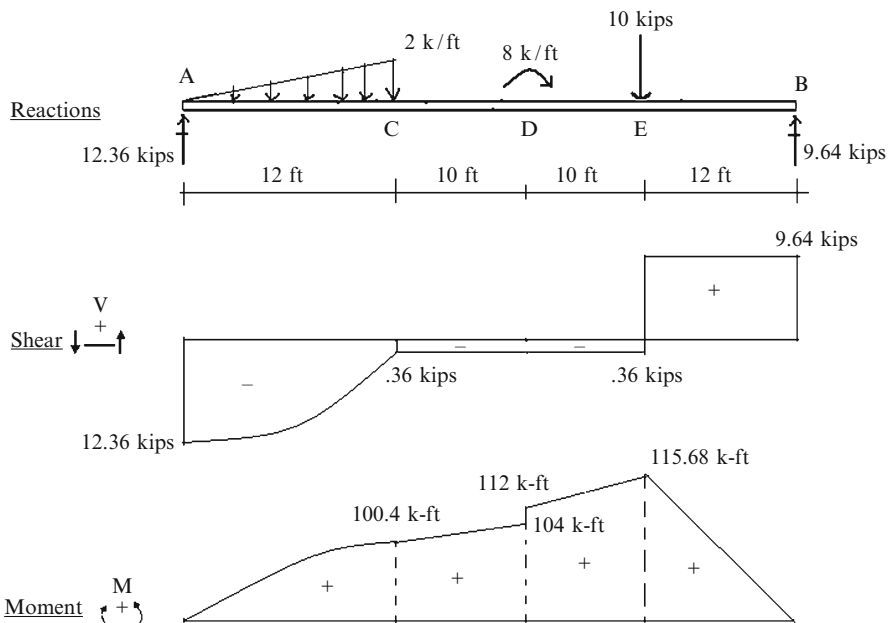


$$\sum F_y = 0 \quad 12.36 - \frac{1}{2} \left(\frac{1}{6} x_1 \right) x_1 = 0 \quad \rightarrow \quad x_1 = 12.18 \text{ ft}$$

$$x_1 = 12.18 \text{ ft} > 12 \text{ ft.}$$

Therefore, shear will not be zero between A and C.

The reactions, shear, and bending moment distributions are listed below (Fig. E3.15c).

**Fig. E3.15c**

3.6 Displacement and Deformation of Slender Beams: Planar Loading

Figure 3.18 shows how a slender beam responds to a transverse planar loading. The geometric quantities that define the movement of the beam from its unloaded position due to an applied loading are defined as the displacements. Displacements are also referred to as deflections. Consider the segment of a homogeneous beam shown in Fig. 3.19. We take the X -axis to coincide with the initial position of the centroidal axis, and the Y -axis to be 90° counterclockwise from the X -axis. When the loading is applied in the $X-Y$ plane, points on the centroidal axis move horizontally and vertically. We assume the cross-section, which is initially normal to the centroidal axis, remains normal to the curve connecting the displaced points. This is a standard assumption for beams known as “Kirchoff’s” hypothesis and implies that the cross-section rotates through the same angle as the tangent to the centroidal axis. Kirchoff’s hypothesis is valid for slender beams, i.e., beams having a depth to span ratio less than about 0.1. With this assumption, the independent geometric measures are the two displacement components, $u(x)$ and $v(x)$, which are functions of x for static loading. Given $v(x)$, we find the cross-sectional rotation, $\theta(x)$, with the geometric relation,

$$\tan\theta = \frac{dv}{dx}$$

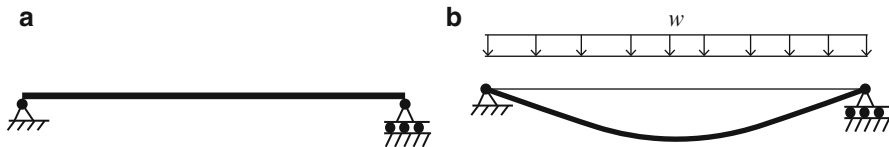


Fig. 3.18

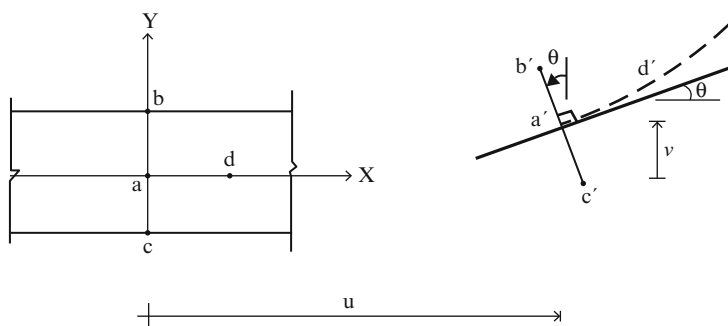


Fig. 3.19 Definition of displacement components

The next assumption that we introduce concerns the magnitude of θ . We assume here that θ^2 is small in comparison to unity, which implies that the tangent is essentially equal to the angle in radians:

$$\tan\theta \approx \theta \quad (3.11)$$

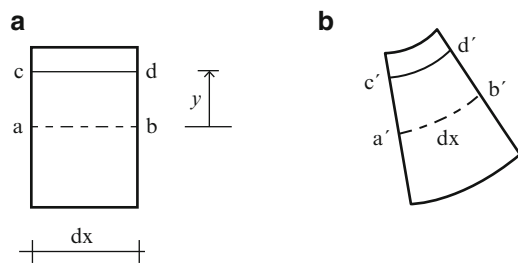
Then the expression for θ reduces to

$$\theta \approx +\frac{dv}{dx} \quad (3.12)$$

Deformations are dimensionless strain measures resulting from displacements. Consider the differential elements shown in Fig. 3.20. The initial rectangular shape is transformed to a quadrilateral shape with curved upper and lower edges. Adjacent cross-sections experience a relative rotation equal to $d\theta/dx dx$, which causes line elements parallel to the centroidal axis to either elongate or contract. These changes in length produce extensional strains. A line element located y units above the centroidal axis experiences a strain $\varepsilon(y)$ equal to

$$\varepsilon(y) = -y \frac{d\theta}{dx} \quad (3.13)$$

Fig. 3.20 Differential beam elements. (a) Initial.
(b) Deformed



According to this model, the strain varies linearly over the cross-section and the peak strain values occur at the upper and lower surfaces; the centroidal axis is not strained.

At this point, we introduce some standard notation for the derivative of the cross-section rotation angle, θ .

$$\chi = \text{curvature} \equiv \frac{d\theta}{dx} \approx \frac{d^2v}{dx^2} \text{ (units of radians/length)} \quad (3.14)$$

$$\rho = \text{radius of curvature} = \frac{1}{\chi} \text{ (units of length)}$$

We prefer to work with the curvature and express the extensional strain as

$$\varepsilon = -y\chi \quad (3.15)$$

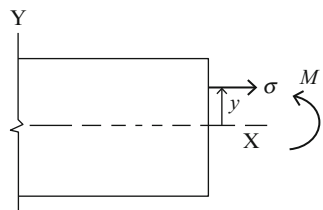
Given χ , one can establish qualitatively the shape of the curve defining the displaced centroidal axis. An analytical solution for the displacement, v , can also be determined by integrating (3.14). We will illustrate both procedures in later sections.

3.6.1 Moment: Curvature Relationship

We have demonstrated how to establish the bending moment distribution corresponding to a given loading. We have also showed how the displacement field can be generated once the curvature is known. To find the displacements due to a given loading, we need to relate the moment and the corresponding curvature along the centroidal axis. Given this relationship, it is a fairly straightforward process to move from prescribed loading to the resulting displacement.

The positive sense of the bending moment on a positive cross-section is defined as counterclockwise. Then noting Fig. 3.21, the moment and normal stress are related by

Fig. 3.21 Definition of normal stress and moment



$$M = \int_A -y\sigma dA \quad (3.16)$$

We determine the stress using the stress-strain relation. In what follows, we assume the material behavior is linear elastic. The stress is a linear function of the strain in this case.

$$\sigma = E\varepsilon = -yE\chi \quad (3.17)$$

where E is Young's modulus for the material. Substituting for σ in (3.16) leads to

$$M = EI\chi \quad (3.18)$$

where $I = \int y^2 dA$. Given M and EI , one finds the curvature (χ) with

$$\chi = \frac{M}{EI} \quad (3.19)$$

and then the displacement v by integrating

$$\frac{d^2v}{dx^2} = \chi = \frac{M}{EI} \quad (3.20)$$

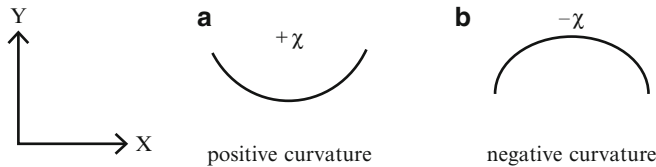
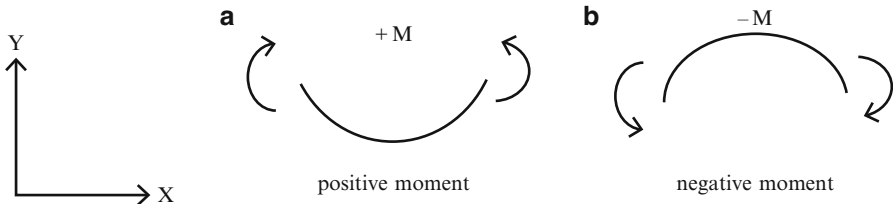
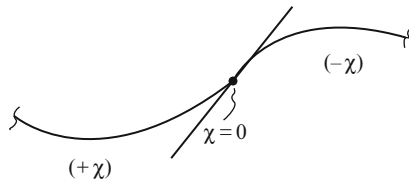
The complete solution of (3.20) consists of a homogenous term and a particular term,

$$v = c_0 + c_1x + v_p \quad (3.21)$$

where v_p is the particular solution corresponding to the function, M/EI , and c_0, c_1 are constants. Two boundary conditions on v are required to determine c_0 and c_1 .

3.6.2 Qualitative Reasoning about Deflected Shapes

Noting (3.18) and the fact that EI is always positive, it follows that the sense of curvature χ is the same as the sense of M . The deflected shapes corresponding to positive and negative curvature are shown in Fig. 3.22. It is more convenient to

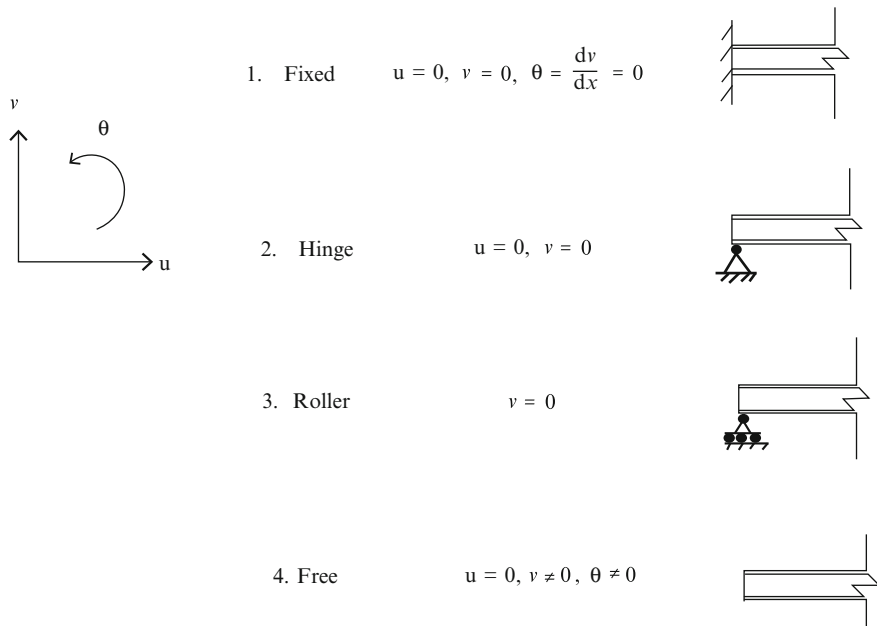
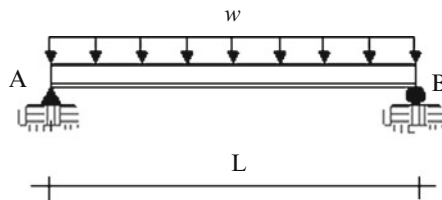
**Fig. 3.22** Deflected shapes for positive and negative curvature**Fig. 3.23** Deflected shape for positive and negative moments**Fig. 3.24** Shape transition at an inflection point

interpret these deflected shapes as the result of applying positive and negative moments. Figure 3.23 illustrates this interpretation.

We divide the moment diagrams into positive and negative moment zones and identify, using Fig. 3.23, the appropriate shape for each zone. Points where the moment changes sign are called inflection points. The curvature is zero at an inflection point, which implies that the curve is locally straight. We deal with inflection points by adjusting the orientation of adjoint shapes such that their tangents coincide at the inflection point. Figure 3.24 illustrates this process.

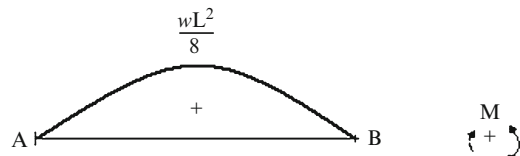
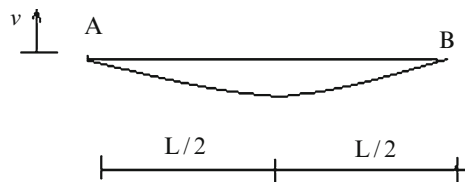
The last step involves enforcing the displacement boundary conditions associated with supports. Figure 3.25 shows three types of supports: full fixity, hinge, and roller. The corresponding displacement measures that are constrained by these supports are as follows.

The deflected shape must pass through a support. If an end is fixed, the cross-section cannot rotate at that point. We need to orient the deflected shape such that the tangent coincides with the initial centroidal axis. In what follows, we present a series of examples which illustrate the process of developing qualitative estimates of deflected shapes given the bending moment distribution.

**Fig. 3.25** Types of supports—displacement measures**Example 3.16** Deflected shape—uniformly loaded, simply supported beam**Given:** The uniformly loaded, simply supported beam shown in Fig. E3.16a.**Determine:** The deflected shape.**Fig. E3.16a****Solution:** The moment is positive throughout the span so Fig. 3.23a applies. The displacement boundary conditions require

$$v(0) = v(L) = 0$$

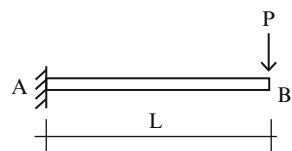
One starts at the left end, sketches a curve with increasing positive curvature up to mid-span and then reverses the process. The deflected shape is symmetrical with respect to mid-span since the moment diagrams and support locations are symmetrical (Figs. E3.16b, c).

Fig. E3.16b Moment diagram**Fig. E3.16c** Deflected shape

Example 3.17 Deflected shape—cantilever beam

Given: The cantilever beam defined in Fig. E3.17a.

Determine: The deflected shape.

Fig. E3.17a

Solution: We note that the moment is negative throughout the span. Point A is fixed and therefore the tangent must be horizontal at this point. The displacement boundary conditions require

$$v(0) = \theta(0) = 0$$

We start at point A and sketch a curve with decreasing negative curvature up to $x = L$ (Figs. E3.17b, c).

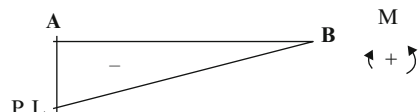
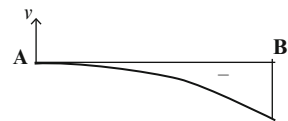
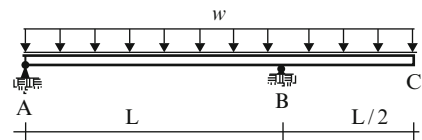
Fig. E3.17b Moment diagram

Fig. E3.17c Deflected shape

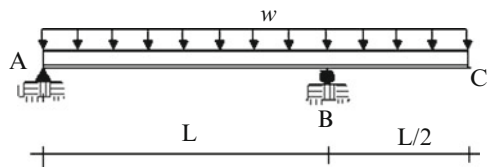
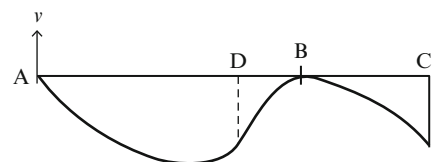
Example 3.18 Deflected shape of a beam with an overhang

Given: The beam with overhang shown in Fig. E3.18a.

Determine: The deflected shape.

Fig. E3.18a

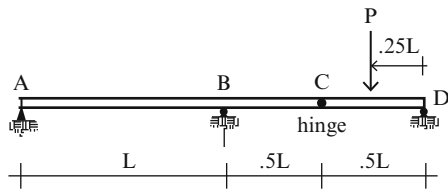
Solution: We note that Fig. E3.18b shows that the moment diagram has both positive and negative regions with an inflection point at $x = 0.75L$. Therefore, it follows that the left segment has positive curvature and the right segment has negative curvature. We need to join these shapes such that the tangent is continuous at point D and the deflections are zero at points A and B (Fig. E3.18c).

Fig. E3.18b Moment diagram**Fig. E3.18c** Deflected shape

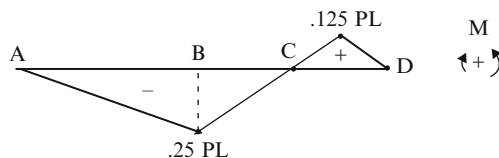
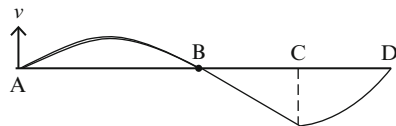
Example 3.19 Deflected shape—beam with a moment release

Given: The beam shown in Fig. E3.19a.

Determine: The deflected shape.

Fig. E3.19a

Solution: Member CD is connected to member ABC with a hinge at point C. A hinge is a physical artifact that allows the members connected to it to rotate freely, i.e., no moment is introduced. A hinge point is different from an inflection point. Although the moment is zero for both hinge and inflection points, the cross-sectional rotation is discontinuous at a hinge, whereas it is continuous at an inflection point. This feature is illustrated in the displacement sketch shown below. The left segment (ABC) has negative curvature. The right segment (CD) has positive curvature (Figs. E3.19b, c).

Fig. E3.19b Moment diagram**Fig. E3.19c** Deflected shape

3.6.3 Moment Area Theorems

The starting point for quantitative analysis is the set of differential equations relating the moment, the cross-sectional rotation, and the deflection.

$$\begin{aligned}\frac{d\theta}{dx} &= \frac{M(x)}{EI} \\ \frac{dv}{dx} &= \theta(x)\end{aligned}\quad (3.22)$$

Given $M(x)/EI$, we integrate $d\theta/dx$ between two points x_1 and x_2 on the x -axis and write the result as

$$\theta(x_2) - \theta(x_1) = \int_{x_1}^{x_2} \frac{M(x)}{EI} dx \quad (3.23)$$

We interpret (3.23) as “*The difference in rotation between 2 points is equal to the area of the M/EI diagram included between these points.*” This statement is referred to as the “First Moment Area” theorem. Taking x_2 as x in (3.23), we can express $\theta(x)$ as

$$\theta(x) = \theta(x_1) + \int_{x_1}^x \frac{M(x)}{EI} dx \quad (3.24)$$

Given $\theta(x)$, we solve for $v(x_2)$.

$$v(x_2) = v(x_1) + \int_{x_1}^{x_2} \theta(x) dx \quad (3.25)$$

Evaluating (3.24) first, and then substituting for $\theta(x)$ in (3.25) leads to

$$v(x_2) - v(x_1) = (x_2 - x_1)\theta(x_1) + \int_{x_1}^{x_2} \left\{ \int_{x_1}^x \frac{M(x)}{EI} dx \right\} dx \quad (3.26)$$

The double integral in (3.26) can be evaluated using integration by parts. First, we note the following identity,

$$d(uv) = u dv + v du \quad (3.27)$$

Integrating between x_1 and x_2 ,

$$\int_{x_1}^{x_2} d(uv) = \int_{x_1}^{x_2} (u dv + v du) \quad (3.28)$$

and rearranging terms leads to

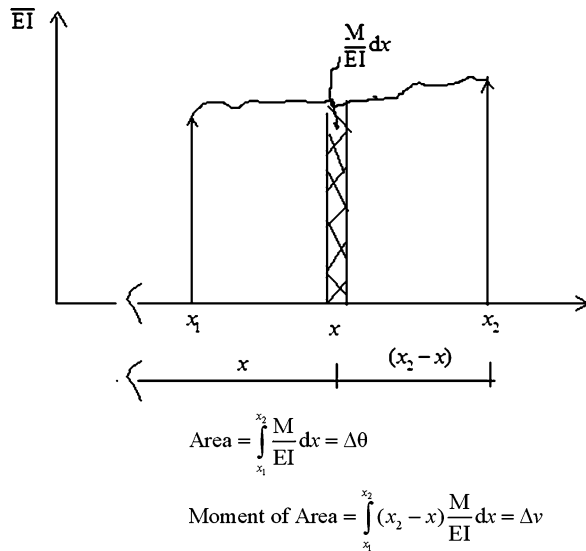
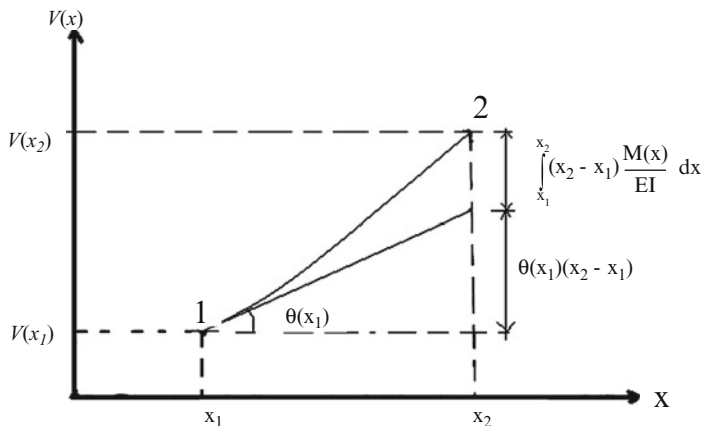
$$\int_{x_1}^{x_2} u dv = uv|_{x_1}^{x_2} - \int_{x_1}^{x_2} v du \quad (3.29)$$

We take

$$\begin{aligned} u &= \int_{x_1}^x \frac{M}{EI} dx \\ dv &= dx \end{aligned} \quad (3.30)$$

in (3.26). Using (3.29), the double integral can be expressed as

$$\begin{aligned} \int_{x_1}^{x_2} \left\{ \int_{x_1}^x \frac{M(x)}{EI} dx \right\} dx &= \left[x \int_{x_1}^x \frac{M(x)}{EI} dx \right]_{x_1}^{x_2} - \int_{x_1}^{x_2} x \frac{M(x)}{EI} dx \\ &= \int_{x_1}^{x_2} (x_2 - x) \frac{M(x)}{EI} dx \end{aligned} \quad (3.31)$$

**Fig. 3.26** Area and moment of area**Fig. 3.27** Graphic interpolation of (3.26)

Finally, an alternate form of (3.26) is

$$v(x_2) - v(x_1) = (x_2 - x_1)\theta(x_1) + \int_{x_1}^{x_2} (x_2 - x) \frac{M(x)}{EI} dx \quad (3.32)$$

This form is referred to as the “Second Moment Area Theorem.” Figure 3.26 shows that the last term can be interpreted as the moment of the M/EI diagram with respect to x_2 . It represents the deflection from the tangent at point 1, as indicated in Fig. 3.27.

Using the Moment Area theorems, one has to evaluate only two integrals,

$$\begin{aligned} J(x) &= \int_{x_1}^x \frac{M(x)}{EI} dx \\ H(x) &= \int_{x_1}^x x \frac{M(x)}{EI} dx \end{aligned} \quad (3.33)$$

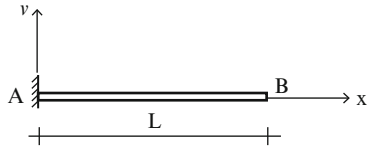
When I is a complicated function of x , these integrals can be evaluated using a symbolic integration scheme or the numerical integration scheme described in Sect. 3.6.6. The final expressions for $v(x)$ and $\theta(x)$ in terms of $v(x_1)$, $\theta(x_1)$, and these integrals are [we take $x_2 = x$ in (3.23) and (3.32)]

$$\begin{aligned} \theta(x) &= \theta(x_1) + J(x) \\ v(x) &= v(x_1) + (x - x_1)\theta(x_1) + xJ(x) - H(x) \end{aligned} \quad (3.34)$$

Example 3.20 Deflected shape—cantilever beam

Given: The cantilever beam shown in Fig. E3.20a. Consider EI is constant.

Fig. E3.20a



Determine: The deflected shapes for various loadings: concentrated moment, concentrated force, and uniform load.

Solution: We measure x from the left support. The displacement boundary conditions are

$$\begin{aligned} v_A &= v(0) = 0 \\ \theta_A &= \theta(0) = 0 \end{aligned}$$

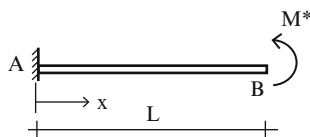
Taking $x_1=0$ and noting the boundary conditions at $x = 0$, (3.34) reduces to

$$\begin{aligned} 0 &\leq x \leq L \\ \theta(x) &= \int_0^x \frac{M(x)}{EI} dx \\ v(x) &= x \int_0^x \frac{M(x)}{EI} dx - \int_0^x x \frac{M(x)}{EI} dx \end{aligned}$$

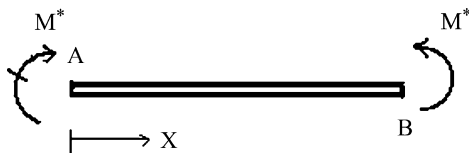
Solutions for various loadings are listed below.

(i) *Concentrated moment* (Fig. E3.20b)

Fig. E3.20b



The expressions for $M(x)$, $\theta(x)$, and $v(x)$ for a concentrated moment are as follows:



$$M(x) = M^* \quad 0 \leq x \leq L$$

$$\theta(x) = \frac{1}{EI} \int_0^x M(x) dx = \frac{M^*}{EI} x$$

$$v(x) = \frac{x}{EI} \int_0^x M(x) dx - \frac{1}{EI} \int_0^x x M(x) dx = \frac{M^* x^2}{EI} - \frac{M^* x^2}{2EI} = +\frac{M^* x^2}{2EI}$$

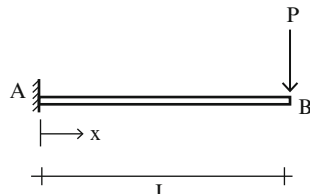
Specific values are

$$\theta_B = \frac{M^* L}{EI}$$

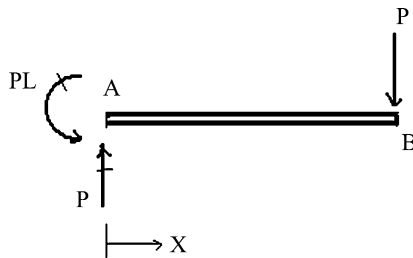
$$v_B = \frac{M^* L^2}{2EI}$$

(ii) *Concentrated Force* (Fig. E3.20c)

Fig. E3.20c



The expressions for $m(x)$, $\theta(x)$, and $v(x)$ for a concentrated load are as follows:



$$M(x) = +P(x - L) \quad 0 \leq x \leq L$$

$$\theta(x) = \frac{1}{EI} \int_0^x M(x) dx = \frac{P}{EI} \left(\frac{x^2}{2} - Lx \right)$$

$$v(x) = \frac{x}{EI} \int_0^x M(x) dx - \frac{1}{EI} \int_0^x xM(x) dx = \frac{P}{EI} \left(\frac{x^3}{6} - \frac{Lx^2}{2} \right)$$

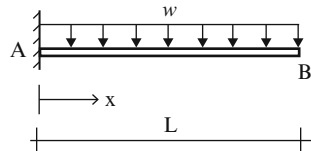
Specific values are

$$\theta_B = -\frac{PL^2}{2EI}$$

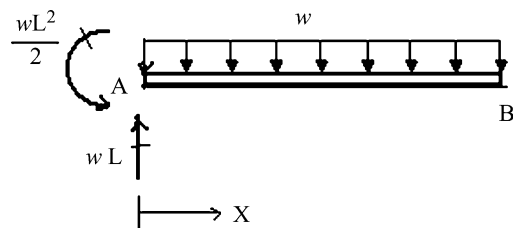
$$v_B = -\frac{PL^3}{3EI}$$

(iii) Uniform Loading (Fig. E3.20d)

Fig. E3.20d



The expressions for $M(x)$, $\theta(x)$, and $v(x)$ for a uniform load are as follows:



$$M(x) = -\frac{wx^2}{2} + wLx - \frac{wL^2}{2} \quad 0 \leq x \leq L$$

$$\theta(x) = \frac{1}{EI} \int_0^x M(x) dx = \frac{w}{6EI} (-x^3 + 3Lx^2 - 3L^2x)$$

$$v(x) = \frac{x}{EI} \int_0^x M(x) dx - \frac{1}{EI} \int_0^x xM(x) dx = \frac{w}{24EI} (-x^4 + 4Lx^3 - 6L^2x^2)$$

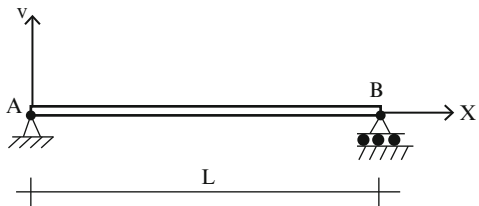
Specific values are

$$\begin{aligned}\theta_B &= -\frac{wL^3}{6EI} \\ v_B &= -\frac{wL^4}{8EI}\end{aligned}$$

Example 3.21 Deflected shape—simply supported beam

Given: The simply supported beam shown in Fig. E3.21a. Consider EI is constant.

Fig. E3.21a



Determine: The deflected shape under different load conditions.

Solution: We measure x from the left support. The displacement boundary conditions are

$$v_A = v(0) = 0$$

$$v_B = v(L) = 0$$

$$\theta_A = \theta(0) \neq 0$$

$$\theta_B = \theta(L) \neq 0$$

Noting the boundary conditions at $x = 0$, the general solution (3.34) for constant EI is given by

$$0 \leq x \leq L$$

$$\theta(x) = \theta(0) + \int_0^x \frac{M(x)}{EI} dx$$

$$v(x) = x\theta(0) + x \int_0^x \frac{M(x)}{EI} dx - \int_0^x x \frac{M(x)}{EI} dx$$

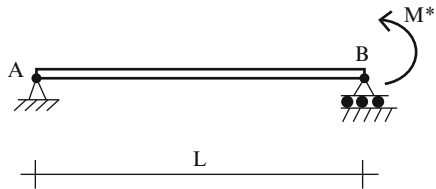
We determine $\theta(0)$ using the remaining boundary condition, $v(L) = 0$. Evaluating $v(x)$ at $x = L$ and equating the result to 0, leads to

$$\theta(0) = - \int_0^L \frac{M(x)}{EI} dx + \frac{1}{L} \int_0^L x \frac{M(x)}{EI} dx$$

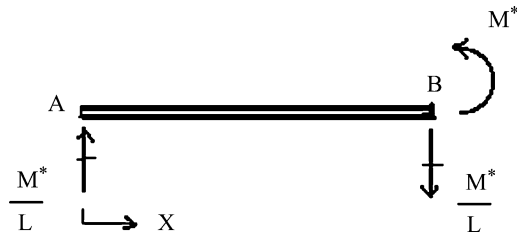
Various loading cases are considered below. We omit the integral details and just present the final solutions.

(i) Concentrated Moment (Fig. E3.21b)

Fig. E3.21b



The expressions for $M(x)$, $\theta(x)$, and $v(x)$ for a concentrated moment are as follows:



$$M(x) = \frac{M^*}{L}x \quad 0 \leq x \leq L$$

$$\begin{aligned} \theta(x) &= - \int_0^L \frac{M(x)}{EI} dx + \frac{1}{L} \int_0^L x \frac{M(x)}{EI} dx + \int_0^x \frac{M(x)}{EI} dx \\ &= \frac{M^* L}{EI} \left(\frac{x^2}{2L^2} - \frac{1}{6} \right) \end{aligned}$$

$$\begin{aligned} v(x) &= -x \int_0^L \frac{M(x)}{EI} dx + \frac{x}{L} \int_0^L x \frac{M(x)}{EI} dx + x \int_0^x \frac{M(x)}{EI} dx - \int_0^x x \frac{M(x)}{EI} dx \\ &= \frac{M^* L^2}{6EI} \left(\frac{x^3}{L^3} - \frac{x}{L} \right) \end{aligned}$$

Specific values are

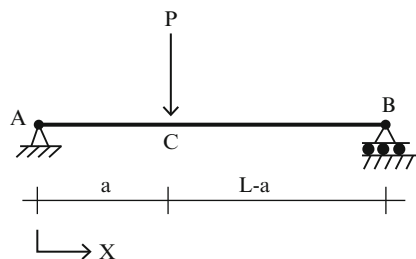
$$\theta_A = -\frac{M^*L}{6EI}$$

$$\theta_B = \frac{M^*L}{3EI}$$

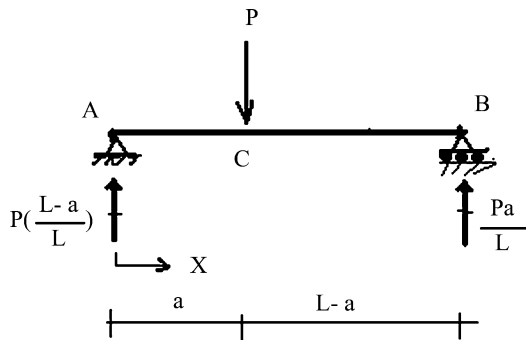
$$v_{\max} = -\frac{\sqrt{3}}{27} \frac{M^*L^2}{EI} \quad \text{at} \quad x = \frac{L}{\sqrt{3}} \approx 0.58L$$

(ii) Concentrated Force (Fig. E3.21c)

Fig. E3.21c



The expressions for $M(x)$, $\theta(x)$, and $v(x)$ for a concentrated load are as follows:



$$M(x) = P \left(\frac{L-a}{L} \right) x \quad 0 \leq x \leq a$$

$$M(x) = \frac{Pa}{L} (L-x) \quad a \leq x \leq L$$

Segment AC $0 \leq x \leq a$

$$\begin{aligned} \theta(x) &= - \int_0^L \frac{M(x)}{EI} dx \frac{1}{L} \int_0^L x \frac{M(x)}{EI} dx + \int_0^x \frac{M(x)}{EI} dx \\ &= -\frac{PL^2}{EI} \left(1 - \frac{a}{L} \right) \left[-\frac{1}{2} \left(\frac{x}{L} \right)^2 + \frac{1}{6} \frac{a}{L} \left(2 - \frac{a}{L} \right) \right] \end{aligned}$$

$$\begin{aligned} v(x) &= -x \int_0^L \frac{M(x)}{EI} dx + \frac{x}{L} \int_0^L x \frac{M(x)}{EI} dx + x \int_0^x \frac{M(x)}{EI} dx - \int_0^x x \frac{M(x)}{EI} dx \\ &= -\frac{PL^3}{EI} \left(1 - \frac{a}{L}\right) \left[-\frac{1}{6} \left(\frac{x}{L}\right)^3 + \frac{1}{6} \frac{a}{L} \frac{x}{L} \left(2 - \frac{a}{L}\right) \right] \end{aligned}$$

Segment CB $a \leq x \leq L$

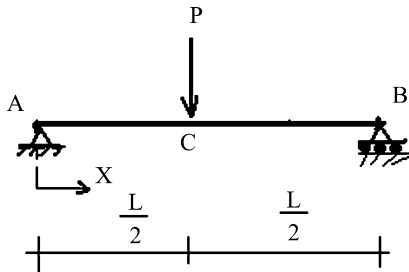
$$\begin{aligned} \theta(x) &= -\frac{PL^2}{EI} \left(\frac{1}{3} + \frac{1}{6} \left(\frac{a}{L}\right)^2 - \frac{x}{L} + \frac{1}{2} \left(\frac{x}{L}\right)^2 \right) \left(\frac{a}{L}\right) \\ v(x) &= -\frac{PL^3}{EI} \left(\frac{1}{6} \frac{a}{L} \right) \left[-\left(\frac{a}{L}\right)^2 + \frac{x}{L} \left(2 + \left(\frac{a}{L}\right)^2\right) - 3\left(\frac{x}{L}\right)^2 + \left(\frac{x}{L}\right)^3 \right] \end{aligned}$$

Specific values are

$$\begin{aligned} \theta_A &= -\frac{Pa(2L^2 - 3aL + a^2)}{6EIL} \\ \theta_B &= \frac{Pa}{6EIL} (L^2 - a^2) \\ v_C &= -\frac{Pa^2(L - a)^2}{3EIL} \end{aligned}$$

The maximum deflection occurs at the point where $\theta(x)=0$. This location depends on a . When $a < L/2$ the peak displacement occurs in segment CB. The location reverses when $a > L/2$.

Special case: $a = L/2$



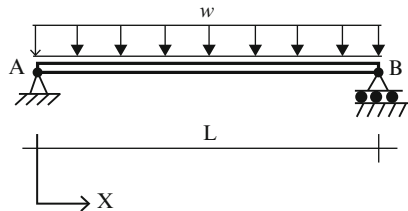
$$\theta_{\max} = \theta_B = -\theta_A = \frac{PL^2}{16EI}$$

$$\theta_C = 0$$

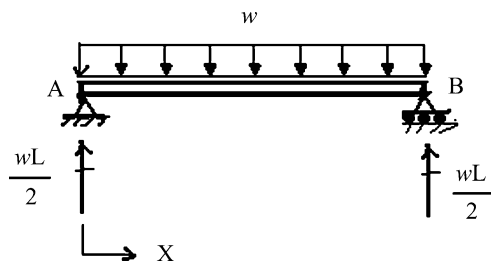
$$v_{\max} = -\frac{PL^3}{48EI} \quad \text{at} \quad x = \frac{L}{2}$$

(iii) Uniform Loading (Fig. E3.21d)

Fig. E3.21d



The expressions for $M(x)$, $\theta(x)$, and $v(x)$ for a uniform load are as follows:



$$M(x) = -\frac{wx^2}{2} + \frac{wL}{2}x \quad 0 \leq x \leq L$$

$$\begin{aligned} \theta(x) &= -\int_0^L \frac{M(x)}{EI} dx = \frac{1}{L} \int_0^L x \frac{M(x)}{EI} dx + \int_0^x \frac{M(x)}{EI} dx \\ &= \frac{wL^3}{24EI} \left(-4 \frac{x^3}{L^3} + 6 \frac{x^2}{L^2} - 1 \right) \end{aligned}$$

$$\begin{aligned} v(x) &= -x \int_0^L \frac{M(x)}{EI} dx + \frac{x}{L} \int_0^L x \frac{M(x)}{EI} dx + x \int_0^x \frac{M(x)}{EI} dx - \int_0^x x \frac{M(x)}{EI} dx \\ &= \frac{wL^4}{24EI} \left(-\frac{x^4}{L^4} + 2 \frac{x^3}{L^2} - \frac{x}{L} \right) \end{aligned}$$

Specific values are

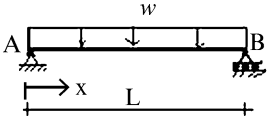
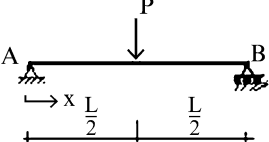
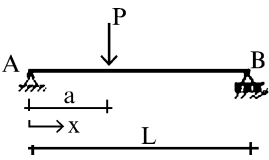
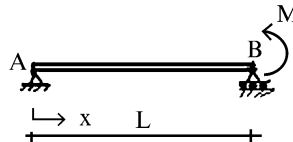
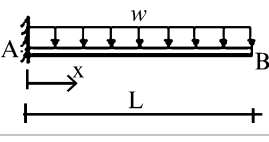
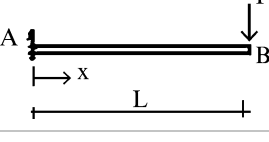
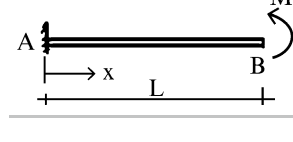
$$\theta_A = -\theta_B = -\frac{wL^3}{24EI}$$

$$v_{\max} = -\frac{5wL^4}{384EI} \quad \text{at } x = \frac{L}{2}$$

Note that the rotation is zero at mid-span since the loading and the structure are symmetrical.

For future reference, the end displacements corresponding to typical loading condition are summarized in Table 3.1. We utilize these results in formulating the Force method to be presented in Chap. 9.

Table 3.1 Catalogue of displacements for various loading condition cases

| Loading | θ^+ Rotation | v^+ ↑ Translation | Reference |
|-------------------------------------------------------------------------------------|------------------------------------------------------------------------------------------|---------------------------------------------------------------------------------------|--------------|
|  | $\theta_B = -\theta_A = \frac{wL^3}{24EI}$ | $v_{max} = -\frac{5wL^4}{384EI}$ at $x = \frac{L}{2}$ | Example 3.21 |
|  | $\theta_B = -\theta_A = \frac{PL^2}{16EI}$ | $v_{max} = -\frac{PL^3}{48EI}$ at $x = \frac{L}{2}$ | Example 3.21 |
|  | $\theta_A = -\frac{Pa(2L^2 - 3aL + a^2)}{EIL}$ $\theta_B = \frac{Pa}{6EI(L^2 - a^2)}$ | $v = -\frac{Pa^2(L - a)^2}{3EI L}$ at $x = a$ | Example 3.21 |
|  | $\theta_A = -\frac{M^*L}{6EI}$ $\theta_B = -\frac{M^*L}{3EI}$ | $v_{max} = -\frac{\sqrt{3}M^*L^2}{27EI}$ at $x = \frac{L}{\sqrt{3}} \approx 0.58L$ | Example 3.21 |
|  | $\theta_B = -\frac{wL^3}{6EI}$ | $v_B = -\frac{wL^4}{8EI}$ | Example 3.20 |
|  | $\theta_B = -\frac{PL^2}{2EI}$ | $v_B = -\frac{PL^3}{3EI}$ | Example 3.20 |
|  | $\theta_B = \frac{M^*L}{EI}$ | $v_B = \frac{M^*L^2}{2EI}$ | Example 3.20 |

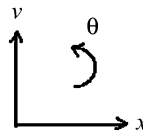
3.6.4 Computing Displacements with the Conjugate Beam Method

The examples listed above illustrate how the moment area theorems defined by (3.34) are applied to compute displacement profiles. Most of the effort involved is concerned with evaluating integrals and specializing the results for different

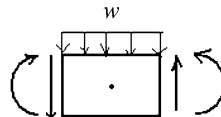
boundary conditions. This approach is straightforward but somewhat tedious. In what follows, we describe a different strategy referred to as the conjugate beam method, which interprets the problem of finding the displacement as an equilibrium problem involving the shear and bending moment in a “Conjugate “beam which is related to the actual beam. Most engineers find it more convenient to work with shear and moment diagrams. The basic geometric equations are (3.22) which are listed below for convenience.

$$\frac{d\theta}{dx} = \frac{M(x)}{EI}$$

$$\frac{dv}{dx} = \theta(x)$$



These equations are similar in form to the differential force equilibrium equations defined by (3.4) and (3.5) that are shown below.



$$\frac{dV}{dx} = w$$

$$\frac{dM}{dx} = -V$$

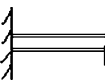
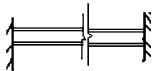
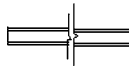
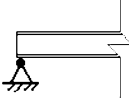
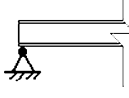
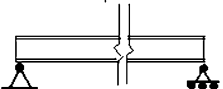
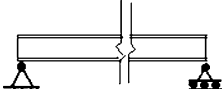
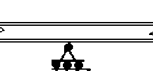
This similarity suggests that one can interpret the geometric variables as force variables for an “equivalent” beam, referred to as the conjugate beam. The relationships between the variables are defined in Table 3.2.

One applies the loading to the conjugate beam and determines the shear and moment distributions. By definition, these variables are related to the rotation (θ) and displacement (v). However, one first must establish the appropriate boundary condition for the conjugate beam. Various types of boundary conditions are listed below (Table 3.3).

Table 3.2

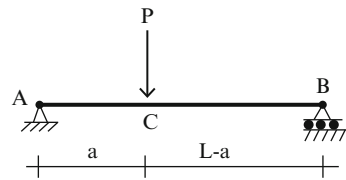
| Actual beam | Conjugate beam |
|----------------------------|-------------------------------------|
| Loading $w \downarrow +$ | Loading $\frac{M}{EI} \downarrow +$ |
| $\theta^+ \curvearrowleft$ | $V \downarrow + \uparrow$ |
| $v^+ \uparrow$ | $-M \curvearrowleft + \uparrow$ |

Table 3.3

| Actual beam | Conjugate beam |
|-----------------------------------------------------------------------------------|------------------------------------------------------------------------------------|
| Fixed $v=0 \theta = 0$ | Free $M=0 V=0$ |
|  |  |
| Fixed-Fixed | Free-Free |
|  |  |
| Hinge $v=0 \theta \neq 0$ | Hinge $M=0 V \neq 0$ |
|  |  |
| Hinge roller | Hinge roller |
|  |  |
| Interior roller $v=0 \theta \neq 0$ | Interior roller $M=0 V \neq 0$ |
|  |  |

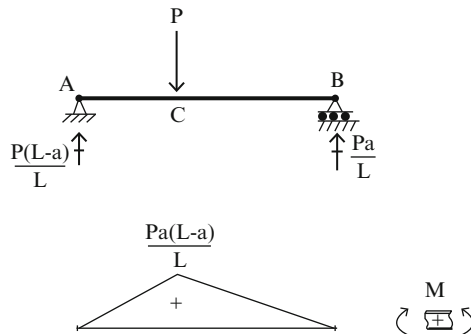
Example 3.22 Deflection computation using the conjugate beam method

Given: The simply supported beam shown in Figs. E3.22a–c. Assume $P = 40 \text{ kN}$, $a = 2 \text{ m}$, $L = 8 \text{ m}$, $I = 160(10^6) \text{ mm}^4$, and $E = 200 \text{ GPa}$.

**Fig. E3.22a**

Determine: The vertical displacement at C and rotations at A and B. Take EI is constant.

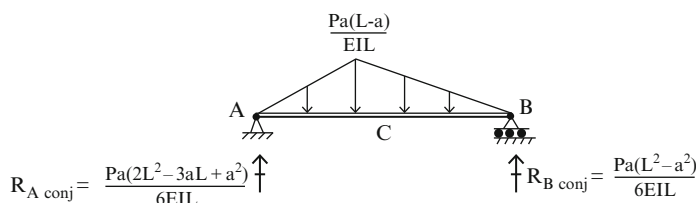
Solution: We determine the bending moment distribution and then apply the M/EI loading to the conjugate beam.

**Fig. E3.22b** Bending moment distribution

The rotation and displacement of the actual beam are computed using

$$\theta = V_{\text{Conj}}$$

$$v = -M_{\text{Conj}}$$

**Fig. E3.22c** Conjugate beam

$$\begin{aligned} \sum M_B &= 0 \quad R_{A \text{ conj}} = \frac{Pa(2L^2 - 3aL + a^2)}{6EIL} \uparrow \\ \sum F_y &= 0 \quad R_{B \text{ conj}} = \frac{Pa(L^2 - a^2)}{6EIL} \uparrow \\ M_{x=a} &= M_{C \text{ conj}} = \frac{Pa^2(L - a)^2}{3EIL} \text{ counterclockwise} \end{aligned}$$

Therefore

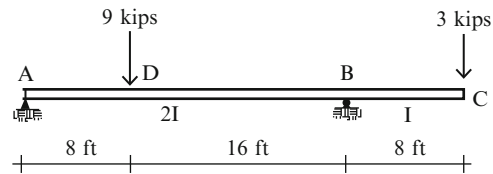
$$\begin{aligned} \theta_A &= V_{A \text{ conj}} = \frac{Pa(2L^2 - 3aL + a^2)}{6EIL} = \frac{40(2)(2(8)^2 - 3(2)(8) + 2^2)10^9}{6(200)(160)(10^6)(8,000)} = 0.0044 \text{ rad clockwise} \\ \theta_B &= V_{B \text{ conj}} = \frac{Pa(L^2 - a^2)}{6EIL} = \frac{40(2)(8^2 - 2^2)10^9}{6(200)(160)(10^6)(8,000)} = 0.0031 \text{ rad counterclockwise} \\ v_C &= -M_{C \text{ conj}} = \frac{Pa^2(L - a)^2}{3EIL} = \frac{40(2)^2(6)^210^{12}}{3(200)(160)(10^6)(8,000)} = 7.5 \text{ mm} \downarrow \end{aligned}$$

We point out that when the M/EI expression is nonlinear, one needs to resort to integration, and the effort involved is similar to that required when the actual geometric equations are used.

Example 3.23 Deflection computation using the conjugate beam method

Given: The beam shown in Fig. E3.23a

Fig. E3.23a



Determine: The vertical displacement at C and rotation at A. Assume $I=200 \text{ in.}^4$ and $E=29,000 \text{ ksi}$.

Solution: First, we determine the bending moment distribution (Fig. E3.23b).

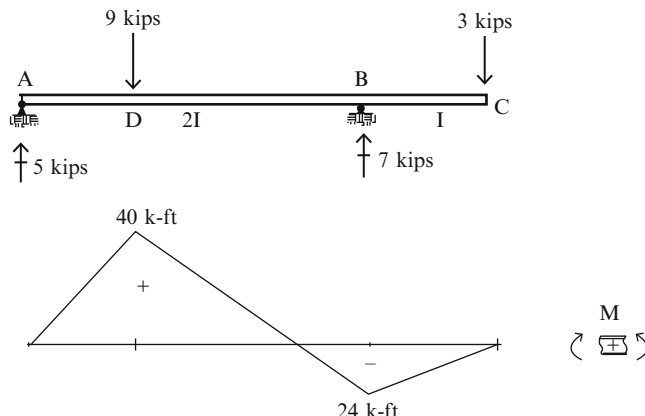


Fig. E3.23b

Next, we apply the M/EI loading to the conjugate beam (Fig. E3.23c).

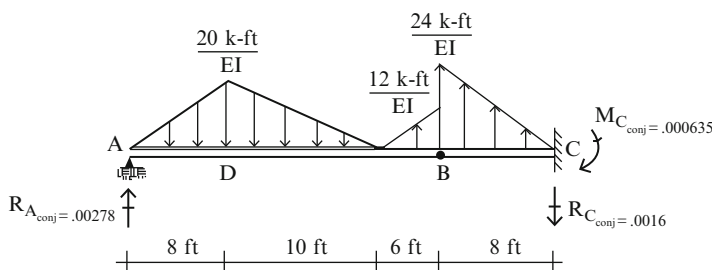


Fig. E3.23c Conjugate beam

$$R_{A\text{ conj}} = \frac{112 \text{ kip ft}^2}{EI} = 0.00278 \uparrow$$

$$R_{C\text{ conj}} = \frac{64 \text{ kip ft}^2}{EI} = 0.0016 \downarrow$$

$$M_{C\text{ conj}} = \frac{256 \text{ kip ft}^3}{EI} = 0.000635 \text{ counterclockwise}$$

Therefore

$$\theta_A = V_{A\text{ conj}} = 0.00278 \text{ rad clockwise}$$

$$\theta_C = V_{C\text{ conj}} = 0.0016 \text{ rad clockwise}$$

$$v_C = -M_{C\text{ conj}} = 0.00635 \text{ in. } \downarrow$$

3.6.5 Computing Displacements with the Method of Virtual Forces

The procedures described in the previous section are intended to generate analytical solutions for the displacement and rotation. In many cases, one is interested only in the motion measures for a particular point. Rather than generate the complete analytical solution and then evaluate it at the point of interest, one can apply the Method of Virtual Forces. The Method of Virtual Forces specialized for bending of slender beams is defined in Ref. [16]. We express the principle as

$$d \delta P = \int_L (\text{bending deformation}) (\delta M(x)) dx \quad (3.35)$$

Where d is the desired displacement measure, δP is the virtual force in the direction of d , and $\delta M(x)$ is the virtual moment due to δP . The deformation due to transverse shear is not included since it is negligible for slender beams. When the behavior is linear elastic, the bending deformation is related to the moment by

$$\text{bending deformation} \equiv \frac{d\theta}{dx} = \frac{M(x)}{EI}$$

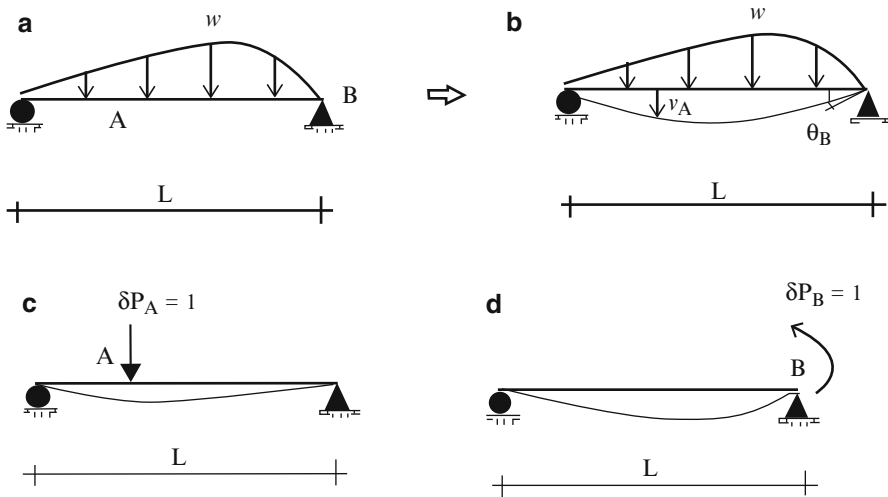


Fig. 3.28 Actual and virtual loads moments. (a) Actual load $M(x)$. (b) Deflected shape. (c) Virtual load $\delta M_v(x)$ for v_A , (d) Virtual load $\delta M_\theta(x)$ for θ_B

and (3.35) takes the form

$$d \delta P = \int_L \frac{M(x)}{EI} \delta M(x) dx \quad (3.36)$$

The steps involved in applying the principle are as follows. We use as an example, the beam shown in Fig. 3.28. To determine a desired vertical displacement or rotation such as v_A or θ_B , one applies the corresponding virtual force or virtual moment in the direction of the desired displacement or rotation, determines the virtual moment $\delta M_v(x)$ or $\delta M_\theta(x)$, and then evaluates the following integrals.

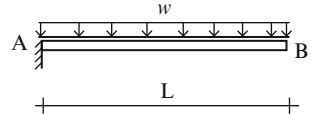
$$v_A = \int_L \frac{M(x)}{EI} \delta M_v(x) dx$$

$$\theta_B = \int_L \frac{M(x)}{EI} \delta M_\theta(x) dx$$

Just as we did for truss structures in Chap. 2, one takes δP to be a unit value. We illustrate the application of this procedure with the following examples.

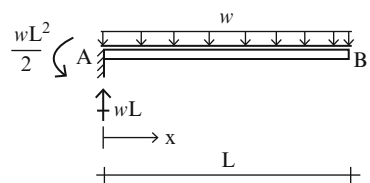
Example 3.24 Deflection computation—method of virtual forces

Given: A uniformly loaded cantilever beam shown in Fig. E3.24a.

Fig. E3.24a

Determine: The vertical displacement and rotation at B. Take EI is constant.

Solution: We start by evaluating the moment distribution corresponding to the applied loading. This is defined in Fig. E3.24b. The virtual moment distributions corresponding to v_B , θ_B are defined in Figs. E3.24c, d. Note that we take δP to be either a unit force (for displacement) or a unit moment (for rotation).

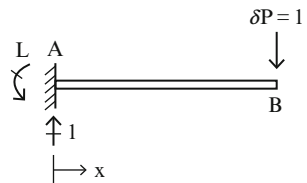
Fig. E3.24b $M(x)$ 

The actual moment $M(x)$ is

$$0 \leq x \leq L \quad M(x) = wLx - w\frac{x^2}{2} - \frac{wL^2}{2} = -\frac{w}{2}(x-L)^2$$

Vertical deflection at B: We apply the virtual vertical force, $\delta P = 1$ at point B and compute the corresponding virtual moment.

$$0 \leq x \leq L \quad \delta M_{v_B}(x) = x - L$$

Fig. E3.24c $\delta M_{v_B}(x)$ 

Then, noting (3.36)

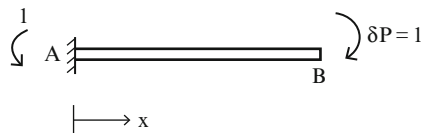
$$\begin{aligned} v_B &= \int_L \frac{M(x)}{EI} \delta M_{v_B}(x) dx = \frac{1}{EI} \int_0^L -\frac{w}{2}(x-L)^2(x-L) dx \\ &= \frac{1}{EI} \int_0^L -\frac{w}{2}(x-L)^3 dx \end{aligned}$$

Integrating leads to

$$v_B = \frac{wL^4}{8EI} \downarrow$$

Rotation at B: We apply the virtual moment, $\delta P = 1$ at point B and determine $\delta M(x)$.

Fig. 3.24d $\delta M_{\theta_B}(x)$



This loading produces a constant bending moment,

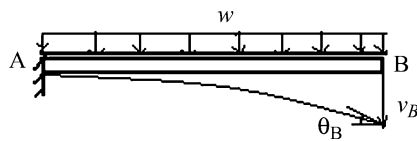
$$0 \leq x \leq L \quad \delta M_{\theta_B}(x) = -1$$

Then, noting (3.36)

$$\theta_B = \int_L \frac{M(x)}{EI} \delta M_{\theta_B}(x) dx = \frac{1}{EI} \int_0^L -\frac{w}{2}(x-L)^2(-1) dx$$

Finally, one obtains

$$\theta_B = \frac{wL^3}{6EI} \text{ clockwise}$$



Example 3.25 Deflection computation—method of virtual forces

Given: The simply supported beam shown in Fig. E3.25a.

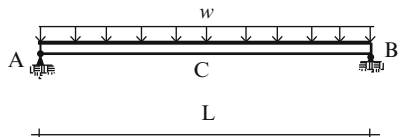


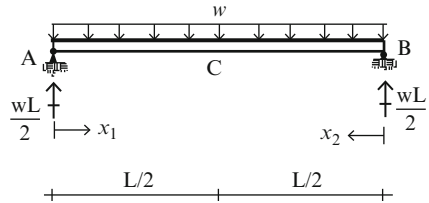
Fig. E3.25a

Determine: The vertical deflection and rotation at point C located at mid-span. Take EI is constant.

Solution: We start by evaluating the moment distribution corresponding to the applied loading. This is defined in Fig. E3.25b. The virtual moment distributions

corresponding to v_C , θ_C are defined in Figs. E3.25c, d. Note that we take δP to be either a unit force (for displacement) or a unit moment (for rotation).

Fig. E3.25b



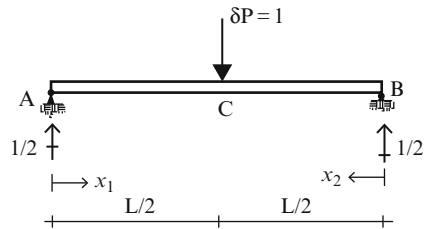
The actual moment is

$$\begin{aligned} 0 < x_1 < \frac{L}{2} \quad M(x) &= \frac{wL}{2}x_1 - \frac{wx_1^2}{2} \\ 0 < x_2 < \frac{L}{2} \quad M(x) &= \frac{wL}{2}x_2 - \frac{wx_2^2}{2} \end{aligned}$$

Vertical displacement at C: We apply a unit virtual load at point C and determine $\delta M(x)$.

$$\begin{aligned} 0 < x_1 < \frac{L}{2} \quad \delta M_{vc}(x) &= \frac{1}{2}x_1 \\ 0 < x_2 < \frac{L}{2} \quad \delta M_{vc}(x) &= \frac{1}{2}x_2 \end{aligned}$$

Fig. E3.25c $\delta M_{vc}(x)$



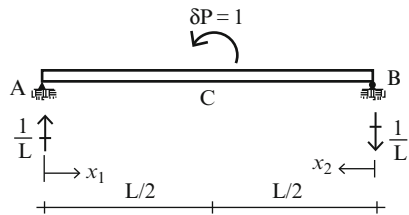
Then, evaluating the integral in (3.36), we obtain

$$\begin{aligned} v_C &= \int_{AC} \left(\frac{M(x_1)}{EI} \delta M_{vc}(x_1) \right) dx_1 + \int_{BC} \left(\frac{M(x_2)}{EI} \delta M_{vc}(x_2) \right) dx_2 \\ &= \frac{1}{EI} \left[\int_0^{L/2} \left(\frac{1}{2}x_1 \right) \left(\frac{wLx_1}{2} - \frac{wx_1^2}{2} \right) dx_1 + \int_0^{L/2} \left(\frac{1}{2}x_2 \right) \left(\frac{wLx_2}{2} - \frac{wx_2^2}{2} \right) dx_2 \right] \\ &= \frac{5wL^4}{384EI} \downarrow \end{aligned}$$

Rotation at C: We apply a unit virtual moment at point C and determine $\delta M(x)$.

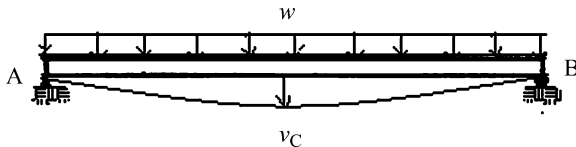
$$\begin{aligned} 0 < x_1 < \frac{L}{2} \quad \delta M_{\theta_C}(x_1) &= \frac{1}{L}x_1 \\ 0 < x_2 < \frac{L}{2} \quad \delta M_{\theta_C}(x_2) &= -\frac{1}{L}x_2 \end{aligned}$$

Fig. E3.25d $\delta M_{\theta_C}(x)$



Then, evaluating the integral in (3.36), we obtain

$$\begin{aligned} \theta_C &= \int_{AC} \left(\frac{M(x_1)}{EI} \delta M_{\theta_C}(x_1) \right) dx_1 + \int_{BC} \left(\frac{M(x_2)}{EI} \delta M_{\theta_C}(x_2) \right) dx_2 \\ &= \frac{1}{EI} \left\{ \int_0^{L/2} \left(\frac{x_1}{L} \right) \left(\frac{wLx_1}{2} - \frac{wx_1^2}{2} \right) dx_1 - \int_0^{L/2} \left(\frac{x_2}{L} \right) \left(\frac{wLx_2}{2} - \frac{wx_2^2}{2} \right) dx_2 \right\} = 0 \end{aligned}$$



Example 3.26 Deflection computation—method of virtual forces

Given: The beam shown in Fig. E3.26a.

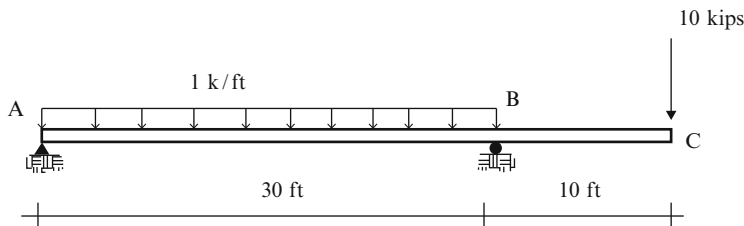
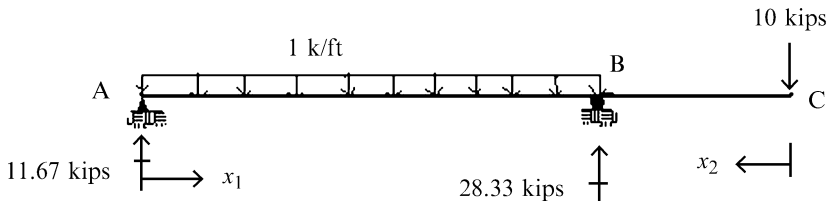


Fig. E3.26a

Determine: Use the virtual force method to determine the vertical deflection and rotation at C. $E = 29,000$ ksi and $I = 300$ in.⁴

Solution: We start by evaluating the moment distribution corresponding to the applied loading.

We divide up the structure into two segments AB and CB and



$$0 < x_1 < 30 \quad M(x) = 11.67x_1 - \frac{x_1^2}{2}$$

$$0 < x_2 < 10 \quad M(x) = -10x_2$$

Vertical deflection at C: We apply a unit virtual load at point C and determine $\delta M(x)$.



$$0 < x_1 < 30 \quad \delta M_{vC}(x) = -\frac{x_1}{3}$$

$$0 < x_2 < 10 \quad \delta M_{vC}(x) = -x_2$$

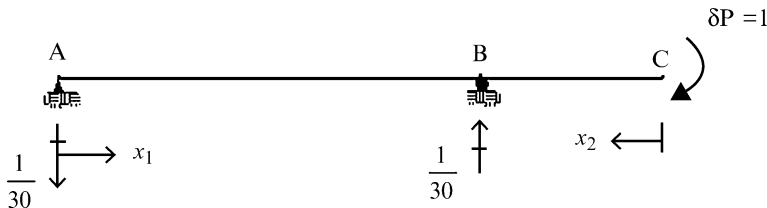
Then, noting (3.36), we divide up the structure into two segments AB and CB and integrate over each segment. The total integral is given by

$$\begin{aligned} v_C &= \int_{AB} \left(\frac{M(x_1)}{EI} \delta M_{vC}(x_1) \right) dx_1 + \int_{CB} \left(\frac{M(x_2)}{EI} \delta M_{vC}(x_2) \right) dx_2 \\ &= \frac{1}{EI} \int_0^{30} \left(11.67x_1 - \frac{x_1^2}{2} \right) \left(-\frac{x_1}{3} \right) dx_1 + \frac{1}{EI} \int_0^{10} (-10x_2)(-x_2) dx_2 \\ &= -\frac{2,073.33 \text{ kip ft}^3}{EI} = \frac{2,073.33(12)^3}{29,000(300)} = -0.41 \text{ in.} \end{aligned}$$

The minus sign indicates the vertical displacement is in the opposite direction of the unit load.

$$\therefore v_C = 0.41 \text{ in. } \uparrow$$

Rotation at C: We apply a unit virtual moment at point C and determine $\delta M(x)$.



$$0 < x_1 < 30 \quad \delta M_{\theta_C}(x) = -\frac{x_1}{30}$$

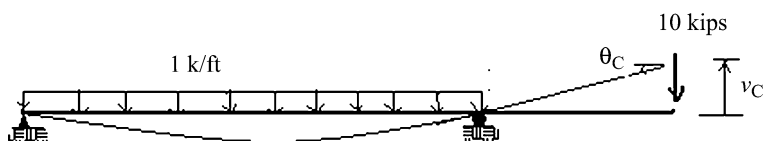
$$0 < x_2 < 10 \quad \delta M_{\theta_C}(x) = -1$$

Then, noting (3.36)

$$\begin{aligned} \theta_C &= \int_{AB} \left(\frac{M(x)}{EI} \delta M_{\theta_C}(x) \right) dx_1 + \int_{CB} \left(\frac{M(x)}{EI} \delta M_{\theta_C}(x) \right) dx_2 \\ &= \frac{1}{EI} \int_0^{30} \left(11.67x_1 - \frac{x_1^2}{2} \right) \left(-\frac{x_1}{30} \right) dx_1 + \frac{1}{EI} \int_0^{10} (-10x_2)(-1) dx_2 \\ &= \frac{374 \text{ kip ft}^2}{EI} = \frac{374(12)^2}{29,000(300)} = +0.0063 \text{ rad} \end{aligned}$$

The positive sign indicates that the rotation is in the direction of the unit moment.

$$\therefore \theta_C = 0.0063 \text{ rad clockwise}$$



Example 3.27 Deflection computation—method of virtual forces

Given: The beam shown in Fig. E3.27a.

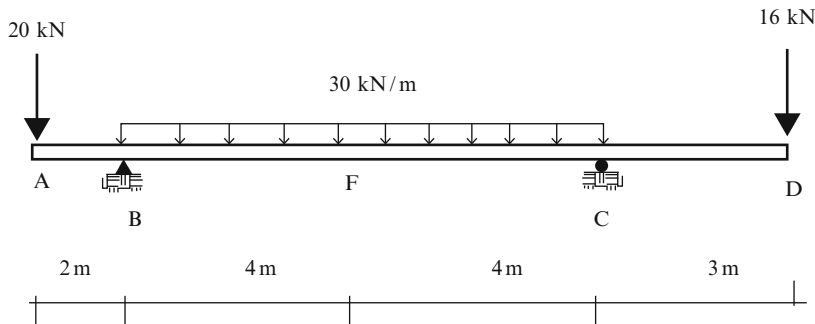
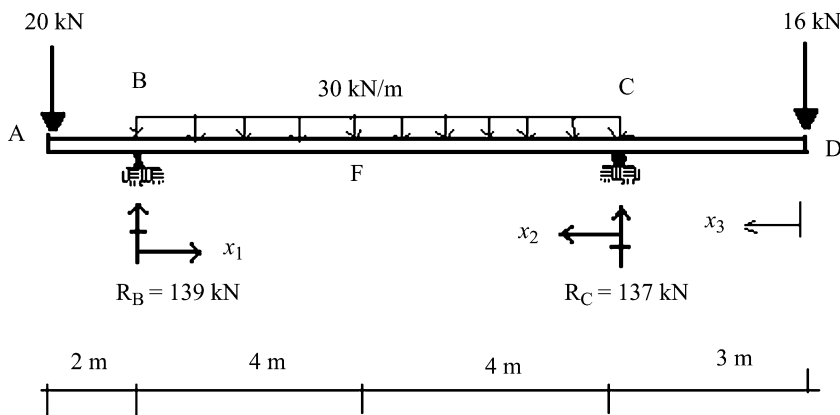


Fig. E3.27a

Determine: Use the virtual force method to determine the vertical deflection at F and rotation at D. Assume $E = 200 \text{ GPa}$ and $I = 120(10)^6 \text{ mm}^4$.

Solution: We start by evaluating the moment distribution corresponding to the applied loading.

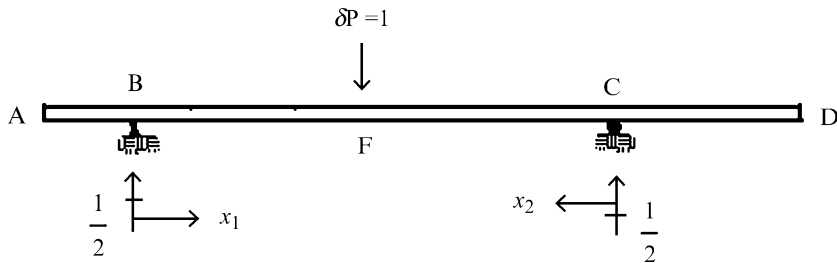


$$0 < x_1 < 8 \quad M(x_1) = -15x_1^2 + 139x_1 - 20(x_1 + 2) = -15x_1^2 + 119x_1 - 40$$

$$0 < x_2 < 8 \quad M(x_2) = -15x_2^2 + 137x_2 - 16(x_2 + 3) = -15x_2^2 + 121x_2 - 48$$

$$0 < x_3 < 3 \quad M(x_3) = -16x_3$$

Vertical deflection at F: We apply a unit virtual load at point F and determine δM .



$$0 < x_1 < 4 \quad \delta M_{v_F}(x_1) = \frac{1}{2}x_1$$

$$0 < x_2 < 4 \quad \delta M_{v_F}(x_2) = \frac{1}{2}x_2$$

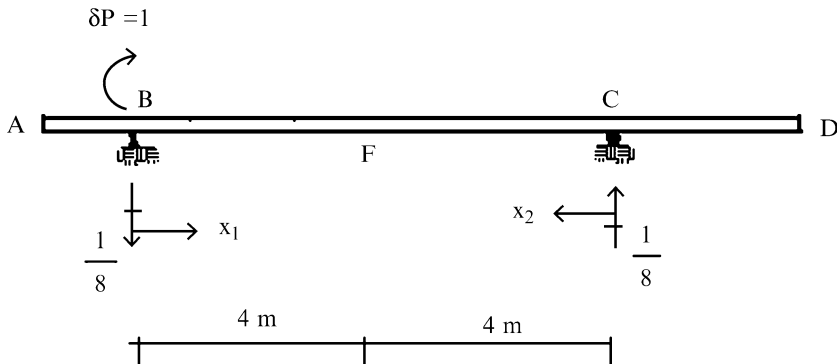
Then, noting (3.36)

$$\begin{aligned} v_E &= \int_{BF} \left(\frac{M(x_1)}{EI} \delta M_{v_F}(x_1) \right) dx_1 + \int_{CF} \left(\frac{M(x_2)}{EI} \delta M_{v_F}(x_2) \right) dx_2 \\ &= \frac{1}{EI} \left\{ \int_0^4 (-15x_1^2 + 119x_1 - 40) \left(\frac{x_1}{2}\right) dx_1 + \int_0^4 (-15x_2^2 + 121x_2 - 48) \left(\frac{x_2}{2}\right) dx_2 \right\} \\ &= \frac{1,248 \text{ kN m}^3}{EI} = \frac{1,248(10)^9}{200(120)(10)^6} = 52 \text{ mm} \end{aligned}$$

The positive sign indicates the vertical displacement is in the direction of the unit load.

$$\therefore v_F = 52 \text{ mm} \downarrow$$

Rotation at B: We apply a unit moment at point B and determine $\delta M(x)$.



$$0 < x_2 < 8 \quad \delta M_{\theta_B}(x_2) = \frac{1}{8}x_2$$

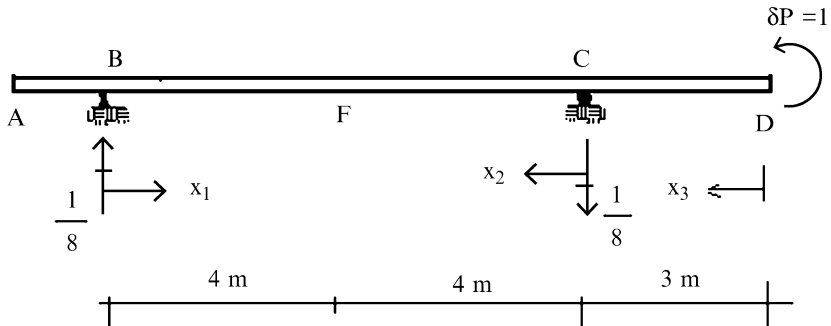
Then, noting (3.36)

$$\begin{aligned}\theta_B &= \int_{CB} \frac{M(x_2)}{EI} \delta M_{\theta_B}(x_2) dx_2 = \frac{1}{EI} \int_0^8 (-15x_2^2 + 121x_2 - 48) \left(\frac{x_2}{8}\right) dx_2 \\ &= \frac{469.3 \text{ kN m}^2}{EI} = \frac{469.3(10)^6}{200(120)(10)^6} = +0.0195 \text{ rad}\end{aligned}$$

The positive sign indicates that the rotation is in the direction of the unit moment.

$$\therefore \theta_B = 0.0195 \text{ rad clockwise}$$

Rotation at D: We apply a unit moment at point D and determine $\delta M(x)$.



$$0 < x_1 < 8 \quad \delta M_{\theta_D}(x_1) = \frac{1}{8}x_1$$

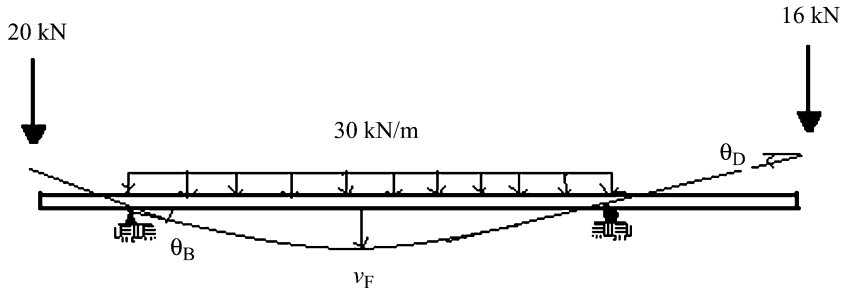
$$0 < x_3 < 3 \quad \delta M_{\theta_D}(x_3) = 1$$

Then, noting (3.36)

$$\begin{aligned}\theta_D &= \int_{BC} \frac{M(x_1)}{EI} \delta M_{\theta_D}(x_1) dx_1 + \int_{DC} \frac{M(x_3)}{EI} \delta M_{\theta_D}(x_3) dx_3 \\ &= \frac{1}{EI} \int_0^8 (-15x_1^2 + 119x_1 - 40) \left(\frac{x_1}{8}\right) dx_1 + \frac{1}{EI} \int_0^3 (-16x_3)(1) dx_3 \\ &= +\frac{386.7 \text{ kN m}^2}{EI} = \frac{386.7(10)^6}{200(120)(10)^6} = 0.016 \text{ rad}\end{aligned}$$

The positive sign indicates that the rotation is in the direction of the unit moment.

$$\therefore \theta_D = 0.016 \text{ rad counterclockwise}$$



3.6.6 Computing Displacements for Non-prismatic Members

When the member is non-prismatic, I is a function of x and it may be difficult to obtain a closed form solution for the integral involving $1/I$. In this case, one can employ a numerical integration scheme. In what follows, we describe a numerical integration procedure which can be easily programmed.

Consider the problem of evaluating the following integral

$$J = \int_{x_A}^{x_B} f(x) dx \quad (3.37)$$

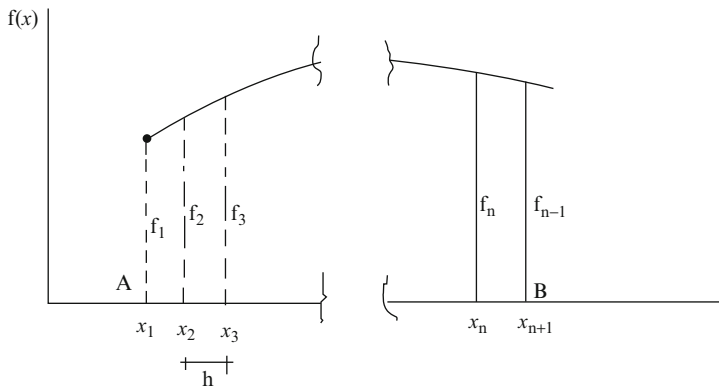
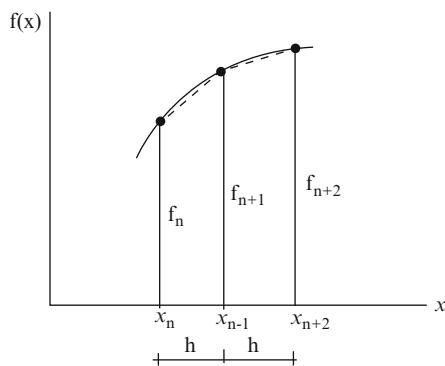
We divide the total interval into n equal segments of length h

$$h = \frac{x_B - x_A}{n} \quad (3.38)$$

and denote the values of x and f at the equally spaced points as

$$x_1, x_2, x_3, \dots, x_{n+1}$$

$$f_1, f_2, f_3, \dots, f_{n+1}$$

**Fig. 3.29****Fig. 3.30**

This notation is illustrated in Fig. 3.29.

The simplest approach is based on approximating the actual curve of $f(x)$ with a set of straight lines connecting (f_1, f_2) , (f_2, f_3) , etc. as shown in Fig. 3.30.

The incremental area between x_n and x_{n+1} is approximated as

$$\Delta J_{n,n+1} = \int_{x_n}^{x_{n+1}} f(x) dx \approx \frac{h}{2} (f_n + f_{n+1}) \quad (3.39)$$

Also, the area between x_1 and x_n is expressed as

$$J_n = \int_{x_1}^{x_n} f(x) dx \quad (3.40)$$

Starting with $J_1=0$, one generates successive areas with

$$J_2 = J_1 + \Delta J_{1,2} = \Delta J_{1,2}$$

$$J_3 = J_2 + \Delta J_{2,3}$$

$$\vdots$$

$$J_n = J_{n-1} + \Delta J_{n-1,n}$$

$$\vdots$$

$$J_{n+1} = J_n + \Delta J_{n,n+1} \quad (3.41)$$

The total integral, J_{n+1} expands to

$$J_{n+1} \approx \int_{x_1}^{x_{n+1}} f(x)dx \approx h \left\{ \frac{1}{2}(f_n + f_{n+1}) + \sum_{j=2}^n f_j \right\} \quad (3.42)$$

Equation is known as the “Trapezoidal’ Rule. One uses (3.41) to evaluate the intermediate integrals when applying the Moment Area Theorems such as (3.33) and (3.34). Equation (3.42) is used with the Virtual Force Method.

We illustrate the application of this approach combined with the Virtual Force Method to the beam defined in Fig. 3.31. Suppose the vertical displacement at point Q is desired. Given $M(x)$ and $I(x)$, we subdivide the X-axis into n equal intervals and evaluate M/I and $\delta M(x)$ at each point.

$$h = \frac{L}{n}$$

$$x_k = (k - 1)h \quad k = 1, 2, \dots, n + 1$$

$$\delta M(x_k) = \left(1 - \frac{x_Q}{L}\right)x_k \quad x < x_Q$$

$$\delta M(x_k) = (L - x_k) \frac{x_Q}{L} \quad x > x_Q$$

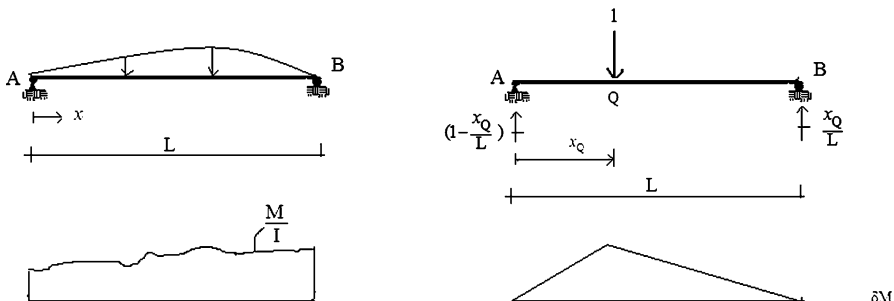


Fig. 3.31

Lastly, we take $f = \frac{M}{I}$ δM in (3.42) and evaluate the summation. The choice of h depends on the ‘smoothness’ of the function M/I , a typical value is $L/20$. One can assess the accuracy by refining the initial choice for h and comparing the corresponding values of the integral.

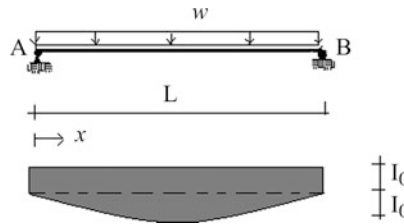
Suppose the deflection at $x=L/2$ is desired. The virtual moment for this case is

$$\begin{cases} \delta M(x) = \left(1 - \frac{1}{2}\right)x_k = \frac{1}{2}x_k & \text{for } x_k < \frac{L}{2} \\ \delta M(x) = (L - x_k)\frac{1}{2} & \text{for } x_k > \frac{L}{2}. \end{cases}$$

We also suppose the loading is uniform and the variation of I is given by

$$I = I_0 \left\{ 1 + 4 \left[\frac{x}{L} - \left(\frac{x}{L} \right)^2 \right] \right\}$$

where I_0 is constant.



The corresponding moment is

$$M = \frac{wL}{2}x - \frac{wx^2}{2} = \frac{wL^2}{8} \left\{ 4 \left[\frac{x}{L} - \left(\frac{x}{L} \right)^2 \right] \right\}$$

Substituting for M , δM , and I , the virtual force expression for the displacement takes the form

$$v\left(x = \frac{L}{2}\right) = \frac{wL^4}{8EI_0} \int_0^1 \left\{ \frac{4 \left[\frac{x}{L} - \left(\frac{x}{L} \right)^2 \right] \frac{\delta M}{L}}{1 + 4 \left[\frac{x}{L} - \left(\frac{x}{L} \right)^2 \right]} \right\} d\left(\frac{x}{L}\right) = \frac{wL^4}{8EI_0} \alpha$$

where α is a dimensionless coefficient that depends on the interval size.

We take the interval as f and subdivide the interval 0-1 into n such intervals. Applying (3.42) and taking a range of values for n leads to

$$\begin{aligned} n &= 10 \quad \alpha = 0.065 \\ n &= 20 \quad \alpha = 0.0559 \\ n &= 30 \quad \alpha = 0.0559 \end{aligned}$$

We note that taking $n = 20$ is sufficiently accurate. We used MATLAB [29] to program the computation associated with (3.42).

3.7 Deformation–Displacement Relations for Deep Beams: Planar Loading

When the depth to span ratio is greater than 0.1, the theory based on Kirchhoff's hypothesis needs to be modified to include the transverse shear deformation. Figure 3.32 illustrates this case: the cross-section remains a plane but is no longer normal to the centroidal axis. Defining β as the rotation of the cross-section, and γ as the transverse shear strain, it follows that

$$\gamma = \theta - \beta \approx \frac{dv}{dx} - \beta \quad (3.43)$$

The extensional strain now involves β rather than θ .

$$\varepsilon(y) = -y \frac{d\beta}{dx} \quad (3.44)$$

Expressions for the internal force variables, V and M , in terms of the deformation measures are derived in a similar way as followed in Sect. 3.6.1. We express them as:

$$\begin{aligned} M &= EI \frac{d\beta}{dx} \\ V &= GA_s \gamma \end{aligned} \quad (3.45)$$

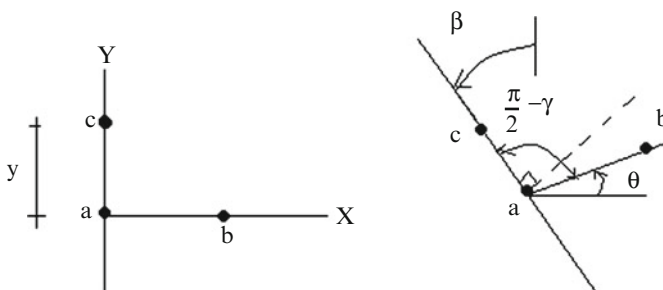
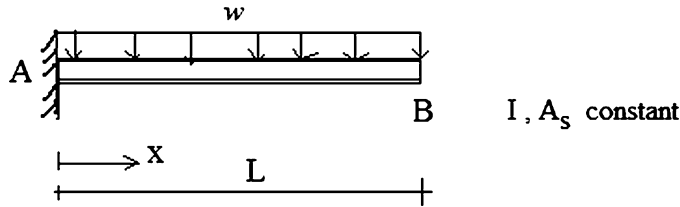


Fig. 3.32

**Fig. 3.33**

where G is the material shear modulus and A_s is the effective shear area, i.e., the cross-sectional area over which the shear stress is essentially uniformly distributed. For an I shape steel section, A_s is taken as the web area.

Given M and V , one first determines β with

$$\beta(x) - \beta(x_A) = \int_{x_A}^x \frac{M}{EI} dx \quad (3.46)$$

If A is a fixed support, $\beta = 0$. Once β is known, we find v by integrating

$$\frac{dv}{dx} = \beta + \frac{V}{GA_s}$$

This leads to

$$v(x) - v(x_A) = \int_{x_A}^x \left(\beta + \frac{V}{GA_s} \right) dx \quad (3.47)$$

In general two boundary conditions are required to specify the two integration constants.

For example, consider the structure and loading defined in Fig. 3.33.

The transverse shear force and moment expressions are

$$V(x) = w(L - x)$$

$$M(x) = -\frac{w}{2}(L - x)^2$$

Point A is a fixed support. Then $\beta(x_A) = v(x_A) = 0$. Noting (3.46),

$$\beta = \int_0^x -\frac{w}{2EI}(L - x)^2 dx$$

↓

$$\beta = \frac{w}{6EI}(L - x)^3 - \frac{w}{6EI}L^3$$

Substituting for β in (3.47) leads to

$$\begin{aligned} v(x) &= \left[\frac{w}{2GA_s} (L-x)^2 \right] + \left[-\frac{w}{24EI} (L-x)^4 - \frac{w}{6EI} L^3 x \right]_0^x \\ &= \frac{w}{2GA_s} \left[(L-x)^2 - L^2 \right] + \frac{w}{6EI} \left[-\frac{1}{4} (L-x)^4 - L^3 x + \frac{L^4}{4} \right] \end{aligned} \quad (3.48)$$

Specializing for $x = L$, the end displacement is equal to

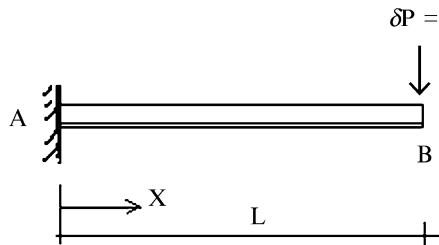
$$v(L) = -\frac{wL^4}{8EI} \left[1 + \frac{4EI}{GA_s L^2} \right]$$

The effect of shear deformation is to “increase” the displacement by a dimensionless factor which is proportioned to the ratio $EI/GA_s L^2$. This factor is usually small with respect to 1 for homogeneous cross-section. It may be large for composite beams that have a “soft” core, i.e., where $G \ll E$.

Rather than work with the deformation–displacement results, one can apply an extended form of the Principle of Virtual Forces. We add the shear deformation term to the integral and also introduce the virtual shear force δV . Then, (3.36) expands to

$$d\delta P = \int_x \left(\frac{M(x)}{EI} \delta M(x) + \frac{V(x)}{GA_s} \delta V(x) \right) dx \quad (3.49)$$

The steps involved are the same as for slender beams. One now has to determine δV as well as δM for a given δP . Revisiting the previous example defined in Fig. 3.33, we compute $v(L)$. The details are as follows.



$$\delta V(x) = 1$$

$$\delta M(x) = L - x$$

$$\begin{aligned}
 + \uparrow v(L) &= \int_0^L \left[-\frac{w}{2EI} (L-x)^2 \right] (L-x) dx + \int_0^L \left[-\frac{w}{GA_s} (L-x) \right] (1) dx \\
 &= \left[\frac{w}{8EI} (L-x)^4 \right]_0^L + \left[-\frac{w}{2GA_s} (L-x)^2 \right]_0^L \\
 &= \frac{w}{8EI} L^4 - \frac{w}{2GA_s} L^2
 \end{aligned}$$

Applying the Principle of Virtual Forces for this example involves less algebra than required for integration.

3.8 Torsion of Prismatic Members

Consider the prismatic member shown in Fig. 3.34. Up to this point, we have assumed the line of action of the external loading passes through the centroidal axis, and consequently the member just bends in the $X-Y$ plane. This assumption is not always true and there are cases where the loading may have some eccentricity with respect to the X -axis. When this occurs, the member twists about the X -axis as well as bends in the $X-Y$ plane.

We deal with an eccentric load by translating its line of action to pass the X -axis. This process produces a torsional moment about X as illustrated in Fig. 3.35.

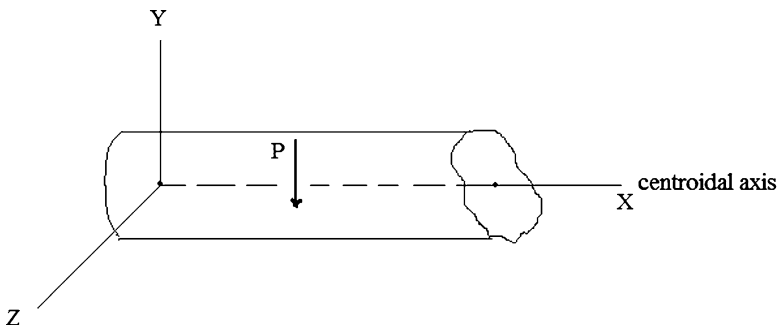


Fig. 3.34 Prismatic member—eccentric load

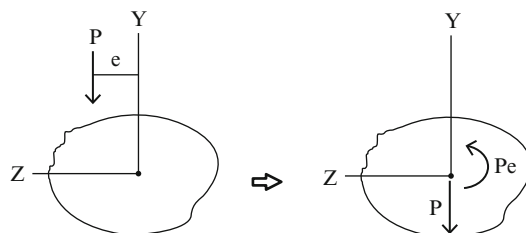


Fig. 3.35

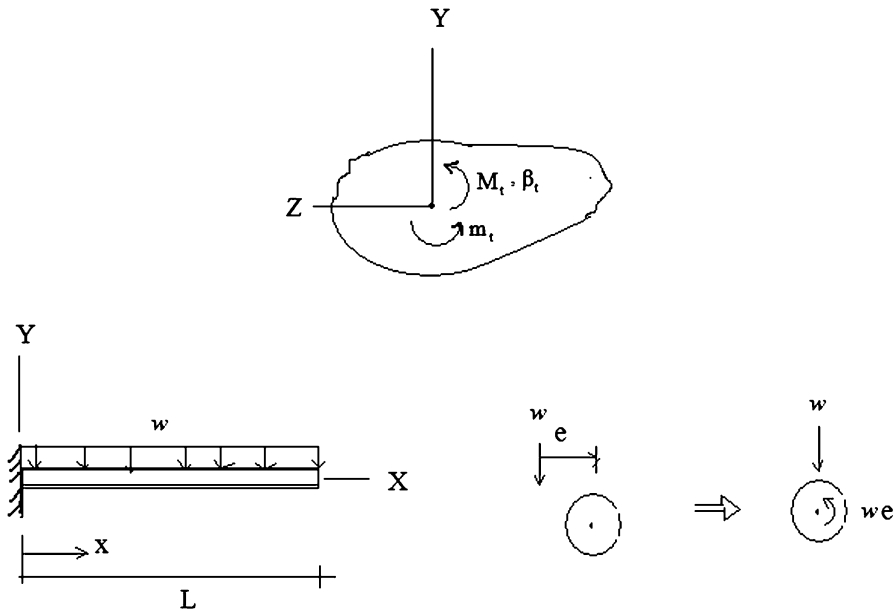


Fig. 3.36

The torsional moment is resisted by shearing stresses acting in the plane of the cross-section, resulting in shear strain and ultimately rotation of the cross-section about the X -axis. Mechanics of Solids texts such as [16] present a detailed theory of torsion of prismatic members so we just list the resultant equations here. First, we introduce the following notation listed in Fig. 3.36

M_t = moment vector about the X -axis (positive sense from Y toward Z)

β_t = rotational vector about the X -axis

m_t = distributed external torsional moment loading

J = torsional cross-sectional property (similar to I for plane bending)

The differential equation of equilibrium for torsion has the form

$$\frac{dM_t}{dx} + m_t = 0 \quad (3.50)$$

One needs to restrain the member at one point for stability. A free end has $M_t=0$. Given M_t , one determines the rotation with

$$M_t = GJ \frac{d\beta_t}{dx} \quad (3.51)$$

Note the similarity between the expression for bending and twisting. We find β_t by integrating (3.51).

$$\beta_t(x) - \beta_t(x_A) = \int_{x_A}^x \frac{M_t}{GJ} dx \quad (3.52)$$

A boundary condition on β_t is required to determine $\beta_t(x)$. Typical boundary conditions are illustrated below.



The principle of Virtual Forces can be extended to deal with combined bending and twisting by adding the twist deformation term to the integration. The general expression which includes all deformation terms is

$$d_A \delta P_A = \int_x \left(\frac{M}{EI} \delta M + \frac{V}{GA_s} \delta V + \frac{M_t}{GJ} \delta M_t \right) dx \quad (3.53)$$

where δM_t is the virtual torsional moment.

When bending and twisting are coupled because of eccentric loading, it is convenient to solve the bending and twisting problems separately, and then combine the solutions.

In what follows, we illustrate this approach.

The eccentric load shown in Fig. 3.36 produces the distributed torsional loading equal to we , and the planar loading w . Noting (3.50), the torsional moment is

$$M_t = we(L - x)$$

We determine the twist with (3.52). The left end is fixed, so $\beta_t(0)=0$. Then

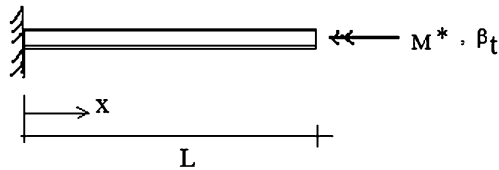
$$\begin{aligned} \beta_t(x) &= \int_0^x \frac{1}{GJ} [we(L - x)] = \frac{we}{2GJ} (L - x)^2 \Big|_0^x \\ \beta_t(x) &= \frac{we}{2GJ} [2Lx - x^2] \end{aligned}$$

The solution for plane bending is generated with (3.22)

$$\frac{d\theta}{dx} = -\frac{w}{2EI} (L - x)^2$$

$$\theta(x) = \left[\frac{w}{6EI} (L - x)^3 \right]_0^x = \frac{w}{6EI} (L - x)^3 - \frac{wL^3}{6EI}$$

$$v(x) = \left[-\frac{w}{24EI} (L - x)^4 - \frac{wL^3 x}{6EI} \right]_0^x = \frac{w}{6EI} \left\{ -\frac{1}{4} (L - x)^4 - L^3 x + \frac{L^4}{4} \right\}$$

Fig. 3.37

The solution for a cantilever beam subjected to a concentrated torsional moment at the free end is needed later when we deal with plane grids.

Noting Fig. 3.37, the torsional moment is constant,

$$M_t = M^*$$

and the twist angle varies linearly with x

$$\beta_t = \frac{M^*}{GJ}x \quad (3.54)$$

3.9 Symmetry and Anti-symmetry

3.9.1 Symmetry and Anti-symmetry: Shear and Moment Diagrams

This section discusses the relationship between certain properties of the shear and moment diagrams and the nature of the loading distribution and support locations. We first introduce some background material on symmetrical and anti-symmetrical functions.

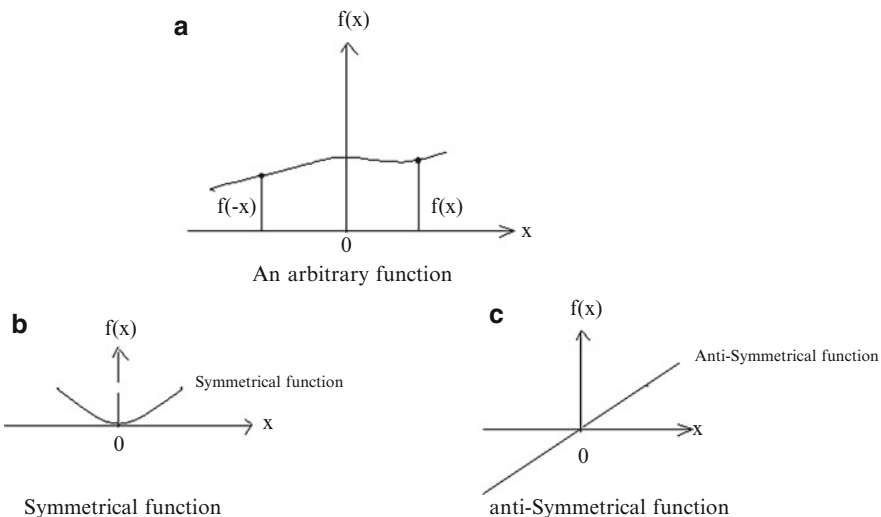
Consider the function $f(x)$ shown in Fig. 3.38. We say the function is symmetrical with respect to $x = 0$ when $f(-x) = f(x)$ and anti-symmetrical when $f(-x) = -f(x)$. Symmetrical functions have $df/dx = 0$ at $x = 0$. Anti-symmetrical functions have $f = 0$ at $x = 0$. One can establish that the derivative of a symmetrical function is an anti-symmetrical function. Similarly, the derivative of an anti-symmetrical function is a symmetrical function. If we know that a function is either symmetrical or anti-symmetrical, then we have to generate only one-half the distribution. The shape of the other half follows by definition of the symmetry properties.

Starting with the basic differential equations relating the shear, moment, and applied distributed loadings:

$$\frac{dV}{dx} = w$$

$$\frac{dM}{dx} = -V$$

$$\frac{dM_t}{dx} + m_t = 0$$

**Fig. 3.38**

We can deduce the following properties for V , M , and M_t , given the nature of the loading

1. w is a symmetrical function
 - V is anti - symmetrical
 - M is symmetrical
 2. w is an anti - symmetrical function
 - V is symmetrical
 - M is anti - symmetrical
 3. m_t is a symmetrical function
 - M_t is anti - symmetrical
 4. m_t is an anti - symmetrical function
 - M_t is symmetrical
- (3.55)

The following cases illustrate these rules.

Symmetrical—planar loading:

Case (a) (Fig. 3.39):

Case (b) (Fig. 3.40):

Note that the center section is in pure bending, i.e. the shear force is zero. This loading scheme is used to test beams in bending

Anti-symmetry—planar loading:

Case (a) (Fig. 3.41):

Case (b) (Fig. 3.42):

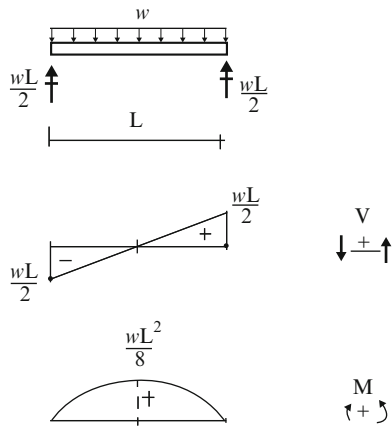
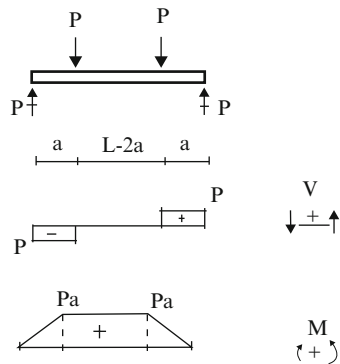
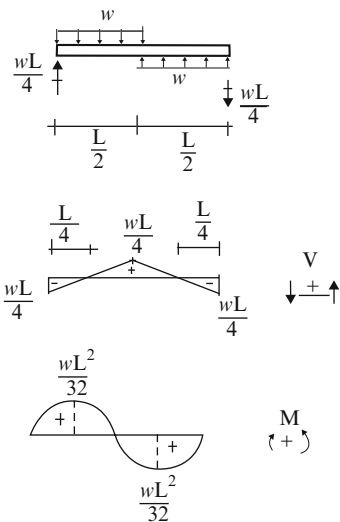
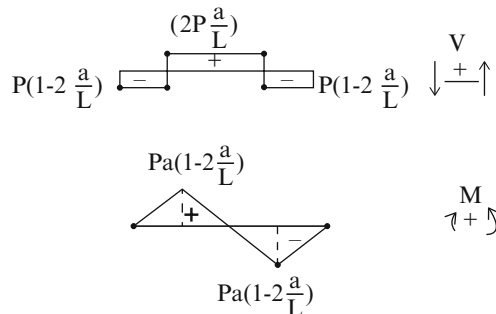
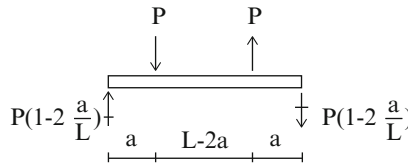
Fig. 3.39 Uniform loading**Fig. 3.40** 2 point loading**Fig. 3.41** Anti-symmetrical uniform loading

Fig. 3.42 Anti-symmetrical 2 point loading



We use the concept of symmetry to represent an arbitrary loading as a superposition of symmetrical and anti-symmetrical loadings. Then, we generate the individual shear and moment diagrams and combine them. As an illustration, consider a simply supported beam with a single concentrated force shown in Fig. 3.43a. We replace it with two sets of forces, one symmetrical and the other anti-symmetrical, as shown in Fig. 3.43b. Then we use the results shown in Figs. 3.40 and 3.42 to construct the shear and moment diagrams.

3.9.2 Symmetry and Anti-Symmetry: Deflected Shapes

A structure is said to be geometrically symmetrical with respect to a particular axis when, if one rotates the portion either to the right or to the left of the axis through 180° , it coincides identically with the other portion. Figure 3.44 illustrates this definition. If we rotate A-B about axis 1-1 it ends up exactly on A-C. A mathematical definition of geometric symmetry can be stated as follows: for every point having coordinates X, Y , there exists a corresponding point with coordinates X, Y .

In addition to geometric symmetry, we also introduce the concept of support symmetry. The supports must be located symmetrically with respect to the axis of geometric symmetry and be of the same nature, e.g., vertical, horizontal, and

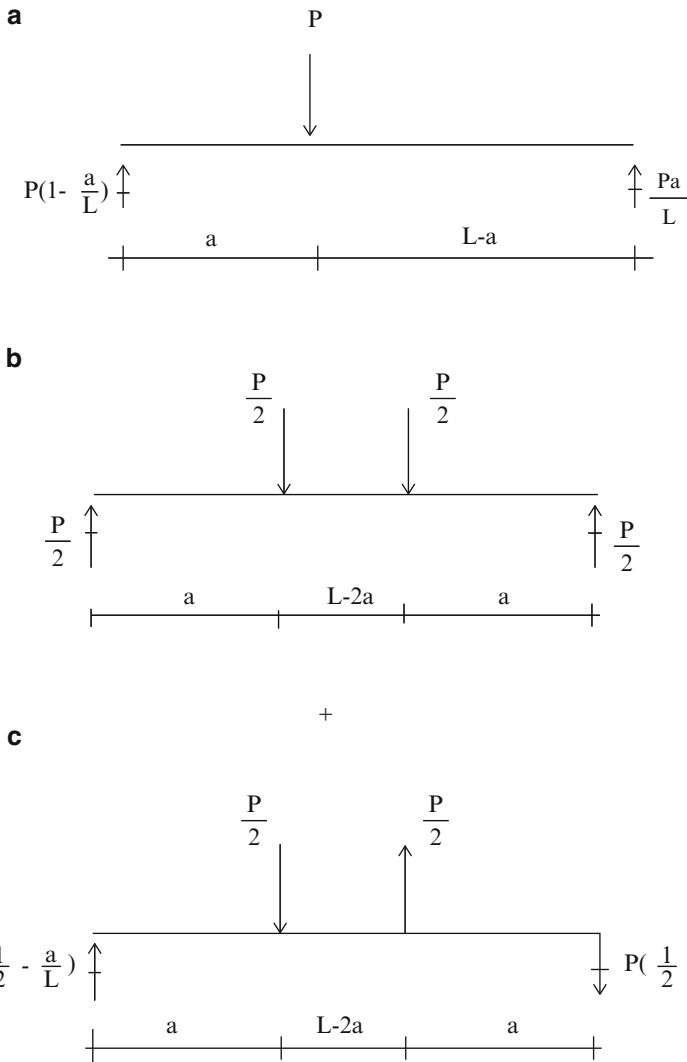


Fig. 3.43 Representation of an arbitrary loading by superposition. (a) Single concentrated load. (b) Set of symmetrical loads. (c) Set of anti-symmetrical loads

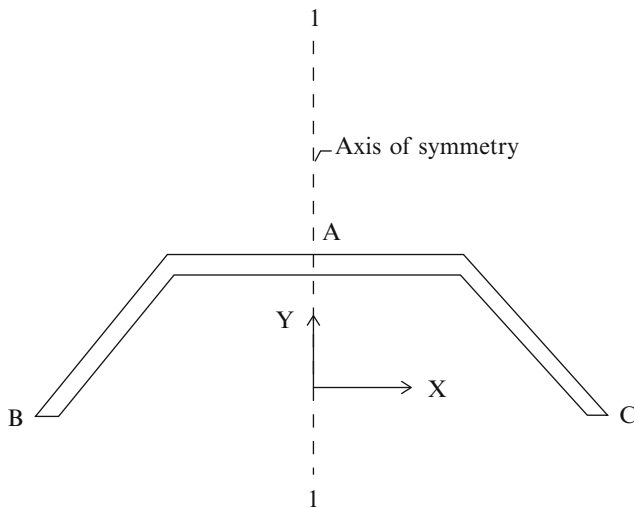


Fig. 3.44 Geometric symmetry



Fig. 3.45 Unsymmetrical support

rotational constraints. Consider Fig. 3.45. There are two vertical restraints at points A and B. The geometric symmetry axis, 1-1, passes through mid-span. For complete symmetry, the roller support at point A needs to be shifted to the end of the span. Another example is shown in Fig. 3.46.

We say a structure is symmetrical when it has both geometric and support symmetry. The symmetry property is very useful since it leads to the following conclusions:

When a symmetrical structure is loaded symmetrically, the resulting deflected shape is also symmetrical. Similarly, a symmetrical structure loaded anti-symmetrically has an anti-symmetric deflected shape.

These conclusions follow from the differential equations listed below and the properties of symmetrical and anti-symmetrical functions:

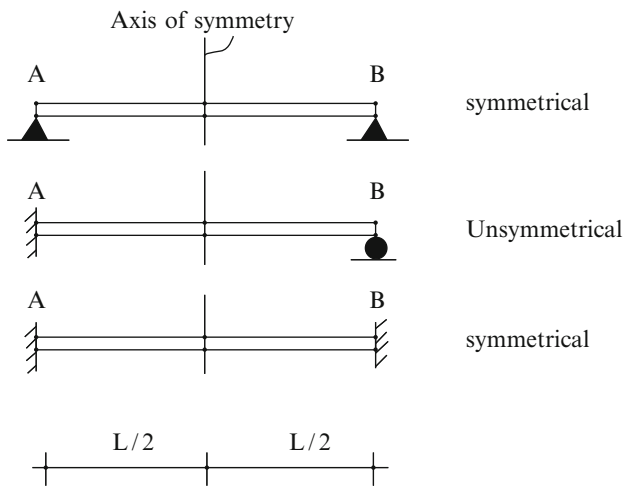


Fig. 3.46 Support symmetry examples

$$\begin{aligned}\frac{dV}{dx} &= w \\ \frac{dM}{dx} &= -V \\ \frac{dM_t}{dx} + m_t &= 0 \\ \frac{d\beta}{dx} &= \frac{M}{EI} \\ \frac{dv}{dx} &= \beta + \frac{V}{GJ} \\ \frac{d\beta_t}{dx} &= \frac{M_t}{GJ}\end{aligned}\tag{3.56}$$

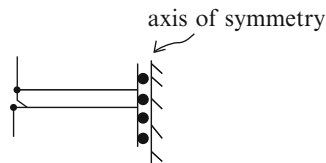
If $f(x)$ is symmetrical, df/dx is anti-symmetrical; If $f(x)$ is anti-symmetrical, df/dx is symmetrical.

Using these properties, we construct the following table relating the response variables to the loading for a symmetrical structure (Table 3.4).

We have placed a lot of emphasis here on symmetry because it is useful for qualitative reasoning. It also allows us to work with only one-half the structure provided that we introduce appropriate boundary conditions on the axis of symmetry. The boundary conditions for the symmetrical case follow from the fact that V , β , and M_l are anti-symmetric functions and therefore vanish at the symmetry axis. We introduce a new support symbol shown in Fig. 3.47, which represents these conditions. The roller support releases V and M_l ; the rigid end plate eliminates β .

Table 3.4 Loading response relationships—symmetrical structure

| Loading | Response variables |
|------------------------|----------------------------------------------------------------------------------------|
| w symmetrical | V anti-symmetrical M symmetrical β anti-symmetrical v symmetrical |
| w anti-symmetrical | V symmetric M anti-symmetrical β symmetrical v anti-symmetrical |
| m_t symmetrical | M_t anti-symmetrical β_t symmetrical |
| m_t anti-symmetrical | M_t symmetrical β_t anti-symmetrical |

Fig. 3.47 Symmetrical boundary conditions on a symmetry axis

For example, consider the symmetrically loaded simply supported beam shown in Fig. 3.48a. We can work with either the left or right segment. We choose to work with the left segment, with an appropriate support at c on the axis of symmetry. The displacement boundary conditions for this segment are

$$v_a = 0, \quad b_c = 0$$

The solution generated with this segment also applies for the other segment (the right portion).

When the loading is anti-symmetrical, the bending moment and displacement are also anti-symmetric functions which vanish at the symmetry axis. The appropriate support on the axis of symmetry, for this case is a roller support. We replace the full beam with the segments shown in Fig. 3.49b, c. We analyze the left segment, and then reverse the sense of the response variables for the other segment.

3.10 Influence Lines and Force Envelopes for Statically Determinate Beams

3.10.1 The Engineering Process

The objective of the engineering process is to define the physical makeup of the beam, i.e., the material, the shape of the cross-section, and special cross-section features such as steel reinforcement in the case of a reinforced concrete beam. Cross-sectional properties are governed by the strength of the material and constraints associated with the specific design codes recommended for the

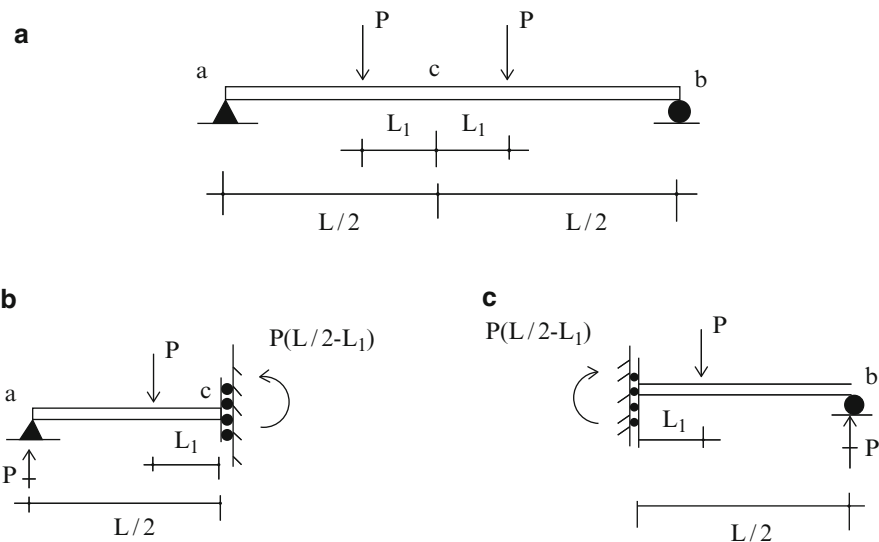


Fig. 3.48 Boundary conditions on symmetry axis—symmetrical planar loading. (a) Symmetrical load. (b) Left segment. (c) Right segment

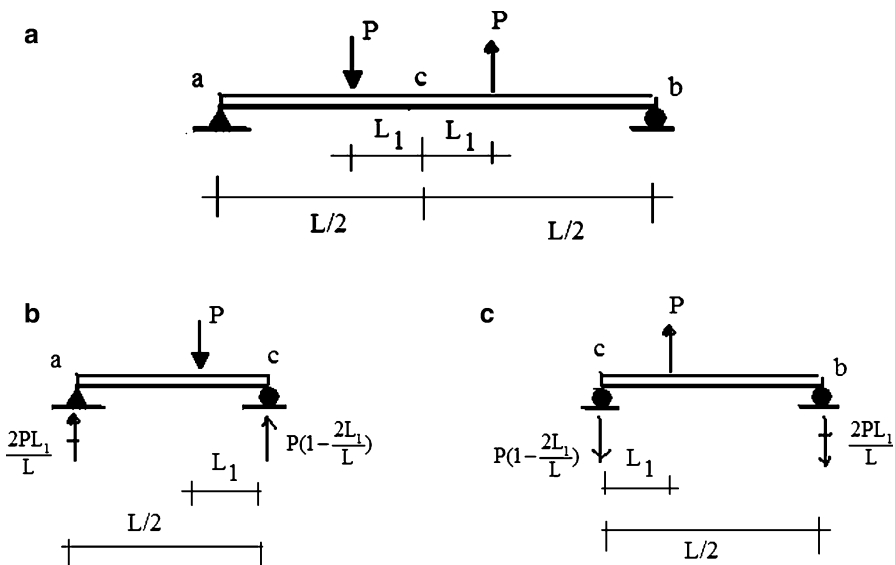


Fig. 3.49 Bending conditions on symmetry axis—anti-symmetrical planar loading. (a) Anti-symmetrical planar load. (b) Left segment. (c) Right segment

different structural materials such as concrete, steel, and wood. Given the maximum values of shear and moment at a particular location, the choice of material, and the general shape of the cross-section, the determination of the specific cross-sectional dimensions involves applying numerical procedures specific to the associated code. This computational aspect of the engineering process is called design detailing. Detailing mostly has been automated and there are an extensive set of computer aided design tools available. *Therefore, we focus here mainly on that aspect of the engineering process associated with the determination of the “maximum” values of shear and moment for statically determinate beams.* Part II extends the discussion to statically indeterminate beams.

Shear and bending moment result when an external loading is applied to a beam. We described in Sect. 3.4 how one can establish the shear and moment distributions corresponding to a given loading. *For statically determinate beams, the internal forces depend only on the external loading and geometry; they are independent of the cross-sectional properties.* Now, the loading consists of two contributions: dead and live. The dead loading is fixed, i.e. its magnitude and spatial distribution are constant over time. Live loading is, by definition, time varying over the life of the structure. This variability poses a problem when we are trying to establish the maximum values of shear and moment. We need to consider all possible live load scenarios in order to identify the live load locations that result in the maximum values of shear and moment.

There are two approaches to treating live loads for statically determinate beams. In the first approach, we select a particular location on the longitudinal axis and determine how the moment and shear at that point vary as the position of the live load is varied. We usually plot these quantities as a function of the position of the live load, which usually is taken as a single concentrated force of unit magnitude and refer to the resulting plot as an *influence line*. With this plot, one can easily identify the critical position of live loading for the cross-section of interest. It is a valuable tool to establish loading patterns.

The current trend is to use beams having a constant cross-section. In this case, we need the absolute maximum values of shear and moment. We are generally not interested in the location of these maxima, just their values. Therefore, in the second approach, we determine for each position of the live load the global maximum values, i.e., the maximum value of the quantity throughout the span. Plots of global maxima vs. live load positions are called *force envelopes*.

It is important to distinguish between influence lines and force envelopes. They display different entities. An influence line relates a *force quantity at a particular point to the position of the live load*, whereas a *force envelope relates the absolute maximum value of the force quantity along the span to the position of the live load*. The following sections illustrate the construction of these plots.

3.10.2 Influence Lines

3.10.2.1 Influence Line for Bending Moment

We consider the simply supported beam with a concentrated load applied a distance x from the left support shown in Fig. 3.50. We view x as a variable and explore how the moment and shear diagrams vary as x ranges from 0 to L . This information allows us to construct both the influence lines at a particular point and the force envelopes.

The bending moment diagram is plotted in Fig. 3.51. We note that the maximum value of moment occurs at the point of application of the force and is related to x by

$$M_{\max} = Px \left(1 - \frac{x}{L}\right) \quad (3.57)$$

We can use the bending moment diagram shown above to establish the influence line for moment at a particular location, say a distance x_1 from the left support. There are two loading regions, $x < x_1$ and $x > x_1$ for P . The corresponding moment at x_1 follows from Fig. 3.52a.

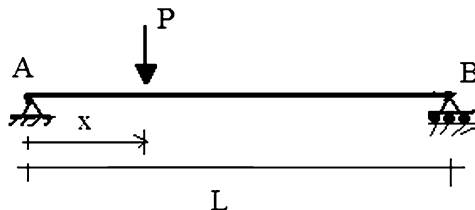


Fig. 3.50 Simply supported beam

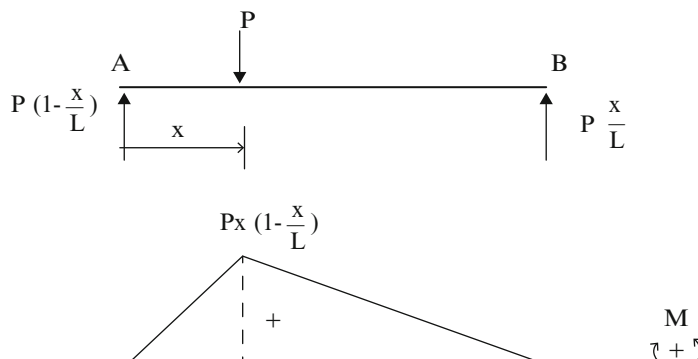


Fig. 3.51 Reactions and bending moment diagram for concentrated load

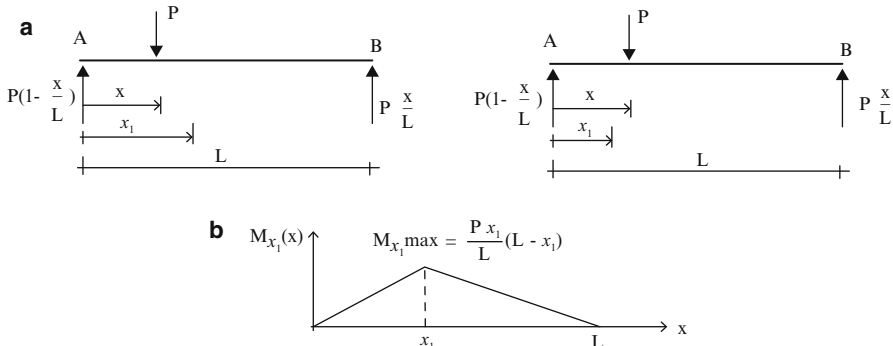


Fig. 3.52 (a) Free body diagrams for $x < x_1$ and $x > x_1$. (b) Influence line for moment at location x_1

$$\begin{aligned} x < x_1 \quad M_{x_1} &= \frac{Px}{L}(L - x_1) \\ x > x_1 \quad M_{x_1} &= Px_1\left(1 - \frac{x}{L}\right) \end{aligned} \quad (3.58)$$

The influence line for M_{x_1} is obtained by varying x in (3.58). The result is plotted in Fig. 3.52. This plot shows that *the maximum value of M_{x_1} as x ranges from 0 to L occurs when the force is applied at x_1 .*

$$M_{x_{1 \max}} = \frac{Px_1}{L}(L - x_1) \quad (3.59)$$

3.10.2.2 Influence Line for Shear Force

We proceed in a similar manner to establish the influence line for the shear force. The shear diagram for a single concentrated force applied at x is shown in Fig. 3.53.

Suppose we want the influence line for the shear at location x_1 . Noting Figs. 3.53 and 3.54, the shear force at x_1 for the different position of the load are

$$\begin{aligned} x < x_1 \quad V|_{x_1} &= +\frac{Px}{L} \\ x > x_1 \quad V|_{x_1} &= -\frac{P(L-x)}{L} \end{aligned} \quad (3.60)$$

These functions are plotted below. At point x_1 , there is a discontinuity in the magnitude of V equal to P and a reversal in the sense. This behavior is characteristic of concentrated forces (Fig. 3.55).

For example, the influence line for shear at a cross-section located at $x_1=0.25L$ is plotted below (Fig. 3.56).

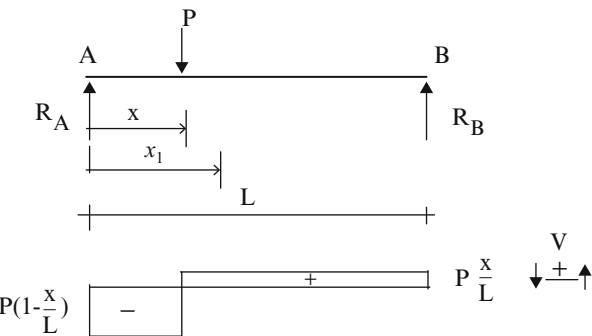


Fig. 3.53 Shear diagram for concentrated load $x < x_1$

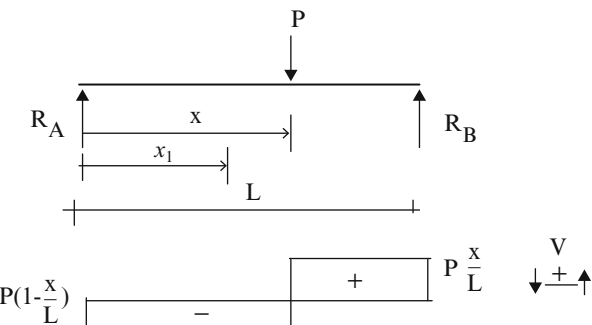


Fig. 3.54 Shear diagram for concentrated load $x > x_1$

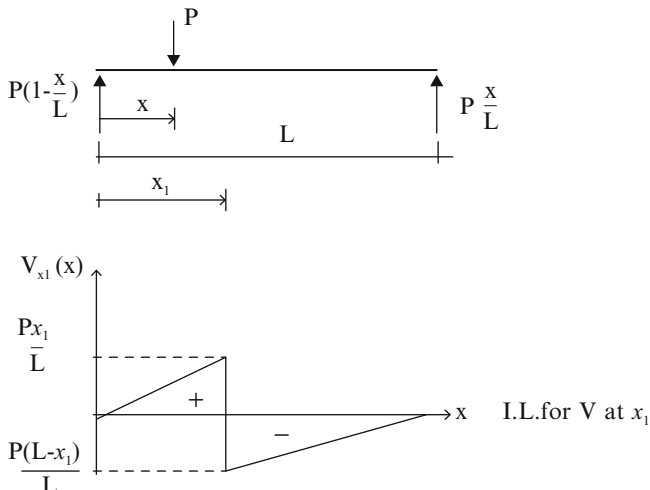


Fig. 3.55 Influence line for shear at location x_1

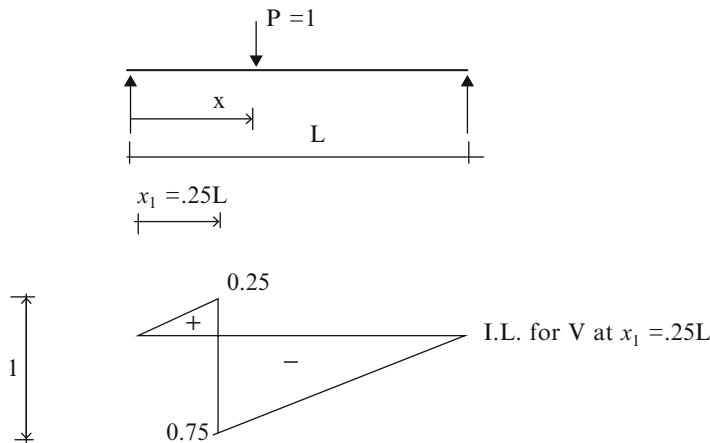


Fig. 3.56 Influence line for shear at $x_1 = 0.25L$ —simply supported beam $P = 1$

Example 3.28 Construction of influence lines

Given: The two-span beam shown in Fig. E3.28a. There is a hinge (moment release) at the midpoint of the second span.

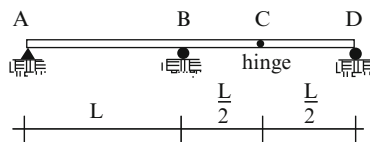


Fig. E3.28a

Determine: The influence lines for the vertical reaction and bending moment at B.

Solution: We consider a unit vertical load moving across the span and use the free body diagrams to determine the reaction and moment at B.

Figure E3.28b shows that when the load is acting on member ABC, the reaction at D equals zero and

$$R_B = \frac{x}{L} \quad \text{for } 0 < x < 1.5.$$

$$R_A = 1 - \frac{x}{L}$$

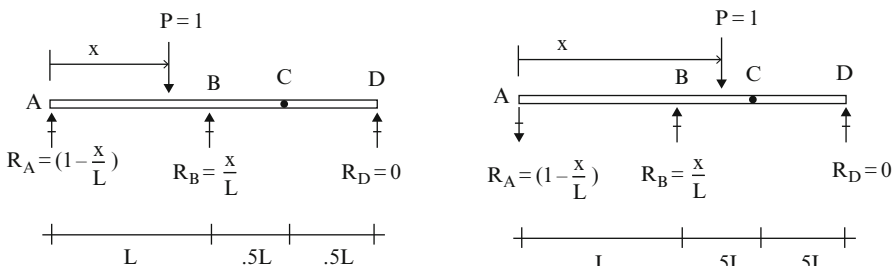


Fig. E3.28b

When the load is applied to the hinge (point C) (Fig. E3.28c), the reaction at D equals zero and

$$\begin{aligned} R_B &= +1.5 \quad \text{for } x = 1.5L \\ R_A &= -0.5 \end{aligned}$$

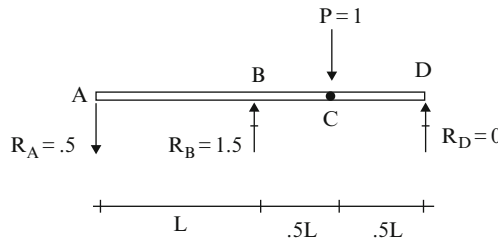


Fig. E3.28c

The behavior changes when the loading passes to member CD. Now there is a reaction at D which releases some of the load on member ABC (see Fig. E3.28d).

$$R_D = 2\left(-1.5 + \frac{x}{L}\right)$$

$$V_C = \frac{(1)(2L-x)}{0.5L} = 2\left(2 - \frac{x}{L}\right) \quad \text{for } 1.5L < x < 2L$$

$$R_B = 1.5V_C = 3\left(2 - \frac{x}{L}\right)$$

$$R_A = -0.5V_C = -\left(2 - \frac{x}{L}\right)$$

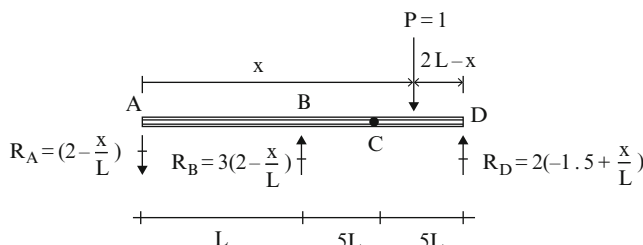


Fig. E3.28d

We determine the influence line for M_B using the same free body diagrams. First, we note that $M_B=0$ when the load is on span AB. The moment increases linearly with $(x-L)$ when the load is on span BC and then decreases linearly to 0 for span CD. The resulting influence lines are plotted below (Fig. E3.28e).

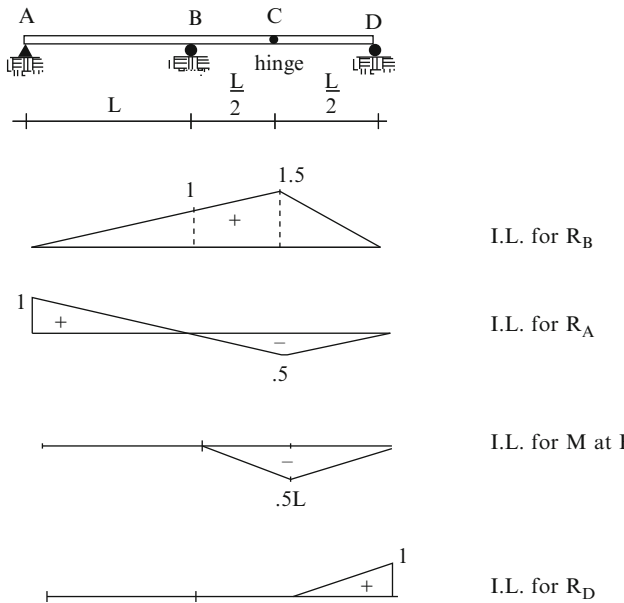


Fig. E3.28e Influence lines for R_B , R_A , R_D , and M_B

Example 3.29 Construction of influence lines

Given: The beam shown in Fig. E3.29a.

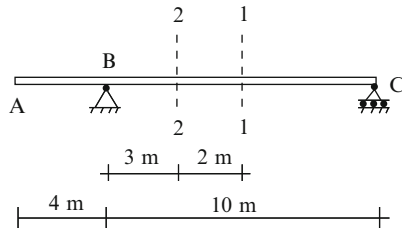
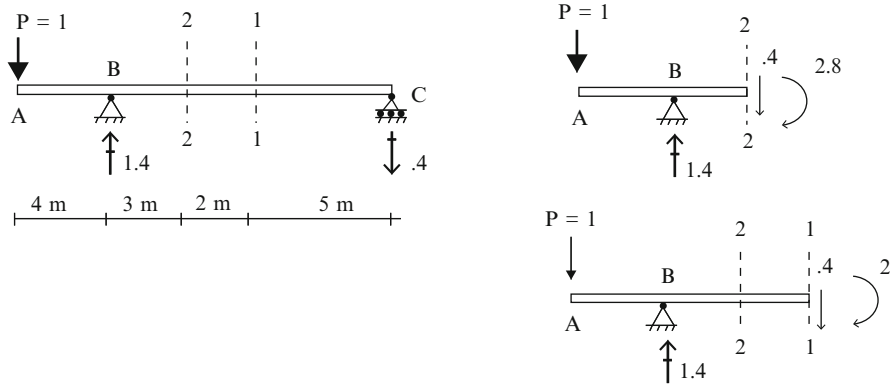
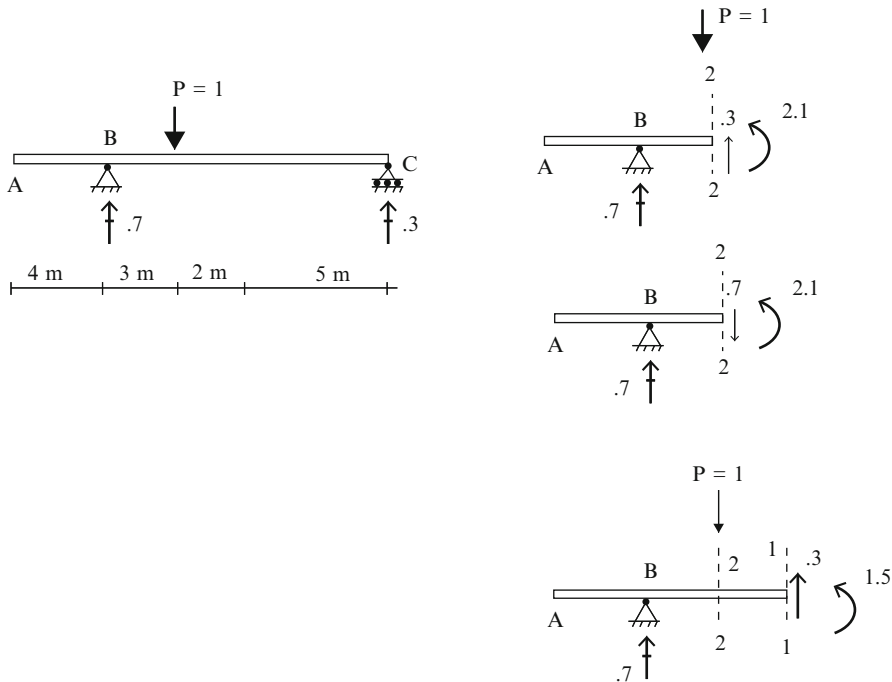
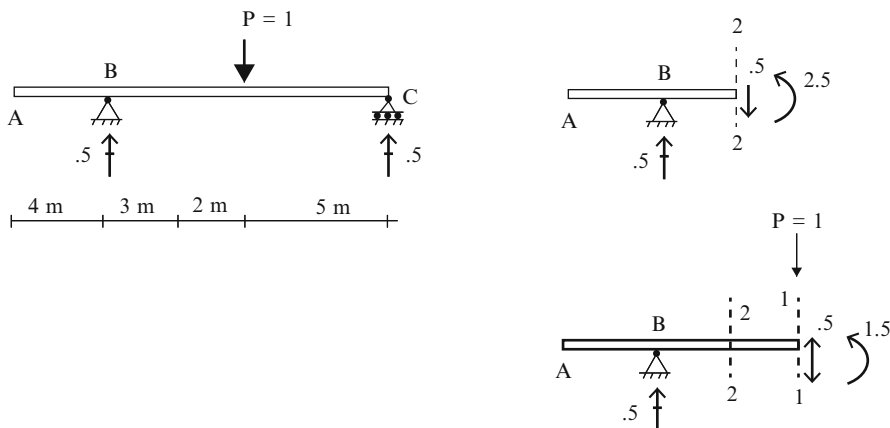


Fig. E3.29a

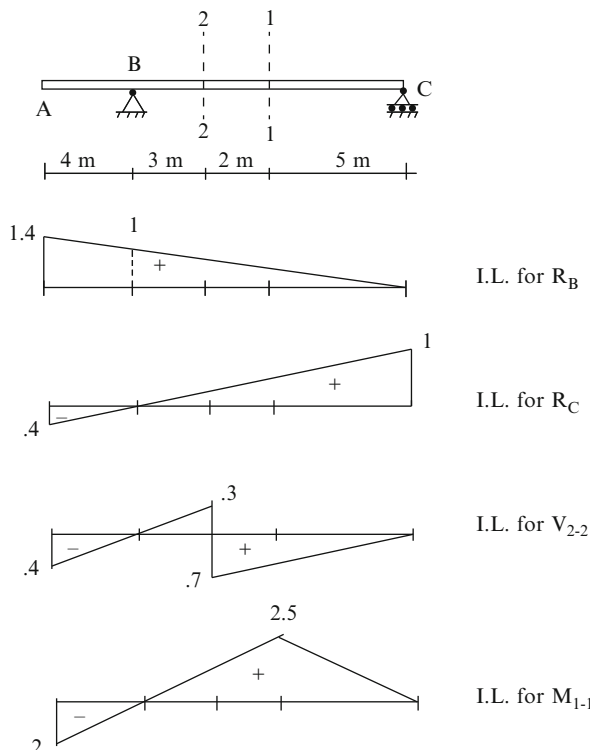
Determine: Draw the influence line for the reaction at B, the reaction at C, the moment at section 1-1, and the shear at section 2-2.

Solution: We consider a unit vertical load moving across the span and use the free body diagrams to determine the shear and moments at sections 1-1 and 2-2. The following figures show the steps (Figs. E3.29b-d).

**Fig. E3.29b** Unit load at A**Fig. E3.29c** Unit load at section 2-2

**Fig. E3.29d** Unit load at section 1-1

The resulting influence lines are plotted below (Fig. E3.29e).

**Fig. E3.29e** Influence lines for R_B , R_C , V_{2-2} , and M_{1-1}

3.10.2.3 Generating Influence Lines with the Principle of Virtual Work

The principle of Virtual work is an alternative way of stating equilibrium conditions for a rigid body. Although the principle is derived in Engineering Mechanics subjects, we assume the reader is not familiar with the topic and therefore present a brief review here.

We consider a rigid body subjected to a set of forces which are in equilibrium. Suppose we introduce a small rigid body displacement of the body from its equilibrium position as indicated in Fig. 3.57. This displacement is called a virtual displacement. According to the principle of Virtual Work, when the forces are in equilibrium, the net work due to these forces during the virtual displacement is equal to zero for all arbitrary virtual displacement patterns. This statement is expressed as a vector dot product,

$$\delta W = \sum \vec{F}_i \bullet \delta \vec{v}_i = 0 \quad (3.61)$$

It is more convenient to work with the scalar form in terms of displacements

$$\delta w = \sum F_i \delta v_i \quad (3.62)$$

where δv_i is the virtual displacement in the direction of F_i .

Requiring (3.62) to be satisfied for *arbitrary rigid body virtual displacement* leads to the force equilibrium equations,

$$\begin{aligned} \sum \vec{F}_i &= \vec{0} \\ \sum \vec{M}_0 &= \vec{0} \end{aligned} \quad (3.63)$$

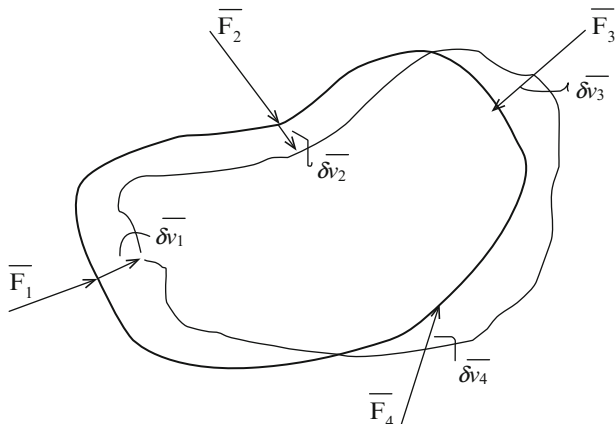
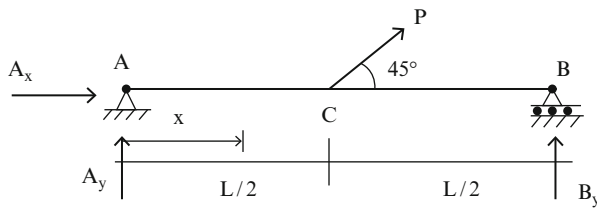


Fig. 3.57 Virtual displacement

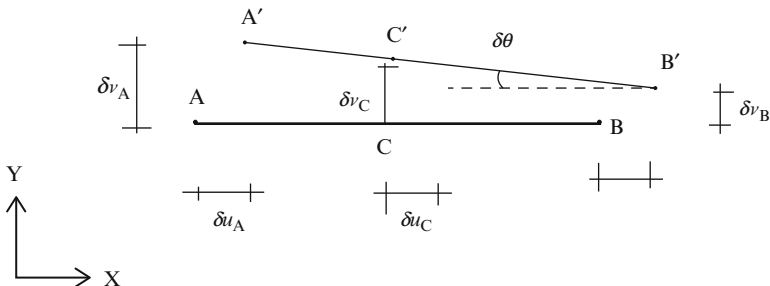
Example 3.30

Given: The rigid body shown in Fig. E3.30a.

**Fig. E3.30a**

Determine: The equilibrium equations using the Principle of Virtual Work.

Solution: We introduce the virtual displacement shown in Fig. E3.30b.

**Fig. E3.30b**

The motion consists of rigid body translations δu^* and δv^* , in the X and Y directions, and a $\delta\theta$ rotation about B. The individual motions are related by the following rigid body conditions,

$$\delta u_A = \delta u_C = \delta u_B = \delta u^*$$

$$\delta v_B = \delta v^*$$

$$\delta v_C = \delta v^* + \frac{L}{2} \delta\theta$$

$$\delta v_A = \delta v^* + L \delta\theta$$

Next, we evaluate the work equation

$$\begin{aligned} \delta W &= (A_x + 0.707P) \delta u^* + B_Y \delta v^* + 0.707P \left(\delta v^* + \frac{L}{2} \delta\theta \right) + A_Y (\delta v^* + L \delta\theta) \\ &= 0 \end{aligned}$$

Rearranging the terms,

$$\delta W = (A_x + 0.707P) \delta u^* + (A_Y + B_Y + 0.707P) \delta v^* + \left(LA_Y + \frac{0.707PL}{2} \right) \delta \theta = 0$$

Requiring the work equations to be satisfied for arbitrary virtual displacements δu^* , δv^* , and $\delta \theta$ leads to the force equilibrium equations

$$A_x + 0.707P = 0$$

$$A_Y + B_Y + 0.707P = 0$$

$$A_y + \frac{1}{2}(0.707P) = 0$$

In the previous section, we established the influence line for a quantity using an equilibrium equation. We can achieve the same result by specializing the choice of a virtual displacement. For example, suppose one wants the influence line for the reaction at A defined in Fig. 3.58.

We select the virtual displacement profile generated by displacing A , holding B fixed as indicated in the figure. Then, applying the work equations,

$$\delta W = R_A \delta v_A - (1) \delta v = 0$$

and solving for R_A leads to

$$R_A = (1) \frac{\delta v}{\delta v_A} = (1) \left(\frac{L-x}{L} \right)$$

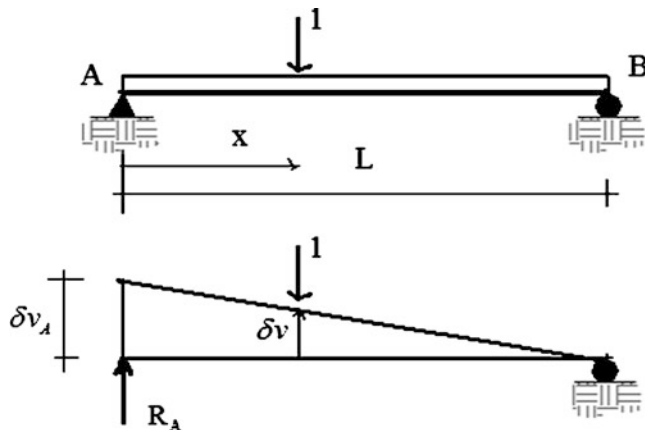


Fig. 3.58

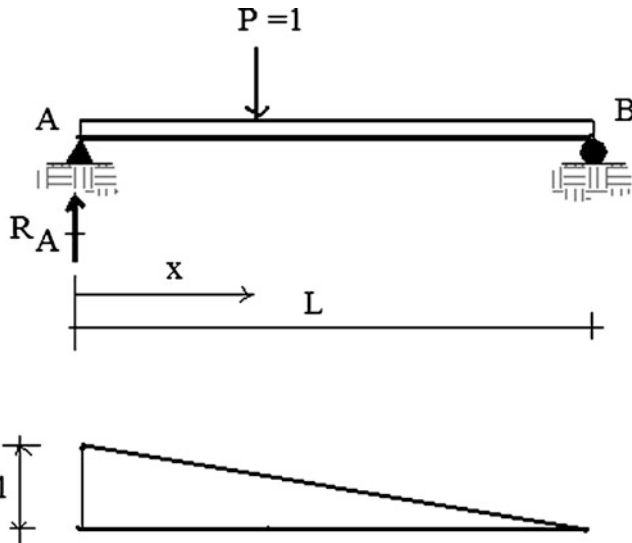


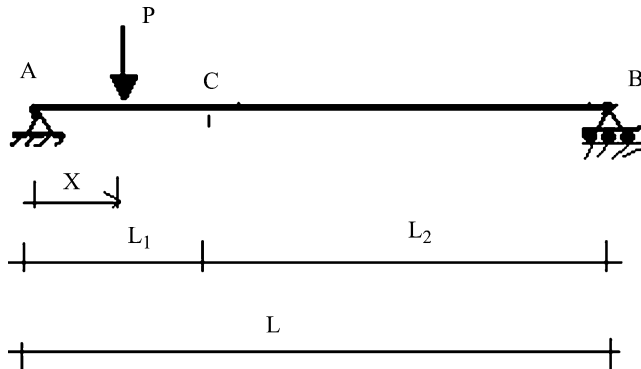
Fig. 3.59 Influence line for reaction at A

Lastly, if we take $\delta v_A=1$, the corresponding virtual displacement pattern is the influence line for R_A . Students prefer working with visual displays rather than with equations and find the virtual work approach more convenient since it is more procedural.

Summarizing, to generate the influence line for a force quantity we remove the restraint corresponding to the quantity and introduce a virtual displacement. The resulting virtual displacement pattern is the influence line for the quantity. Examples of typical cases are listed below.

Reaction at A (Fig. 3.59):

Internal moment at point C (Fig. 3.60):



We introduce a hinge at C, and then apply a unit rotation, $\delta\theta_C$, which generates a triangular displacement profile.

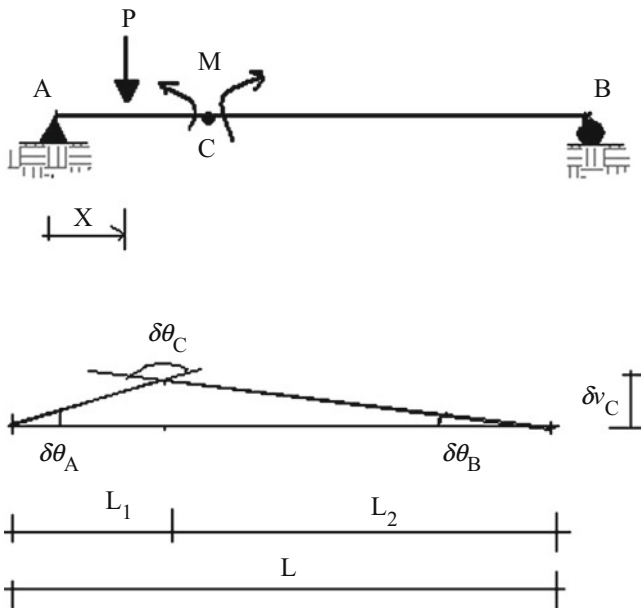


Fig. 3.60 Influence line for moment at C

The geometric parameters are related by

$$\delta\theta_A = \frac{\delta v_c}{L_1} \quad \delta\theta_B = \frac{\delta v_c}{L_2}$$

$$\delta\theta_C = \delta\theta_A + \delta\theta_B = \left(1 + \frac{L_1}{L_2}\right) \delta\theta_A$$

We suppose $\delta\theta$ is small. Substituting in the work equation leads to

$$-P(x \delta\theta_A) + M \delta\theta_C = 0$$

↓

$$-Px \delta\theta_A + M \left(\frac{L_1 + L_2}{L_2}\right) \delta\theta_A = 0$$

↓

$$M = \frac{PL_2x}{L}$$

This result confirms that the virtual displacement profile is a *scaled version* of the influence line for moment.

Internal shear at C (Fig. 3.61):

We introduce a shear release at C and apply a differential displacement of the adjacent cross-sections.

This motion produces the displacement profile shown below.

Assuming $\delta\theta$ is small, the virtual motion parameters are related by

$$\delta_1 = L_1 \delta\theta \quad \delta_2 = L_2 \delta\theta$$

$$\delta = \delta_1 + \delta_2 = L \delta\theta$$

Using these results, the work equation takes the following form,

$$\delta W = VL \delta\theta - P(x \delta\theta) = 0$$

⇓

$$V = P \frac{x}{L}$$

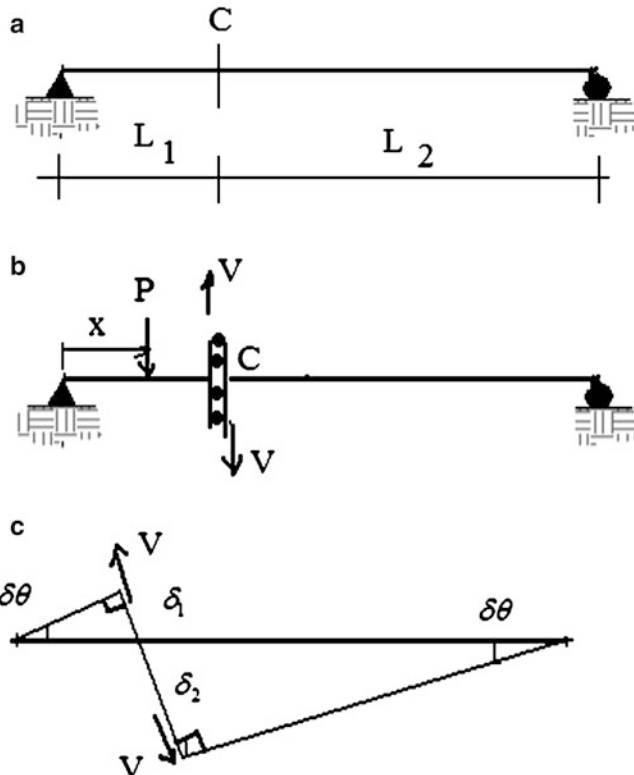
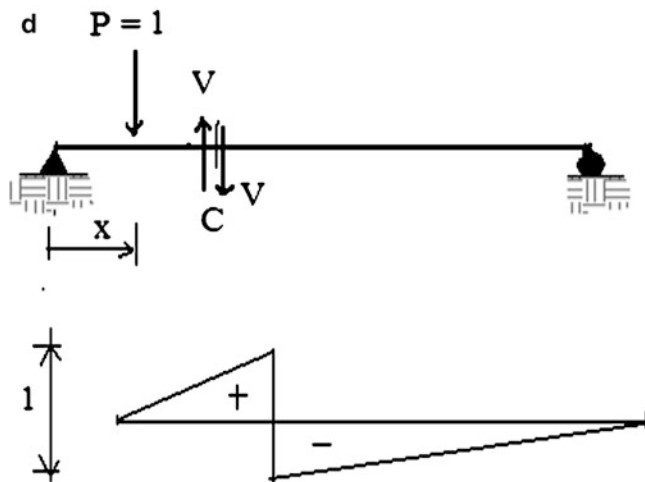


Fig. 3.61 Influence line for shear at C

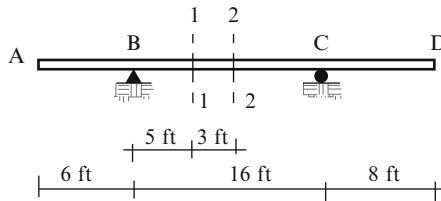
**Fig. 3.61** (continued)

Since $\delta\theta$ is small, we sketch the influence line as shown below.

These examples show that one can determine the analytical solution for an influence line with the principle of Virtual Work. However, we use the Principle mainly to generate a qualitative estimate of the overall shape of the influence line. Given the shape, one can identify the critical loading pattern and then generate a quantitative estimate. The following example illustrates this point.

Example 3.31 Construction of influence lines

Given: The beam shown in Fig. E3.31a.

**Fig. E3.31a**

Determine: The influence lines for the vertical reactions at B and C, moment at section 2-2, and the moment and shear forces at section 1-1 using the Principle of

Virtual Work. Suppose a uniformly distributed live load of $w_L = 1.2 \text{ kip/ft}$ and uniformly distributed dead load of $w_D = 0.75 \text{ kip/ft}$ are placed on the beam. Using these results, determine the maximum value of the vertical reaction at B and the maximum and minimum values of moment at section 2-2.

Solution: The vertical displacement patterns corresponding to the force quantities of interest are plotted in Fig. E3.31b.

By definition, these displacement patterns are scaled versions of the influence lines. We determine the appropriate scale factors using force body diagrams shown in Fig. E3.31c. We take the load placed at A to calibrate the diagrams.

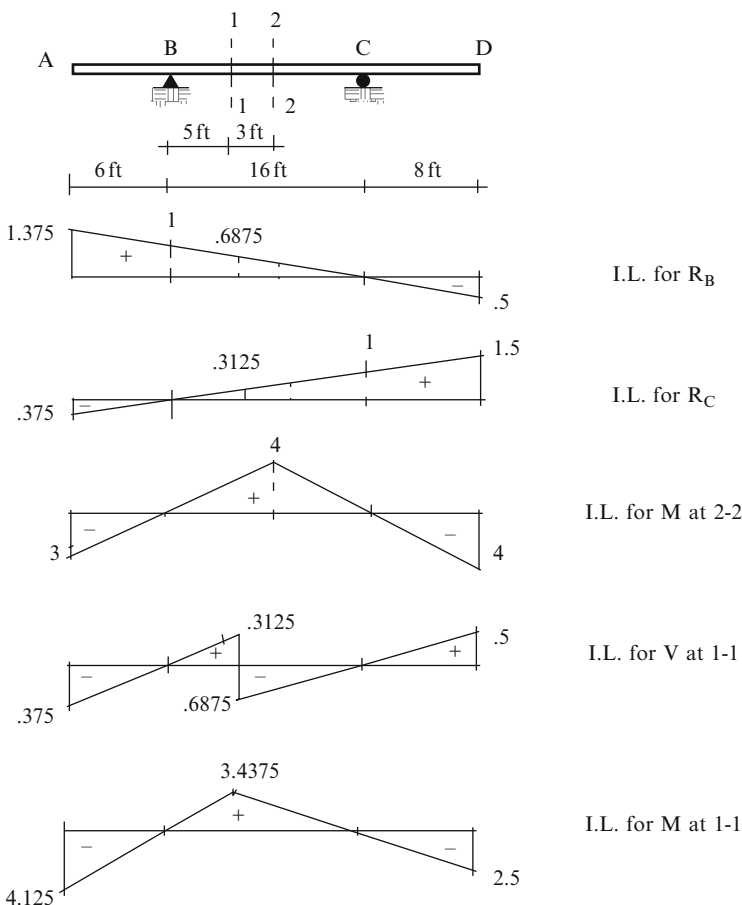
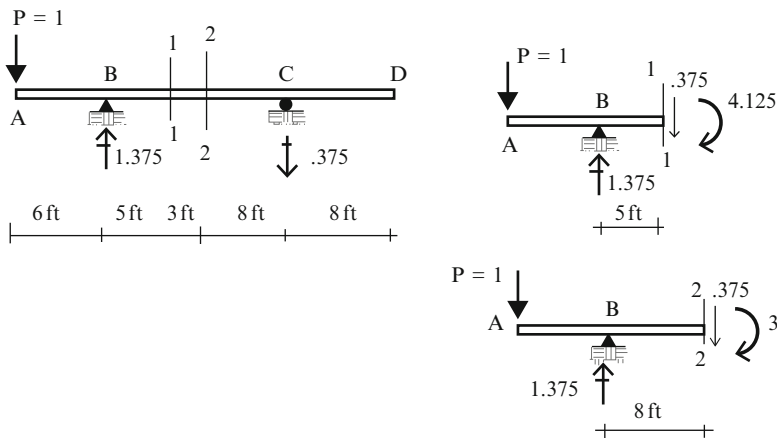
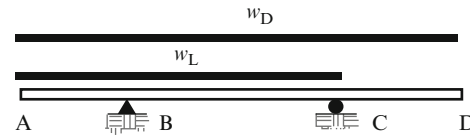


Fig. E3.31b Influence lines for R_B , R_C , V_{1-1} , M_{2-2} , and M_{1-1}

**Fig. E3.31c**

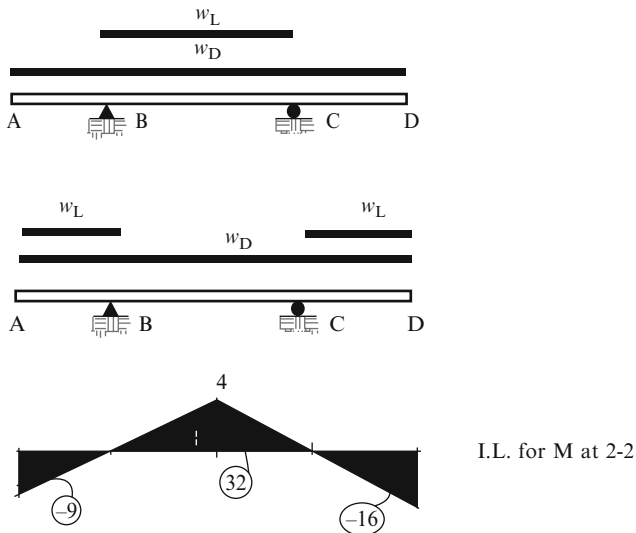
Then, the peak value of R_B is determined using data shown in Fig. E3.31d.

$$R_{B\max} = 1.2(15.125) + 0.75(15.125 - 2) = 28 \text{ kip}$$

**Fig. E3.31d** Maximum and minimum values of R_B

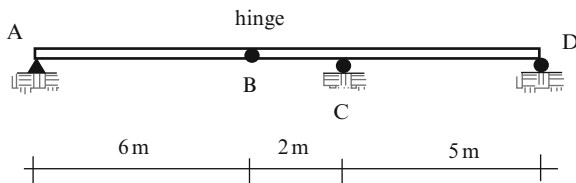
Similarly, the peak values of moment at section 2-2 are generated using the data shown in Fig. E3.31e.

$$\begin{cases} M_{\max} \text{ at } 2-2 = 1.2(32) + 0.75(32 - 9 - 16) = 43.65 \text{ kip ft} \\ M_{\min} \text{ at } 2-2 = 1.2(-9 - 16) + 0.75(32 - 9 - 16) = -24.75 \text{ kip ft} \end{cases}$$

**Fig. E3.31e**

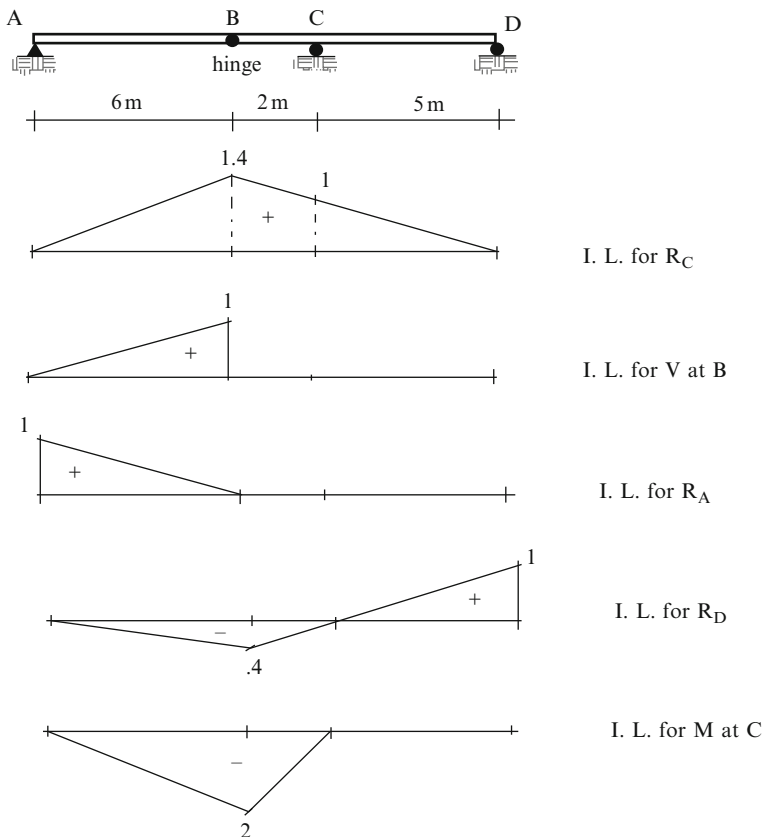
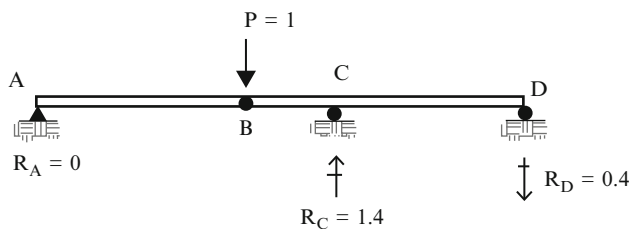
Example 3.32 Construction of influence lines

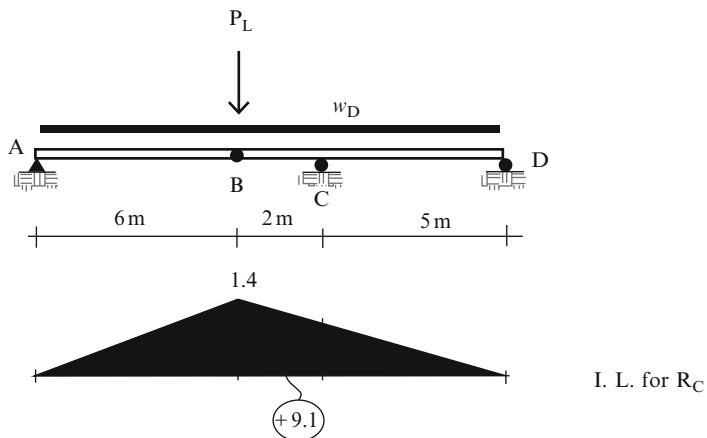
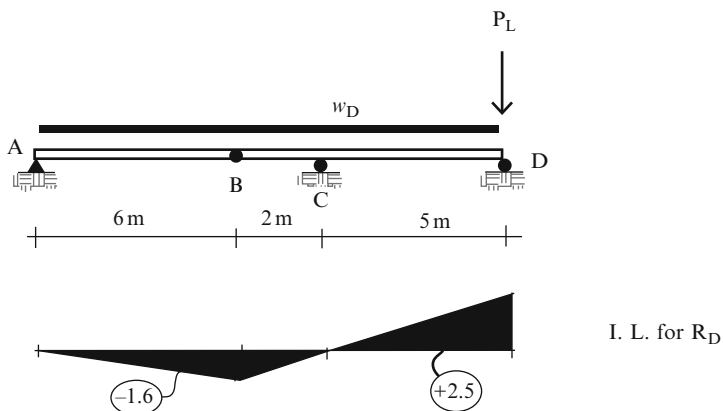
Given: The beam shown in Fig. E3.32a.

**Fig. E3.32a**

Determine: The influence lines for the vertical reactions at C, A, and D, the internal shear force at B, and the internal moment at C using Principle of Virtual Work. Suppose a concentrated live load of $P_L=50 \text{ kN}$ and uniformly distributed dead load of $w_D=12 \text{ kN/m}$ is placed on the beam. Determine the maximum value of the vertical reactions at D and C.

Solution: The calibrated vertical displacement patterns corresponding to the force quantities of interest are plotted in Fig. E3.32b. By definition, these scaled displacement patterns are the influence lines (Fig. E3.32c). The peak values are determined using Figs. E3.32d, e.

**Fig. E3.32b****Fig. E3.32c**

**Fig. E3.32d****Fig. E3.32e**

$$R_{C\max} = 12(9.1) + 50(1.4) = 179.2 \text{ kN}$$

$$R_{D\max} = (2.5 - 1.6)(12) + 50(1) = 60.8 \text{ kN}$$

Example 3.33 Cantilever construction-concentrated loading

Given: The three-span symmetrical scheme shown in Fig. E3.33a. There are two moment releases located symmetrically with respect to the centerline of the center span. This structure is statically determinate: Member cd functions as a simply supported member; segments bc and de act as cantilevers in providing support for member cd. The structural arrangement is called cantilever construction and is used for spanning distances which are too large for a single span or a combination of two spans.

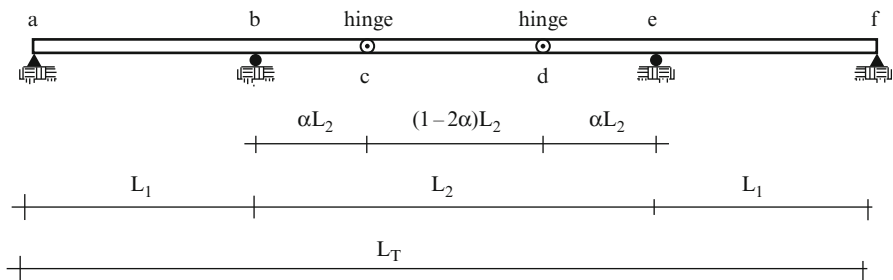


Fig. E3.33a

Determine: A method for selecting L_1 , given L_T , and the location of the moment releases.

Solution: The optimal geometric arrangement is determined by equating the maximum moments in the different spans. Given the total crossing length, L_T , one generates a conceptual design by selecting L_1 , and α which defines the location of the hinges. The remaining steps are straightforward. One applies the design loading, determines the maximum moments for each beam segment, and designs the corresponding cross-sections. The local topography may control where the interior supports may be located. We assume here that we are not constrained in choosing L_1 and describe below how one can utilize moment diagrams to arrive at an optimal choice for L_1 and α .

We consider the design load to be a single concentrated force that can act on any span. The approach that we follow is to move the load across the total span and generate a sequence of moment diagrams. This calculation provides information on the location of the load that generates the maximum moment for each span.

When the load is on ab, member ab functions as a simply supported beam, and we know from the previous example that the critical location is at mid-span. As the load moves from b to c, bc acts like a cantilever, and the critical location is point c. Lastly, applying the load at the midpoint of c, d produces the maximum moment for cd. Since the structure is symmetrical we need to move the load over only one-half the span. Moment diagrams for these cases are shown in Figs. E3.33b–d.

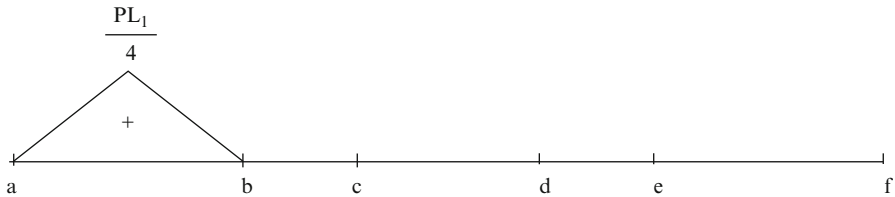
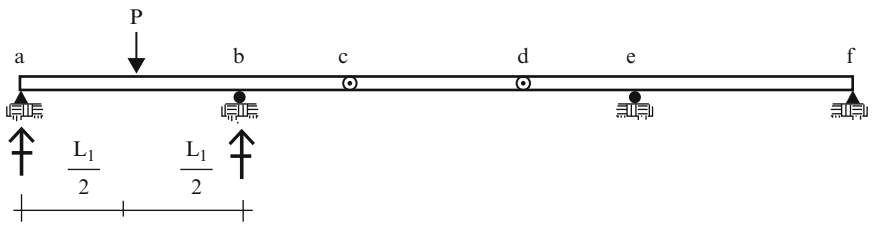


Fig. E3.33b Moment diagram—load on member AB

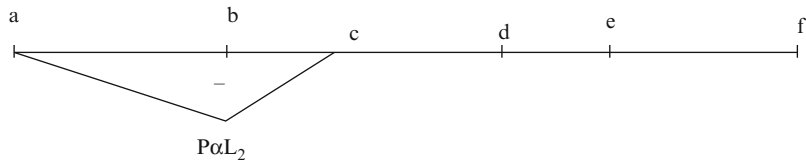
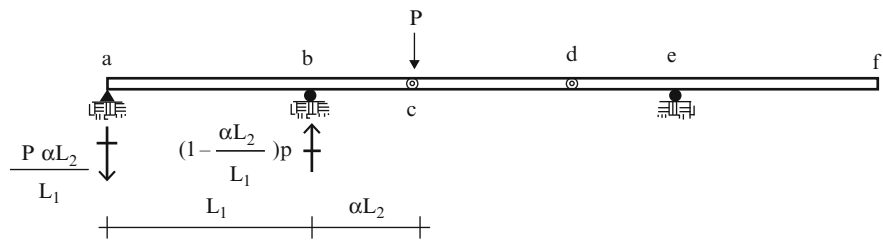


Fig. E3.33c Moment diagram—load on member BC

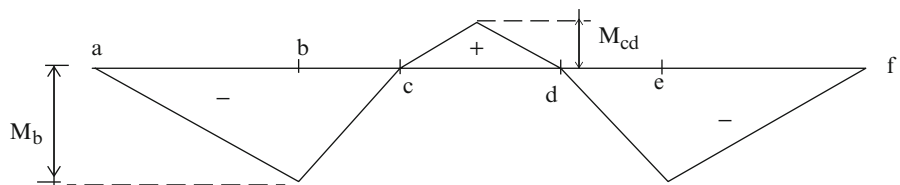
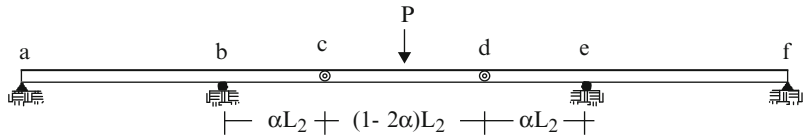


Fig. E3.33d Moment diagram—load on member CD

Based on these analyses, the design moments for the individual spans are

$$M|_{ab} = \frac{PL_1}{4} \quad M|_{fe} = M|_{ab}$$

$$M|_{bc} = P\alpha L_2 \quad M|_{ed} = M|_{bc}$$

$$M|_{cd} = \frac{PL_2(1-2\alpha)}{4}$$

$$M_b = \frac{P}{2}\alpha L_2 \quad M_e = M_b$$

From a constructability perspective, a constant cross-section throughout the total span is desirable. This goal is achieved by equating the design moments and leads to values for L_1 and α . Starting with $M|_{bc}=M|_{cd}$, one obtains

$$\begin{aligned} P\alpha L_2 &= \frac{PL_2(1-2\alpha)}{4} \\ \Downarrow \\ \alpha &= \frac{(1-2\alpha)}{4} \\ \Downarrow \\ \alpha &= \frac{1}{6} \end{aligned}$$

Next we equate $M|_{ab}$ and $M|_{bc}$, resulting in

$$\begin{aligned} \frac{PL_1}{4} &= P\alpha L_2 \\ \Downarrow \\ L_1 &= \frac{2}{3}L_2 \end{aligned}$$

The “optimal” center span is

$$2L_1 + L_2 = L_T$$

$$\Downarrow$$

$$L_2 = \frac{3}{7}L_T = 0.429L_T$$

If the interior supports can be located such that these span lengths can be realized, the design is *optimal for this particular design loading*. We want to emphasize here that analysis is useful for gaining insight about behavior, which provides the basis for rational design. One could have solved this problem by iterating through various geometries, i.e., assuming values for α and L_1 , but the strategy described above is a better structural engineering approach.

Example 3.34 Cantilever construction—uniform design loading

Given: The three-span symmetrical structure shown in Fig. E3.34a.

Determine: The optimal values of L_1 and α corresponding to a uniform live loading w .

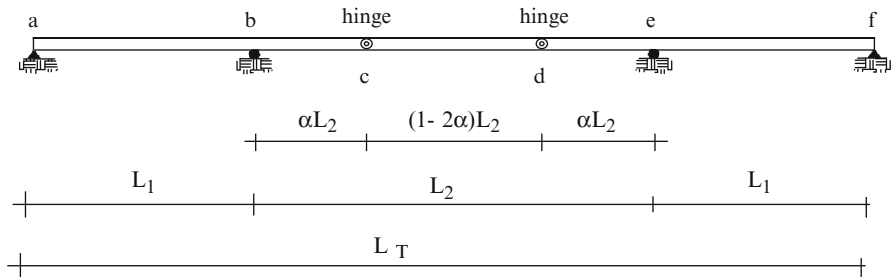


Fig. E3.34a

Solution: Using the results of the previous example, first, we establish the influence lines for the moment at mid-span of ab (M_{1-1}), at point b (M_b), and at mid-span of member cd (M_{2-2}). They are plotted below (Figs. E3.34b–e).

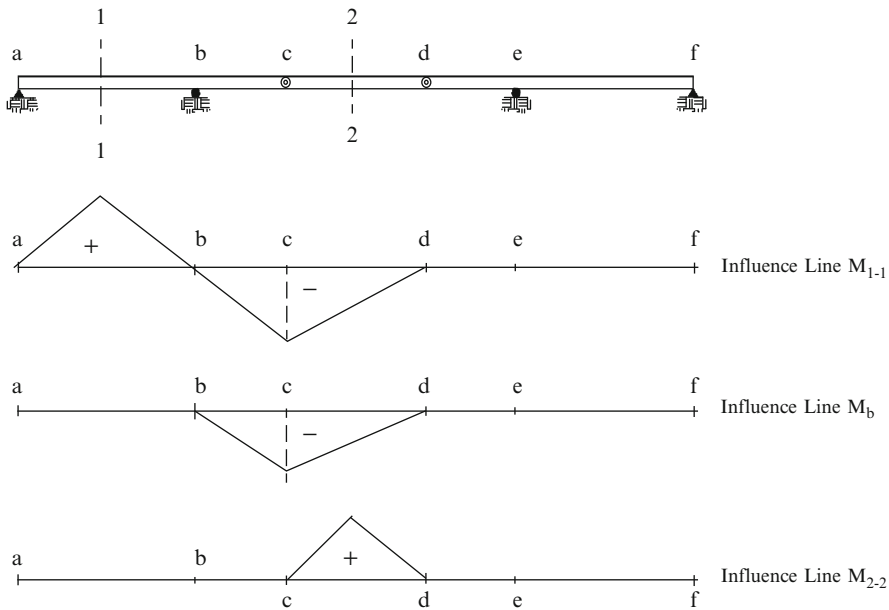


Fig. E3.34b Influence lines

We suppose that the uniformly distributed loading can be applied on an arbitrary segment of a span. We start with the side span, ab. Based on the influence line, we load span ab.

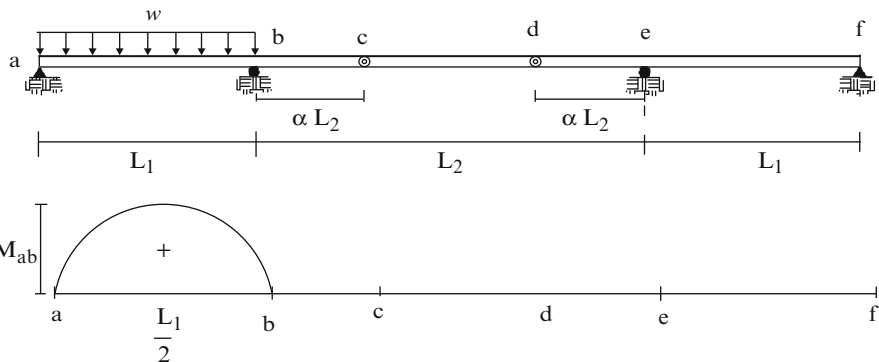


Fig. E3.34c Moment diagram

Next, we load the center span. Loading the segment bcd produces the maximum values for M_b and M_{cd} . The third option is to load the center span.

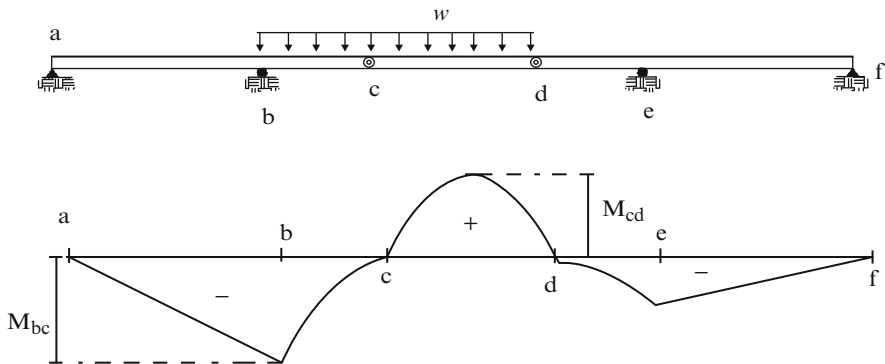


Fig. E3.34d Moment diagram

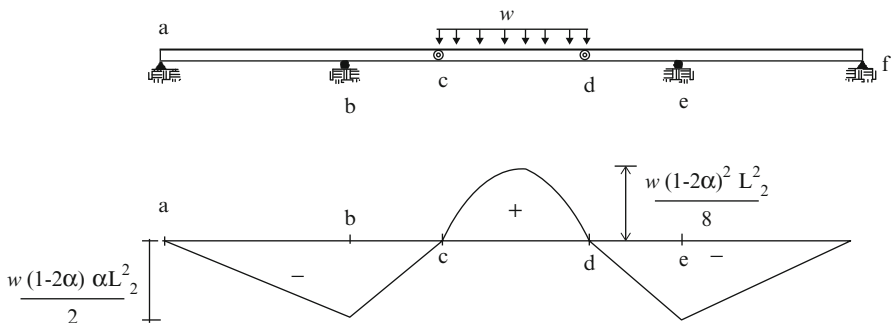


Fig. E3.34e Moment diagram

The peak values for these loading schemes are

$$M_{ab} = \frac{wL_1^2}{8}$$

$$M_{cd} = \frac{wL_2^2}{8} [1 - 2\alpha]^2$$

$$M_{bc} = \frac{wL_2^2}{2} [\alpha^2 + \alpha(1 - 2\alpha)]$$

The remaining steps are the same as for the previous example. We want to use a constant cross-section for the total span and therefore equate the design moments. This step results in values for α and L_1 .

Setting $M_{bc}=M_{cd}$ results in

$$\begin{aligned} \frac{1}{8}[1 - 2\alpha]^2 &= [\alpha^2 + \alpha(1 - 2\alpha)] \\ 8\alpha^2 - 8\alpha + 1 &= 0 \\ \Downarrow \\ \alpha &= \frac{1}{2} \left[1 - \frac{\sqrt{2}}{2} \right] = 0.147 \end{aligned}$$

Setting $M_{ab}=M_{cd}$ leads to

$$\begin{aligned} \frac{wL_1^2}{8} &= \frac{wL_2^2}{8} [1 - 2\alpha]^2 = \frac{wL_2^2}{8} \left[\frac{\sqrt{2}}{2} \right]^2 \\ \therefore L_1 &= \frac{\sqrt{2}}{2} L_2 = 0.707L_2 \end{aligned}$$

Lastly, L_2 is related to the total span by

$$\begin{aligned} 2L_1 + L_2 &= L_T \\ \Downarrow \\ (1 + \sqrt{2})L_2 &= L_T \\ \Downarrow \\ L_2 &= 0.414L_T \end{aligned}$$

These results are close to the values based on using a single concentrated load.

Examples 3.33 and 3.34 illustrate an extremely important feature of statically determinate structures. The reactions and internal forces produced by a specific loading depend only on the *geometry* of the structure. They are independent of the properties of the components that comprise the structure. This fact allows one to obtain a more favorable internal force distribution by adjusting the geometry as we did here.

These examples also illustrate the use of cantilever construction combined with internal moment releases. In Part II of the text, we rework those problems using beams which are continuous over all three spans, i.e., we remove the moment releases. The resulting structures are statically indeterminate.

3.10.3 Force Envelopes

3.10.3.1 A Single Concentrated Force

Figure 3.62 defines the bending moment distribution for a single concentrated load. We note that M_{\max} is a quadratic function of x . One can plot M_{\max} vs. x and determine the location of the maximum value of M_{\max} .

Alternatively, one can apply the following analytical approach. Differentiating $M_{x_{\max}}$ with respect to x and setting the result equal to zero leads to the desired value of x .

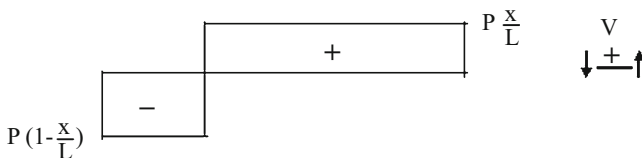
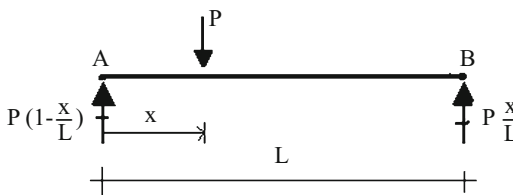
$$\frac{\partial}{\partial x}(M_{\max}) = 0$$

↓

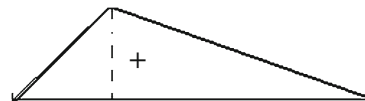
$$P\left(1 - \frac{2x}{L}\right) = 0$$

↓

$$x = \frac{L}{2}$$

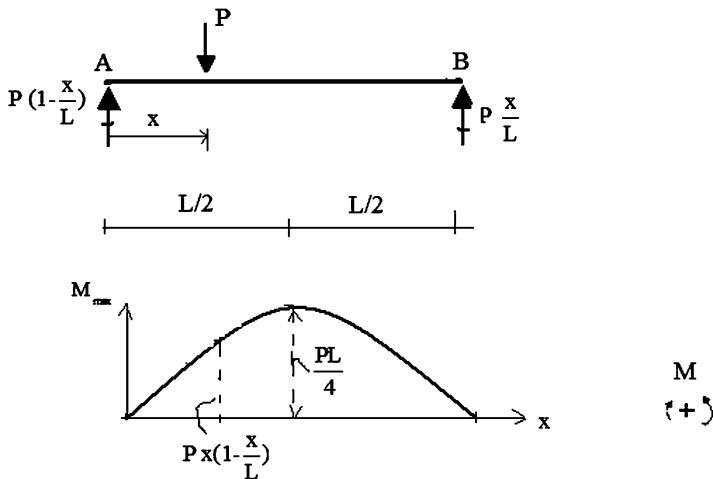
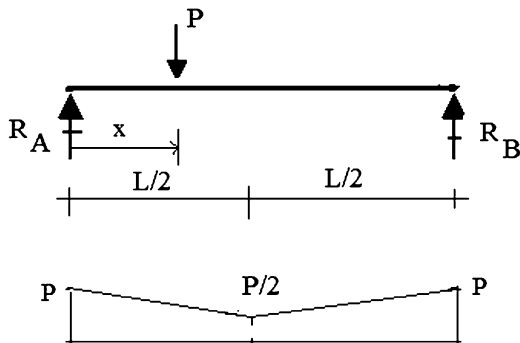


$$M_{\max} = P x \left(1 - \frac{x}{L}\right)$$



$$M = \frac{1}{2} +$$

Fig. 3.62 Reactions, shear and bending moment diagrams for concentrated load at x

**Fig. 3.63** Moment envelope for a single concentrated load P **Fig. 3.64** Shear envelope for a single concentrated load P

According to the above equation, the absolute maximum value of bending moment occurs when the force is applied at mid-span.

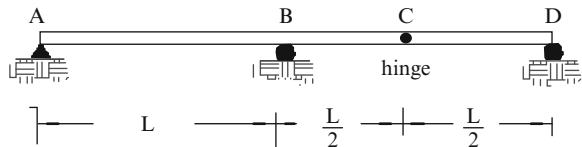
$$M_{\max}|_{\max} = \frac{PL}{4}$$

Figure 3.63 shows the moment envelope for the case where there is only a single concentrated force.

We note from Fig. 3.62 that the absolute maximum shear force is equal to the applied force, P , and either V_A or V_B controls depending on the location of the load with respect to mid-span. Figure 3.64 shows the shear envelope for the case where there is only a single concentrated force.

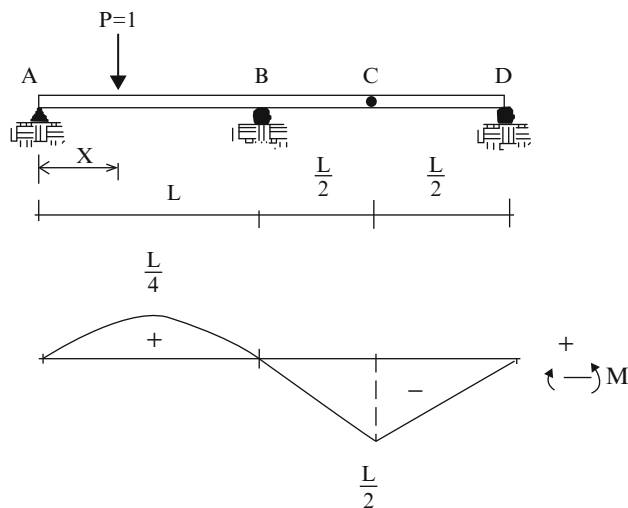
Example 3.35 Construction of moment envelope

Given: The two-span beam shown in Fig. E3.35a. There is a hinge (moment release) at the midpoint of the second span.

Fig. E3.35a

Determine: The moment envelope corresponding to a single concentrated load moving across the span.

Solution: The analytical information that is related to the bending moment distributions generated in Example 3.28 is utilized to construct the moment envelope shown in Fig. E3.35b. One can also use the computer to generate these results.

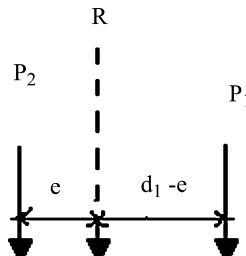
**Fig. E3.35b** Moment envelope for a concentrated unit load

The moment envelope is useful for identifying the position of the load that controls the design. For this example, we see that the load applied at the midpoint of span AB produces the largest positive moment and the load applied at C produces the largest negative moment.

3.10.3.2 Multiple Concentrated Loads

We consider next the case where there are two concentrated forces. This loading can simulate the load corresponding to a two axle vehicle. The notation is defined in Fig. 3.65.

The resultant force $R = P_1 + P_2$ is located e units from the line of action of P_2 .



where

$$e = \frac{P_1}{P_1 + P_2} d_1$$

The moment diagram for a set of concentrated forces is piecewise linear with peak values at the points of application of the forces. Figure 3.66 shows the result for this loading case. Analytical expressions for the reactions and the moments at points ① and ② are

$$\begin{aligned} R_A &= (P_1 + P_2) \frac{1}{L} (L - x) - P_1 \frac{d_1}{L} \\ R_B &= (P_1 + P_2) \frac{x}{L} + P_1 \frac{d_1}{L} \\ M_1 &= (P_1 + P_2) \frac{x}{L} (L - x - d_1) + P_1 \frac{d_1}{L} (L - x - d_1) \\ M_2 &= (P_1 + P_2) \frac{x}{L} (L - x) - P_1 \frac{d_1}{L} x \end{aligned} \quad (3.64)$$

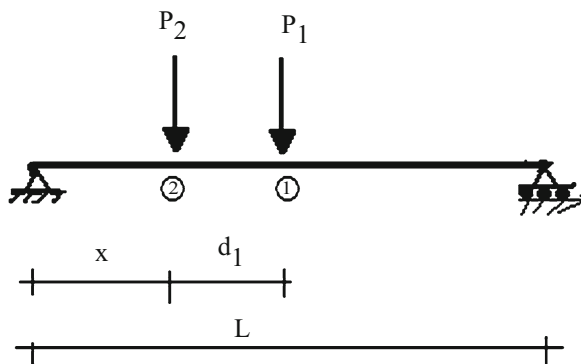


Fig. 3.65 Two concentrated forces

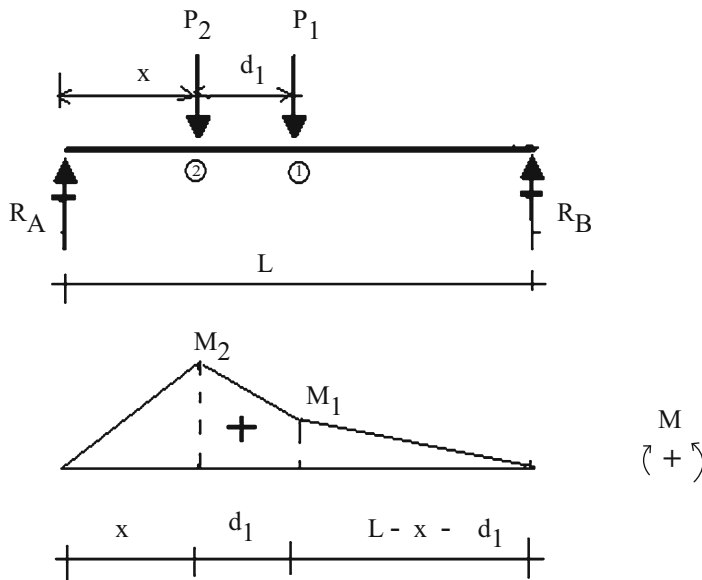


Fig. 3.66 Moment diagram—arbitrary position of loading

These moments are quadratic functions of x . One can compute M_1 and M_2 for a range of x values and determine the values of x corresponding to the peak values. Alternatively, one can determine the value of x corresponding to a maximum value of a particular moment by differentiating the corresponding moment expression with respect to x and setting the result equal to zero.

Maximum value of M_2

$$\begin{aligned} \frac{\partial M_2}{\partial x} &= 0 \\ (P_1 + P_2)\left(1 - 2\frac{x}{L}\right) - P_1\frac{d_1}{L} &= 0 \quad (3.65) \\ x|_{M_2 \text{ max}} &= \frac{L}{2} - \frac{d_1}{2} \left(\frac{P_1}{P_1 + P_2}\right) = \frac{L}{2} - \frac{e}{2} \end{aligned}$$

Maximum value of M_1

$$\begin{aligned} \frac{\partial M_1}{\partial x} &= 0 \\ (P_1 + P_2)(L - 2x - d_1) - P_1d_1 &= 0 \\ x|_{M_1 \text{ max}} &= \frac{L}{2} - \frac{d_1}{2} - \frac{e}{2} \quad (3.66) \end{aligned}$$

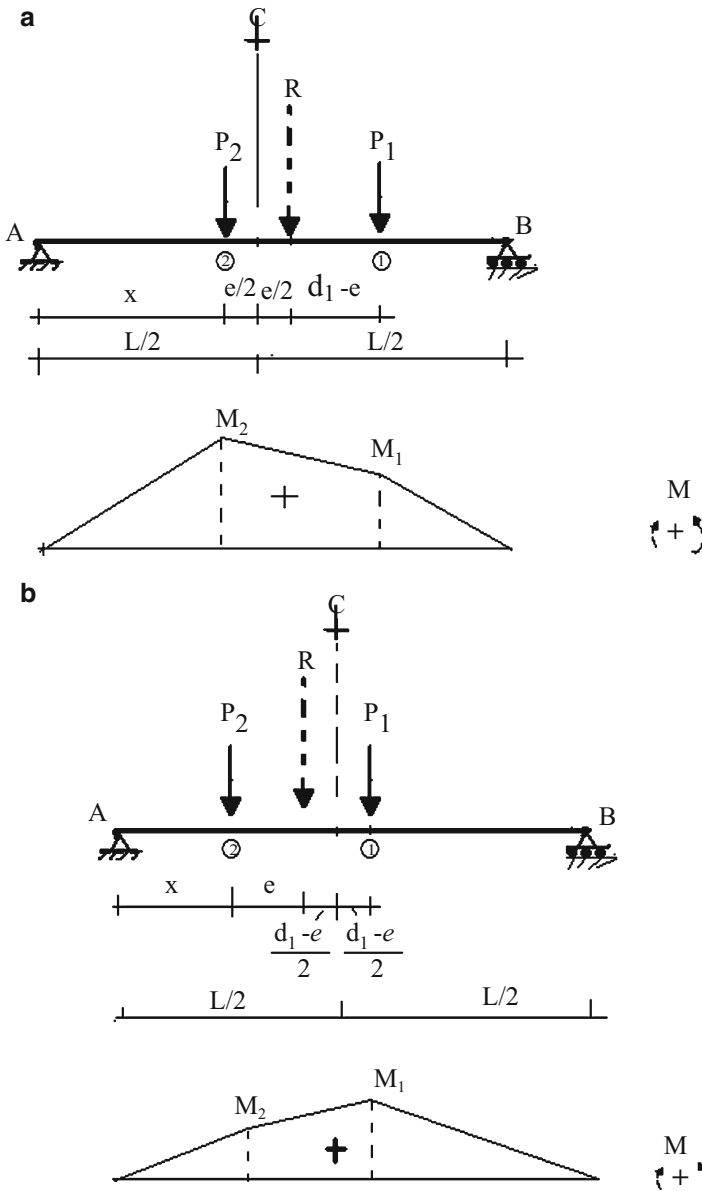


Fig. 3.67 Critical location of loading for maximum bending moments. (a) $x|_{M_{2 \max}}$. (b) $x|_{M_{1 \max}}$

We can interpret the critical location for the maximum value of M_2 from the sketch shown in Fig. 3.67a. The force P_2 is located $e/2$ units to the left of mid-span and the line of action of the resultant is $e/2$ units to the right of mid-span. A similar result applies for M_1 . P_1 is positioned such that P_1 and R are equidistant from mid-span as shown in Fig. 3.67b.

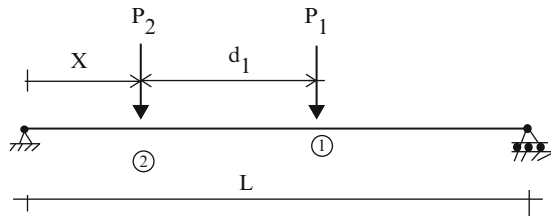
The absolute maximum live load moment is found by evaluating M_1 and M_2 using the corresponding values of $x|_{M_{1\max}}$ and $x|_{M_{2\max}}$. In most cases, the absolute maximum moment occurs at the point of application of the *largest force* positioned according to (3.66) and (3.67).

Example 3.36 Illustration of Computation of Maximum Moments for two-force loading

Given: The beam shown in Fig. E3.36a and the following data

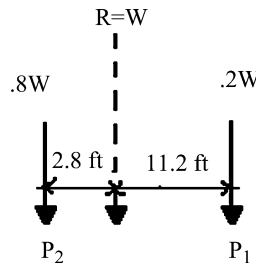
$$R = W \quad P_1 = 0.2W \quad P_2 = 0.8W \quad d_1 = 14 \text{ ft} \quad L = 40 \text{ ft}$$

Fig. E3.36a



Determine: The maximum possible moment in the beam as the two-force loading system moves across the span.

Solution: The resultant is located $e = \frac{0.2W}{W}(14) = 2.8 \text{ ft}$ from P_2 .



Using (3.65)

$$x|_{M_{2\max}} = \frac{L}{2} - \frac{e}{2} = 20 - 1.4 = 18.6 \text{ ft}$$

Using (3.64) and the above value for x , the reactions and bending moments are

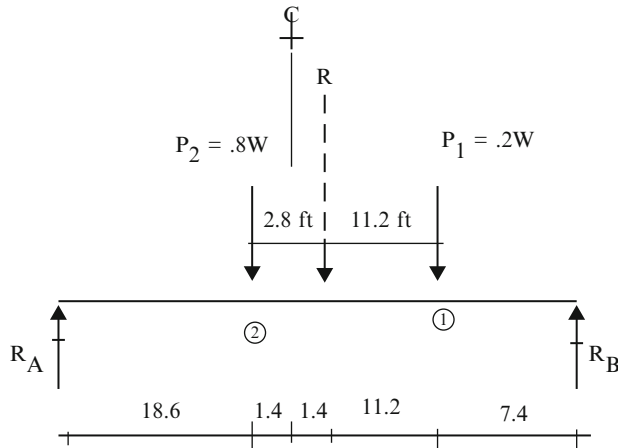
$$R_A = 0.465W$$

$$R_B = 0.535W$$

$$M_1 = 3.96W$$

$$M_2 = 8.69W$$

The critical loading position for M_2 is shown in Fig. E3.36b.

**Fig. E3.36b**

We compute \$M_1\$ in a similar way. The critical location is found using (3.66).

$$x|_{M_1\max} = \frac{L}{2} - \frac{d_1}{2} - \frac{e}{2} = 20 - 7 - 1.4 = 11.6 \text{ ft}$$

Next we apply (3.64).

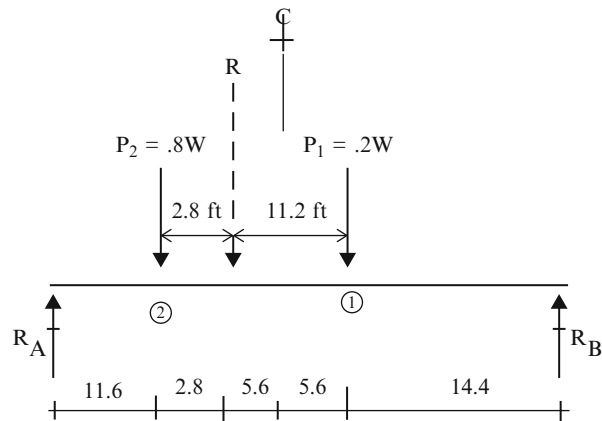
$$R_A = 0.64W$$

$$R_B = 0.36W$$

$$M_1 = 5.184W$$

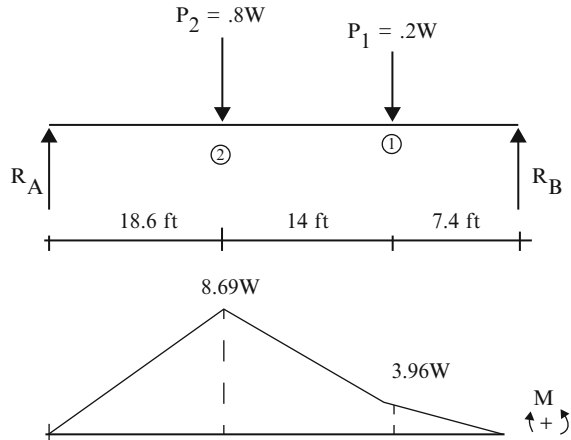
$$M_2 = 7.424W$$

The critical loading position for \$M_1\$ is shown in Fig. E3.36c.

**Fig. E3.36c**

It follows that the absolute maximum live load moment occurs when P_2 is positioned 18.6 ft from the left support. This point is close to mid-span (Fig. E3.36d).

Fig. E3.36d



The analysis for the case of three concentrated loads proceeds in a similar way. Figure 3.68 shows the notation used to define the loading and the location of the resultant force. The moment diagram is piecewise linear with peaks at the point of application of the concentrated loads.

We generate expressions for the bending moments at points 1, 2, and 3 for an arbitrary position of the loading defined by x and then determine the locations of maximum moment by differentiating these expressions. First, we locate the resultant force

$$R = P_1 + P_2 + P_3 \quad (3.67)$$

$$e = \frac{d_2 P_2 + (d_1 + d_2) P_1}{R}$$

The moments at locations 1, 2, and 3 are functions of x .

$$M_3 = \frac{R}{L} (L - x - e)x \quad (3.68)$$

$$M_2 = \frac{R}{L} (L - x - e)(x + d_2) - P_3 d_2$$

$$M_1 = \frac{R}{L} (L - x - d_2 - d_1)(x + e)$$

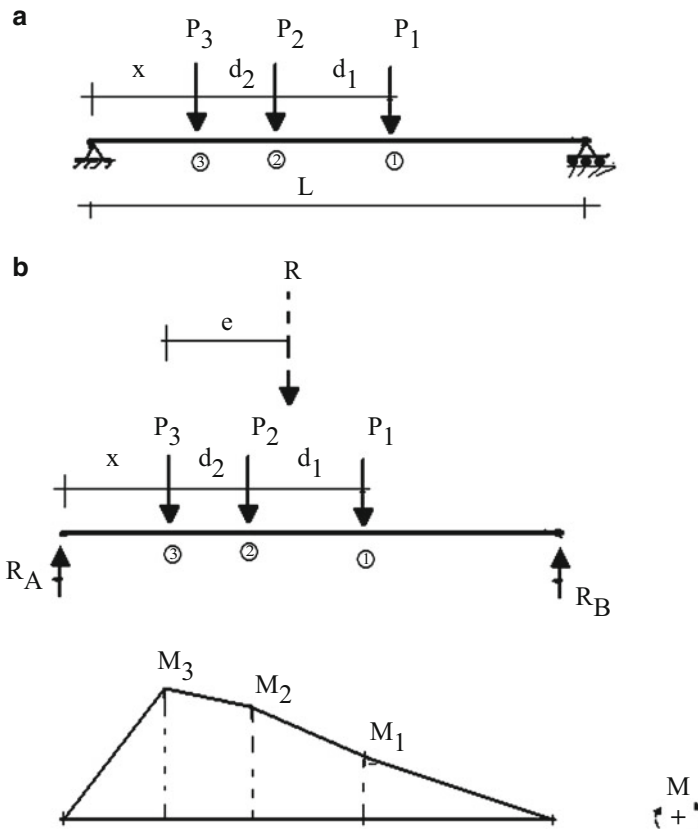


Fig. 3.68 Notation and moment diagram—three concentrated loads

Differentiating each expression with respect to x and equating the result to zero leads to the equations for the critical values of x that correspond to relative maximum values of the moments.

$$\begin{aligned}
 \text{For } M_3|_{\max} \quad & x = \frac{1}{2}(L - e) \\
 \text{For } M_2|_{\max} \quad & x = \frac{1}{2}(L - e - d_2) \\
 \text{For } M_1|_{\max} \quad & x = \frac{1}{2}(L - d_2 - d_1 - e)
 \end{aligned} \tag{3.69}$$

The positions of the loading corresponding to these three values of x are plotted in Fig. 3.69. Note that the results are similar to the two concentrated load case. We need to evaluate (3.68) for each value of x in order to establish the absolute maximum value of the bending moment.

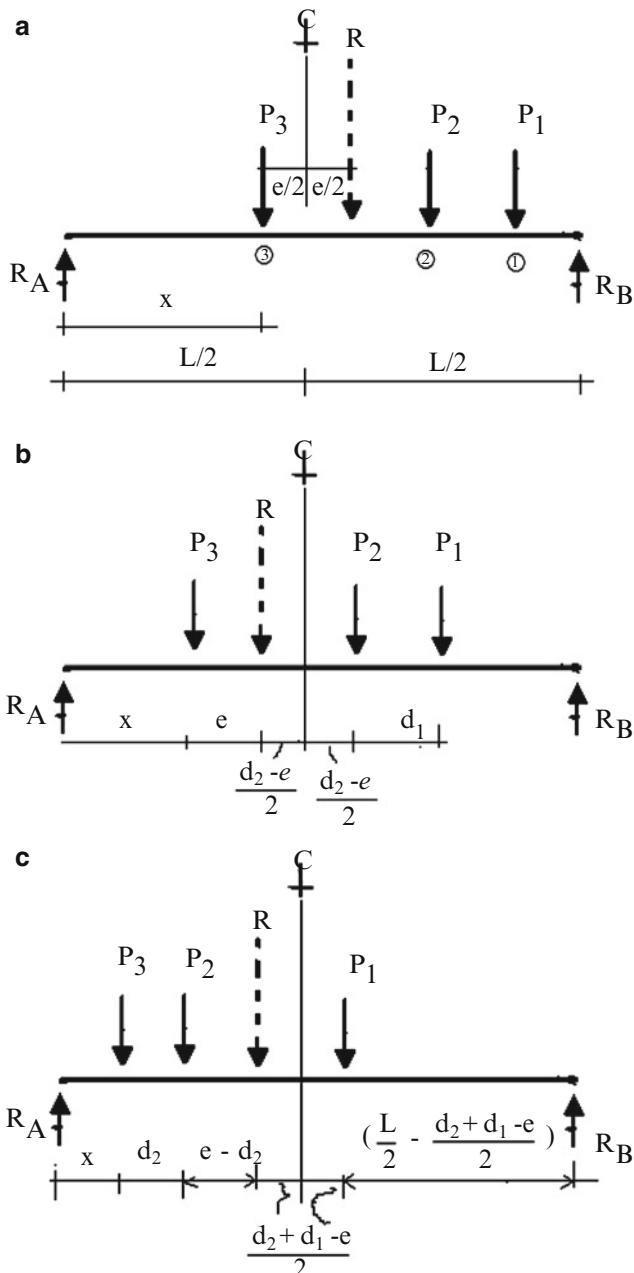
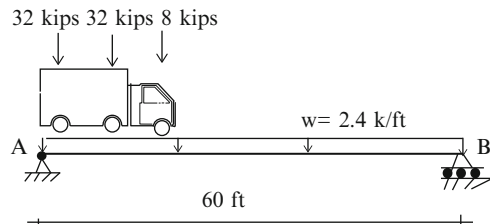


Fig. 3.69 Possible locations of loading for maximum moment

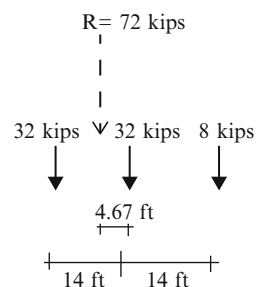
Example 3.37

Given: The beam shown in Fig. E3.37a.

Fig. E3.37a

Determine: The maximum possible moment in the beam caused by

- (1) A truck moving across the span (Fig. E3.37b).

Fig. E3.37b

- (2) A uniformly distributed dead load of $w = 2.4 \text{ kip/ft}$ in addition to the truck loading.

Solution:

Part (1): The critical truck loading position is defined by Fig. E3.37c. The corresponding bending moment diagram is plotted below; the maximum moment occurs 2.3 ft from the center of the span. $M_{\max} = 806.7 \text{ kip ft}$.

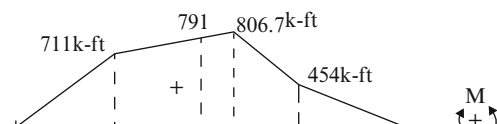
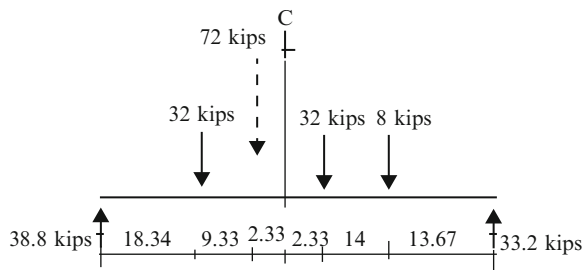
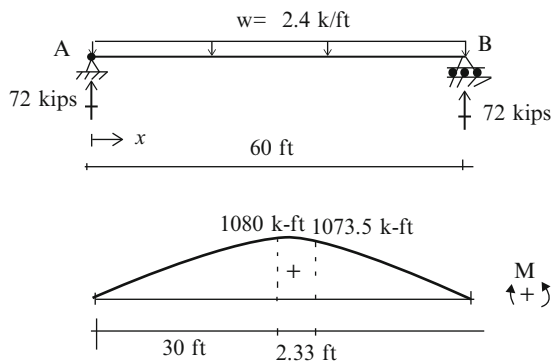


Fig. E3.37c Moment distribution for moving truck load

Part (2): The bending moment diagram for uniform loading is parabolic, with a maximum value at mid-span.

Fig. E3.37d Moment distribution for dead load



$$M_{\text{dead}}(x) = 72x - 1.2x^2 \quad 0 \leq x \leq 60$$

We estimate the peak moment due to the combined loading by adding corresponding moment values from Figs. E3.37c, d.

$$\left. \begin{aligned} M_{\text{combined}} &= (M_{\text{dead}} + M_{\text{truck}})_{\text{at } x=32.33 \text{ ft}} = 1,073.5 + 806.7 \approx 1880 \text{ kip ft} \\ M_{\text{combined}} &= (M_{\text{dead}} + M_{\text{truck}})_{\text{at } x=30 \text{ ft}} = 1,080 + 791 \approx 1,871 \text{ kip ft} \end{aligned} \right\} M_{\text{max}} = 1,880 \text{ kip ft}$$

When there are multiple loadings, it is more convenient to generate discrete moment envelope using a computer-based analysis system. The discrete moment envelope for the combined (dead + truck) loading is plotted below (Fig. E3.37e). Scanning the envelope shows that the maximum moment occurs at $x = 30.9$ ft and $M_{\text{max}} = 1,882.6$ kip ft. This result shows that it was reasonable to superimpose the moment diagrams in this example.

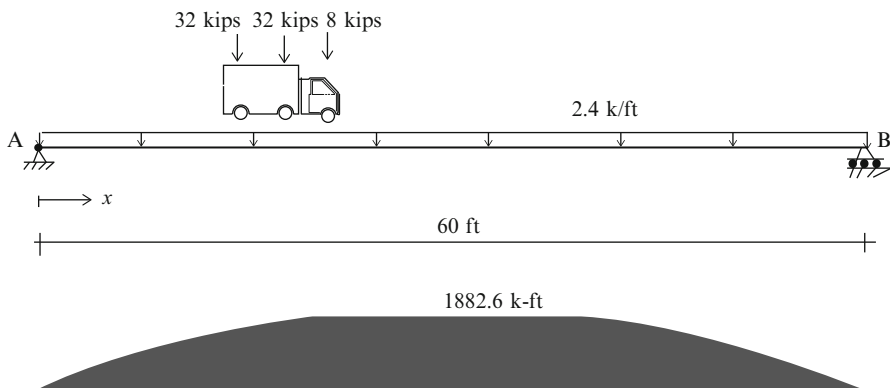


Fig. E3.37e Discrete moment envelope for the combined (dead + truck) loading

3.11 Summary

3.11.1 Objectives of the Chapter

- To develop analytical and computational methods for quantifying the behavior of beams subjected to transverse loading. Of particular interest are the reactions, the internal forces (shear, bending, and twisting moments), and the displacements.
- To introduce the concepts of influence lines and force envelopes which are needed to establish design values for beam cross-sections.

3.11.2 Key Facts and Concepts

- A stable statically determinate beam requires three nonconcurrent displacement restraints. There are three reaction forces which are determined using the static equilibrium equations.
- External loads are resisted by internal forces acting on a cross-section. For planar loading, these quantities consist of an axial force, F , a transverse shear force, V , and a bending moment, M . One can establish the magnitude of these variables using the static equilibrium equations. Alternatively, one can start with the following differential equilibrium equations,

$$\frac{dV}{dx} = w$$

$$\frac{dM}{dx} = -V$$

Integrating between points 1 and 2 leads to

$$V_2 - V_1 = \int_{x_1}^{x_2} w \, dx$$

$$M_2 - M_1 = - \int_{x_1}^{x_2} V \, dx$$

The first equation states that the difference in shear is equal to the area under the loading diagram. The second equation states that the change in moment is equal to the area under the shear diagram.

- Planar bending results in a transverse displacement, $v(x)$. When the beam is slender, these variables are related by

$$\frac{d^2v}{dx^2} = \frac{M}{EI}$$

where I is the second moment of area for the section. Given $M(x)$, one determines $v(x)$ by integrating this expression and noting the two boundary conditions on v .

- The transverse displacement at a particular point can also be determined using the Principle of Virtual Forces specialized for planar bending of slender beams.

$$d \delta P = \int_x \frac{M}{EI} \delta M v(x) dx$$

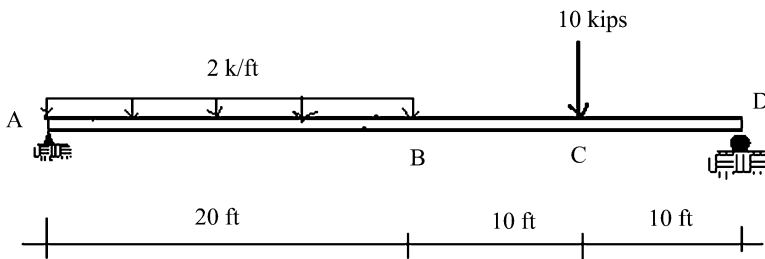
Here, d is the desired displacement, δP is a virtual force in the direction of d , and δM is the virtual moment corresponding to δP . One usually employs numerical integration when the integral is complex.

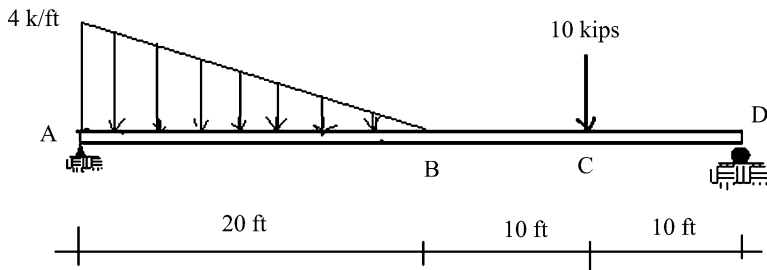
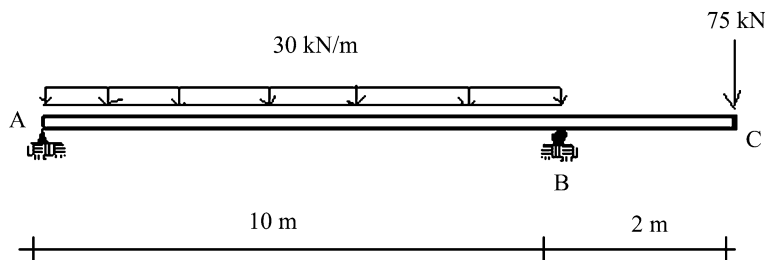
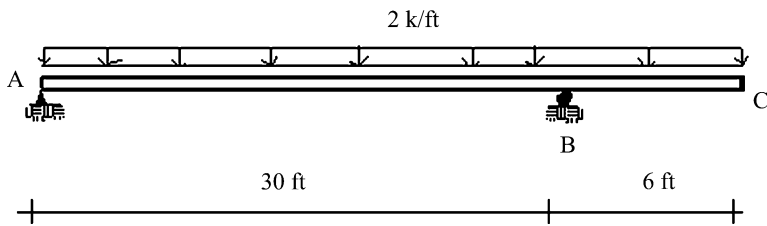
- An influence line is a plot of the magnitude of a particular internal force quantity; say the bending moment at a specific location vs. the position of a unit concentrated load as it moves across the span. It is useful for establishing the peak magnitude of the force quantity at that location.
- A force envelope is a plot of the maximum value of a force quantity, say the bending moment along the span vs. position of the load. It is used when the cross-section is taken as constant along the span and the absolute maximum value is required for design.

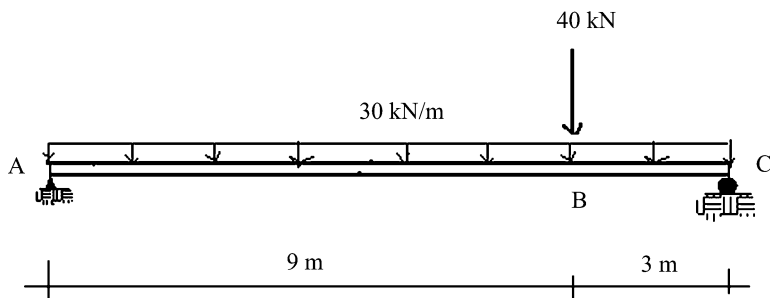
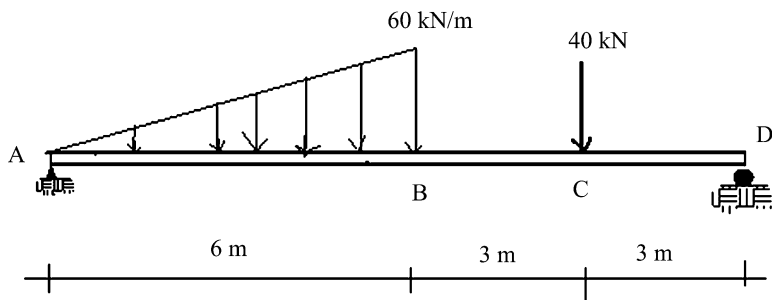
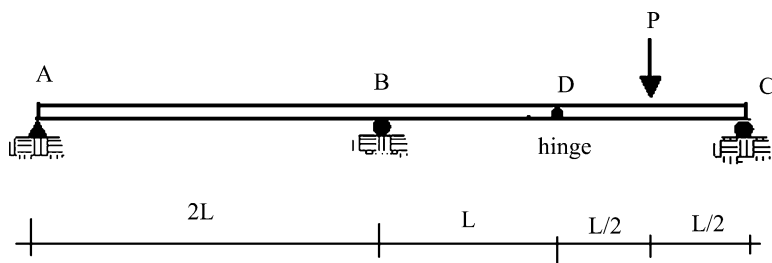
3.12 Problems

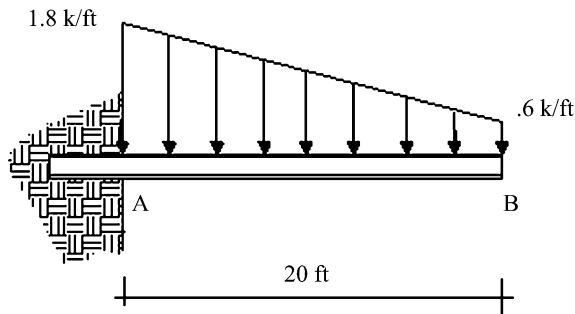
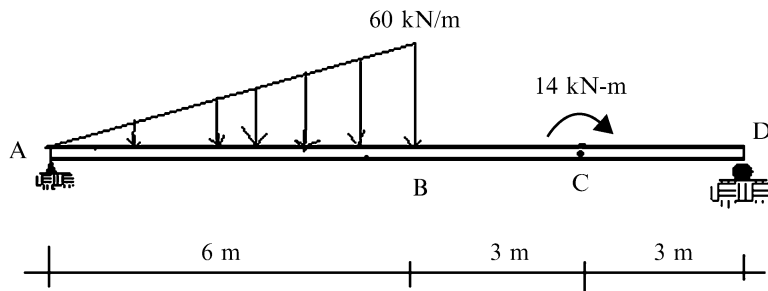
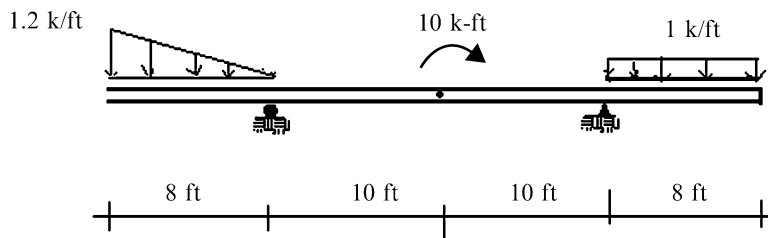
For the beams defined in Problems 3.1–3.22, compute the reactions and draw the shear and moment diagrams.

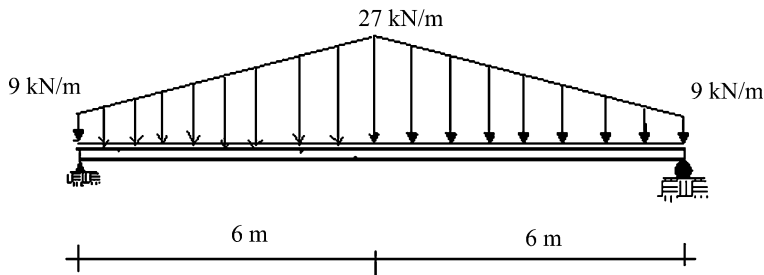
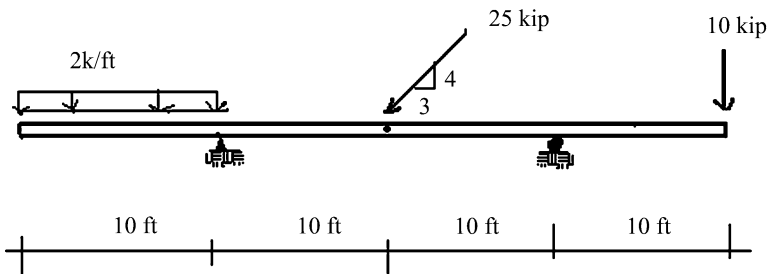
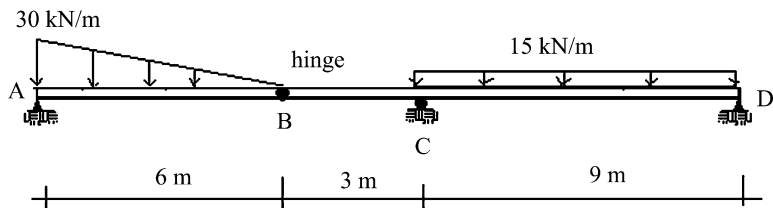
Problem 3.1

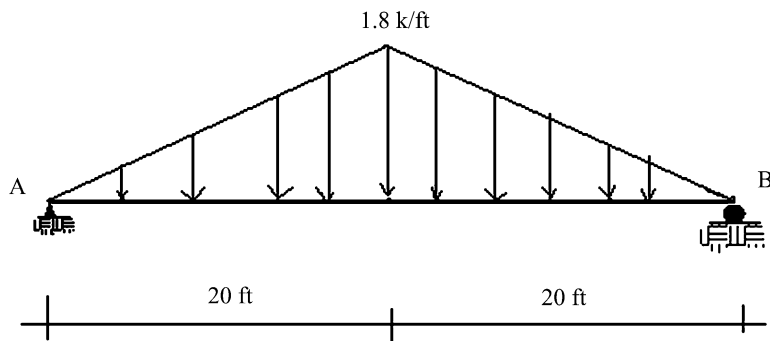
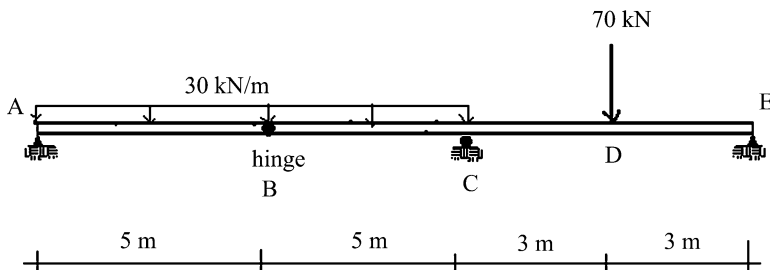
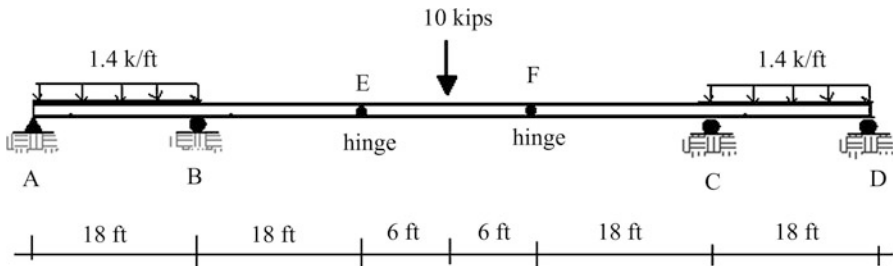


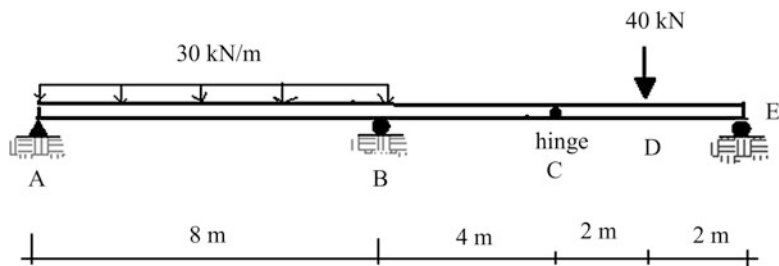
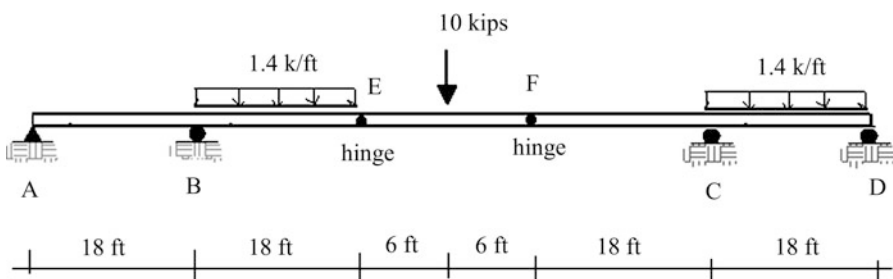
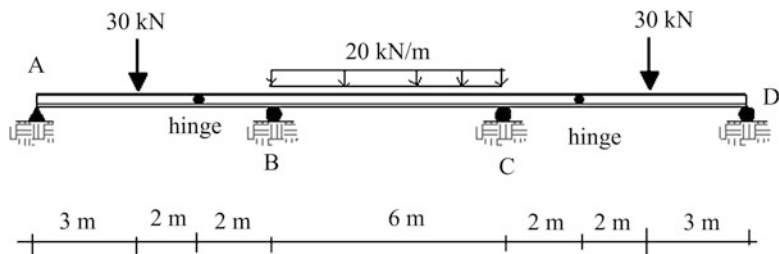
Problem 3.2**Problem 3.3****Problem 3.4**

Problem 3.5**Problem 3.6****Problem 3.7**

Problem 3.8**Problem 3.9****Problem 3.10**

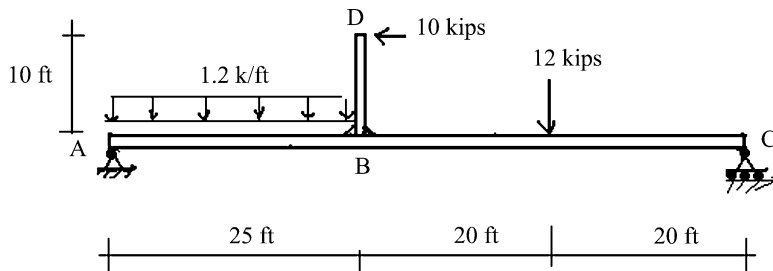
Problem 3.11**Problem 3.12****Problem 3.13**

Problem 3.14**Problem 3.15****Problem 3.16**

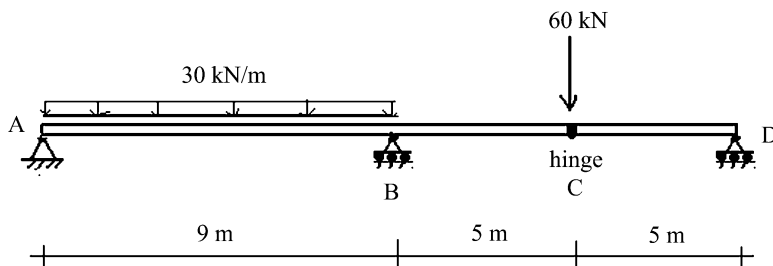
Problem 3.17**Problem 3.18****Problem 3.19**

Problem 3.20

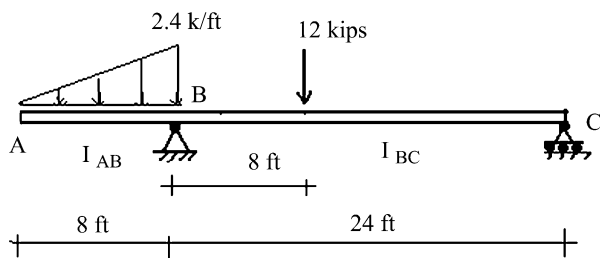
Member BD is rigidly attached to the beam at B.

**Problem 3.21**

Determine the maximum bending moment. Take EI is constant.

**Problem 3.22**

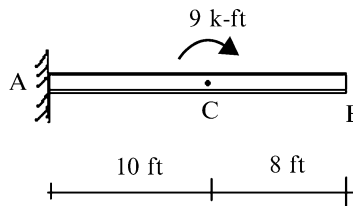
Determine the maximum bending moment. Does the bending moment distribution depend on either E or I ? Justify your response.



For the beams defined in Problems 3.23–3.27, use the conjugate beam method to determine the vertical deflection and rotation measures indicated. Take EI is constant.

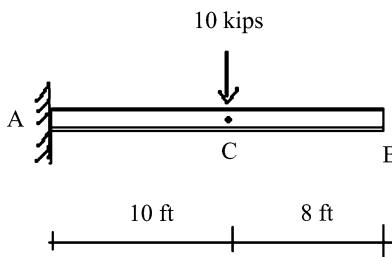
Problem 3.23

$$\theta_B, v_B \quad I = 200 \text{ in}^4, E = 29,000 \text{ kip/in}^2$$



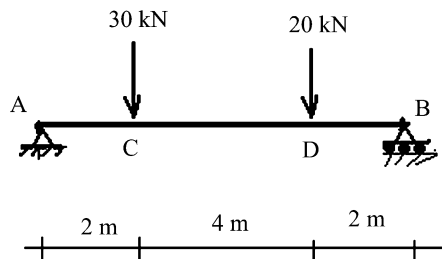
Problem 3.24

$$\theta_B, v_B \quad I = 200 \text{ in}^4, E = 29,000 \text{ ksi}$$

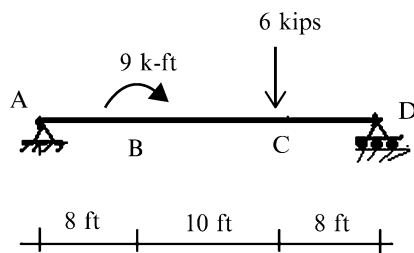


Problem 3.25

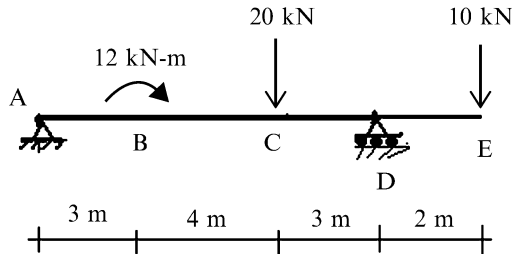
$$\theta_A, v_C \quad I = 80(10^6) \text{ mm}^4, E = 200 \text{ GPa}$$

**Problem 3.26**

$$\theta_D, v_C \quad I = 200 \text{ in}^4, E = 29,000 \text{ ksi}$$

**Problem 3.27**

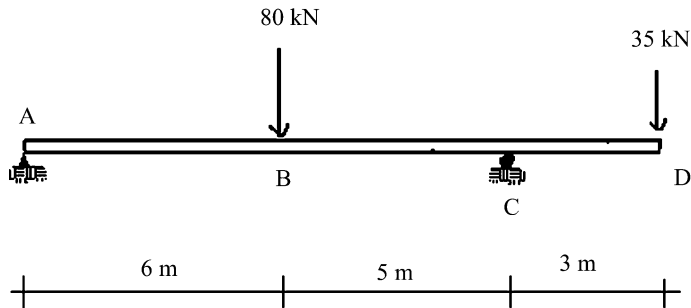
$$\theta_D, v_C \quad I = 80(10^6) \text{ mm}^4, E = 200 \text{ GPa}$$



For the beams defined in Problems 3.28–3.35, use the virtual force method to determine the vertical deflection and rotation measures indicated.

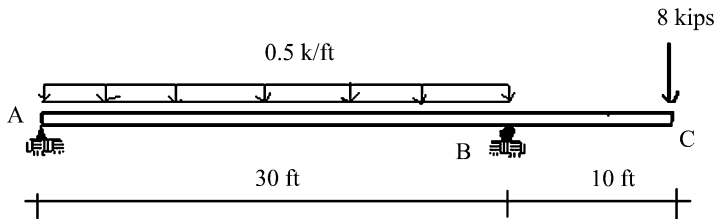
Problem 3.28

$$\theta_B, v_D \quad I = 120(10^6) \text{ mm}^4, E = 200 \text{ GPa}$$



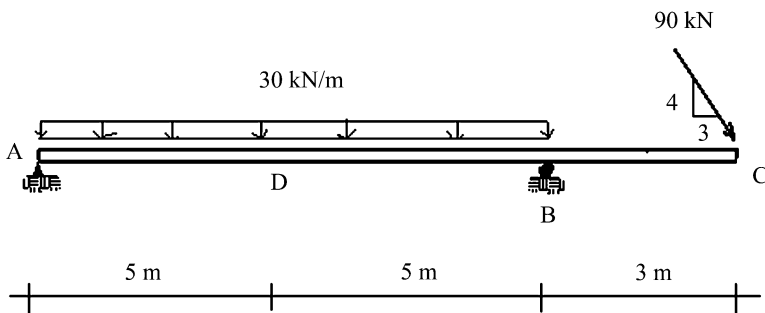
Problem 3.29

$$\theta_A, v_C \quad I = 300 \text{ in}^4, E = 29,000 \text{ ksi}$$

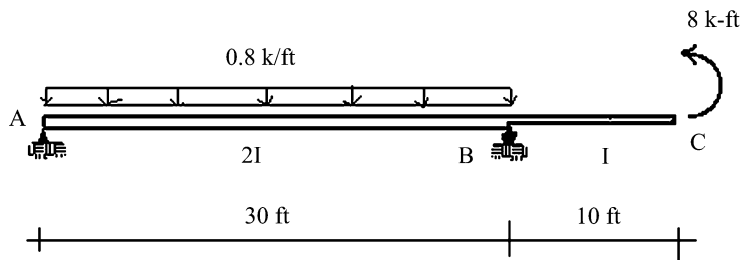


Problem 3.30

$$\theta_C, v_D \quad I = 120(10^6) \text{ mm}^4, E = 200 \text{ GPa}$$

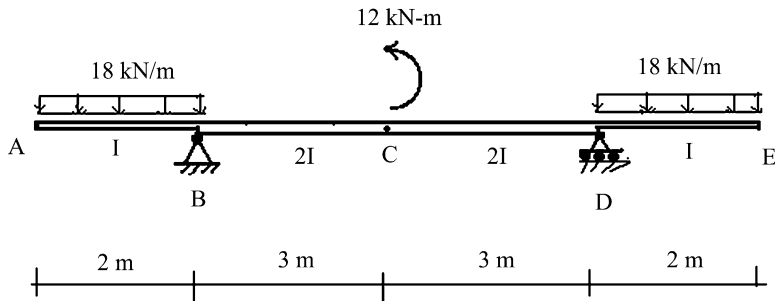
**Problem 3.31**

$$\theta_C, v_C \quad I = 200 \text{ in}^4, E = 29,000 \text{ ksi}$$

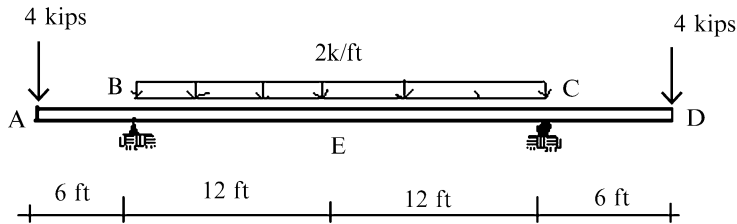


Problem 3.32

$$\theta_C, v_C I = 100(10^6) \text{ mm}^4, E = 200 \text{ GPa}$$

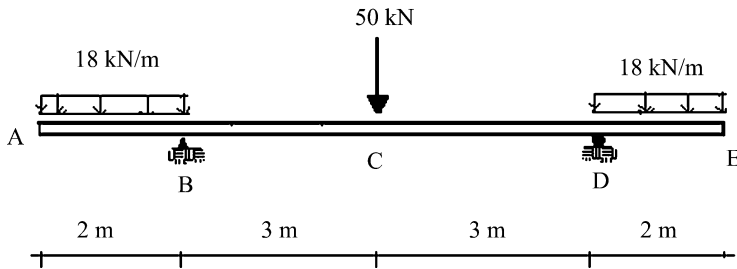
**Problem 3.33**

$$\theta_B, v_E I = 300 \text{ in}^4, E = 29,000 \text{ ksi}$$

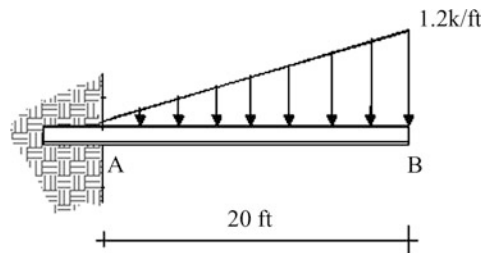


Problem 3.34

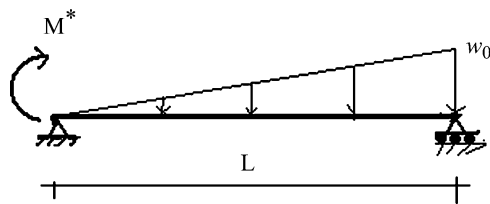
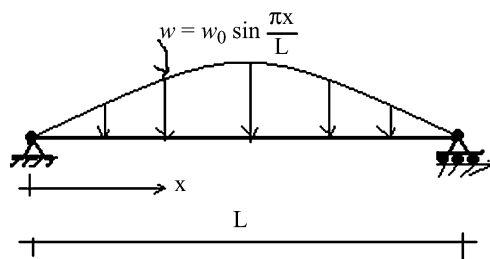
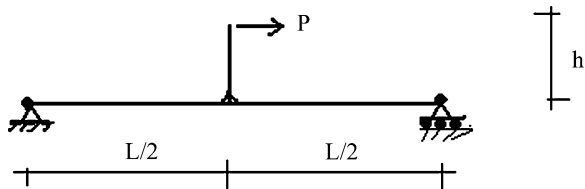
$$\theta_C, \theta_E, \text{ and } v_E \quad I = 160(10^6) \text{ mm}^4, E = 200 \text{ GPa}$$

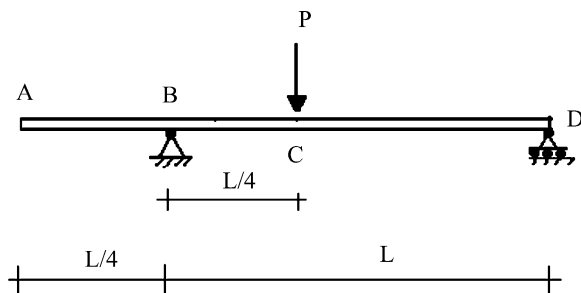
**Problem 3.35**

$$\theta_B, v_B \quad I = 120 \text{ in}^4, E = 29,000 \text{ ksi}$$

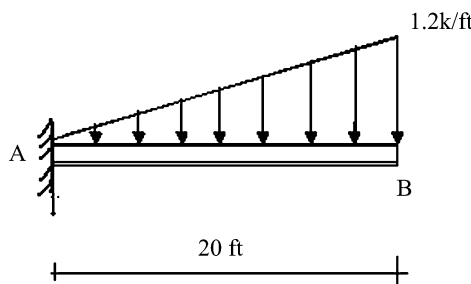


Determine the analytical solutions for the deflected shape for the beams defined in Problems 3.36–3.39. Assume EI is constant.

Problem 3.36**Problem 3.37****Problem 3.38**

Problem 3.39**Problem 3.40**

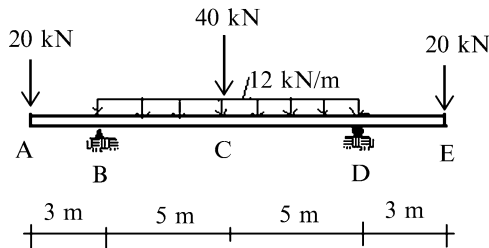
Determine the value of I required to limit the vertical deflection at B to $1/2$ in. $E = 29,000$ ksi.

**Problem 3.41**

- Solve Problem 3.39 using computer software. Consider different sets of values for EI . Show that the magnitude of the deflection varies as $1/EI$. Assume $P = 100$ kN, $L = 8$ m.
- Suppose the peak deflection is specified. How would you determine the appropriate value of I ?

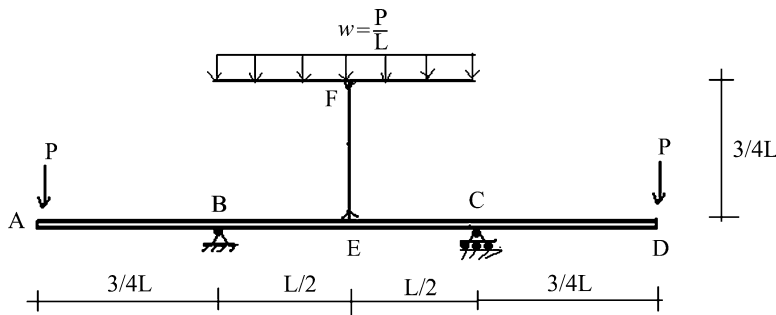
Problem 3.42

Utilize symmetry to sketch the deflected shape. EI is constant. Assume $E = 200$ GPa and $I = 160(10)^6 \text{ mm}^4$.



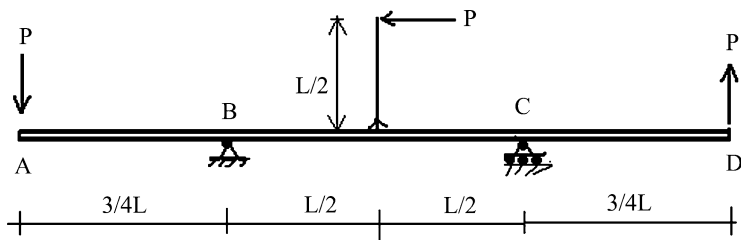
Problem 3.43

Determine the vertical deflection of point A. Sketch the deflected shape of the beam. EI is constant.



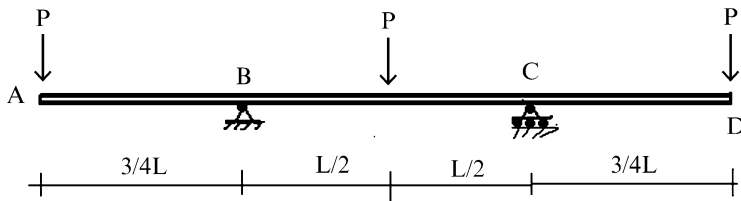
Problem 3.44

Determine the vertical deflection of point A. Sketch the deflected shape of the beam. EI is constant.

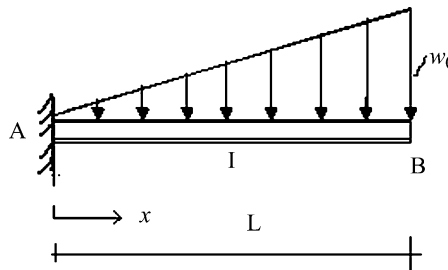


Problem 3.45

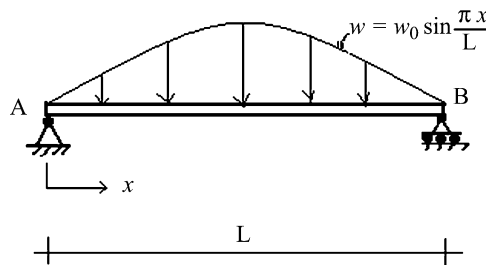
Determine the vertical deflection of point A. Sketch the deflected shape. EI is constant.

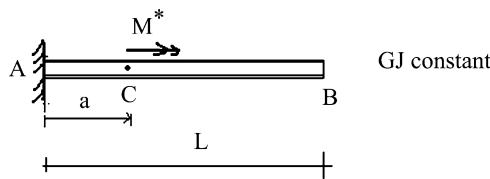
**Problem 3.46**

Consider the cantilever beam shown below. Determine the displacement at B due to the loading. Use the principle of Virtual Forces and evaluate the corresponding integral with the trapezoidal rule. Take $w_0=10 \text{ kip}/\text{ft}$, $L=20 \text{ ft}$, $I_0=1,000 \text{ in.}^4$, $E=29,000 \text{ ksi}$, $I=I_0(1+\cos \frac{\pi x}{2L})$.

**Problem 3.47**

Assume AB is a “deep” beam. I and A are constant. Determine the analytical solution for β (the rotation of the cross-section) and v .



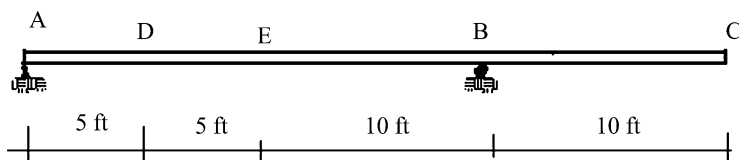
Problem 3.48

- (1) Determine β_t (the rotation of the cross-section about the longitudinal axis) at B due to the concentrated torque at C.
- (2) Suppose a distribution torque, m_t , is applied along A–B. Determine $M_t(x)$.
Take $m_t = \sin \frac{\pi x}{2L}$
- (3) Determine β_t at B due to the distributed torsional loading.

Problem 3.49

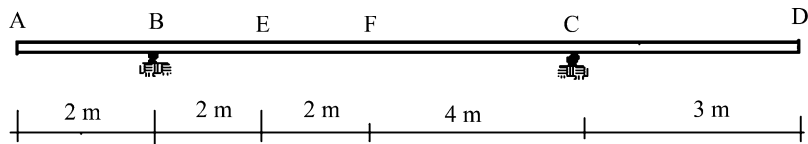
Draw the influence lines for:

- (a) Reaction at A
- (b) Moment at E
- (c) Shear at D

**Problem 3.50**

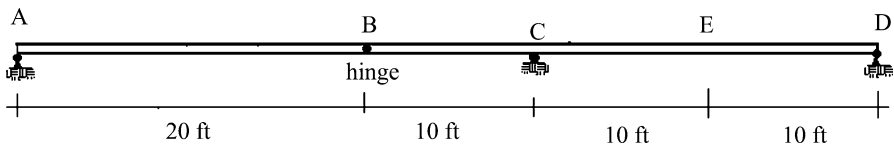
Draw the influence lines for:

- (a) Reaction at B
- (b) Reaction at C
- (c) Moment at E
- (d) Shear at F

**Problem 3.51**

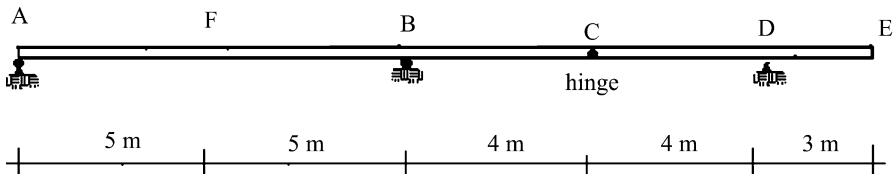
Draw the influence lines for:

- Reaction at A
- Reaction at C
- Reaction at D
- Moment at E

**Problem 3.52**

Draw the influence lines for:

- Vertical reaction at A
- Vertical reaction at B
- Moment at point F
- Shear at point F

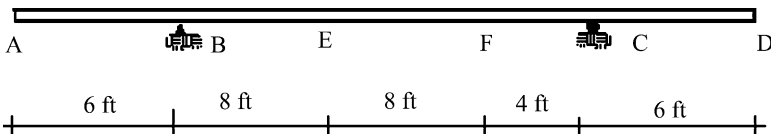


Suppose a uniformly distributed dead load of 18 kN/m and uniformly distributed live load of 30 kN/m are placed on the beam. Use the above results to determine the maximum values for the vertical reaction at A and the moment at point F. Also show the position of the live load on the beam.

Problem 3.53

Draw the influence line for:

- The reaction at B
- The moment at E
- The shear at F
- The moment at F

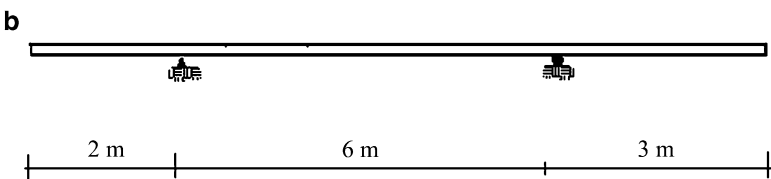
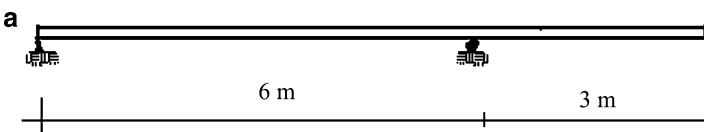


Suppose a uniformly distributed live load of 1.2 kip/ft and uniformly distributed dead load of 0.8 kip/ft are placed on the beam. Use the above results to determine:

- The maximum value of the vertical reaction at B
- The maximum and minimum values of shear at F
- The maximum and minimum values of moment at F

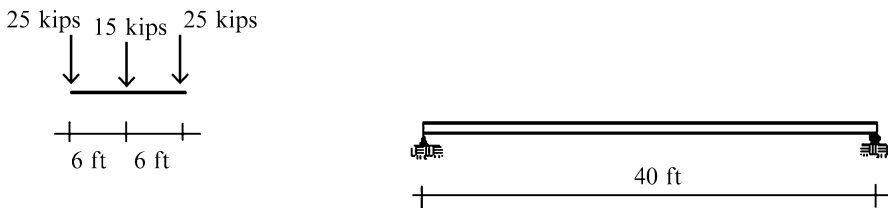
Problem 3.54

For the beams shown, determine the moment and shear envelopes corresponding to a single concentrated load moving across the span.

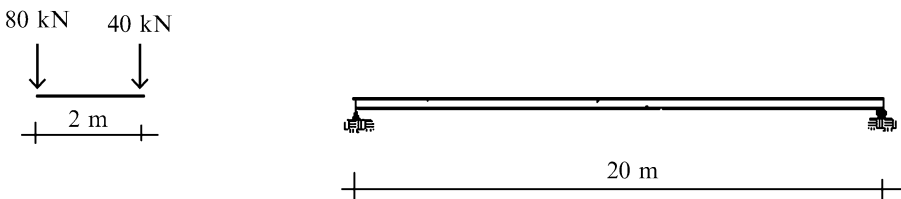


Problem 3.55

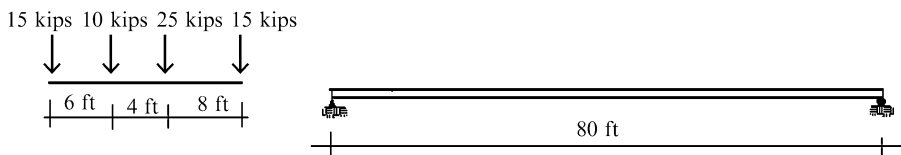
Determine the maximum possible moment in the 40 ft span beam as the loading system shown moves across the span.

**Problem 3.56**

Determine the location of the maximum possible moment in the 20 m span beam as the loading system shown moves across the span.

**Problem 3.57**

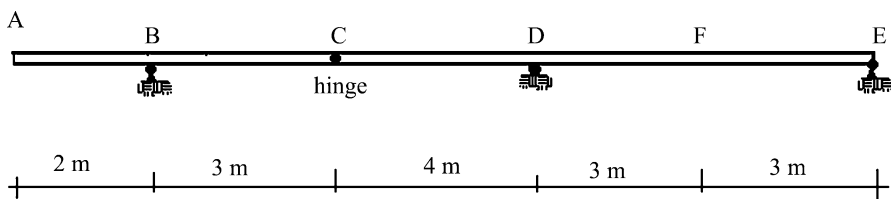
Determine the maximum possible moment in a 80 ft span beam as the loading system shown moves across the span. Assume a uniform load of 2 kip/ft also acts on the span. Use computer software.

**Problem 3.58**

For the beam shown:

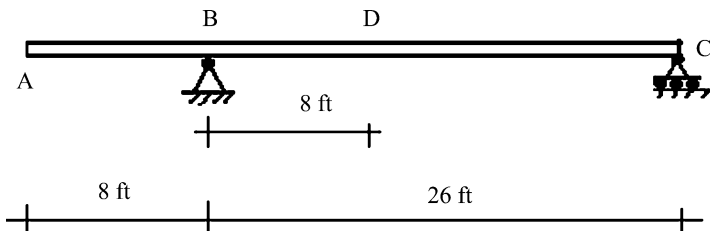
- Draw the influence lines for the vertical reaction at support D, the moment at point F, and the shear at point C.
- For a uniformly distributed live load of 20 kN/m, use the above results to determine the maximum values of the reaction at D, moment at F, and shear at point F. Also show the position of the live load on the beam.

- (c) Establish the moment envelope corresponding to a single concentrated vertical load.



Problem 3.59

For the beam shown below



Draw the influence line for:

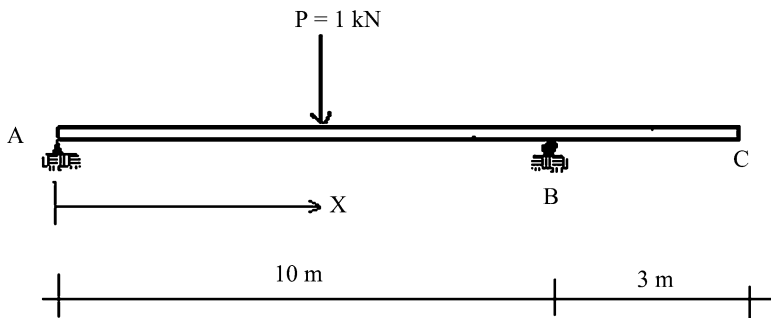
- (a) The vertical reaction at B
- (b) The moment at D
- (c) The vertical reaction at C

If a uniformly distributed live load of 1.8 kip/ft and uniformly distributed dead load of 1.4 kip/ft are placed on the beam, use the above results to determine the maximum and minimum values of

- (a) The vertical reaction at C
- (b) The moment at D

Problem 3.60

Using computer software, determine the influence line for the vertical displacement at $x = 5$ m. Assume EI is constant.



Hint: Apply a unit load at $x = 5 \text{ m}$ and determine the deflected shape. This is a scaled version of the influence line. Verify by moving the load and recomputing the displacement at $x = 5 \text{ m}$.

Overview

Plane frame structures are composed of structural members which lie in a single plane. When loaded in this plane, they are subjected to both bending and axial action. Of particular interest are the shear and moment distributions for the members due to gravity and lateral loadings. We describe in this chapter analysis strategies for typical statically determinate single story frames. Numerous examples illustrating the response are presented to provide the reader with insight as to the behavior of these structural types. We also describe how the Method of Virtual Forces can be applied to compute displacements of frames. The theory for frame structures is based on the theory of beams presented in Chap. 3. Later in Chaps. 9, 10, and 15, we extend the discussion to deal with statically indeterminate frames and space frames.

4.1 Definition of Plane Frames

The two dominant planar structural systems are plane trusses and plane frames. Plane trusses were discussed in detail in Chap. 2. Both structural systems are formed by connecting structural members at their ends such that they are in a single plane. The systems differ in the way the individual members are connected and loaded. Loads are applied at nodes (joints) for truss structures. Consequently, the member forces are purely axial. Frame structures behave in a completely different way. The loading is applied directly to the members, resulting in internal shear and moment as well as axial force in the members. Depending on the geometric configuration, a set of members may experience predominately bending action; these members are called “beams.” Another set may experience predominately axial action. They are called “columns.” The typical building frame is composed of a combination of beams and columns.

Frames are categorized partly by their geometry and partly by the nature of the member/member connection, i.e., pinned vs. rigid connection. Figure 4.1 illustrates

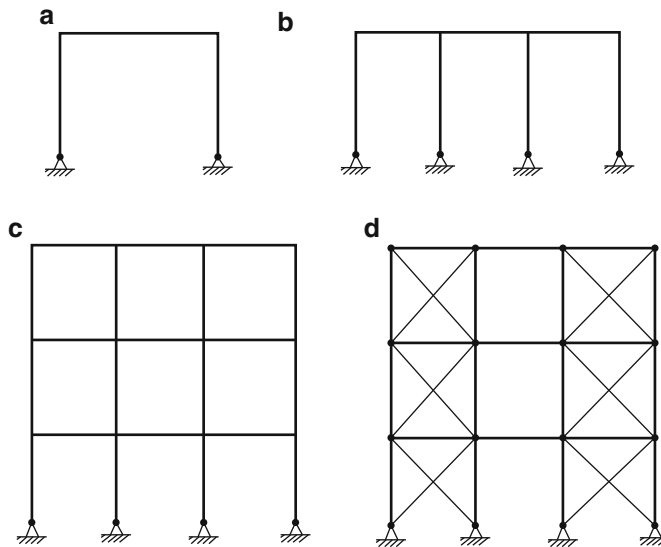


Fig. 4.1 Typical plane building frames. (a) Rigid Portal frame. (b) Rigid multi-bay portal frame. (c) Multistory rigid frame. (d) Multistory braced frame

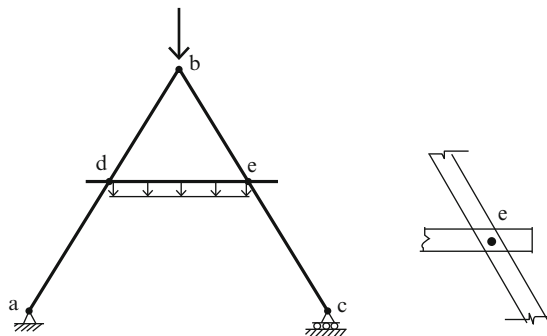


Fig. 4.2 A-frame

some typical rigid plane frames used mainly for light manufacturing factories, warehouses, and office buildings. We generate three dimensional frames by suitably combining plane frames.

Figure 4.2 shows an A-frame, named obviously for its geometry. This frame has three members ab, bc, and de that are pinned together at points d, b, and e. Loads may be applied at the connection points, such as b, or on a member, such as de. A-frames are typically supported at the base of their legs, such as at a and c. Because of the nature of the loading and restraints, the members in an A-frame generally experience bending as well as axial force.

To provide more vertical clearance in the interior and also to improve the aesthetics, a more open interior space is created by pitching the top member as

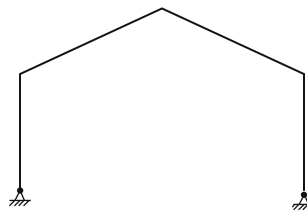


Fig. 4.3 Gable (pitched roof) frames

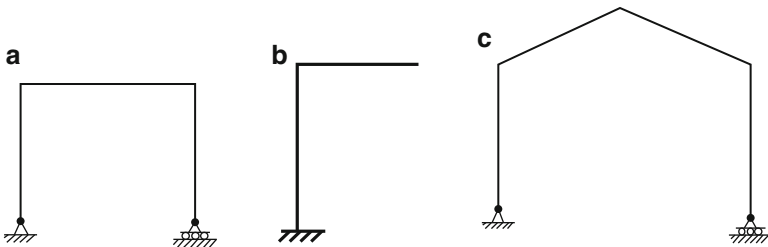


Fig. 4.4 Statically determinate support schemes for planar frames

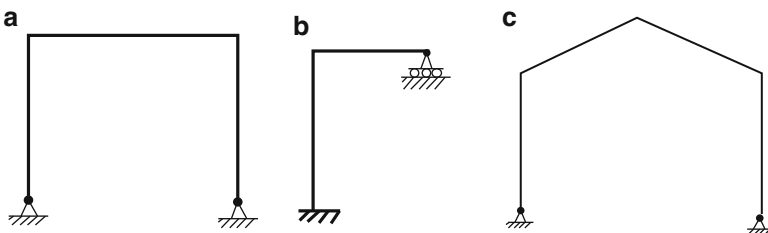


Fig. 4.5 Statically indeterminate support schemes—planar frames

illustrated in Fig. 4.3. Pitched roof frames are also referred to as gable frames. Architects tend to prefer them for churches, gymnasias, and exhibition halls.

4.2 Statical Determinacy: Planar Loading

All the plane frames that we have discussed so far can be regarded as rigid bodies in the sense that if they are adequately supported, the only motion they will experience when a planar load is applied will be due to deformation of the members. Therefore, we need to support them with only three nonconcurrent displacement restraints. We can use a single, fully fixed support scheme, or a combination of hinge and roller supports. Examples of “adequate” support schemes are shown in Fig. 4.4. All these schemes are statically determinate. In this case, one first determines the reactions and then analyzes the individual members.

If more than three displacement restraints are used, the plane frames are statically indeterminate. In many cases, two hinge supports are used for portal and gable

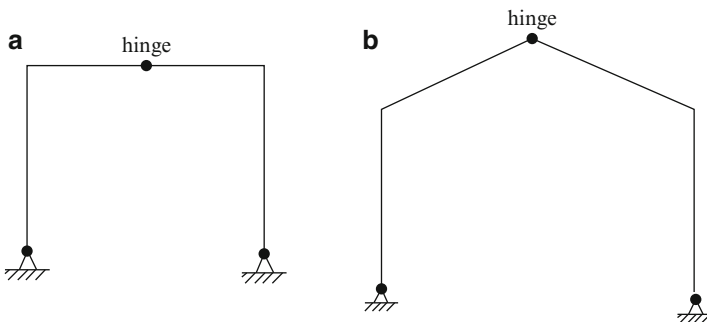


Fig. 4.6 3-Hinge plane frames

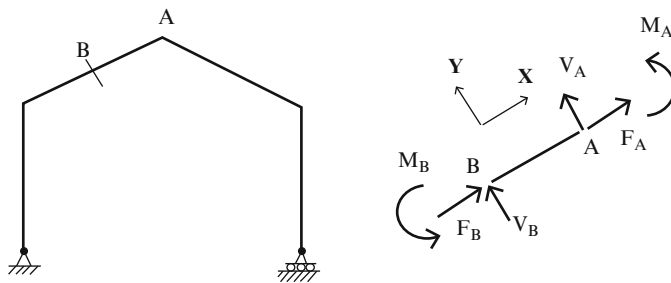


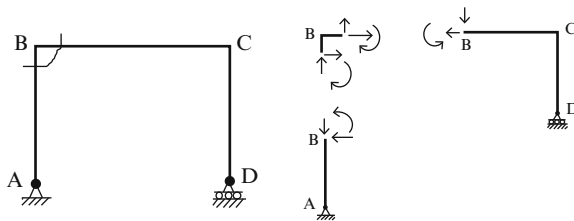
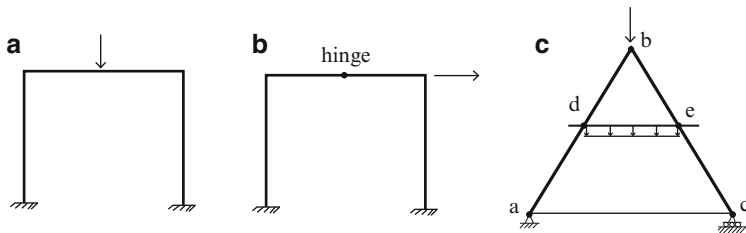
Fig. 4.7 Free body diagram—member forces

frames (see Fig. 4.5). We cannot determine the reaction forces in these frame structures using only the three available equilibrium equations since there are now four unknown reaction forces. They are reduced to statically determinate structures by inserting a hinge which acts as a moment release. We refer to these modified structures as 3-hinge frames (see Fig. 4.6).

Statistical determinacy is evaluated by comparing the number of unknown forces with the number of equilibrium equations available. For a planar member subjected to planar loading, there are three internal forces: axial, shear, and moment. Once these force quantities are known at a point, the force quantities at any other point in the member can be determined using the equilibrium equations. Figure 4.7 illustrates this computation for the member segment AB. Therefore, it follows that there are only *three force unknowns for each member* of a rigid planar frame subjected to planar loading.

We define a node (joint) as the intersection of two or more members, or the end of a member connected to a support. A node is acted upon by member forces associated with the members' incident on the node. Figure 4.8 illustrates the forces acting on node B.

These nodal forces comprise a general planar force system for which there are three equilibrium equations available; summation of forces in two nonparallel directions and summation of moments. Summing up force unknowns, we have three for each member plus the number of displacement restraints. Summing up

**Fig. 4.8** Free body diagram—node B**Fig. 4.9** Indeterminate portal and A-frames

equations, there are three for each node plus the number of force releases (e.g., moment releases) introduced. Letting m denote the number of members, r the number of displacement restraints, j the number of nodes, and n the number of releases, the criterion for statical determinacy of *rigid plane frames* can be expressed as

$$3m + r - n = 3j \quad (4.1)$$

We apply this criterion to the portal frames shown in Figs. 4.4, 4.5, and 4.6. For the portal frame in Fig. 4.4a

$$m = 3, r = 3, j = 4$$

For the corresponding frame in Fig. 4.5a

$$m = 3, r = 4, j = 4$$

This structure is indeterminate to the 1st degree. The 3-hinge frame in Fig. 4.6b has

$$m = 4, r = 4, n = 1, j = 5$$

Inserting the moment release reduces the number of unknowns and now the resulting structure is statically determinate.

Consider the plane frames shown in Fig. 4.9. The frame in Fig. 4.9a is indeterminate to the 3rd degree.

$$m = 3, r = 6, j = 4$$

The frame in Fig. 4.9b is indeterminate to the 2nd degree.

$$m = 4, r = 6, j = 5 n = 1$$

Equation (4.1) applies for rigid plane frames, i.e., where the members are rigidly connected to each other at nodes. The members of an A-frame are connected with pins that allow relative rotation and therefore A-frames are *not* rigid frames. We establish a criterion for A-frame type structures following the same approach described above. Each member has three equilibrium equations. Therefore, the total number of equilibrium equations is equal to $3m$. Each pin introduces two force unknowns. Letting n_p denote the number of pins, the total number of force unknowns is equal to $2n_p$ plus the number of displacement restraints. It follows that

$$2n_p + r = 3m \quad (4.2)$$

for static determinacy of A-frame type structures. Applying this criterion to the structure shown in Fig. 4.2, one has $n_p = 3, r = 3, m = 3$ and the structure is statically determinate. If we add another member at the base, as shown in Fig. 4.9c, $n_p = 5, r = 3, m = 4$, and the structure becomes statically indeterminate to the 1st degree.

4.3 Analysis of Statically Determinate Frames

In this section, we illustrate with numerous examples the analysis process for statically determinate frames such as shown in Fig. 4.10a. In these examples, our primary focus is on the generation of the internal force distributions. Of particular interest are the

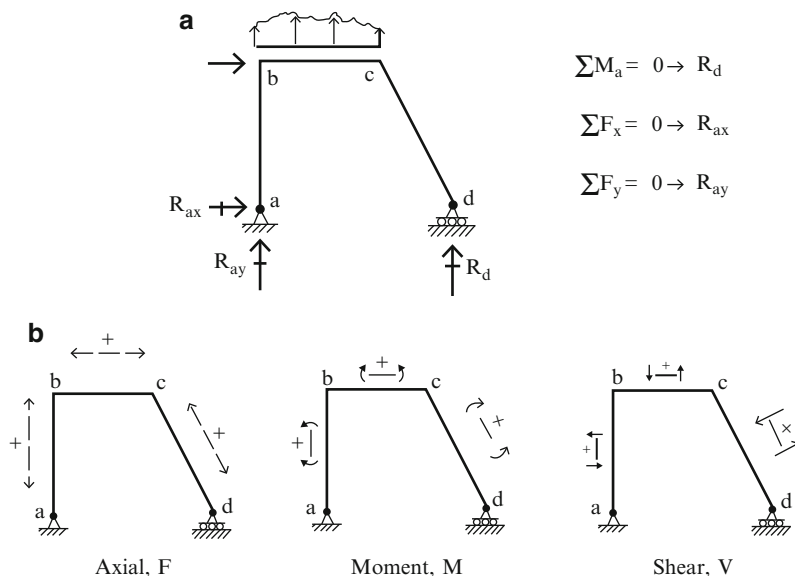


Fig. 4.10 (a) Typical frame. (b) Sign convention for the bending moment, transverse shear, and axial force

location and magnitude of the peak values of moment, shear, and axial force since these quantities are needed for the design of the member cross-sections.

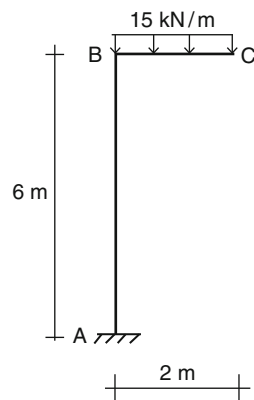
The analysis strategy for these structures is as follows. We first find the reactions by enforcing the global equilibrium equations. Once the reactions are known, we draw free body diagrams for the members and determine the force distributions in the members. *We define the positive sense of bending moment according to whether it produces compression on the exterior face.* The sign conventions for bending moment, transverse shear, and axial force are defined in Fig. 4.10b.

The following examples illustrate this analysis strategy. Later, we present analytical solutions which are useful for developing an understanding of the behavior.

Example 4.1 Unsymmetrical cantilever frame

Given: The structure defined in Fig. E4.1a.

Fig. E4.1a



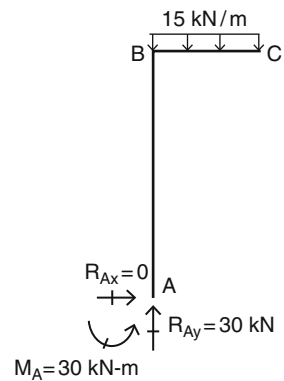
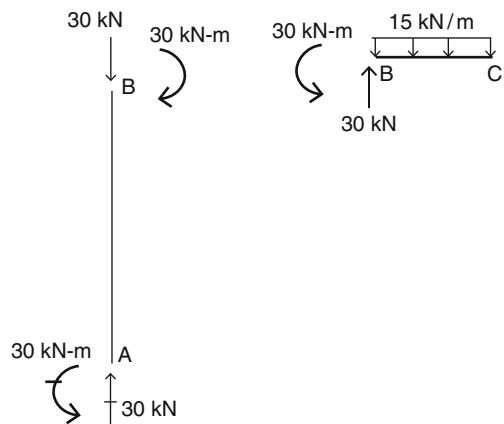
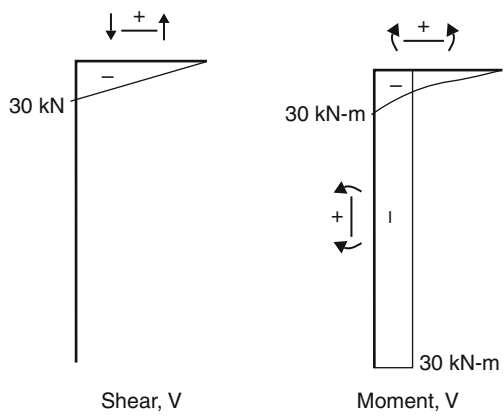
Determine: The reactions and draw the shear and moment diagrams.

Solution: We first determine the reactions at A, and then the shear and moment at B. These results are listed in Figs. E4.1b, c. Once these values are known, the shear and moment diagrams for members CB and BA can be constructed. The final results are plotted in Fig. E4.1d.

$$\sum F_x = 0 \quad R_{Ax} = 0$$

$$\sum F_y = 0 \quad R_{Ay} - (15)(2) = 0 \quad R_{Ay} = 30 \text{ kN} \uparrow$$

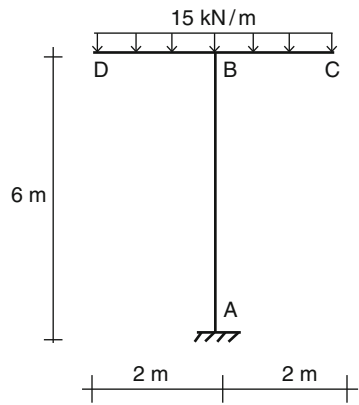
$$\sum M_A = 0 \quad M_A - (15)(2)(1) = 0 \quad M_A = 30 \text{ kN m counter clockwise}$$

Fig. E4.1b Reactions**Fig. E4.1c** End actions**Fig. E4.1d** Shear and moment diagrams

Example 4.2 Symmetrical cantilever frame

Given: The structure defined in Fig. E4.2a.

Fig. E4.2a



Determine: The reactions and draw the shear and moment diagrams.

Solution: We determine the reactions at A and shear and moment at B. The results are shown in Figs. E4.2b, c.

$$\sum F_x = 0 \quad R_{Ax} = 0$$

$$\sum F_y = 0 \quad R_{Ay} - (15)(4) = 0 \quad R_{Ay} = 60 \text{ kN } \uparrow$$

$$\sum M_A = 0 \quad M_A - (15)(2)(1) + (15)(2)(1) = 0 \quad M_A = 0$$

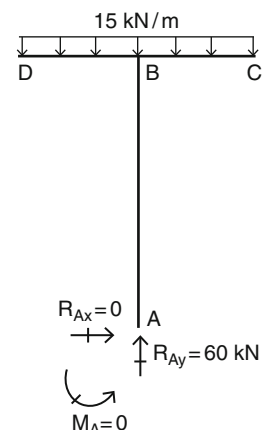
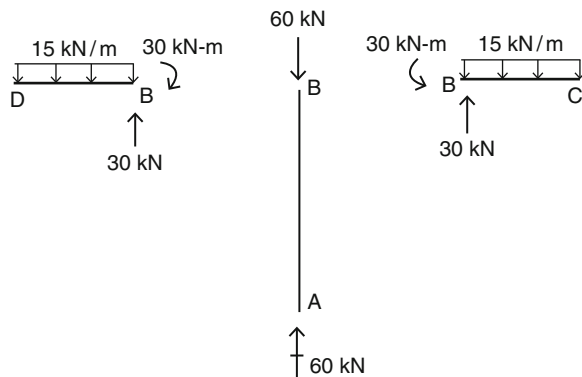
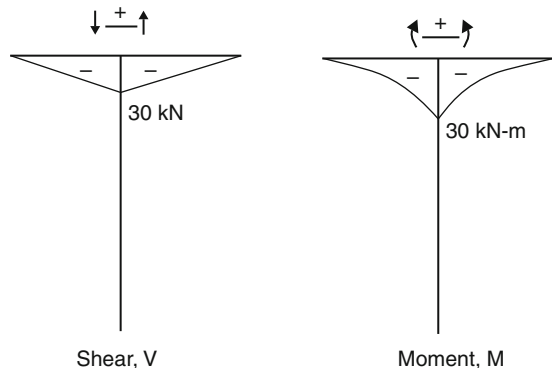


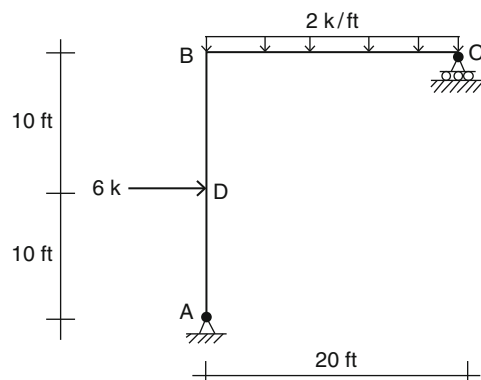
Fig. E4.2b Reactions

Fig. E4.2c End actions

Finally the shear and moment diagrams for the structures are plotted in Fig. E4.2d. Note that member AB now has no bending moment, just axial compression of 12 kip.

Fig. E4.2d Shear and moment diagrams*Example 4.3 Angle-type frame segment*

Given: The frame defined in Fig. E4.3a.

**Fig. E4.3a**

Determine: The reactions and draw the shear and moment diagrams.

Solution: We determine the vertical reaction at C by summing moments about A. The reactions at A follow from force equilibrium considerations (Fig. E4.3b).

$$\begin{aligned}\sum M_A = 0 \quad 2(20)(10) + 6(10) - R_C(20) &= 0 \quad R_C = 23 \text{ kip } \uparrow \\ \sum F_x = 0 \quad R_{Ax} &= 6 \text{ kip } \leftarrow \\ \sum F_y = 0 \quad R_{Ay} - 2(20) + 23 &= 0 \quad R_{Ay} = 17 \text{ kip } \uparrow\end{aligned}$$

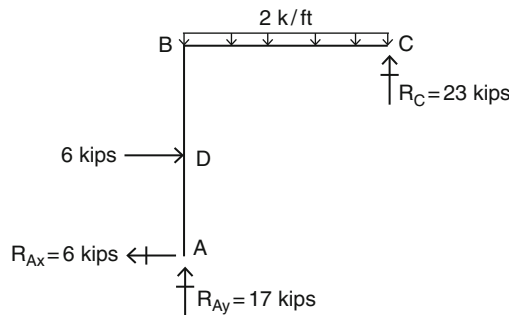


Fig. E4.3b Reactions

Next, we determine the end moments and end shears for segments CB and BA using the equilibrium equations for the members. Figure E4.3c contains these results.

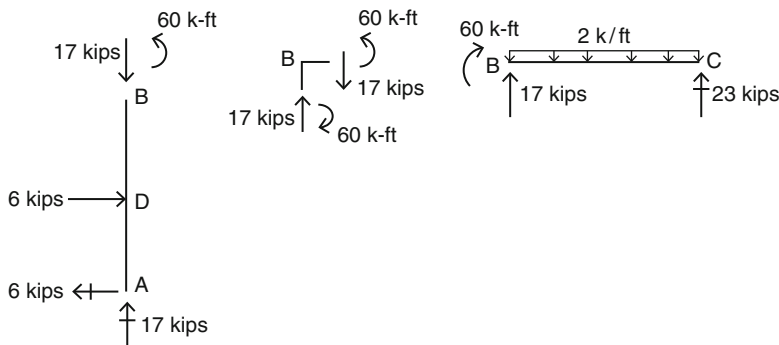
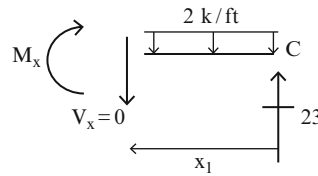


Fig. E4.3c End actions

Lastly, we generate the shear and bending moment diagrams (Fig. E4.3d). The maximum moment occurs in member BC. We determine its location by noting that the moment is a maximum when the shear is zero.



$$23 - (2)x_1 = 0 \rightarrow x_1 = 11.5 \text{ ft}$$

Then $M_{\max} = 23(11.5) - \frac{2(11.5)^2}{2} = 132.25 \text{ kip ft}$

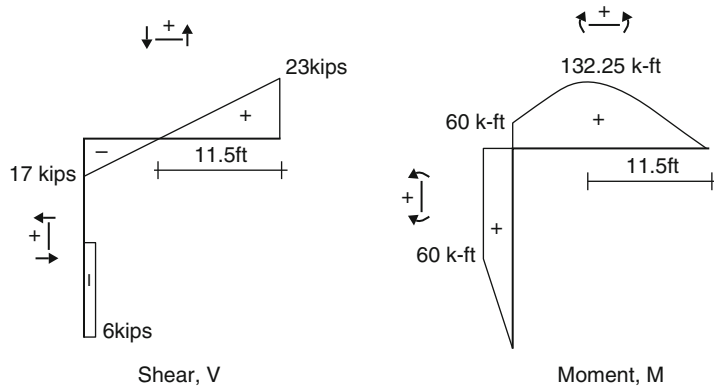


Fig. E4.3d Shear and moment diagrams

Example 4.4 Simply supported portal frame

Given: The portal frame defined in Fig. E4.4a which is similar to that discussed in the text.

Determine: The shear and moment distributions.

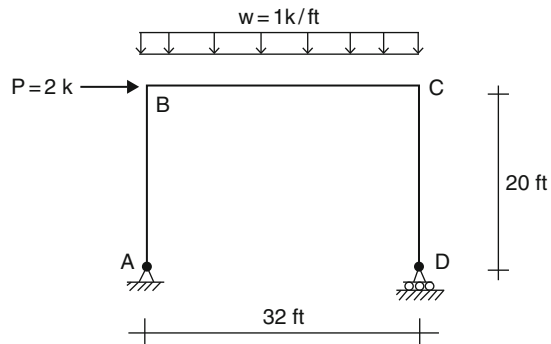
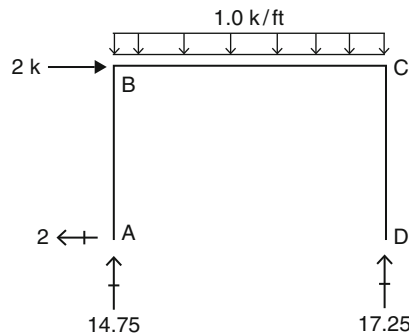


Fig. E4.4a

Solution: The reaction at D is found by summing moments about A. We then determine the reactions at A using force equilibrium considerations. Figure E4.4b shows the result.

$$\begin{aligned}\sum M_A = 0 \quad 1(32)(16) + 2(20) - R_D(32) &= 0 & R_D &= 17.25 \uparrow \\ \sum F_x = 0 \quad R_{Ax} &= 2 \leftarrow \\ \sum F_y = 0 \quad R_{Ay} - 1(32) + 17.25 &= 0 & R_{Ay} &= 14.75 \uparrow\end{aligned}$$

Fig. E4.4b Reactions



Isolating the individual members and enforcing equilibrium leads to the end forces and moments shown in Fig. E4.4c.

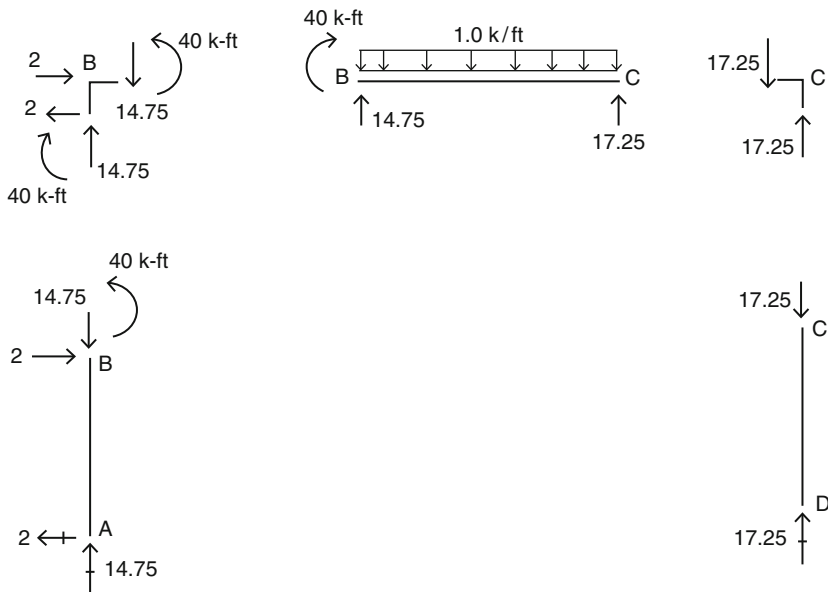
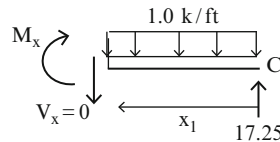


Fig. E4.4c End actions

We locate the maximum moment in member BC. We suppose the moment is a maximum at $x = x_1$. Setting the shear at this point equal to zero lead to



$$17.25 - x_1(1) = 0 \rightarrow x_1 = 17.25 \text{ ft}$$

$$\text{Then } M_{\max} = 17.25(17.25) - \frac{(1)(17.25)^2}{2} = 148.78 \text{ kip ft}$$

The shear and moment diagrams are plotted in Fig. E4.4d.

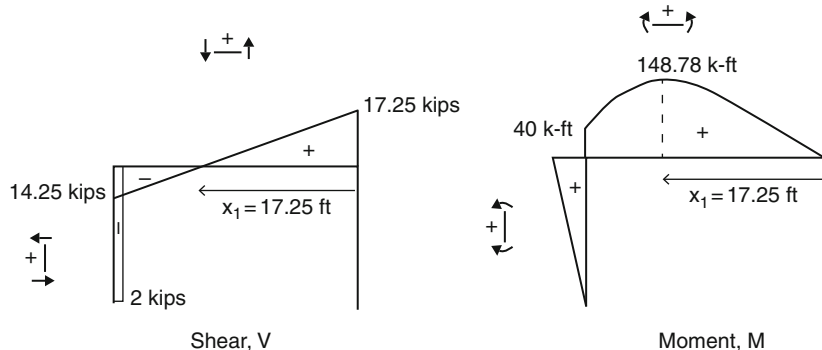


Fig. E4.4d Shear and moment diagrams

Example 4.5 3-Hinge portal frame

Given: The 3-hinge frame defined in Fig. E4.5a.

Determine: The shear and moment distributions.

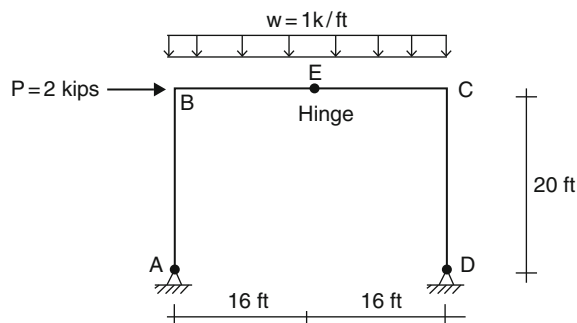


Fig. E4.5a

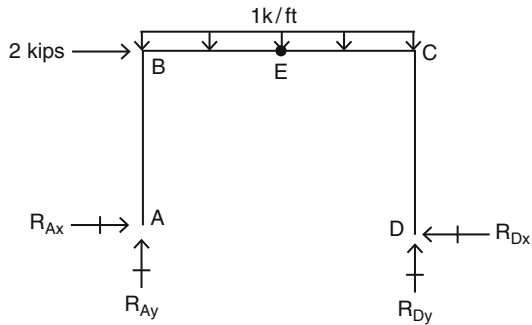
Solution: Results for the various analysis steps are listed in Figs. E4.5b–g.

Step 1: Reactions at D and A

The vertical reaction at D is found by summing moments about A.

$$\sum M_A = 0 \quad R_{Dy}(32) - (1)(32)(16) - 2(20) = 0 \quad R_{Dy} = 17.25 \text{ kip } \uparrow$$

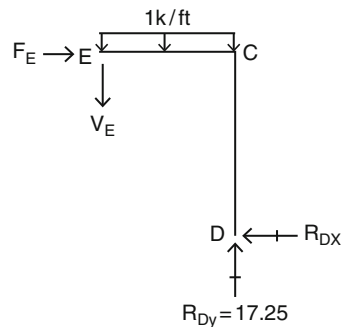
Fig. E4.5b



Next, we work with the free body diagram of segment ECD. Applying the equilibrium conditions to this segment results in

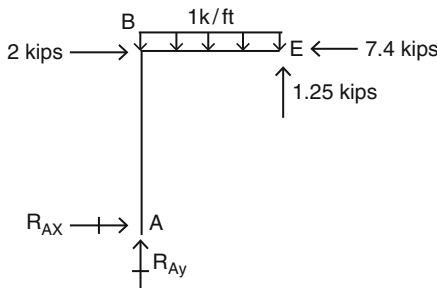
$$\begin{aligned}\sum M_E &= 0 & 17.25(16) - (1)(16)(8) - R_{DX}(20) &= 0 & R_{DX} &= 7.4 \leftarrow \\ \sum F_x &= 0 & F_E = -R_{DX} &= 7.4 \text{ kips } \rightarrow \\ \sum F_y &= 0 & -V_E + 17.25 - (1)(16) &= 0 & V_E &= 1.25 \text{ kips } \downarrow\end{aligned}$$

Fig. E4.5c

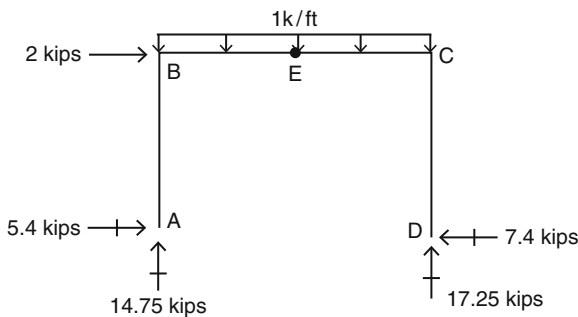


With the internal forces at E known, we can now proceed with the analysis of segment ABE.

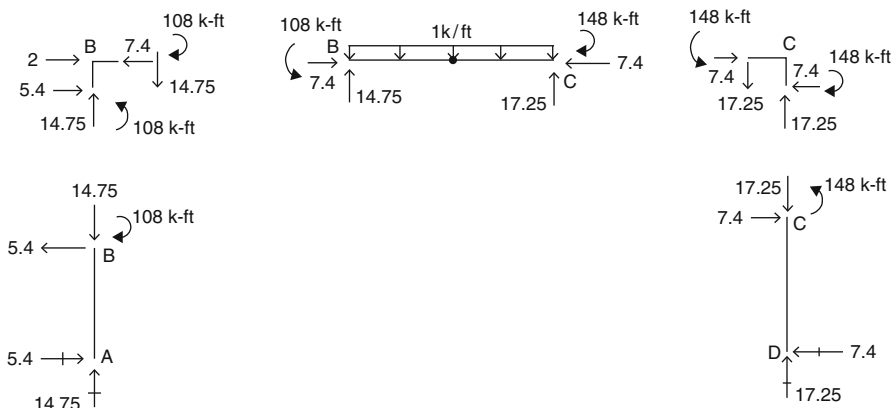
$$\begin{aligned}\sum F_x &= 0 & R_{Ax} + 2 - 7.4 &= 0 & R_{Ax} &= 5.4 \text{ kip } \rightarrow \\ \sum F_y &= 0 & R_{Ay} + 17.25 - (1)(32) &= 0 & R_{Ay} &= 14.75 \text{ kip } \uparrow\end{aligned}$$

**Fig. E4.5d**

Reactions are listed below

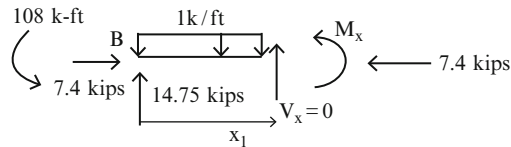
**Fig. E4.5e** Reactions

Step 2: End actions at B and C

**Fig. E4.5f** End actions

Step 3: Shear and moment diagrams

First, we locate the maximum moment in member BC.



$$14.75 - (1)x_1 = 0 \rightarrow x_1 = 14.75 \text{ ft}$$

$$\text{Then } M_{\max} = 14.75(14.75) - \frac{1(14.75)^2}{2} - 108 = 0.78 \text{ kip ft}$$

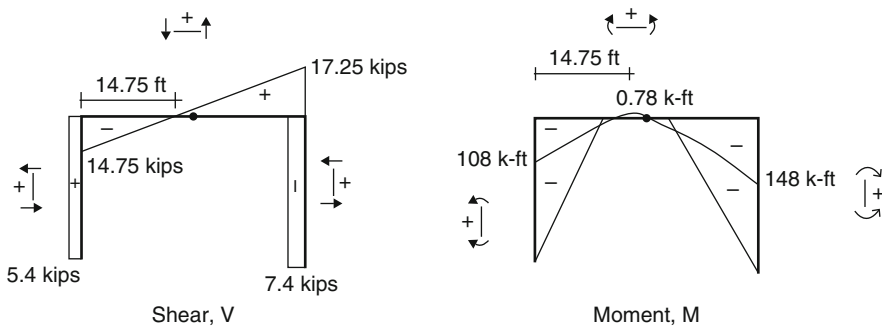


Fig. E4.5g Shear and moment diagrams

Example 4.6 Portal frame with overhang

Given: The portal frame defined in Fig. E4.6a.

Determine: The shear and moment diagrams.

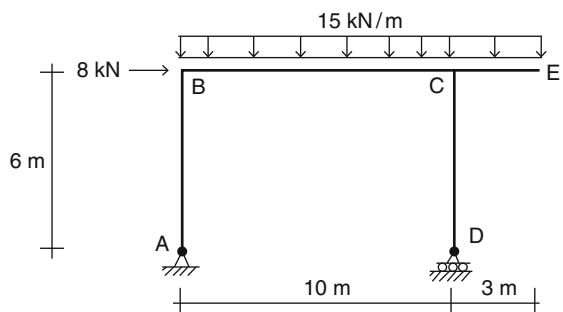


Fig. E4.6a

Solution: Results for the various analysis steps are listed in Figs. E4.6b–d.

$$\begin{aligned}\sum M_A = 0 \quad R_D(10) - 8(6) - (15)(13)(6.5) &= 0 & R_D &= 131.55 \text{ kN} \uparrow \\ \sum F_x = 0 \quad R_{Ax} &= 8 \text{ kN} \leftarrow \\ \sum F_y = 0 \quad R_{Ay} + 131.55 - (15)(13) &= 0 & R_{Ay} &= 63.45 \text{ kN} \uparrow\end{aligned}$$

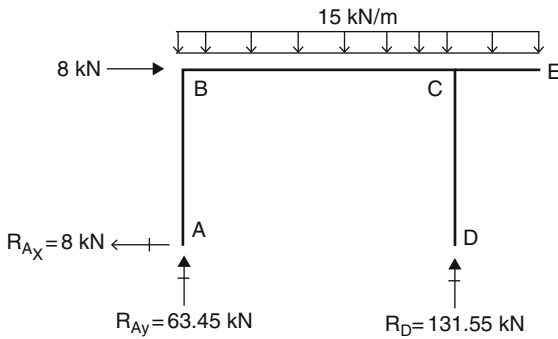


Fig. E4.6b Reactions

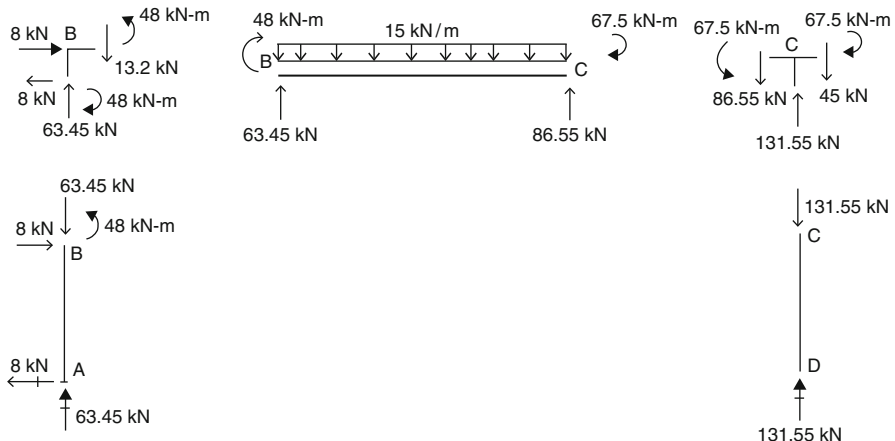
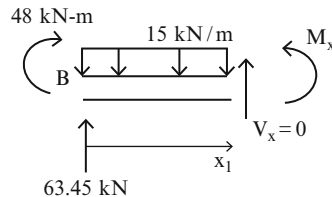


Fig. E4.6c End actions

First, we locate the maximum moment in member BC.



$$63.45 - (15)x_1 = 0 \rightarrow x_1 = 4.23 \text{ m}$$

$$\text{Then } M_{\max} = 63.45(4.23) - \frac{(15)(4.23)^2}{2} + 48 = 182 \text{ kN m}$$

The corresponding shear and moment diagrams are listed in Fig. E4.6d.

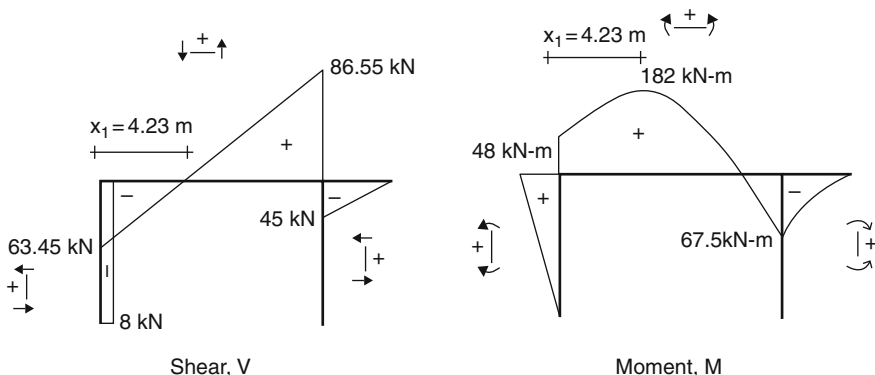


Fig. E4.6d Shear and moment diagrams

4.3.1 Behavior of Portal Frames: Analytical Solution

The previous examples illustrated numerical aspects of the analysis process for single story statically determinate portal frames. For future reference, we list below the corresponding analytical solutions. We consider both gravity and lateral loading. These solutions are useful for reasoning about the behavior of this type of frame when the geometric parameters are varied.

Portal frame—Gravity loading: Shown in Fig. 4.11

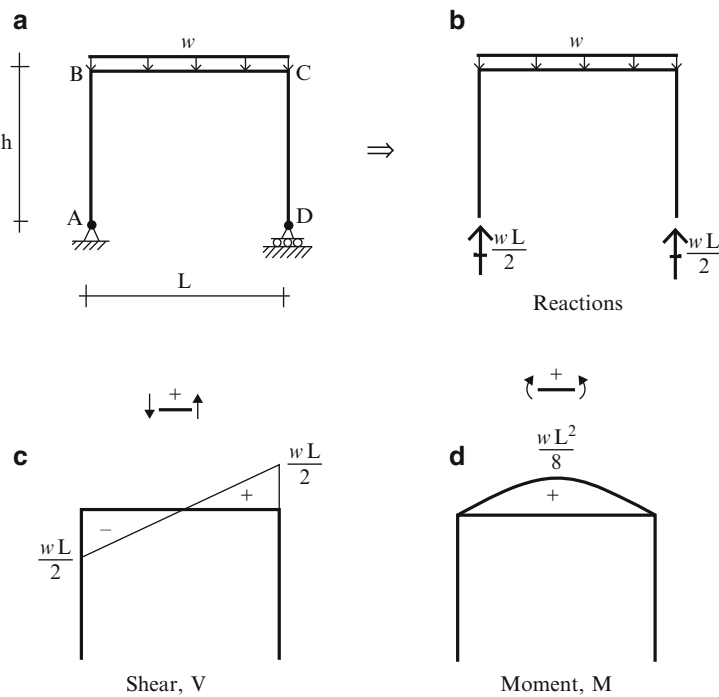


Fig. 4.11 Statically determinate portal frame under gravity loading. (a) Geometry and loading. (b) Reactions. (c) Shear diagram. (d) Moment diagram

Portal frame—Lateral loading: Shown in Fig. 4.12

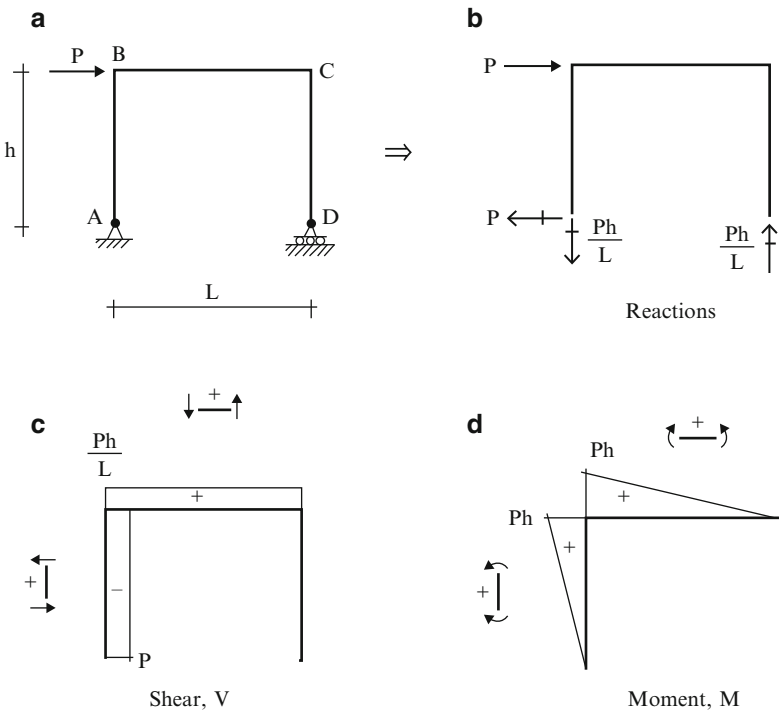


Fig. 4.12 Statically determinate portal frame under lateral loading. (a) Geometry and loading. (b) Reactions. (c) Shear diagram. (d) Moment diagram

3-hinge portal frame—gravity loading: Shown in Fig. 4.13

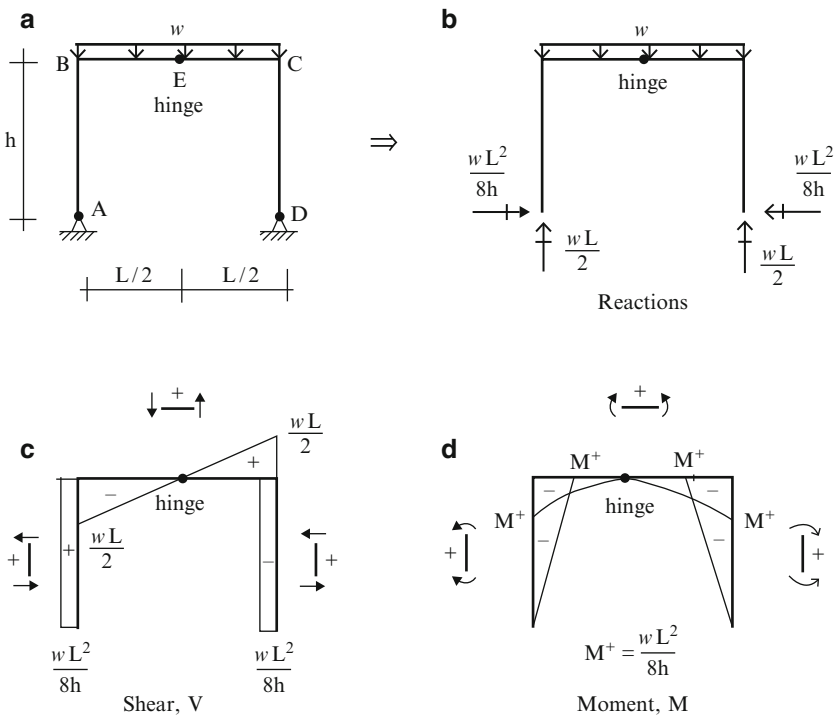


Fig. 4.13 Statically determinate 3-hinge portal frame under gravity loading. (a) Geometry and loading. (b) Reactions. (c) Shear diagram. (d) Moment diagram

3-hinge portal frame—lateral loading: Shown in Fig. 4.14

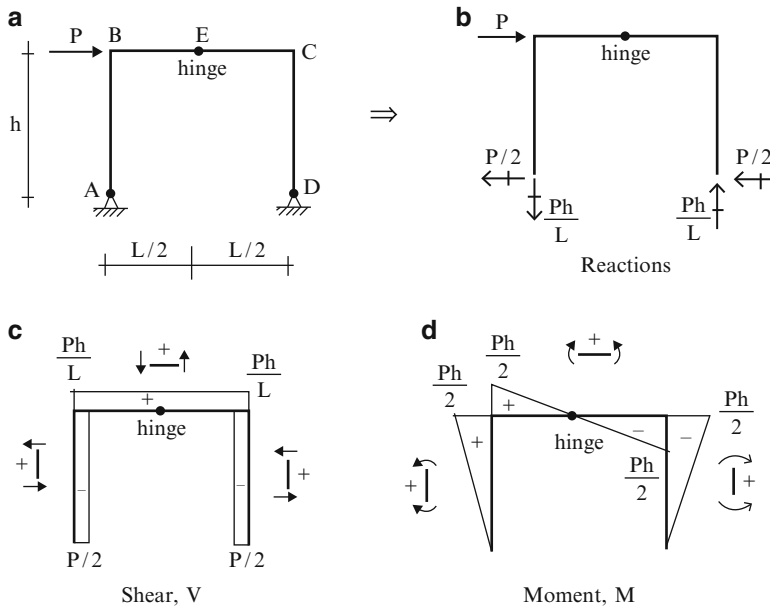


Fig. 4.14 Statically determinate 3-hinge portal frame under lateral loading. (a) Geometry and loading. (b) Reactions. (c) Shear diagram. (d) Moment diagram

These results show that the magnitude of the peak moment due to the uniform gravity load is the *same* for both structures but of opposite sense. The peak moment occurs at the corner points for the 3-hinge frame and at mid-span for the simply supported beam which behaves as a simply supported beam. The response under lateral loading is quite different. There is a 50 % *reduction* in peak moment for the 3-hinge case due to the inclusion of an additional horizontal restraint at point d.

For the 3-hinge frame, we note that the bending moment diagram due to gravity loading is symmetrical. In general, a symmetrical structure responds symmetrically when the loading is symmetrical. We also note that the bending moment diagram for lateral loading applied to the 3-hinge frame is anti-symmetrical.

Both loadings produce moment distributions having peaks at the corner points. In strength-based design, the cross-sectional dimensions depend on the design moment; the deepest section is required by the peak moment. Applying this design approach to the 3-hinge frame, we can use variable depth members with the depth increased at the corner points and decreased at the supports and mid-span. Figure 4.15 illustrates a typical geometry. Variable depth 3-hinge frames are quite popular. We point out again here that the internal force distribution in statically determinate structures depends only on the loading and geometry and is independent of the cross-sectional properties of the members. Therefore provided we keep the same geometry (centerline dimensions), we can vary the cross-section properties for a 3-hinge frame without changing the moment distributions.

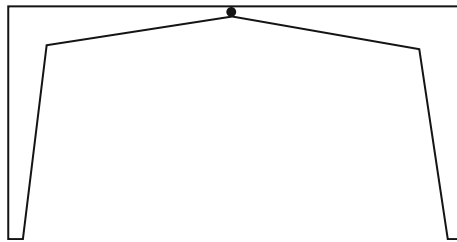


Fig. 4.15 Variable cross-section 3-hinge frame

4.4 Pitched Roof Frames

In this section, we deal with a different type of portal frame structure: the roof members are sloped upward to create a pitched roof. This design creates a more open interior space and avoids the problem of rain water pounding or snow accumulating on flat roofs. Figure 4.16 shows the structures under consideration. The first structure is a rigid frame with a combination of pin and roller supports; the second structure is a 3-hinge frame. Both structures are analyzed by first finding the reactions and then isolating individual members to determine the member end forces, and the internal force distributions.

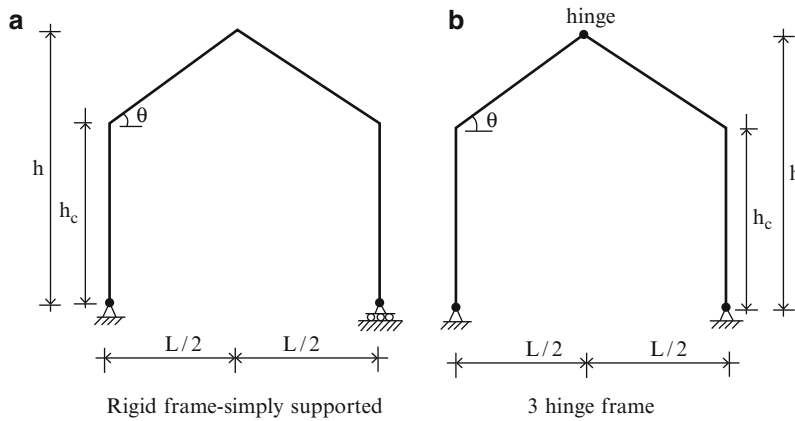


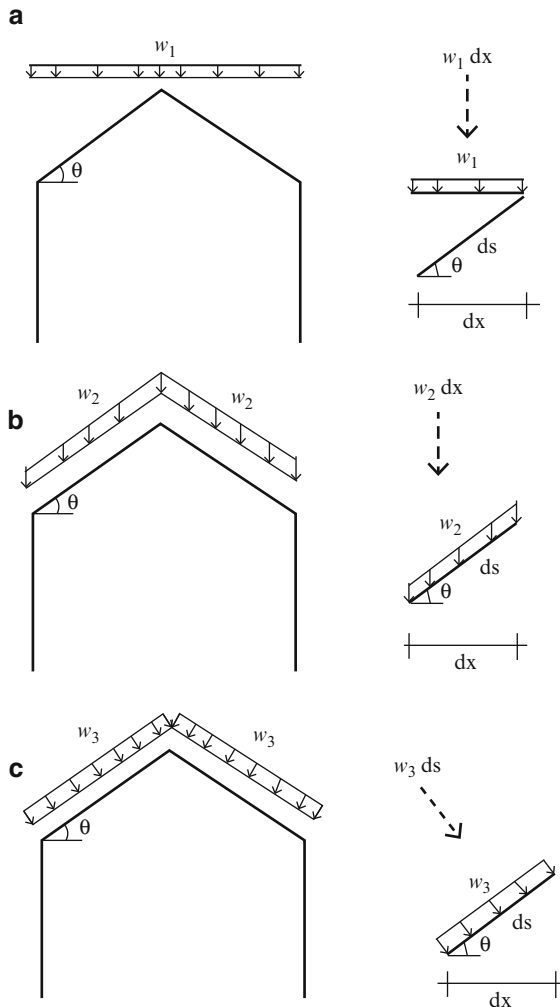
Fig. 4.16 Pitched roof frames

4.4.1 Member Loads

Typical loads that may be applied to an inclined member are illustrated in Fig. 4.17. They may act either in the vertical direction or normal to the member. In the vertical direction, they may be defined either in terms of the horizontal projection of the length of the member or in terms of the length of the member.

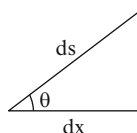
Fig. 4.17 Loading on an inclined member.

- (a) Vertical load per horizontal projection.
- (b) Vertical load per length.
- (c) Normal load per length



When computing the reactions, it is convenient to work with loads referred to horizontal and vertical directions and expressed in terms of the horizontal projection. The w_1 loading is already in this form. For the w_2 load, we note that

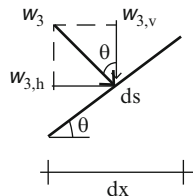
$$dx = ds \cos\theta$$



Then

$$\begin{aligned} w_2 \, ds &= \frac{w_2 \, dx}{\cos \theta} \\ w_{2,v} &= \frac{w_2}{\cos \theta} \end{aligned} \quad (4.3)$$

The w_3 load is normal to the member. We project it onto the vertical and horizontal directions and then substitute for ds .



$$(w_3 \, ds) \cos \theta = w_{3,v} \, dx$$

$$\begin{aligned} w_3 \, ds \sin \theta &= w_{3,h} \, dx \\ w_3 \frac{dx}{\cos \theta} \sin \theta &= w_{3,h} \, dx \end{aligned}$$

The final result is

$$\begin{aligned} w_{3,v} &= w_3 \\ w_{3,h} &= w_3 \tan \theta \end{aligned} \quad (4.4)$$

It follows that the equivalent vertical loading per horizontal projection is equal to the normal load per unit length. These results are summarized in Fig. 4.18.

When computing the axial force, shear, and moment distribution along a member, it is more convenient to work with loads referred to the normal and tangential directions of the member and expressed in terms of the member arc length.

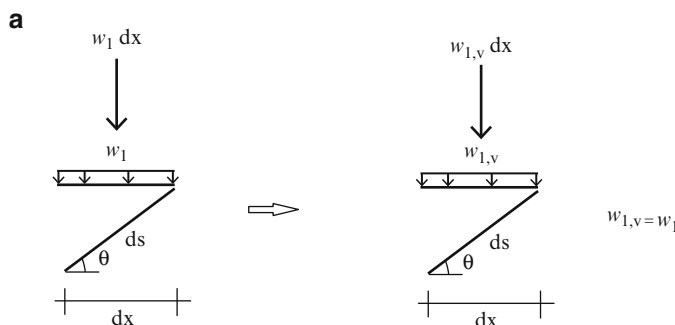
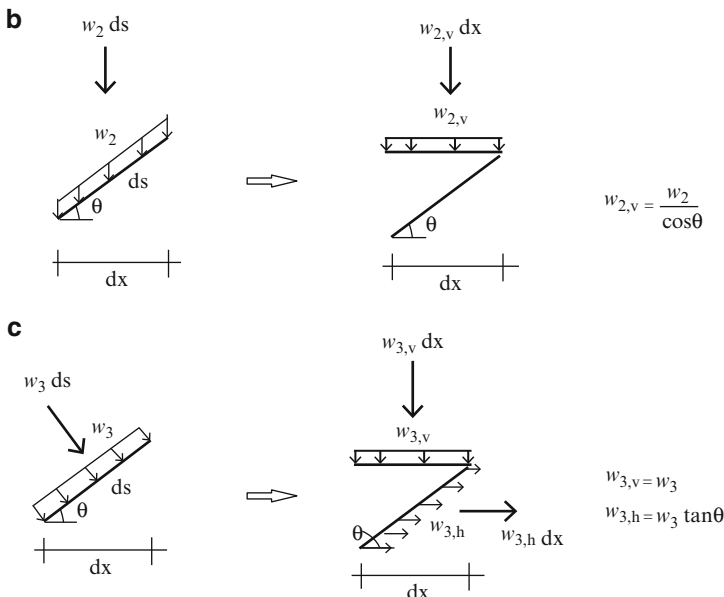


Fig. 4.18 Equivalent vertical member loadings

**Fig. 4.18** (continued)

The approach is similar to the strategy followed above. The results are summarized below (Fig. 4.19).

Vertical–horizontal projection loading:

$$\begin{aligned} w_{1,n} &= w_1 \cos \theta^2 \\ w_{1,t} &= w_1 \cos \theta \sin \theta \end{aligned} \quad (4.5)$$

Vertical member loading:

$$\begin{aligned} w_{2,n} &= w_2 \cos \theta \\ w_{2,t} &= w_2 \sin \theta \end{aligned} \quad (4.6)$$

w_3 loading:

$$\begin{aligned} w_{3,n} &= w_3 \\ w_{3,t} &= 0 \end{aligned}$$

4.4.2 Analytical Solutions for Pitched Roof Frames

Analytical solutions for the bending moment distribution are tabulated in this section. They are used for assessing the sensitivity of the response to changes in the geometric parameters.

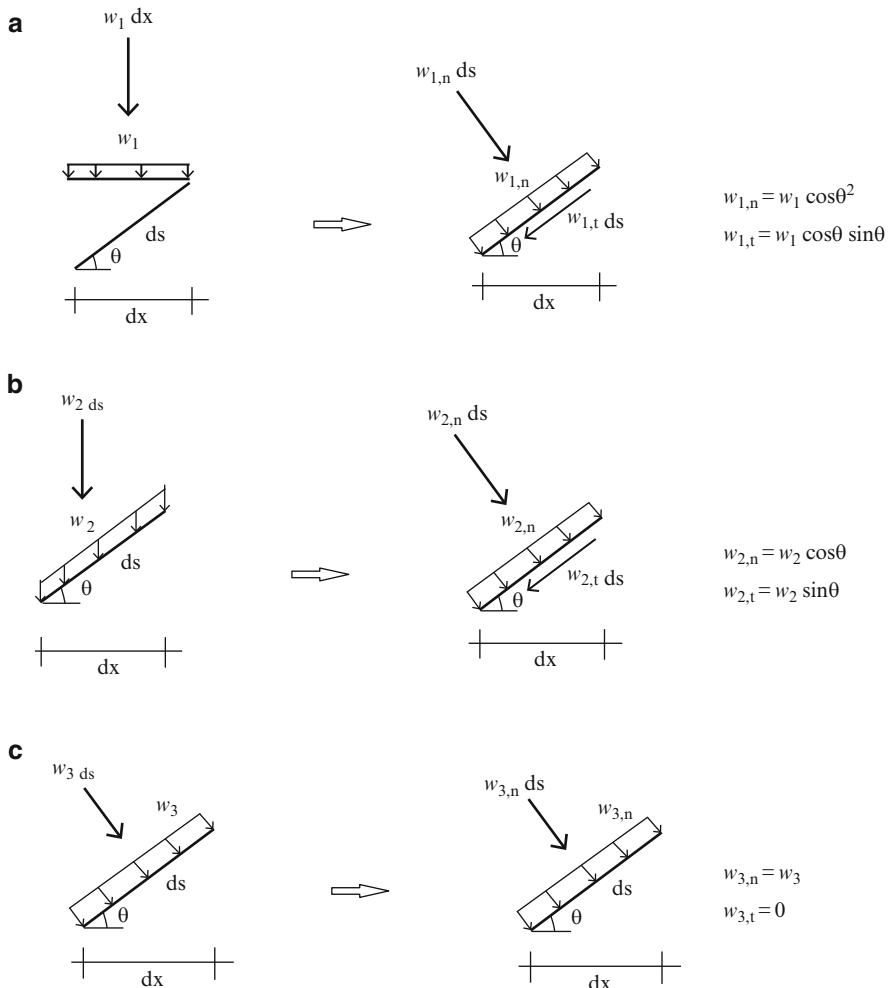


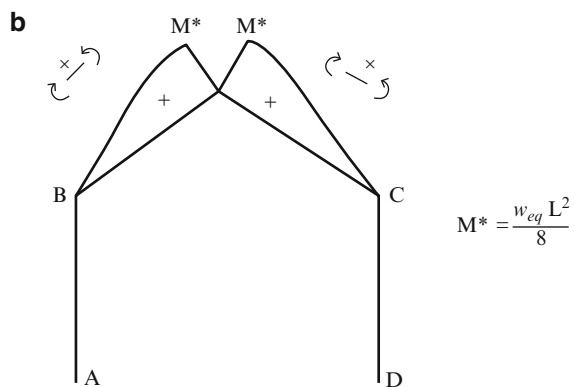
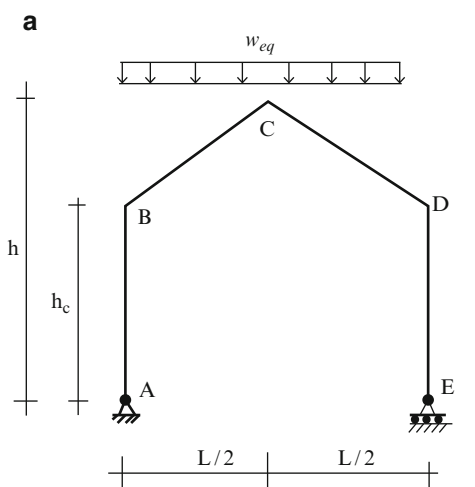
Fig. 4.19 Equivalent normal and tangential member loadings

Gravity loading per unit horizontal projection: Results are listed in Figs. 4.20 and 4.21.

Lateral Loading: Results are listed in Figs. 4.22 and 4.23.

Fig. 4.20 Simply supported gable rigid frame.

- (a) Structure and loading.
- (b) Moment diagram



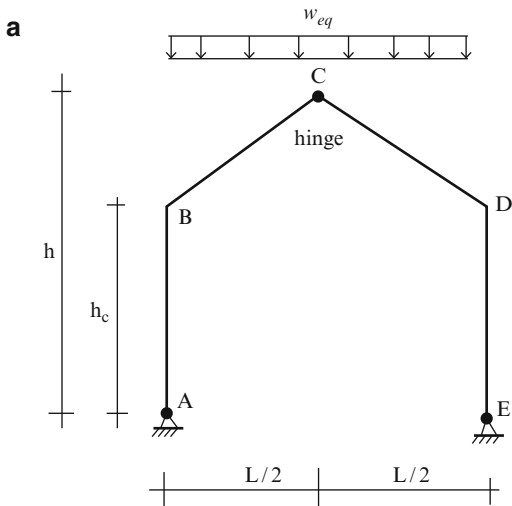
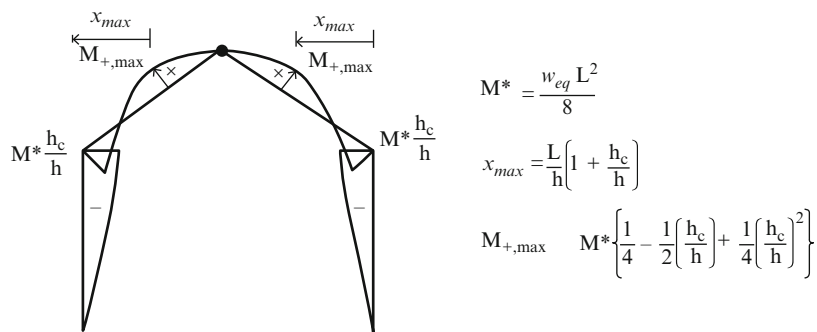
**b**

Fig. 4.21 3-Hinge frame under gravity loading. (a) Structure and loading. (b) Moment diagram

Fig. 4.22 Simply supported rigid frame—lateral loading.
(a) Structure and loading.
(b) Moment diagram

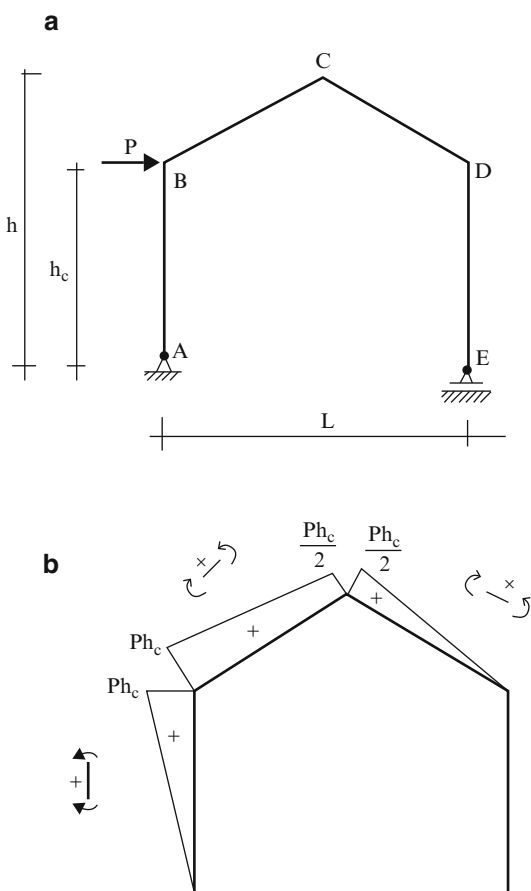
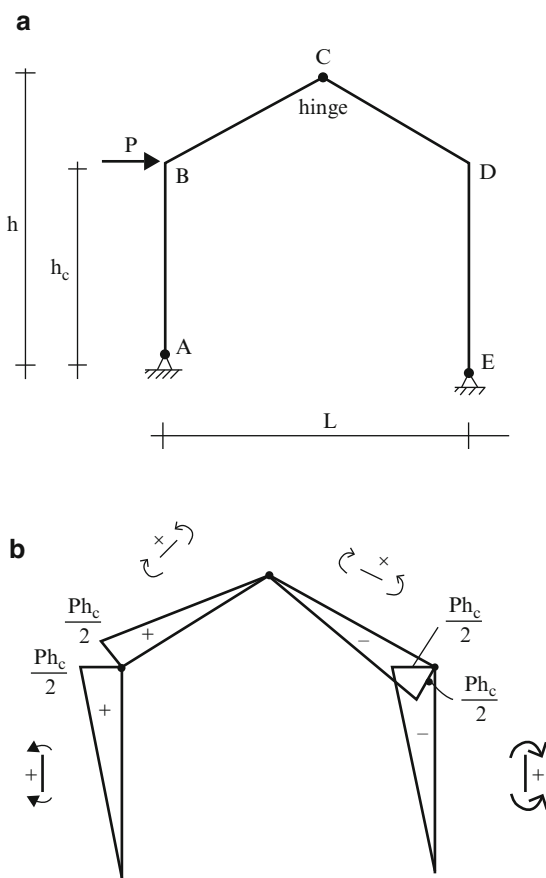


Fig. 4.23 3-hinge frame—lateral loading. (a) Structure and loading. (b) Moment diagram



Example 4.7 Simply supported gable frame—lateral load

Given: The gable frame with the lateral load defined in Fig. E4.7a.

Determine: The shear, moment, and axial force diagrams.

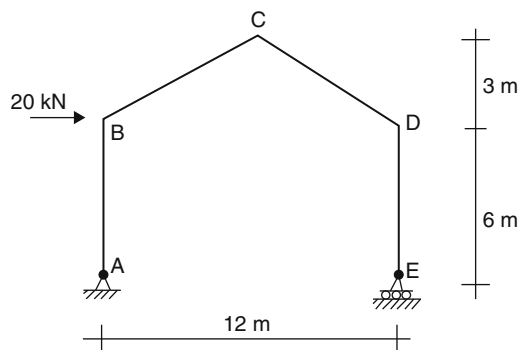


Fig. E4.7a

Solution: Moment summation about A leads to the vertical reaction at E. The reactions at A follow from force equilibrium considerations. Next, we determine the end forces and moments for the individual members. Lastly, we generate the shear and moment diagrams. Results for the various analysis steps are listed in Figs. E4.7b–e.

Step 1: Reactions

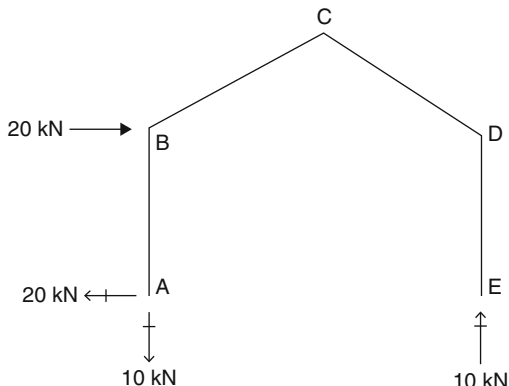


Fig. E4.7b Reactions

Step 2: End forces

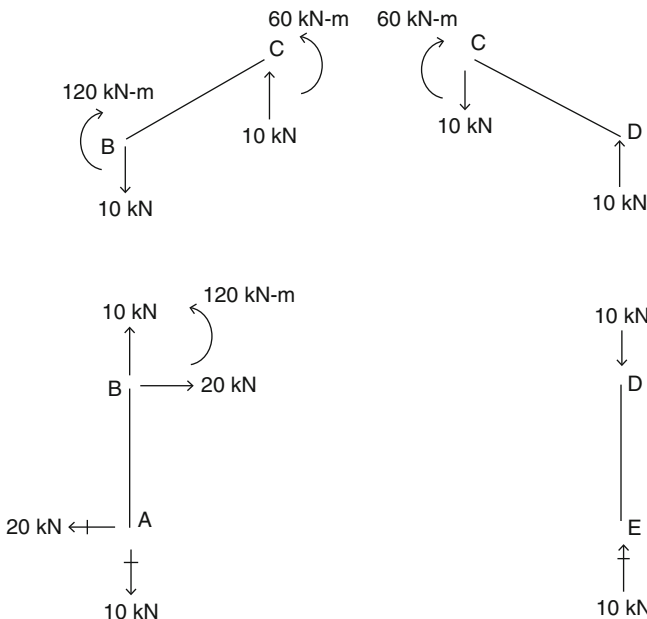


Fig. E4.7c End forces—global frame

Step 3: Member forces—member frames

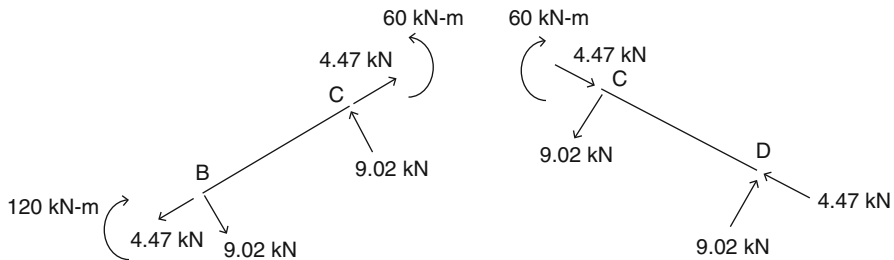


Fig. E4.7d End forces in local member frame

Step 4: Internal force diagrams

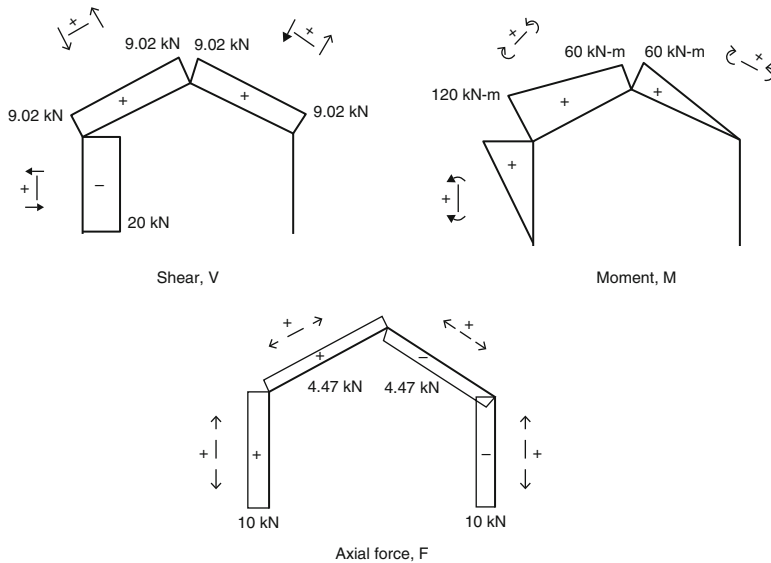


Fig. E4.7e Force distributions

Example 4.8 3-Hinge gable frame—lateral loading

Given: The 3-hinge gable frame shown in Fig. E4.8a.

Determine: The shear, moment, and axial force diagrams.

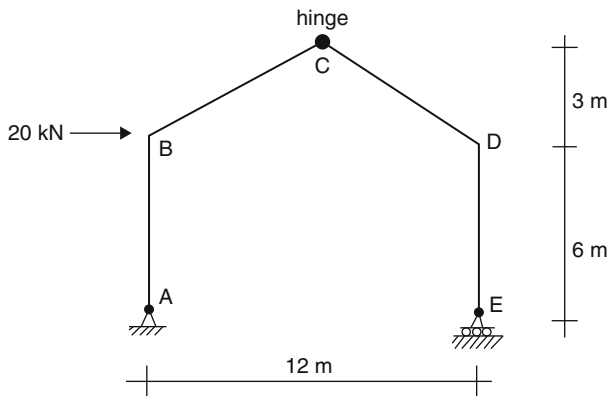


Fig. E4.8a

Solution:

Step 1: Reactions

The reactions (Fig. E4.8b) are determined by summing moments about A and C and applying the force equilibrium conditions.

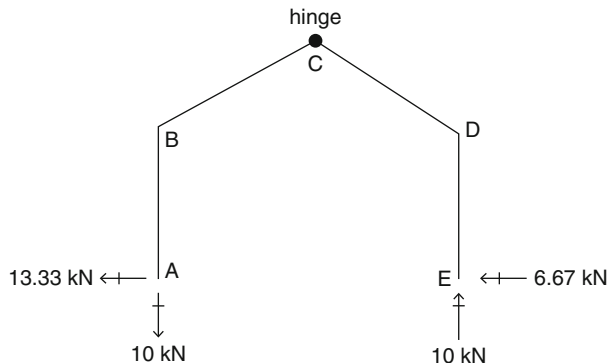


Fig. E4.8b Reactions

Step 2: End forces—global frame (Fig. E4.8c)

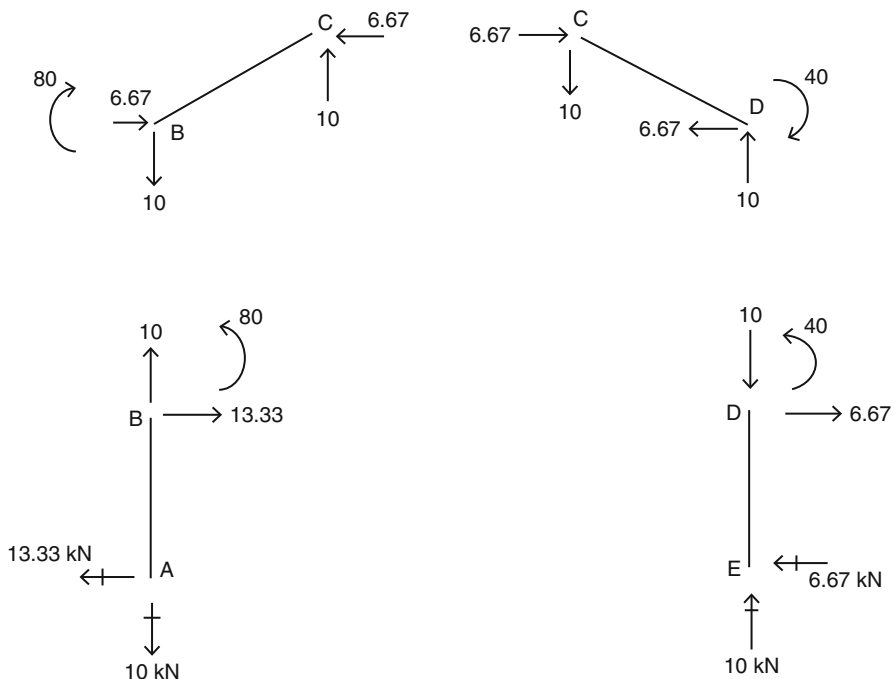


Fig. E4.8c End forces

Step 3: End forces—local member frame

Figure E4.8d shows the end forces and moments resolved into components referred to the local member frame.

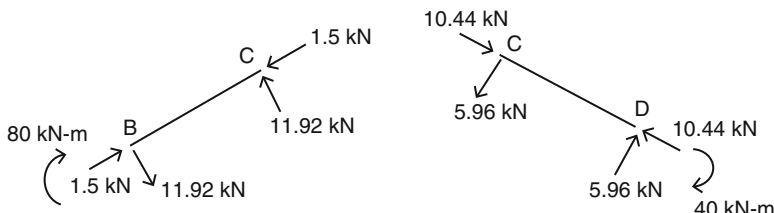


Fig. E4.8d End actions in local member frame

Step 4: Internal force distribution (Fig. E4.8e)

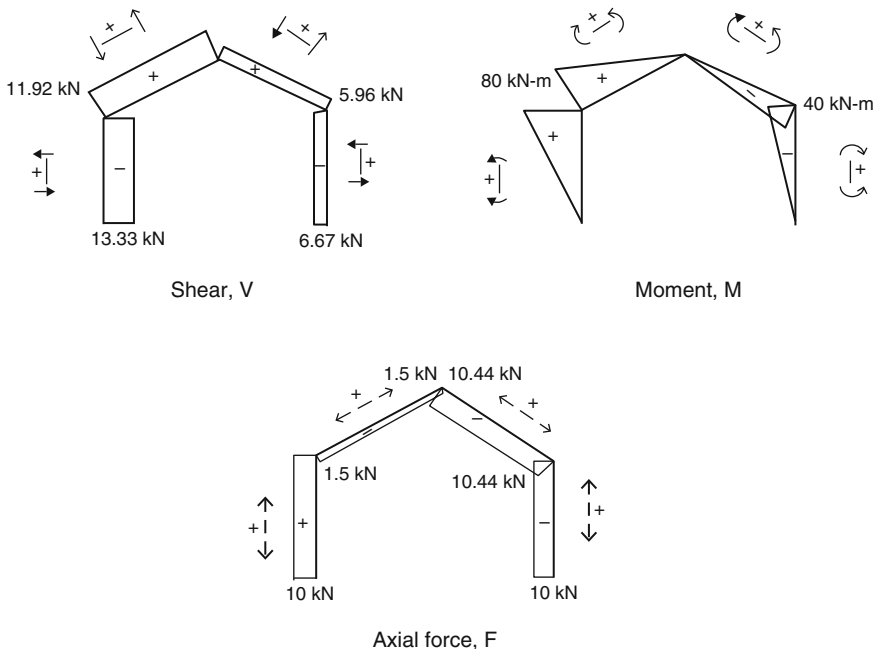


Fig. E4.8e Force distributions

Note that the 3-hinge gable structure has a lower value of peak moment.

Example 4.9 Simply supported gable frame—unsymmetrical loading

Given: The frame defined in Fig. E4.9a. The loading consists of a vertical load per horizontal projection applied to member BC.

Determine: The member force diagrams.

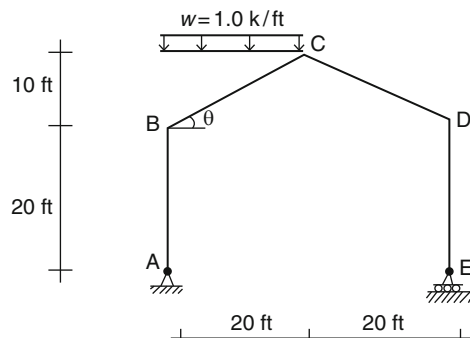
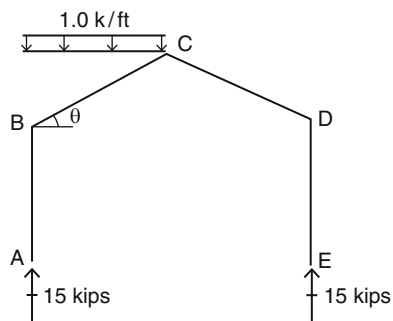


Fig. E4.9a

Solution: The reactions at E and A are determined by summing moments about A and by enforcing vertical equilibrium. Figure E4.9b shows the results.

Fig. E4.9b Reactions



Next we determine the end forces and moments for the individual members. Then, we need to resolve the loading and the end forces for members BC and CD into normal and tangential components. The transformed quantities are listed in Figs. E4.9c, d.

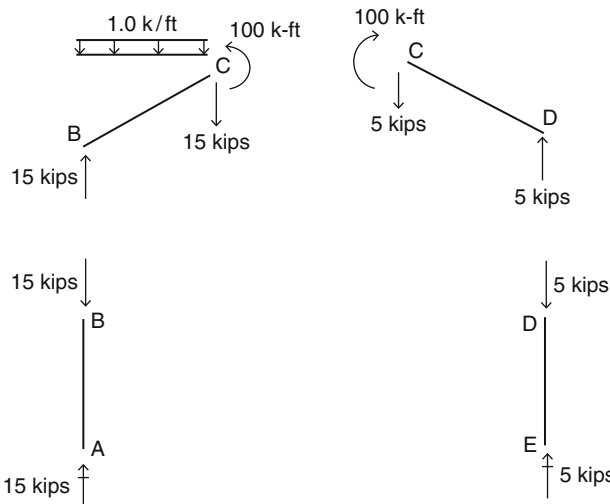


Fig. E4.9c End actions—global frame

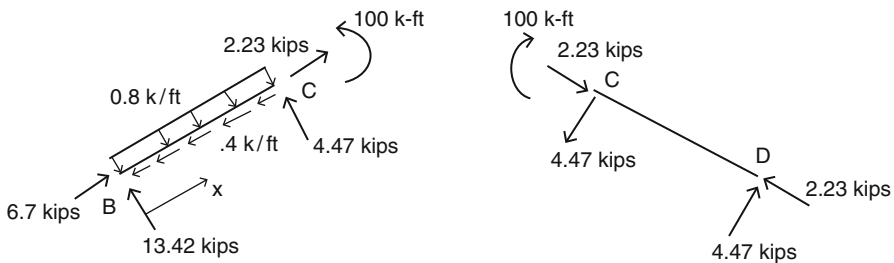


Fig. E4.9d End actions—local frame

The maximum moment in member BC occurs at x_1 . We determine the location by setting the shear equal to zero.

$$13.42 - 0.8x_1 = 0 \Rightarrow x_1 = 16.775$$

Then $M_{\max} = 13.42(16.775) - 0.8(16.775)^2(\frac{1}{2}) = 112.56 \text{ kip ft}$

Figure E4.9e contains the shear, moment, and axial force diagrams.

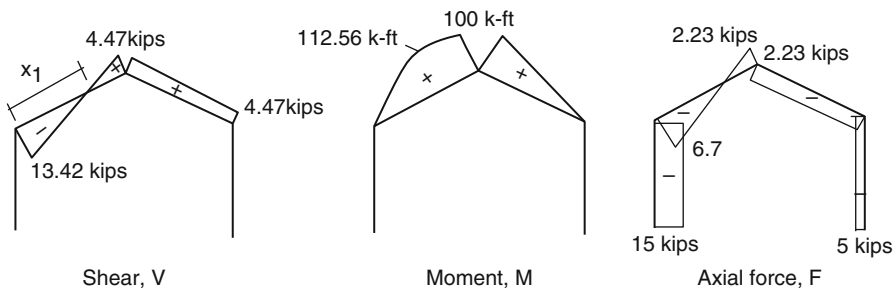


Fig. E4.9e

Example 4.10 3-Hinge gable frame

Given: The 3-hinge gable frame shown in Fig. E4.10a.

Determine: The shear and moment diagrams.

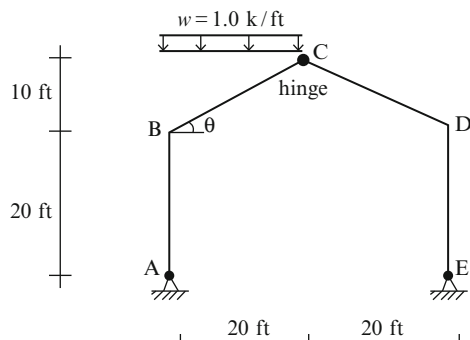


Fig. E4.10a

Solution: We analyzed a similar loading condition in Example 4.9. The results for the different analysis phases are listed in Figs. E4.10b–d. Comparing Fig. E4.10e with Fig. E4.9e shows that there is a substantial *reduction* in the magnitude of the maximum moment when the 3-hinged gable frame is used.

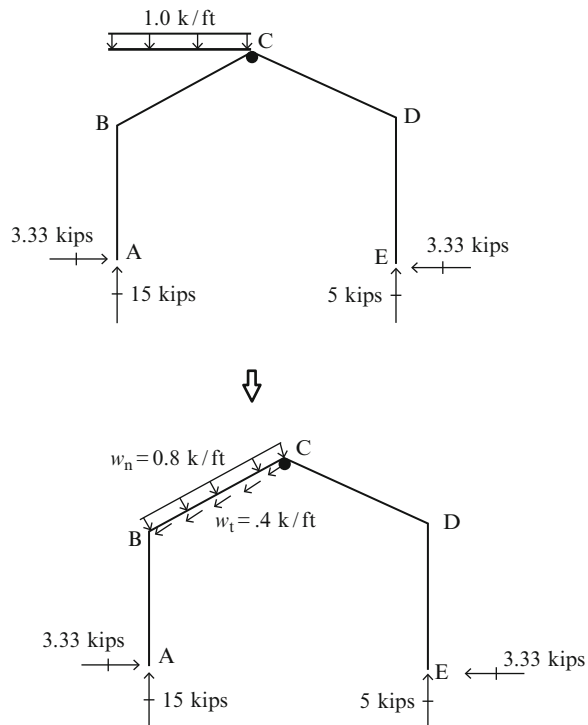
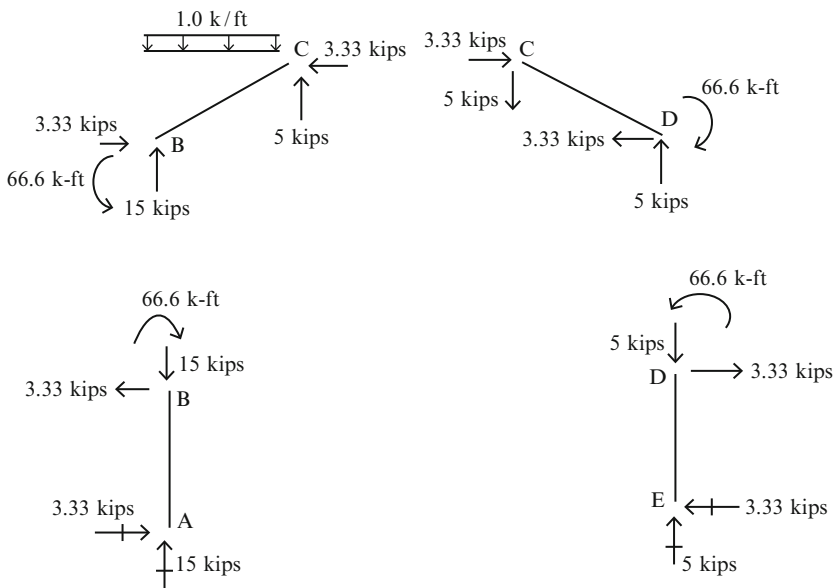
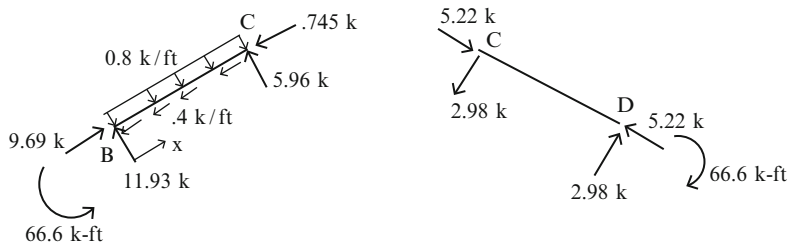


Fig. E4.10b Reactions

**Fig. E4.10c** End forces**Fig. E4.10d** End forces in local frame

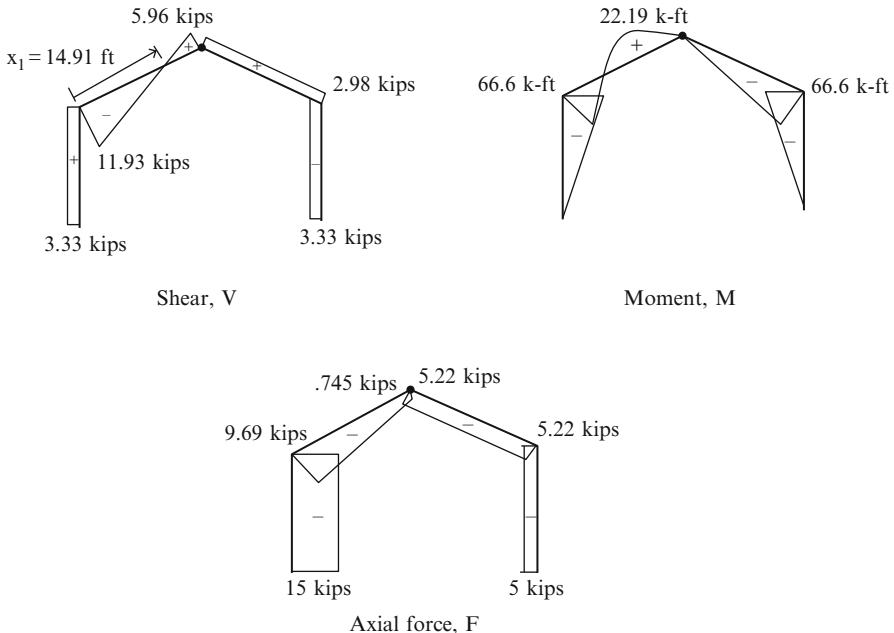


Fig. E4.10e Shear and moment diagrams

4.5 A-Frames

A-frames are obviously named for their geometry. Loads may be applied at the connection points or on the members. A-frames are typically supported at the base of their legs. Because of the nature of the loading and restraints, the members in an A-frame generally experience bending as well as axial force.

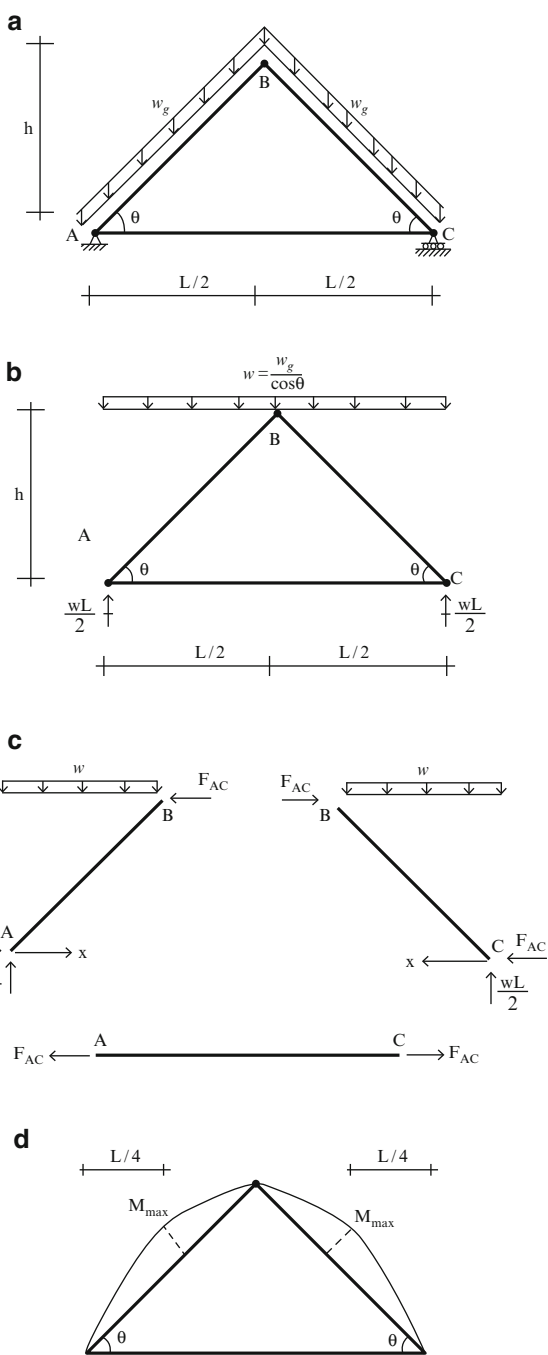
We consider first the triangular frame shown in Fig. 4.24. The inclined members are subjected to a uniform distributed loading per unit length w_g which represents the self-weight of the members and the weight of the roof that is supported by the member.

We convert w_g to an equivalent vertical loading per horizontal projection w using (4.3). We start the analysis process by first finding the reactions at A and C.

Next, we isolate member BC (see Fig. 4.24c).

$$\begin{aligned} \sum M_{\text{at } B} &= -\frac{w}{2} \left(\frac{L}{2}\right)^2 + \frac{wL}{2} \left(\frac{L}{2}\right) - hF_{AC} = 0 \\ &\Downarrow \\ F_{AC} &= \frac{wL^2}{8h} \end{aligned}$$

Fig. 4.24 (a) Geometry and loading. (b) A-frame loading and reactions. (c) Free body diagrams. (d) Moment diagram



The horizontal internal force at B must equilibrate F_{AC} . Lastly, we determine the moment distribution in members AB and BC. Noting Fig. 4.24c, the bending moment at location x is given by

$$M(x) = \frac{wL}{2}x - F_{AC}\left(\frac{2h}{L}\right)x - \frac{wx^2}{2} = \frac{wL}{4}x - \frac{wx^2}{2}$$

The maximum moment occurs at $x = L/4$ and is equal to

$$M_{\max} = \frac{wL^2}{32}$$

Replacing w with w_g , we express M_{\max} as

$$M_{\max} = \left(\frac{w_g}{\cos\theta}\right)\frac{L^2}{32}$$

As θ increases, the moment increases even though the projected length of the member remains constant.

We discuss next the frame shown in Fig. 4.25a. There are two loadings: a concentrated force at B and a uniform distributed loading applied to DE.

We first determine the reactions and then isolate member BC.

Summing moments about A leads to

$$P\left(\frac{L}{2}\right) + \frac{wL}{2}\left(\frac{L}{2}\right) = R_C L \quad R_C = \frac{P}{2} + \frac{wL}{4}$$

The results are listed below.

Noting Fig. 4.25d, we sum moments about B to determine the horizontal component of the force in member DE.

$$\begin{aligned} \frac{L}{2}\left(\frac{P}{2} + \frac{wL}{4}\right) &= \frac{wL}{4}\frac{L}{4} + \frac{h}{2}F_{de} \\ F_{de} &= \frac{PL}{2h} + \frac{wL^2}{8h} \end{aligned}$$

The bending moment distribution is plotted in Fig. 4.25e. Note that there is bending in the legs even though P is applied at node A. This is due to the location of member DE. If we move member DE down to the supports A and C, the moment in the legs would vanish.

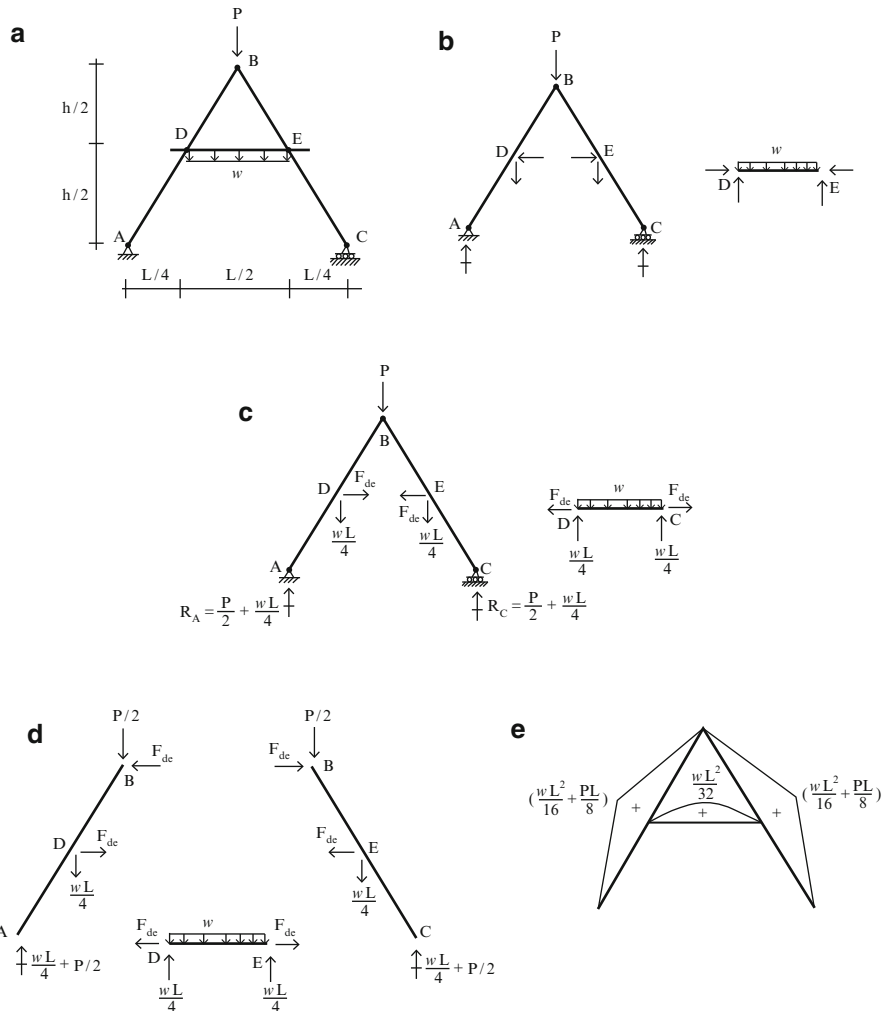


Fig. 4.25 (a) A-frame geometry and loading. (b), (c), (d) Free body diagrams. (e) Bending moment distribution

4.6 Deflection of Frames Using the Principle of Virtual Forces

The Principle of Virtual Forces specialized for a planar frame structure subjected to planar loading is derived in Ref. [16]. The general form is

$$\delta \delta P = \sum_{\text{members}} \int_s \left\{ \frac{M}{EI} \delta M + \frac{F}{AE} \delta F + \frac{V}{GA_s} \delta V \right\} ds \quad (4.7)$$

Frames carry loading primarily by bending action. Axial and shear forces are developed as a result of the bending action, but the contribution to the displacement produced by shear deformation is generally small in comparison to the displacement associated with bending deformation and axial deformation. Therefore, we neglect this term and work with a reduced form of the principle of Virtual Forces.

$$d \delta P = \sum_{\text{members}} \int_s \left\{ \frac{M}{EI} \delta M + \frac{F}{AE} \delta F \right\} ds \quad (4.8)$$

where δP is either a unit force (for displacement) or a unit moment (for rotation) in the direction of the desired displacement d ; δM and δF are the virtual moment and axial force due to δP . The integration is carried out over the length of each member and then summed up.

For low-rise frames, i.e., where the ratio of height to width is on the order of unity, the axial deformation term is also small. In this case, one neglects the axial deformation term in (4.8) and work with the following form

$$d \delta P = \sum_{\text{members}} \int_s \left(\frac{M}{EI} \right) (\delta M) ds \quad (4.9)$$

Axial deformation is significant for tall buildings, and (4.8) is used for this case. In what follows, we illustrate the application of the Principle of Virtual Forces to some typical low-rise structures. We revisit this topic later in Chap. 9, which deals with statically indeterminate frames.

Example 4.11 Computation of deflections—cantilever-type structure

Given: The structure shown in Fig. E4.11a. Assume EI is constant.

$$E = 29,000 \text{ ksi}, I = 300 \text{ in.}^4$$

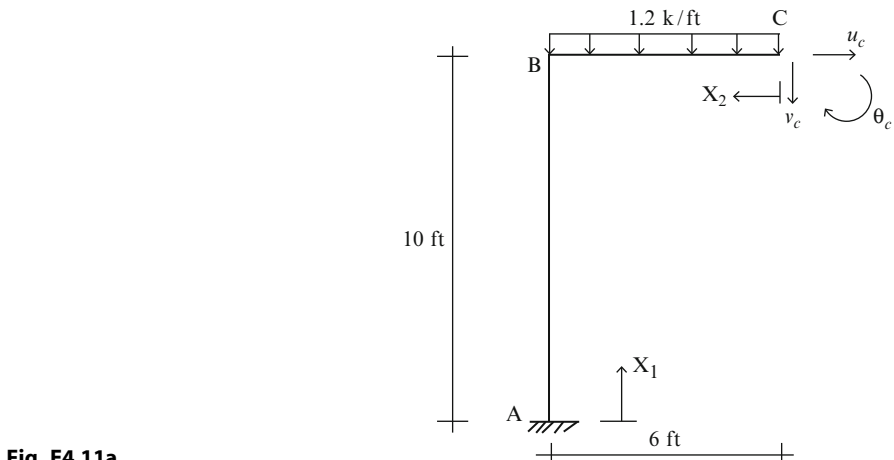


Fig. E4.11a

Determine: The horizontal and vertical deflections and the rotation at point C, the tip of the cantilever segment.

Solution: We start by evaluating the moment distribution corresponding to the applied loading. This is defined in Fig. E4.11b. The virtual moment distributions corresponding to u_c , v_c , θ_c are defined in Figs. E4.11c–e. Note that we take δP to be either a unit force (for displacement) or a unit moment (for rotation).

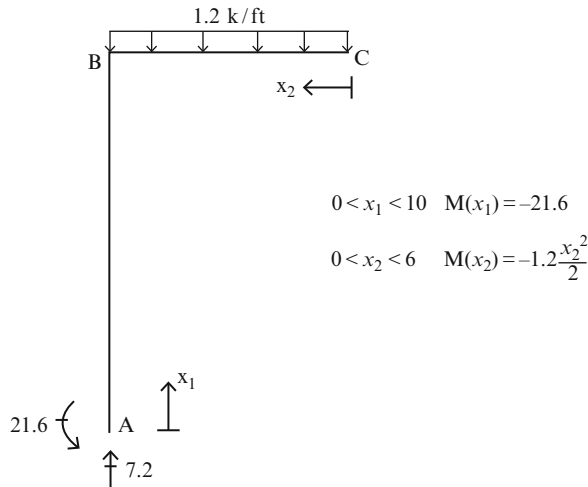


Fig. E4.11b $M(x)$

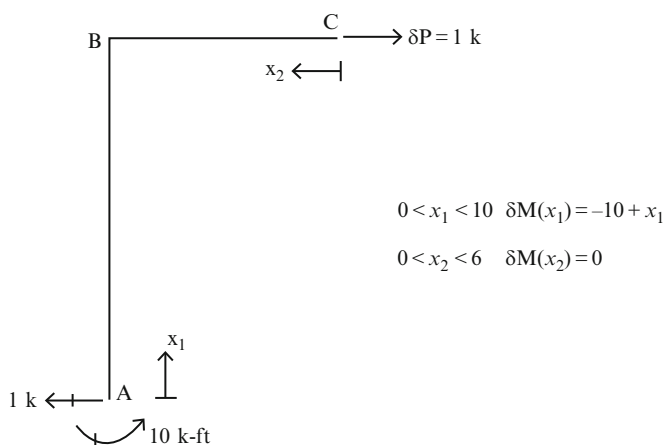
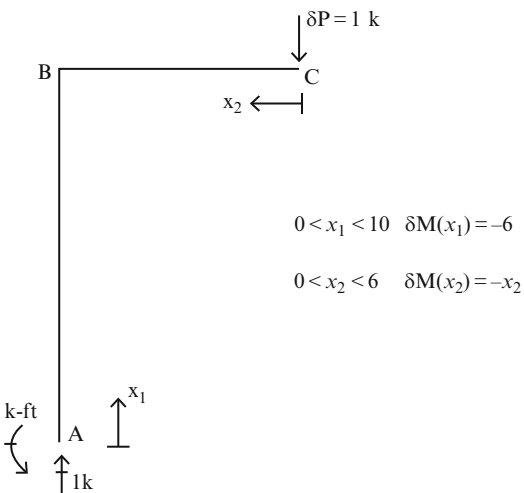
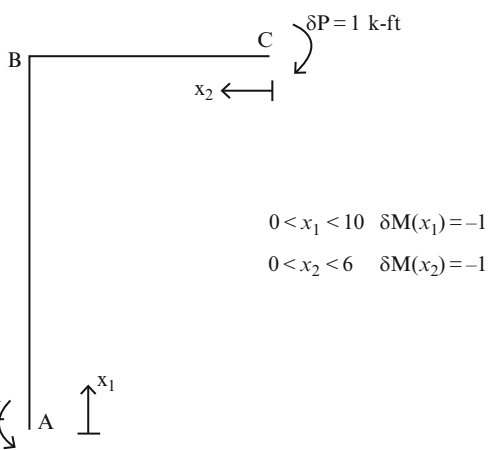


Fig. E4.11c $\delta M(x)$ for u_c

Fig. E4.11d $\delta M(x)$ for v_c **Fig. E4.11e** $\delta M(x)$ for θ_c 

We divide up the structure into two segments AB and CB and integrate over each segment. The total integral is given by

$$\sum_{\text{members}} \int_s \left(\frac{M}{EI} \delta M \right) ds = \int_{AB} \left(\frac{M}{EI} \delta M \right) dx_1 + \int_{AB} \left(\frac{M}{EI} \delta M \right) dx_2$$

The expressions for u_c , v_c , and θ_c are generated using the moment distributions listed above.

$$EIu_C = \int_0^{10} (-21.6)(-10 + x_1) dx_1 = 1,080 \text{ kip ft}^3$$

$$u_C = \frac{1,080(12)^3}{29,000(300)} = 0.2145 \text{ in.} \rightarrow$$

$$EIv_C = \int_0^{10} (-21.6)(-6) dx_1 + \int_0^6 \left(-\frac{1.2}{2}x_2^2\right)(-x_2) dx_2 = 1,490 \text{ kip ft}^3$$

$$v_C = \frac{1,490(12)^3}{29,000(300)} = 0.296 \text{ in.} \downarrow$$

$$EI\theta_C = \int_0^{10} (-21.6)(-1) dx_1 + \int_0^6 \left(-\frac{1.2}{2}x_2^2\right)(-1) dx_2 = 259 \text{ kip ft}^2$$

$$\theta_C = \frac{259(12)^2}{29,000(300)} = 0.0043 \text{ rad clockwise}$$

Example 4.12 Computation of deflections

Given: The structure shown in Fig. E4.12a. $E = 29,000 \text{ ksi}$, $I = 900 \text{ in.}^4$

Determine: The horizontal displacements at points C and D and the rotation at B.

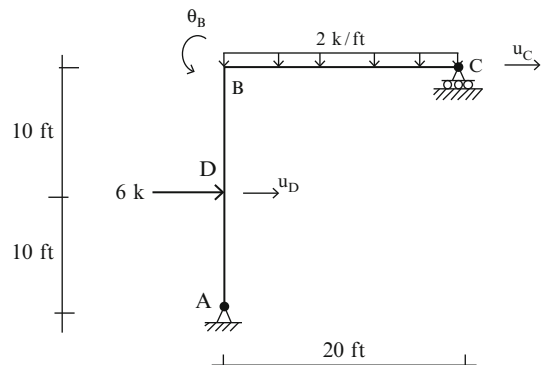
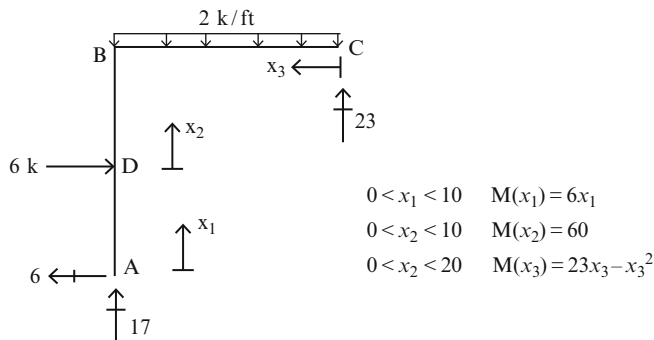
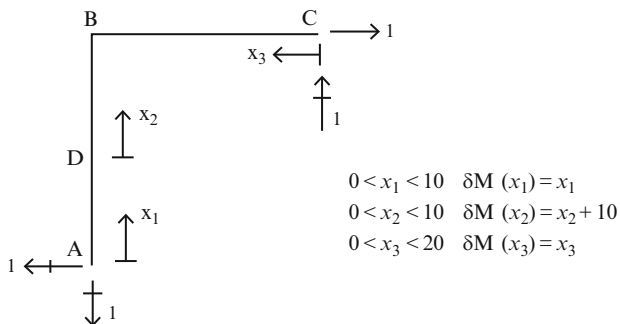
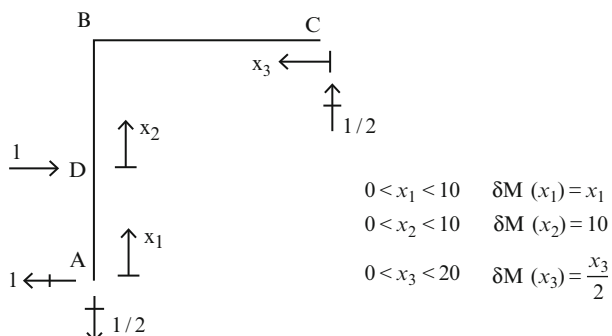


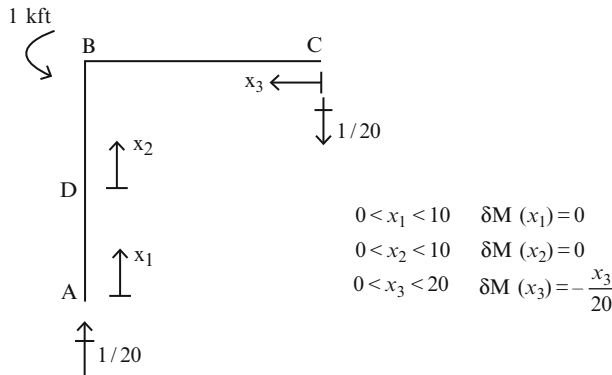
Fig. E4.12a

Solution: We start by evaluating the moment distribution corresponding to the applied loading. This is defined in Fig. E4.12b.

**Fig. E4.12b** $M(x)$

The virtual moment distributions corresponding to u_c and u_D are listed in Figs. E4.12c, d.

**Fig. E4.12c** δM for u_C **Fig. E4.12d** δM for u_D

**Fig. E4.12e** δM for θ_B

We express the total integral as the sum of three integrals.

$$\sum_{\text{members}} \int_s \left(\frac{M}{EI} \delta M \right) ds = \int_{AD} \left(\frac{M}{EI} \delta M \right) dx_1 + \int_{DB} \left(\frac{M}{EI} \delta M \right) dx_2 + \int_{CB} \left(\frac{M}{EI} \delta M \right) dx_3$$

The corresponding form for u_c is

$$\begin{aligned}
 EIu_C &= \int_0^{10} 6x_1(x_1) dx_1 + \int_0^{10} (x_2 + 10)(60) dx_2 + \int_0^{20} (23x_3 - x_3^2)(x_3) dx_3 \\
 &= |2x_1^3|_0^{10} + |30x_2^2 + 600x_2|_0^{10} + \left| \frac{23x_3^3}{3} - \frac{x_3^4}{4} \right|_0^{20} = 32,333 \text{ kip ft}^3 \\
 u_C &= \frac{32,333 \times (12)^3}{(29,000)(900)} = 2.14 \text{ in.} \rightarrow
 \end{aligned}$$

Following a similar procedure, we determine u_D

$$\begin{aligned}
 EIu_D &= \int_0^{10} 6x_1(x_1) dx_1 + \int_0^{10} 60(10) dx_2 + \int_0^{20} (23x_3 - x_3^2) \left(\frac{x_2}{3} \right) dx_3 \\
 &= |2x_1^3|_0^{10} + |600x_2|_0^{10} + \left| \frac{23x_3^3}{6} - \frac{1}{8}x_3^4 \right|_0^{20} = 18,667 \text{ kip ft}^3 \\
 u_D &= \frac{18,667(12)^3}{(29,000)(300)} = 3.7 \text{ in.} \rightarrow
 \end{aligned}$$

Lastly, we determine θ_B (Fig. E4.12e)

$$EI\theta_B = \int_0^{20} (23x_3 - x_3^2) \left(-\frac{x_3}{20} \right) dx_3$$

$$= \left| -\frac{23x_3^3}{60} + \frac{x_3^4}{80} \right|_0^{20} = -1,066.67 \text{ kip ft}^2$$

$$\theta_B = -\frac{1,066.67(12)^2}{(29,000)(900)} = -0.0059$$

The minus sign indicates the sense of the rotation is opposite to the initial assumed sense.

$$\theta_B = .0059 \text{ rad} \quad \curvearrowleft$$

Example 4.13 Computation of deflection

Given: The steel structure shown in Figs. E4.13a–c. Take $I_b = \frac{4}{3}I_c$, $h_C = 4 \text{ m}$, $L_b = 3 \text{ m}$, $P = 40 \text{ kN}$, and $E = 200 \text{ GPa}$.

Determine: The value of I_c required to limit the horizontal displacement at C to be equal to 40 mm.

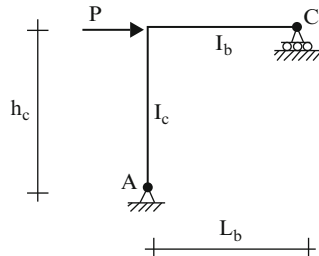
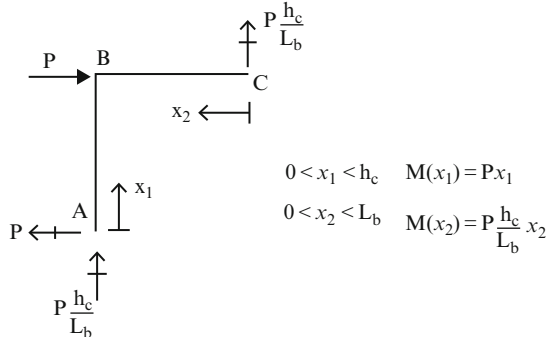
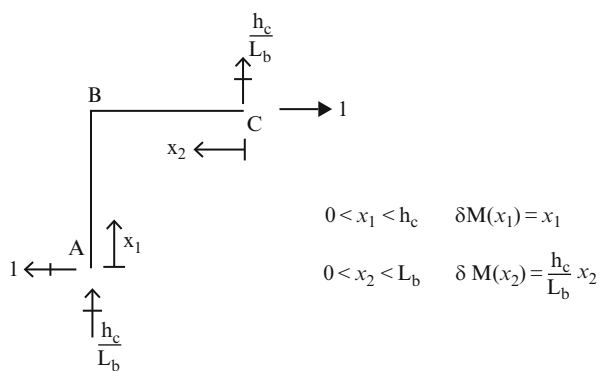


Fig. E4.13a

Solution: We divide up the structure into two segments and express the moments in terms of the local coordinates x_1 and x_2 .

Fig. E4.13b $M(x)$ **Fig. E4.13c** δM for u_C 

We express the total integral as the sum of two integrals.

$$\sum_{\text{members}} \int_s \left(\frac{M}{EI} \delta M \right) ds = \int_{AB} \left(\frac{M}{EI} \delta M \right) dx_1 + \int_{CB} \left(\frac{M}{EI} \delta M \right) dx_2$$

The corresponding expression for u_C is

$$\begin{aligned}
 u_C &= \frac{1}{EI_c} \int_0^{h_c} (Px_1)(x_1) dx_1 + \frac{1}{EI_b} \int_0^{L_b} \left(P \frac{h_c}{L_b} x_2 \right) \left(\frac{h_c}{L_b} x_2 \right) dx_2 \\
 &\Downarrow \\
 u_C &= \frac{P}{EI_c} \int_0^{h_c} (x_1)^2 dx_1 + \frac{P}{EI_b} \left(\frac{h_c}{L_b} \right)^2 \int_0^{L_b} (x_2)^2 dx_2 \\
 &\Downarrow \\
 u_C &= \frac{Ph_c^3}{3EI_c} + \frac{PL_b^3}{3EI_b} \left(\frac{h_c}{L_b} \right)^2
 \end{aligned}$$

Then, for $I_b = \frac{4}{3}I_c$, the I_c required is determined with

$$\begin{aligned} u_C &= \frac{Ph_c^2}{3E} \left(\frac{h_c}{I_c} + \frac{L_b}{I_b} \right) = \frac{40(4,000)^2}{3(200)} \left(\frac{4,000}{I_c} + \frac{3,000}{(4/3)I_c} \right) = 40 \rightarrow I_c \\ &= 166(10)^6 \text{ mm}^4 \end{aligned}$$

Example 4.14 Computation of Deflection—non-prismatic member

Given: The non-prismatic concrete frame shown in Figs. E4.14a–d.

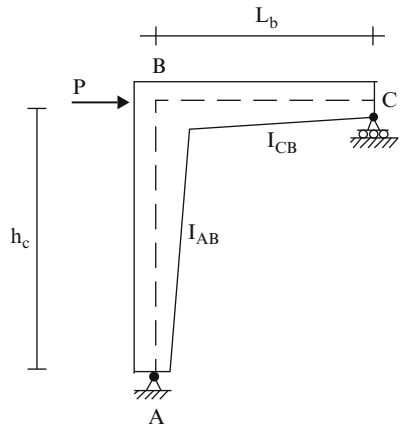


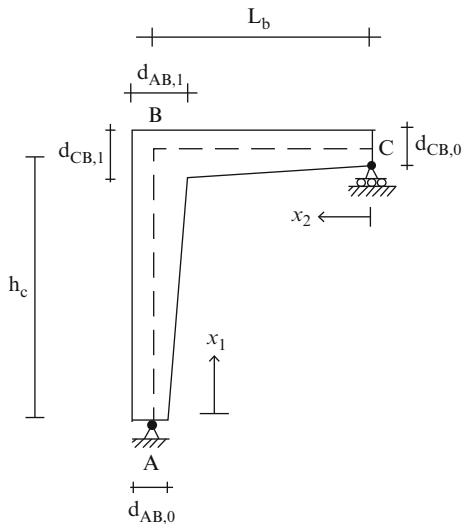
Fig. E4.14a

Take $h_c = 12 \text{ ft}$, $L_b = 10 \text{ ft}$, $P = 10 \text{ kip}$, and $E = 4 \text{ ksi}$. Consider the member depths (d) to vary linearly and the member widths (b) to be constant. Assume the following geometric ratios::

$$d_{AB,1} = 2d_{AB,0}$$

$$d_{CB,1} = 1.5d_{CB,0}$$

$$b = \frac{d_{AB,0}}{2}$$

Fig. E4.14b**Determine:**

- A general expression for the horizontal displacement at C. Use numerical integration to evaluate \$u_C\$ as a function of \$d_{AB,0}\$.
- The value of \$d_{AB,0}\$ for which \$u_C = 1.86\$ in.

Solution:

Part (a): The member depth varies linearly. For member AB,

$$\begin{aligned} d(x_1) &= d_{AB,0} \left(1 - \frac{x_1}{h} \right) + d_{AB,1} \left(\frac{x_1}{h} \right) = d_{AB,0} \left\{ 1 + \frac{x_1}{h} \left(\frac{d_{AB,1}}{d_{AB,0}} - 1 \right) \right\} \\ &= d_{AB,0} g_{AB} \left(\frac{x_1}{h} \right) \end{aligned}$$

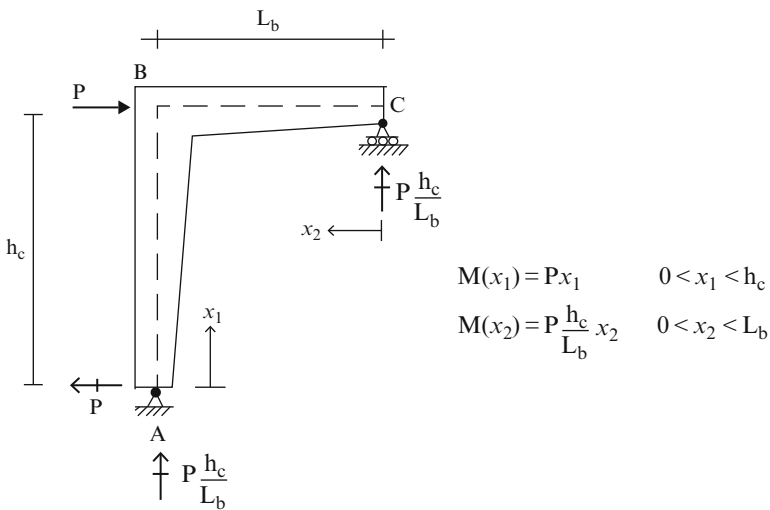
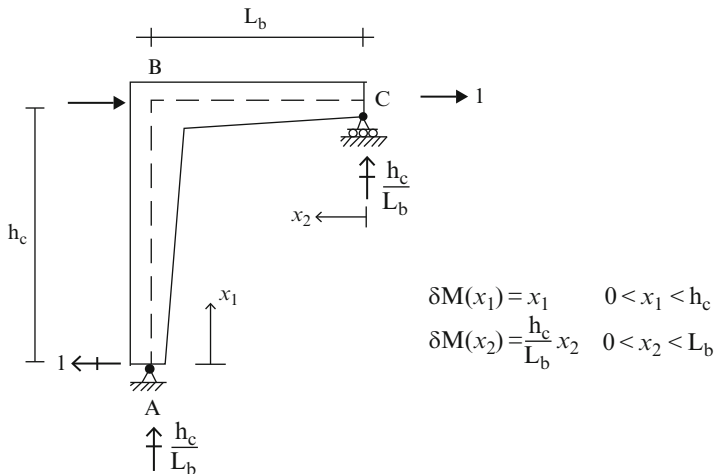
Then

$$I_{AB} = d_{AB,0} (g_{AB})^3$$

Similarly, for member BC

$$\begin{aligned} d(x_2) &= d_{CB,0} \left\{ 1 + \frac{x_2}{L_b} \left(\frac{d_{CB,1}}{d_{CB,0}} - 1 \right) \right\} = d_{CB,0} g_{CB} \left(\frac{x_2}{L_b} \right) \\ I_{CB} &= d_{CB,0} (g_{CB})^3 \end{aligned}$$

We express the moments in terms of the local coordinates \$x_1\$ and \$x_2\$.

**Fig. E4.14c** $M(x)$ **Fig. E4.14d** δM for u_C

We express the total integral as the sum of two integrals.

$$\sum_{\text{members}} \int_s \left(\frac{M}{EI} \delta M \right) ds = \int_{AB} \left(\frac{M}{EI} \delta M \right) dx_1 + \int_{CB} \left(\frac{M}{EI} \delta M \right) dx_2$$

The corresponding expression for u_C is

$$u_C = \frac{1}{E} \int_0^{h_c} \frac{1}{I_{AB}} (Px_1)(x_1) dx_1 + \frac{1}{E} \int_0^{L_b} \frac{1}{I_{CB}} \left(P \frac{h_c}{L_b} x_2 \right) \left(\frac{h_c}{L_b} x_2 \right) dx_2$$

Substituting for I_{AB} and I_{CB} and expressing the integral in terms of the dimensionless values $x_1/h = \bar{x}_1$ and $x_2/L_b = \bar{x}_2$, the expression for u_C reduces to

$$u_C = \frac{P(h_c)^3}{EI_{AB,0}} \int_0^1 \frac{(\bar{x}_1)^2 d\bar{x}_1}{(g_{AB})^3} + \frac{P(h_c/L_b)^2 (L_b)^3}{EI_{CB,0}} \int_0^1 \frac{(\bar{x}_2)^2 d\bar{x}_2}{(g_{CB})^3}$$

Taking $g_{AB} = g_{CB} = 1$ leads to the values for the integrals obtained in Example 3.13, i.e., 1/3.

Part (b): Using the specified sections, the g functions take the form

$$\begin{aligned} g_{AB} &= 1 + \frac{\bar{x}_1}{h} = 1 + \bar{x}_1 \\ g_{CB} &= 1 + \frac{1}{2} \frac{\bar{x}_2}{L_b} = 1 + \frac{1}{2} \bar{x}_2 \end{aligned}$$

Then, the problem reduces to evaluating the following integrals:

$$J_1 = \int_0^1 \frac{(\bar{x}_1)^2 d\bar{x}_1}{(1 + \bar{x}_1)^3} \quad \text{and} \quad J_2 = \int_0^1 \frac{(\bar{x}_2)^2 d\bar{x}_2}{(1 + (1/2)\bar{x}_2)^3}$$

We compute these values using the trapezoidal rule. Results for different interval sizes are listed below.

| N | J_1 | J_2 |
|-----|--------|--------|
| 10 | 0.0682 | 0.1329 |
| 20 | 0.0682 | 0.1329 |
| 25 | 0.0682 | 0.1329 |
| 30 | 0.0682 | 0.1329 |

Next, we specify the inertia terms

$$\begin{aligned} I_{AB,0} &= \frac{b(d_{AB,0})^3}{12} \\ I_{BC,0} &= \frac{b(d_{CB,0})^3}{12} \end{aligned}$$

For $I_{AB,0} = (3/4)I_{CB,0}$, the expression for u_C reduces to

$$u_C = \frac{P}{EI_{AB,0}} \left\{ h_c^3 J_1 + \left(\frac{h_c}{L_b}\right)^2 (L_b)^3 \left(\frac{3}{4}\right) (J_2) \right\}$$

Then, setting $u_C = 1.86$ in. and solving for $I_{AB,0}$ leads to

$$I_{AB,0} = \frac{P}{Eu_C} \left\{ h_c^3 J_1 + \left(\frac{h_c}{L_b}\right)^2 (L_b)^3 \left(\frac{3}{4}\right) (J_2) \right\} = 606.2 \text{ in.}^2$$

Finally

$$d_{AB,0} = \{24I_{AB,0}\}^{1/4} = 10.98 \text{ in.}$$

$$d_{CB,0} = \left\{\frac{4}{3}\right\}^{1/3} d_{AB,0} = 12.1 \text{ in.}$$

4.7 Deflection Profiles: Plane Frame Structures

Applying the principle of Virtual Forces leads to specific displacement measures. If one is more interested in the overall displacement response, then it is necessary to generate the displacement profile for the frame. We dealt with a similar problem in Chap. 3, where we showed how to sketch the deflected shapes of beams given the bending moment distributions.

We follow essentially the same approach in this section. Once the bending moment is known, one can determine the curvature, as shown in Fig. 4.26.

In order to establish the deflection profile for the entire frame, one needs to construct the profile for each member, and then join up the individual shapes such as that the displacement restraints are satisfied. We followed a similar strategy for planar beam-type structures; however, the process is somewhat more involved for plane frames.

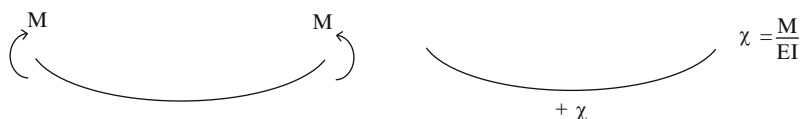
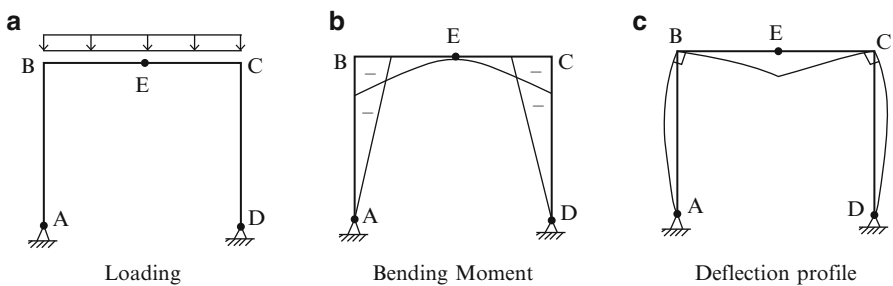
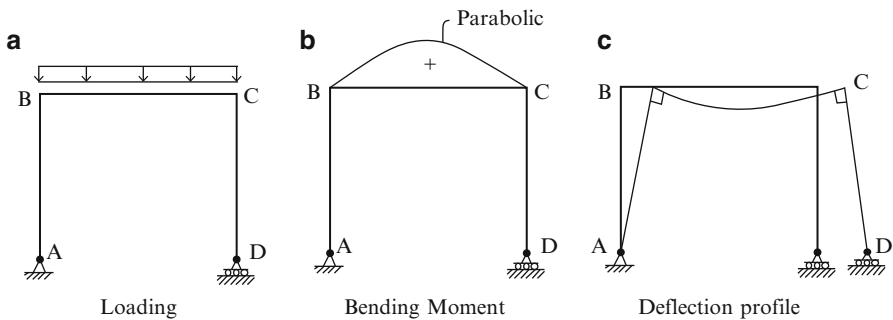


Fig. 4.26 Moment-curvature relationship



Consider the portal frame shown in Fig. 4.27. Bending does not occur in AB and CD since the moment is zero. Therefore, these members must remain straight. However, BC bends into a concave shape. The profile consistent with these constraints is plotted below. Note that B, C, and D move laterally under the vertical loading.

Suppose we convert the structure into the 3-hinge frame defined in (Fig. 4.28). Now, the moment diagram is negative for all members.

In this case, the profile is symmetrical. There is a discontinuity in the slope at E because of the moment release.

Gable frames are treated in a similar manner. The deflection profiles for simply supported and 3-hinge gable frames acted upon by gravity loading are plotted below (Figs. 4.29 and 4.30).

The examples presented so far have involved gravity loading. Lateral loading is treated in a similar way. One first determines the moment diagrams, and then establishes the curvature patterns for each member. Lateral loading generally produces lateral displacements as well as vertical displacements. Typical examples are listed below (Figs. 4.31, 4.32, and 4.33).

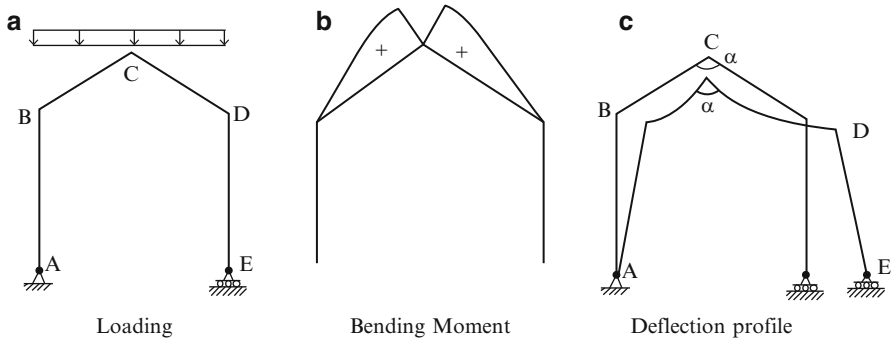


Fig. 4.29 Simply supported gable frame

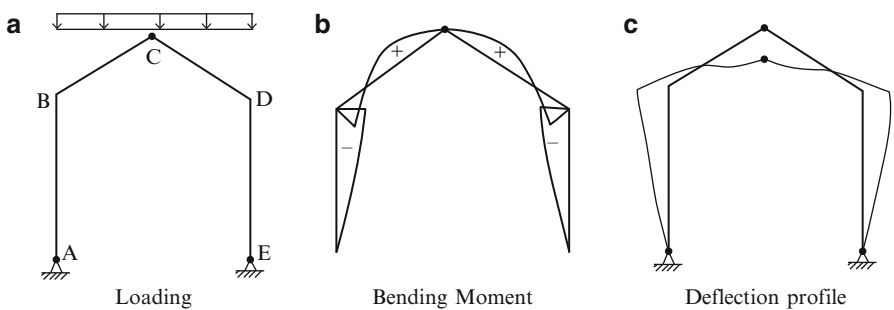


Fig. 4.30 3-Hinge gable frame

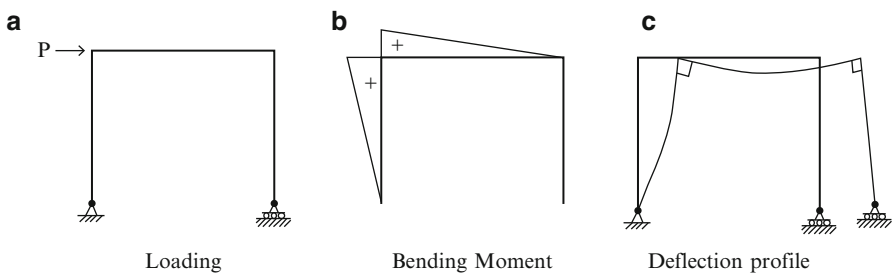


Fig. 4.31 Portal frame

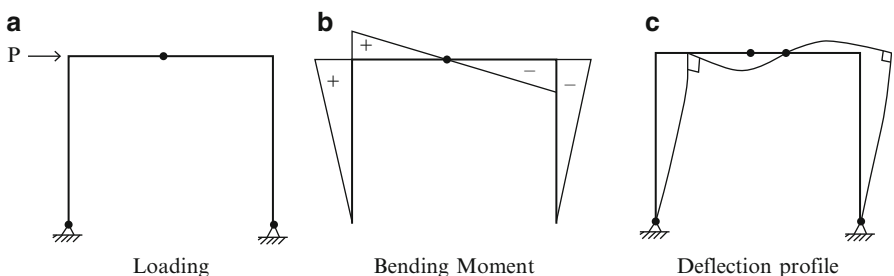


Fig. 4.32 3-Hinge frame

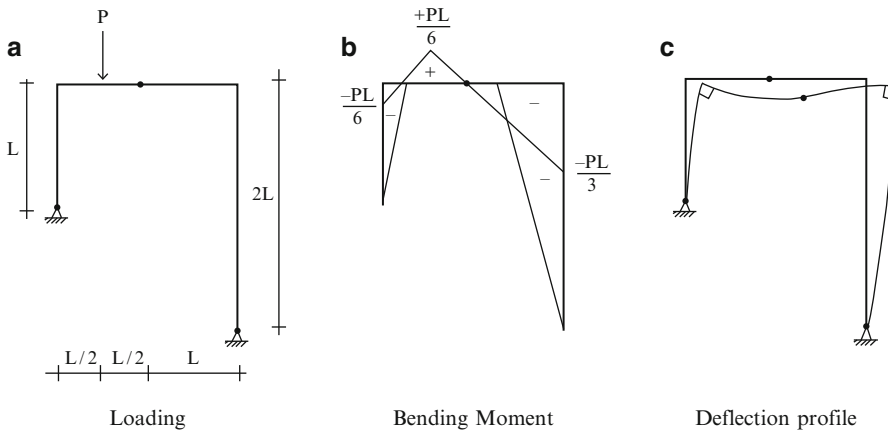


Fig. 4.33 3-Hinge frame

4.8 Computer-Based Analysis: Plane Frames

When there are multiple loading conditions, constructing the internal force diagrams and displacement profiles is difficult to execute manually. One generally resorts to computer-based analysis methods specialized for frame structures.

Consider the gable plane frame shown in Fig. 4.34. One starts by numbering the nodes and members, and defines the nodal coordinates and member incidences. Next, one specifies the nodal constraints. For plane frames, there are two coordinates and three displacement variables for each node (two translations and one rotation). Therefore, there are three possible displacement restraints at a node. For this structure, there are two support nodes, nodes 1 and 5. At node 1, the X and Y translations are fully restrained, i.e., they are set to zero. At node 5, the Y translation is fully restrained.

Next, information related to the members, such as the cross-sectional properties (A, I), loading applied to the member, and releases such as internal moment releases are specified. Finally, one specifies the desired output. Usually, one is interested in shear and moment diagrams, nodal reactions and displacements, and the deflected shape. Graphical output is most convenient for visualizing the structural response. Typical output plots for the following cross-sectional properties $I_1 = 100 \text{ in.}^4$, $I_2 = 1,000 \text{ in.}^4$, $I_3 = 300 \text{ in.}^4$, $E = 29,000 \text{ ksi}$, $A_1 = 14 \text{ in.}^2$, $A_2 = 88 \text{ in.}^2$, and $A_3 = 22 \text{ in.}^2$ are listed in Fig. 4.35.

4.9 Plane Frames: Out of Plane Loading

Plane frames are generally used to construct three dimensional building systems. One arranges the frames in orthogonal patterns and connects them with bracing to form a stable system. Figure 4.36 illustrates this scheme. Gravity load is applied to

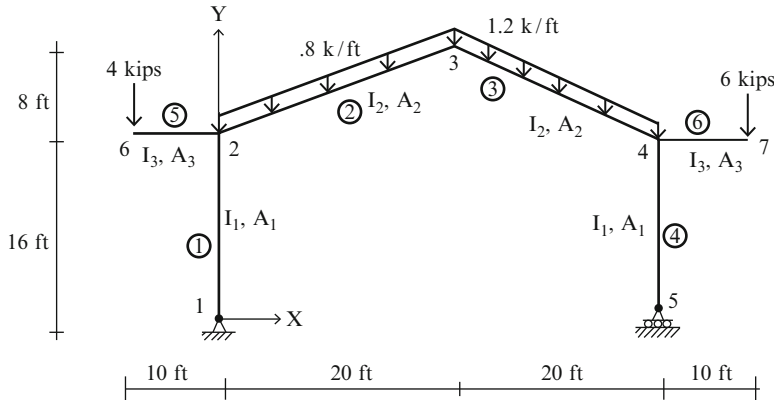


Fig. 4.34 Geometry and loading

the floor slabs. They transfer the load to the individual frames resulting in each frame being subjected to a planar loading. This mechanism is discussed in detail in Chap. 15.

Our interest here is the case where the loading acts normal to the plane frame. One example is the typical highway signpost shown in Fig. 4.37. The sign and the supporting member lie in a single plane. Gravity load acts in this plane. However, the wind load is normal to the plane and produces a combination of bending and twisting for the vertical support. One deals separately with the bending and torsion responses and then superimposes the results.

The typical signpost shown in Fig. 4.37 is statically determinate. We consider the free body diagram shown in Fig. 4.38. The wind load acting on the sign produces bending and twisting moment in the column. We use a double-headed arrow to denote the torsional moment.

$$\uparrow M_{tB} = P_w b$$

Of interest is the Y displacement at C. This motion results from the following actions:

Member BC bends in the $X-Y$ plane

$$v_c = \frac{P_w \left(\frac{b}{2}\right)^3}{3EI_2}$$

Member AB bends in the Y-Z plane

Fig. 4.35 Graphical output for structure defined in Fig. 4.34. (a) Displacement profile. (b) Bending moment, M . (c) Shear, V . (d) Axial force, F . (e) Reactions

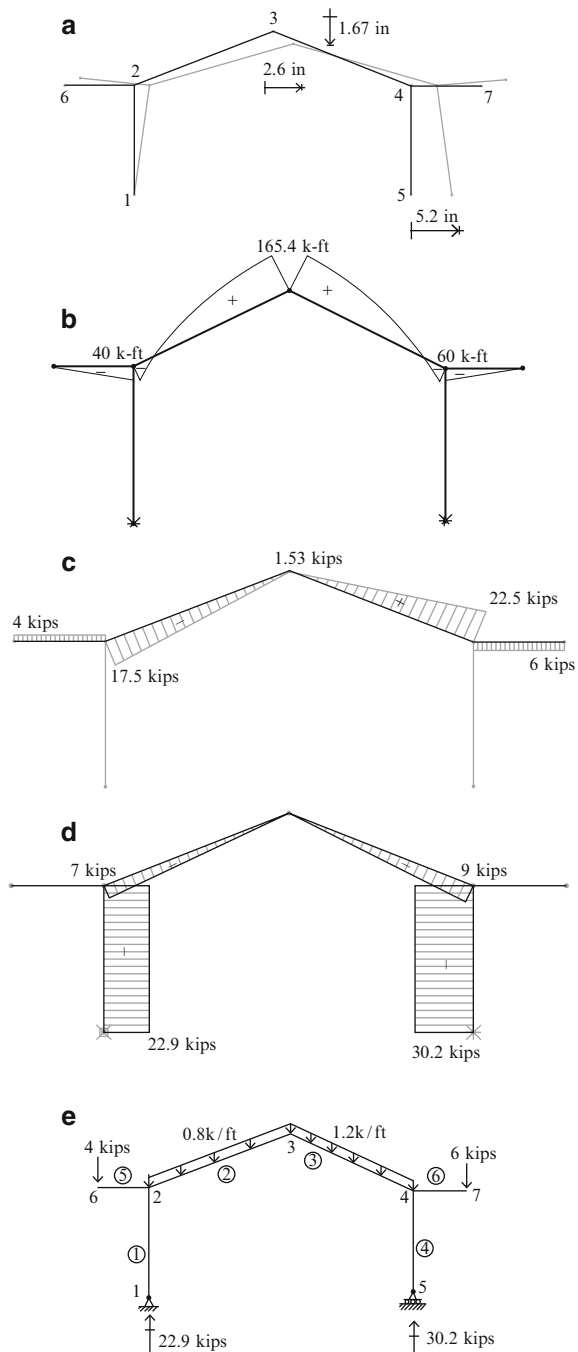


Fig. 4.36 A typical 3-D system of plane frames

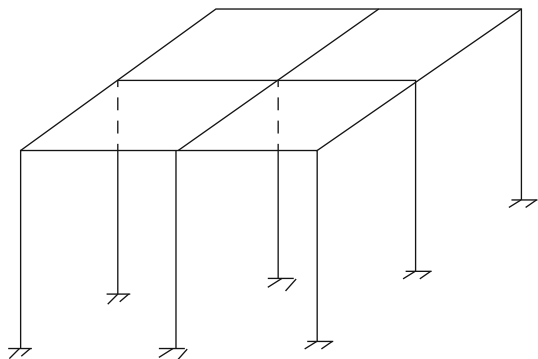


Fig. 4.37 Sign post structure

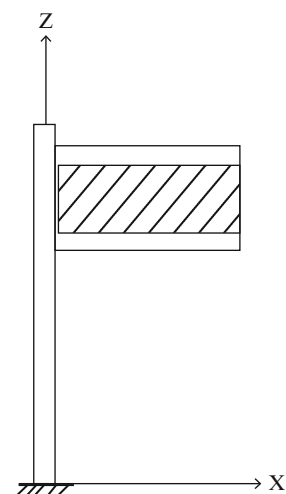
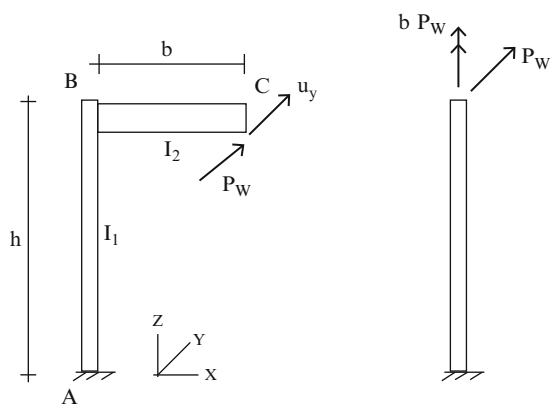


Fig. 4.38 Free body diagrams



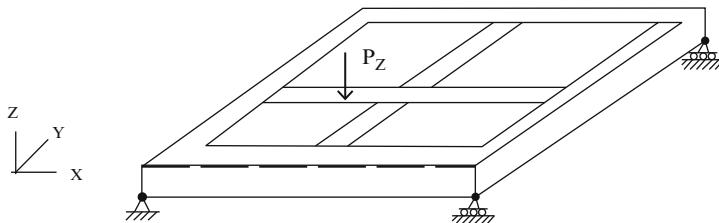


Fig. 4.39 Plane grid structure

$$v_B = \frac{P_w h^3}{3EI_1}$$

Node C displaces due to the rotation at B

$$v_c = \left(\frac{b}{2}\right)^2 \left(P_w \frac{h}{GJ}\right)$$

Summing the individual contributions leads to

$$v_{c \text{ total}} = P_w \left[\frac{b^3}{24EI_2} + \frac{h^3}{3EI_1} + \frac{b^2 h}{4GJ} \right]$$

Another example is the transversely loaded grid structure shown in Fig. 4.39. The members are rigidly connected at their ends and experience, depending on their orientation, bending in X-Z plane or the Y-Z plane, as well as twist deformation. Plane grids are usually supported at their corners. Sometimes, they are cantilevered out from one edge. Their role is to function as plate-type structures under transverse loading.

Plane grids are *statically indeterminate* systems. Manual calculations are not easily carried out for typical grids so one uses a computer analysis program. This approach is illustrated in Chap. 10.

4.10 Summary

4.10.1 Objectives

- To develop criteria for static determinacy of planar rigid frame structures
- To develop criteria for static determinacy of planar A-frame structures
- To present an analysis procedure for statically determinate portal and pitched roof plane frame structures subjected to vertical and lateral loads
- To compare the bending moment distributions for simple vs. 3-hinged portal frames under vertical and lateral loading

- To describe how the Principle of Virtual Forces is applied to compute the displacements of frame structures
- To illustrate a computer-based analysis procedure for plane frames
- To introduce the analysis procedure for out-of-plane loading applied to plane frames.

4.10.2 Key Concepts

- A planar rigid frame is statically determinate when $3m + r = 3j$, where m is the number of members, r is the number of displacement restraints, and j is the number of nodes.
- A planar A-frame is statically determinate when $3m = r + 2n_p$, where n_p is the number of pins, m is the number of members, and r is the number of displacement restraints.
- The Principle of Virtual Forces specialized for frame structures has the general form

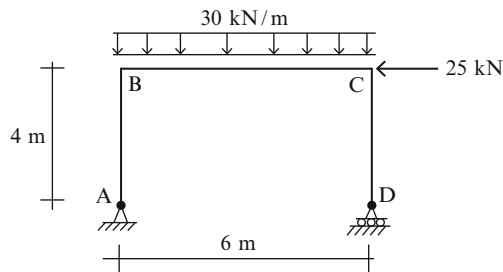
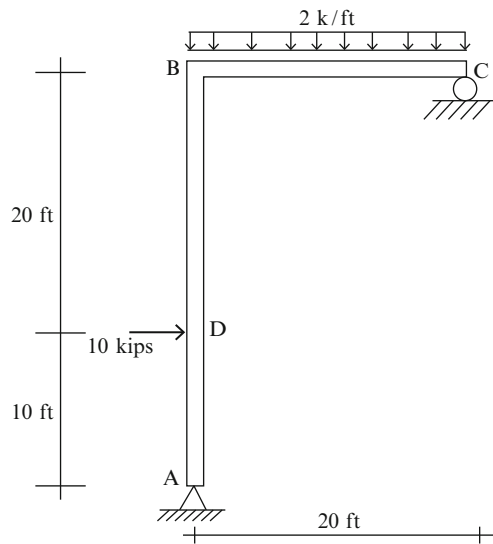
$$d \delta P = \sum_{\text{members}} \int \frac{M}{EI} \delta M ds + \sum_{\text{members}} \int \frac{F}{AE} \delta F ds$$

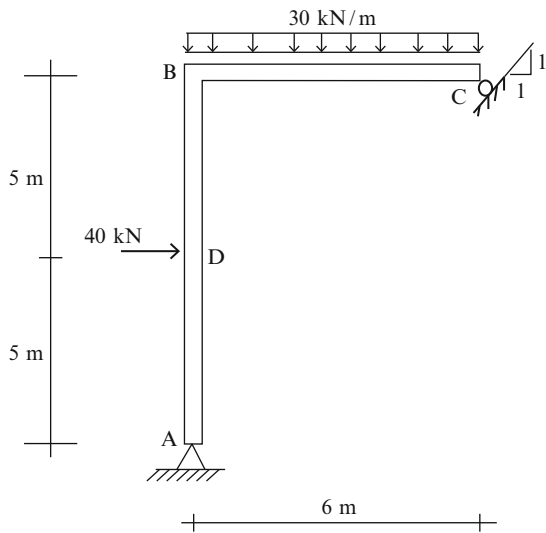
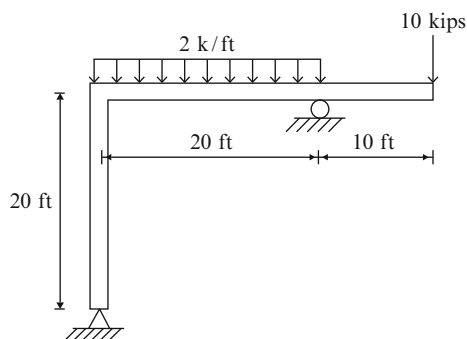
For low-rise frames, the axial deformation term is negligible.

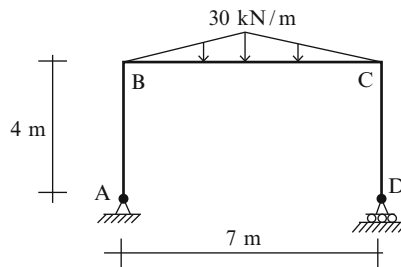
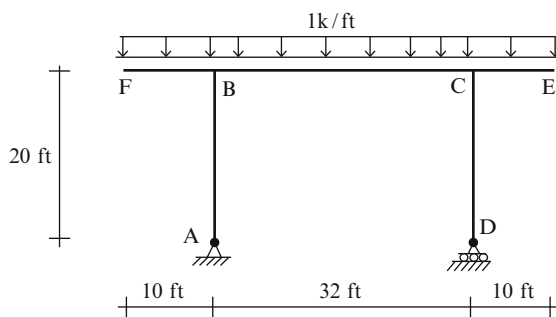
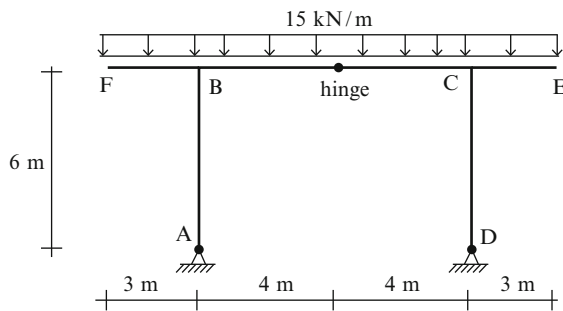
- The peak bending moments generated in 3-hinged frames by lateral loading are generally less than for simple portal frames.

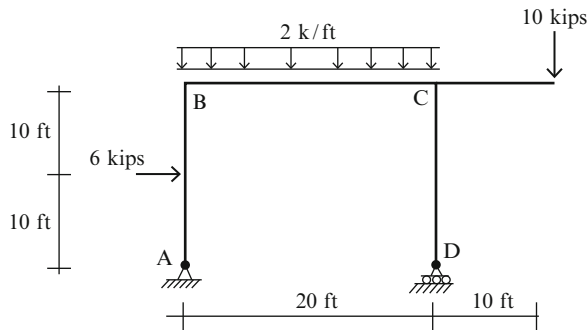
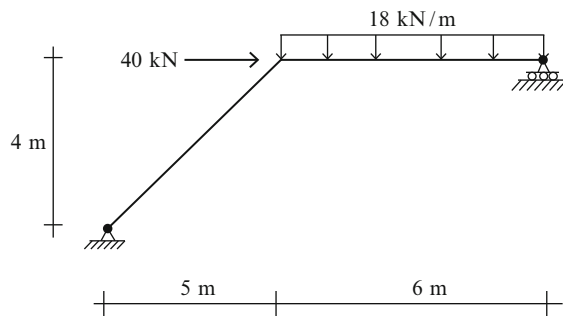
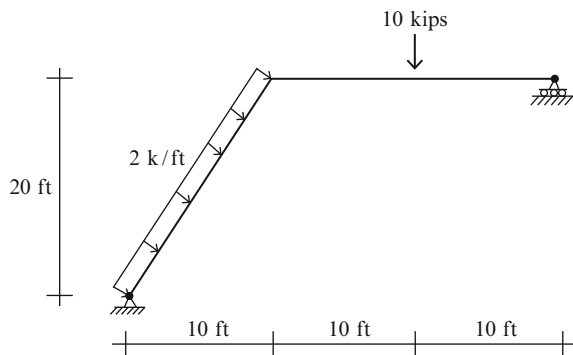
4.11 Problems

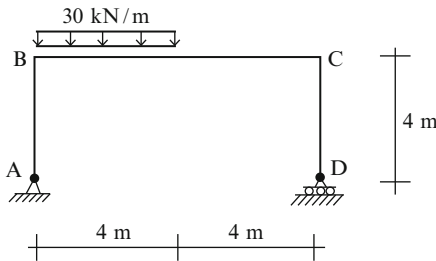
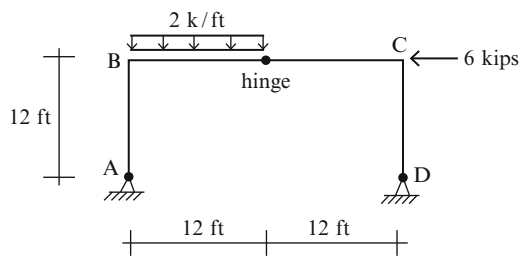
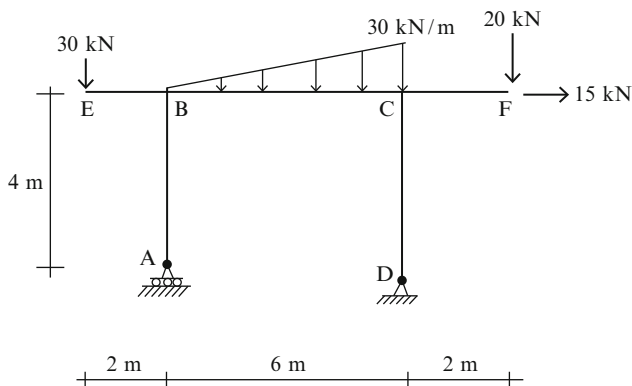
For the plane frames defined in Problems 4.1–4.20, determine the reactions, and shear and moment distributions.

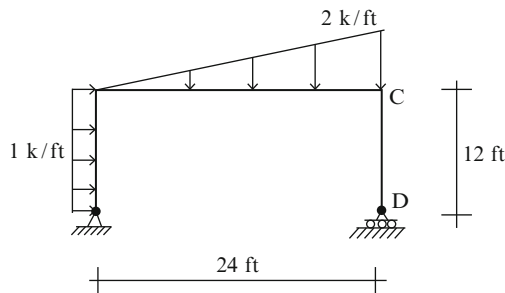
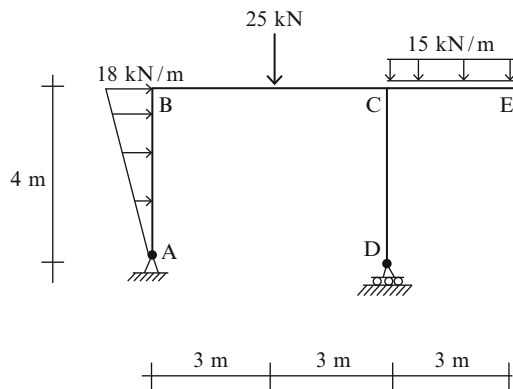
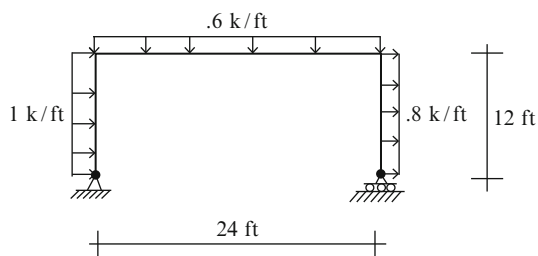
Problem 4.1**Problem 4.2**

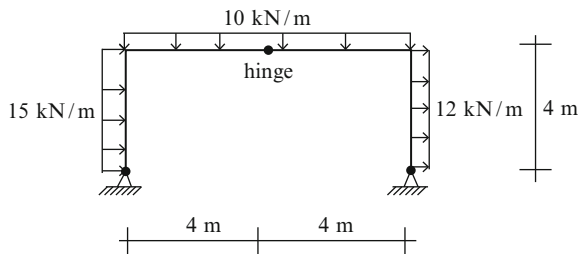
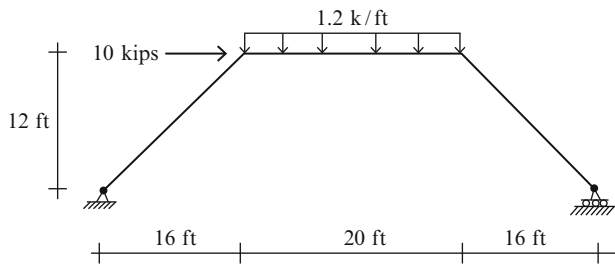
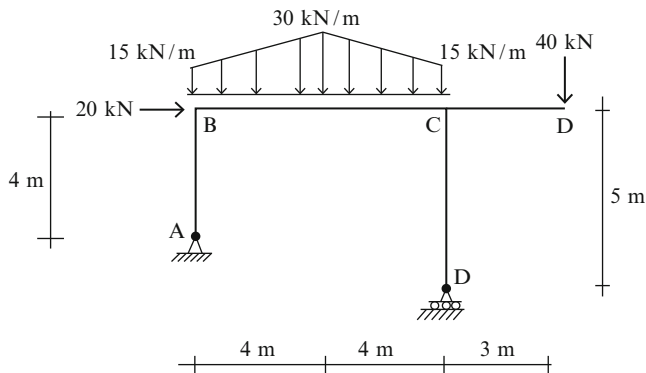
Problem 4.3**Problem 4.4**

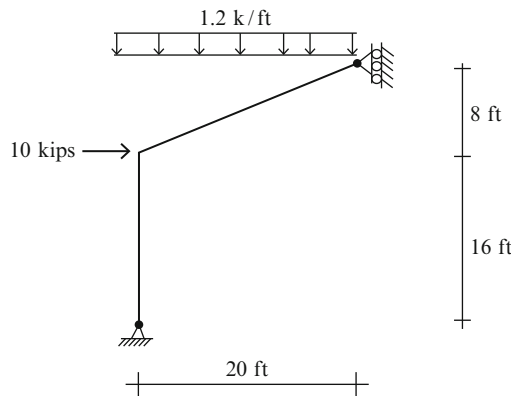
Problem 4.5**Problem 4.6****Problem 4.7**

Problem 4.8**Problem 4.9****Problem 4.10**

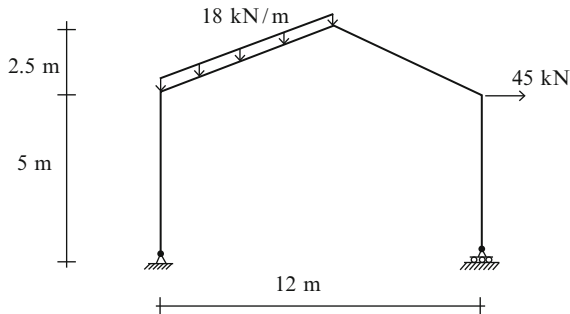
Problem 4.11**Problem 4.12****Problem 4.13**

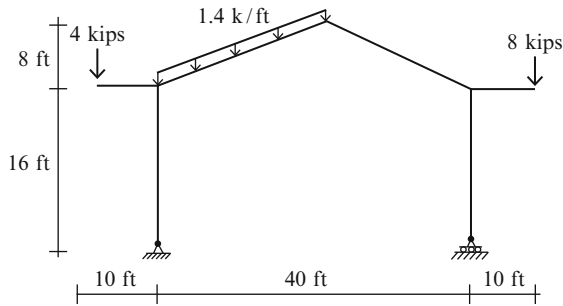
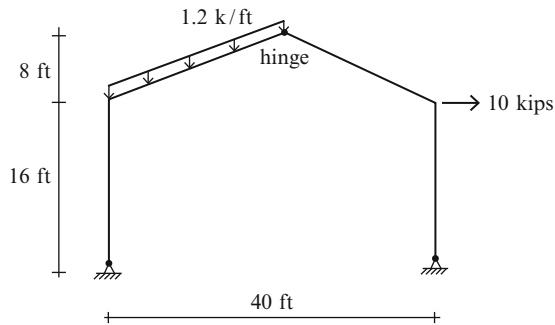
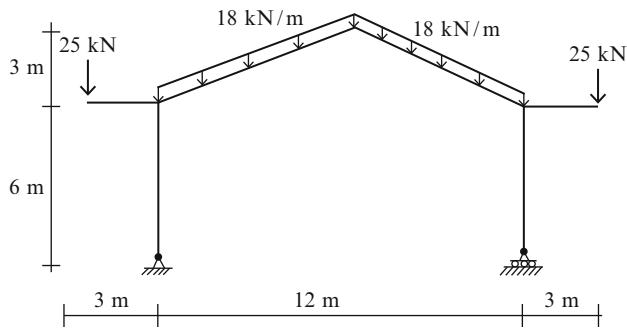
Problem 4.14**Problem 4.15****Problem 4.16**

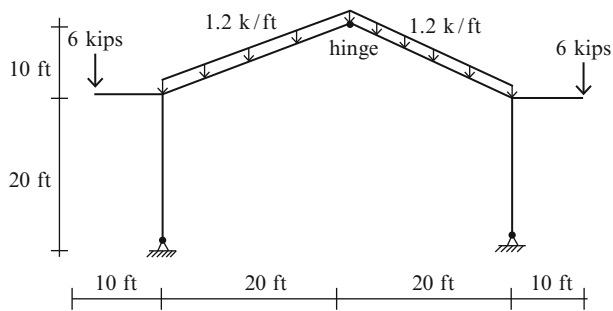
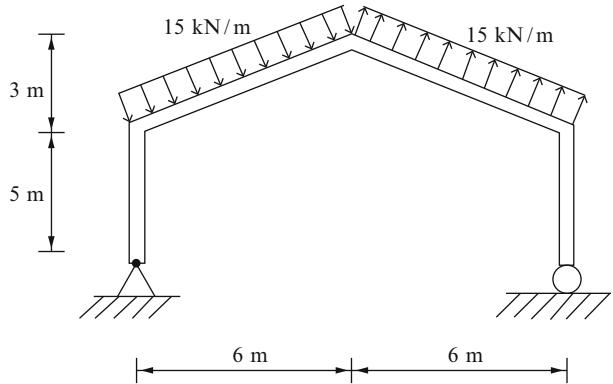
Problem 4.17**Problem 4.18****Problem 4.19**

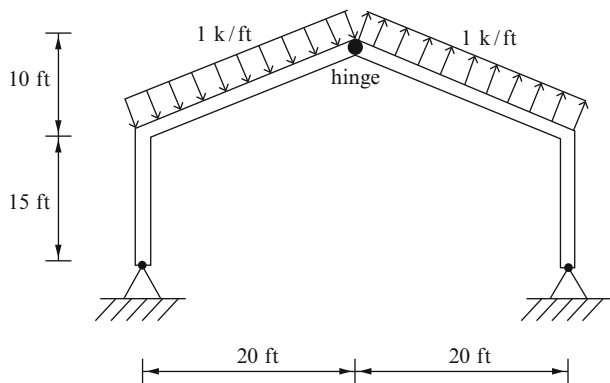
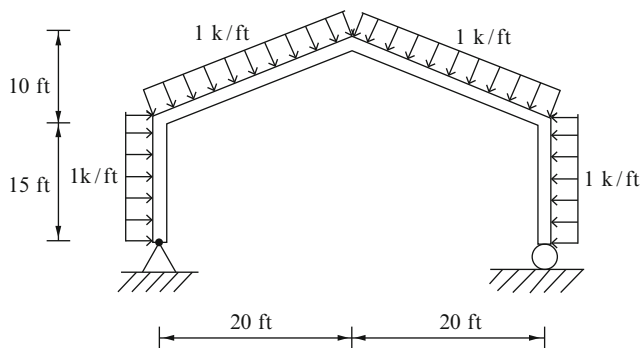
Problem 4.20

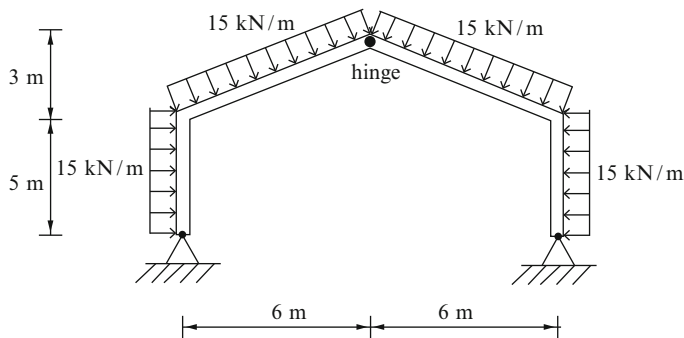
For the gable frames defined in Problems 4.21–4.29, determine the bending moment distributions.

Problem 4.21

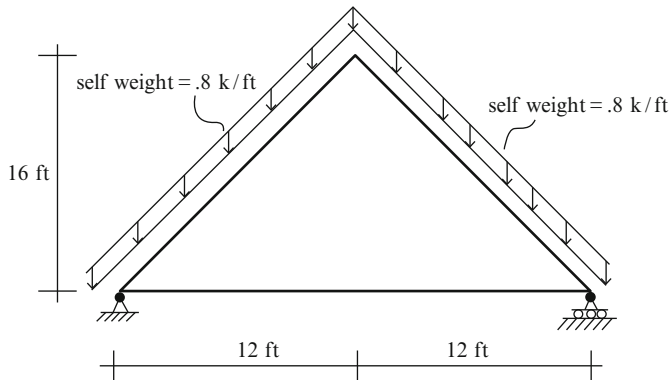
Problem 4.22**Problem 4.23****Problem 4.24**

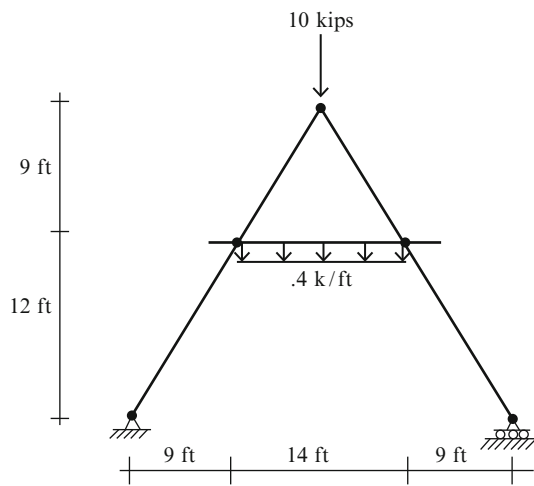
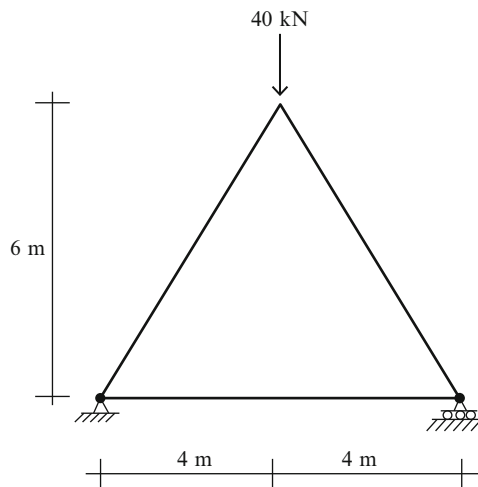
Problem 4.25**Problem 4.26**

Problem 4.27**Problem 4.28**

Problem 4.29

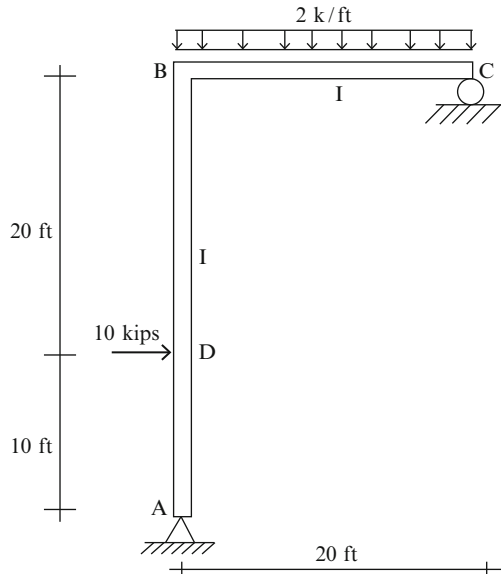
For the A-frames defined in Problems 4.30–4.32, determine the reactions and bending moment distribution.

Problem 4.30

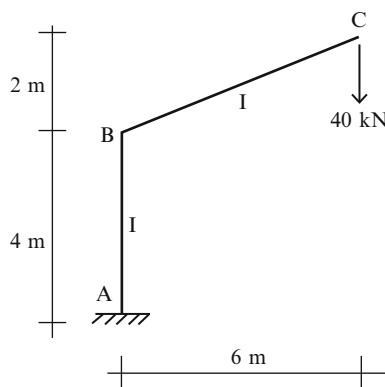
Problem 4.31**Problem 4.32**

Problem 4.33

Determine the horizontal deflection at D and the clockwise rotation at joint B. Take $E = 29,000$ ksi. Determine the I required to limit the horizontal displacement at D to 2 inches. Use the Virtual Force method.

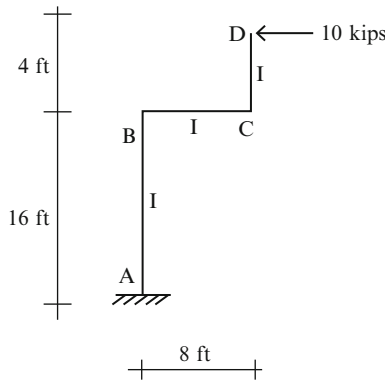
**Problem 4.34**

Determine the value of I to limit the vertical deflection at C to 30 mm. Take $E = 200$ GPa. Use the Virtual Force method.

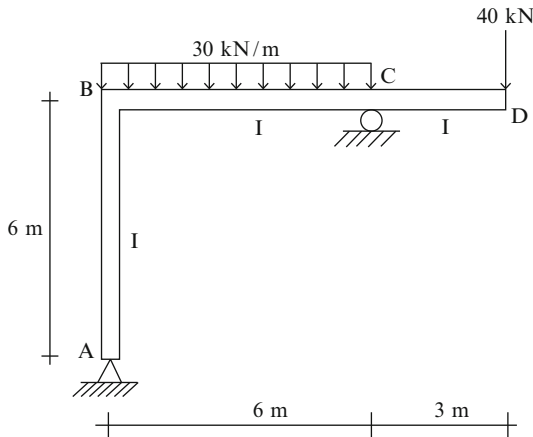


Problem 4.35

Determine the value of I required limiting the horizontal deflection at D to $\frac{1}{2}$ in. Take $E = 29,000$ ksi. Use the Virtual Force method.

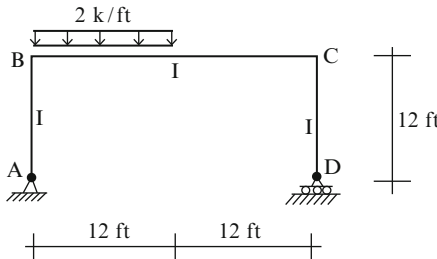
**Problem 4.36**

Determine the vertical deflection at D and the rotation at joint B. Take $E = 200$ GPa and $I = 60(10)^6$ mm 4 . Use the Virtual Force method.

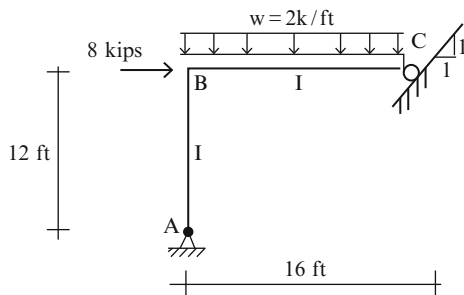


Problem 4.37

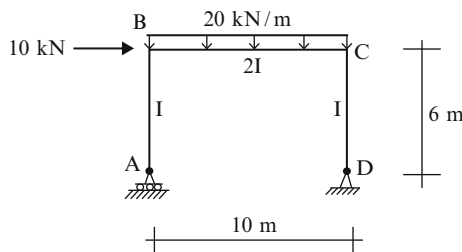
Determine the horizontal displacement at joint B. Take $E = 29,000$ ksi and $I = 200$ in.⁴ Use the Virtual Force method.

**Problem 4.38**

Determine the displacement at the roller support C. Take $E = 29,000$ ksi and $I = 100$ in.⁴ Use the Virtual Force method.

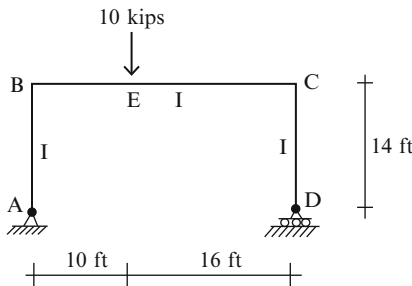
**Problem 4.39**

Determine the horizontal deflection at C and the rotation at joint B. Take $E = 200$ GPa and $I = 60(10)^6$ mm⁴. Use the Virtual Force method.

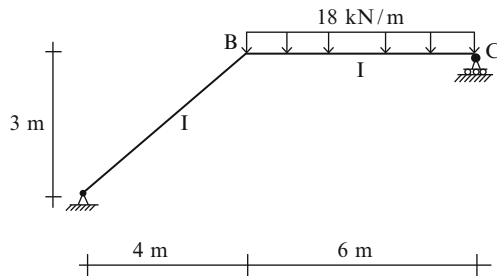


Problem 4.40

Determine the horizontal deflection at C and the vertical deflection at E. Take $E = 29,000$ ksi and $I = 160$ in.⁴ Use the Virtual Force method.

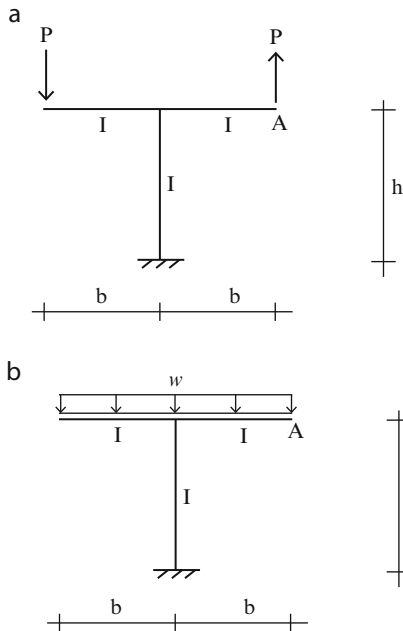
**Problem 4.41**

Determine the horizontal deflection at C. $I = 100(10)^6$ mm⁴ and $E = 200$ GPa. Sketch the deflected shape. Use the Virtual Force method.

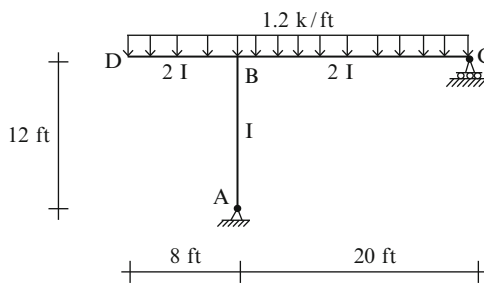


Problem 4.42

Sketch the deflected shapes. Determine the vertical deflection at A. Take $I = 240 \text{ in.}^4$, $E = 29,000 \text{ ksi}$, and $h = 2b = 10 \text{ ft}$. Use the Virtual Force method.

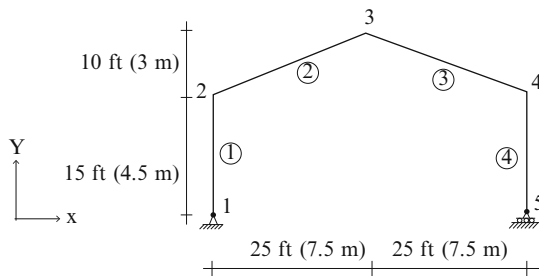
**Problem 4.43**

Determine the deflection profile for member DBC. Estimate the peak deflection. Use computer software. Note that the deflection is proportional to $1/EI$.

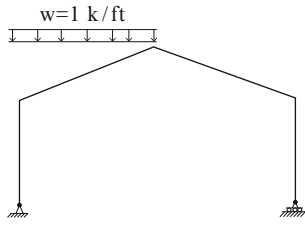


Problem 4.44

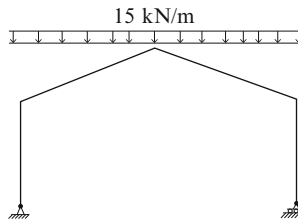
Consider the pitched roof frame shown below and the loadings defined in cases (a)–(f). Determine the displacement profiles and shear and moment diagrams. EI is constant. Use a computer software system.



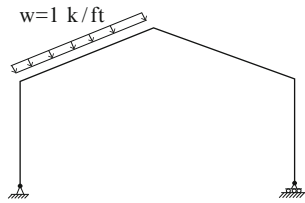
$$a \quad w=1 \text{ k/ft}$$



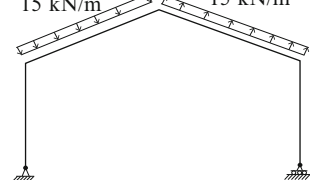
$$b$$



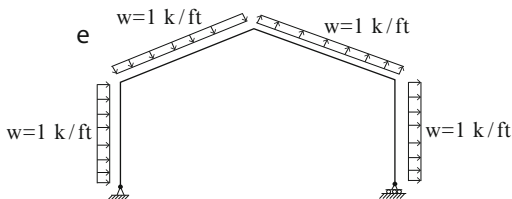
$$c \quad w=1 \text{ k/ft}$$



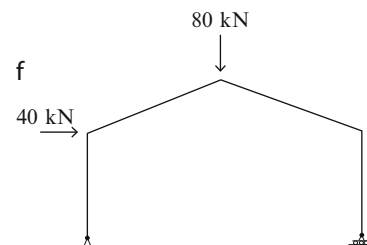
$$d \quad 15 \text{ kN/m} \quad 15 \text{ kN/m}$$



$$e \quad w=1 \text{ k/ft} \quad w=1 \text{ k/ft}$$

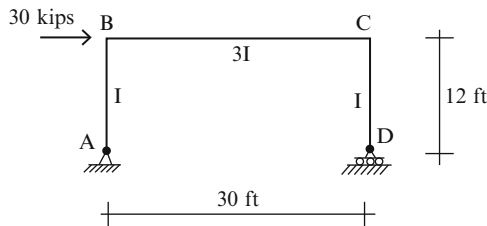


$$f$$

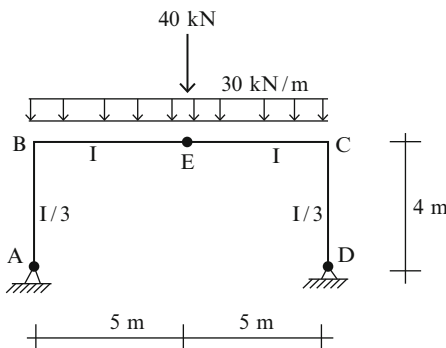


Problem 4.45

Consider the frame shown below. Determine the required minimum I for the frame to limit the horizontal deflection at C to 0.5 in. The material is steel. Use computer software.

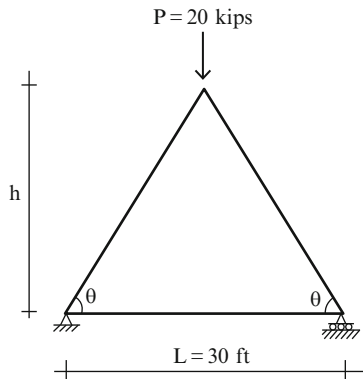
**Problem 4.46**

Consider the frame shown below. Determine the required minimum I for the frame to limit the vertical deflection at E to 15 mm. The material is steel. Use computer software.



Problem 4.47

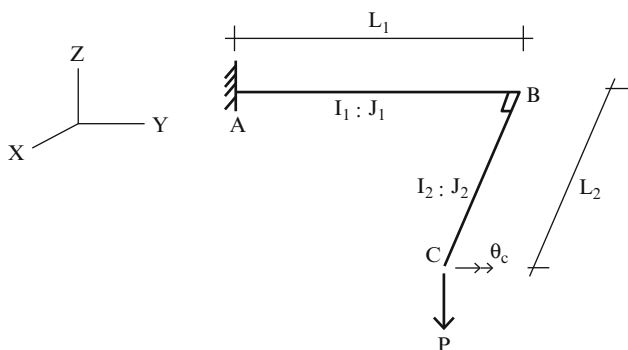
Consider the triangular rigid frame shown below. Assume the member properties are constant. $I = 240 \text{ in.}^4$, $A = 24 \text{ in.}^2$. Use computer software to determine the axial forces and end moments for the following range of values of $\tan\theta = 2h/L = 0.1, 0.2, 0.3, 0.4, 0.5$



Compare the solution with the solution based on assuming the structure is an ideal truss.

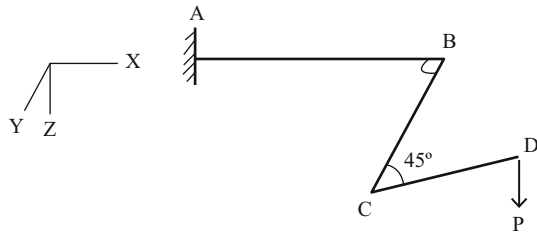
Problem 4.48

Consider the structure consisting of two members rigidly connected at B. The load P is applied perpendicular to the plane ABC. Assume the members are prismatic. Determine θ_y at point C.



Problem 4.49

Members AB, BC, and CD lie in the X-Y plane. Consider the cross-sectional properties to be constant. Determine the z displacement at B and D. Take $L_{AB} = L$, $L_{BC} = \frac{L}{2}$, $L_{CD} = L\sqrt{2}$.



Overview

Historically, cables have been used as structural components in bridge structures. In this chapter, we first examine how the geometry of a cable is related to the loading that is applied to it. We treat concentrated loadings first and then incorporate distributed loadings leading up to a theory for continuously loaded inclined cables. We also analyze the effect of temperature on the cable geometry. Lastly, we develop an approximate formula for estimating the stiffness of a cable modeled as an equivalent straight member. This modeling strategy is used when analyzing cable-stayed structures.

5.1 Introduction

A cable is a flexible structural component that offers no resistance when compressed or bent into a curved shape. Technically, we say a cable has zero bending rigidity. It can support only tensile loading. The first cables were made by twisting vines to form a rope-like member. There are many examples of early cable suspension bridges dating back several thousand years. With the introduction of iron as a structural material, cables were fabricated by connecting wrought iron links. Figure 5.1 shows an example of an iron link suspension bridge, the Clifton Suspension bridge near Bristol England built in 1836–1864 and designed by Isambard Brunel.

When high-strength steel wires became available, steel replaced wrought iron as the material of choice for cables. Modern cables are composed of multiple wires (up to 150 wires) clustered in a circular cross-section and arranged in a parallel pattern, as illustrated in Fig. 5.2. This arrangement is used for cable-stayed bridges and suspension bridges. The cable is normally coated with a protective substance such as grease and wrapped or inserted in a plastic sheathing.

One of the most notable early applications of steel cables was the Brooklyn Bridge built in 1870–1883 and designed by John Roebling and Wilhelm Hildebrandt. John Roebling also invented and perfected the manufacture of steel



Fig. 5.1 Clifton Suspension Bridge, England

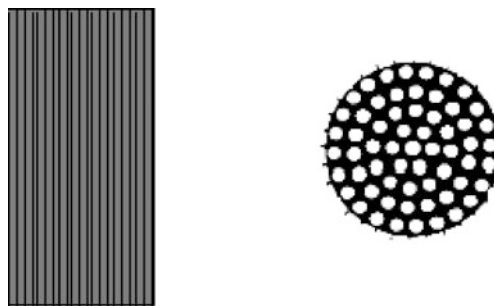


Fig. 5.2 Cable–strand arrangements

wire cable which was used for the bridge. At the time of completion, the total length of the Brooklyn Bridge was 50 % greater than any existing suspension bridge, an extraordinary advancement in bridge engineering (Fig. 5.3).

Cable-stayed structures employ cables fabricated from ultra high-strength steel to allow for the high level of tension required for stiffness. The cable-stayed bridge concept has emerged as the predominant choice for main spans up to about 1,000 m, replacing the conventional truss structural system. Figure 5.4 shows the Normandy Bridge, with a main span of 856 m. Built in 1995, it held the record for the largest main span until 1999, when it was exceeded by the Tatara bridge in Japan.

Cable nets are also used as the primary structural elements for long-span horizontal roof structures. Figure 5.5 shows a single-layer cable net structure with a double-curved saddle-shaped surface designed by Schlaich Bergermann and partners for a stadium in Kuwait.



Fig. 5.3 Brooklyn Bridge, USA

5.2 Cables Subjected to Concentrated Loads

5.2.1 Horizontal Cables

Suppose we conduct the following experiment shown in Fig. 5.6. We start with a horizontally aligned cable that is pin connected at A, supported with a roller support at B, and tensioned with a force H . We then apply a concentrated load, P , at mid-span. The cable adopts the triangular shape shown under the action of P . Two questions are of interest. Firstly, why a triangular shape? Secondly, how is the downward vertical displacement at mid-span related to P and H ? Historically, the term “sag” is used to describe the vertical motion of a cable.

We answer these questions by noting that the magnitude of the moment at any section along the length of the cable must be zero since a cable has no resistance to bending. Summing moments about B

$$\sum_{\text{at } B} M = R_A L - P \frac{L}{2} = 0 \rightarrow R_A = \frac{P}{2} \uparrow$$

Next, we consider the free body diagram for the arbitrary segment shown in Fig. 5.7. Setting the moment at x equal to zero leads to an expression for the sag, $v(x)$.

$$\sum M_{\text{at } x} = \frac{P}{2}x - Hv(x) = 0 \quad (5.1)$$



Fig. 5.4 Normandy Bridge, France

$$v(x) = \frac{P}{2H}x \quad (5.2)$$

Finally, evaluating $v(x)$ at $x = L/2$ results in an equation relating v_C and P .

$$v_C = \frac{PL}{4H} \quad (5.3)$$

Fig. 5.5 Doubly curved single-layer cable net, Kuwait



Fig. 5.6 Transverse loading on pretensioned cable.

(a) Axial load. (b) Transverse load added. (c) Free body diagram

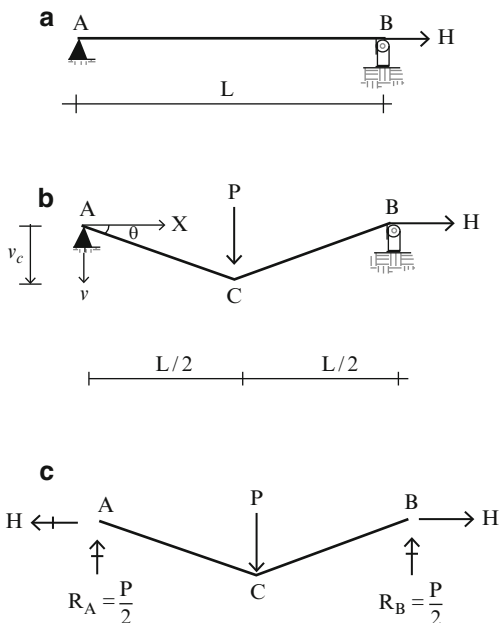
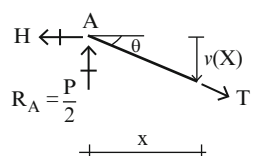
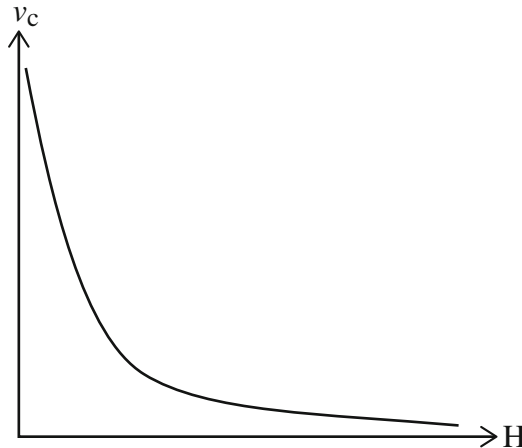


Fig. 5.7 Free body diagram of cable segment

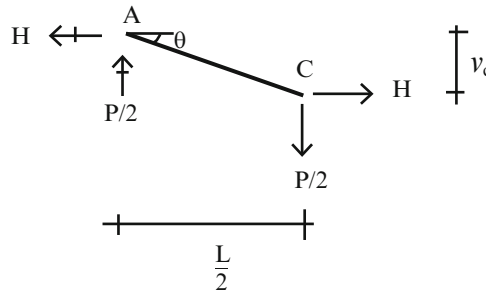


The relationship between v_C and H is plotted below. Usually, one specifies H and determines v_C . However, there are cases where one specifies v_C , and determines the required value of H . In general for cable systems, one needs to specify either a force or a sag in order to define solution.



The tension in the cable is given by

$$T = \sqrt{H^2 + \left(\frac{P}{2}\right)^2} = H\sqrt{1 + \left(\frac{P}{2H}\right)^2} \quad (5.4)$$



Noting that the angle of inclination of the cable is related to the sag by

$$\tan \theta = \frac{v_c}{L/2} = \frac{P/2}{H} \quad (5.5)$$

leads to an alternative expression for the tension,

$$T = H\sqrt{1 + \left(\frac{P}{2H}\right)^2} = H\sqrt{1 + \tan^2 \theta} = \frac{H}{\cos \theta} \quad (5.6)$$

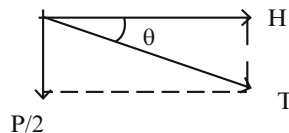
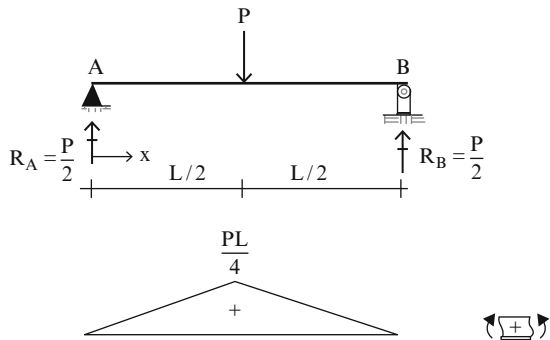


Fig. 5.8 Moment distribution for simply supported beam $M_0(x)$



When θ is small, T is approximately equal to H .

Equation (5.1) combines two moment distributions, one due to the transverse loading P and the other due to H . The moment due to P can be interpreted as the moment in a simply supported beam spanning between points A and B, the support points for the cable. Figure 5.8 shows this distribution.

We express (5.1) as

$$M_0(x) - v(x)H = 0 \quad (5.7)$$

where $M_0(x)$ is the moment due to the transverse loading acting on the simply supported beam spanning between A and B. Then, the expression for the sag can be written as

$$v(x) = \frac{M_0(x)}{H} \quad (5.8)$$

We interpret this result as follows. *The shape of the vertical sag of the cable from the horizontal chord is a scaled version of the moment diagram for the transverse loading acting on a simply supported beam spanning between the cable supports.*

We extend this reasoning to a cable subjected to multiple concentrated loads. Figure 5.9a illustrates this case. The moment diagram for a set of concentrated loads is piecewise linear, with peak values at the points of application of the concentrated loads. It follows from (5.8) that the shape of the cable is also piecewise linear. Details are listed below. One generates $M_0(x)$, the corresponding shear $V_0(x)$, the displacement v , and the tension T . Note that one has to specify either H or one of the vertical coordinates (v_C or v_D) in order to compute the shape.

$$T = \sqrt{V_0^2 + H^2} = \frac{H}{\cos \theta}$$

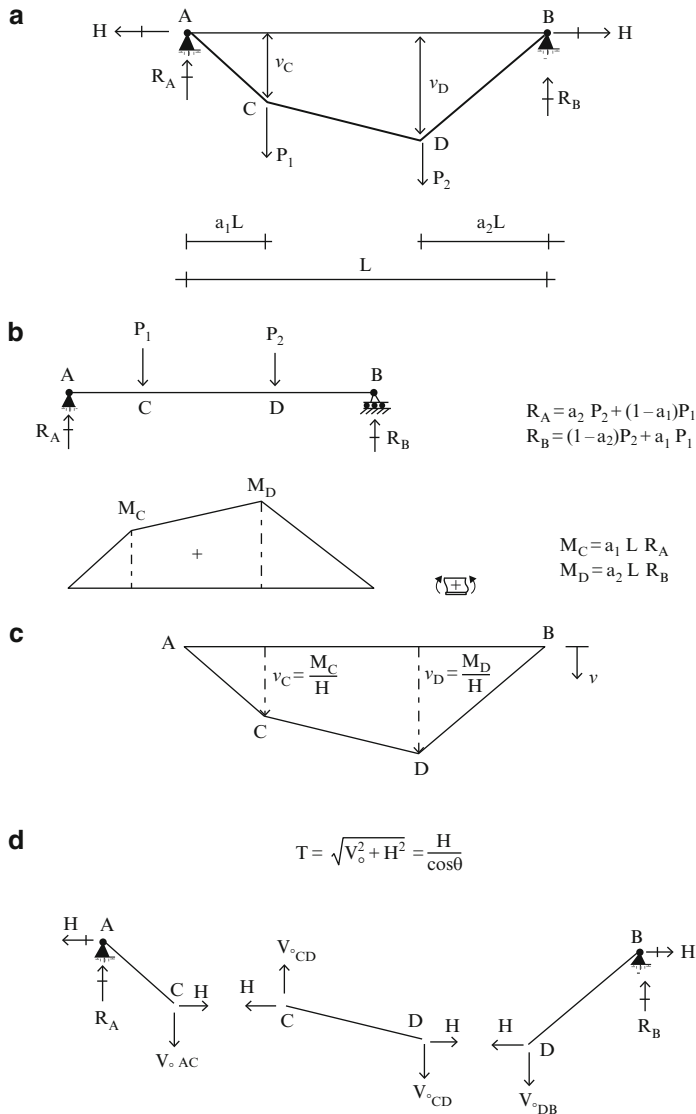
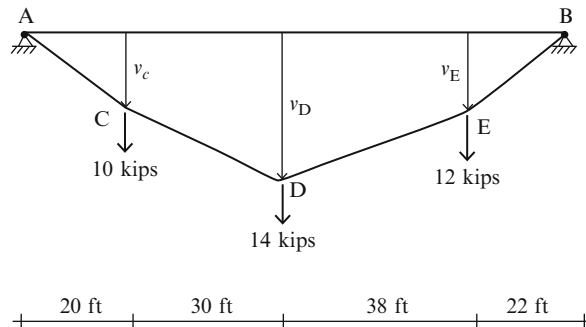


Fig. 5.9 Cable with two concentrated loads. (a) Loading. (b) $M_0(x)$ diagram. (c) Cable sag profile. (d) Cable tension computation

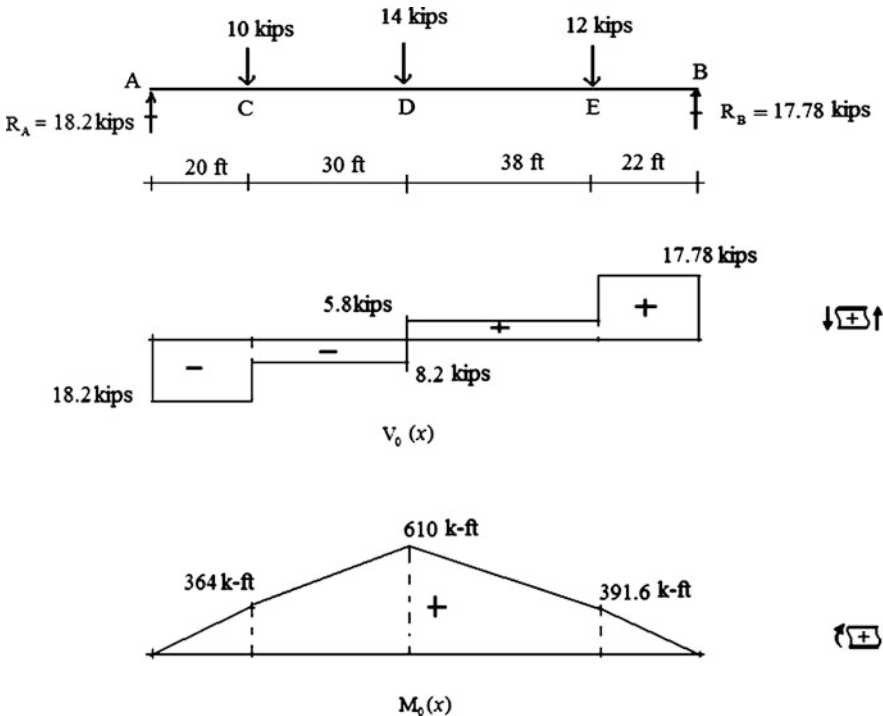
Example 5.1 Cable with multiple concentrated loads

Given: The cable and loading shown in Fig. E5.1a.

Determine: The shape corresponding to this loading. Assume (a) $v_D = 6$ ft
(b) $v_D = 12$ ft.

**Fig. E5.1a** Cable geometry and loading

Solution: First, we find the vertical reactions and generate the shear diagram $V_0(x)$ and moment diagram, $M_0(x)$, treating chord AB as a simply supported beam acted upon by the three vertical forces (Fig. E5.1b).

**Fig. E5.1b** Simply supported beam results

The downward vertical sag from the chord AB is determined with (5.8).

$$+ \downarrow \quad v(x) = \frac{M_0(x)}{H}$$

In order to compute $v(x)$, we need the horizontal force, H .
 (a) Taking $v_D = 6$ ft results in

$$6 = \frac{610}{H} \Rightarrow H = 101.67 \text{ kip}$$

The remaining sags are

$$v_C = \frac{364}{101.67} = 3.58 \text{ ft}$$

$$v_E = \frac{391.6}{101.67} = 3.85 \text{ ft}$$

The final results for the shape are plotted below (Fig. E5.1c).

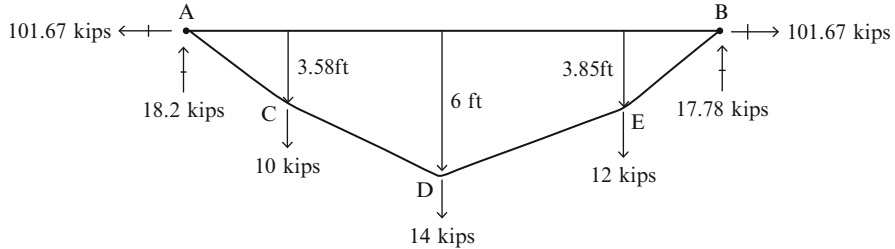


Fig. E5.1c Sag profile for $v_D = 6$ ft

Once the shape is known, one can find the tension in the various segments using (Fig. E5.1d)

$$T = \sqrt{V_o^2 + H^2} = \frac{H}{\cos\theta}$$

Fig. E5.1d Force decomposition

$$T_{AC} = \sqrt{18.2^2 + 101.67^2} = 103.3 \text{ kip}$$

$$T_{CD} = \sqrt{8.2^2 + 101.67^2} = 102 \text{ kip}$$

$$T_{DE} = \sqrt{5.8^2 + 101.67^2} = 101.8 \text{ kip}$$

$$T_{EA} = \sqrt{17.8^2 + 101.67^2} = 103.2 \text{ kip}$$

(b) Taking $v_D = 12$ ft results in

$$H = \frac{610}{12} = 50.83 \text{ kip}$$

$$v_C = \frac{364}{50.83} = 7.16 \text{ ft}$$

$$v_E = \frac{391.6}{50.83} = 7.7 \text{ ft}$$

and

$$T_{AC} = 54 \text{ kip}$$

$$T_{CD} = 51.5 \text{ kip}$$

$$T_{DE} = 51.16 \text{ kip}$$

$$T_{EB} = 53.85 \text{ kip}$$

The sag profile is plotted below (Fig. E5.1e)

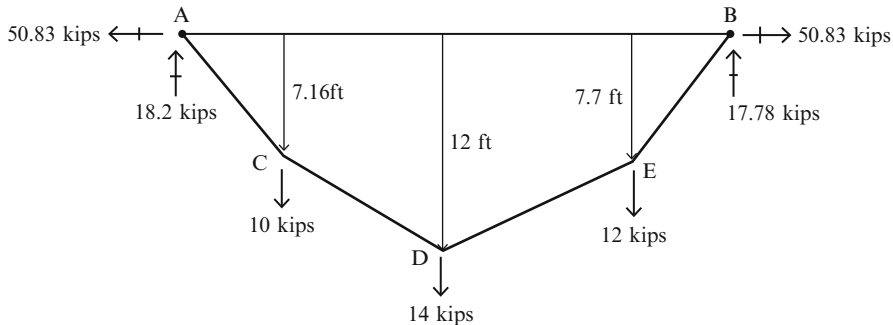


Fig. E5.1e Sag profile for $v_D = 12$ ft

Note that increasing the prescribed value of v_D decreases the cable forces.

5.2.2 Inclined Cables

When the cable is inclined, we follow the same approach except that now we measure the *cable sag with respect to the inclined chord*. Consider the cable defined in Fig. 5.10. This example differs from the previous examples only with respect to the inclination of the chord AB.

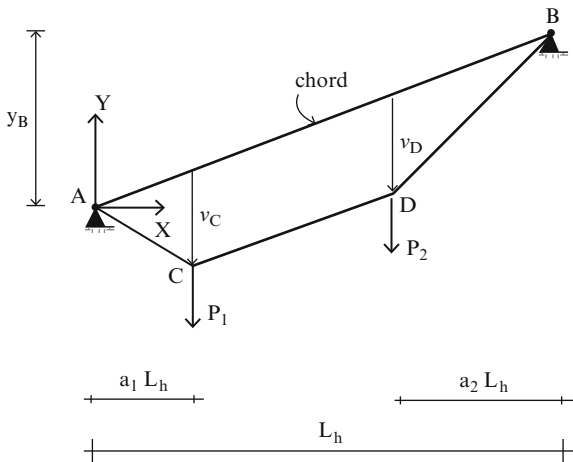


Fig. 5.10 Inclined cable with concentrated loads

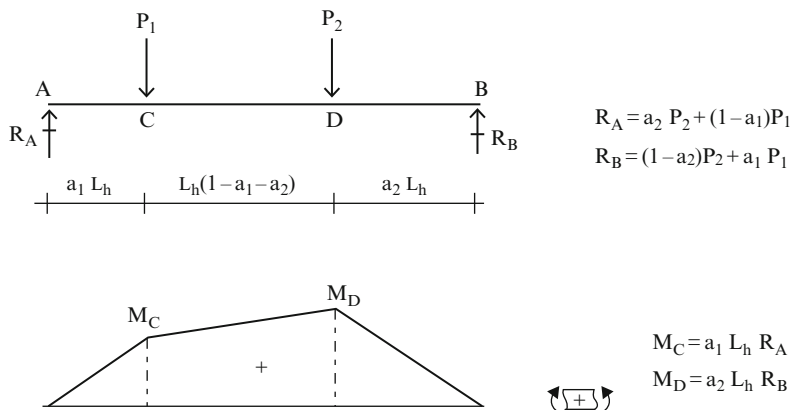
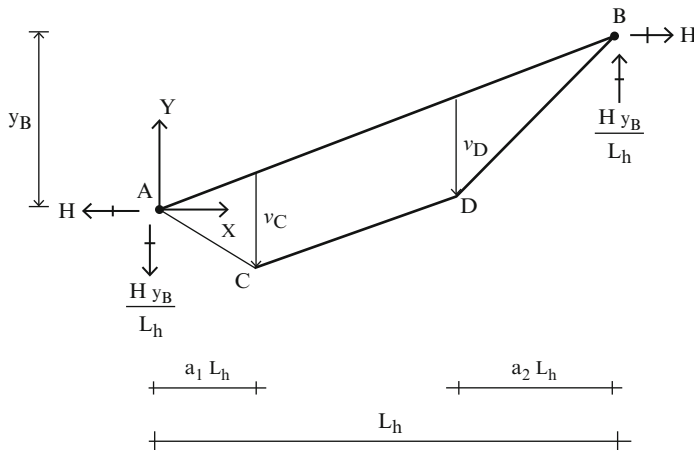


Fig. 5.11 Moment due to vertical loads, $M_0(x)$

The reactions and corresponding bending moment distribution generated by the vertical loads are shown in Fig. 5.11. Note that these moment results are identical to the results for the case of a horizontal chord orientation.

The reactions generated by the horizontal cable force, H are defined in Fig. 5.12. Setting the total moment equal to zero leads to

$$\begin{aligned} M_0(x) - H \frac{y_B}{L_h} x + Hy(x) &= 0 \\ \Downarrow \\ M_0(x) &= H \left(\frac{y_B}{L_h} x - y(x) \right) \equiv Hv(x) \\ \Downarrow \\ v(x) &= \frac{M_0(x)}{H} \end{aligned}$$

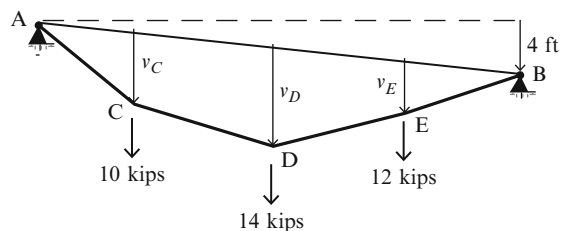
**Fig. 5.12** Reactions due to horizontal force, H

Note that the solution for $v(x)$ is identical to the results for the horizontal cable except that now one measures the sag from the inclined chord.

Example 5.2 Analysis of an inclined cable

Given: The inclined cable and loading shown in Fig. E5.2a.

Determine: The sag of the cable. Assume $v_D = 6$ ft.

**Fig. E5.2a** Inclined geometry

Solution: According to the theory presented above, the sag with respect to the inclined chord is given by

$$+ \downarrow \quad v(x) = \frac{M_0(x)}{H}$$

where $V_0(x)$ and $M_0(x)$ are the simply supported beam shear and moment (Fig. E5.2b). The $V_0(x)$ and $M_0(x)$ results are

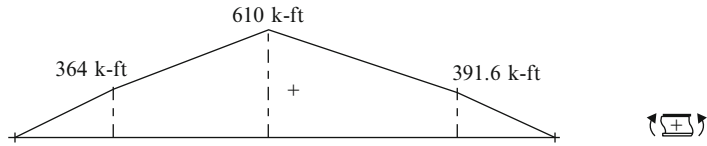
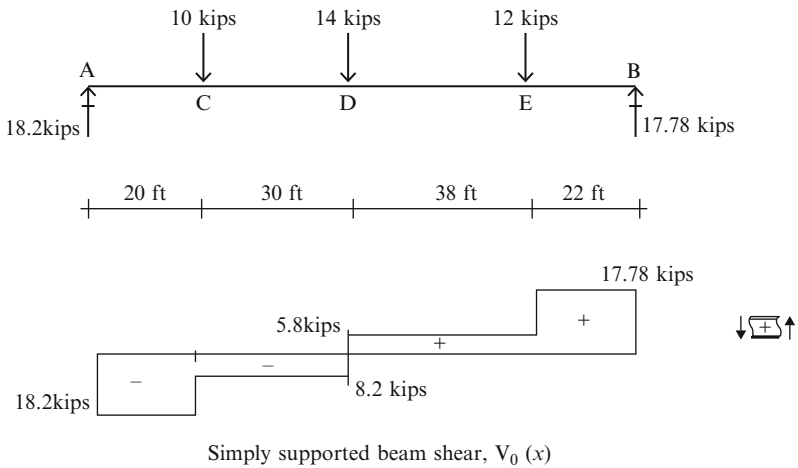


Fig. E5.2b Simply supported beam results

Then

$$v_C = \frac{364}{H} \quad v_D = \frac{610}{H} \quad v_E = \frac{391.6}{H}$$

For $v_D = 6$ ft, the value of H follows from

$$H = \frac{M_{0D}}{v_D} = \frac{610}{6} = 101.67 \text{ kip}$$

Finally, the values of sag at C and E are

$$v_C = \frac{364}{101.67} = 3.58 \text{ ft}$$

$$v_E = \frac{391.6}{101.67} = 3.85 \text{ ft}$$

To determine the tension, we need to compute the vertical shear in each panel.

The vertical reactions due to H (Fig. E5.2c) are

$$\frac{Hy_B}{L} = \frac{101.67(4)}{110} = 3.7 \text{ kip}$$

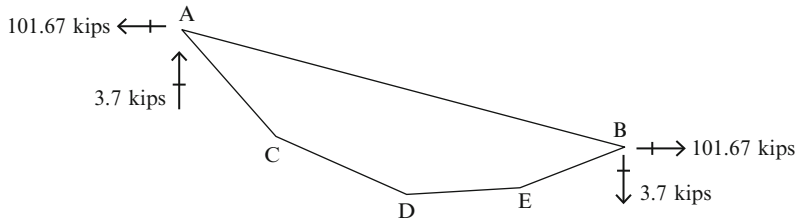


Fig. E5.2c Vertical reactions due to H

The net results for vertical shear are shown in Fig. E5.2d.

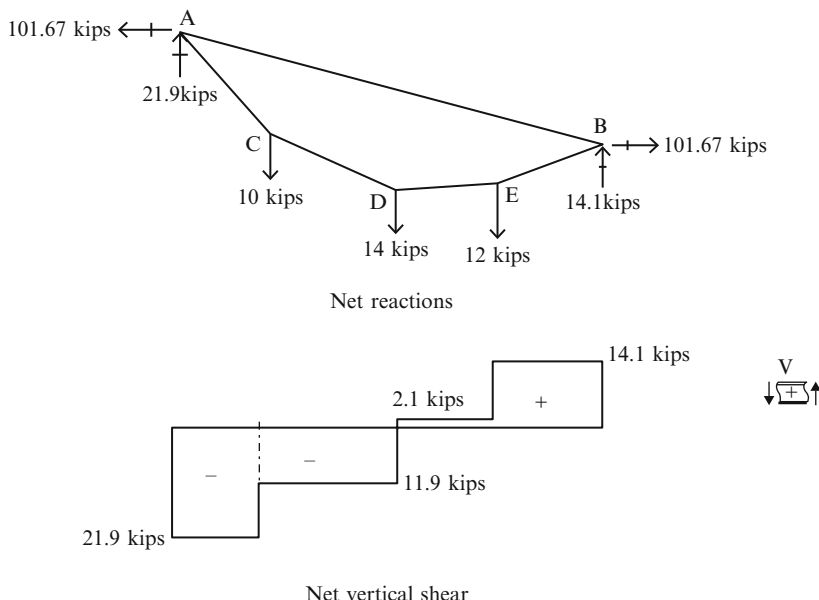


Fig. E5.2d Vertical shear

Lastly, the tension in each segment is computed using these values for V and H . The maximum tension is in segment AC.

$$T_{AC} = \sqrt{21.9^2 + 101.67^2} = 104 \text{ kip}$$

$$T_{CD} = \sqrt{11.9^2 + 101.67^2} = 102.4 \text{ kip}$$

$$T_{DE} = \sqrt{2.1^2 + 101.67^2} = 102.7 \text{ kip}$$

$$T_{EA} = \sqrt{14.09^2 + 101.67^2} = 102.6 \text{ kip}$$

5.3 Cables Subjected to Distributed Loading

5.3.1 Horizontal Cable: Uniform Loading per Horizontal Projection

We consider next the cable system shown in Fig. 5.13. The cable supports a horizontal platform, which in turn, supports a uniform vertical loading. We represent the action of the closely spaced vertical hangers on the cable *as a uniform downward loading per unit horizontal projection*. The self weight of the cable, which is usually small in comparison to the applied loading, is neglected. Following the procedure described in the previous section, we determine the moment diagram for a simply supported beam spanning between the end supports. *The sag of the cable with respect to the horizontal chord AB is an inverted scaled version of the moment diagram.* The details are shown in Fig. 5.14.

The sag, $\tan \theta$, and T are given by

$$\begin{aligned} v(x) &= \frac{M_0(x)}{H} = \frac{(wL/2)x - (wx^2/2)}{H} = \frac{w}{2H}(Lx - x^2) \\ \tan \theta &= \frac{dv}{dx} = \frac{1}{H} \frac{dM_0(x)}{dx} = \frac{w}{2H}(L - 2x) \\ T &= \frac{H}{\cos \theta} \end{aligned} \quad (5.9)$$

It follows that the shape due to a uniform load is parabolic and the maximum sag occurs at mid-span, point c.

$$v_C = h = \frac{w}{2H}(L^2/2 - L^2/4) = \frac{wL^2}{8H} \quad (5.10)$$

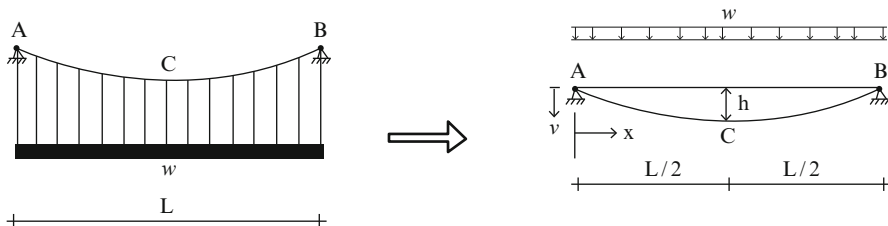


Fig. 5.13 Cable with a uniformly distributed loading

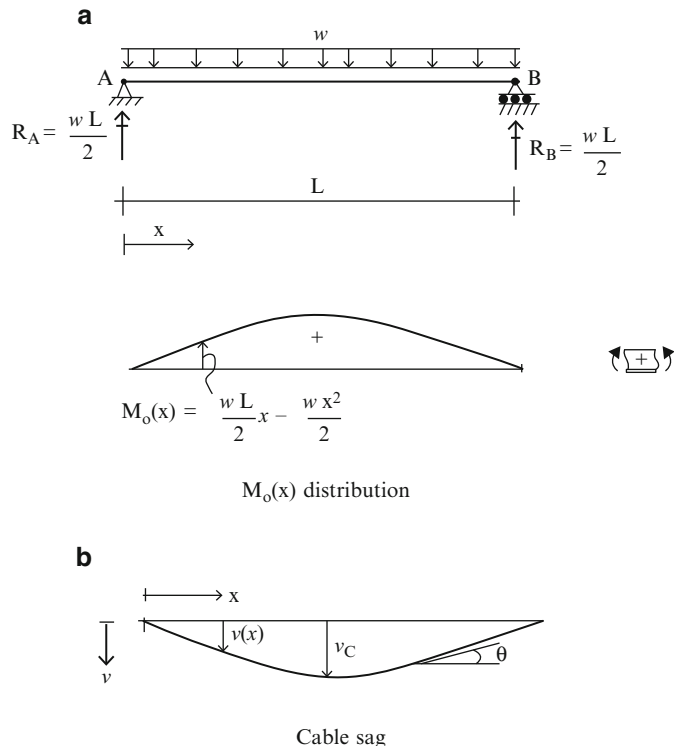


Fig. 5.14 Horizontal cable. (a) Simply supported beam results. (b) Cable sag

Example 5.3 Determine the tension for specified cable geometry.

Given: The cable shown in Fig. E5.3a. The loading and desired cable geometry is specified.

Determine: The value of the horizontal tension force, H , which produces this geometry under the given loading.

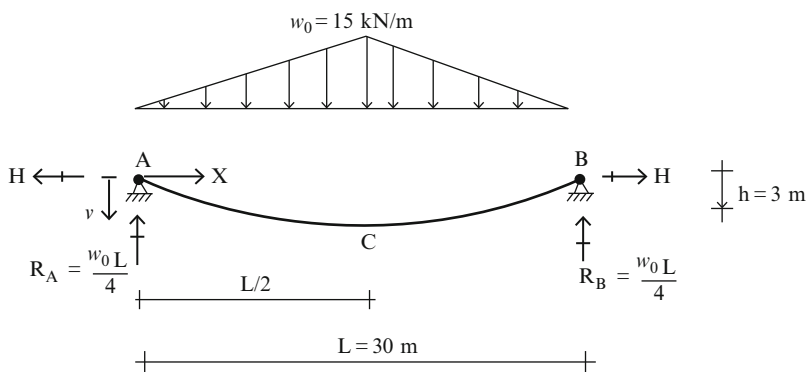
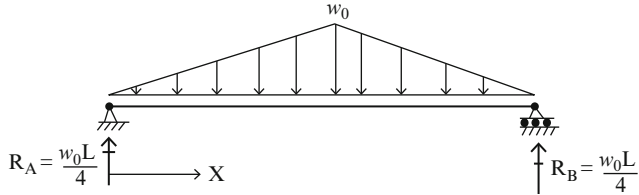


Fig. E5.3a

Solution: We note that the maximum value of v occurs at $x = L/2$. Then, specializing (5.9) for this value of x leads to the value of H :



$$M_o(x) = \frac{w_0 L}{4}x - \frac{w_0}{3L}x^3$$

$$\tan \theta = \frac{1}{H} \frac{dM_o(x)}{dx} = \frac{1}{H} \left(\frac{w_0 L}{4} - \frac{w_0}{L}x \right)^2$$

$$H = \frac{M_o(x = L/2)}{v_C} = \frac{w_0 L^2}{12} \frac{1}{v_C} = \frac{(15)(30)^2}{12(3)} = 375 \text{ kN}$$

The tension is related to H by:

$$T = \frac{H}{\cos \theta}$$

The peak values of θ occur at $x = 0$ and $x = L$.

$$\tan \theta_{\text{at } x=0} = \frac{1}{H} \left(\frac{w_0 L}{4} \right) = \frac{(15)(30)}{(375)(4)} = 0.3$$

$$\theta_{\text{at } x=0} = 16.7^\circ$$

It follows that

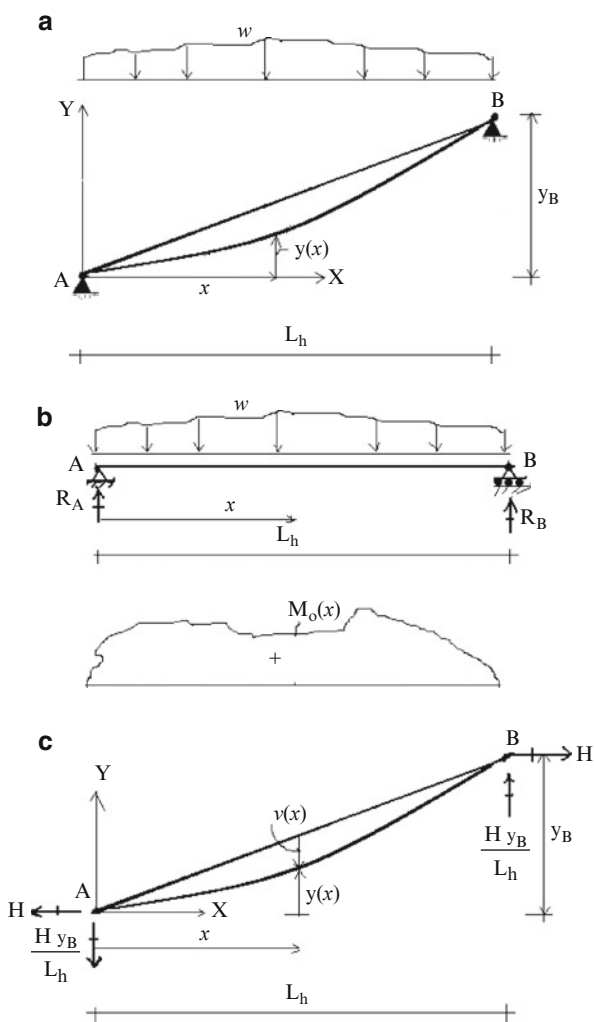
$$\theta_{\max} = \pm 16.7^\circ$$

$$T_{\max} = \frac{H}{\cos \theta} = 391.5 \text{ kN}$$

5.3.2 Inclined Cables

Suppose the cable is inclined, and subjected to an arbitrary loading. We define the shape by the function $y(x)$. Figure 5.15 defines this notation.

Fig. 5.15 Inclined cable geometry—arbitrary loading.
(a) Geometry-arbitrary loading.
(b) Simply supported beam results.
(c) Reactions due to horizontal force, H .



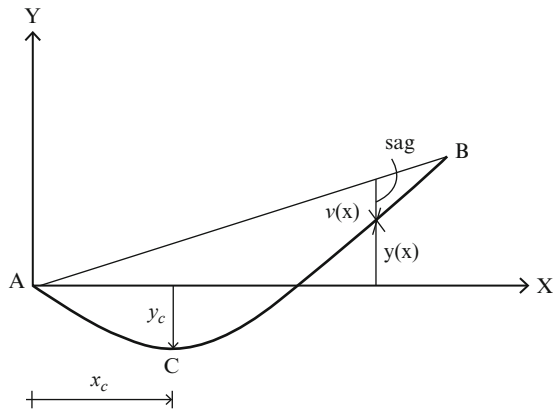
Since the cable has no bending rigidity, the shape of the cable must adjust itself so that the resultant moment due to the vertical load and H vanishes at all points along the cable. Then, setting the total moment at x equal to zero leads to

$$\sum M_{\text{at } x} = M_0(x) + Hy(x) - \frac{Hy_B}{L_h}x = 0$$

$$\Downarrow$$

$$y(x) = \frac{y_B}{L_h}x - \frac{M_0(x)}{H} \quad (5.11)$$

Fig. 5.16 Cable geometry—lowest point



We note from Fig. 5.15 that

$$\frac{y(x) + v(x)}{x} = \frac{y_B}{L_h}$$

$$\Downarrow$$

$$y(x) = \frac{y_B}{L_h}x - v(x) \quad (5.12)$$

Finally, equating (5.11) and (5.12) leads to the expression for the sag,

$$v(x) = \frac{M_0(x)}{H} \quad (5.13)$$

We observe that the solution for the sag is identical to the result that we obtained for the horizontal chord orientation *except now one measures the sag from the inclined chord*. The solution is also similar to the case of a set of concentrated loads.

The lowest point on the cable (point C in Fig. 5.16) is determined by setting the slope equal to zero.

$$\frac{dy}{dx} \Big|_{x_c} = 0 \quad (5.14)$$

Noting (5.11),

$$\frac{y_B}{L_h} - \frac{1}{H} \frac{dM_0(x)}{dx} = 0 \quad (5.15)$$

For the case where the distributed load is uniform, $M_0(x)$ is parabolic, and (5.15) expands to

$$\frac{y_B}{L_h} - \frac{1}{H} \left(-wx_C + \frac{wL_h}{2} \right) = 0 \quad (5.16)$$

Solving for x leads to

$$x_C = \frac{L_h}{2} - \frac{y_B}{L_h} \frac{H}{w} \quad (5.17)$$

For an arbitrary loading, we need to use (5.15).

Example 5.4 Determine the tension for specified inclined cable geometry

Given: The inclined cable defined in Fig. E5.4a. Point C is the lowest point of the cable.

Determine: The coordinates of point C and the peak values of cable tension.

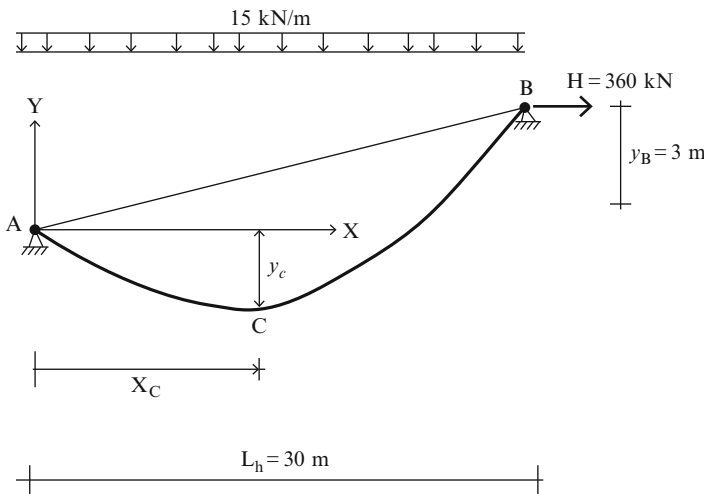


Fig. E5.4a

Solution: Noting (5.17)

$$x_C = \frac{L_h}{2} - \frac{y_B}{L_h} \frac{H}{w} = \frac{30}{2} - \frac{3}{30} \left(\frac{360}{15} \right) = 12.6 \text{ m}$$

Applying (5.11) for point C,

$$\begin{aligned} y_C &= x_C \frac{y_B}{L_h} - \frac{w}{2H} \left\{ L_h x_C - (x_C)^2 \right\} = 12.6 \left(\frac{3}{30} \right) - \frac{15}{2(360)} \left(30(12.6) - (12.6)^2 \right) \\ &= -3.3 \text{ m} \end{aligned}$$

Given H , we can find the cable tension at any point with:

$$T = \frac{H}{\cos \theta}$$

where

$$\tan \theta = \frac{dy}{dx} = \frac{y_B}{L_h} - \frac{wL_h}{2H} + \frac{wx}{H}$$

The critical locations are at the support points A and B.

$$\tan \theta_A = \frac{3}{30} - \frac{15(30)}{2(360)} = -0.525 \quad \theta_A = -27.7^\circ$$

$$\tan \theta_B = \frac{3}{30} - \frac{15(30)}{2(360)} + \frac{15(30)}{360} = +0.725 \quad \theta_B = +35.9^\circ$$

$$T_A = \frac{H}{\cos \theta_A} = 406.6 \text{ kN}$$

$$T_{\max} = T_B = \frac{H}{\cos \theta_B} = 444.4 \text{ kN}$$

5.4 Advanced Topics

This section deals with the calculation of arch length, the axial stiffness and the effect of temperature. We also discuss a modeling strategy for cable-stayed structures such as guyed towers and cable-stayed bridges.

5.4.1 Arc Length

We consider first the uniformly loaded horizontal cable shown in Fig. 5.17. We have shown that the sag profile due to a uniform load is parabolic,

$$v(x) = \frac{wL}{2H}x - \frac{wx^2}{2H}$$

and the maximum sag occurs at mid-span,

$$v_{\max} \equiv h = \frac{wL^2}{8H}$$

Given H and L , of interest is the total arc length of the cable. We need this quantity in order to determine the effect on the cable geometry of a temperature increase in the cable. Figure 5.17 shows the initial and loaded shapes of the cable. Note that the initial length is greater than L . We denote this quantity as $L + \Delta$.

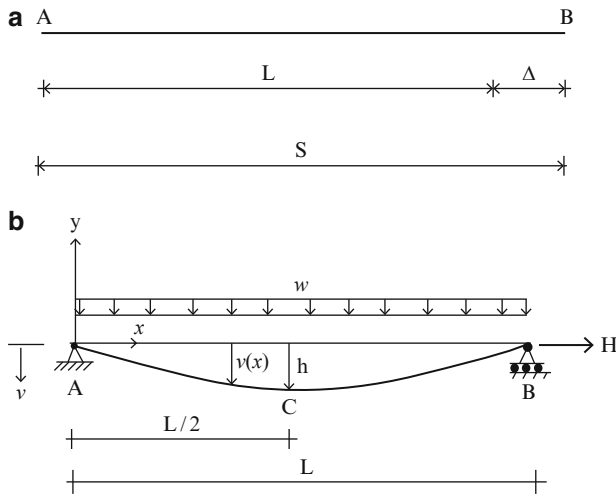


Fig. 5.17 Cable geometry. (a) Initial unloaded. (b) Loaded shape

The differential arc length, ds , is related to its horizontal and vertical projections by

$$ds = \sqrt{dx^2 + dy^2} = dx \sqrt{1 + \left(\frac{dy}{dx}\right)^2} \quad (5.18)$$

Integrating between 0 and L leads to an expression for the total arc length

$$S = \int_0^L \left\{ 1 + \left(\frac{dy}{dx}\right)^2 \right\}^{\frac{1}{2}} dx \quad (5.19)$$

Given $y(x)$, one evaluates the integral using either symbolic or numerical integration.

When the cable is horizontal, $y(x) = -v(x)$.

When the maximum sag h is small with respect to L , we can assume that dy/dx is small with respect to 1 and simplify the integral in (5.19) using the following binomial series expression,

$$(1 + f)^{\frac{1}{2}} = 1 + \frac{1}{2}f - \frac{1}{8}f^2 + \dots \quad (5.20)$$

$|f| < 1$

Taking $f = (\frac{dy}{dx})^2$ and retaining only the first two terms, we obtain the following approximation for S :

$$S \approx \int_0^L \left\{ 1 + \frac{1}{2} \left(\frac{dy}{dx} \right)^2 \right\} dx \quad (5.21)$$

Noting Fig. 5.17a, we see that $\Delta = \frac{1}{2} \int_0^L \left(\frac{dy}{dx} \right)^2 dx$ for this approximation.

Lastly, we evaluate S for the case when the loading is uniform. Retaining the first three terms in (5.20) leads to

$$S \approx L \left\{ 1 + \frac{8}{3} \left(\frac{h}{L} \right)^2 - \frac{32}{5} \left(\frac{h}{L} \right)^4 \right\} \quad (5.22)$$

We refer to h/L as the sag ratio. Equation (5.22) shows that the effect of decreasing the sag ratio is to transform the “curved” cable to essentially a straight segment connecting the two end points. *The cables used for guyed towers and cable-stayed bridges have small sag ratios, and are approximated as equivalent straight axial elements. We will discuss this topic in a later section.*

Example 5.5

Given: The cable defined in Fig. E5.5a.

Determine: The length of the cable corresponding to this geometry. Also determine the change in geometry due to a temperature increase of 150°F . Take $\alpha = 6.6 \times 10^{-6}/^\circ\text{F}$.

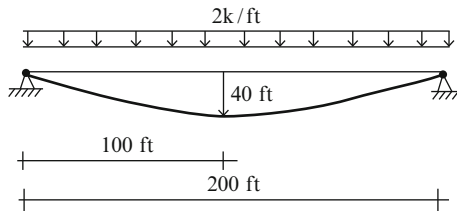


Fig. E5.5a

Solution: The horizontal reaction due to the loading shown is

$$H = \frac{wL^2}{8h} = 250 \text{ kip}$$

We evaluate S using (5.22),

$$S = 200 \left\{ 1 + \frac{8}{3} \left(\frac{40}{200} \right)^2 - \frac{32}{5} \left(\frac{40}{200} \right)^4 \right\} = 200 \{ 1 + 0.107 - 0.01 \}$$

$$S = 219.4 \text{ ft}$$

The change in cable length due to a temperature increase is

$$\Delta S = S(\alpha \Delta T) \approx 219.4(6.6 \times 10^{-6})(150) \approx 0.217 \text{ ft}$$

This length change produces a change in the sag. We differentiate (5.22) with respect to h ,

$$\frac{dS}{dh} \approx \frac{16}{3} \frac{h}{L} - \frac{128}{5} \left(\frac{h}{L} \right)^3$$

and solve for dh .

$$dh \approx \frac{dS}{(16/3)(h/L)\{1 - 4.8(h/L)^2\}}$$

Substituting for dS leads to

$$dh \approx \frac{0.217}{(16/3)(40/200)\{1 - 4.8(40/200)^2\}} = 0.25 \text{ ft}$$

Finally, we update H using the new values for $h = 40 + 0.25 = 40.25 \text{ ft}$

$$H = \frac{wL^2}{8h} = \frac{2(200)^2}{8(40.25)} = 248.5 \text{ kip}$$

The effect of temperature increase on H is small for this geometry.

Example 5.6

Given: The uniformly loaded inclined cable shown in Fig. E5.6a.

Determine: The sag profile and total arc length.

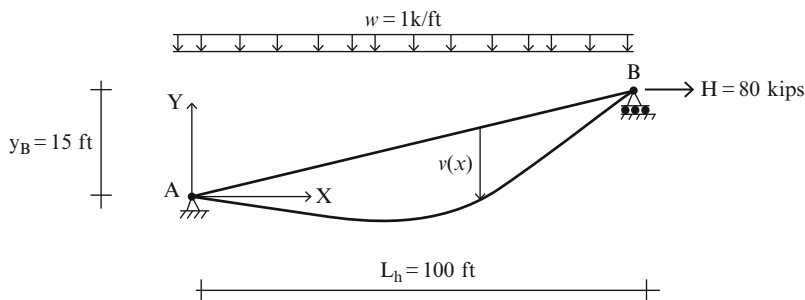


Fig. E5.6a

Solution: The profile defined in terms of $y(x)$ is given by (5.11). For the given dimensions, it expands to

$$\begin{aligned} y(x) &= \frac{y_B}{L_h}x - \frac{M_0(x)}{H} \\ &= \frac{15}{100}x - \left(50x - \frac{x^2}{2}\right)\frac{1}{80} \end{aligned}$$

Then, the sag profile is given by

$$v(x) = +\left(50x - \frac{x^2}{2}\right)\frac{1}{80} = \frac{5}{8}x - \frac{x^2}{160}$$

We determine the total arc length using (5.19).

$$S = \int_0^{L_h} ds \int_0^{L_h} \left\{ 1 + \left(\frac{dy}{dx} \right)^2 \right\}^{1/2} dx$$

Substituting for $y(x)$ leads to

$$S = \int_0^{100} \left\{ 1 + \left[\frac{15}{100} - \frac{1}{80}(50 - x) \right]^2 \right\}^{1/2} dx$$

We evaluate the integral using numerical integration. The result is

$$S = 107.16 \text{ ft}$$

5.4.2 Equivalent Axial Stiffness

In what follows, we establish a procedure for modeling a shallow horizontal cable as an equivalent straight axial member. Consider the cable shown in Fig. 5.18. Suppose the horizontal force, H , is increased a small amount, say ΔH . This action causes the support at B to displace horizontally an amount Δu . The ratio $\Delta H / \Delta u$ is a measure of the axial stiffness for the cable. We interpret it as the tangent stiffness since we perturbed the system from a “loaded” state.

We generate an expression for the tangent stiffness in the following way. We start with the straight unloaded cable shown in Fig. 5.19 and apply a horizontal force. The cable stretches an amount u_1 . Next, we apply the uniform

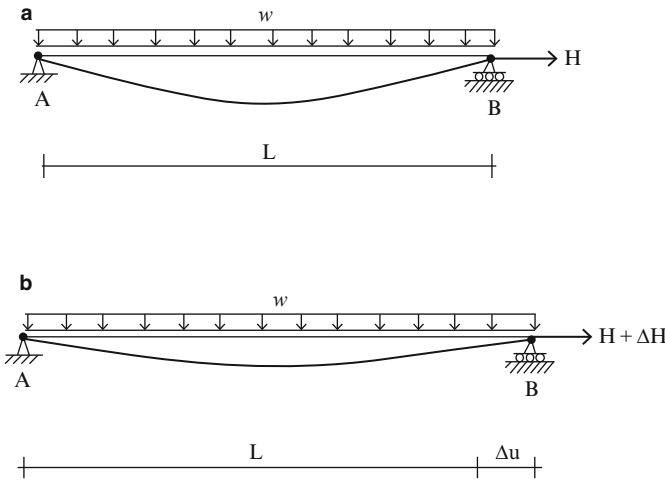


Fig. 5.18 Actual and perturbed configurations

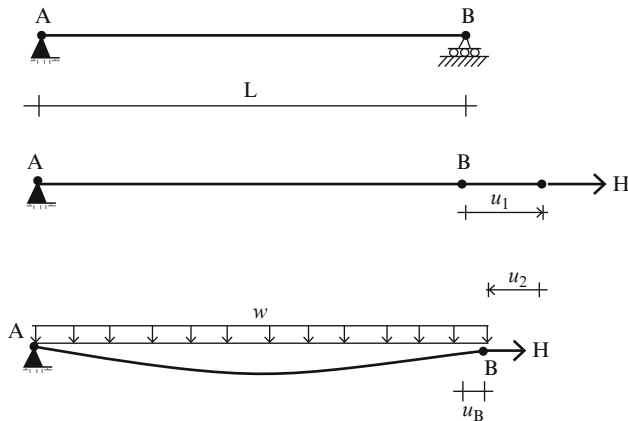


Fig. 5.19 Deflection patterns

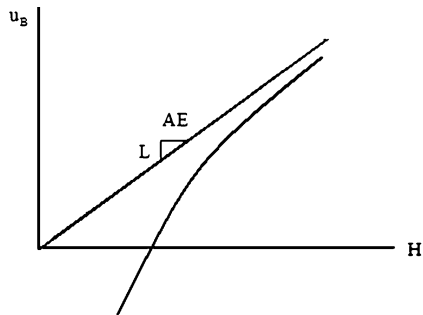
downward load, holding H constant. Point B moves to the left an amount u_2 . We estimate u_2 using (5.21) specified for a parabolic shape and small sag ratio,

$$u_2 \approx \int_0^L \frac{1}{2} \left(\frac{dv}{dx} \right)^2 dx = \frac{w^2 L^3}{24 H^2}$$

The net motion of B is u_B .

$$u_B = u_1 - u_2 = \frac{HL}{AE} - \frac{w^2 L^3}{24 H^2} \quad (5.23)$$

Fig. 5.20 u_B vs. H relationship



Equation (5.23) is plotted in Fig. 5.20. For large H , the first term dominates and the behavior approaches the behavior of an axial member. We want to determine dH/du . Since u_B is a nonlinear function of H , we first find the derivative du/dH , and then invert.

$$\begin{aligned} \frac{du_B}{dH} &= \frac{L}{AE} + \frac{w^2 L^3}{12H^3} = \frac{L}{AE} \left\{ 1 + \frac{1}{12} \frac{AE}{H} \left(\frac{wL}{H} \right)^2 \right\} \\ &\downarrow \\ \frac{dH}{du_B} &= k_t = \left(\frac{1}{1 + (1/12)(AE/H)(wL/H)^2} \right) \frac{AE}{L} \end{aligned} \quad (5.24)$$

Note that AE/L is the axial stiffness of a straight member. Equation (5.24) shows that the tangent stiffness for the horizontal cable approaches AE/L as the tension H is increased.

The tangent stiffness k_t can also be expressed in terms of a modified elastic modulus E_{eq} .

We write (5.24) as $k_t = (A/L)E_{eq}$. Then, the definition equation for E_{eq} follows:

$$E_{eq} = \frac{E}{1 + (1/12)(AE/H)(wL/H)^2} \quad (5.25)$$

In general, $E_{eq} < E$. Substituting the terms,

$$\begin{aligned} \frac{A}{H} &= \frac{1}{\sigma} \\ \frac{wL}{H} &= 8 \left(\frac{h}{L} \right) \end{aligned}$$

transforms (5.25) to

$$E_{eq} = \frac{E}{1 + (16/3)(E/\sigma)(h/L)^2} \quad (5.26)$$

where σ is the stress in the cable. It follows that the equivalent modulus depends on the initial stress in the cable and the sag ratio. A typical value of initial stress is on the order of 50–100 ksi ($344,700$ – $1,034,100$ kN/m 2). Values of sag ratio range from 0.005 to 0.02. The corresponding variation in E_{eq} for a steel cable with $\sigma = 50$ ksi ($344,700$ kN/m 2) is tabulated below.

| E/σ | h/L | E_{eq}/E |
|------------|-------|-------------------|
| 580 | 0.005 | 0.928 |
| | 0.01 | 0.764 |
| | 0.02 | 0.447 |

Note that a typical sag ratio of 0.01 results in a 25% reduction in E . One uses high-strength steel strands, on the order of 150 ksi ($1,034,100$ kN/m 2) yield stress, for cable-stayed structures in order to minimize their loss of stiffness due to cable sag.

5.4.3 Equivalent Axial Stiffness for an Inclined Cable

In this section, we extend the modeling strategy to deal with shallow inclined cables. Inclined cables with *small sag* ratios are used in cable-stayed bridges and also as supports for guyed towers. Figure 5.21 shows the Millau Viaduct Bridge in France. Figure 5.22 illustrates a two-cable scheme for a guyed tower subjected to wind loading.

We model each cable as a straight axial member with a modulus of elasticity, E_{eq} which depends on the initial tension and geometry of the cable. This approach is reasonable when the changes in geometry and tension due to the applied load are small in comparison to the initial properties.



Fig. 5.21 Millau Viaduct Bridge in France

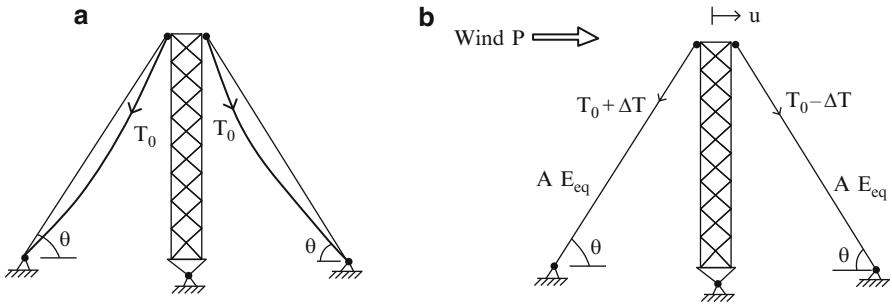


Fig. 5.22 Guyed tower modeling scheme. (a) Initial position. (b) Loaded position

Equilibrium of the tower requires

$$2\Delta T \cos \theta = P \quad (5.27)$$

The corresponding extension of the “equivalent” straight member due to ΔT is:

$$\Delta e = \frac{\Delta TL}{AE_{eq}} \quad (5.28)$$

Lastly, we relate Δe to the horizontal displacement u .

$$\Delta e = u \cos \theta$$

Combining these equations leads to an expression relating P and u .

$$P = \left[\frac{2AE_{eq}}{L} (\cos \theta)^2 \right] u \quad (5.29)$$

The bracketed terms represents the lateral stiffness of the tower for a lateral load applied at the top of the tower. Given E_{eq} , one can evaluate the lateral response of the tower with (5.29).

We develop an expression for E_{eq} by modifying (5.25). Figure 5.23 shows a typical inclined cable and the notation introduced here. The loading acting on the cable is assumed to be the self weight, w_g . Also when the cable is rotated from the horizontal position up to the inclined position, H is now the cable tension, T ; the normal distributed load w becomes $w_g \cos \theta$; and the loading term becomes

$$wL \Rightarrow (w_g \cos \theta)L = w_g L_h \quad (5.30)$$

Substituting for these terms in (5.25) leads to

$$E_{eq} \approx \frac{E}{1 + (1/12)(AE/T)(w_g L_h / T)^2} \quad (5.31)$$

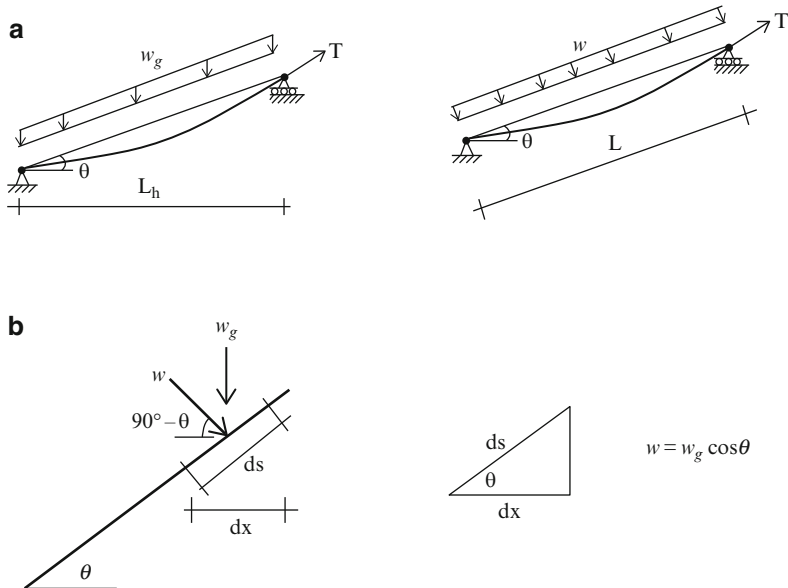


Fig. 5.23 Inclined cable geometry. (a) Vertical versus normal loading. (b) Loading components

Lastly, we introduce the following definitions involving the initial stress and weight density,

$$\frac{A}{T} = \frac{1}{\sigma} \quad (5.32)$$

$$w_g = \gamma_g A$$

The final form of (5.31) for an individual cable is

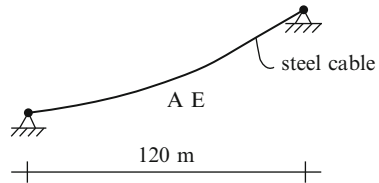
$$E_{eq} = \frac{E}{1 + (1/12)(E/\sigma)(\gamma_g L_h/\sigma)^2} \quad (5.33)$$

Equation (5.33) is known as Ernst's Formula. This expression is used when modeling the cables in a cable-stayed scheme with equivalent axial member properties.

Example 5.7

Given: The steel cable shown in Fig. E5.7a. Take the initial stress as 700 MPa.

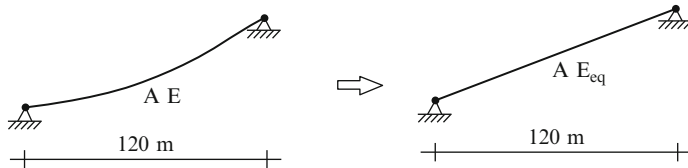
Determine: The equivalent modulus, E_{eq} .

Fig. E5.7a

Solution: properties of steel are $E = 200 \text{ GPa}$ and $\gamma_g = 77 \text{ kN/m}^3$. Substituting these values in (5.33) leads to

$$\frac{E_{\text{eq}}}{E} = \frac{1}{1 + (1/12)(200(10^3)/700)(77(120)/700,000)^2} = 0.996$$

One uses E_{eq} when specifying the properties of the “equivalent” straight axial member.



5.4.4 Cable Shape Under Self Weight: Catenary

There are cases where the loading on a cable is due only to self weight. Electrical transmission lines are one example. The previous analyses have assumed the loading is defined in terms of the horizontal projection (dx). This assumption is reasonable when the slope of the cable is small. In order to investigate the case when the slope is not small, we need to work with the exact equilibrium equation.

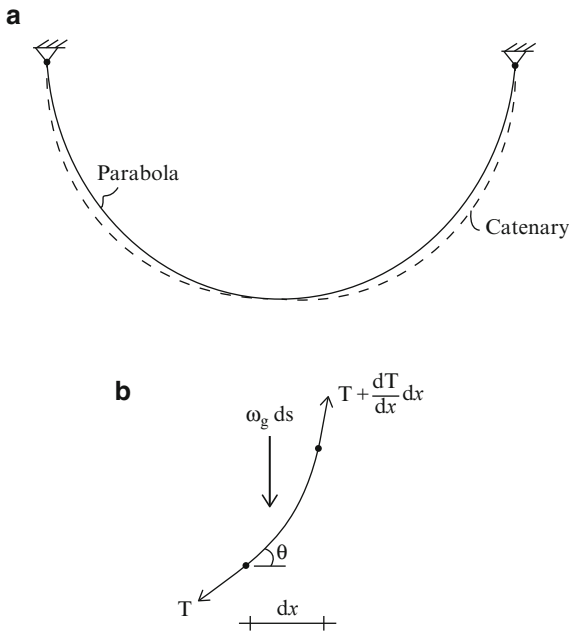
Consider the segment shown in Fig. 5.24. Enforcing equilibrium and noting that the loading is vertical leads to following equations:

$$\begin{aligned}\sum F_y &= 0 \quad \frac{d}{dx}(T \sin \theta) dx = w_g ds \\ \sum F_x &= 0 \quad \frac{d}{dx}(T \cos \theta) = 0 \Rightarrow T \cos \theta = \text{Constant} = H\end{aligned}\tag{5.34}$$

Substituting for T

$$T = \frac{H}{\cos \theta} \Rightarrow T \sin \theta = H \tan \theta = H \frac{dy}{dx}$$

Fig. 5.24 (a) Cable shape under self weight—Catenary. (b) Differential segment



in the first equation in (5.34) leads to

$$H \frac{d^2y}{dx^2} = \omega_g \frac{ds}{dx} = \omega_g \left\{ 1 + \left(\frac{dy}{dx} \right)^2 \right\}^{\frac{1}{2}} \quad (5.35)$$

The general solution of (5.35) is

$$y = \frac{H}{\omega_g} \cosh \left(\frac{\omega_g}{H} x + c_1 \right) + c_2 \quad (5.36)$$

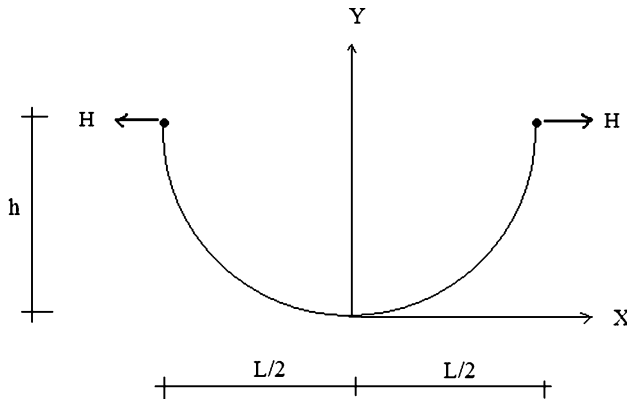
where c_1 and c_2 are integration constants which are determined using the coordinates of the support points.

We consider the symmetrical case shown in Fig. 5.25. We locate the origin at the lowest point. Then for this choice,

$$\begin{aligned} c_1 &= 0 \\ c_2 &= -\frac{H}{\omega_g} \end{aligned}$$

and

$$y = \frac{H}{\omega_g} \left\{ \cosh \left(\frac{\omega_g}{H} x \right) - 1 \right\}$$

**Fig. 5.25**

The force H is determined from the condition $y(L/2) = h$

$$h = \frac{H}{w_g} \left\{ \cosh \left(\frac{w_g L}{2H} \right) - 1 \right\} \quad (5.37)$$

We need to solve (5.38) using iteration since it is a transcendental equation.
We expand the cosh term,

$$\begin{aligned} \cosh x &= 1 + \frac{x^2}{2} + \frac{x^4}{24} + \cdots + \frac{x^n}{n!} \\ &= 1 + \frac{x^2}{2} \left\{ 1 + \frac{x^2}{12} + \cdots + 2 \frac{x^{(n-2)}}{n!} \right\} \end{aligned} \quad (5.38)$$

When x^2 is small with respect to 1, we approximate the expression as

$$\cosh x \approx 1 + \frac{x^2}{2} \left\{ 1 + \frac{x^2}{12} \right\}$$

Taking $x = \frac{w_g L}{2H}$ and substituting for $\cosh x$ in (5.37) leads to

$$h \approx \frac{w_g L^2}{8H} \left\{ 1 + \frac{1}{12} \left(\frac{w_g L}{2H} \right)^2 \right\} \quad (5.39)$$

When the loading is assumed to be per unit projected length, the corresponding expression for h is $h = wL^2/8H$. For a given H , h is larger for the self weight case. Also for a given h , H is larger for the self weight case. The difference increases with the sag ratio, h/L .

We find the arc length using (5.35).

$$H \frac{d^2y}{dx^2} dx = \omega_g ds$$

Integrating,

$$\begin{aligned} S &= 2 \int_0^{\frac{L}{2}} \left(\frac{1}{\omega_g} \right) H \frac{d^2y}{dx^2} dx = \frac{2}{\omega_g} H \frac{dy}{dx} \Big|_0^{\frac{L}{2}} \\ S &= \frac{2H}{\omega_g} \sinh \left(\frac{\omega_g L}{2H} \right) \end{aligned} \quad (5.40)$$

We determine the maximum tension which occurs at $x = \pm(L/2)$ using

$$T_{\max} = H \cosh \left(\frac{\omega_g L}{2H} \right) \quad (5.41)$$

Example 5.8

Given: The cable shown in Fig. E5.8a has a self weight of 1.2 kip/ft.

Determine: The arc length, h and maximum tension in the cable using the catenary equations. Also the percent of error in the maximum tension value when using parabolic equations. Consider the following values for H : $H = 75, 100$, and 250 kip.

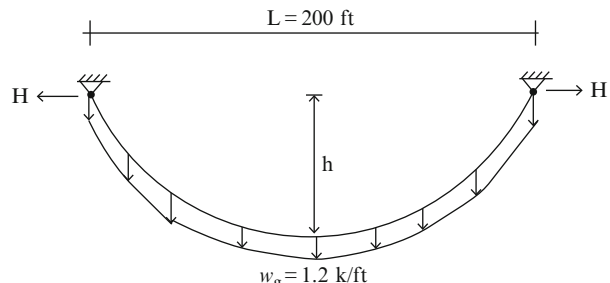


Fig. E5.8a

Solution: The relevant equations are listed below.

$$h = \frac{H}{w_g} \left\{ \cosh \left(\frac{w_g L}{2H} \right) - 1 \right\}$$

$$h_{\text{ap}} \approx \frac{w_g L^2}{8H} \left\{ 1 + \frac{1}{12} \left(\frac{w_g L}{2H} \right)^2 \right\}$$

$$S = \frac{2H}{\omega_g} \sinh\left(\frac{\omega_g L}{2H}\right)$$

$$T_{\max} = H \cosh\left(\frac{\omega_g L}{2H}\right)$$

These equations are evaluated using a digital computer. The results are summarized in the table below. Note that when h/L is large, the error introduced by the parabolic approximation is significant.

| H | Catenary | | | | Parabola | | % error T_{\max} |
|-----|----------|------|------------------|------------|----------|------------|--------------------|
| | S | h | $h_{\text{ap.}}$ | T_{\max} | h | T_{\max} | |
| 75 | 296.9 | 98.6 | 97 | 193 | 80 | 141.5 | 27% |
| 100 | 251.6 | 67.5 | 67.2 | 181 | 60 | 156.2 | 14% |
| 250 | 207.7 | 24.5 | 24.5 | 279 | 24 | 277.3 | 1% |

5.5 Summary

5.5.1 Objectives

- To describe how a cable adjusts its geometry when subjected to a single vertical concentrated load.
- To extend the analysis to a cable subjected to multi concentrated vertical loads.
- To derive an expression for the deflected shape of the cable when subjected to an arbitrary vertical loading.
- To present a series of examples which illustrate the computational procedure for finding the deflected shape of a cable.
- To derive an approximate expression for the equivalent axial stiffness of a cable modeled as a straight member.

5.5.2 Key Concepts

- Given a cable supported at two points, A and B, and subjected to a vertical loading. The vertical deflection from the chord connecting points A and B is proportional to the bending moment M in a simply supported beam spanning between A and B. One finds the bending moment diagram using a simple equilibrium analysis. The deflection of the cable with respect to the chord AB is an inverted scaled version of the moment diagram.
- Under vertical loading, the horizontal component of the cable force is constant.

- The length of the cable is determined by integrating

$$S = \int_0^L ds = \int_0^L \sqrt{1 + \left(\frac{dy}{dx}\right)^2} dx$$

where

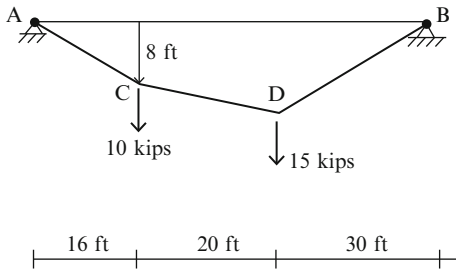
$$y = -\frac{M_0(x)}{H} + \frac{y_B}{L_h}x$$

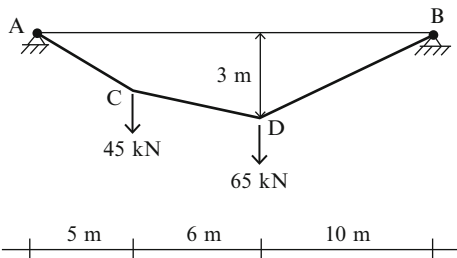
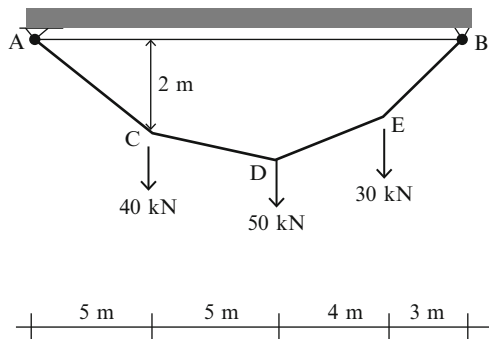
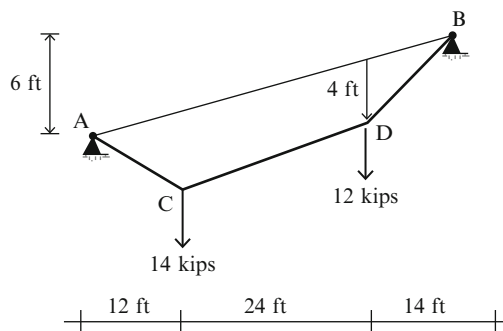
One usually approximates the integrand with $ds \approx 1 + (1/2)(dy/dx)^2$ when $(dy/dx)^2$ is small in comparison to 1.

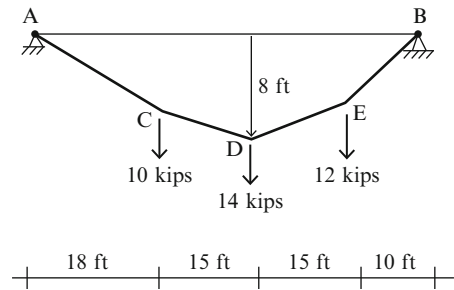
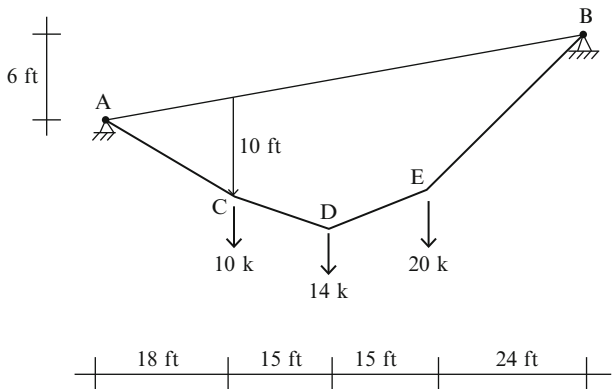
5.6 Problems

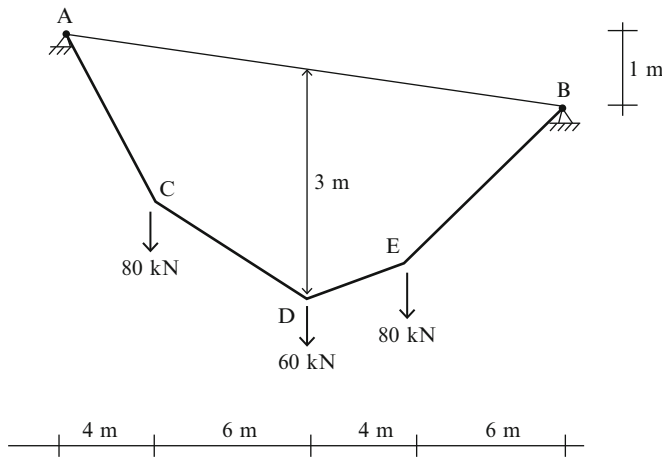
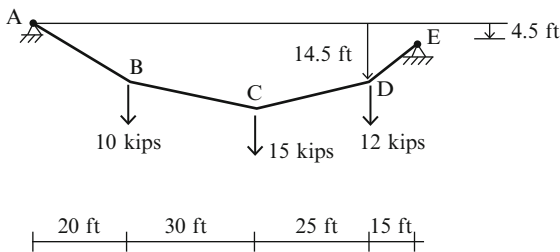
For Problems 5.1–5.8, determine the reactions at the supports, and the tension in each segment of the cable.

Problem 5.1

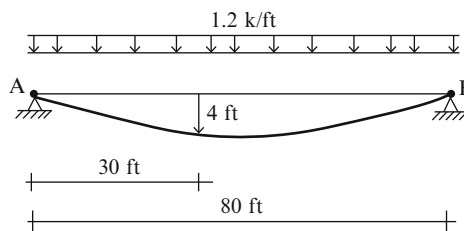


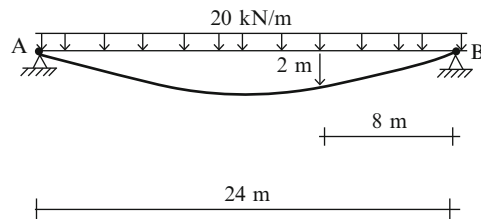
Problem 5.2**Problem 5.3****Problem 5.4**

Problem 5.5**Problem 5.6**

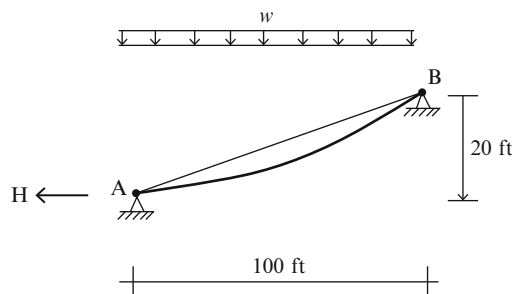
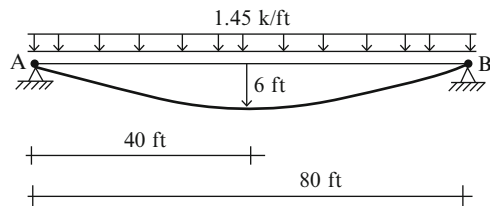
Problem 5.7**Problem 5.8**

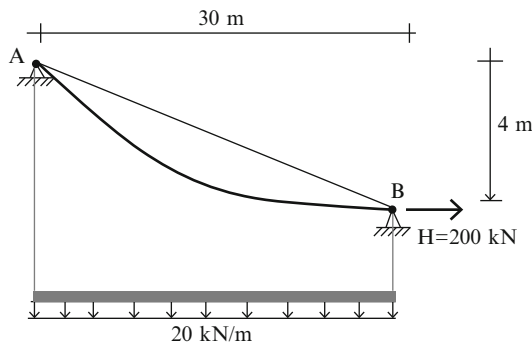
For Problems 5.9–5.14, determine the maximum tension.

Problem 5.9

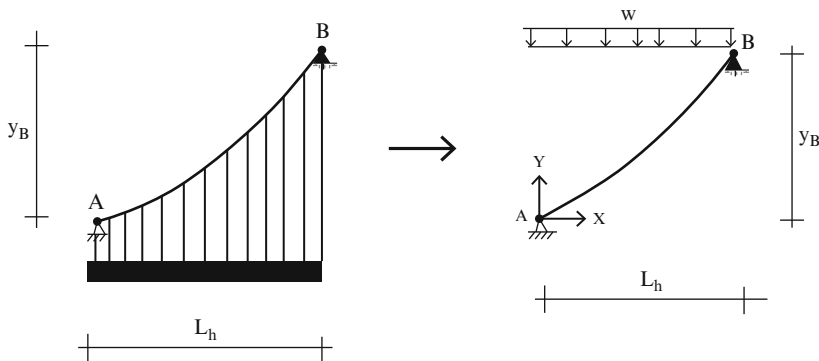
Problem 5.10**Problem 5.11**

Assume $w = 1.7 \text{ kip/ft}$ and $H = 40 \text{ kip}$.

**Problem 5.12**

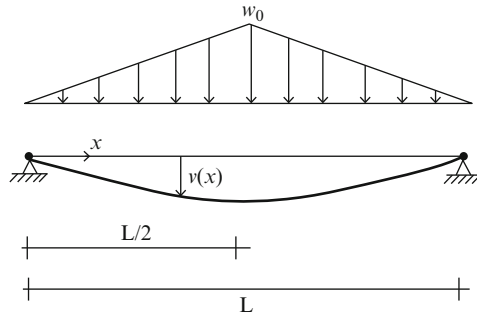
Problem 5.13**Problem 5.14**

Assume $w = 1.4 \text{ kip/ft}$, $y_B = 10 \text{ ft}$, $H = 100 \text{ k}$, and $L_h = 40 \text{ ft}$.

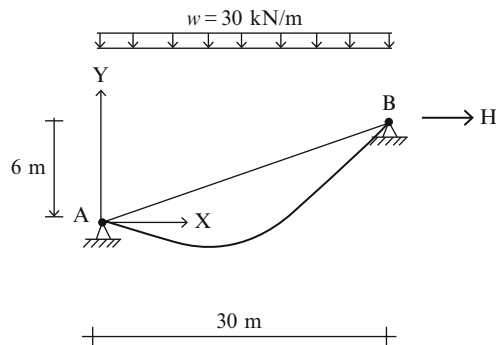


Problem 5.15

Assume $w_0 = 1.8 \text{ k/ft}$, $v_{\text{at } x=20 \text{ ft}} = 2 \text{ ft}$ and $L = 80 \text{ ft}$. Determine the deflected shape.

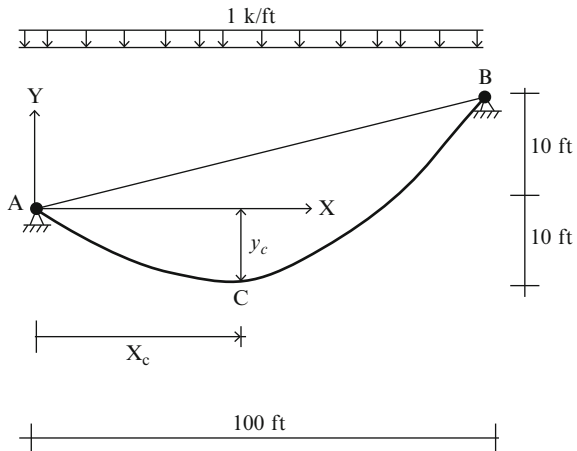
**Problem 5.16**

Determine the coordinates of the lowest point on the cable for $H = 650 \text{ kN}$

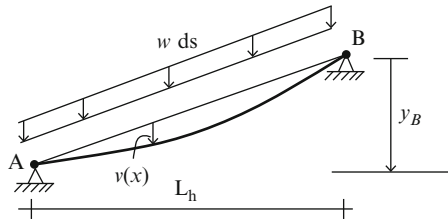


Problem 5.17

Determine the peak values of cable tension.

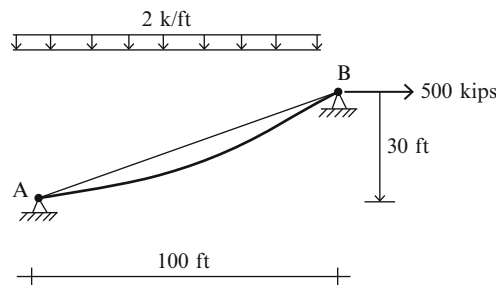
**Problem 5.18**

Consider the case where the loading is defined in terms of per unit arc length. Derive the expression for the deflected shape, $v(x)$.

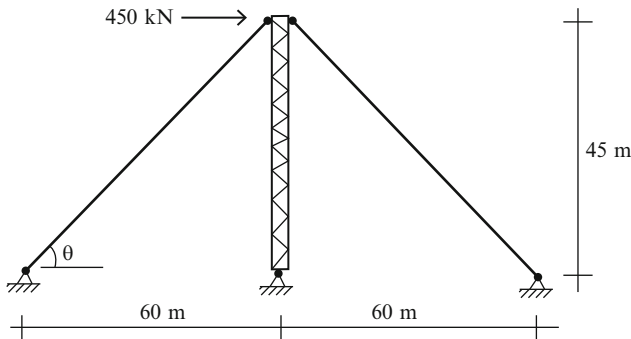


Problem 5.19

- (a) Determine the total arc length for this geometry.
 (b) Determine the effect of a temperature increase of 100°F. Assume the cable material is steel.

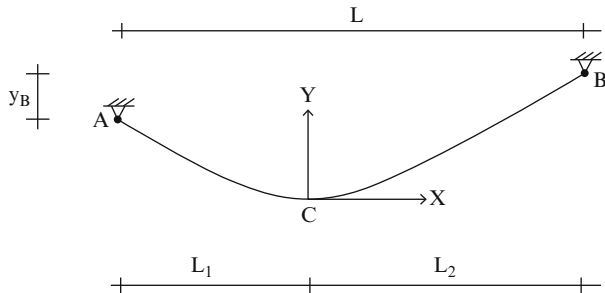
**Problem 5.20**

Consider the guyed tower scheme shown in the sketch below. Assume the guys are steel cables that are stressed initially to 520 MPa. Determine the cable cross-sectional area required to limit the lateral motion at the top of the tower to 10 mm.



Problem 5.21

The cable shown below carries its own weight. Determine the arc length and maximum tension in the cable. Point C is the lowest point. Assume $w = 0.8 \text{ kip per foot of cable}$, $L_1 = 60 \text{ ft}$, $L_2 = 80 \text{ ft}$, $y_B = 8 \text{ ft}$, and $H = 150 \text{ kip}$.



Overview

Chapter 3 dealt with beams, which are *straight* members subjected to transverse loading. We showed there that transversely loaded beams respond by bending, i.e., they equilibrate the loading by developing internal shear and moment quantities. When the centroidal axis is curved, the behavior of a curved member subjected transverse loading, depending on how the ends are restrained, can undergo a dramatic change from predominately bending action to predominately axial action. This characteristic of curved members makes them more efficient than straight members for spanning moderate to large scale openings. A typical application is an arch structure, which is composed of curved members restrained at their ends.

In this chapter, we first develop the general solution for the internal forces in a planar curved member and apply it to members having parabolic and circular shapes. Next, we introduce the method of virtual forces specialized for planar curved members and illustrate its application to compute displacements for various geometries. The last section of the chapter deals with the optimal shape for an arch and the analysis of three-hinged arches, a popular form of arch structure. The material presented here also provides the basis for the analysis of statically indeterminate arches treated in Chap. 9.

6.1 A Brief History of Arch-Type Structures

We define an arch as a curved member that spans an opening and is restrained against movement at its ends by abutments. Figure 6.1 illustrates this definition. Arches are designed to carry a vertical loading which, because of the curved nature of the member, is partially resisted by horizontal forces provided by the abutments. Arches generally are more efficient than straight beam-type structures for spanning an opening since their geometry can be modified so that they carry the transverse loading almost completely by axial action, i.e., by compression. However,

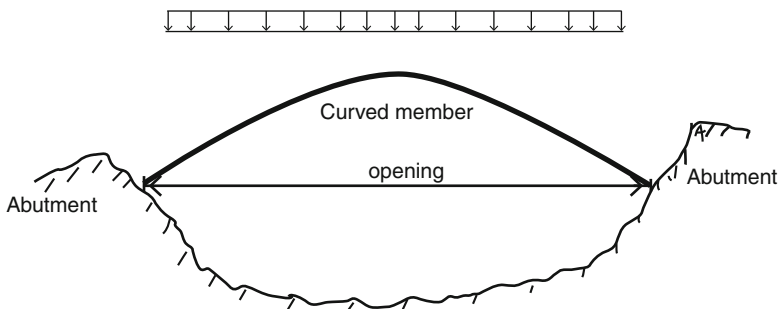


Fig. 6.1 Definition of an arch

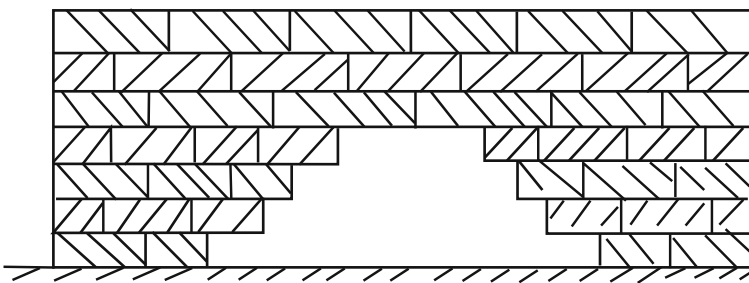


Fig. 6.2 Corbel arch

abutments are required to develop the compression type behavior and this requirement sometimes limits the applicability of the arch for a particular site.

In what follows, we briefly discuss the historical development of arch structures and then present the underlying theory for statically determinate curved members. This theory is similar to the theory for gable roof structures presented in Chap. 4. Later, in Chap. 9, we discuss the theory of statically indeterminate curved members.

Arches have many applications. They are used for openings in walls, for crossing gorges and rivers, and as monumental structures such as the Arc de Triumph. The first application of arch-type construction in buildings occurred around 4,000BC in Egypt and Greece. Openings in walls were spanned using the scheme shown in Fig. 6.2. Large flat stones were stacked in layers of increasing width until they met at the top layer. Each layer was stabilized by the weight applied above the layer. The concept is called a Corbel arch. No formwork is required to construct the structure. Also, no horizontal thrust and therefore no abutments are needed. The term “false arch” is sometimes used to describe this type of structure. False arches were used almost exclusively in ancient Greece where the techniques of masonry construction were perfected.

The type of arch construction shown in Fig. 6.3 for carrying vertical loading across an opening was introduced by the Egyptians around 3,000BC. It employs tapered stones, called voussoirs, which are arranged around a curved opening in such a manner that each brick is restrained by compressive and frictional forces. The system is unstable until the last stone, called the “keystone,” is placed. Consequently, temporary framework is required during construction.

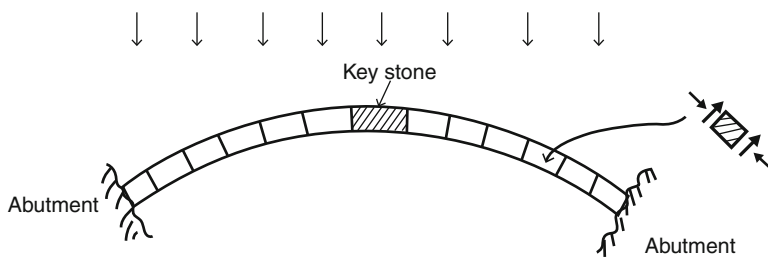


Fig. 6.3 Key stone arch construction



Fig. 6.4 Pont du Gard crossing

Starting around 300BC, the Romans perfected masonry arch construction and built some unique structures, many of which are still functioning after 2,000 years. They preferred circular arches and included them in buildings, bridges, and aqueducts. One of the most famous examples is the Pont du Gard, shown in Fig. 6.4; a bridge/aqueduct over the river Gard built in 19BC. Some of the stones weigh up to 6 t.

Another example of a second century multiple span Roman masonry bridge is shown in Fig. 6.5. The typical span length is 98 ft. This bridge crosses the Tagus River in Spain and was a key element in the transportation network connecting the outer Roman Provinces with Rome.

Masonry materials are ideal for arch construction since they are strong under compression and also very durable. However, it is difficult to construct long span masonry arch bridges. With the development of alternate structural materials such as cast iron and steel at the end of the eighteenth century, there was a shift toward arches formed with metal members. Figure 6.6 shows the Iron Bridge built in 1781.



Fig. 6.5 Alcantara Toledo bridge

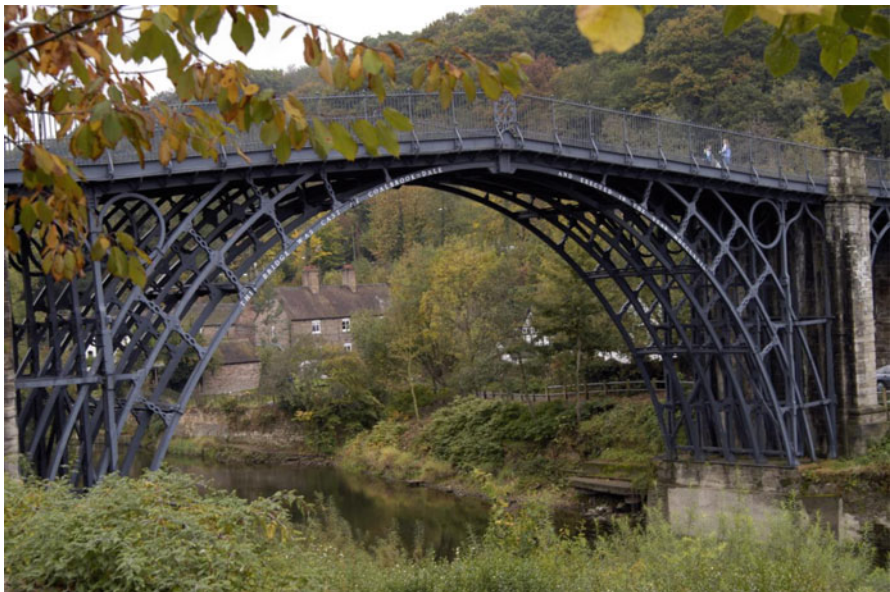


Fig. 6.6 Iron Bridge, England



Fig. 6.7 Eads Bridge, USA

The main span is 100 ft and crosses the Severn Gorge in the UK. Each of the members was formed using cast iron technology which was evolving at the time. Since cast iron is weak in tension and tends to fail in a brittle manner, it was shortly replaced as the material of choice by steel.

The development of railroads created a demand for bridges with more load capacity and longer spans. During this time period, there were many arch bridges constructed. Figure 6.7 shows the Eads Bridge built in 1874 across the Mississippi River in St. Louis, Missouri. This bridge has ribbed steel arch spans of 520 ft, fabricated with tubular structural alloy steel members; the first use of steel in a major bridge project. Today, the bridge is still carrying pedestrian, vehicular, and light rail traffic across the Mississippi.

At the end of the nineteenth century, reinforced concrete emerged as a major competitor to steel as a structural material. Reinforced concrete allowed one to form arch geometries that were aesthetically more pleasing than conventional steel arch geometries, and therefore became the preferred material. Most of this surge in popularity was due to the work of Robert Maillart, a Swiss Engineer (1872–1940), who developed arch concepts that revolutionized the design practice for reinforced concrete arches. An example is the Salginatobel Bridge, shown in Fig. 6.8. This bridge, built in 1930, crosses the Salgina Valley Ravine in Switzerland with a span of 270 ft. It is the ideal solution for this picturesque site and has been recognized by ASCE as a landmark project.



Fig. 6.8 Salginatobel Bridge, Switzerland

A unique arch bridge in the USA is the New Gorge Steel Arch Bridge located in West Virginia. Opened in 1977, it has the longest main span (1,700 ft) and highest height (876 ft) of all arch bridges in North and South America. It held the world record for span and height until 2003 when the Lupu Arch Bridge in Shanghai (1,800 ft span) was opened. A type of weathering steel called Corten was used in the New Gorge Arch structure in order to avoid the need for periodic painting.

Another unique arch bridge in the USA is the Hoover Dam Bypass Bridge. Segmented concrete construction was used to fabricate the concrete box elements in situ. The construction process employed a complex tieback scheme, as illustrated in Fig. 6.9b–d. The bridge was completed in 2010.

6.2 Modeling of Arch Structures

We idealize an arch structure as a curved member restrained at its ends with a combination of fixed, hinged, and roller supports. Figure 6.10 illustrates various types of end conditions. Case (a) corresponds to full end fixity, a condition that is difficult to achieve. The more common case is (b) where the abutments can prevent translation but not rotation. We refer to this structure as a two-hinged arch. The third case, (c), corresponds to a “tied arch structure” where the ends are interconnected with a tension member. This scheme is used when the abutments are not capable of resisting the horizontal thrust action of the arch.

If the arch is a bridge, the roadway may be connected above the structure as in Fig. 6.11a, or below the structure as in Fig. 6.11b. When placed above, the deck weight is transmitted by compression members to the arch. Decks placed below the arch are supported by cables. Both loading cases are idealized as a uniform loading *per horizontal projection* as shown in Fig. 6.11c. In some cases, soil backfill is

placed between the roadway and the arch. The soil loading is represented as a non uniform loading whose shape is defined by the arch geometry. Figure 6.11d, e illustrate this case.

The structures in Fig. 6.10 are statically indeterminate. We can reduce the two-hinge arch to a statically determinate structure by converting it to a three-hinge arch. The additional hinge is usually placed at mid-span as shown in Fig. 6.12.

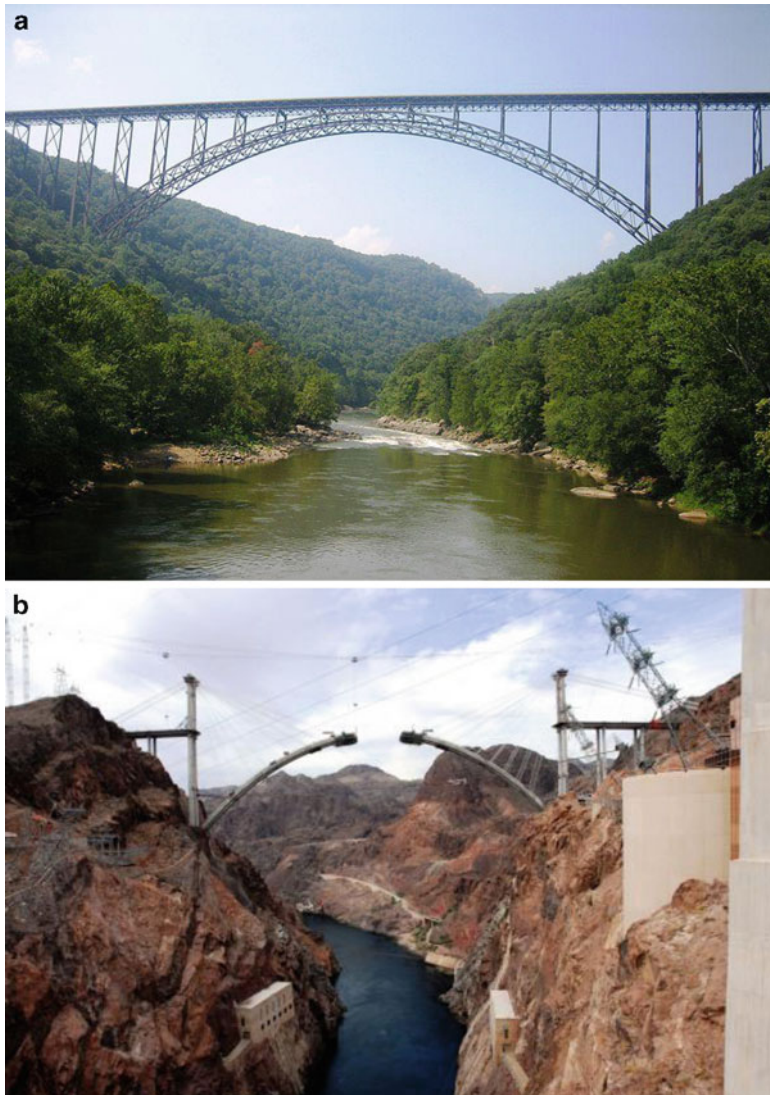


Fig. 6.9 Modern Arch Bridges in the USA. (a) New Gorge Arch, West Virginia. (b) Hoover Dam Bypass—under construction. (c) Hoover Dam Bypass—under construction. (d) Hoover Dam Bypass—under construction. (e) Hoover Dam Bypass—completed

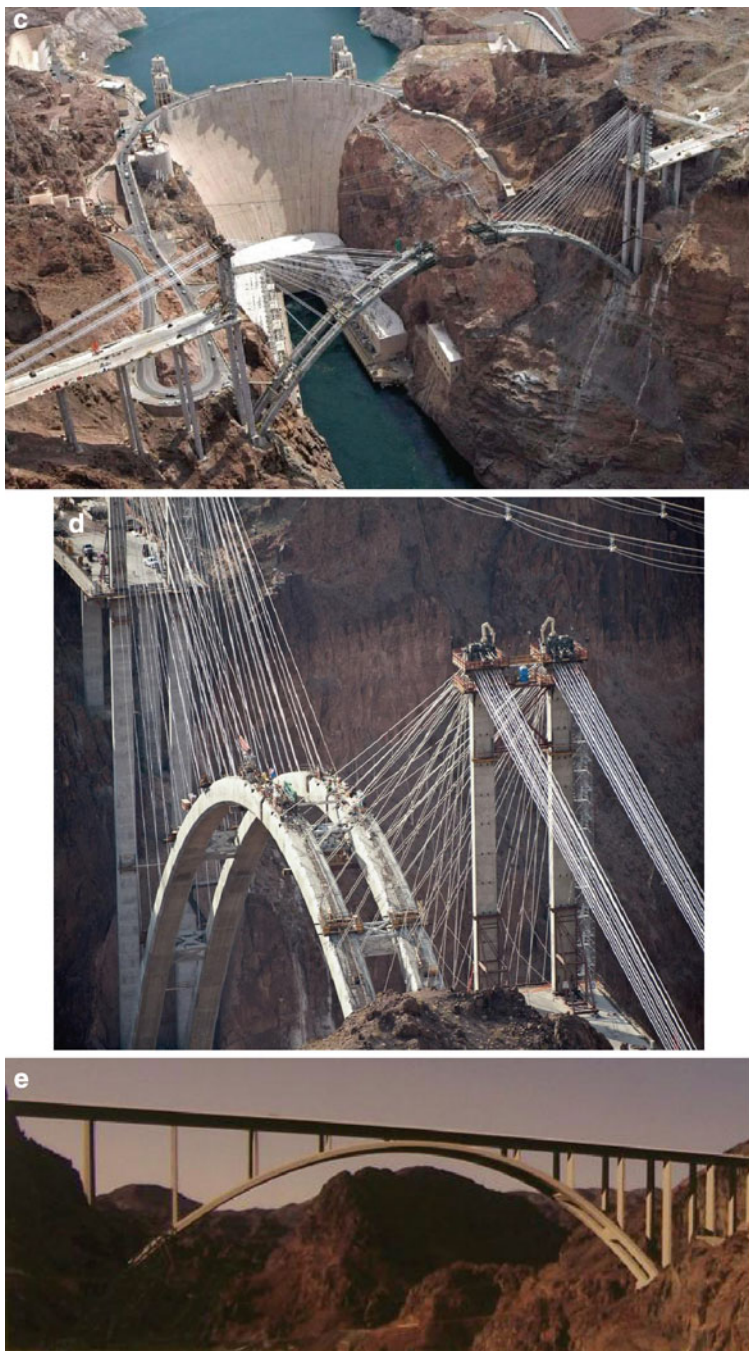


Fig. 6.9 (continued)

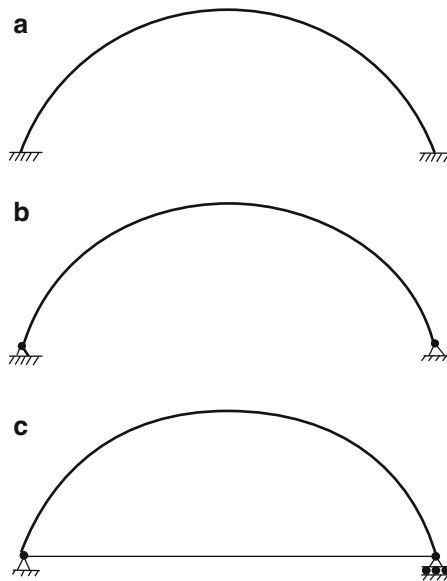


Fig. 6.10 Indeterminate Arch structures with various end fixity conditions. (a) Fully fixed Arch—three degree indeterminate. (b) Two-hinged arch—one degree indeterminate. (c) Tied arch—one degree indeterminate

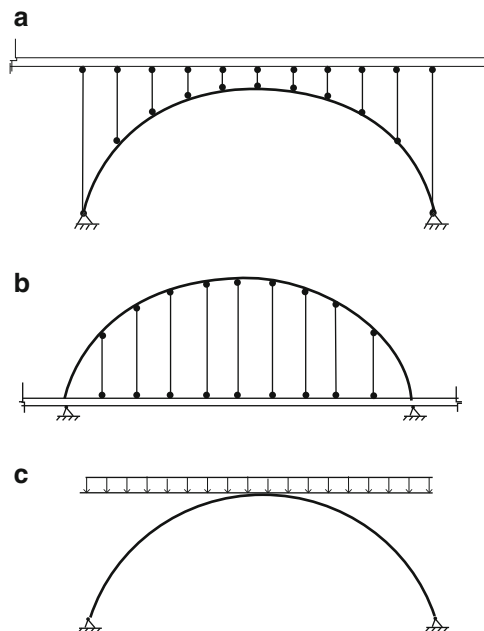


Fig. 6.11 Different roadway arrangements—idealized loading. (a) Roadway above the arch. (b) Roadway below the arch. (c) Idealized uniform dead loading. (d) Soil backfill above the arch. (e) Idealized soil loading

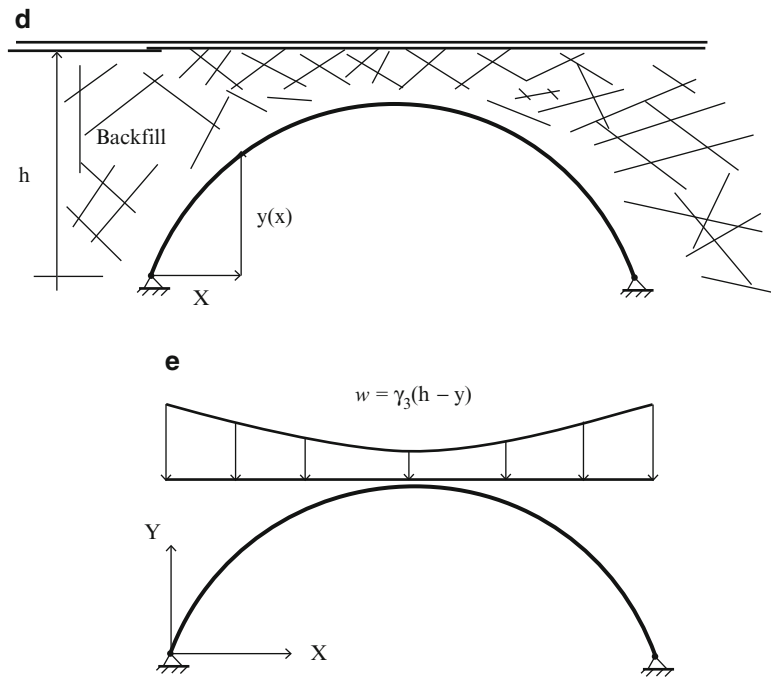


Fig. 6.11 (continued)

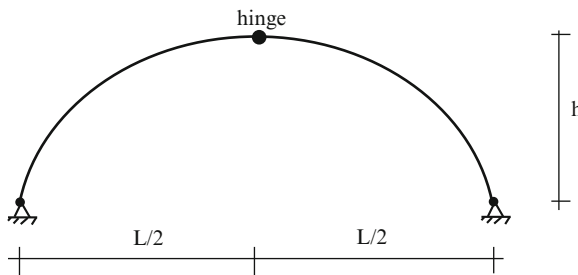


Fig. 6.12 Three-hinge arch

In this chapter, we first present a general theory of statically determinate curved members and then specialize the general theory for three-hinge arches. We treat statically indeterminate arches later in Chap. 9.

6.3 Internal Forces in Curved Members

We consider the statically determinate curved member shown in Fig. 6.13a. We work with a Cartesian reference frame having axes X and Y and define the centroidal axis of the member by the function, $y = y(x)$. The vertical loading is

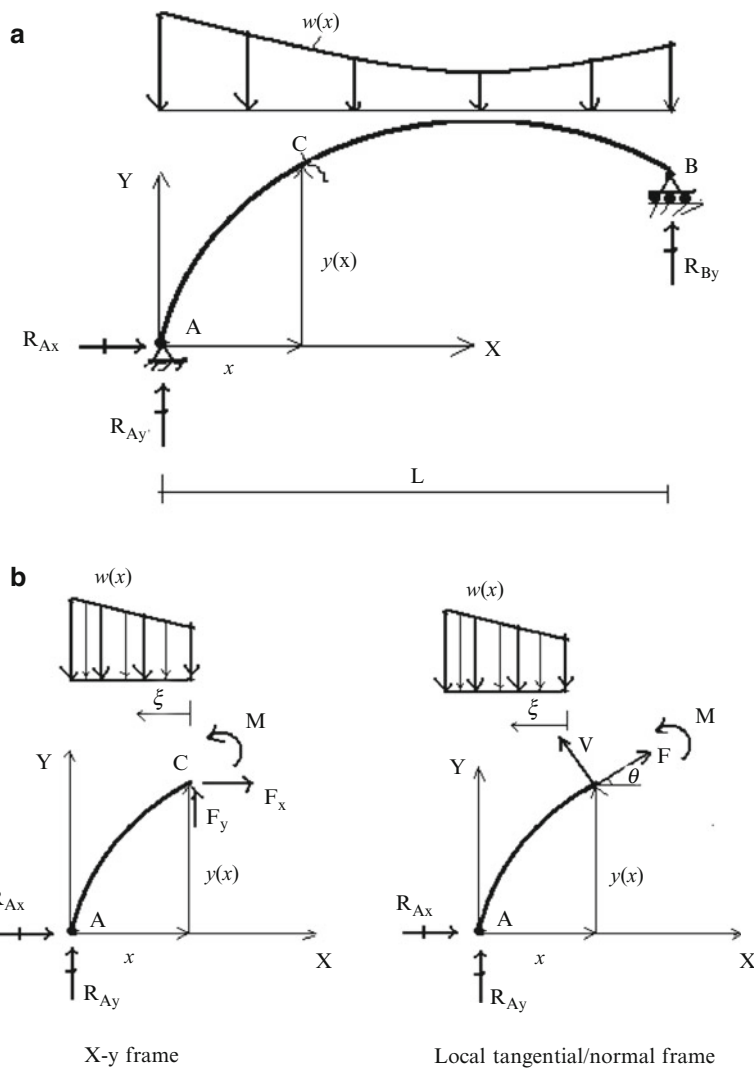


Fig. 6.13 (a) Notation for statically determinate curved member. (b) Free body diagram—curved beam. x - y frame. Local tangential/normal frame

assumed to be expressed in terms of the horizontal projected length. These choices are appropriate for the arch structures described in the previous section. We determine the reactions using the global equilibrium equations.

The applied load is equilibrated by internal forces, similar to the behavior of a straight beam under transverse load. To determine these internal forces, we isolate an arbitrary segment such as AC defined in Fig. 6.13b. We work initially with the internal forces referred to the X - Y frame and then transform them over to the local tangential/normal frame. Note that now there may be a longitudinal force component as well as a transverse force component, whereas straight beams subjected to transverse loading have no longitudinal component.

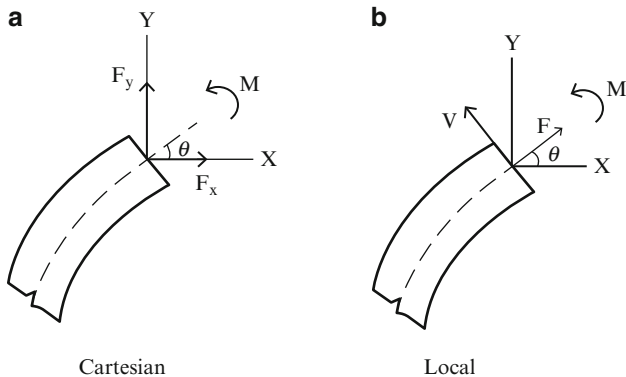


Fig. 6.14 Cartesian—local force components

Enforcing equilibrium leads to the general solution for the internal forces.

$$\begin{aligned} F_x &= -R_{Ax} \\ F_y &= -R_{Ay} + \int_0^x w(\xi) d\xi \\ M &= xR_{Ay} - yR_{Ax} - \int_0^x w(\xi)\xi d\xi \end{aligned} \quad (6.1)$$

Lastly, we transform the Cartesian force components (F_x, F_y) over to the tangential/normal frame (F, V). Noting Fig. 6.14, the transformation law is

$$\begin{aligned} F &= F_y \sin\theta + F_x \cos\theta \\ V &= F_y \cos\theta - F_x \sin\theta \\ \tan\theta &= \frac{dy}{dx} \end{aligned} \quad (6.2)$$

In order to evaluate the axial (F) and shear forces (V), we need to specify the angle θ between the tangent and the horizontal axis. This quantity depends on $y(x)$, the function that defines the shape of the centroidal axis.

We specialize the above set of equations for a symmetrical curved member where the loading consists of

- (a) A uniform vertical loading per projected length defined in Fig. 6.15.
- (b) A concentrated load at the crown defined in Fig. 6.16.

- (a) *Uniformly distributed load:*

Enforcing equilibrium and symmetry leads to

$$\begin{aligned} R_{Ax} &= 0 & R_{Ay} = R_{By} &= \frac{wL}{2} \\ F_x &= 0 & F_y &= -\frac{wL}{2}wx \\ M &= \frac{wL}{2}x - \frac{wx^2}{2} \end{aligned}$$

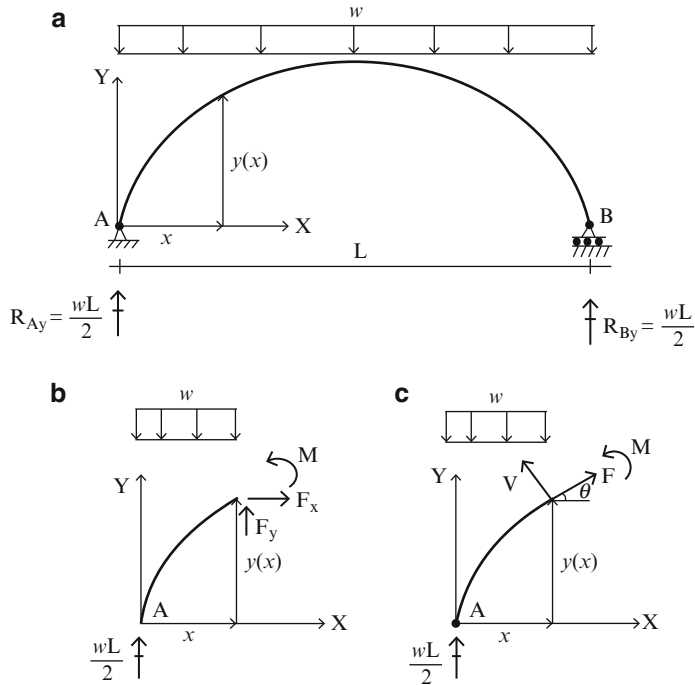


Fig. 6.15 Curved member—uniform vertical loading. (a) Reactions. (b) Internal forces—Cartesian frame. (c) Internal forces—local frame

Note that these results are the *same* as for a simply supported straight beam subjected to transverse loading.

Substituting for F_x and F_y in (6.2) results in the internal forces (F , V , M) due to a uniform vertical loading,

$$\begin{aligned} F &= \left(-\frac{wL}{2} + wx \right) \sin \theta \\ V &= \left(-\frac{wL}{2} + wx \right) \cos \theta \\ M &= \frac{wL}{2}x - \frac{wx^2}{2} \end{aligned} \quad (6.3)$$

(b) *Concentrated load:*

The internal forces referred to the Cartesian frame are
Segment AC $0 \leq x < L/2$

$$F_x = 0$$

$$F_y = -\frac{P}{2}$$

$$M = \frac{P}{2}x$$

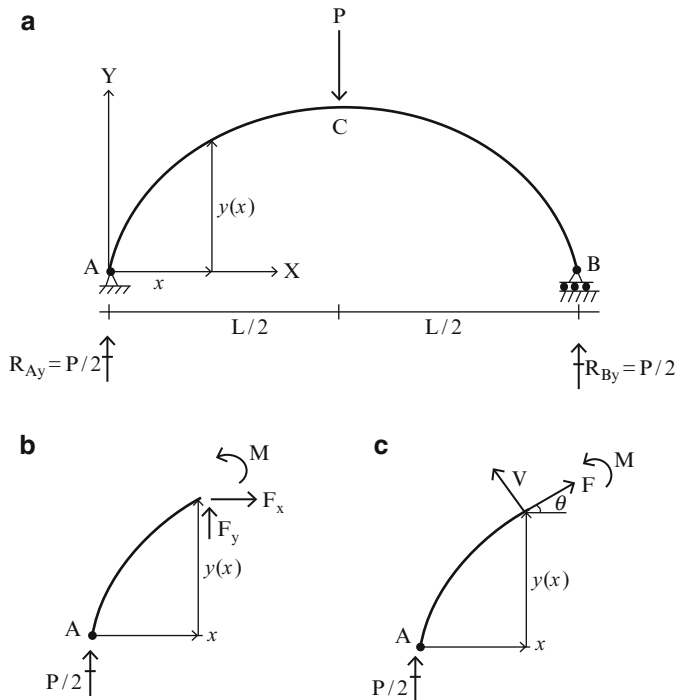
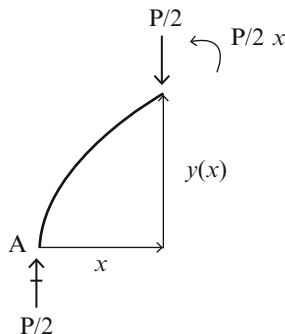


Fig. 6.16 Curved member—concentrated load. (a) Reactions. (b) Internal forces—Cartesian frame. (c) Internal forces—local frame

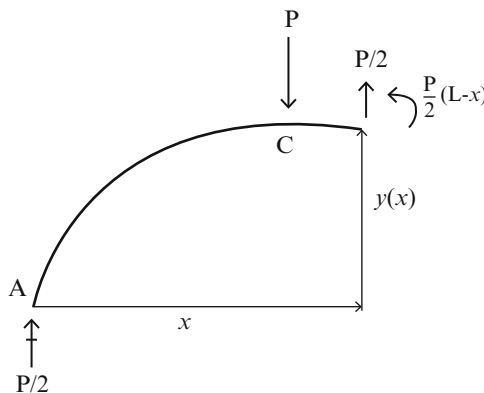


Segment CB $L/2 < x \leq L$

$$F_x = 0$$

$$F_y = \frac{P}{2}$$

$$M = \frac{P}{2}(L - x)$$



Substituting for F_x and F_y in (6.2) results in the internal forces (F, V, M) in the local frame,

$$\text{For } 0 \leq x < L/2 \quad \text{For } L/2 < x \leq L$$

$$\begin{aligned} F &= -\frac{P}{2} \sin \theta & F &= -\frac{P}{2} \sin \theta \\ V &= -\frac{P}{2} \cos \theta & V &= +\frac{P}{2} \cos \theta \\ M &= \frac{P}{2}x & M &= \frac{P}{2}(L-x) \end{aligned} \tag{6.4}$$

6.4 Parabolic Geometry

We will show later that a parabolic arch is the optimal shape for a uniform vertical loading, in the sense that there is essentially no bending, only axial force, introduced by this loading. Using the notation defined in Fig. 6.17, the parabolic curve is expressed in terms of h , the height at mid-span, and the dimensionless coordinate, x/L .

$$y(x) = 4h \left[\frac{x}{L} - \left(\frac{x}{L} \right)^2 \right] \tag{6.5}$$

Differentiating $y(x)$ leads to

$$\tan \theta = \frac{dy}{dx} = 4 \frac{h}{L} \left(1 - 2 \frac{x}{L} \right) \tag{6.6}$$

The maximum value of θ is at $x = 0, L$

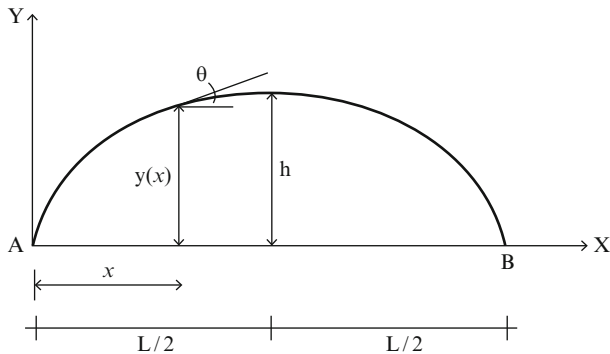


Fig. 6.17 Notation for parabolic shape function

$$\theta_{\max} = \pm \tan^{-1} \left(4 \frac{h}{L} \right)$$

Values of θ_{\max} vs. h/L are tabulated in the table below.

| $\frac{h}{L}$ | θ_{\max} (°) | $\tan \theta_{\max}$ | $\cos \theta_{\max}$ | $\sin \theta_{\max}$ |
|---------------|---------------------|----------------------|----------------------|----------------------|
| 0 | 0 | 0 | 1 | 0 |
| 0.01 | ± 2.3 | ± 0.04 | 0.999 | ± 0.04 |
| 0.025 | ± 5.7 | ± 0.1 | 0.995 | ± 0.099 |
| 0.05 | ± 11.3 | ± 0.2 | 0.98 | ± 0.196 |
| 0.1 | ± 21.8 | ± 0.4 | 0.93 | ± 0.37 |
| 0.15 | ± 30.9 | ± 0.6 | 0.86 | ± 0.51 |
| 0.2 | ± 38.6 | ± 0.8 | 0.78 | ± 0.62 |
| 0.25 | ± 45 | ± 1 | 0.7 | ± 0.7 |
| 0.3 | ± 50.2 | ± 1.2 | 0.64 | ± 0.77 |
| 0.35 | ± 54.4 | ± 1.4 | 0.58 | ± 0.81 |
| 0.4 | ± 58 | ± 1.6 | 0.53 | ± 0.85 |
| 0.45 | ± 60.9 | ± 1.8 | 0.48 | ± 0.87 |
| 0.5 | ± 63.4 | ± 2 | 0.45 | ± 0.89 |

The parameter h/L is a measure of the steepness of the curved member. Deep curved members have $h/L \geq \approx 0.25$. A curved member is said to be shallow when h/L is small with respect to unity, on the order of 0.1. The trigonometric measures for a shallow curved member are approximated by

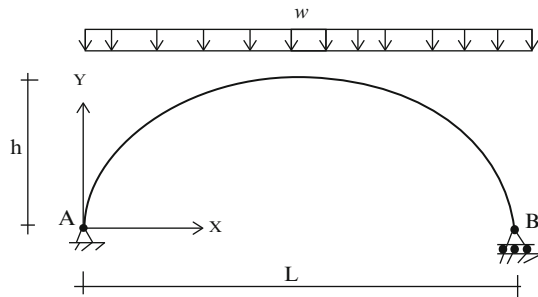
$$\text{shallow parabolic curve} \left\{ \begin{array}{l} \tan \theta = \frac{dy}{dx} \approx \theta \text{ (rad)} \\ \cos \theta = \frac{1}{\sqrt{1 + \tan^2 \theta}} \approx 1 \\ \sin \theta = \frac{\tan \theta}{\sqrt{1 + \tan^2 \theta}} \approx \tan \theta \approx \theta \text{ (rad)} \end{array} \right. \quad (6.7)$$

Example 6.1 Shallow vs. deep parabolic curved members

Given: The parabolic curved beam defined in Fig. E6.1a.

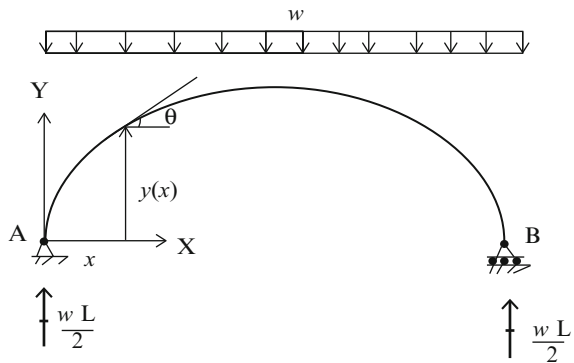
Determine: The axial, shear, and moment distributions for (a) $h/L = 0.1$, (b) $h/L = 0.5$.

Fig. E6.1a Parabolic geometry



Solution: Enforcing equilibrium and symmetry leads to the reactions listed in Fig. E6.1b.

Fig. E6.1b Reactions



Applying (6.3) and (6.5), the internal forces in the local frame are

$$F = \left(-\frac{wL}{2} + wx \right) \sin \theta$$

$$V = \left(-\frac{wL}{2} + wx \right) \cos \theta$$

$$M = \frac{wL}{2}x - \frac{wx^2}{2}$$

where

$$\cos \theta = \frac{1}{\sqrt{1 + \left(4 \frac{h}{L} \left(1 - 2 \frac{x}{L}\right)\right)^2}}$$

$$\sin \theta = \frac{4 \frac{h}{L} \left(1 - 2 \frac{x}{L}\right)}{\sqrt{1 + \left(4 \frac{h}{L} \left(1 - 2 \frac{x}{L}\right)\right)^2}}$$

The internal forces are listed in the table below and plotted in Figs. E6.1c–e for $h/L = 0.1$ and $h/L = 0.5$:

| $\frac{x}{L}$ | $\frac{h}{L} = 0.1$ | | $\frac{h}{L} = 0.5$ | | |
|---------------|---------------------|----------------|---------------------|----------------|----------------|
| | $\frac{M}{wL^2}$ | $\frac{V}{wL}$ | $\frac{F}{wL}$ | $\frac{V}{wL}$ | $\frac{F}{wL}$ |
| 0 | 0 | -0.464 | -0.186 | -0.224 | -0.447 |
| 0.1 | 0.045 | -0.381 | -0.122 | -0.212 | -0.339 |
| 0.2 | 0.08 | -0.292 | -0.07 | -0.192 | -0.125 |
| 0.3 | 0.105 | -0.197 | -0.032 | -0.156 | -0.125 |
| 0.4 | 0.12 | -0.1 | -0.008 | -0.093 | -0.037 |
| 0.5 | 0.125 | 0 | 0 | 0 | 0 |
| 0.6 | 0.12 | 0.1 | -0.008 | 0.093 | -0.037 |
| 0.7 | 0.105 | 0.197 | -0.032 | 0.156 | -0.125 |
| 0.8 | 0.08 | 0.292 | -0.07 | 0.192 | -0.23 |
| 0.9 | 0.045 | 0.381 | -0.122 | 0.212 | -0.339 |
| 1 | 0 | 0.464 | -0.186 | 0.224 | -0.447 |

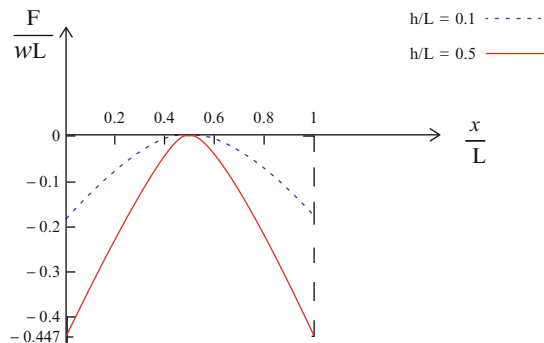
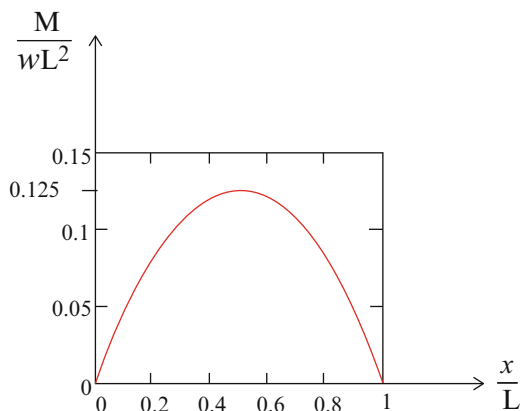
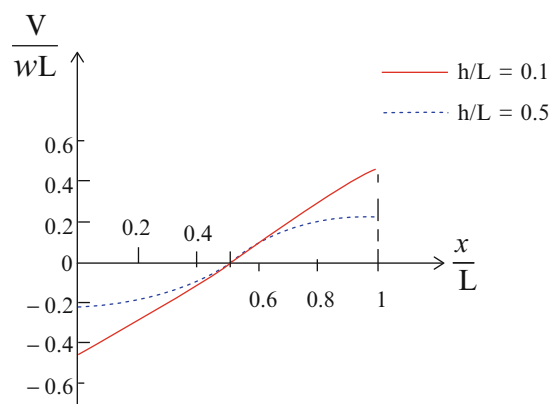


Fig. E6.1c Axial force, F

Fig. E6.1d Moment, M **Fig. E6.1e** Shear, V 

The axial force is compressive and the maximum value occurs at the supports. The maximum shear force also occurs at the supports. The maximum moment occurs at the mid-span. These maximum values are listed below.

$$F_{\max} = \begin{cases} 0.186 wL & \text{for } \frac{h}{L} = 0.1 \\ 0.447 wL & \text{for } \frac{h}{L} = 0.5 \end{cases}$$

$$V_{\max} = \begin{cases} 0.464 wL & \text{for } \frac{h}{L} = 0.1 \\ 0.224 wL & \text{for } \frac{h}{L} = 0.5 \end{cases}$$

$$M_{\max} = 0.125 wL^2$$

Example 6.2 Shallow vs. deep parabolic curved members

Given: The parabolic curved beam defined in Fig. E6.2a

Determine: The axial, shear, and moment distributions for (a) $h/L = 0.1$, (b) $h/L = 0.5$.

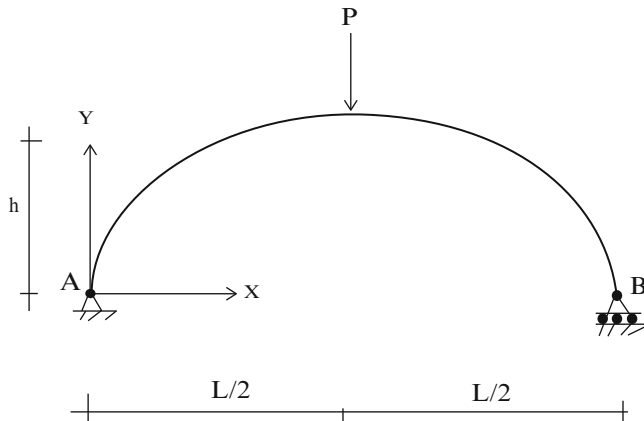


Fig. E6.2a

Solution: Enforcing equilibrium and symmetry leads to the reactions listed in Fig. E6.2b.

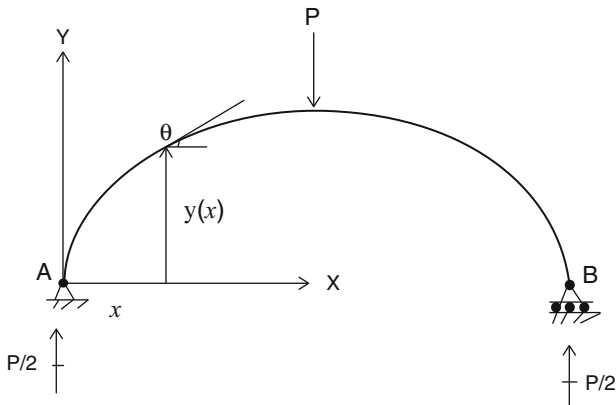


Fig. E6.2b Reactions

Applying (6.4) and (6.5), the internal forces in the local frame are

For $0 \leq x < L/2$ For $L/2 < x \leq L$

$$F = -\frac{P}{2} \sin \theta \quad F = -\frac{P}{2} \sin \theta$$

$$V = -\frac{P}{2} \cos \theta \quad V = +\frac{P}{2} \cos \theta$$

$$M = \frac{P}{2}x \quad M = +\frac{P}{2}(L-x)$$

where

$$\cos \theta = \frac{1}{\sqrt{1 + \left(4 \frac{h}{L} \left(1 - 2 \frac{x}{L}\right)\right)^2}}$$

$$\sin \theta = \frac{4 \frac{h}{L} \left(1 - 2 \frac{x}{L}\right)}{\sqrt{1 + \left(4 \frac{h}{L} \left(1 - 2 \frac{x}{L}\right)\right)^2}}$$

The internal forces are plotted in Figs. E6.1c–e and listed in the table which follows for $h/L = 0.1$ and $h/L = 0.5$.

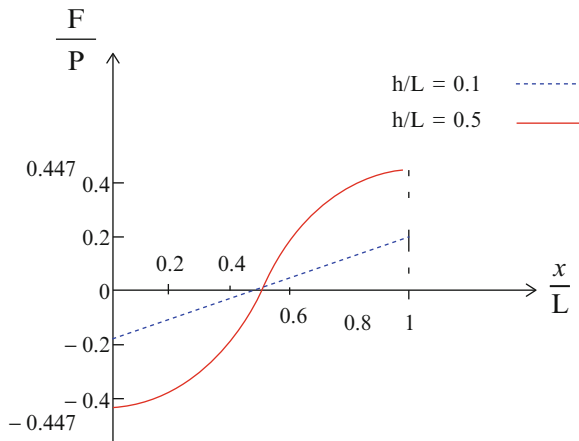


Fig. E6.2c Axial force, F

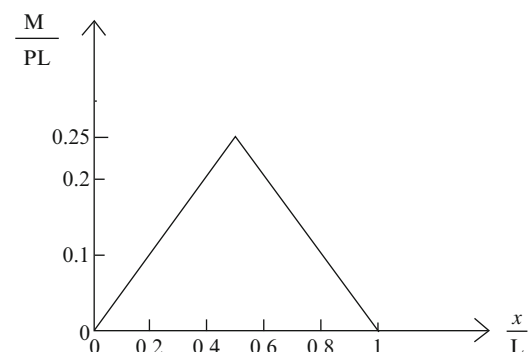
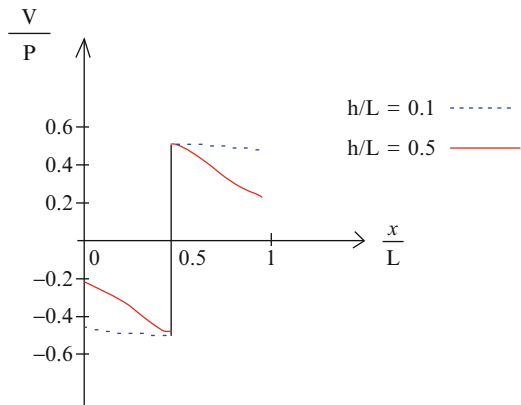


Fig. E6.2d Moment, M

Fig. E6.2e Shear, V 

The axial force is compressive and the maximum value occurs at the supports. The maximum shear force and maximum moment occurs at the mid-span.

| $\frac{x}{L}$ | $\frac{M}{PL}$ | $\frac{h}{L} = 0.1$ | | $\frac{h}{L} = 0.5$ | |
|---------------|----------------|---------------------|---------------|---------------------|---------------|
| | | $\frac{V}{P}$ | $\frac{F}{P}$ | $\frac{V}{P}$ | $\frac{F}{P}$ |
| 0 | 0 | -0.464 | -0.186 | -0.224 | -0.447 |
| 0.1 | 0.05 | -0.476 | -0.152 | -0.265 | -0.424 |
| 0.2 | 0.1 | -0.486 | -0.117 | -0.32 | -0.384 |
| 0.3 | 0.15 | -0.494 | -0.079 | -0.39 | -0.312 |
| 0.4 | 0.2 | -0.498 | -0.04 | 0.464 | -0.186 |
| 0.5 | 0.25 | 0.5 | 0 | 0.5 | 0 |
| 0.6 | 0.2 | 0.498 | 0.04 | 0.464 | 0.186 |
| 0.7 | 0.15 | 0.494 | 0.079 | 0.39 | 0.312 |
| 0.8 | 0.1 | 0.486 | 0.177 | 0.32 | 0.384 |
| 0.9 | 0.05 | 0.476 | 0.152 | 0.265 | 0.424 |
| 1 | 0 | 0.464 | 0.186 | 0.244 | 0.447 |

6.5 Method of Virtual Forces for Curved Members

Displacements are determined using the form of the Method of Virtual Forces specialized for curved members [16]:

$$d \delta P = \int_s \left\{ \frac{F}{AE} \delta F + \frac{V}{GA_s} \delta V + \frac{M}{EI} \delta M \right\} ds \quad (6.9)$$

where d is the desired displacement, δP , δF , δV , δM denote the virtual force system, and the various terms represent the contribution of axial, shear, and bending deformation. As discussed in Chaps. 3 and 4, the contributions of axial and shear deformation are usually small and only the bending deformation term is retained for slender straight beams and frames composed of slender straight members.

$$d \delta P \approx \int_x \frac{M \delta M}{EI} dx$$

For curved members, we distinguish between “non-shallow” and “shallow” members.

6.5.1 Non-shallow Slender Curved Members

For non-shallow slender curved members subjected to transverse loading, the contributions of axial and shear deformation are usually small and only the bending deformation term is retained. In this case, we approximate (6.9) with

$$d \delta P \approx \int_s \frac{M}{EI} \delta M ds = \int_x \frac{M \delta M}{EI \cos \theta} dx \quad (6.10)$$

6.5.2 Shallow Slender Curved Members

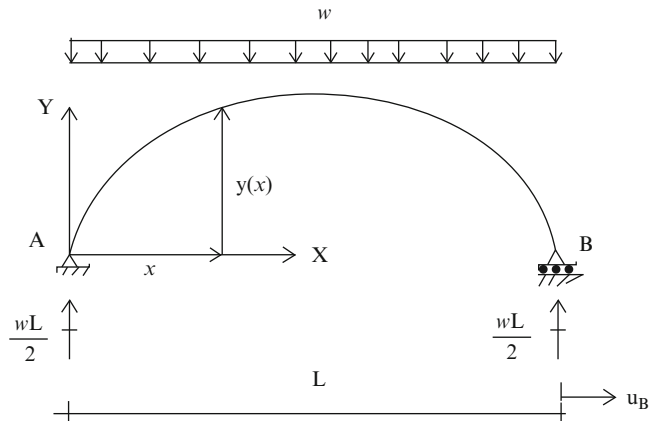
For shallow slender curved members subjected to transverse loading, the axial deformation may be as significant as the bending deformation and therefore *must be retained*. In this case, we use

$$d \delta P \approx \int_s \left\{ \frac{F}{AE} \delta F + \frac{M}{EI} \delta M \right\} ds = \int_x \left\{ \frac{F}{AE} \delta F + \frac{M}{EI} \delta M \right\} \frac{dx}{\cos \theta} \quad (6.11)$$

Example 6.3 Deflection of Parabolic curved beam—shallow vs. deep

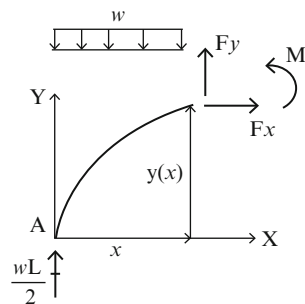
Given: The parabolic curved beam defined in Fig. E6.3a. Consider EI is constant.

Determine: The horizontal displacement at B for (a) non-shallow beam and (b) shallow beam.

**Fig. E6.3a**

The internal forces for this loading are

$$\begin{aligned} F_x &= 0 & F &= \left(-\frac{wL}{2} + wx \right) \sin \theta \\ F_y &= -\frac{wL}{2} + \frac{wx}{2} & \rightarrow & V = \left(-\frac{wL}{2} + wx \right) \cos \theta \\ M &= \frac{wL}{2}x - \frac{wx^2}{2} & M &= \frac{wL}{2}x - \frac{wx^2}{2} \end{aligned}$$



If the horizontal displacement at support B is desired, we select the virtual force system shown in Fig. E6.3b.

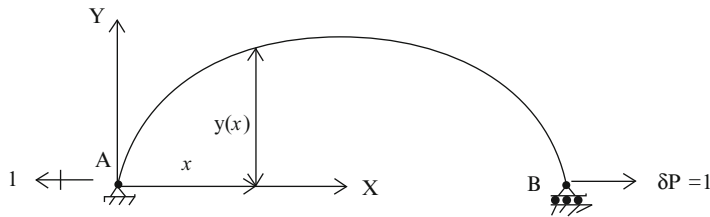


Fig. E6.3b Virtual force system for u_B

The internal virtual forces are

$$\delta F_x = 1$$

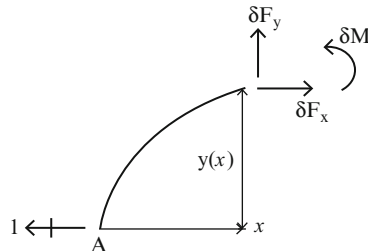
$$\delta F_y = 0$$

$$\delta F = \delta F_y \sin\theta + \delta F_x \cos\theta = \cos\theta$$

$$\delta V = \delta F_y \cos\theta - \delta F_x \sin\theta = -\sin\theta$$

$$\delta M = y(x)$$

$$\tan\theta = \frac{dy}{dx}$$



(a) *Non-shallow curved member:*

We use the approximate form defined by (6.10) for a non-shallow curved member.

$$u_B = \int_0^L \frac{M \delta M}{EI \cos\theta} dx$$

Substituting for M , δM , and $\cos\theta$, this expression expands to

$$u_B = \int_0^L \left(\frac{wL}{2}x - \frac{wx^2}{2} \right) \left\{ 4h \left(\frac{x}{L} - \left(\frac{x}{L} \right)^2 \right) \right\} \sqrt{1 + (\tan\theta)^2} \frac{dx}{EI}$$

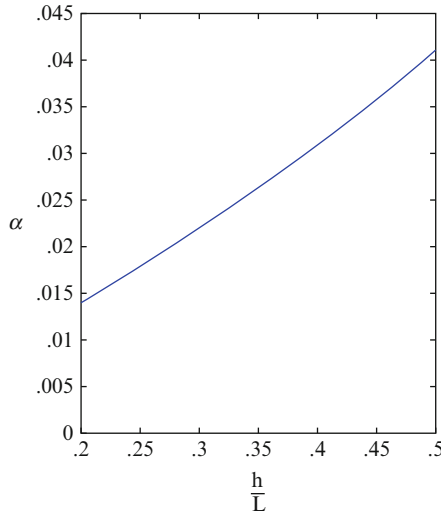
where

$$\tan\theta = 4 \frac{h}{L} \left(1 - 2 \frac{x}{L} \right)$$

For EI constant, the solution is expressed as

$$u_B = \frac{wL^4}{EI}(\alpha)$$

where α is a function of h/L . We evaluate α using numerical integration. The result is plotted below.



(b) *Shallow curved member:*

When the parabola is shallow ($\cos\theta \approx 1$), we need to include the axial deformation term as well as the bending deformation term. Starting with the form specified for a shallow member, (6.11),

$$u_B = \int_x \left(\frac{F}{AE} \delta F + \frac{M}{EI} \delta M \right) dx$$

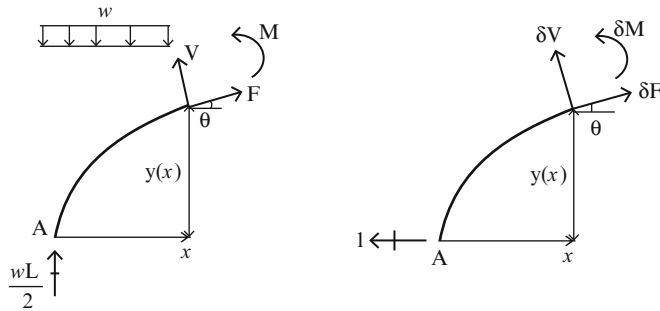
and noting that

$$F \approx \left(-\frac{wL}{2} + wx \right) \frac{dy}{dx} = -\frac{2wh}{L^2} (L - 2x)^2 \quad \delta F \cos\theta \approx 1$$

$$\delta F = \delta F_x$$

$$\delta V = 0$$

$$M = \frac{wL}{2}x - \frac{wx^2}{2} \quad \delta M = y = 4h \left\{ \frac{x}{L} - \left(\frac{x}{L} \right)^2 \right\}$$



Leads to

$$u_B = -\frac{2}{3} \frac{wLh}{AE} + \frac{1}{15} \frac{whL^3}{EI}$$

Note that the axial deformation causes the ends to move together, whereas the bending deformation causes the ends to move apart.

6.5.3 Circular Curved Member

When the arch geometry is a circular segment, it is more convenient to work with polar coordinates. We consider the segment shown in Fig. 6.18. In this case R is constant and θ is the independent variable. The differential arc length ds is equal to $Rd\theta$.

We assume the member is slender and retain only the bending deformation term. Equation (6.10) takes the following form

$$d\delta P = \int_0^{\theta_B} \frac{M \delta M}{EI} R d\theta \quad (6.12)$$

When EI is constant, the equation simplifies to

$$d\delta P = \frac{R}{EI} \int_0^{\theta_B} M \delta M d\theta \quad (6.13)$$

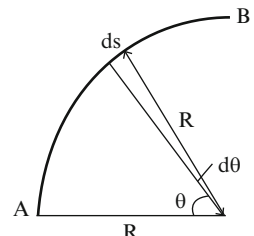
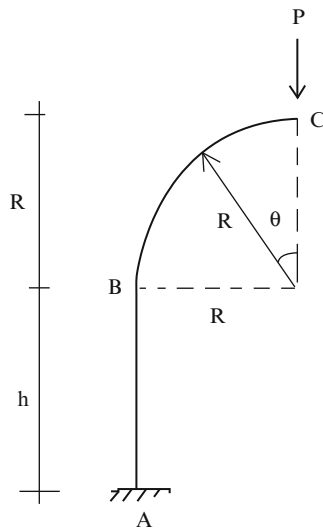


Fig. 6.18 Geometry—Circular arch

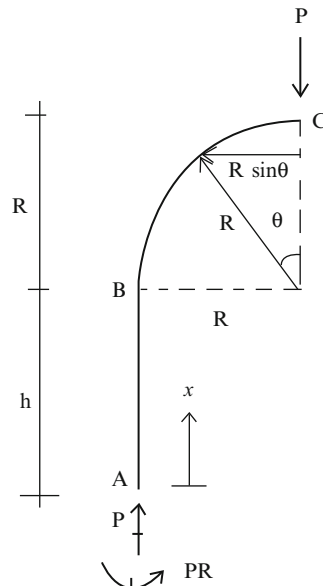
Example 6.4 Deflection of a light pole

Given: The light pole structure defined in Figs. E6.4a–d. Consider EI is constant.
Determine: The horizontal and vertical displacements at C.

Fig. E6.4a

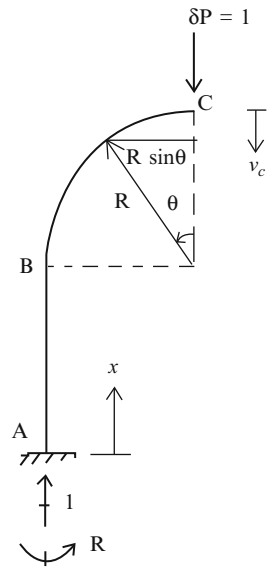
Solution: Member AB is straight and BC is a circular arc. We take the polar angle from C toward B. The bending moment distribution due to P is

$$\begin{array}{ll} \text{Segment B - C} & M = -PR\sin\theta \quad 0 < \theta < \pi/2 \\ \text{Segment A - B} & M = -PR \quad 0 < x < h \end{array}$$

Fig. E6.4b

The vertical displacement at C is determined with the following virtual force system

Fig. E6.4c



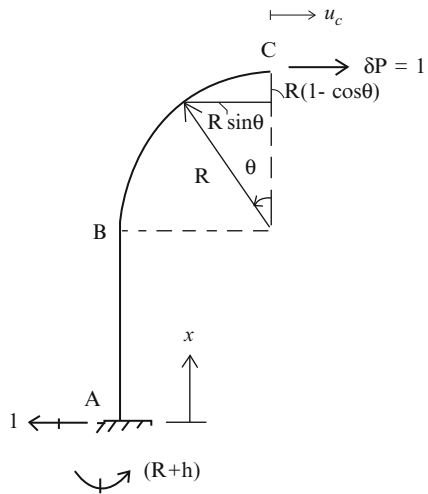
$$\begin{array}{lll} \text{Segment B - C} & \delta M = -R \sin \theta & 0 < \theta < \pi/2 \\ \text{Segment A - B} & \delta M = -R & 0 < x < h \end{array}$$

Considering only bending deformation terms, the displacement is given by

$$\begin{aligned} v_c &= v_c|_{AB} + v_c|_{CB} \\ &= \frac{1}{EI} \int_0^h (-PR)(-R)dx + \frac{1}{EI} \int_0^{\pi/2} (-PR \sin \theta)(-R \sin \theta)R d\theta \\ &= \frac{PR^2 h}{EI} + \frac{1}{EI} \int_0^{\pi/2} PR^3 (\sin \theta)^2 d\theta \\ &= \frac{PR^2}{EI} \left(h + \frac{\pi}{4} R \right) \end{aligned}$$

Following a similar approach, the virtual force system corresponding to the horizontal displacement at C is evaluated

Fig. E6.4d



$$\text{Segment B} - \text{C} \quad \delta M = -R(1 - \cos \theta) \quad 0 < \theta < \pi/2$$

$$\text{Segment A} - \text{B} \quad \delta M = -(R + h) + x \quad 0 < x < h$$

Then

$$\begin{aligned} u_c &= u_c|_{AB} + u_c|_{BC} \\ &= \frac{1}{EI} \int_0^h (-PR)(-R - h + x) dx + \frac{1}{EI} \int_0^{\pi/2} (-PR \sin \theta) R(-1 + \cos \theta) R d\theta \\ &= \frac{PRh^2}{2EI} + \frac{PR^2h}{EI} + \frac{1}{EI} \int_0^{\pi/2} PR^3(1 - \cos \theta) \sin \theta d\theta \\ &= \frac{P}{EI} \left(\frac{R^3}{2} + \frac{h^2R}{2} + R^2h \right) \end{aligned}$$

6.6 Analysis of Three-Hinged Arches

An arch is a particular type of curved member that is restrained against movement at its ends. These restraints produce longitudinal forces which counteract the action of vertical loads. Arch structures are generally more efficient than straight

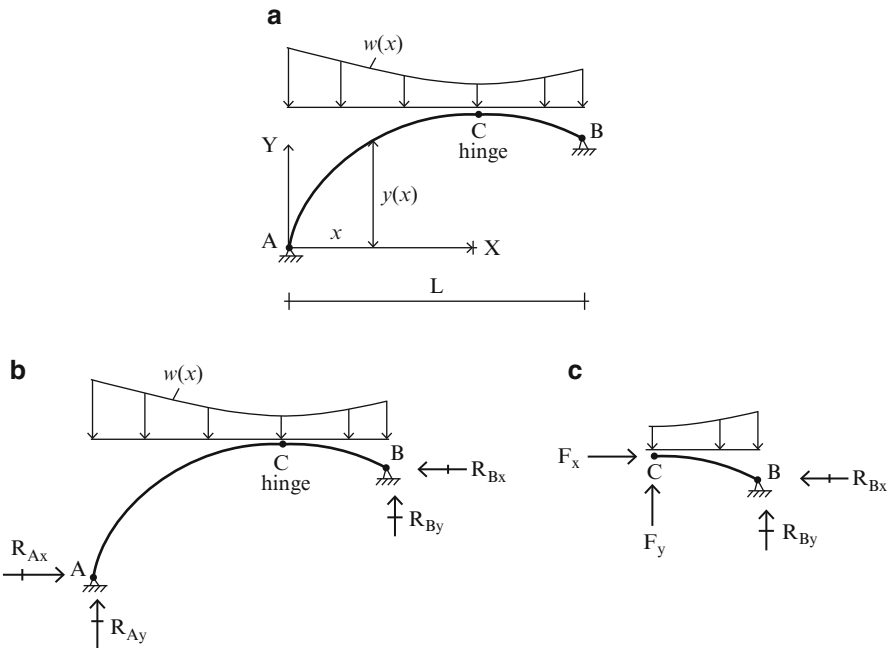


Fig. 6.19 Geometry and reactions—three-hinged arch. (a) Geometry. (b) Reactions. (c) Right segment

members. In this section, we examine three-hinged arches, which are a popular form of arch structure. These structures are statically determinate. A more detailed study of statically indeterminate arches is presented in Chap. 9.

Consider the arch shown in Fig. 6.19. This structure is statically determinate since there is a moment release at C. The overall analysis strategy is as follows:

Step 1: Moment summation about A

Step 2: Moment summation about C for segment CB of the arch

These steps results in two equations relating R_{Bx} and R_{By} , which can be solved.

Step 3: X force summation $\rightarrow R_{Ax}$

Step 4: Y force summation $\rightarrow R_{Ay}$

Once the reactions are known, one can work in from either end and determine the internal forces and moment using the equations derived in the previous section. The following examples illustrate the approach.

Example 6.5 Three-Hinged parabolic Arch

Given: The three-hinged arch shown in Fig. E6.5a.

Determine: The reactions. Assume $L_1 = 30 \text{ m}$, $w = 15 \text{ kN/m}$.

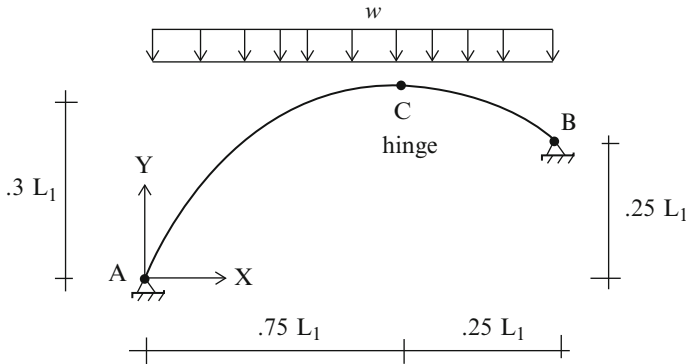


Fig. E6.5a

Solution: Summing moments about A and C leads to (Figs. E6.5b, c)

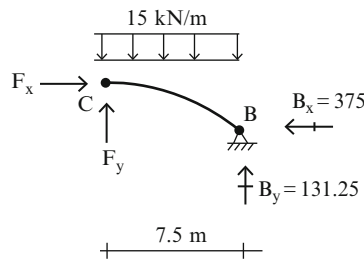
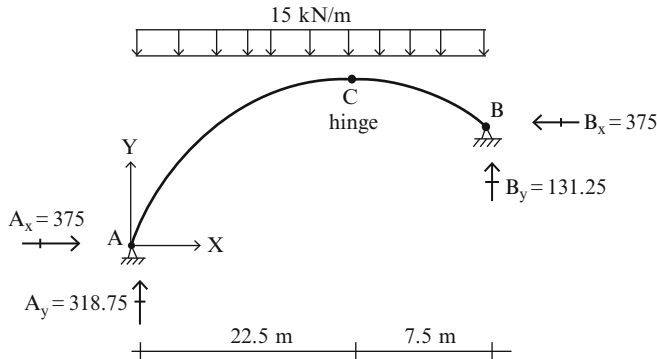
$$\begin{aligned}\sum M_{\text{at A}} &= 0 \quad -w \frac{(L_1)^2}{2} + B_x(0.25L_1) + B_y(L_1) = 0 \\ \sum M_{\text{at C}} &= 0 \quad -w \frac{(0.25L_1)^2}{2} - B_x(0.05L_1) + B_y(0.25L_1) = 0\end{aligned}$$

The solution of the above equations leads to

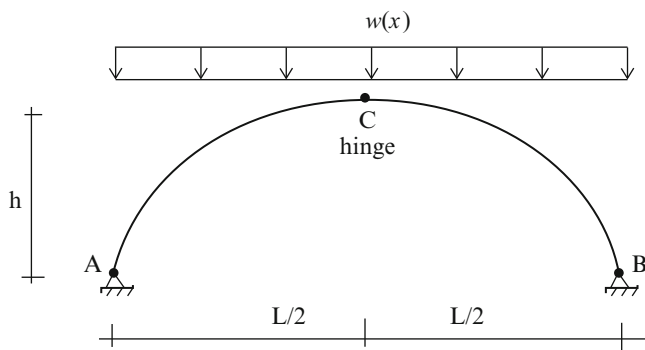
$$\begin{aligned}B_x &= \frac{5}{6}wL_1 = 375 \text{ kN} \leftarrow \\ B_y &= \frac{7}{24}wL_1 = 131.25 \text{ kN} \uparrow\end{aligned}$$

Lastly, the reactions at A are determined using force equilibrium:

$$\begin{aligned}\sum F_y &= 0 \quad A_y = -B_y + wL_1 = \frac{17}{24}wL_1 = 318.75 \text{ kN} \uparrow \\ \sum F_x &= 0 \quad A_x = -B_x = 375 \text{ kN} \rightarrow\end{aligned}$$

**Fig. E6.5b****Fig. E6.5c**

Example 6.6 Three-Hinged parabolic Arch—uniform vertical loading
Given: The parabolic arch shown in Fig. E6.6a.

**Fig. E6.6a**

Determine: The internal forces and the vertical displacement at C (v_c).

Solution: The loading and arch geometry are symmetrical with respect to mid-span. It follows that the vertical reactions are equal to $wL/2$. Setting the moment at C equal to zero, we obtain an expression for R_{Bx} (Fig. E6.6b).

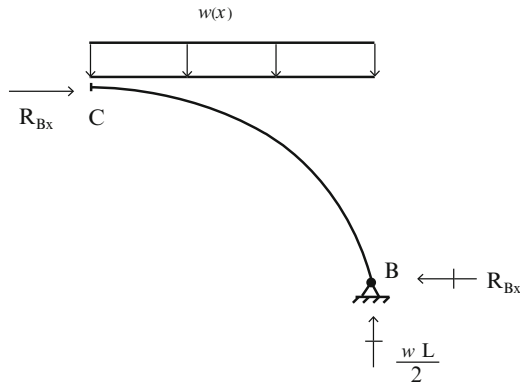


Fig. E6.6b

$$\sum M_c = 0$$

$$\frac{w}{2} \left(\frac{L}{2}\right)^2 + hR_{Bx} = \frac{wL}{2} \frac{L}{2} \rightarrow R_{Bx} = \frac{wL^2}{8h} \leftarrow$$

Then, summing X forces,

$$\begin{aligned} \sum F_x &= 0 \\ R_{Ax} &= \frac{wL^2}{8h} \rightarrow \end{aligned}$$

The results are listed below (Figs. E6.6b, c).

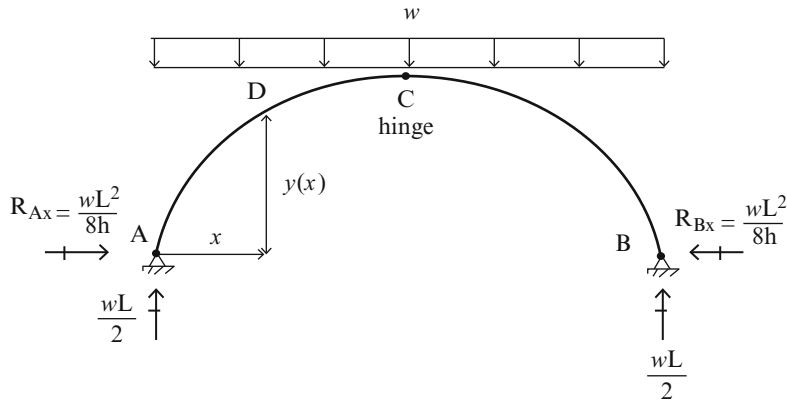


Fig. E6.6c

Cutting the member at D, isolating the segment AD, and applying the equilibrium conditions leads to:

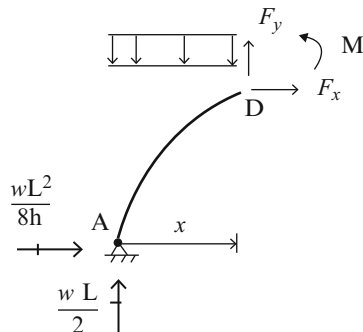


Fig. E6.6d

$$F_x = -\frac{wL^2}{8h}$$

$$F_y = wx - \frac{wL}{2}$$

$$M = \frac{wL}{2}x - \frac{wL^2}{8h}y - \frac{wx^2}{2}$$

Substituting for y , the expression for M reduces to

$$M = \frac{wL}{2}x - \frac{wL^2}{8h} \left\{ 4h \left[\frac{x}{L} - \left(\frac{x}{L} \right)^2 \right] \right\} - \frac{wx^2}{2} = 0$$

It follows that there is *no* bending moment in a three-hinged parabolic arch subjected to uniform loading per horizontal projection.

We could have deduced this result from the theory of cables presented in Chap. 5. We showed there that a cable subjected to a uniform vertical loading adopts a parabolic shape. A cable, by definition, has no moment. Therefore, if one views a parabolic arch as an inverted cable, it follows that the moment in the arch will be zero. This result applies only for uniform vertical loading; there *will* be bending for other types of loading applied to a parabolic arch.

The axial force and transverse shear are determined with the following transformation equations:

$$F = F_x \cos \theta + F_y \sin \theta = -\frac{wL^2}{8h} \cos \theta + \left(wx - \frac{wL}{2} \right) \sin \theta$$

$$V = -F_x \sin \theta + F_y \cos \theta = \frac{wL^2}{8h} \sin \theta + \left(wx - \frac{wL}{2} \right) \cos \theta$$

where

$$\tan \theta = \frac{4h}{L} \left(1 - 2 \frac{x}{L} \right)$$

$$\cos \theta = \frac{1}{\sqrt{1 + \tan^2 \theta}}$$

$$\sin \theta = \frac{\tan \theta}{\sqrt{1 + \tan^2 \theta}}$$

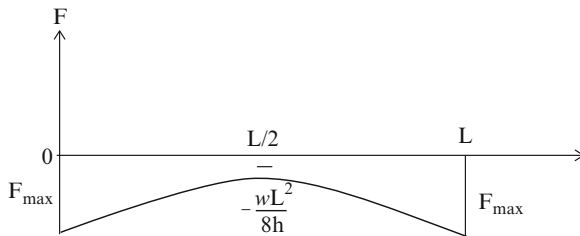
Expanding the expression for V and substituting for $\tan \theta$, one finds

$$V = \left[\tan \theta \frac{wL^2}{8h} + wx - \frac{wL}{2} \right] \cos \theta \equiv 0$$

The shear must be zero since the moment is zero. Only axial force exists for this loading.

The axial force distribution is plotted below. The maximum value is also tabulated as a function of h/L .

| h/L | F_{\max} |
|-------|------------|
| 0.1 | $-1.35wL$ |
| 0.2 | $-0.8wL$ |
| 0.3 | $-0.65wL$ |
| 0.4 | $-0.59wL$ |
| 0.5 | $-0.56wL$ |



The solution, $M = V = 0$, is valid for a uniformly loaded three-hinged parabolic arch, i.e., it applies for both *deep and shallow* arches.

If we use the approximate form of the method of Virtual Forces specialized for a “deep” arch,

$$v_c = \int_S \frac{M \delta M}{EI} ds$$

it follows that the arch does not displace due to bending deformation. However, there will be displacement due to the axial deformation. We need to start with exact expression,

$$v_c = \int_S \left(\frac{M \delta M}{EI} + \frac{F \delta F}{EA} \right) ds$$

and then set $M = 0$

$$v_c \cong \int_S \frac{F \delta F}{EA} ds$$

Suppose the vertical displacement at mid-span is desired. The virtual force system for $\delta P = 1$ is

$$\begin{aligned} \delta F_x &= -\frac{L}{4h} \\ \Rightarrow \quad \delta F &= \left(-\frac{L}{4h} \right) \cos \theta + \left(-\frac{1}{2} \right) \sin \theta \\ \delta F_y &= -\frac{1}{2} \end{aligned}$$

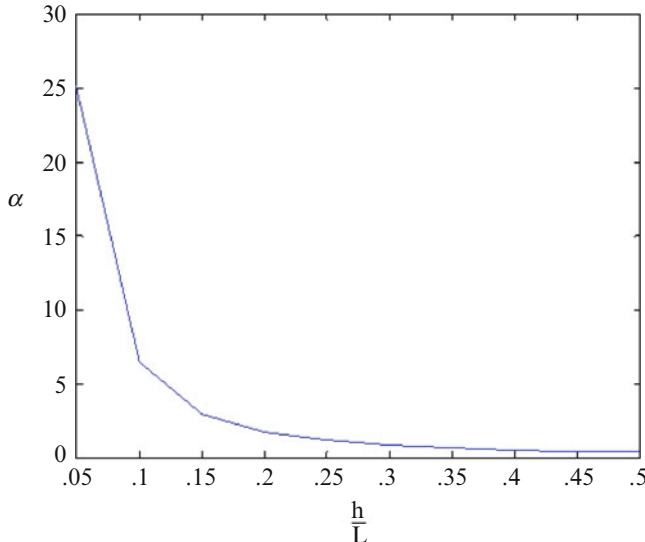
Substituting for the forces and assuming AE is constant results in the following integral

$$v_c = \frac{1}{AE} \int_0^L \left\{ \left(-\frac{wL^2}{8h} \right) + \left(-\frac{wL}{2} + wx \right) \tan \theta \right\} \left(-\frac{L}{4h} - \frac{1}{2} \tan \theta \right) \cos \theta dx$$

We express the solution as

$$v_c = \frac{wL^2}{AE} \{\alpha\}$$

where α is a function of h/L . The following plot shows the variation of α . Note that v_c approaches 0 for a deep arch.



Example 6.7 Three-Hinged parabolic Arch—concentrated load applied at mid-span

Given: The parabolic arch defined in Fig. E6.7a

Determine: The internal forces and vertical displacement at C (v_c).

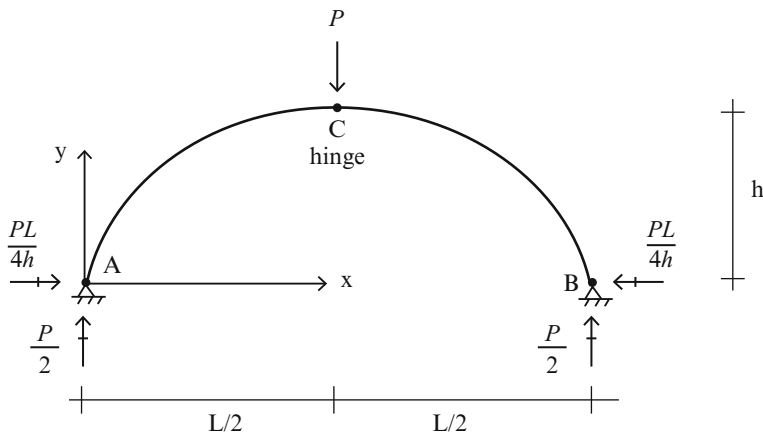


Fig. E6.7a

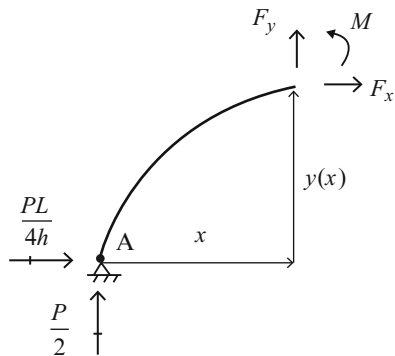
Solution: Enforcing equilibrium leads to the following expressions for the internal forces (Fig. E6.7b):

Segment AC $0 \leq x < L/2$

$$\begin{aligned} F_x &= -\frac{PL}{4h} \\ F_y &= -\frac{P}{2} \\ M &= \frac{P}{2}x - \frac{PL}{4h}y \end{aligned}$$

Segment CB $L/2 < x \leq L$

$$\begin{aligned} F_x &= -\frac{PL}{4h} \\ F_y &= \frac{P}{2} \\ M &= -\frac{P}{2}x - \frac{PL}{4h}y + \frac{PL}{2} \end{aligned}$$

Fig. E6.7b

The corresponding transformed internal forces are

Segment AC $0 \leq x < L/2$

$$\begin{aligned} F &= -\frac{P}{2} \sin \theta - \frac{PL}{4h} \cos \theta \\ V &= -\frac{P}{2} \cos \theta + \frac{PL}{4h} \sin \theta \\ M &= \frac{P}{2}x - PL \left[\frac{x}{L} - \left(\frac{x}{L} \right)^2 \right] = PL \left(-\frac{x}{2L} + \frac{x^2}{L^2} \right) \end{aligned}$$

Segment CB $L/2 < x \leq L$

$$\begin{aligned} F &= \frac{P}{2} \sin \theta - \frac{PL}{4h} \cos \theta \\ V &= \frac{P}{2} \cos \theta + \frac{PL}{4h} \sin \theta \\ M &= PL \left(-\frac{3x}{2L} + \frac{x^2}{L^2} + \frac{1}{2} \right) \end{aligned}$$

The values of F , V , and M are listed below.

| X/L | M/PL | $h/L = 0.5$ | | $h/L = 0.1$ | |
|-------|--------|-------------|-----------|-------------|-----------|
| | | F/P | V/P | F/P | V/P |
| 0 | 0 | -0.67 | 0.22 | -2.51 | 0.46 |
| 0.1 | -0.04 | -0.69 | 0.16 | -2.53 | 0.3 |
| 0.2 | -0.06 | -0.7 | 0.06 | -2.55 | 0.1 |
| 0.3 | -0.06 | -0.7 | -0.08 | -2.55 | -0.1 |
| 0.4 | -0.04 | -0.065 | 0.28 | -2.53 | -0.3 |
| 0.5 | 0 | -0.5 | ∓ 0.5 | -2.5 | ∓ 0.5 |
| 0.6 | -0.04 | -0.65 | 0.28 | -2.53 | 0.3 |
| 0.7 | -0.06 | -0.7 | 0.08 | -2.55 | 0.1 |
| 0.8 | -0.06 | -0.7 | 0.06 | -2.55 | -0.1 |
| 0.9 | -0.04 | -0.69 | -0.16 | -2.53 | -0.3 |
| 1 | 0 | -0.67 | -0.22 | -2.51 | -0.46 |

The maximum moment occurs at the location, where $dM/dx = 0$. Note that $M_{\max} = +PL/4$ for a straight member.

$$\frac{dM}{dx} = 0 \quad \Rightarrow \quad x|_{M_{\max}} = \frac{L}{4} \quad \Rightarrow \quad M_{\max} = -\frac{PL}{16}$$

The distribution of F , V , and M are plotted below. The reversal in sense of M is due to the influence of the horizontal thrust force on the bending moment (Figs. E6.7c–e).

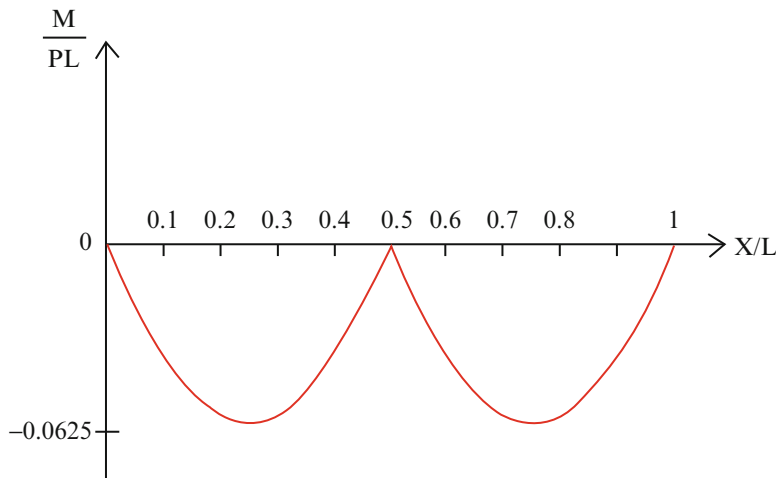


Fig. E6.7c

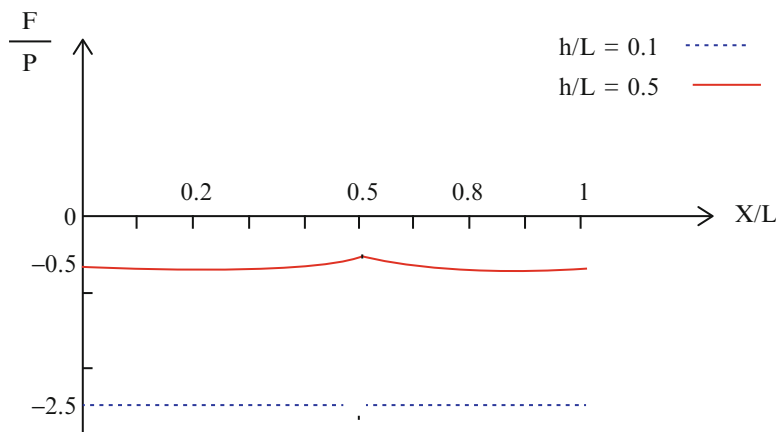
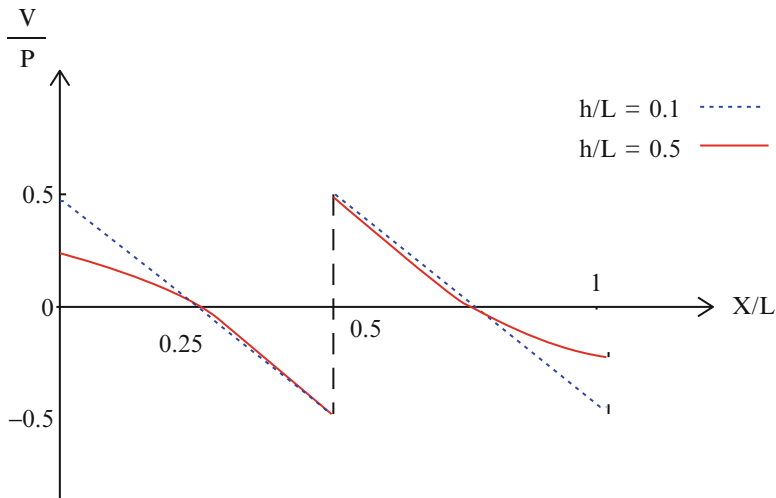
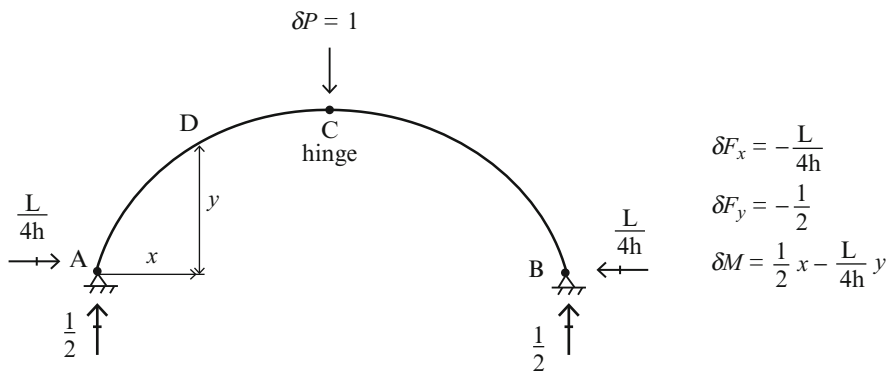


Fig. E6.7d

**Fig. E6.7e**

The virtual forces for the computation of v_c are (Fig. E6.7f)

**Fig. E6.7f**

We consider only bending deformation. The displacement at C is given by

$$v_c = 2 \int_0^{L/2} \frac{P}{2} \left(x - \frac{L}{2h} y \right) \frac{1}{2} \left(x - \frac{L}{2h} y \right) \frac{dx}{EI \cos\theta}$$

When I is a function of x , we use either symbolic or numerical integration. However, when I is taken as $I_0/\cos\theta$, the integral simplifies and one can obtain an analytical solution. The analytical solution corresponding to this assumption is

$$v_c = \frac{PL^3}{EI} \left(\frac{1}{30} \right)$$

Example 6.8 Three-Hinged parabolic arch with horizontal and vertical loads

Given: The parabolic arch and loading defined in Fig. E6.8a.

Determine: (a) Determine the analytical expressions for the axial force, shear force, and bending moment. (b) Using computer software, determine the vertical and horizontal displacements at C due to the loading. Take $E = 29,000$ ksi, $I = 5,000$ in.⁴, and $A = 500$ in.². Discretize the arch using segments of length $\Delta x = 1$ ft. Also determine profiles for displacement, moment, and axial force.

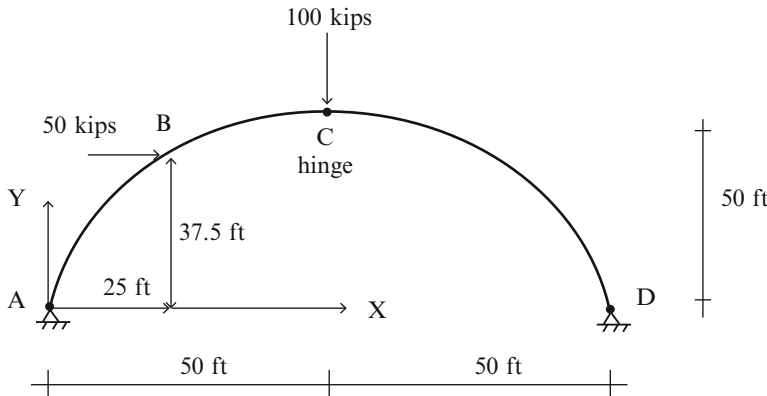


Fig. E6.8a

Solution: (a) The reactions are listed on Fig. E6.8b.

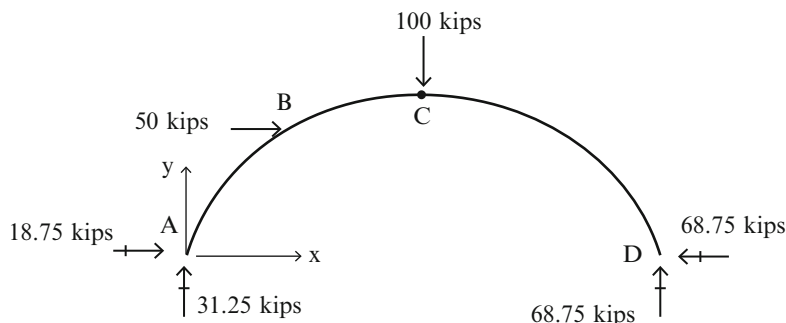


Fig. E6.8b

Noting that $y = 2(x - x^2/100)$ and isolating different segments along the centroidal axis leads to the following expressions for Moment (M), axial force (F), and shear (V).

Segment AB $0 \leq x < 25$

$$\begin{aligned} F_x &= -18.75 & F &= -18.75 \cos \theta - 31.25 \sin \theta \\ F_y &= -31.25 & \Rightarrow & V = -18.75 \sin \theta - 31.25 \cos \theta \\ M &= 31.25x - 18.75y & M &= 31.25x - 18.75y \end{aligned}$$

Segment BC $25 < x < 50$

$$\begin{aligned} F_x &= -68.75 & F &= -68.75 \cos \theta - 31.25 \sin \theta \\ F_y &= -31.25 & \Rightarrow & V = -68.75 \sin \theta - 31.25 \cos \theta \\ M &= 31.25x - 18.75y - 50(y - 37.5) & M &= 31.25x - 18.75y - 50(y - 37.5) \end{aligned}$$

Segment CD $50 < x \leq 100$

$$\begin{aligned} F_x &= -68.75 & F &= -68.75 \cos \theta + 68.75 \sin \theta \\ F_y &= 68.75 & \Rightarrow & V = 68.75 \sin \theta + 68.75 \cos \theta \\ M &= 68.75(100 - x) - 68.75y & M &= 68.75(100 - x) - 68.75y \end{aligned}$$

(b) The computer generated moment, axial force, and deflection profiles are listed below (Figs. E6.8c–e). Hand computation is not feasible for this task.

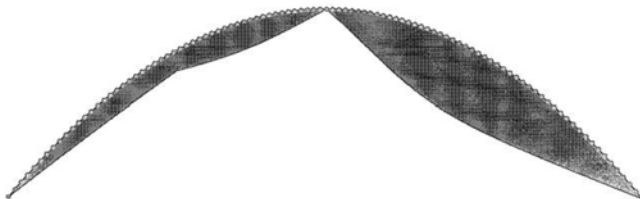


Fig. E6.8c Moment, M



Fig. E6.8d Axial, F

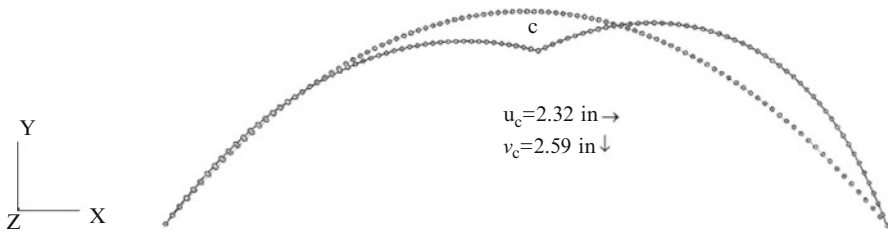


Fig. E6.8e Deflection profile

Example 6.9 Optimal shape for a statically determinate arch

Given: The loading defined in Fig. E6.9a and support locations A and B. Assume H is a variable.

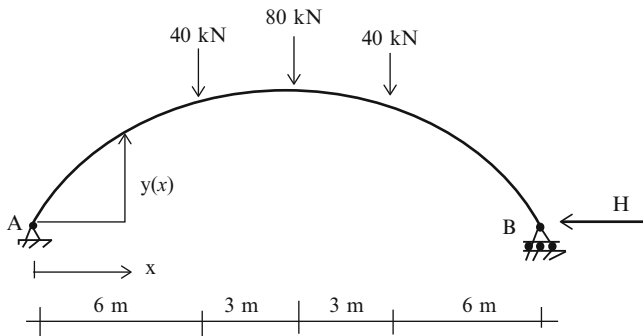


Fig. E6.9a

Determine: The optimal shape of the arch passing through A and B. Consider H to vary from 80 to 200 kN. Note that the optimum shape corresponds to zero bending moment.

Solution: We first generate the bending moment distribution in a simply supported beam spanning between A and B (Fig. E6.9b).

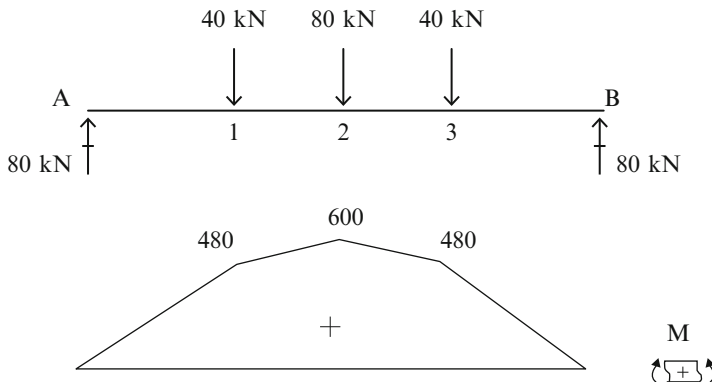


Fig. E6.9b

Requiring the bending moment to vanish at points 1, 2, 3 leads to the following y coordinates of points 1, 2, and 3:

$$y_1 = \frac{480}{H} \quad y_2 = \frac{600}{H} \quad y_3 = \frac{480}{H}$$

This piecewise solution is the general solution for the optimal shape (Fig. E6.9c). One specifies H and then determines the coordinates. The value of H selected depends on the capacity of the supports to resist lateral loading.

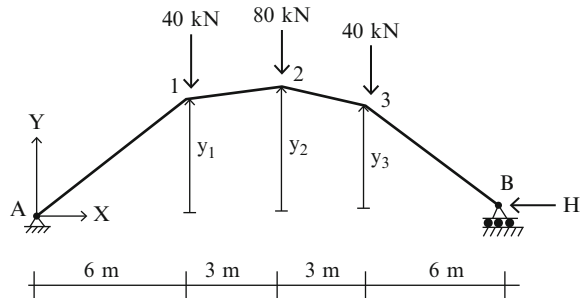


Fig. E6.9c Optimal shape

Configurations corresponding to various values of H are listed below. Note that as H increases, the shape becomes shallower.

| H kN | y_1 m | y_2 m | y_3 m |
|--------|---------|---------|---------|
| 80 | 6 | 7.5 | 6 |
| 120 | 4 | 5 | 4 |
| 160 | 2 | 3.75 | 3 |
| 200 | 1.4 | 3 | 2.4 |

6.7 Summary

6.7.1 Objectives

- To develop the equilibrium equations for planar curved members and illustrate their application to parabolic and circular arches.
- To introduce and apply the Principle of Virtual Forces for planar curved members.
- To describe the analysis process for three-hinged arches.
- To illustrate the behavior of statically determinate parabolic arches subjected to vertical and lateral loading.

6.7.2 Key Factors and Concepts

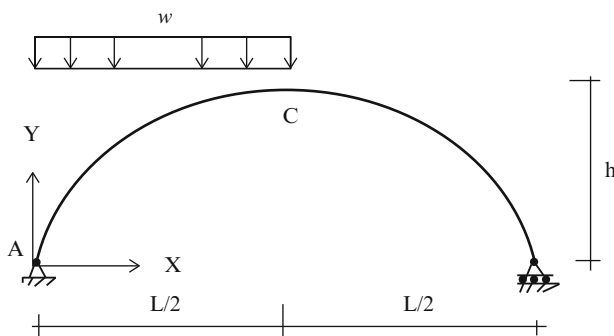
- Depending upon the loading distribution, the geometry of the member, and the support conditions, a curved member may support transverse loading mainly by axial action. This feature makes curved members very attractive for long span structures.
- Curved members are classified as either shallow or non-shallow, depending upon the ratio of height to span length. For shallow members, bending and axial action are coupled. In the limit, a shallow curved member reduces to a beam.
- When applying the principle of virtual forces to compute displacements of a slender non-shallow (deep) curved member, the contributions due to axial and shear deformation are usually negligible compared to the contribution from bending deformation.
- In general, three-hinged arches carry load through both bending and axial action. However, when the arch shape is parabolic and the vertical loading is uniform, there is no bending moment in the three-hinged arch.
- Two-Hinged curved members are statically indeterminate. A general theory for these structures is presented in Chap. 9. One can show that, based on this theory, a moment free state can be obtained for an arbitrary loading, by adjusting the shape of the curved member. In this case, two-hinged curved members can behave similar to cables.

6.8 Problems

Problem 6.1

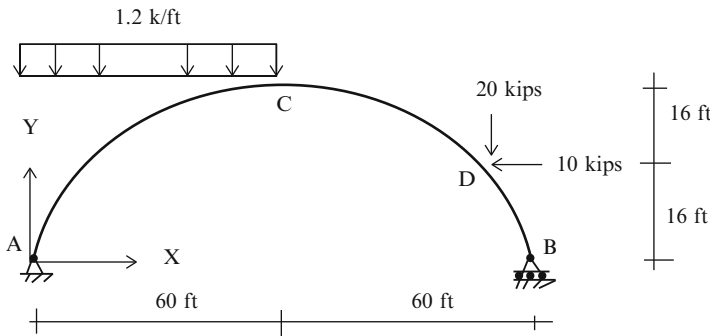
Consider the parabolic member shown below. Find the reactions and member forces (F , V , and M).

- Assume $w = 1.2 \text{ kip/ft}$, $h = 24 \text{ ft}$, $L = 120 \text{ ft}$
- Assume $w = 18 \text{ kN/m}$, $h = 7 \text{ m}$, $L = 36 \text{ m}$

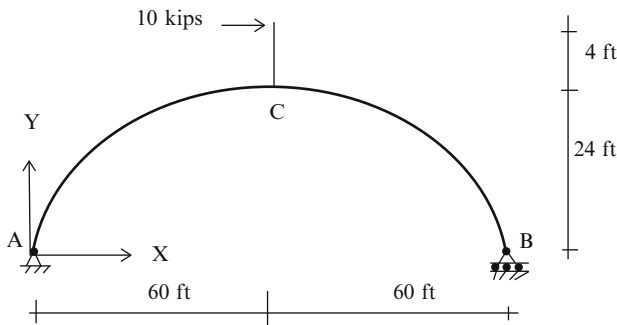


Problem 6.2

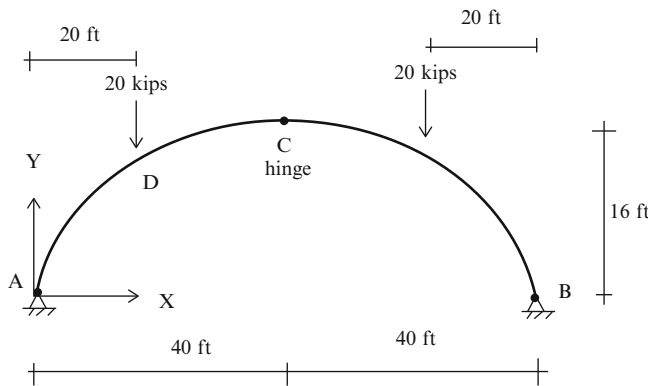
Consider the parabolic member shown below. Find the reactions and member forces at $x = 20$ and 80 ft.

**Problem 6.3**

Consider the parabolic member shown below. Find the reactions and member forces (F , V , and M).

**Problem 6.4**

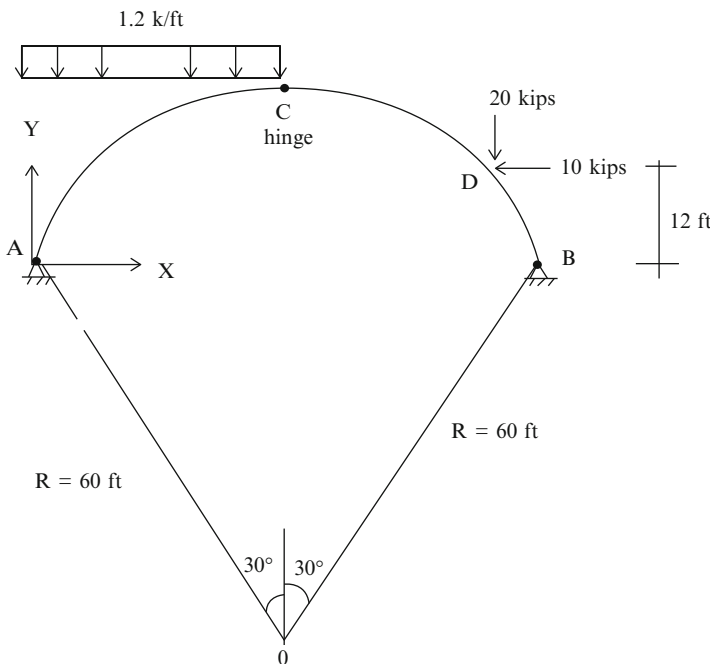
Determine the reactions, the axial and shear forces, and the moments at $x = 30$ ft for the three-hinged parabolic arch shown below.



Problem 6.5

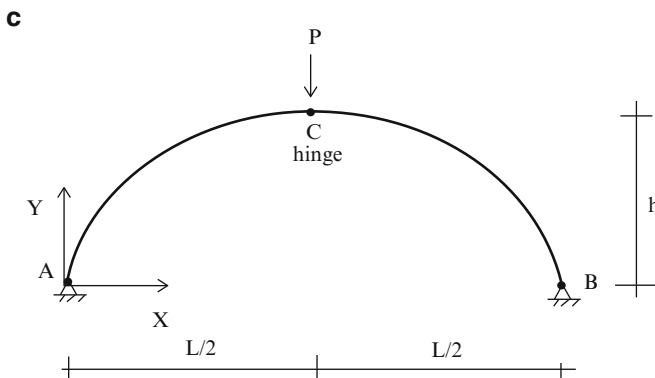
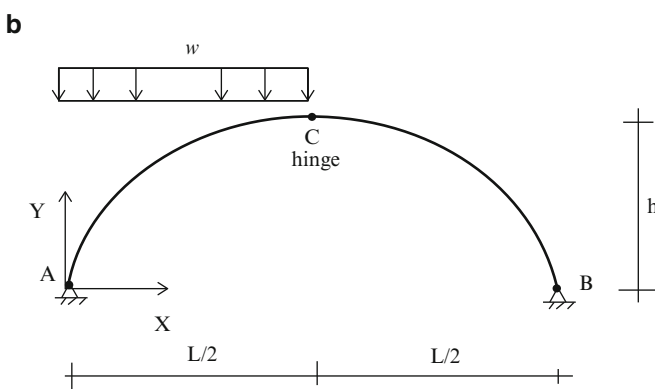
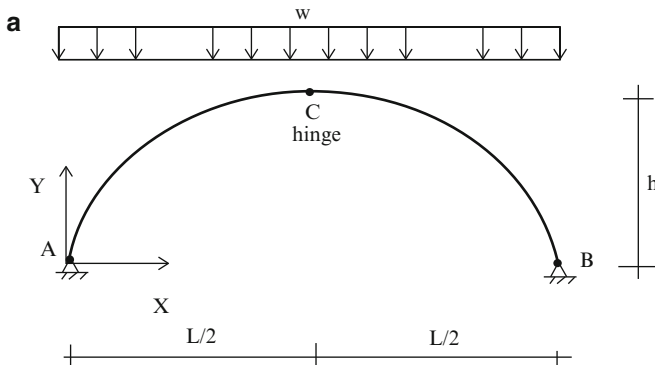
Consider the three-hinged circular arch shown below

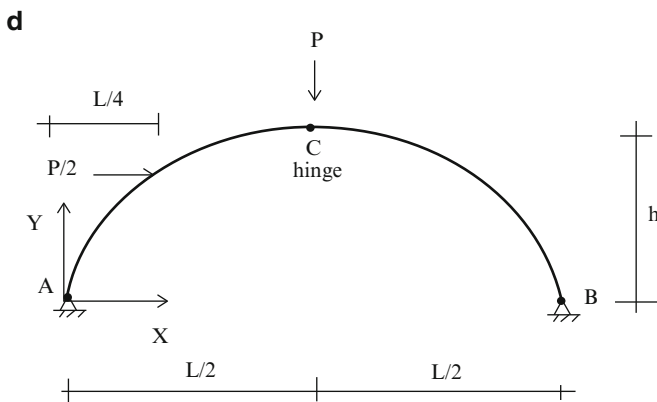
- (a) Find the reactions
- (b) Determine the axial and shear forces and the moments at $x = 20$ ft and $x = 40$ ft.



Problem 6.6

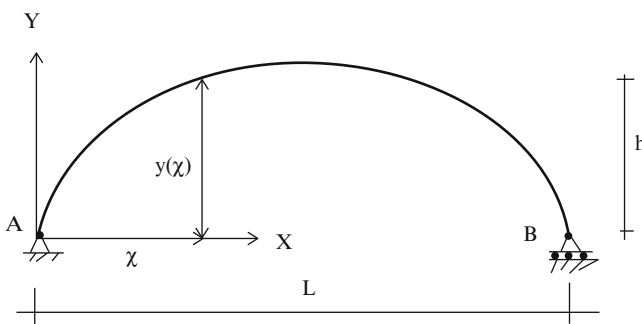
Consider the three-hinged parabolic arches shown below. Determine analytical expression for the axial force, shear force, and bending moment. Using computer software, determine displacement profiles. Take $h = 9 \text{ m}$, $L = 30 \text{ m}$, $P = 450 \text{ kN}$, $w = 30 \text{ kN/m}$, $E = 200 \text{ GPa}$, $I = 160(10^6) \text{ mm}^4$, and $A = 25,800 \text{ mm}^2$





Problem 6.7

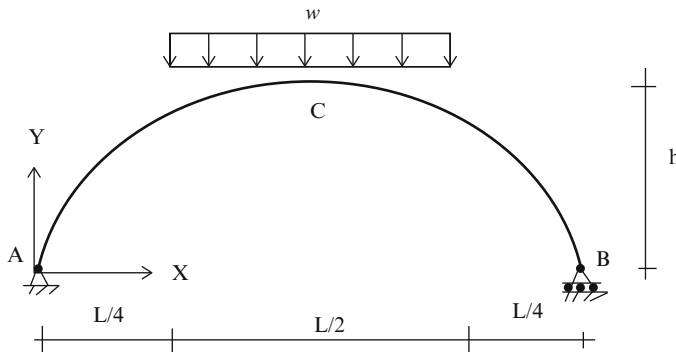
Consider the simply supported curved member shown below. Assume the shape is defined by an arbitrary function, $y = y(x)$. Suppose the member experiences a uniform temperature increase, ΔT , over its entire length. Determine the horizontal displacement of B .



Problem 6.8

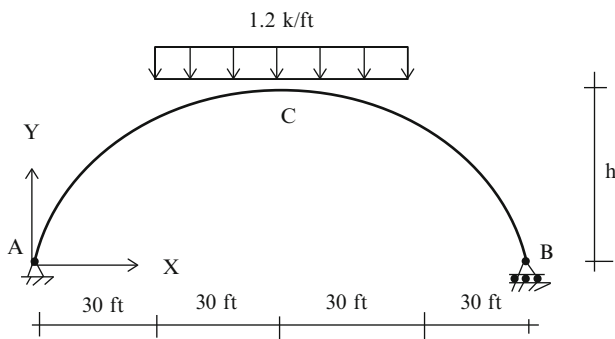
Consider the parabolic member shown below. Determine the horizontal displacement at B .

- (a) Assume $w = 1.2 \text{ kip/ft}$, $h = 24 \text{ ft}$, $L = 120 \text{ ft}$, $E = 29,000 \text{ ksi}$
- (b) Assume $w = 18 \text{ kN/m}$, $h = 7 \text{ m}$, $L = 36 \text{ m}$, $E = 200 \text{ GPa}$

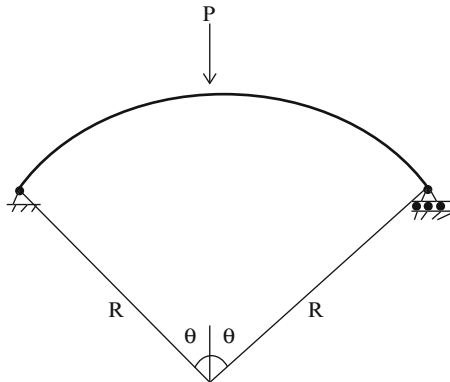
**Problem 6.9**

Consider the parabolic member shown below. Determine the vertical displacement at C. Take $I = 400 \text{ in}^4$, $A = 40 \text{ in}^2$, $E = 29,000 \text{ kip/in}^2$

- (a) $h = 10 \text{ ft}$
- (b) $h = 30 \text{ ft}$

**Problem 6.10**

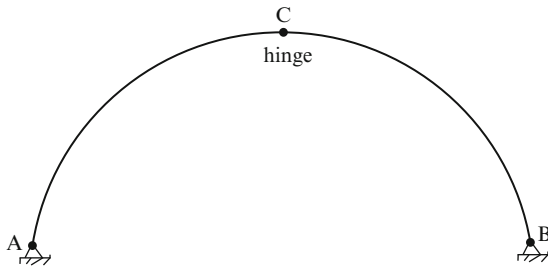
- (a) Determine analytical expressions for the member forces for the circular curved member shown below. Take $R = 40 \text{ ft}$, $P = 10 \text{ kip}$, and $\theta = 30^\circ$.
- (b) Repeat part using a computer software package. Discretize the arc length into 3° segments. Assume the following values for the member properties: $E = 29,000 \text{ ksi}$, $I = 400 \text{ in.}^4$, and $A = 40 \text{ in.}^2$. Compare the analytical and computer generated values for moment and axial force.



Problem 6.11

Consider the three-hinged arch shown below. Discuss how the arch behaves when:

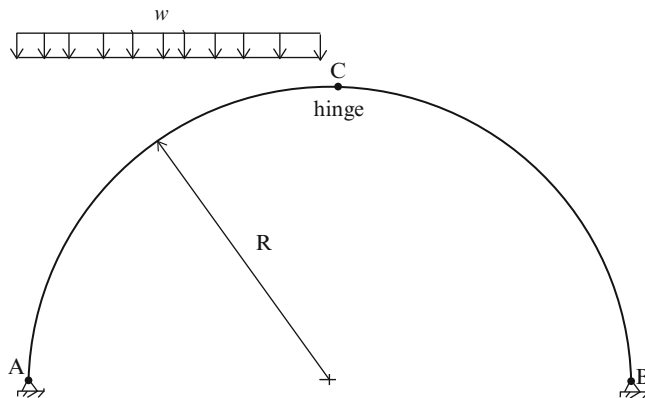
- (a) There is a uniform temperature increase.
- (b) The support at B settles.



Problem 6.12

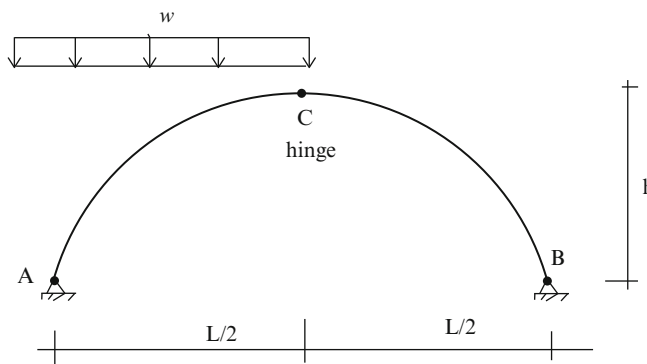
Consider the semicircular three-hinged arch shown below. Determine the vertical and horizontal displacements at C due to the loading.

- (a) Assume $E = 29,000$ ksi, $I = 400$ in.⁴, $A = 40$ in.², $R = 50$ ft, and $w = 2$ kip/ft
- (b) Assume $E = 200$ GPa, $I = 160(10^6)$ mm⁴, $A = 25,800$ mm², $R = 15$ m, and $w = 30$ kN/m

**Problem 6.13**

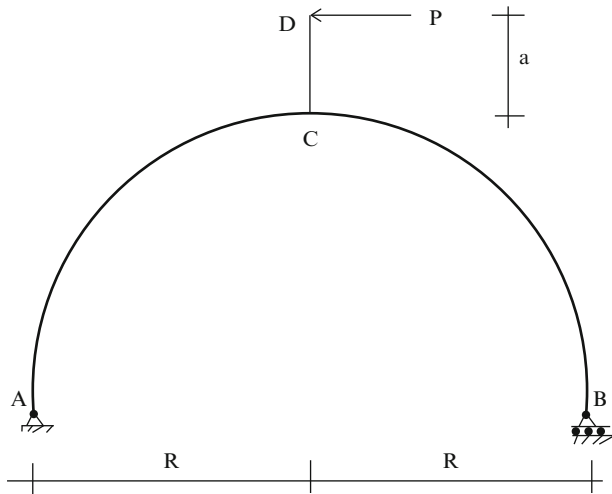
Consider the parabolic three-hinged arch shown below. Using computer software, determine the vertical and horizontal displacements at C due to the loading. Discretize the arch using segments of length $\Delta x = L/10, L/20$, and $L/40$. Compare the convergence rate for these segment sizes.

- Take $E = 29,000$ ksi, $I = 400$ in.⁴, $A = 40$ in.², $L = 120$ ft, $h = 60$ ft, and $w = 2$ kip/ft
- Take $E = 200$ GPa, $I = 160(10^6)$ mm⁴, $A = 2,500$ mm², $L = 36$ m, $h = 18$ m, and $w = 30$ kN/m



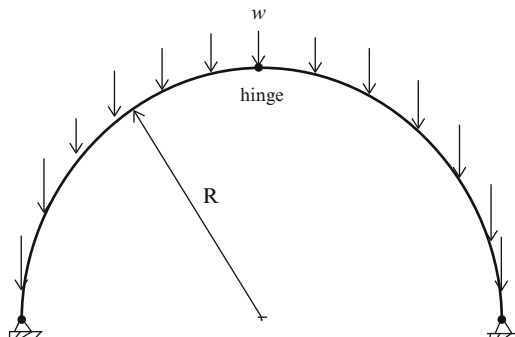
Problem 6.14

Consider the semicircular arch shown below. Member CD is rigidly attached to the arch at C. Determine an expression for the horizontal displacement at D due to P.



Problem 6.15

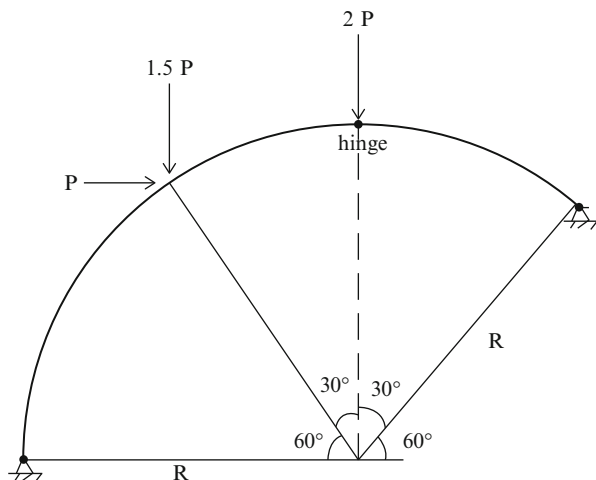
- Determine analytical solutions for the axial, shear, and moment distribution for the three-hinged semicircular arch shown. Consider the loading to be due to self-weight w . Take $w = 0.6 \text{ kip}/\text{ft}$ and $R = 40 \text{ ft}$.
- Apply computer software using the following discretization: $\Delta\theta = 9^\circ, 4.5^\circ, 2.25^\circ$. Compare the convergence rate of the solution. Take $E = 29,000 \text{ ksi}$, $I = 400 \text{ in.}^4$, and $A = 40 \text{ in.}^2$.



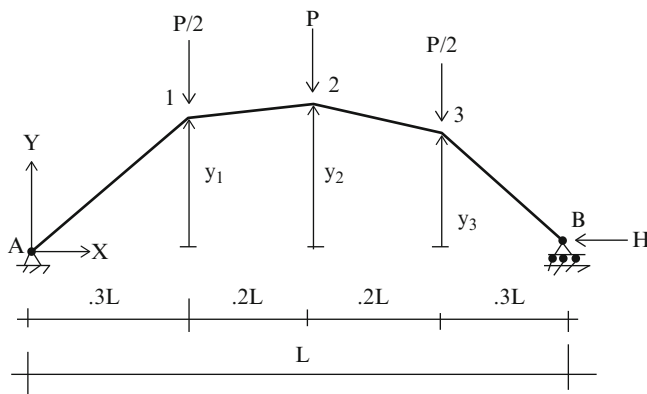
Problem 6.16

Determine the member forces for the three-hinged circular arch shown. Use computer software.

- Take $E = 29,000$ ksi, $R = 40$ ft, $P = 4$ kip, $I = 400$ in. 4 , and $A = 40$ in. 2
- Take $E = 200$ GPa, $R = 12$ m, $P = 18$ kN, $I = 160(10^6)$ mm 4 , and $A = 25,800$ mm 2

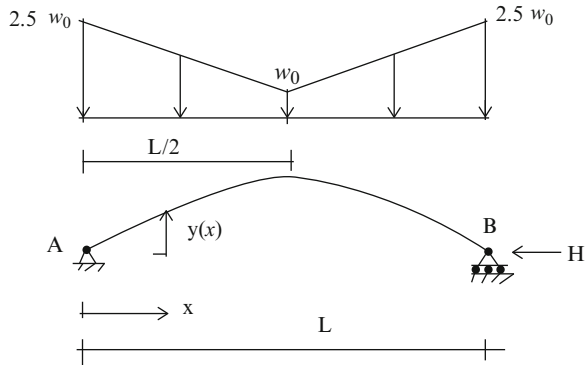
**Problem 6.17**

Determine the optimal shape of the arch passing through A and B for given value of H . Note that optimum shape corresponds to zero moment. Assume $L = 120$ ft and $P = 25$ kip.



Problem 6.18

Determine the optimal shape of the arch for a given value of H . Assume $L = 30\text{ m}$ and $\omega_0 = 15\text{ kN/m}$.

**Problem 6.19**

Consider the three-hinged arch shown below. Determine the reactions and the internal forces.

